An Investigation of a Novel Cyclin-Dependent Kinase Inhibitor as a Treatment Option for Acute Myeloid Leukaemia

Wittawat Chantkran

MD, MSc, FRCPath (Thailand)

Thesis submitted in fulfilment of the requirements for the degree of Doctor of Philosophy

Institute of Cancer Sciences

College of Medical, Veterinary and Life Sciences

University of Glasgow

April 2020

This thesis is dedicated to the scholarship provider, my country, Thailand

Abstract

Acute myeloid leukaemia (AML) is one of the most common haematological malignancies, characterised by the clonal expansion of abnormal or poorly differentiated myeloid cells, infiltrating the bone marrow (BM), blood or extramedullary tissues. Although treatment of AML has progressed over the past few decades, in some patients, particularly elderly patients, usually defined as older than 60-65 years of age, the outcome is dismal due to the remarkable genetic complexity, epigenetic alterations, and the dynamics of the disease. In this study, a newly developed CDK2/9 inhibitor CYC065 was investigated as a treatment option for AML.

OCI-AML3, MOLM-13, and MV4-11 AML cell lines were used, aiming to encompass the stratifications of major risk profiles according to the European LeukemiaNet (ELN) recommendations, to assess the effects of CYC065 on growth and survival of AML cells. It was observed that AML cells were sensitive to the treatment with CYC065. The longer CYC065 exposure, the greater the cytotoxic/anti-metabolic effect on the cells, with a reduction of the IC50. This was consistent with apoptosis results, which were induced over the 72h investigated. The percentage of active caspase-3-positive cells was also increased and correlated with an increase in the percentage of annexin V-positive cells across higher CYC065 concentrations. In cell cycle analysis, Gap 1 (G1) arrest was observed at 4h in OCI-AML3 and MV4-11 cell lines, indicating that cell cycle arrest occurred at an early time point which precedes the induction of cell death at 24h.

The effects of CYC065 on proteins and gene expression were interrogated in the three cell lines. By using Western blotting, a downregulation of RNA polymerase II (RNAPII) was observed following treatment with CYC065 for 4h. Among the B-cell lymphoma 2 (BCL-2) family, a dramatic reduction of short half-life myeloid cell leukemia 1 (MCL-1) level was seen at both gene and protein level, highlighting a potential target inhibition of CYC065. A decrease in extracellular signal-regulated protein kinases 1 and 2 (ERK1/2) was mutually observed in all cell lines, potentially reducing MCL-1 stability. The reduction of MCL-1 results in rapid induction of apoptosis. A decrease in gene expression of E2F transcription factor 1 (*E2F1*) was demonstrated, which potentially leads to G1 arrest.

CYC065 in combination with other therapeutics; the selective BCL-2 inhibitor venetoclax, the conventional chemotherapy cytarabine, or the hypomethylating agent azacitidine was assessed for synergistic activity. Combination studies using CompuSyn software were performed to investigate the most efficacious drug combination ratios which were utilised for further synergistic investigations. Using various methods, the synergistic effect of CYC065/venetoclax, CYC065/cytarabine, and CYC065/azacitidine combinations were observed in all cell lines tested in this study. Rationally, the combination studies using these partners were continued in primary human AML samples.

Primary human AML and normal haematopoietic cells were treated with two different concentrations of each therapeutic drug to encompass sensitive and resistant AML responses. The doses used were; 0.25μM or 0.5μM of CYC065, 0.025μM or 0.5μM of venetoclax, 0.01μM or 0.1μM of cytarabine, and 0.5μM or 2μM of azacitidine as a single agent or in combination for 72h. The data from six primary AML and three normal control samples are summarised aiming to observe a global effect of the treatments. Although not statistically significant, a decrease in cell number synchronously with an increase in annexin V-positive cells in the apoptosis assays, active caspase-3-positive cells in the active caspase-3 assays and an increase in the percentage of sub G0 population in cell cycle analysis was seen in the combination arms as compared with the single arms at both low and high concentrations in a dose-dependent manner. By contrast, normal cells experienced toxicity only at high concentrations of single and combination treatments with the exception of a single treatment of CYC065 and venetoclax. In the cell proliferation assays, at high concentrations, CYC065/azacitidine combination showed the synergistic effect in cell division arrest in primary AML but not in normal control samples, thus, a favourable therapeutic window was observed. Nevertheless, the concentrations of CYC065 and azacitidine needed to be tapered in order to reduce toxicity to normal cells. For the colony-forming unit (CFU) assays, although representing a small proportion of primary AML samples, a decrease in colony number, in which the majority of the colonies were CFU-monocyte (CFU-M), was seen in combination arms as compared with single treatments in a dose-dependent manner. The same effect was observed in normal samples in which a decline in colony number was seen regardless of colony type.

High diversity of genetic mutations was observed for primary human AML samples. Considering the responses to the treatment of each sample as an individual, it was observed that the more complex the molecular genetic lesions or complexity of karyotype, the less efficacious the combination therapy responses observed. A variable response of these primary samples was the most plausible explanation for statistically insignificant results when a global effect of the treatments was evaluated. Nonetheless, an insufficient number of cases could introduce overinterpretation. Consequently, although the results were promising, it is inappropriate to draw any conclusions at present, with a larger cohort of patient samples required in order to fully evaluate the findings.

In summary, our studies indicate the efficacy of the novel CDK2/9 inhibitor CYC065 as a single agent or in conjunction with frontline AML chemotherapeutics highlighting the potential of CYC065 for a novel therapeutic approach. Our work implicates the importance of individual genetic profiling as a critical step prior to initiating therapy for AML, highlighting the need for a more personalised medicine approach to improve outcomes in AML.

Table of contents

List of Tables

List of Figures

Publication in preparation

Chantkran, W., Zheleva, D., Frame, S., Hsieh, Y., Wheadon, H., Copland, M. CYC065, a novel CDK2/9 inhibitor - a potential therapeutic approach for acute myeloid leukemia.

Presentations

European School of Haematology, 4th International Conference on Acute Myeloid Leukemia "Molecular and Translational": Advances in Biology and Treatment, Estoril, Portugal, 2017
Type: Poster presentation
Title: Characterisation of the Mechanism of Action of CYC065, a Novel CDK Inhibitor, in Acute Myeloid Leukaemia (AML)
Authors: Wittawat Chantkran, Sheelagh Frame, Daniella Zheleva, Ya-Ching Hsieh and Mhairi Copland

European School of Haematology, 5th International Conference on Acute Myeloid Leukemia "Molecular and Translational": Advances in Biology and Treatment, Estoril, Portugal, 2019
Type: Poster presentation
Title: Combination of CYC065, a Second Generation CDK2/9 Inhibitor, with Venetoclax or Standard Chemotherapies – a Novel Therapeutic Approach for Acute Myeloid Leukaemia (AML)
Authors: Wittawat Chantkran, Sheelagh Frame, Daniella Zheleva, Ya-Ching Hsieh and Mhairi Copland

61st American Society of Hematology Annual Meeting & Exposition, Orlando, Florida, The USA, 2019
Type: Poster presentation
Title: Combination of CYC065, a Second Generation CDK2/9 Inhibitor, with Venetoclax or Standard Chemotherapies – a Novel Therapeutic Approach for Acute Myeloid Leukaemia (AML)
Authors: Wittawat Chantkran, Sheelagh Frame, Daniella Zheleva, Ya-Ching Hsieh, Helen Wheadon and Mhairi Copland

Acknowledgements

This PhD degree was sponsored by Ministry of Science and Technology. I am grateful to Thailand for this fully funded scholarship. The completion of this study was made possible by Paul O'Gorman Leukaemia Research Centre, University of Glasgow, thank you very much. I would like to express my sincere gratitude and appreciation to my supervisor Professor Mhairi Copland for your guidance, motivation and patience (especially for my English writing). Thank you for being my role model and showing me how to be "a good clinician" and "a great scientist" at the same time. I am greatly indebted to Professor Helen Wheadon, my co-supervisor, for your generous, supportive and encouragement. Thank you for your solutions for all of technical problems in laboratory (which I know that I will definitely get answers if I run to you). You are "always" there for me. Thank you both of you, by heart not just a word, for showing me how to be a nice supervisor and how to treat your student properly. This is also one of the transferable skills that I've learnt.

I would like to thank Dr Alison Michie and Dr Karen Keeshan for those three consecutive annual reviews. Your comments and tips are really useful and applicable. I would like to thank Dr Alan Hair for primary sample processing, Jennifer Cassels for your guidance in flow cytometry and for preparing culture media as well. I thank Dr Heather Jørgensen for your support as a convener of the institute, Joana Silvestre for creating the heatmaps, Diane Verrecchia and Angela Newlands for facilitating administrative processes. Special thanks to Dr Daniella Zheleva and Dr Sheelagh Frame from Cyclacel Pharmaceuticals.

Back to the first day at POG in 2016, Dr Chinmay Munje, as a postdoc, was the first person who taught me how to use pipettes from the first drop as I know "absolutely" nothing, many thanks. Caroline Busch, thank you for your support, in particular, in terms of entertaining (I will never ever forget our trips in Mumbai and Disneyland in Florida). Narissa Parry, as a native speaker, thank you for being my advisor in English. Kudzai Nyamondo, you are so kind, generous and funny. Dr Gillian Horne, Dr Rebecca Mitchell, Lauren Hope and Chidchanok Chornkrathok, thank you for your help.

Finally, I would like to thank anyone who reads this thesis. I hope you will gain the benefits from my results and be able to apply them for further studies.

Declaration of authorship

I declare that, except for where noted, all work contained in this thesis was performed and composed by myself. Where others have contributed to elements of the work, this is stated clearly in the text. No element of this work has been submitted for any other degree of professional qualification.

Wittawat Chantkran

Abbreviations

% Annexin V, Percentage of annexin V-positive cells (apoptosis assay)
% Caspase-3, Percentage of active caspase-3-positive cells (active caspase-3 assay)
% Sub G0, Percentage of sub G0 population (cell cycle analysis)
7-AAD, 7-Aminoactinomycin D (apoptosis assay)
AFF1 or AF4, ALL1-fused gene from chromosome 4 (AF4)/FMR2 Family Member 1
Akt, Protein kinase B
ALL, Acute lymphoblastic leukaemia
AML, Acute myeloid leukaemia
AML-MRC, Acute myeloid leukaemia with myelodysplasia-related changes
AP1, Activator protein 1
Apaf-1, Apoptotic protease activating factor-1
APC/C, Anaphase-promoting complex/cyclosome
APL, Acute promyelocytic leukaemia
AraC, Cytarabine
AraC1, 0.01μM of cytarabine
AraC2, 0.1μM of cytarabine
ARF, Alternative reading frame
ASR, Worldwide age-standardised rate
ASXL1, Additional sex combs-like 1
ATCC, American Type Culture Collection
ATF3, Activating transcription factor 3
ATL, Adult T-cell leukaemia/lymphoma
ATM, Ataxia telangiectasia-mutated
ATP, Adenosine triphosphate
ATR, Ataxia telangiectasia and Rad3-related protein
ATRA, All-trans retinoic acid
AV, Annexin V (apoptosis assay)
AZA, Azacitidine
AZA1, 0.5μM of azacitidine
AZA2, 2μM of azacitidine
BAD, B-cell lymphoma 2-associated death promoter
BAK, B-cell lymphoma 2 homologous antagonist/killer
BAK1, B-cell lymphoma 2 antagonist/killer 1
BAX, B-cell lymphoma 2-associated X
BCL-2, B-cell lymphoma 2
BCL2L1, B-cell lymphoma 2 like 1
BCL-w, B-cell lymphoma 2-like protein 2
BCL-xL, B-cell lymphoma-extra large
BCR-ABL, Breakpoint cluster region protein-Abelson murine leukemia viral oncogene homolog
BET, Bromodomain (BRD) and extra-terminal
BFU-E, Burst-forming unit-erythrocyte
BH, B-cell lymphoma 2 homology
BID, B-cell lymphoma 2 homology 3 interacting-domain death agonist
BIM(EL), B-cell lymphoma 2-like protein 11-extra long
BIM, B-cell lymphoma 2-like protein 11
BIRC5, Baculoviral inhibitor of apoptosis repeat-containing 5 (survivin)
BM, Bone marrow

BMF, B-cell lymphoma 2 modifying factor
BrdU, bromodeoxyuridine
BSA, Bovine serum albumin
b-ZIP, C-terminal basic leucine zipper
CAD, Caspase-activated DNase
CAK, Cyclin-dependent kinase-activating kinase
CAMK, Ca2+/calmodulin-dependent protein kinase
Cancer stem cell, CSC
CBF, Core-binding factor
CD, Cluster of differentiation
CDC25, Cell division cycle 25
CDK, Cyclin-dependent kinase
CDKI, Cyclin-dependent kinase inhibitor
CDKN1A, Cyclin-depend kinase inhibitor 1A ($p21^{Cip1}$)
CDKN2C, Cyclin-depend kinase inhibitor 2C ($p18^{INK4C}$)
CDKN2D, Cyclin-depend kinase inhibitor 2D ($p19^{INK4D}$)
CDKN3, Cyclin-depend kinase inhibitor 3
CEBPA, CCAAT/enhancer-binding protein alpha
cFLIP, cellular Fas-associated protein with death domain-like IL-1ß converting enzyme (FLICE)-like inhibitory protein
CFU, Colony-forming unit
CFU-E, Colony-forming unit-erythrocyte
CFU-F, Colony-forming unit-fibroblast
CFU-G, Colony-forming unit-granulocyte
CFU-GEMM, Colony-forming unit-granulocyte, erythrocyte, monocyte, and megakaryocyte
CFU-GM, Colony-forming unit-granulocyte, monocyte
CFU-M, Colony-forming unit-monocyte
CFU-S, Colony-forming unit-spleen
CHIP, Clonal haematopoiesis of indeterminate potential
ChIP-qPCR, chromatin immunoprecipitation and quantitative polymerase chain reaction
CHK, Checkpoint kinase
cIAP, cellular inhibitors of apoptosis
Cip/Kip, Cyclin-dependent kinase interacting protein/kinase inhibitor proteins
CLL, Chronic lymphocytic leukaemia
CML, Chronic myeloid leukaemia
CMML, Chronic myelomonocytic leukaemia
CMP, Common myeloid progenitor
CR, Complete remission
CRi, Complete remission with incomplete recovery
CSF, Colony-stimulating factor
CT, Cycle threshold
CTD, Carboxy-terminal domain
CTV, CellTrace™ Violet (cell proliferation assay)
CV, Coefficient of variation
CYC1, 0.25µM of CYC065
CYC2, 0.5µM of CYC065
CYLD, Cylindromatosis (de-ubiquitinating enzyme)
Cyt c, Cytochrome c
DAPI, 4′,6-diamidino-2-phenylindole (apoptosis assay)
DC, Dendritic cell

Diablo, Direct inhibitor of apoptosis-binding protein with low isoelectric point
DIFP, Diisopropylfluorophosphate
DISC, Death-inducing signaling complex
Div, Division
DLBCL, Diffuse large B-cell lymphoma
DMSO, Dimethylsulphoxide
DNA, Deoxyribonucleic acid
DNMT3A, DNA methyltransferase 3 alpha
DOT1-L, H3K79 histone methyltransferase disruptor of telomeric silencing 1-like
DR, Death receptor
DSIF, 5,6-dichloro-1-ß-D-ribofuranosylbenzimidazole (DRB) sensitivity-inducing factor
EFS, Event-free survival
EGFR, Epidermal growth factor receptor
ELL, Elongation factor for ribonucleic acid polymerase II
ELN, European LeukemiaNet
EphA1, Ephrin-receptor A1
EPO, Erythropoietin
ERK, Extracellular signal-regulated kinase
EZH2, Enhancer of zeste homolog 2
FA, Fanconi anaemia
FADD, Fas-associated death domain
Fas, Fas receptor
FasL, Fas ligand
FBS, Foetal bovine serum
Fbw7γ, F-box protein component to the E3 ubiquitin ligase complex
FDA, U.S. Food and Drug Administration
FLT3, FMS-like tyrosine kinase 3
FLT3-ITD, FMS-like tyrosine kinase 3-internal tandem duplication
FLT3L, FMS-like tyrosine kinase 3 ligand
FLT3-TKD, FMS-like tyrosine kinase 3-tyrosine kinase domain
G0 phase, Quiescence state
G1 phase, Gap 1 phase
G2 phase, Gap 2 phase
G-CSF, Granulocyte colony-stimulating factor
GM-CSF, Granulocyte-macrophage colony-stimulating factor
GO, anti-CD33 Gemtuzumab ozogamicin
GSK3ß, Glycogen synthase kinase 3 beta
H3K27me3, Tri-methylation of histone H3 lysine 27
H3K4me2, Di-methylation of histone H3 lysine 4
HBSS, Hank's Balanced Salt Solution
hCNT, human concentrative nucleoside transporters
HDAC, Histone deacetylase
HDACI, Histone deacetylase inhibitor
hENT, Human equilibrative nucleoside transporters
Hh, Hedgehog
HHMS, Hereditary myeloid malignancy syndrome
HIDAC, High-dose cytarabine
HLA-DR, Human leukocyte antigen–DR isotype
HMA, Hypomethylating agent
hMOF, MOZ, Ybf2/ Sas3, Sas2 and Tip60 (MYST) protein Male Absent on the First
HOX, Homeobox

HPC, Haematopoietic progenitor cell
HR, Hazard ratio
HSC, Haematopoietic stem cell
HSCT, Haematopoietic stem cell transplantation
HSPC, Haematopoietic stem and progenitor cell
HTLV-1, Human T-lymphotropic virus 1
HtrA2 , High-temperature requirement A serine peptidase 2
IAP, Inhibitors of apoptosis
IBMFS, Inherited bone marrow failure syndrome
IC, Intensive chemotherapy
ICAD, Inhibitor of caspase-activated DNase
IDAC, Intermediate-dose cytarabine
IDH, Isocitrate dehydrogenase
IgVH, Immunoglobulin variable heavy chain gene
IL, Interleukin
IMDM, Iscove's Modified Dulbecco's Medium
INF, Interferon
INK4, Inhibitors of cyclin-dependent kinase 4
IκBα, Nuclear factor of kappa light polypeptide gene enhancer in B-cells inhibitor, alpha
JAK, Janus kinase
JNK, c-Jun N-terminal kinase
KIT, Tyrosine-protein kinase Kit
KL, Tyrosine-protein kinase KIT ligand
KMT2A or *MLL*, Lysine-specific methyltransferase 2A or Mixed lineage leukaemia
KMT2A-PTD, Lysine-specific methyltransferase 2A-partial tandem duplication
KMT2A-R, Lysine-specific methyltransferase 2A/Mixed lineage leukaemia rearrangement
LDAC, Low-dose cytarabine
LFS, Leukaemia-free survival
Lin, Lineage
LSC, Leukaemic stem cell
LSD-1, Lysine-specific demethylase 1
LTC-IC, Long-term culture initiating cell
M phase, Mitosis phase
mAb, Monoclonal antibody
MAPK, Mitogen-activated protein kinase
MBL, Monoclonal B-lymphocytosis
MCL-1, Myeloid cell leukemia 1
MCM7, Minichromosome maintenance complex component 7
M-CSF, Macrophage colony-stimulating factor
MDM2, Mouse double minute 2 homolog
MDS, Myelodysplastic syndromes
MEF, Mouse embryonic fibroblast
MEIS1, Meis Homeobox 1
MEK, Mitogen-activated protein kinase kinase
MFC, Multi-parameter flow cytometry
MGUS, Monoclonal gammopathy of undetermined significance
MLLT1 or ENL, Myeloid/lymphoid or mixed-lineage leukaemia; translocated to, 1 or eleven nineteen leukaemia
MLLT10 or AF10, Myeloid/lymphoid or mixed-lineage leukaemia; translocated to, 10 or ALL1-fused gene from chromosome 10

MLLT3 or AF9, Myeloid/lymphoid or mixed-lineage leukaemia; translocated to, 3 or ALL1-fused gene from chromosome 9
MLP, Multilymphoid progenitor
MM, Multiple myeloma
MOMP, Mitochondrial outer membrane permeabilisation
MPN, Myeloproliferative neoplasm
mTOR, mammalian target of rapamycin
MTT, 3-(4,5-dimethylthiazol-2-yl)-2,5-diphenyltetrazolium bromide
MYC, Myelocytomatosis oncogene
MYCN, Neuroblastoma myelocytomatosis oncogene
MYH11, Myosin heavy chain 11
NCRI, UK National Cancer Research Institute
NDC, No drug control
NELF, Negative elongation factor
NES, Nuclear export signal
NF-κB, Nuclear factor kappa-light-chain-enhancer of activated B cells
NGS, Next-generation sequencing
NOD/SCID, Non-obese diabetic/severe combined immunodeficient
Non-SCLC, Non-small cell lung cancer
NOXA, Phorbol-12-myristate-13-acetate-induced protein 1
NPM1, Nucleophosmin 1
OS, Overall survival
PB, Peripheral blood
PBS, Phosphate-buffered saline
PCNA, Proliferating cell nuclear antigen
PCR, Polymerase chain reaction
PDX, Patient-derived xenograft
Pen/Strep, Penicillin-streptomycin
PGE2, Prostaglandin E2
PHD, Plant homology domain
PI, Propidium iodide (cell cycle analysis)
PI3K, Phosphoinositide-3-kinase
PKC, Protein kinase C
PLK, Polo-like kinase
PNH, Paroxysmal nocturnal haemoglobinuria
PP1, Protein phosphatase 1
PPP1R10, Protein phosphatase 1 regulatory subunit 10
PR, Partial remission
PRC2, Polycomb repressive complex 2
pre-LSC, pre-leukaemic stem cell
P-TEFb, Positive transcription elongation factor b
PTEN, Phosphatase and tensin homolog
PTK, Protein tyrosine kinase
PUMA, p53 upregulated modulator of apoptosis
qPCR, Quantitative polymerase chain reaction
RAS, Rat sarcoma viral oncogene homolog
Rb, Retinoblastoma protein
RHD, Runt homology domain
RNA, Ribonucleic acid
RNAPII, Ribonucleic acid polymerase II
ROS, Reactive oxygen species
RPMI, Roswell Park Memorial Institute media

RRM1/2, Ribonucleoside-diphosphate reductase large subunit and subunit M2
RT, Room temperature
RTK, Receptor tyrosine kinase
RUNX1, Runt-related transcription factor 1
RUNX1T1, Runt-related transcription factor 1 partner transcriptional co-repressor 1
S phase, Synthesis phase
S2, Serine 2
S473, Serine 473
S5, Serine 5
S62, Serine 62
S70, Serine 70
S780, Serine 780
S807/S811, Serine 807/Serine 811
S9, Serine 9
s-AML, Acute myeloid leukaemia secondary to myelodysplastic syndromes
SC, Stem cell
SCF, Stem cell factor
SCLC, small cell lung cancer
SD, Standard deviation
SF3B1, Splicing Factor 3b Subunit 1
SH-PTP2, Src homology 2 protein-tyrosine phosphatase
shRNA, short hairpin RNA
siRNA, short interfering RNA
Smac, Second mitochondria-derived activator of caspase
SMC, Structural maintenance of chromosomes
SMO, Sonic hedgehog receptor smoothened
Src, Sarcoma tyrosine kinase
SRSF2, Serine arginine-rich splicing factor 2
ST6Gal1, Beta-galactoside alpha-2,6-sialyltransferase 1
STAG2, Stromal antigen 2
STAT, Signal transducers and activators of transcription
STK, Serine/Threonine kinase
SWOG, US Southwest Oncology Group
T160, Threonine 160
T180/Y182, Threonine 180/Tyrosine 182
T202/Y204, Threonine 202/Tyrosine 204
T320, Threonine 320
T390, Threonine 390
t-AML, therapy-related AML
TET2, Ten-eleven translocation methylcytosine dioxygenase 2
TFIIH, Transcription factor II H
TGF-β, Transforming growth factor β
Thy-1 or CD90, Thy-1 cell surface antigen
TLR, Toll-like receptor
TNFR1, Tumour necrosis factor-α receptor 1
TNF-α, Tumour necrosis factor-α
TOX4, Thymocyte selection-associated high mobility group box family member 4
TP53, Tumour protein p53
TPO, Thrombopoietin
TRADD, Tumour necrosis factor receptor-associated death domain
TRAF, Tumour necrosis factor receptor-associated factor

TRAIL, Tumour necrosis factor-related apoptosis-inducing ligand
TRM, Treatment related mortality
TST, Timed sequential therapy
U2AF1, U2 small nuclear RNA auxiliary factor 1
Ub, Ubiquitin
UCK1/2, Uridine-cytidine kinases 1 and 2
VAF, Variant allele frequency
VEN, Venetoclax
VEN1, 0.025μM of venetoclax
VEN2, 0.5μM of venetoclax
vs, versus
WDR82, Typtophan-aspartate (WD) repeat-containing protein 82
WHO, World Health Organization
WT1, Wilms' tumour suppressor gene1
XIAP, X-linked inhibitor of apoptosis protein
ZRSR2, Zinc finger CCCH-type, ribonucleic acid-binding motif and serine/arginine rich 2

Chapter 1 Introduction

1.1 Cell biology

1.1.1 The cell cycle

The majority of 10^{13}–10^{14} cells in human body are outside of an active cell cycle and are non-dividing. Some of these non-dividing cells are irreversibly arrested and become terminally differentiated or senescent, whereas, a subset of them called quiescent cells, e.g. stem and progenitor cells, hepatocytes, fibroblasts, lymphocytes and some of epithelial cells (Yao, 2014) can re-enter the proliferative cell cycle in response to physiological growth signals.

Cell cycling begins from a quiescence state (G0) in which a cell stops dividing and is then followed by the interphase, comprised of Gap 1 (G1), Synthesis (S), and Gap 2 (G2) phases. In the G1 phase, a cell increases in size (to about double its original size) and a high amount of transcriptional and translational machineries are synthesised for further protein synthesis and DNA duplication. In addition, more organelles are produced and the volume of the cytoplasm also increases. Crucially, G1 checkpoint control is a necessary mechanism to ensure that a cell is ready for DNA synthesis in the S phase where the amount of DNA is doubled but the number of chromosomes remains constant. After that, a cell progresses to the G2 phase. The mitochondria divide and the cell continues to grow in preparation for division and G2 checkpoint occurs before entering the mitosis (M) phase. At this point, a cell's growth is temporarily halted. Mitosis consists of five morphologically distinct phases, including prophase, prometaphase, metaphase, anaphase, and telophase (Maton et al., 1997; O'Connor, 2008). During prophase, the chromatin coils and becomes increasingly compact, resulting in the formation of visible chromosomes. The replicated chromosomes have an X shape called sister chromatids which are pairs of identical copies of DNA joined at centromere. Then, the mitotic spindle made of microtubules begins to form at opposite ends of the cell and is responsible for separating the sister chromatids into two cells. Next, during prometaphase, the nuclear envelope breaks down and frees the sister chromatids from the nucleus. A kinetochore is developed around the centromere where kinetochore filaments from the spindle poles attach. During metaphase, the kinetochore microtubules pull the sister chromatids back and forth until they align along the equator of the cell called the equatorial plane. Again, there is a metaphase checkpoint in

the middle of the M phase to guarantee a completeness of cell division (Cooper, 2000). Next, during anaphase, each pair of chromosomes is separated into two identical, independent chromosomes and pulled to opposite poles of the cell by the mitotic spindle, ensuring that each daughter cell receives an identical set of chromosomes. The final phase of mitosis is telophase where a nuclear membrane forms around each set of chromosomes to separate the nuclear DNA from the cytoplasm. The chromosomes begin to uncoil, which makes them diffuse and less compact. Cytokinesis starts during anaphase and continues through telophase. The contractile ring, a ring of protein filament, forms around the equator of the cell beneath the plasma membrane. It shrinks at the equator of the cell and pinches the plasma membrane inward to form a cleavage furrow which, eventually, results in a complete separation of two daughter cells each bound by its own plasma membrane.

There are various proteins which control cell cycling. The key protein families include twenty cyclin-dependent kinases (CDKs) and twenty-nine cyclins (Cao et al., 2014), the pocket protein family i.e. retinoblastoma protein (Rb) and the Rb-related p107 and p130 proteins (Henley & Dick, 2012), eight E2F family members in which only E2Fs 1-5 are capable of binding to pocket proteins (Classon & Harlow, 2002), and the two main classes of cyclin-dependent kinase inhibitors (CDKIs) which are the inhibitors of CDK4 (INK4) family and the CDK interacting protein/kinase inhibitor proteins (Cip/Kip) as detailed below. CDKs are heterodimeric serine/threonine kinases composed of a catalytic kinase characterised by needing a separate cyclin subunit which provides domains essential for enzymatic activity (Santo, Siu, & Raje, 2015). At the DNA level, most members of the kinase superfamily of CDKs share the presence of the catalytic eukaryotic protein kinase domain of approximately 250 amino acids (Z. Li et al., 2009). In general, cyclins show less sequence similarity than the CDKs. The cyclin family are categorised into three major groups, including group I (cyclin B group: A-, B-, D-, E-, F-, G-, J-, I- and O-), group II (cyclin Y group i.e. a partner of the CDK5 subfamily), and group III (cyclin C group: C-, H-, K-, L- and T- major partners of transcriptional CDKs) (Cao et al., 2014; Z. Ma et al., 2013). CDKs, cyclin partners and their functions are summarised in Table 1.1.1.1.

Table 1.1.1.1 CDKs, their cyclin partners and functions.

CDKs	Partners	Functions	References
CDK1	Cyclin A/B	Associates with the M phase	(Chen et al., 2009; Marais et al., 2010)
CDK2	Cyclin A/E	Associates with the G1/S phase transition	(Marais et al., 2010)
CDK3	Cyclin C	Associates with G0/G1 and G1/S phase transition	(Ren & Rollins, 2004)
CDK4/6	Cyclin D	Associates with the G1/S phase transition	(Santo, Siu, & Raje, 2015)
CDK5	p35 and p39	Drives progression from G1/S and in RB phosphorylation	(Dorand et al., 2016; Pozo et al., 2013)
CDK7	Cyclin H	Associates with CAK and RNAPII transcription	(Li et al., 2017)
CDK8	Cyclin C	Regulates the transcriptional initiation	(Nemet, Jelicic, Rubelj, & Sopta, 2014)
CDK9	Cyclin T	Promotes the transcriptional elongation	(Peterlin & Price, 2006)
CDK10	Cyclin M	Associates with the ETS2 transcription factor and modulates its transactivation activity	(Guen, Gamble, Lees, & Colas, 2017)
CDK11	Cyclin L	Regulates RNA transcription and splicing, autophagy, and apoptosis	(Dos Santos Paparidis & Canduri, 2018)
CDK12	Cyclin K	Controls alternative last exon splicing; regulates the expression of DNA damage, stress, and heat shock genes	(Blazek et al., 2011; Kohoutek & Blazek, 2012; Liang et al., 2015)
CDK13	Cyclin K	Transcript synthesis toward the middle and 3′ end of the emerging RNA	(Kohoutek & Blazek, 2012; Liang et al., 2015)
CDK14	Cyclin Y	Promotes Wnt/β -catenin signaling through phosphorylation of the LRP6 co-receptor	(Ou-Yang, Huang, & Sun, 2017)
CDK15	Cyclin Y	Participates in hepatitis B virus-driven transformation	(Shiraishi et al., 2014)
CDK16	Cyclin Y	Regulates mitosis, apoptosis, and growth; Synaptic tra cking and remodelling	(Ou et al., 2010; Yanagi & Matsuzawa, 2015)
CDK17	Cyclin Y	Promotes amyloid precursor protein-dependent Alzheimer; Inhibits autophagy	(Chaput, Kirouac, Stevens, & Padmanabhan, 2016; Leonardi, Perna, Tronnolone, Colecchia, & Chiariello, 2019)
CDK18	Cyclin Y	Promotes amyloid precursor protein-dependent Alzheimer; Inhibits autophagy; promotes DNA replication stress and stability	(Chaput et al., 2016; Leonardi et al., 2019)
CDK19	Cyclin C	CDK8 paralog, with a similar role to CDK8, but seems to perform some distinct roles	(Galbraith et al., 2013)
CDK20	Cyclin H	Activates intestinal cell kinase or β -catenin/T-cell factor transcription factors signalling to stimulate cell-cycle progression	(Malumbres, 2014)

The cell cycle is driven in the precise order described above. The activation and degradation of regulatory protein complexes are in a sequential manner. Among these, some CDKs and their regulatory partners play a key role. A schematic diagram of the cell cycle is shown in Figure 1.1.1.1. Initially, CDK3/cyclin C phosphorylates the retinoblastoma protein (Rb), resulting in the release of various transcription factors of the E2F group from the paused state which drives the cell from G0 to G1 phase (Ren & Rollins, 2004). Following this, cyclin D is expressed in response to early response genes, including activator protein 1(*AP1*), activating transcription factor 3 (*ATF3*), and myelocytomatosis oncogene (*MYC*), upon mitogenic stimulation (Allan, Albanese, Pestell, & LaMarre, 2001; Loyer et al., 1996; Mateyak, Obaya, & Sedivy, 1999). At the early G1 phase, CDK4/6-cyclin D phosphorylates Rb and its family member p107 and p130. The de-repressed E2F transcription factors induce G1/S-regulated genes e.g. cyclin E and cyclin A (Bartek, Bartkova, & Lukas, 1997; Hinds et al., 1992). At the late G1 phase, CDK2/cyclin E further phosphorylates Rb to strengthen its own expression and trigger the transition of the G1 to S phase via E2F transcriptional activities.

CDK2/cyclin E induces centrosome duplication and histone expression at the late G1 phase (Ma et al., 2000; Okuda et al., 2000; Zhao et al., 2000) and also promotes initiation of DNA replication at the early S phase (E. Liu, Li, Yan, Zhao, & Wu, 2004; Mailand & Diffley, 2005). Following this, during progression from S to G2 phase, E2F is switched off by CDK2/cyclin A and CDK1/cyclin A, which are activated by CDK7/cyclin H (CDK-activating kinase, CAK). To enter the M phase, CDK1/cyclin B must be activated via dephosphorylation by CDC25 at its threonine residue. CDK1 reaches its peak activity in the late prophase (Gavet & Pines, 2010) and inhibits protein phosphatase 1 (PP1) activity (Nasa & Kettenbach, 2018), resulting in attenuation of its dephosphorylation activity for Rb which ultimately leads to the release of the E2F transcription factors. Cyclin B is then ubiquitinated by anaphase-promoting complex/cyclosome (APC/C), resulting in entry to anaphase until mitosis and cytokinesis are completed (Bose, Simmons, & Grant, 2013; Santo et al., 2015). By contrast, CDK inhibitors suppress CDK/cyclin activities. During the late G1 phase, the INK4 family proteins $p16^{INK4A}$, $p15^{INK4B}$, $p18^{INK4C}$ and $p19^{INK4D}$ compete with cyclin D, preventing formation of further CDK4/6-cyclin D complexes (Jeffrey, Tong, & Pavletich, 2000). Although the Cip/Kip $p21^{Cip1}$, $p27^{Kip1}$ and $p57^{Kip2}$ support an active CDK4/6-cyclin D complex (Sherr & Roberts, 1999), they potentially inhibit CDK2/cyclin E, and this inhibitory threshold must be overcome for progression of cell cycle (Santo et al., 2015).

The aim of G1 and G2 checkpoints is to prevent replication errors and ensure that the genomic materials are correctly separated during cell division. To address this issue, serine/threonine kinases ataxia telangiectasia-mutated (ATM) and ataxia telangiectasia and Rad3-related protein (ATR) detect DNA double strand breaks and DNA damage caused by ultraviolet irradiation, respectively (Abraham, 2001). At the G1 checkpoint, the activated checkpoint kinase 2 (CHK2) and the checkpoint kinase 1 (CHK1) phosphorylated by ATM and ATR, respectively, inhibit cell division cycle 25 (CDC25) and halts its activity i.e. removing inhibitory phosphates from CDK1 (Timofeev, Cizmecioglu, Settele, Kempf, & Hoffmann, 2010) and CDK2 (Santo et al., 2015). ATM/CHK2 promotes G1 arrest through the tumour suppressor protein p53 (TP53) (Cao et al., 2006; Hirao et al., 2002). Indeed, p53 activates the transcription of $p21^{Cip1}$ (Bose et al., 2013) which potently inhibits CDK2 (Hengst, Göpfert, Lashuel, & Reed, 1998)

but, on the other hand, can also bind to caspase-3 preventing apoptosis (Shapiro, 2006). In addition, p53 also induces a transcriptional expression of the Fas receptor and death receptor 5 (DR5) in the extrinsic apoptosis pathway; and the p53 upregulated modulator of apoptosis (PUMA) in the intrinsic apoptosis pathway (Haupt, Berger, Goldberg, & Haupt, 2003) (detailed in section 1.1.2). For the G2 checkpoint, in addition to upregulation of ATM-CHK2-CDC25 and ATR-CHK1-CDC25 pathways, Wee1 kinase is also upregulated which synergistically constrains the removal of inhibitory phosphates from CDK1, keeping it inactivated (Harvey, Charlet, Haas, Gygi, & Kellogg, 2005).

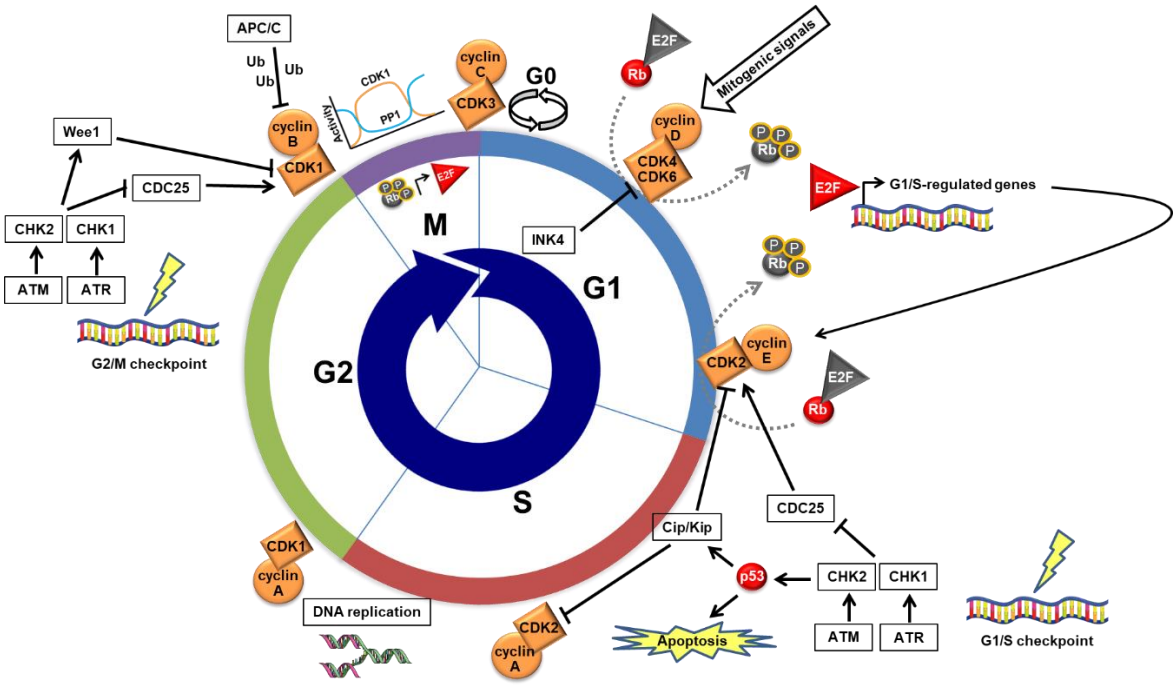

Figure 1.1.1.1 A schematic diagram of the cell cycle.
Driven by CDKs and their regulatory partners, activation and degradation take place in a sequential manner. The G1 and G2 checkpoints are necessary to prevent the accumulation of DNA damage. Cyclin-dependent kinase (CDK). Retinoblastoma protein (Rb). Serine/threonine kinase ataxia telangiectasia-mutated protein (ATM). Serine/threonine kinase ataxia telangiectasia and Rad3-related protein (ATR). Checkpoint kinase (CHK). Cell division cycle 25 (CDC25). Anaphase-promoting complex/cyclosome (APC/C). Ubiquitinate (Ub). Inhibitors of cyclin-dependent kinase 4 (INK4). Cyclin-dependent kinase interacting protein/kinase inhibitor protein (Cip/Kip).

In terms of cellular transcription, the major transcriptional CDKs are CDK7/cyclin H and CDK9/cyclin T (Santo et al., 2015). A schematic diagram of cellular transcription is shown in Figure 1.1.1.2. During transcriptional initiation, transcription factor II H (TFIIH)/CDK7/cyclin H are recruited to the proximal promoter. CDK7/cyclin H activates CDK9 and phosphorylates the serine 5 (S5)

residue on the carboxy-terminal domain (CTD) of ribonucleic acid (RNA) polymerase II (RNAPII), which supports the binding of the 5´mRNA capping enzyme. Then, positive transcription elongation factor b (P-TEFb)/CDK9/cyclin T complex induces progressive transcriptional elongation. Indeed, P-TEFb phosphorylates and inactivates negative elongation factor (NELF) and 5,6-dichloro-1-ß-D-ribofuranosylbenzimidazole (DRB)-sensitivity inducing factor (DSIF) rendering a release of elongation complex from its paused state; whereas CDK9/cyclin T phosphorylates serine 2 (S2) residue on the CTD of RNAPII in order to optimise its function as a platform of several transcription factors (Santo et al., 2015; Thiel, Huang, Lei, & Hua, 2012). On the other hand, CDK8/cyclin C suppresses transcription through inhibitory phosphorylation of the CTD of RNAPII and prevents it from binding to a gene promoter (H. Liu, Cheng, & Hsieh, 2009).

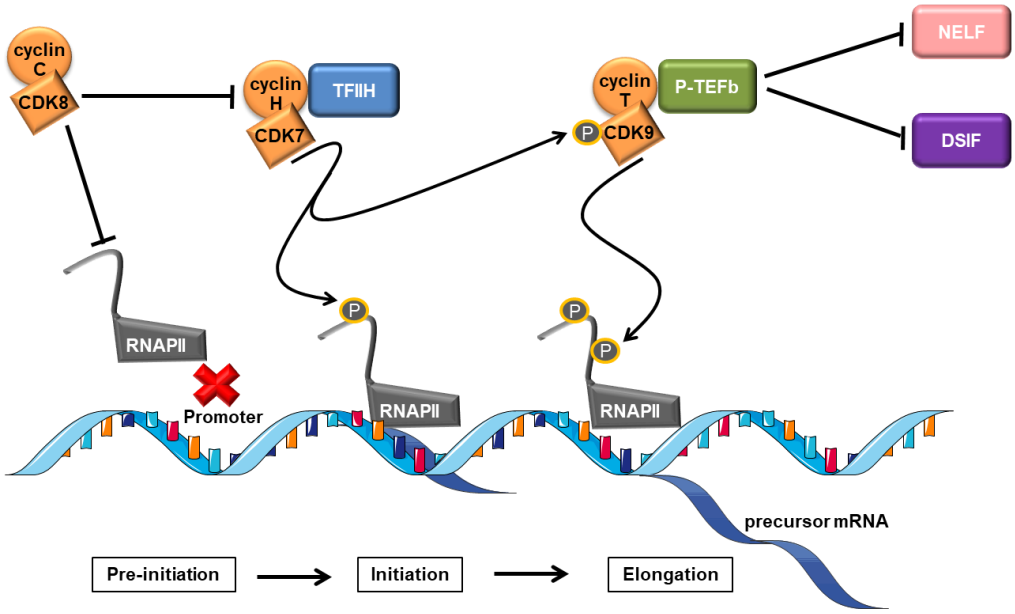

Figure 1.1.1.2 A schematic diagram of cellular transcription.
CDK7/cyclin H and CDK9/cyclin T are the major transcriptional CDKs. CDK7/cyclin H, as a part of TFIIH, phosphorylates serine at the 5 position of the CTD of RNAPII to initiate transcription. For transcriptional elongation, P-TEFb inactivates NELF and DSIF to release the elongation complex and CDK9/Cyclin T phosphorylates serine at the 2 position of the CTD of RNAPII for progressive transcriptional elongation. By contrast, CDK8/Cyclin C suppresses the transcription by inhibiting cyclin H and preventing RNAPII from binding to a gene promoter. Cyclin-dependent kinase (CDK). Transcription factor II H (TFIIH). Positive transcription elongation factor b (P-TEFb). Negative elongation factor (NELF). 5,6-dichloro-1-ß-D-ribofuranosylbenzimidazole (DRB)-sensitivity inducing factor (DSIF). Ribonucleic acid (RNA) polymerase II (RNAPII).

1.1.2 Apoptosis pathway

Recently, a number of cell death mechanisms has been categorised. These include mitotic catastrophe, immunogenic cell death, autophagy-dependent cell death, lysosome-dependent cell death, NETotic cell death, entotic cell death, parthanatos, pyroptosis, ferroptosis, necroptosis, mitochondrial permeability transition-driven necrosis, and apoptosis (Galluzzi et al., 2018). Diametrically, these can be divided into two main groups. On the one hand, cell death which originates from perturbation by intracellular or extracellular stresses e.g. infection, toxins, or trauma which is too prolonged or too intense for cells to restore their homeostasis (Galluzzi, Bravo-San Pedro, Kepp, & Kroemer, 2016). On the other hand, cell death is mediated by an intracellular programme, generally referred to as "programmed cell death" (Fuchs & Steller, 2011). Apoptosis is a form of programmed cell death that occurs in multicellular organisms. In terms of macroscopic morphological manifestations, apoptosis exhibits shrinkage of cell; chromatin condensation (pyknosis); nuclear fragmentation (karyorrhexis); the loss of cellular membrane asymmetry i.e. phosphatidylserine residues located in the inner plasma membrane are externalised (Y. Zhang, Chen, Gueydan, & Han, 2018). This is followed by plasma membrane blebbing and the formation of apoptotic bodies which are engulfed by phagocytic cells and ultimately degraded within lysosomes (Leist & Jäättelä, 2001). Apoptosis can be initiated through **a**) the extrinsic apoptosis pathway; and **b**) the intrinsic apoptosis pathway.

1.1.2.1 The extrinsic apoptosis pathway

A schematic diagram of the extrinsic apoptosis pathway is shown in Figure 1.1.2.1.1. Primarily, the binding of ligands and transmembrane death receptors facilitates the extrinsic apoptosis pathway. Various ligands and their cognate receptors have been identified, including Fas ligand and Fas receptor (FasL/Fas or cluster of differentiation [CD]178/CD95) (J. E. Kim et al., 2017), tumour necrosis factor-α and its receptor 1 (TNF-α/TNFR1), TNF-related apoptosis-inducing ligand and death receptors 4 and 5 (TRAIL or Apo2L/DR4/5) (Samali, Zhivotovsky, Jones, Nagata, & Orrenius, 1999; Schütze, Tchikov, & Schneider-Brachert, 2008; Tibbetts, Zheng, & Lenardo, 2003; Yamada, Arakaki, Saito, Kudo, & Ishimaru, 2017). The binding of FasL/Fas and TRAIL/DR4/5 results in the

recruitment of the adaptor protein Fas-associated death domain (FADD) which binds to pro-caspase-8 to form a membrane-bound matrix death-inducing signaling complex (DISC). By contrast, the binding of TNF-α/TNFR1 results in the transient recruitment of TNF receptor-associated death domain (TRADD), TNF receptor-associated factor 2 and 5 (TRAF2 and TRAF5), receptor-interacting protein 1 (RIP1), and ubiquitin-ligase cellular inhibitors of apoptosis 1 and 2 (cIAP1/2), which ubiquitinate RIP1, to form pro-survival complex I (Hsu, Xiong, & Goeddel, 1995; Micheau & Tschopp, 2003). Complex I then upregulates the pro-survival cellular Fas-associated protein with death domain-like IL-1ß converting enzyme (FLICE)-like inhibitory protein (cFLIP) via the nuclear factor kappa-light-chain-enhancer of activated B cells (NF-κB) and the c-Jun N-terminal kinase (JNK) pathways (Z. G. Liu, Hsu, Goeddel, & Karin, 1996; Micheau & Tschopp, 2003). cFLIP competitively displaces caspase-8 from DISC, halting the apoptosis process. However, this effect is reversible when RIP1 is de-ubiquitinated by de-ubiquitinating enzyme cylindromatosis (CYLD) during an induction of oxidative stress (Ganjam et al., 2018) or a degradation of cIAP1/2 (Zhou & Li, 2015). TRADD and RIP1 are then dissociated from complex I and bind to pro-caspase-8 to form cytoplasmic death complex II (Micheau & Tschopp, 2003; Zhou & Li, 2015), resulting in activation of caspase-8. Indeed, the membrane-bound DISC and the cytoplasmic complex II serve as a platform to increase the local concentration of pro-caspases-8, resulting in their activation by dimerisation in which individual procaspase-8 molecules associate with each other through their protease domains (①). Then, two sequential cleavage events occur which are the separation of the large and small subunits (②), followed by the separation of the large subunit and the platform to free a mature caspase-8 (③). Activated caspase-8 then cleaves and activates caspases-3, 6 and 7. While caspase-6 and 7 preferentially cleave only lamin A and PARP, respectively, it has been reported that caspase-3 is globally required for multiple proteolytic events, suggesting that it is the primary executioner (Slee, Adrain, & Martin, 2001). The substrates of caspase-3 include fodrin which is highly similar to spectrin, gelsolin which is an actin-binding protein, inhibitor caspase-activated DNase (ICAD) which leads to an activation of DNase, U1 small nuclear ribonucleoprotein, type III intermediate filament vimentin, Rb, STAT1, type I topoisomerase, RIP1, XIAP (survivin), lamin B and PARP.

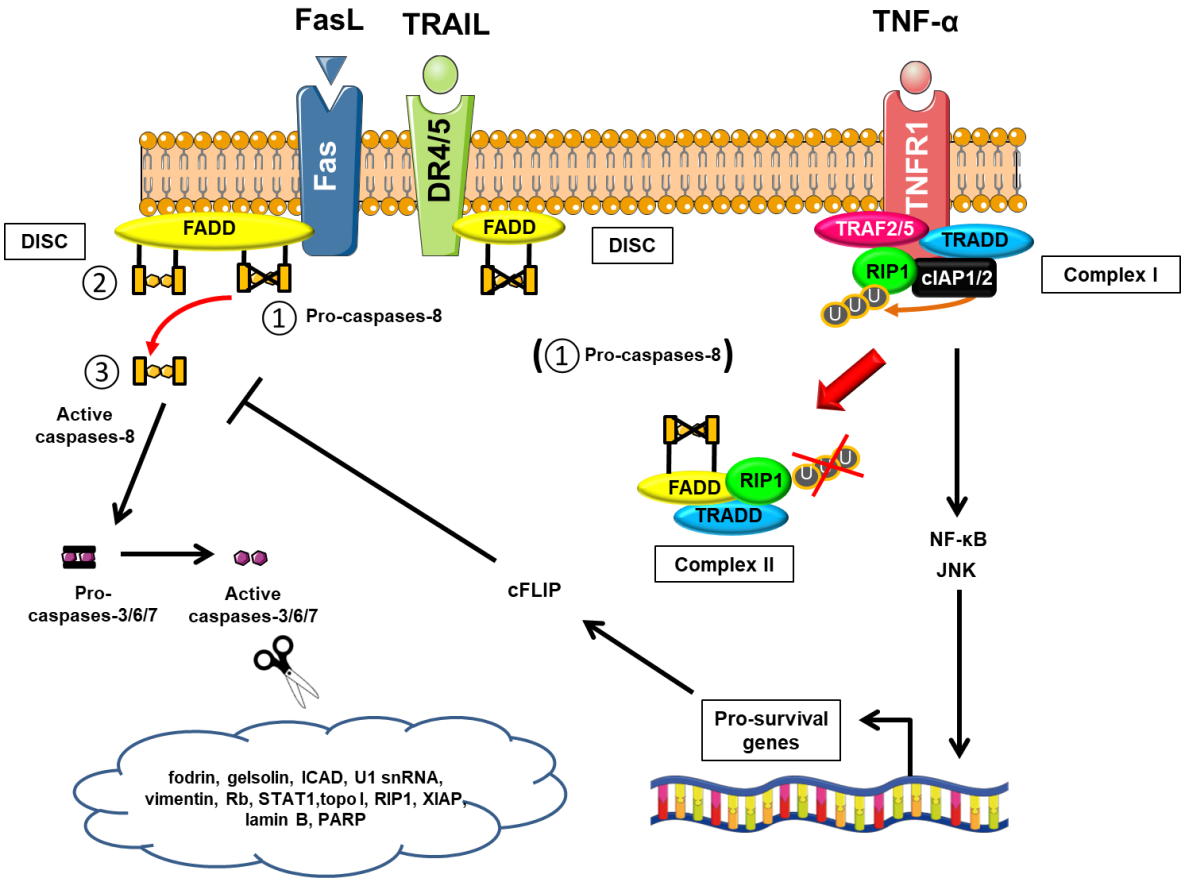

Figure 1.1.2.1.1 A schematic diagram of the extrinsic apoptosis pathway.
The pathway is initiated by the binding of ligands and transmembrane death receptors. FADD and TRADD play a critical role in transmitting the death signaling to the downstream intracellular apoptotic machinery. The binding of FasL/Fas and TRAIL/DR4/5 mediates the formation of DISC which activates caspases, culminating with cleavage of numerous cellular substrates. In contrast, the binding of and TNF-α/TNFR1 results in transient formation of pro-survival complex I, followed by the formation of death complex II which similarly activate caspases. Fas ligand (FasL). Fas receptor (Fas). Tumour necrosis factor (TNF). Tumour necrosis factor receptor (TNFR). Tumour necrosis factor-related apoptosis-inducing ligand (TRAIL). Death receptor (DR). Fas-associated death domain (FADD). Tumour necrosis factor receptor-associated death domain (TRADD). Death-inducing signaling complex (DISC). Cellular inhibitors of apoptosis (cIAP). Receptor interacting protein 1 (RIP1). Ubiquitination (U). Tumour necrosis factor receptor-associated factor (TRAF). Nuclear factor kappa-light-chain-enhancer of activated B cells (NF-κB). c-Jun N-terminal kinase (JNK). Cellular Fas-associated protein with death domain-like IL-1β converting enzyme-like inhibitory protein (cFLIP).

1.1.2.2 The intrinsic apoptosis pathway

The BCL-2 family comprises four groups of proteins based on their domain composition, including BCL-2 homology (BH) one to four (Renault & Chipuk, 2014). In terms of function, the BCL-2 family members can be divided into four groups, including; pro-apoptotic effectors, pro-apoptotic activators, pro-apoptotic sensitisers, and anti-apoptotic proteins. A schematic diagram of the intrinsic apoptosis pathway is shown in Figure 1.1.2.2.1. The critical step for

intrinsic apoptosis is irreversible and widespread mitochondrial outer membrane permeabilisation (MOMP) which results from a homo-oligomerisation of the pro-apoptotic effectors; BCL-2 homologous antagonist/killer (BAK) and BCL-2-associated X protein (BAX) (Galluzzi, Kepp, & Kroemer, 2016). In order to initiate MOMP, the structure of BAK and BAX needs to be rearranged which can be triggered by, crucially, protein-protein interactions with the BH3 only pro-apoptotic activators e.g. PUMA, BCL-2-like protein 11 (BIM), and BH3 interacting-domain death agonist (BID) (Gavathiotis et al., 2008; Kuwana et al., 2005; Letai et al., 2002). These pro-apoptotic activators bind directly to BAX and BAK either at the N-terminus or a core hydrophobic region of them, resulting in conformational changes (Czabotar et al., 2013; Desagher et al., 1999; Gavathiotis et al., 2008). By contrast, anti-apoptotic proteins, e.g. BCL-2, BCL-2-like protein 2 (BCL-w), B-cell lymphoma-extra large (BCL-xL), and MCL-1, directly inhibit BAK and BAX or trigger sequestration of the pro-apoptotic activators (Kuwana et al., 2005; Letai et al., 2002). Indeed, BCL-xL interacts with both BAK and BAX, whereas, BCL-2 preferentially binds to BAX and MCL-1 preferentially binds to BAK (Gillissen et al., 2007). The BH-3 only pro-apoptotic sensitisers, e.g. BCL-2-associated death promoter (BAD), BCL-2 modifying factor (BMF), and phorbol-12-myristate-13-acetate-induced protein 1 (NOXA) (Chipuk et al., 2008; Kuwana et al., 2005), can bind to anti-apoptotic proteins and prevent them from interacting with the BH-3 only pro-apoptotic activators. In another scenario, pro-apoptotic sensitisers can displace and free pro-apoptotic activators, then competitively bind to anti-apoptotic proteins. This is often termed “de-repression” (Elkholi, Floros, & Chipuk, 2011). Of note, NOXA specifically binds and inhibits MCL-1 (Gélinas & White, 2005). Indeed, NOXA mediates the ubiquitylation and proteasomal degradation of MCL-1 (Kotschy et al., 2016).

Following MOMP, the inner mitochondrial membrane and cristae junctions undergo extensive remodeling (Frezza et al., 2006; Scorrano et al., 2002; R. Yamaguchi et al., 2008) and several pro-apoptotic proteins within the mitochondrial inter-membrane space are released, including cytochrome c (Cyt c), second mitochondria-derived activator of caspase (SMAC, also known as direct inhibitor of apoptosis-binding protein with low isoelectric point [DIABLO]), and high-temperature requirement A serine peptidase 2 (HTRA2). Cyt c binds to

apoptotic protease activating factor-1 (APAF-1) to form the apoptosome. Once formed, the apoptosome can then recruit pro-caspases-9 which leads to their dimerisation. Unlike other initiator or effector caspases, the activation loop which links the large and small subunits of pro-caspase-9 is particularly long so that cleavage is not required for activation as the loop is predicted to move and allow access to the active site (Bratton & Salvesen, 2010). The catalytic activity of pro-caspase-9 starts immediately after binding to the apoptosome (Renatus, Stennicke, Scott, Liddington, & Salvesen, 2001; Stennicke et al., 1999) and stops once autocatalytic cleavage is finished, and the processed caspased-9 dissociates from the apoptosome which allows new pro-caspase-9 to bind. Hence, rather than an actual activation, the pro-caspase-9 autoprocessing acts as a molecular timer for the apoptosome/caspase-9 catalytic activity (Bratton & Salvesen, 2010). Following this, pro-caspases-3, 6, and 7 are cleaved which results in subsequent multiple proteolytic events as described in section 1.1.2.1. At the same time, SMAC and HTRA2 inhibit the inhibitors of apoptosis (IAP) family members X-linked inhibitor of apoptosis protein (XIAP) and baculoviral inhibitor of apoptosis repeat-containing 5 (BIRC5, also known as survivin), releasing caspases from their repressed state. Phosphatidylserine externalisation also results from the activity of these active caspases (Elkholi, Renault, Serasinghe, & Chipuk, 2014) which signals and elicits the recruitment of phagocytic cells (I. K. Poon, Lucas, Rossi, & Ravichandran, 2014; Segawa et al., 2014).

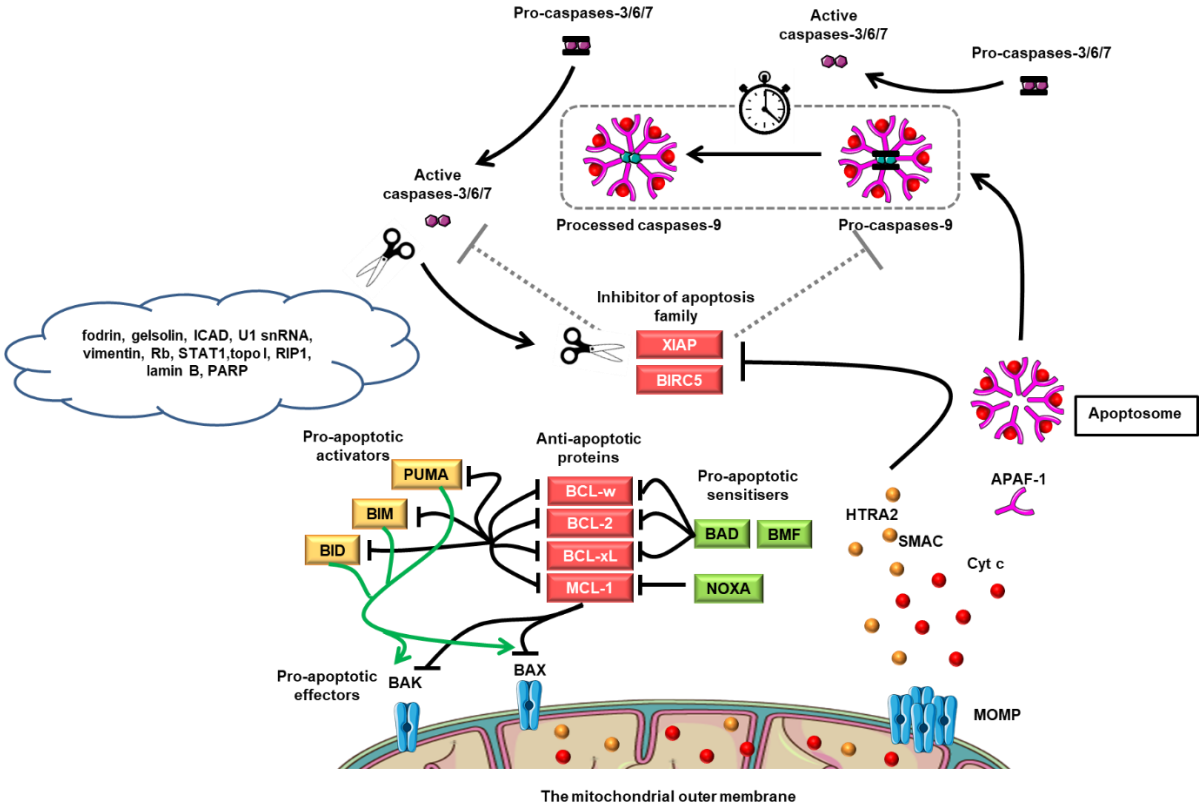

Figure 1.1.2.2.1 A schematic diagram of the intrinsic apoptosis pathway.
The BCL-2 family members which can be divided into four functional groups, including pro-apoptotic effectors, pro-apoptotic activators, pro-apoptotic sensitisers, and anti-apoptotic proteins, play a key role in controlling this pathway. The critical step is a homo-oligomerisation of BAK and BAX, resulting in MOMP. Following MOMP, several pro-apoptotic proteins are released. Among these, Cyt c is a key protein that mediate the formation of apoptosome which activates caspases, culminating with cleavage of numerous cellular substrates. B-cell lymphoma 2-like protein 2 (BCL-w). B-cell lymphoma 2 (BCL-2). B-cell lymphoma-extra large (BCL-xL). Myeloid cell leukemia 1 (MCL-1). B-cell lymphoma 2-associated death promoter (BAD). B-cell lymphoma 2 modifying factor (BMF). phorbol-12-myristate-13-acetate-induced protein 1 (NOXA). B-cell lymphoma 2-like protein 11 (BIM). BH3 interacting-domain death agonist (BID). p53 upregulated modulator of apoptosis (PUMA). B-cell lymphoma 2 homologous antagonist/killer (BAK). B-cell lymphoma 2-associated X protein (BAX). Mitochondrial outer membrane permeabilisation (MOMP). Cytochrome c (Cyt c). Second mitochondria-derived activator of caspase (SMAC). High-temperature requirement A serine peptidase 2 (HTRA2). Apoptotic protease activating factor-1 (APAF-1).

1.1.3 Haematopoietic hierarchy

The concept of the haematopoietic stem cell (HSC) was first described in 1961 from experiments using a mouse model of spleen and BM irradiation (Till & McCulloch, 1961). Colonies of HSCs were seen in the spleens of these aplastic mice at day 7-8 after they were intravenously injected with BM cells. The colonies were called CFU-spleen (CFU-S) at the time, these are currently known as CFU-granulocyte, erythrocyte, monocyte, and megakaryocyte (CFU-GEMM) (Quigley, Means, & Glader, 2014) or common myeloid progenitor cells (CMPs).

The ability of self-renewal, pluripotentiality and the capability of generating differentiated progeny are characteristics of HSCs (Mirza, 2019). They are able to restore the haematopoietic system of a lethally irradiated host. In the BM, the ratio of HSCs to nucleated blood cells is approximately 1:1000 (Rossmann, Orkin, & Chute, 2018) with a capability of BM to produce approximately $2.5x10^{12}$ red blood cells, $2.5x10^{12}$ platelets, and $1x10^{12}$ white blood cells per kilogram of body weight per day (Dave & Koury, 2016). The long-term culture-initiating cell (LTC-IC) assay is an *in vitro* functional assay used to quantify the primitive haematopoietic progenitor cells which are capable of initiating and sustaining myelopoiesis for several weeks (Hogge, Lansdorp, Reid, Gerhard, & Eaves, 1996). The LTC-IC shares functional and phenotypic properties with the BM microenvironment, which supports *in vivo* repopulating stem cells (SCs) (Hogge et al., 1996; Sutherland, Hogge, & Eaves, 1993). Briefly, test cells are co-cultured with BM cells for 5 weeks, then all cells are harvested and transferred into methylcellulose culture (CFU assay) for a further 10-14 days. Any CFUs detected represent the progeny of LTC-IC as CFUs present in the input cell suspension have undergone terminal differentiation by this time. Lin-CD38-CD34+CD45RA-CD90+CD49f+CD7-CD10-FLT3+ cells are the earliest identifiable human HSCs capable of initiating long-term cultures (Hua et al., 2019; Notta et al., 2016). Alternatively, *in vivo* assays to evaluate HSC engraftment and functionality are available (Dick, Bhatia, Gan, Kapp, & Wang, 1997). Briefly, test cells are transplanted into syngeneic, lethally irradiated animals e.g. non-obese diabetic/severe combined immunodeficient (NOD/SCID) mice. Following this, the engrafted BM cells are transferred to a secondary recipient to promote the proliferation and differentiation of HSCs, thus allowing them to be characterised (Verfaillie, 2003).

Historically, when HSCs were first discovered, little was known about their regulation and self-renewal and differentiation and it was perceived to be a random process (Till & McCulloch, 1961). However, extensive research indicates that the BM microenvironmental cues play a fundamental role in HSCs maintenance, self-renewal, and differentiation (Metcalf, 2007). Several key molecular regulators have been identified. These include stem cell factor (SCF, also known as the tyrosine-protein kinase KIT ligand [KL]), thrombopoietin (TPO), and FMS-like tyrosine kinase 3 ligand (FLT3L) (Mirza, 2019) which

facilitate HSC proliferation and differentiation. By contrast, transforming growth factor beta (TGF-ß) (Verfaillie, 2003), prostaglandin E2 (PGE2) (Durand & Zon, 2010), angiopoietin1 (Arai et al., 2004), and osteopontin (Nilsson et al., 2005) promote HSC quiescence. Morphogenic signaling pathways also play a key role, with the effects of Wnt signaling being dependent on the amount of Wnt ligands present (Luis et al., 2011). Whereas, Notch-1 regulatory signaling factors mediate the response of HSCs to the signals from microenvironment and play a key role in HSC quiescence and maintenance (Verfaillie, 2003). In addition, interferon alpha (INF-α) (Essers et al., 2009) and interferon gamma (INF-γ) (Baldridge, King, Boles, Weksberg, & Goodell, 2010) have been reported to stimulate HSC proliferation. Following this, myeloid-lymphoid lineage segregation is under the influence of various cytokines, colony-stimulating factors (CSFs) and interleukins (ILs) as shown in Figure 1.1.3.1.

In the classical myeloid-lymphoid segregation model, granulocyte-macrophage (GM)-CSF, FLT3L, SCF, IL-1, IL-3, IL-6, and IL-11 are required for myeloid lineage commitment (Mirza, 2019). IL-3 is important for development of granulocytes, monocytes, megakaryocytes, and erythroid cells. Originating from megakaryocyte/erythroid progenitor cells, erythropoiesis demands erythropoietin (EPO), mainly produced from the renal peritubular interstitial cells (Kaushansky, 2016), SCF, GM-CSF, and IL-3, whereas, megakaryopoiesis requires TPO mainly produced from the liver (Wolber et al., 1999), GM-CSF, SCF, IL-3, IL-6, and IL-11. Factors that promote differentiation of the CMP into neutrophils, monocytes, eosinophils, and basophils include GM-CSF, granulocyte CSF (G-CSF), macrophage CSF (M-CSF), SCF, IL-3, IL-5, and IL-6 (Mirza, 2019). Stimulated by GM-CSF, CFU-granulocyte, monocyte (CFU-GM) undergo further differentiation into CFU-granulocyte (CFU-G) and CFU-monocyte (CFU-M). G-CSF stimulates neutrophil differentiation from CFU-G, whereas, M-CSF stimulates monocyte differentiation from CFU-M (Kaushansky, 2016). Eosinophils require GM-CSF, IL-5, and IL-3, whereas, basophils potentially require GM-CSF, SCF, and IL-3 for differentiation (Mirza, 2019). Growth factors promoting lymphoid differentiation include SCF, FLT3L, IL-2, IL-3, IL-4, IL-7, and IL-15 (Mirza, 2019).

Interestingly, it has been reported that, while myeloid commitment follows the classical rigid myeloid-lymphoid segregation model, human multi-lymphoid

progenitor cells (MLP) are not lymphoid restricted but, indeed, nearly half of the MLP compartment is biased towards dendritic cells (DCs), monocytes and macrophages (Naik et al., 2013) (Figure 1.1.3.1, red lines). Nowadays, an improvement of sorting scheme by fluorescence-activated cell sorting (FACS) and the rapid expansion of microfluidic technology has transformed the research capabilities for study at the single-cell level. For example, single-cell RNA-sequencing (scRNA-seq) is increasingly being used to determine lymphocyte fate (Stubbington et al., 2016), myoblast differentiation (Trapnell et al., 2014), describe cell lineage relationships in early development (Petropoulos et al., 2016), and reconstruct cell hierarchy (Hwang, Lee, & Bang, 2018). Notta et al used FACS to resolve myeloid, erythroid and megakaryocytic fates from single CD34+ cells in combination with single-cell functional analysis, performed scRNA-seq and then mapped the progenitor hierarchy across human development (Notta et al., 2016). They reported that the blood progenitor architecture is not identical across development i.e. oligopotent progenitors with myeloid-erythroid-megakaryocyte and erythroid-megakaryocyte activity are a prominent component of the hierarchy in foetal liver, whereas, the BM is dominated by unilineage progenitors with primarily myeloid, erythroid, and lymphoid/monocytic potential with the megakaryocyte lineage being closely tied to the fate of multipotent cells (Figure 1.1.3.1, green lines). Studying at the single-cell level thus challenges the previous understanding about haematopoietic hierarchy.

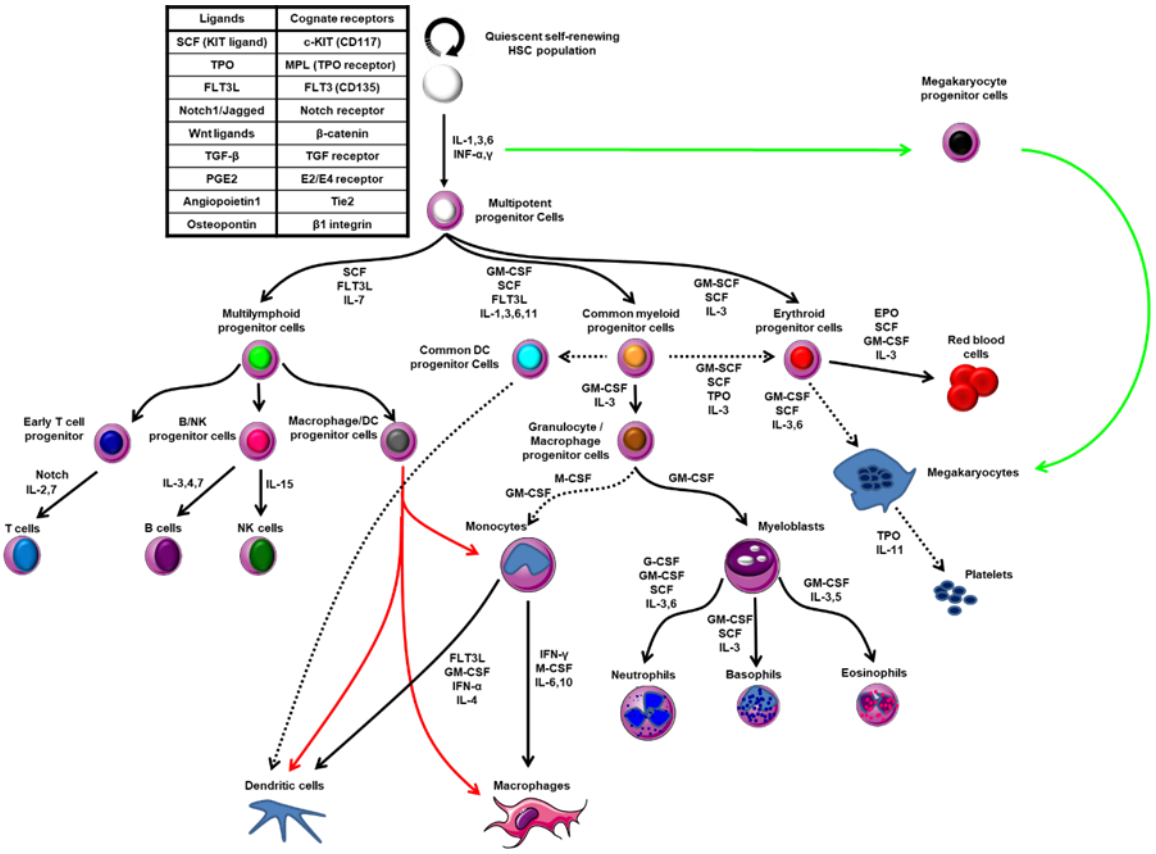

Figure 1.1.3.1 A schematic diagram of haematopoietic hierarchy.
HSCs differentiate into all blood cell lineages. Myeloid commitment follows the classical myeloid-lymphoid segregation model, whereas, the MLPs are not lymphoid restricted and, indeed, give rise to the monocytic lineage (red lines). In addition, redefined model of human blood development reveals that megakaryocyte/erythroid progenitors exist in foetal liver, whereas, the origin of the megakaryocyte lineage is switched to be closely tied to the fate of multipotent cells in adult bone marrow (green lines). B cell/natural killer cell progenitor (B/NK). natural killer cell (NK). Dendritic cell (DC). Stem cell factor (SCF). Thrombopoietin (TPO). Erythropoietin (EPO). FMS-like tyrosine kinase 3 ligand (FLT3L). Transforming growth factor (TGF). Prostaglandin E2 (PGE2). Interferon (INF). Interleukin (IL). Granulocyte-macrophage colony-stimulating factor (GM-CSF). Granulocyte colony-stimulating factor (G-CSF). Macrophage colony-stimulating factor (M-CSF).

1.2 Clonal evolution from normal haematopoiesis to acute myeloid leukaemia and relapsed disease after treatment

Genomic instability is a hallmark of cancer. As life advances, each HSC repeatedly undergoes replication cycles in which some of the mutations occurring at each replication may be irreparable (Stratton, Campbell, & Futreal, 2009). In another scenario, HSC exhaustion due to telomere loss or apoptosis can diminish diversity and increase competition between the various HSCs (Heuser, Thol, & Ganser, 2016; Yoshizato et al., 2015), resulting in inequality or clonal

haematopoiesis. Key somatic mutations that confer growth advantage on the cancer cell are called “driver mutations” (Stratton et al., 2009). By contrast, “passenger mutations” have been shown to occur in HSCs with age, these generally do not contribute to clonal growth advantage and are not involved in the cancer development. As these biologically inert somatic mutations often occur during cell division, therefore, pre-leukaemic stem cells (pre-LSC) that obtain a driver mutation and expand into leukaemic stem cells (LSC) will already have a passenger mutation(s) within its genome, which will be carried along in the clonal expansion and will be present in all cells of the final cancer (Stratton et al., 2009).

A schematic model of clonal evolution from normal HSCs to AML LSCs is shown in Figure 1.2.1. Clonal haematopoiesis of indeterminate potential (CHIP) is predominantly defined by evidence of **a**) Clonal haematopoiesis i.e. somatic mutations with a variant allele frequency of at least 2% (Steensma et al., 2015) which is just above the limit of detection of the high throughput sequencing techniques (Haferlach et al., 2014). Therefore, it is recommended a reading depth of at least 500 copies and repeating the sequencing (Heuser et al., 2016). **b**) Absence of haematopoietic dysplasia. c) Absence of blast increase in BM. Monoclonal gammopathy of undetermined significance (MGUS), monoclonal B-lymphocytosis (MBL), and paroxysmal nocturnal haemoglobinuria (PNH) must be ruled out. Although not indicated in the criteria, CHIP is one of the most common differential diagnosis of patients with cytopaenia (haemoglobin <10 g/dL, platelets $<1x10^5$/μL, neutrophils $<1x10^3$/μL). CHIP is age-related phenomenon. It is seen in <1%, 9.5-13.9%, and 16.4% of patients under the age of 40, between 71 to 80 and over 80, respectively (Genovese et al., 2014; Heuser et al., 2016; Jaiswal et al., 2014; Xie et al., 2014). Recent studies suggest that DNA methyltransferase 3 alpha (*DNMT3A*), ten-eleven translocation methylcytosine dioxygenase 2 (*TET2*), and additional sex combs-like 1 (*ASXL1*) are the three most commonly mutated genes observed in patients with CHIP (Genovese et al., 2014; Jaiswal et al., 2014; Xie et al., 2014). HSCs bearing only these mutations are considered as pre-LSCs which have a potential of clonal expansion without inducing leukaemia (Heuser et al., 2016; Sato, Wheat, Steidl, & Ito, 2016). However, the risk of developing haematological malignancies was 11 to 13 times higher for the patients with CHIP in which 60% of them develop

myeloid neoplasm, including myelodysplastic syndromes (MDS), AML, chronic myelomonocytic leukaemia (CMML), myeloproliferative neoplasm (MPN), whereas, 40% develop a lymphoid neoplasm, including chronic lymphocytic leukaemia (CLL), multiple myeloma (MM), and B-cell lymphoma (Genovese et al., 2014; Heuser et al., 2016). For the management of CHIP, when it is found in patients without cytopaenia, a differential blood count at 3 months later, and after that every 12 months is recommended (Heuser et al., 2016). By contrast, initial BM biopsy and a differential blood count once a month for 3 months and then every 3 months should be performed if cytopaenia is observed in patients diagnosed with CHIP. If cytopaenias worsen or there is the appearance of blasts in the differential blood count, repeat BM biopsy is indicated for further investigations e.g. histology, cytomorphology, cytogenetic, and molecular genetic studies (Heuser et al., 2016) to exclude the development of an overt myeloid malignancy.

MDS are malignant diseases which are a transition state between CHIP to AML. pre-LSCs acquire a driver mutation, e.g. serine arginine-rich splicing factor 2 (*SRSF2*), stromal antigen 2 (*STAG2*), or isocitrate dehydrogenase 1 and 2 (*IDH1* and *IDH2*) mutations (Estey, 2018), and then expand into AML LSCs. MDS are defined by **a**) dysplastic cells or ring sideroblasts or increase of myeloblasts up to 19% in BM or peripheral blood (PB); **b**) cytopaenia in PB; and **c**) absence of reactive causes of the cytopaenia (Thol, Heuser, & Ganser, 2015). AML is an extreme case of clonal haematopoiesis, in which one LSC carrying multiple driver mutations takes over almost all of the abnormal haematopoiesis and drives it into a suppression of normal haematopoiesis. This results in anaemia, neutropaenia, thrombocytopaenia, and severe disorders of myeloid differentiation. AML secondary to MDS (s-AML) have often acquired additional runt-related transcription factor 1 (*RUNX1*), CCAAT/enhancer-binding protein alpha (*CEBPA*) or FMS-like tyrosine kinase 3 (*FLT3*) mutations, whereas, *de novo* AML often have *RUNX1*, *CEBPA*, *FLT3 or* lysine-specific methyltransferase 2A (*KMT2A*, previously termed mixed lineage leukaemia [*MLL*]) mutations without mutations associated with prior MDS (M. J. Walter, 2015). Importantly, a problem for the treatment of AML is that quiescent LSCs are resistant to conventional chemotherapeutic agents (Hodgson & Bradley, 1979) and radiation (Ploemacher, van Os, van Beurden, & Down, 1992).

Apart from this paradigm, germline mutations are mutations present in all HSCs at birth which characterise hereditary myeloid malignancy syndromes (HHMSs), including inherited BM failure syndromes (IBMFSs) like Fanconi anaemia (FA). Evidence for these BM failure syndromes is often been present with features that are readily recognised in childhood (University of Chicago, 2016). Germline mutations frequently culminate in MDS/AML (Godley & Shimamura, 2017). Diagnostic criteria, incidence, and molecular landscape in mutations of AML will be described in more detail in section 1.3.

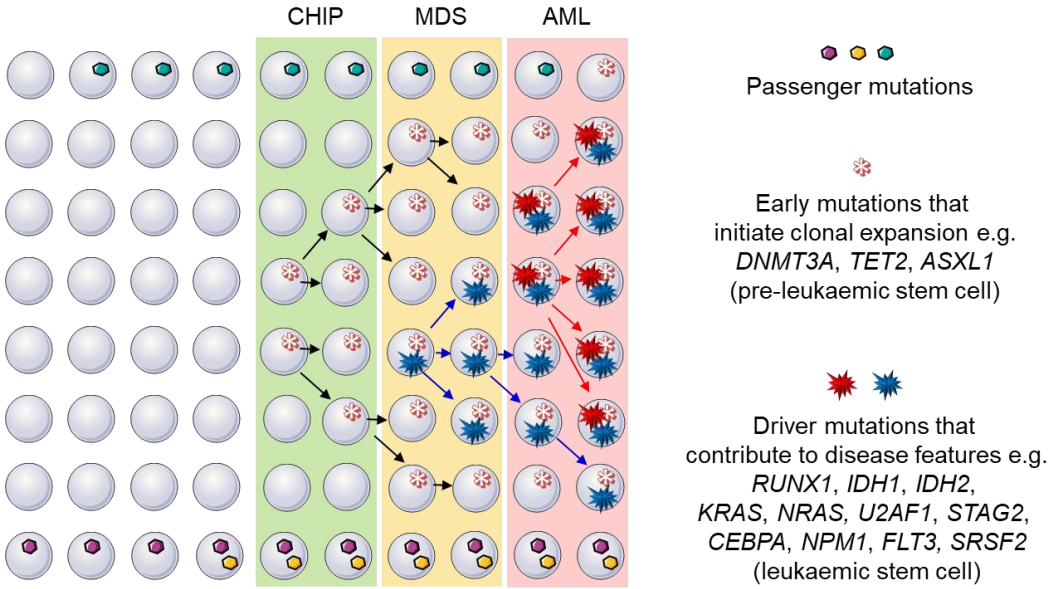

Figure 1.2.1 A schematic model of clonal expansion and clonal evolution from normal HSCs to AML LSCs. The structure of the model is adapted from (Becker, 2016). Clonal haematopoiesis of indeterminate potential (CHIP). Myelodysplastic syndromes (MDS). Acute myeloid leukaemia (AML). Haematopoietic stem cell (HSC). Leukaemic stem cell (LSC). DNA methyltransferase 3 alpha (DNMT3A). Ten-eleven translocation methylcytosine dioxygenase 2 (TET2). Additional sex combs-like 1 (ASXL1). Runt-related transcription factor 1 (RUNX1). Isocitrate dehydrogenase (IDH). Kirsten rat sarcoma viral oncogene homolog (KRAS). Neuroblastoma rat sarcoma viral oncogene homolog (NRAS). U2 small nuclear RNA auxiliary factor 1 (U2AF1). Stromal antigen 2 (STAG2). CCAAT/enhancer-binding protein alpha (CEBPA). Nucleophosmin 1 (NPM1). FMS-like tyrosine kinase 3 (FLT3). Serine arginine-rich splicing factor 2 (SRSF2).

The concept of clonal evolution from diagnosis to relapse is shown in Figure 1.2.2 (Vosberg & Greif, 2019). During therapy, a few residual AML cells may escape from treatment, hide in a niche, and eventually grow out again resulting in relapsed disease. The variant allele frequency (VAF), defined as the percentage of sequence reads harbouring the mutation divided by the total number of reads (Strom, 2016), is used to categorise the mutational clones. In linear evolution, residual cells from a dominant clone acquires additional driver or passenger mutations mediating therapy resistance (Figure 1.2.2A) (Grove & Vassiliou, 2014; Vosberg & Greif, 2019). By contrast, in branching evolution, after the dominant clone is eradicated, there is an outgrowth of a subclone either with additional mutations (Figure 1.2.2B top panel) or without additional mutations (Figure 1.2.2B bottom panel) (Grove & Vassiliou, 2014; Vosberg & Greif, 2019). Hence, the loss of a dominant clone at relapse is the hallmark of branching evolution. In another scenario, the model of evolution remains unclear in AML patients if there is no difference (Figure 1.2.2C left box), or if it is completely different (Figure 1.2.2C right box) between the mutational profiles at diagnosis and at relapse (Vosberg & Greif, 2019). Clonal evolution occurs not only at genetic level but also at epigenetic level. It has been reported that a lack of genetic evolution can be compensated by an increase in epigenetic evolution, resulting in epigenetic profiles that confer therapy resistance and subsequent relapsed disease (S. Li et al., 2016). In addition, cytogenetic alterations at relapse not present at initial diagnosis has been identified as potential mechanism of relapsed disease (Bacher et al., 2010). Mostly, the cytogenetic alterations at relapse are a more complex karyotype, e.g. deletions of the long arm of chromosomes 5 or 7, which is associated with poor outcome (Grimwade et al., 2010; Papaemmanuil et al., 2016).

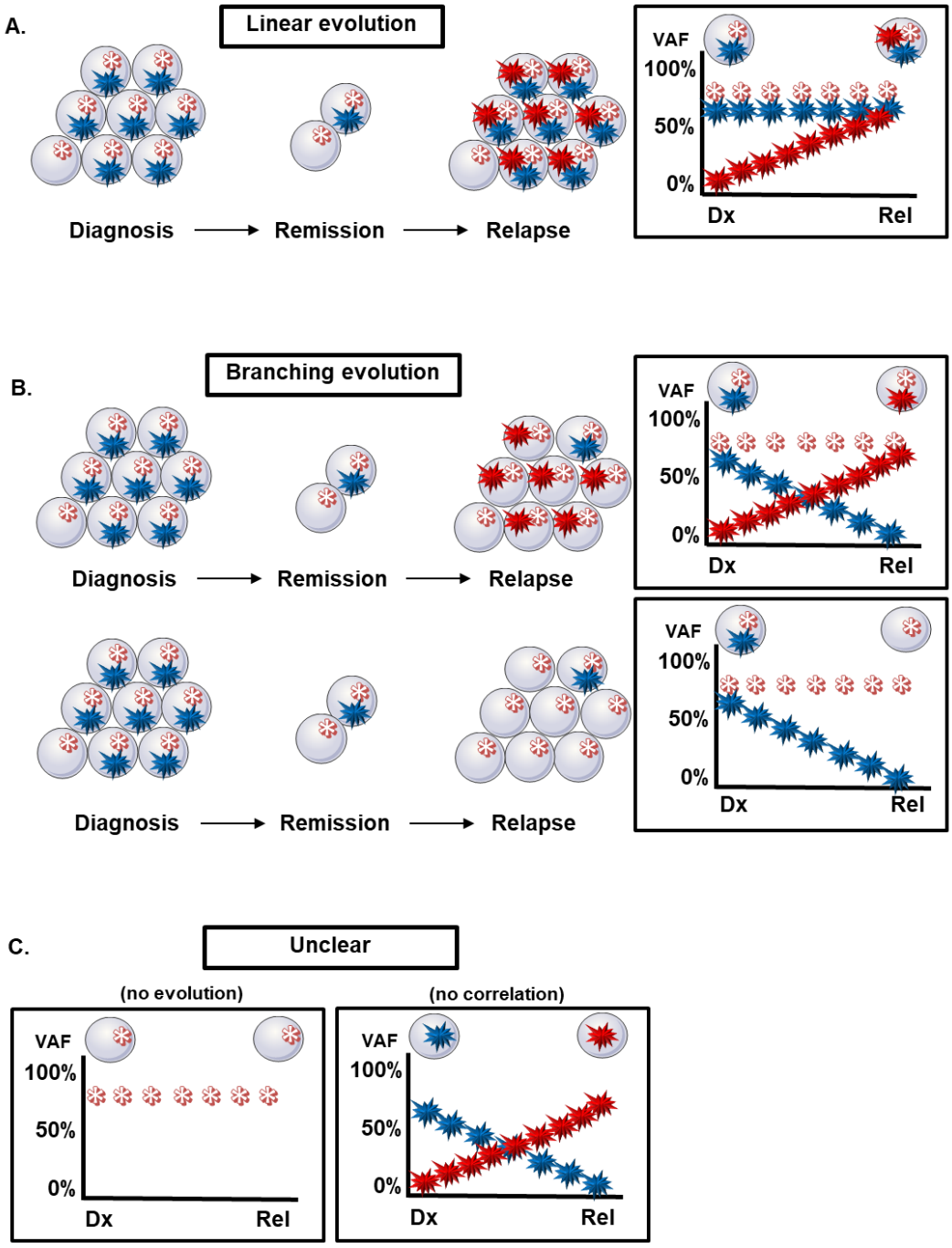

Figure 1.2.2 A schematic model of clonal evolution from diagnosis to relapse.
The structure of the model is adapted from (Vosberg & Greif, 2019). (A) Linear evolution is characterised by the presence of a dominant clone with additional mutations at relapse; (B) Branching evolution is characterised by the loss of a dominant clone and an outgrowth of a subclone either with additional mutations (top panel) or without additional mutations (bottom panel) at relapse; (C) The model of evolution remains unclear in AML patients if there is no difference (left box, no evolution), or if it is completely different (right box, no correlation) between the mutational profiles at diagnosis and at relapse. Diagnosis (Dx). Relapse (Rel). Variant allele frequency (VAF).

1.3 Acute myeloid leukaemia

1.3.1 Diagnosis criteria and incidence

AML is a disease in which the clonal expansion of abnormal or poorly differentiated myeloid cells infiltrate the BM, blood or extramedullary tissues (H. Döhner, Weisdorf, & Bloomfield, 2015). Patients usually present with fever, anaemia and a bleeding tendency. It is the most common malignant myeloid disorder in adults. The main criteria of the World Health Organization (WHO) for AML, revised in 2016, are the presence of ≥50% erythroid precursors plus ≥20% myeloblasts of all cells in BM or PB (Arber et al., 2016). As summarised in Table 1.3.1.1 (Arber et al., 2016), this can be subcategorised into AML with recurring genetic abnormality; AML with myelodysplasia-related changes (AML-MRC); and AML, not otherwise specified (Arber et al., 2016). Additionally, AML with recurrent genetic abnormalities of chromosomal rearrangements between chromosomes 8 and 21 [t(8;21)], within chromosome 16 [inv(16)/t(16;16)] or chromosomal rearrangements between chromosomes 15 and 17 [t(15;17)] is diagnosed regardless of blast percentage (Swerdlow, Campo, & Harris, 2008).

In 2012, the Global Cancer Incidence, Mortality and Prevalence (GLOBOCAN) revealed that the worldwide age-standardised rate (ASR) of AML is 4.7 per 100,000 with a mortality rate of 3.4 per 100,000 and a male-to-female ratio of approximately 1.4:1 (GLOBOCAN, 2012). In the UK, an overall incidence rate is 5.2 per 100,000 with 4.3 per 100,000 for mortality rate (CRUK, 2016). The age-specific incidence rate rises steadily from age 50-54 and more steeply from age 60-64. In 2013-2015, the highest rates were 39 and 22 per 100,000 in the 85-89 year old age group for males and females, respectively, with a male-to-female ratio of approximately 6.4:4.2 (CRUK, 2016).

Table 1.3.1.1 Diagnostic criteria for AML and MDS according to the 2016 revision to the WHO classification of myeloid neoplasms and acute leukaemia (Arber et al., 2016).

BM erythroid precursors	Myeloblast % of all cells in BM (or PB)	Prior therapy	Recurring WHO genetic abnormality	Meets criteria for AML-MRC	Diagnosis
≥50%	NA	Yes	NA	NA	Therapy-related myeloid neoplasm
≥50%	≥20%	No	Yes*	No	AML with recurring genetic abnormality
≥50%	≥20%	No	No	Yes†	AML with myelodysplasia-related changes
≥50%	≥20%	No	No	No	AML, not otherwise specified (non erythroid subtype)
≥50%	<20%	No	No	NA	Myelodysplastic syndromes
>80% immature erythroid precursors with ≥30% Proerythroblasts	<20%	No	No	NA	AML, not otherwise specified, acute erythroid leukemia (pure erythroid type)

*AML with recurrent genetic abnormalities
AML with t(8;21)(q22;q22.1); *RUNX1-RUNX1T1*
AML with inv(16)(p13.1q22) or t(16;16)(p13.1;q22); *CBFB-MYH11*
APL with t(15;17)(q22;q21); *PML-RARA*
AML with t(9;11)(p21.3;q23.3); *MLLT3-KMT2A*
AML with t(6;9)(p23;q34.1); *DEK-NUP214*
AML with inv(3)(q21.3q26.2) or t(3;3)(q21.3;q26.2); *GATA2, MECOM*
AML (megakaryoblastic) with t(1;22)(p13.3;q13.3); *RBM15-MKL1*
Provisional entity: AML with *BCR-ABL1*
AML with mutated *NPM1*
AML with biallelic mutations of *CEBPA*
Provisional entity: AML with mutated *RUNX1*

†Criteria for AML with myelodysplasia-related changes must meet at least 1 of 3 criteria
1) Prior history of myelodysplastic syndromes (MDS) or myelodysplastic/myeloproliferative neoplasm (MDS/MPN)
2) Multilineage dysplasia : ≥50% of cells dysplastic in at least 2 lineages
3) MDS-associated cytogenetic abnormality 3.1) Complex karyotype (≥3 abnormalities) 3.2) Unbalanced translocations -7/del(7q) del(5q)/t(5q) i(17q)/t(17p) -13/del(13q) del(11q) del(12p)/t(12p) idic(X)(q13) 3.3) Balanced translocations t(11;16)(q23.3;p13.3) t(3;21)(q26.2;q22.1) t(1;3)(p36.3;q21.2) t(2;11)(p21;q23.3) t(5;12)(q32;p13.2) t(5;7)(q32;q11.2) t(5;17)(q32;p13.2) t(5;10)(q32;q21.2) t(3;5)(q25.3;q35.1)

Bone marrow (BM). Peripheral blood (PB). Acute myeloid leukaemia (AML). Myelodysplastic syndromes (MDS). Myelodysplasia-related changes (MRC). Runt-related transcription factor 1 (RUNX1). Runt-related transcription factor 1 partner transcriptional co-repressor 1 (RUNX1T1). Core-binding factor subunit beta (CBFB). Myosin Heavy Chain 11 (MYH11). Promyelocytic leukaemia (PML). Retinoic acid receptor alpha (RARA). Myeloid/lymphoid or mixed-lineage leukaemia; translocated to 3 (MLLT3). Lysine methyltransferase 2A (KMT2A). DEK Proto-Oncogene (DEK). Nucleoporin 214 (NUP214). GATA-binding factor 2 (GATA2). MDS1 And EVI1 Complex Locus (MECOM). RNA Binding Motif Protein 15 (RBM15). Megakaryoblastic leukaemia 1 (MKL1). Breakpoint cluster region (BCR). Abelson murine leukaemia viral oncogene homolog 1 (ABL1). Nucleophosmin 1 (NPM1). CCAAT/enhancer-binding protein alpha (CEBPA).

1.3.2 Molecular landscape of mutations in acute myeloid leukaemia

AML is renowned for its complex clonal heterogeneity and adaptation potential. Mutational profiling with a spectrum of cooperating mutations of adult patients, up to the age of approximately 65 years, with AML is shown in Figure 1.3.2.1 (H. Döhner et al., 2017). The classification is based on WHO subgroups with the additional groups of chromatin–spliceosome mutation, chromosomal aneuploidy, and IDH2 mutation at arginine 172 residue (*IDH2*^{R172}) (Papaemmanuil et al., 2016). Mutational frequencies are gathered from the databases of the German-Austrian AML Study Group, the British Medical Research Council, and selected publications (Duployez et al., 2016; Faber et al., 2016; Gröschel et al., 2015; Papaemmanuil et al., 2016).

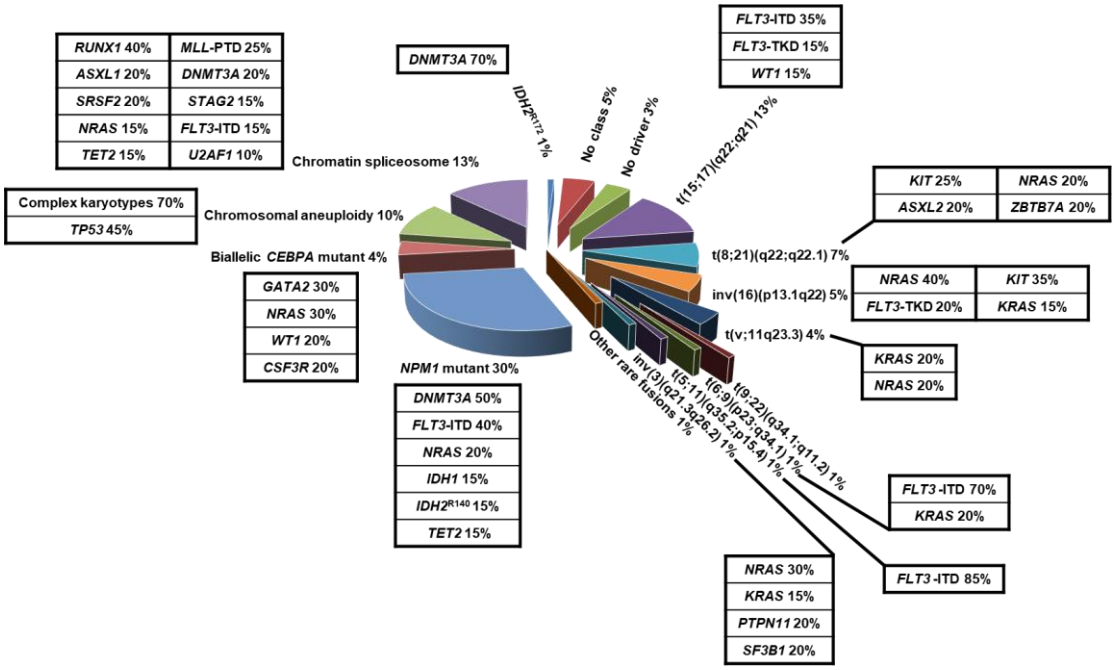

Figure 1.3.2.1 Molecular classes of AML and concurrent gene mutations in adult patients up to the age of approximately 65 years (H. Döhner et al., 2017). CCAAT/enhancer-binding protein alpha (CEBPA). Nucleophosmin 1 (NPM1). Runt-related transcription factor 1 (RUNX1). Mixed lineage leukaemia-partial tandem duplication (MLL-PTD). Additional sex combs-like 1 and 2 (ASXL1 and ASXL2). DNA methyltransferase 3 alpha (DNMT3A). Serine arginine-rich splicing factor 2 (SRSF2). Stromal antigen 2 (STAG2). Kirsten rat sarcoma viral oncogene homolog (KRAS). Neuroblastoma rat sarcoma viral oncogene homolog (NRAS). FMS-like tyrosine kinase 3-internal tandem duplication (FLT3-ITD). FMS-like tyrosine kinase 3- tyrosine kinase domain (FLT3-TKD). Methylcytosine dioxygenase 2 (TET2). U2 small nuclear RNA auxiliary factor 1 (U2AF1). GATA-binding factor 2 (GATA2). Wilms tumour 1 (WT1). Colony Stimulating Factor 3 Receptor (CSF3R). Isocitrate dehydrogenase 1 and 2 (IDH1 and IDH2). Isocitrate dehydrogenase 2 mutation at arginine 140 or 172 residue (IDH2^{R140} or IDH2^{R172}). Protein tyrosine phosphatase non-receptor type 11 (PTPN11). Splicing factor 3B subunit 1 (SF3B1). Tyrosine-protein kinase Kit (KIT). Zinc finger and BTB domain containing 7A (ZBTB7A).

In addition, mutated genes could be classified according to their functional categories (H. Döhner et al., 2017; He, Oliveira, Hoyer, & Viswanatha, 2018) as detailed below.

1.3.2.1 Signalling genes

FLT3 encodes FLT3 receptor which is part of a family of receptor tyrosine kinases (RTKs). RTKs transmit signals from the cell surface into the cell through a process called signal transduction. The FLT3 protein is found in the outer membrane of certain cell types where FLT3L can bind to it. This binding activates the FLT3 protein, which subsequently activates a series of proteins inside the cell that are part of multiple signalling pathways e.g. the phosphoinositide-3-kinase/protein kinase B (PI3K/AKT), the Janus kinase/signal transducers and activators of transcription 5 (JAK/STAT5), and the rat sarcoma viral oncogene homolog (RAS) pathways (Takahashi, 2011). The signalling pathways stimulated by the FLT3 protein control many important cellular processes such as the growth, proliferation and survival of cells, particularly of early blood cells called haematopoietic progenitor cells. The most frequent *FLT3* mutation is an internal tandem duplication (ITD) in exon 14 (Schwartz et al., 2019), occurring in approximately 25% of patients with AML (Levis & Small, 2003) and characterised by high white blood cell and BM blast counts as well as a high risk of relapse after standard chemotherapy (Boissel et al., 2002; Whitman et al., 2010). *FLT3*-ITD-positive patients are also less likely to respond to salvage chemotherapy and have shorter survival following relapse than *FLT3*-ITD-negative patients (Boissel et al., 2002; Ravandi et al., 2010). Mutations in the tyrosine kinase domain (TKD) of *FLT3* occur in an additional 5-10% (Estey, 2018). The most common mutation is the substitution of aspartic acid with tyrosine at codon 835 (*FLT3*^{D835Y}) (Mead et al., 2007).

The tyrosine-protein kinase Kit gene (*KIT*) which encodes the KIT protein, another RTKs, also known as CD117. The KIT protein is found in the cell membrane of certain cell types where SCF binds and activates it, resulting in the activation of multiple signalling pathways including PI3/AKT, JAK/STAT1,3 and 5, RAS and Src family (Linnekin, 1999). *KIT* is expressed by myeloblasts in approximately 60% to 80% of patients with AML (Ikeda et al., 1991). The overall

reported frequency of *KIT* mutations in adults and children with AML is 17% (Boissel et al., 2006), but it occurs in 52% of patients with core binding factor (CBF) AML (Paschka et al., 2006) which is associated with t(8;21) and inv(16)/t(16;16) and corresponding molecular rearrangements *RUNX1*/RUNX1 partner transcriptional co-repressor 1 (*RUNX1T1*) and core-binding factor subunit beta (*CBFB*)/myosin heavy chain 11 (*MYH11*) genes. Two of these genes, *RUNX1* and *CBFB*, provide instructions for making CBF which attaches to certain regions of DNA and turns on genes that help control haematopoiesis. The substitution of aspartic acid with valine at codon 816 (KIT^{D816V}) missense mutations (DiNardo & Cortes, 2016) and ITD involving exon 11 and exon 12 (Malaise, Steinbach, & Corbacioglu, 2009) are the most common form of *KIT* mutations and are frequently associated with an adverse prognosis, although this has not been universally observed (Klein et al., 2015).

1.3.2.2 Nucleophosmin genes

Nucleophosmin 1 (*NPM1*) encodes nucleophosmin which belongs to the nucleophosmin/nucleoplasmin family of proteins. The frequency of *NPM1* mutation in AML is approximately 30% (Heath et al., 2017) with associated clinical features including high BM blasts, white blood cells and platelet counts at diagnosis (K. Döhner et al., 2005). NPM1 is a ubiquitously expressed phosphoprotein, containing 12 exons and encoding a protein that shuttles between the nucleus and cytoplasm (Federici & Falini, 2013). The current knowledge states that there are four main functions of NPM1 (Heath et al., 2017) including: **a)** a role in ribosome biogenesis i.e. mediating nuclear export of 5S ribosomal RNA for incorporation into 60S ribosomal subunits (Yu et al., 2006); **b)** a role in maintenance of genomic stability, i.e., binding to unduplicated centrosomes to prevent their duplication. At the G1/S boundary, phosphorylation at Thr199 inactivates NPM1 activity rendering centrosome duplication (Okuda et al., 2000). It re-associates with centrosomes at mitosis where a daughter cell receives a single NPM1-bound centrosome following cytokinesis; **c)** a role in stress response i.e. interacting with p53 and increasing its stability (Colombo, Marine, Danovi, Falini, & Pelicci, 2002), inhibiting mouse double minute 2 homolog (MDM2) (Kurki et al., 2004) which is an E3 ubiquitin-protein ligase that causes proteolytic degradation of p53, and regulating growth

arrest and DNA-damage-inducible protein 45 alpha (GADD45A) (Gao et al., 2005), a pro-apoptotic protein, enhancing p53-dependent cell cycle arrest; **d)** a role in modulation of growth suppressive pathways i.e. binding to the alternative reading frame (ARF) tumour suppressor protein. In a p53-independent manner, ARF disrupts ribosomal RNA precursor processing and suppresses ribosome biogenesis upon cellular stress (Sherr, 2006). In a p53-dependent manner, ARF also interacts with and localises MDM2 to the nucleolus and ceases its p53-inhibitory activity (Weber, Taylor, Roussel, Sherr, & Bar-Sagi, 1999). *NPM1* mutations usually occur in exon 12 (Falini et al., 2005). Approximately 80% are a type A mutation in which the TCTG at position 956-959 is duplicated (Verhaak et al., 2005). This creates the new nuclear export signal (NES) motif rendering cytoplasmic localisation of the protein (NPM1c). However, *NPM1* mutations are always heterozygous as the wild-type is crucial for cell survival (Heath et al., 2017). NPM1c causes uncontrolled centrosome duplication and aneuploidy (Sportoletti et al., 2008). It sequesters ARF to the cytoplasm resulting in degradation. MDM2 is relieved causing p53 to be ubiquitinated and degraded. NPM1c delocalises an F-box protein component to the E3 ubiquitin ligase complex (Fbw7γ), which promotes Myc degradation, to the cytoplasm rendering its destabilisation/degradation and Myc activation (Bonetti et al., 2008). In addition, NPM1c retains the proteolytic activities of cleaved caspase-6 and -8, thus perturbing the apoptotic process (Leong et al., 2010). Nonetheless, although *NPM1* mutation is an AML-driving lesion, alone it could not initiate leukaemia (Cheng et al., 2010). *NPM1* mutations likely precede *FLT3*-ITD, as *FLT3*-ITD is approximately twice as frequent in *NPM1*-mutated AML compared with AML with wild-type *NPM1* (Falini et al., 2005; Verhaak et al., 2005). The evidence suggests that *NPM1* mutations are usually secondary to *DNMT3A* mutations in which *NPM1* mutations co-exist in approximately 60% of cases (L. Yang, Rau, & Goodell, 2015). The presence of an *NPM1* mutation, without *FLT3*-ITD, is associated with relatively favourable clinical outcome (He et al., 2018).

1.3.2.3 Cohesin complex genes

The cohesin complex is a multi-subunit ring-like structure composed of structural maintenance of chromosomes (SMC) family i.e. SMC1A and SMC3, double-strand-break repair protein rad21 (RAD21), and stromal antigen 1 and 2 (STAG1 and

STAG2) proteins (He et al., 2018), and functions in the processes of meiosis and mitosis i.e. to keep the sister chromatids connected with each other during metaphase, ensuring that each sister chromatid segregates to opposite poles, facilitating spindle attachment onto chromosomes, and thus, recombinational DNA repair, and controlling transcriptional processes (Mehta, Kumar, Srivastava, & Ghosh, 2013). Mutations of this complex result in an increased proliferation potential which is one of the key processes for every malignant cell including AML blasts. Cohesin complex gene mutations are present in approximately 13% of AML patients (Ley et al., 2013). The mutations are prognostically neutral and commonly associated with *NPM1* (Thol et al., 2014), *RUNX1* and *ASXL1* mutations (He et al., 2018).

1.3.2.4 Chromatin-modifying genes

KMT2A encodes a large multi-domain protein. Previously, it was stated that the histone 3 lysine 4 (H3K4) methyltransferase activity of the Su(var)3-9, enhancer of zeste, trithorax (SET) domain at the C-terminal fragment is required for *KMT2A* target gene activation (Krivtsov & Armstrong, 2007). However, it has recently been revealed that recruitment of the histone acetyltransferases CBP/p300 and the human MOZ, Ybf2/ Sas3, Sas2 and Tip60 (MYST) protein Male Absent on the First (hMOF) to the promoter of the target genes is crucial for gene expression (Mishra et al., 2014; Winters & Bernt, 2017), particularly the Homeobox (*HOX*) gene which is involved in the development of multiple tissues including haematopoiesis (Alharbi, Pettengell, Pandha, & Morgan, 2013; Mallo & Alonso, 2013).

KMT2A rearrangement (*KMT2A*-R) usually occurs at the 8.3 kb breakpoint cluster region (BCR) between exons 8 and 13, resulting in the novel KMT2A fusion proteins (*KMT2A*-FPs) (Ayton & Cleary, 2001). There are more than 80 different partner proteins for *KMT2A* (Meyer et al., 2013), but more than 80% of them are one of the following: the nuclear binding proteins *ALL1*-fused gene from chromosome 4 (AF4, also known as AF4/FMR2 Family Member 1 [AFF1]), *ALL1*-fused gene from chromosome 9 (AF9, also known as myeloid/lymphoid or mixed-lineage leukaemia; translocated to, 3 [MLLT3]), eleven nineteen leukaemia (ENL, also known as myeloid/lymphoid or mixed-lineage leukaemia; translocated to, 1 [MLLT1]), *ALL1*-

fused gene from chromosome 10 (AF10, also known as myeloid/lymphoid or mixed-lineage leukaemia; translocated to, 10 [MLLT10]) and elongation factor for RNAPII (ELL). Mostly, *KMT2A-AFF1* (*MLL-AF4*) results in ALL whereas *KMT2A-MLLT3* (*MLL-AF9*) predominantly causes AML (Swerdlow et al., 2008). The AFF1 protein is shown to directly interact with the P-TEFb/cyclin T/CDK9 complex, which phosphorylates the S2 position of the CTD of RNAPII (Santo et al., 2015), and the H3K79 histone methyltransferase disruptor of telomeric silencing 1-like (DOT1L) (Bitoun, Oliver, & Davies, 2007). H3K79 is broadly distributed across the promoter and the open reading frame (Krivtsov & Armstrong, 2007). Consequently, the broad methylation marks may lead to aberrant expression of *HOX* genes. MLLT3 and MLLT1 have highly similar structures (Winters & Bernt, 2017) and have been shown to interact with AFF1-containing complexes, thus also binding to P-TEFb and DOT1L (Bitoun et al., 2007; Mueller et al., 2007), whereas MLLT10 is shown to directly interact with DOT1L (Okada et al., 2005). Overall, the outcome of *KMT2A* binding is transcriptional activation. Another type of *KMT2A*-R is *KMT2A*-partial tandem duplication (*KMT2A*-PTD). Unlike KMT2A-FPs, *KMT2A*-PTD results from a duplicated genomic region insertion i.e. a varied number of exons 5-12 are inserted before exons 11 or 12, rendering duplicated AT-hook domains (Krivtsov & Armstrong, 2007; Whitman et al., 2005). However, it is currently unclear what the mechanism is by which *KMT2A*-PTD induces leukaemogenesis.

ASXL1 is a chromatin-binding protein which regulates epigenetic marks and transcription. ASXL1 interacts with the polycomb repressive complex 2 (PRC2) complex and facilitates tri-methylation of histone H3 lysine 27 (H3K27me3) resulting in gene silencing (Wiles & Selker, 2017). Truncating and frameshift mutations in the C-terminal plant homology domain (PHD) are the most common mutations and have been associated with secondary AML, *RUNX1* mutations, and poor prognosis (He et al., 2018).

1.3.2.5 DNA-methylation related genes

DNMT3A encodes DNA methyltransferase, and is recurrently mutated in approximately 18-25% of AML patients (He et al., 2018; Thol et al., 2011). It is more commonly observed in patients with advanced age e.g. patients with CHIP as discussed in section 1.2. The most common mutation is the substitution of arginine

with histidine at codon 882 (*DNMT3A*^{R882H}) (Koya et al., 2016), resulting in the loss of its methyltransferase function which causes hypomethylation. However, R882H appears to minimally perturb the methylation of CpG islands (Ley et al., 2010) but may alter the methylation of non promoter-associated CpG regions, affecting gene expression indirectly (H. Wu et al., 2010). A recent study revealed that *DNMT3A* mutation may contribute to leukaemia initiation by allowing the self-renewing haematopoietic stem and progenitor cell (HSPC) pool to slowly expand (Spencer et al., 2017). Single cell RNA sequencing of haematopoietic progenitor cells (HPC) bearing *DNMT3A*^{R878H} in mice, which is comparable with *DNMT3A*^{R882H} in human, has shown dysregulated genes with pathway analyses suggesting dysregulation of the apoptotic and proliferative, proteasome, chemokine and inflammatory signaling pathways (A. M. Smith et al., 2019). Mostly, it has been stated that the prognostic significance of the *DNMT3A* mutation is poor (Ley et al., 2010; Marcucci et al., 2012; Ostronoff et al., 2013). However, recent cohort study has revealed that *DNMT3A* R882 mutation (*DNMT3A*^{R882}) had no impact either on the leukaemia-free survival (LFS) ($P = 0.37$) or overall survival (OS) rates ($P = 0.63$) in elderly patients with AML (fifteen patients with *DNMT3A*^{R882} vs eighty-three patients with wild-type *DNMT3A*) undergoing non-myeloablative conditioning haematopoietic stem cell transplantation (HSCT) (Schmalbrock et al., 2018).

TET2 encodes a methylcytosine dioxygenase. The enzyme is crucial for the DNA demethylation process i.e. converting methylcytosine (5mC) to 5-hydroxymethylcytosine (5hmC) (Cimmino et al., 2017). *TET2* mutations, consequently, result in DNA hypermethylation which plays a role in establishing CHIP (see section 1.2) and additional gene mutations. *TET2* mutations are mutually exclusive of isocitrate dehydrogenase 1 and 2 (*IDH1* and *IDH2*) gene mutations. IDH1 and IDH2 are the mitochondrial and cytosolic/peroxisomal enzymes which catalyse oxidative decarboxylation of isocitrate to α-ketoglutarate (α-KG). *IDH1* and *IDH2* mutations are found in 7-14% and 8-19% of AML, respectively (Medeiros et al., 2017). The most common mutational sites are arginine 132 for *IDH1* (*IDH1*^{R132}) and arginine 140 or arginine 172 for *IDH2* (*IDH2*^{R140} or *IDH2*^{R172}) (Kato et al., 2014), which results in a new enzymatic function to convert α-KG to oncometabolite 2-hydroxyglutarate (2-HG). Accumulation of 2-HG results in a block of differentiation and promotes leukaemogenesis (Shafer & Grant, 2016). 2-HG is a competitive inhibitor of multiple α-KG-dependent

dioxygenases, including TET2 (Xu et al., 2011). Hence, *IDH* mutation causes DNA hypermethylation.

Recently, it has been demonstrated that the IDH2 inhibitor enasidenib induces differentiation of AML blasts (Stein, 2018) and has been approved by the U.S. Food and Drug Administration (FDA) for relapsed/refractory (R/R) AML (see section 1.4.2.1.1). The prognostic impact of *TET2* and *IDH1/2* alterations remains controversial (He et al., 2018; Rakheja, Konoplev, Medeiros, & Chen, 2012).

Wilms' tumour suppressor gene1 (*WT1*) encodes a transcription factor which has an essential role in the normal development of the urogenital system. WT1 binds and stabilises p53 (Maheswaran et al., 1993). Heat shock protein 90 (Hsp90) is a chaperone which stabilises WT1 which then binds to signal transducer and activator of transcription 3 (STAT3) resulting in enhancement of Wilms' tumour development (Y. Rong et al., 2006). In AML, WT1 is usually overexpressed which is associated with resistance to therapy, a high incidence of relapse, and poor OS (Barragán et al., 2004). *WT1* mutations occur in approximately 6-15% of AML cases (Hou et al., 2010). The most common mutations are truncation and frameshift mutations (He et al., 2018). Mutated WT1 fails to properly direct TET2 to its target rendering DNA hypermethylation. The mutations are associated with *FLT3*-ITD and CCAAT/enhancer-binding protein alpha (*CEBPA*) mutations. Clinical outcomes of *WT1* mutations are mostly poor, independent of the presence of *FLT3*-ITD (Rampal & Figueroa, 2016).

1.3.2.6 Spliceosome complex genes

Splicing Factor 3b Subunit 1 (*SF3B1*), U2 small nuclear RNA auxiliary factor 1 (*U2AF1*), serine arginine-rich splicing factor 2 (*SRSF2*), and zinc finger CCCH-type, RNA-binding motif and serine/arginine rich 2 (*ZRSR2*) encode protein components of the splicing machinery. Spliceosome mutations are found in approximately 10% of AML cases with poor clinical outcomes (He et al., 2018). The mutations contribute to a splicing abnormality during gene transcription, with impacts on epigenetic modification, transcription, and genome integrity. For instance, Kim *et al*. revealed that enhancer of zeste homolog 2 (EZH2), a component of PRC2 complex which is responsible for the addition of methyl groups to H3K27, is

impaired due to *SRSF2* mutation. This results in impaired haematopoietic differentiation (E. Kim et al., 2015).

1.3.2.7 Transcription factor fusions

RUNX1 encodes core binding factor alpha (CBFα) which forms a heterodimeric complex with its partner CBFß and targets promoter regions through the conserved Runt homology domain (RHD) which regulates transcription at multiple genes involved in normal haematopoietic development. There are two main categories of *RUNX1* mutations. These are chromosomal translocations and somatic mutations with an incidence rate of 5-16% in AML (Jalili et al., 2018). The most common chromosomal translocations are t(8;21)(q22;q22) in *de novo* AML, generating fusion proteins RUNX1-RUNX1T1 which confers a favourable prognosis (Bellissimo & Speck, 2017). By contrast, *RUNX1* somatic mutations including deletions, missense, splicing, frameshift, and nonsense mutations are associated with a poor prognosis (Bellissimo & Speck, 2017). The mutations are distributed across the gene and usually mutually exclusive of *NPM1* and *CEBPA* mutations (He et al., 2018).

1.3.2.8 Myeloid transcription factor genes

CEBPA gene encodes a transcription factor which controls myeloid progenitor differentiation and proliferation and promotes granulocytic maturation. It is expressed in myeloid progenitors and granulocytes, but not macrophages, and is shown to regulate the expression of many myeloid genes (Gruber & Rubnitz, 2018). *CEBPA* mutations are found in 5-14% of AML (Wouters et al., 2009). Only biallelic *CEBPA* mutations are considered as a favourable prognosis (Wouters et al., 2009) which typically occur in the N-terminal and C-terminal. The N-terminal (amino acids 1-120) frameshift/nonsense mutation renders a truncated wild-type p42 CEBPA protein which leads to re-initiation of translation from a second downstream ATG codon and results in a dominant-negative p30 isoform that inhibits the function of the wild-type protein (He et al., 2018). The C-terminal basic leucine zipper (bZIP) (amino acids 278-358) in-frame/missense mutation results in disruption of CEBPA DNA binding and dimerisation (Nerlov, 2004).

1.3.2.9 Tumour suppressor genes

TP53 encodes p53, the guardian of the genome (Read & Strachan, 1999). Normal p53 is upregulated in response to a variety of cellular proliferative stress and DNA damage signals. At the G1 checkpoint, ATM/CHK2 promotes G1 arrest through p53 (Cao et al., 2006; Hirao et al., 2002) which activates the transcription of $p21^{Cip1}$ that inhibits CDK2/cyclin E and stabilises the interaction between the Rb/E2F complex, keeping it inactivated (Bose et al., 2013). In addition, p53 induces the upregulation of DNA repair machinery (Bartek & Lukas, 2001) and pro-apoptotic factors enhancing apoptosis via the extrinsic and intrinsic pathways (Haupt et al., 2003). Somatic *TP53* mutations are seen in approximately 6-8% of AML (He et al., 2018) and are more associated with s-AML or therapy-related AML (t-AML) compared to *de novo* AML (Pedersen-Bjergaard, Christiansen, Desta, & Andersen, 2006). Interestingly, *TP53* mutations often coexist with complex karyotypes (He et al., 2018) and chromosomal aneuploidy in which 45% of the cases bear *TP53* mutations (H. Döhner et al., 2017). The majority are missense mutations in exons 5–8 (Hou et al., 2015; Nigro et al., 1989). *TP53* mutations confer chemoresistance with poor prognosis (He et al., 2018).

1.3.2.10 The stratifications of major risk profiles according to the European LeukemiaNet recommendations

Karyotypes and the genetic mutational status are the most important predictor of resistance (Estey, 2018). Nowadays, molecular genetics and cytogenetic alterations are stratified for risk profile according to the ELN recommendations as summarised in Table 1.3.2.10.1 (H. Döhner et al., 2017), which probably are the most widely used source. Although numerous studies have investigated other genetic lesions, for example, *DNMT3A*, *IDH1/2*, or genes in the chromatin/spliceosome group other than *ASXL1* and *RUNX1*, there is not enough evidence to assign them into an individual ELN prognostic group.

Table 1.3.2.10.1 The stratification of genetic lesions for risk profile according to the ELN recommendations 2017 (H. Döhner et al., 2017).

Risk category	Genetic abnormality
Favorable	t(8;21)(q22;q22); *RUNX1-RUNX1T1*
	inv(16)(p13.1q22) or t(16;16)(p13.1;q22); *CBFB-MYH11*
	Mutated *NPM1* without *FLT3*-ITD or with *FLT3*-ITD^{low}
	Biallelic mutated *CEBPA*
Intermediate	Mutated *NPM1* and *FLT3*-ITD^{high}
	Wild-type *NPM1* without or with *FLT3*-ITD^{low} (without adverse-risk genetic lesions)
	t(9;11)(p21.3;q22.3); *MLLT3-KMT2A*
	Cytogenetic abnormalities not classified as favorable or adverse
Adverse	t(6;9)(p23;q34.1); *DEK-NUP214*
	t(v;11)(v;q23.3); *KMT2A* rearranged (MLLr)
	t(9;22)(q34.1;q11.2); *BCR-ABL1*
	inv(3)(q21.3q26.2) or t(3;3)(q21.3;q26.2); *GATA2*, *MECOM*
	−5 or del(5q); −7; −17/abn(17p)
	Complex karyotype, monosomal karyotype
	Wild-type *NPM1* and *FLT3*-ITD^{high}
	Mutated *RUNX1*
	Mutated *ASXL1*
	Mutated *TP53*

Runt-related transcription factor 1 (RUNX1). Runt-related transcription factor 1 partner transcriptional co-repressor 1 (RUNX1T1). Core-binding factor subunit beta (CBFB). Myosin Heavy Chain 11 (MYH11). Nucleophosmin 1 (NPM1). FMS-like tyrosine kinase 3-internal tandem duplication (FLT3-ITD). CCAAT/enhancer-binding protein alpha (CEBPA). Myeloid/lymphoid or mixed-lineage leukaemia; translocated to, 3 (MLLT3). Lysine methyltransferase 2A (KMT2A). DEK Proto-Oncogene (DEK). Nucleoporin 214 (NUP214). GATA-binding factor 2 (GATA2). MDS1 And EVI1 Complex Locus (MECOM). Additional sex combs-like 1 (ASXL1).

1.4 Management of acute myeloid leukaemia

1.4.1 Standard therapy

i) Induction therapy

The purpose of induction therapy is to eradicate the active disease. The complete remission (CR) rate is defined as less than 5% of blasts in BM and blood count returning to normal i.e. neutrophils ≥1x10^3/μL and platelets ≥1x10^5/μL and absence of transfusion requirements (Cheson et al., 2003; H. Döhner et al., 2010; R. B. Walter et al., 2010). In contrast, CR with residual neutropaenia or thrombocytopaenia is determined as CR with incomplete recovery (CRi) (Cheson et al., 2003; H. Döhner et al., 2010). Partial remission (PR) is defined as

a reduction by at least 50% of blasts in BM to 5-25% of cellularity, and blood count returning to normal (H. Döhner et al., 2010).

An evaluation of eligibility to receive the standard "7+3" intensive chemotherapy (IC) (discussed below) remains a difficult task for clinicians, but is usually defined as patients younger than 70-75 years plus WHO performance status 0-1 and absence of cardiac, hepatic, or renal dysfunction, and serum albumin >3.5g/dl (Estey, 2018). Clinical trials of novel agents or less intensive therapy should be offered if patients are ineligible for IC (discussed in Chapter 6). The efficacy of less intensive therapy has been impressively described in one clinical study in which four Southwest Oncology Group (SWOG) studies were analysed, including two groups of elderly patients with MDS or AML who were ineligible for IC and given azacitidine and two groups of patents aged less than 60 years given a "7+3" regimen (Othus et al., 2016). The purposes of this study were: i) to evaluate whether CR is associated with OS in elderly patients with MDS or AML given azacitidine; and ii) to evaluate the impact of CR on OS comparing azacitidine regimens with the standard "7+3" regimen. It was observed that CR is associated with an overall 60% improvement in OS and the impact of CR on OS was similar with azacitidine as with more intense regimens. The details of azacitidine therapy will be further described in Chapter 5.

The standard IC is often termed "7+3 induction" because it consists of receiving low dose continuous-infusion cytarabine (100-200mg/m^2) for 7 days, along with short infusions of an anthracycline e.g. idarubicin dosed at 12mg/m^2 on each of the first 3 days. In the UK, the induction course is usually given as two cycles of 3 days of the topoisomerase inhibitor daunorubicin and 10 days of cytarabine known as "DA 3+10" (NICE, 2018). Cytarabine combines a cytosine base with an arabinose sugar which is similar enough to human deoxycytidine to be incorporated into human DNA, but different enough that it interferes with DNA synthesis (Konda, Arvind, & Shah, 2013). After absorption, it is rapidly converted into cytosine arabinoside triphosphate, which damages DNA when the cell cycle arrests in S phase (Kwok, Vincent, & Gibson, 2017). Rapidly dividing cells, which require DNA replication for mitosis, are therefore most affected. Cytarabine also inhibits both DNA and RNA polymerases and nucleotide reductase enzymes needed for DNA synthesis (Perry, 2008). Clinically, the most important

anthracyclines include daunorubicin, doxorubicin, idarubicin and epirubicin (Weiss, 1992). The main mechanisms of anthracyclines include intercalating DNA which interferes with its metabolism; interfering in the production of RNA; and inhibiting topoisomerase II (Kwok et al., 2017) which manages DNA tangles and supercoils by simultaneously cutting both strands of the DNA helix (Shen, 2019). After the enzyme induces a DNA double-strand break, inhibition of topoisomerase II by anthracyclines prevents re-ligation of the break which leads to cytotoxicity (Shen, 2019). A CR is achieved in 60-85% and 40-60% of patients younger and older than 60 years, respectively (H. Döhner et al., 2015). If CR is not achieved, re-induction with intensive multi-agent salvage chemotherapies or clinical trials are usually offered as a specific standard regimen is not currently available for refractory AML. Alternatively, palliative treatment is the other choice for unfit elderly patients.

CPX-351 is liposome-encapsulated combination of cytarabine and daunorubicin at a fixed molar ratio of 5:1 which leads to a longer exposure to the two drugs in the BM (Nikanjam, Capparelli, Lancet, Louie, & Schiller, 2018). In a phase 3 clinical trial, the efficacy of CPX-351 was compared with a "7+3" regimen in patients with AML with prior cytotoxic therapy or antecedent MDS or CMML (NCT01696084). As compared with the standard IC, CPX-351 showed a higher CR+CRi rate (47.7% vs 33.3%, P = 0.016), longer event-free survival (EFS) (hazard ratio [HR] = 0.74, P = 0.02), and an improvement of median OS (HR = 0.69, P = 0.05) (Lancet et al., 2018). CPX-351 has been approved by the FDA in 2017 for patients with t-AML or AML-MRC.

ii) Consolidation therapy

Following induction and achievement of CR/CRi, consolidation therapy is introduced, aiming to clear up all residual disease often termed "measurable residual disease" (MRD) and prevent relapse. The methods currently widely applied to assess MRD include multi-parameter flow cytometry (MFC), and quantitative polymerase chain reaction (qPCR). In addition, newer technologies e.g. next-generation sequencing (NGS) are emerging and reserved for clinical trials at this time (Ravandi, Walter, & Freeman, 2018; Schuurhuis et al., 2018). In terms of sensitivity, qPCR is more sensitive than MFC with a detection range of $1:10^4$ to $1:10^6$ (Del Principe et al., 2016; Schuurhuis et al., 2018) and $1:10^3$ to

$1:10^5$ (Del Principe et al., 2016), respectively. Using MFC, MRD positivity is commonly defined as $<1:10^3$ white blood cells (Luskin & Stone, 2017). However, residual leukaemia may still be problematic at this cut off. Hence, several studies use a cutoff of below $<1:10^3$ (e.g. $<1:10^4$) instead (Freeman et al., 2013; Ossenkoppele & Schuurhuis, 2016; Quek et al., 2016; R. B. Walter et al., 2013). According to the ELN recommendations, patients with favourable genetic risk should receive intermediate-dose cytarabine (IDAC), 1-1.5g/m^2, for 6 days whereas those with other genetic risks should receive HSCT (H. Döhner et al., 2010). However, only patients sufficiently fit and with a suitable donor undergo HSCT. Receiving re-induction therapy, taking part in clinical trials, or receiving palliative treatment are choices for the patients with relapse after HSCT.

The CR rate for induction therapy is 60-85% and 40-60% in patients younger and older than 60 years, respectively (H. Döhner et al., 2015). Following consolidation therapy, the achievement of long-term remission is much poorer, with the cure rate of 35-40% and 5-15% in patients younger and older than 60 years, respectively (H. Döhner et al., 2015). Over the last 50 years, there has been a steady improvement in treatment outcome of AML. Nevertheless, the prognosis of AML is globally poor, with a 5-year OS of 28% (SEER, 2015), especially in the elderly. Treatment-related mortality and resistance to chemotherapy are two major causes of treatment failure. Older people are prone to poor tolerability which often leads to them being ineligible for intensive chemotherapy because of the presence of comorbid disease, decreased ability for clearance of chemotherapy, poor performance status and poor tolerance and susceptibility to systematic bacterial and fungal infections (Klepin & Balducci, 2009).

AML is renowned for its complex clonal heterogeneity and adaptation potential. Therefore, there are many efforts to improve the standard AML treatment regimens, especially in older patients, aiming to lessen adverse drug effects. The possible interventions include intensity reduction, introducing a new class of chemotherapy and more personalised medicine i.e. introducing targeted therapy for individuals. Combination studies are another point of interest to exploit opportunities for reduced drug resistance development, decrease toxicity as a result of dose reduction, and improve efficacy (Foucquier & Guedj, 2015). In

addition, targeting parallel mechanisms potentially reduces the risk of relapse and improves the depth of response and overall response rate. Combination studies are potentially beneficial for patients with adverse-risk cytogenetics and patients with R/R AML for which a specific salvage regimen is not available.

1.4.2 Targeted therapy

A high diversity of genetic mutations is the nature of AML. Rationally, various targeted therapies have been developed as summarised in Table 1.4.2.1.

Table 1.4.2.1 Current targeted therapy options approved or in clinical trials for AML.

Drug class	Drug	Phase of development in AML
Epigenetic modifiers		
IDH1 inhibitor	Ivosidenib	FDA approved
IDH2 inhibitor	Enasidenib	FDA approved
BET inhibitor	Birabresib	1
HDAC inhibitor	Valproic acid	2
	Vorinostat	1
	Entinostat	2
	Panobinostat	1b/2
LSD1 inhibitor	GSK2879552	1 (Terminated)
DOT1L inhibitor	Pinometostat	1b/2
Other Agents		
Anti-CD33 immunoconjugate	Gemtuzumab ozogamicin	FDA approved
Anti-CD70 monoclonal antibody	Cusatuzumab	1/2
FLT3 inhibitor	Midostaurin	FDA approved
	Gilteritinib	FDA approved
Neddylation inhibitor	Pevonedistat	1b
Aminopeptidase inhibitor	Tosedostat	2
BH-3 mimetic drugs		
Pan-BCL-2 inhibitor	Obatoclax mesylate	Discontinued
Dual BCL-2/BCL-xL inhibitor	ABT-737	No clinical trial data in AML
Selective BCL-2 inhibitor	Venetoclax	FDA approved
Selective BCL-xL inhibitor	WEHI-539	No clinical trial data in AML
Selective MCL-1 inhibitor	MIK665	1
Cell cycle and signaling inhibitors		
Hedgehog inhibitor	Glasdegib	FDA approved
Polo-like kinases inhibitor	Volasertib	FDA approved
	Rigosertib	1/2
Wee1 inhibitor	Adavosertib	2 (Terminated)
MDM2 inhibitor	AMG 232	1b
	Idasanutlin	3
Aurora kinase inhibitor	Alisertib	1
	Barasertib	2
	AMG 900	1
CDK inhibitor	see Table 1.4.2.8.6.1	

Isocitrate dehydrogenase (IDH). Bromodomain and extra-terminal (BET). Histone deacetylase (HDAC). Lysine-specific demethylase 1 (LSD1). H3K79 histone methyltransferase disruptor of telomeric silencing 1-like (DOT1L). Cluster of differentiation (CD). FMS-like tyrosine kinase 3 (FLT3). B-cell lymphoma 2 (BCL-2). B-cell lymphoma-extra large (BCL-xL). Myeloid cell leukemia 1 (MCL-1). Mouse double minute 2 homolog (MDM2). Cyclin-dependent kinase (CDK). U.S. Food and Drug Administration (FDA).

1.4.2.1 Epigenetic modifiers

1.4.2.1.1 IDH inhibitor

In a phase 1/2 clinical study, the efficacy of the IDH2 inhibitor enasidenib was evaluated in patients with R/R AML harbouring *IDH2* mutations (NCT01915498). The CR+CRi rate was 26.6% and median survival was 9.3 months (Stein et al., 2017) as compared with 3.3 months in patients with R/R AML given one or more of seven available salvage treatments (Roboz et al., 2014). The FDA approved enasidenib for use as a single agent for treatment of R/R AML harbouring *IDH2* mutations in 2017. A phase 3 clinical trial is ongoing in patients with R/R AML harbouring *IDH2* mutations, aiming to evaluate the efficacy of enasidenib as compared with conventional care regimens, including best supportive care, azacitidine, low-dose cytarabine (LDAC) or IDAC (NCT02577406).

An ongoing phase 1 dose-escalation and dose-expansion study is evaluating the safety and efficacy of the IDH1 inhibitor ivosidenib in patients with R/R AML harbouring *IDH1* mutations (NCT02074839). The preliminary CR+CRi rate was 30.4% and the overall response rate was 41.6% (DiNardo, Stein, et al., 2018). One fifth of patients who achieved a CR/CRi had no residual detectable *IDH1* mutations. Based on these data, the FDA granted “breakthrough” therapy designation for ivosidenib for use as a single agent for patients with R/R AML harbouring *IDH1* mutations in 2018; and for treatment of newly diagnosed AML harbouring *IDH1* mutations in 2019.

1.4.2.1.2 BET inhibitor

The bromodomain (BRD) and extra-terminal (BET) family is a distinct group of BRD proteins, including BRD2, BRD3, BRD4 (Coudé et al., 2015), and testis-specific BRDT. The proteins bind to acetylated lysines in histones and control gene expression (Z. Yang, Zheng, Thiriet, & Hayes, 2005). In particular, BRD2 controls expression of cyclin A and D1, acts as an atypical kinase, and is also involved with transcriptional co-activators and co-repressors (LeRoy, Rickards, & Flint, 2008). In mice, overexpression of *BRD2* in B-cell progenitors induces B-cell lymphomas (Romesser et al., 2009). BRD4 recruits P-TEFb to active promoters via its affinity to acetylated histones (Z. Yang, He, & Zhou, 2008). shRNA-

mediated *BRD4* knockdown results in anti-leukaemic activity *in vitro* and *in vivo* (Zuber et al., 2011). Birabresib, a thienotriazolodiazepine, specifically binds to BRDs 2, 3 and 4, thus inhibiting binding to acetylated histones, resulting in a downregulation of gene expression. A dose-escalation, phase 1 clinical trial, aiming to evaluate the safety and find a recommended dose of birabresib in patients with *de novo* AML, s-AML, acute lymphoblastic leukaemia (ALL), diffuse large B-cell lymphoma (DLBCL), and MM (NCT01713582), has been completed. The results are not yet available. In a phase 1b study, the safety of birabresib was evaluated in patients with advanced solid tumours (NCT02259114). The PR rate was 6.5% (Lewin et al., 2018).

1.4.2.1.3 HDAC inhibitor

Histone deacetylase (HDAC) is the enzyme that removes acetyl groups from lysine on a histone, enabling the histones to tightly wrap DNA around it. The expression of HDAC is frequently deregulated (mostly upregulation) in AML cells (Abdel-Wahab & Levine, 2013), affecting genes involved with haematopoiesis, signal transduction and transcriptional regulation (Tickenbrock et al., 2011). HDAC inhibitors (HDACIs) inhibits the enzyme, resulting in hyperacetylation of histones which releases DNA for transcription (Elmer et al., 2016). However, as a single agent, the efficacy of HDACIs is low (Shafer & Grant, 2016). Consequently, HDACIs as a conjunctive therapy is preferred, particularly with the hypomethylating agents (HMAs) which results in a synergism between histone deacetylase inhibition and demethylation (Gore et al., 2006). In a phase 2 clinical trial, the efficacy of this treatment approach was assessed by comparing decitabine plus HDACI valproic acid vs decitabine alone in elderly patients with AML or MDS (NCT00414310). It was observed that the CR rate of patients given the drug combination was not different from those given decitabine alone (37% vs 31%, $P = 0.497$) (Issa et al., 2015). In a phase 1 clinical study, the efficacy of decitabine in combination with concurrent vs sequential HDACI vorinostat was compared in patients with R/R AML or MDS (NCT00479232). The CR rate was higher in the concurrent group (22.6% vs 6.7%) (Kirschbaum et al., 2014). In a phase 2 clinical trial, the efficacy of the treatment regimen was compared between azacitidine with or without vorinostat in patients with newly diagnosed AML, R/R AML, or MDS who are ineligible for IC (NCT01617226). The CR+CRi rate

was not statistically significant different between patients given azacitidine plus vorinostat and those given azacitidine alone (26% vs 22%, *P* = 0.49) (Craddock et al., 2017). The median OS was slightly higher in the combination arm as compared with the single arm (11 vs 9.6 months, *P* = 0.32). Interestingly, it was observed that mutations in the genes *IDH1* (*P* = 0.004), CDK inhibitor 2A (*CDKN2A*) (*P* = 0.0001), and *TP53* (*P* = 0.003) are associated with reduced OR. In a phase 2 clinical trial, the efficacy of treatment was compared between azacitidine with or without the HDACI entinostat in patients with AML or MDS (NCT00313586). It was observed that the CR rate is slightly higher in patients given azacitidine alone as compared with those given the drug combination (12.2% vs 8%) (Prebet et al., 2014). In a phase 1b/2 study, the efficacy of azacitidine in combination with HDACI panobinostat in patients with AML (Australian and New Zealand Clinical Trials Registry: ACTRN12610000924055) was assessed. The CR+CRi rate was 10.3% (Tan et al., 2014). In addition, it was observed that an increase in blood mononuclear cell histone H3 and H4 acetylation following treatment with panobinostat is dose-dependent. Interestingly, there was a strong correlation between an increase in acetylation from baseline and clinical response, with a response rate of 44-46% as compared with a response rate of 0% in patients whose acetylation level remained unchanged.

1.4.2.1.4 LSD1 inhibitor

Lysine-specific demethylase 1 (LSD1) is histone-modifying enzyme which is frequently overexpressed in human cancer, including AML (Shafer & Grant, 2016; Smitheman et al., 2019). shRNA-mediated *LSD1* knockdown results in a remarkable transcriptional activation of myeloid lineage marker genes, including CD11b and CD86, in THP-1 cell lines bearing *KMT2A-MLLT3* and also demonstrates the anti-tumour activities in a THP-1 mouse xenograft model (Fang et al., 2017). In addition, using chromatin immunoprecipitation and quantitative PCR (ChIP-qPCR), it was observed that there is an increase in histone H3 lysine 4 di-methylation (H3K4me2) modification at the CD11b promoter region, whereas, global H3K4me2 level remains unchanged. The expression of CD11b is an indicator of differentiation to a mature myeloid cell (van Lochem et al., 2004). CD86 is co-expressed with CD80 on mature macrophages and dendritic cells, and

is essential for an interaction with CD4+ T cells (L. Chen & Flies, 2013). In a phase 1 clinical study, the safety of a LSD1 inhibitor GSK2879552 with or without all-trans retinoic acid (ATRA) was evaluated in patients with R/R AML (NCT02177812). However, the trial was terminated due to an unfavourable risk for the patients.

1.4.2.1.5 DOT1L inhibitor

An ongoing phase 1b/2 clinical study is evaluating the combination effect of a DOT1L inhibitor pinometostat in combination with a "7+3" regimen in patients with AML harbouring *KMT2A*-R (NCT03724084); and pinometostat in combination with azacitidine in patients with AML harbouring *KMT2A-MLLT3* or R/R AML (NCT03701295).

1.4.2.2 Anti-CD33 immunoconjugate

CD33 is a cell surface antigen which is commonly expressed on AML and normal myeloid cells (R. B. Walter, Appelbaum, Estey, & Bernstein, 2012). Gemtuzumab ozogamicin (GO) is an antibody-drug conjugate combining an anti-CD33 antibody with the toxic antibiotic calicheamicin, an anti-tumour antibiotic which is extremely toxic to all cells. GO is highly effective against acute promyelocytic leukaemia (APL), potentially, resulting from its high expression of CD33 (Lo-Coco et al., 2004). However, as a single agent, the efficacy against other AML subtypes was low with the CR+CRi rate of 13% in relapsed AML (Larson et al., 2005). Consequently, GO as part of a combination therapy approach is preferred. An individual-patient meta-analysis of five studies was performed in patients with AML (excluding APL), including two UK National Cancer Research Institute (NCRI), French Goelams group, French Alfa group, and US SWOG group (Hills et al., 2014). The efficacy of treatment regimen was compared between IC alone (a "7+3" regimen or fludarabine (antimetabolite) + high-dose cytarabine (HIDAC) + G-CSF + idarubicin (anthracyclines) [FLAG-ida] regimen) vs IC plus GO. It was observed that there is no significant effect of combining GO on CR rate (P = 0.3). However, a 5-years survival rate was higher in the combination therapy arm as compared with the single arm (76.3% vs 55.2%, P = 0.0005 in AML patients with favourable cytogenetics; and 39.4% vs 34.1%, P = 0.007 in AML patients with intermediate cytogenetics). A dose of 3mg/m^2 on days 1, 4, and 7 of induction

therapy and 3mg/m^2 on day 1 of consolidation therapy is recommended for the least toxicity and greatest benefit (Castaigne et al., 2012). GO, as a single agent or in combination with a "7+3" regimen or FLAG-ida, has been approved by the FDA in 2017 for patients with new diagnosed or R/R AML which is CD33 positive. It is recommended to be used in AML patients with ELN favourable or intermediate risk (Estey, 2018).

1.4.2.3 Anti-CD70 monoclonal antibody

It has been reported that the TNF superfamily ligand–receptor pair CD70/CD27 is expressed on AML blasts, progenitors and SCs activating a SC gene expression programme (Riether et al., 2017). In newly diagnosed AML patients, soluble CD27 was found to be a strong independent negative prognostic biomarker for OS. Blocking CD70/CD27 by monoclonal antibody (mAb) promoted differentiation in AML blasts and prolonged survival in murine AML xenografts. CD70/CD27 was not detected on HSPCs from healthy BM donors, hence, a therapeutic window was seen. In a phase 1/2 clinical trial, the efficacy of anti-CD70 mAb cusatuzumab in combination with azacitidine was evaluated in patients with newly diagnosed AML (NCT03030612). The study has not been completed yet but preliminary data showed that the CR+CRi rate was 82% (Ochsenbein et al., 2018).

1.4.2.4 FLT3 inhibitor

Midostaurin is an oral multitargeted tyrosine kinase inhibitor (TKI) active in patients with a FLT3 mutation. In a phase 3 randomised double-blind study, the efficacy of the treatment regimen was compared between the standard "7+3" regimen with or without midostaurin in patients aged less than 60 with AML harbouring *FLT3* mutation (NCT00651261). Although the CR rate in the combination therapy arm was similar to the single arm (58.9% vs 53.5%, P = 0.15), the median OS was higher in the combination therapy arm (74.7 vs 25.6 months, P = 0.009) (Stone et al., 2017). However, the independent effect of maintenance therapy has not been determined in this trial and the reason behind the superior OS in men compared with women is unexplained. Midostaurin in combination with a "7+3" regimen and HIDAC has been approved by the FDA in 2017 for patients with new diagnosed AML harbouring *FLT3* mutation.

Gilteritinib is a newer potent FLT3 inhibitor with preclinical activity against *FLT3*^{D835} mutation (L. Y. Lee et al., 2017). In a phase 3 clinical trial, the efficacy of gilteritinib was compared with salvage chemotherapy in patients with R/R AML harbouring *FLT3*-ITD, *FLT3*^{D835} or *FLT3*^{I836} mutation (NCT02421939). The CR+CRi rate was higher in the gilteritinib group as compared with the salvage chemotherapy group (21.1% vs 10.5%, *P* = 0.0106) and the median OS was higher in the former group (9.3 vs 5.6 months, *P* = 0.0004) (Perl et al., 2019). Gilteritinib, as a single agent, has been approved by the FDA in 2018 for patients with R/R AML harbouring *FLT3*-ITD, *FLT3*^{D835} or *FLT3*^{I836} mutation.

1.4.2.5 Neddylation inhibitor

Neddylation is the process by which the neural-precursor-cell-expressed developmentally down-regulated 8 (NEDD8) is conjugated to its target proteins. NEDD8 binds specifically to the Cullin subunit of ubiquitin protein ligase (E3) and activate it (Z. Q. Pan, Kentsis, Dias, Yamoah, & Wu, 2004). The activated E3 enzyme then forms a complex with a ubiquitin carrier (E2) enzyme and catalyses the transfer of ubiquitin from the E2 enzyme to the protein substrate (Suresh, Lee, Kim, & Ramakrishna, 2016). Inhibiting neddylation results in an inactivation of ubiquitination which leads to an accumulation of various proteins, including substrates with role in the stress response, DNA damage, and cell cycle progress (Shafer & Grant, 2016). It has been reported that the neddylation inhibitor pevonedistat blocks degradation of nuclear factor of kappa light polypeptide gene enhancer in B-cells inhibitor, alpha (IκBα), keeping NF-κB inactivated (Swords et al., 2010). NF-κB is known to be crucial for the survival of LSCs and their proliferation (Kagoya et al., 2014). In a phase 1, dose-escalation study, the safety of pevonedistat was evaluated in patients with R/R AML or MDS (NCT00911066). Two different dosing schedules were administrated, including schedule A (on days 1, 3 and 5), or schedule B (on days 1, 4, 8 and 11) of a three-week cycle. For the patients treated at or below the maximum tolerated dose, the CR rate was 8.7% in schedule A and 0% in schedule B (Swords et al., 2015). In a phase 1b clinical trial, the safety and efficacy of pevonedistat in combination with azacitidine was evaluated in elderly patients with newly diagnosed AML (NCT01814826). The CR+CRi rate was 39.1% (Swords et al., 2018).

1.4.2.6 Aminopeptidase inhibitor

Aminopeptidases facilitate protein degradation by catalysing amino acid cleavage from the N-terminus of protein substrates (Taylor, 1993). It has been reported that inhibiting aminopeptidases results in an accumulation of protein and a decrease in free amino acids which leads to a stress response, including an activation of pro-apoptotic regulators NOXA and PUMA in MM cell lines (Moore et al., 2009). In a phase 2 clinical trial, the efficacy of the aminopeptidase inhibitor tosedostat was evaluated in elderly patients with R/R AML (NCT00780598). Two dosage regimens were administrated, including regimen A (120mg once daily for 6 months), or regimen B (240mg once daily for 2 months followed by 120mg once daily for 4 months).The CR+CRi rates were 5.3% and 14.3% in regimen A and B, respectively (J. Cortes et al., 2013). In a phase 2 clinical study, the efficacy of tosedostat in combination with either IDAC or decitabine was evaluated in elderly patients with AML or MDS (NCT01567059). The CR+CRi rate was 52.9% in both combinations (Mawad et al., 2016). However, the median OS was higher in patients given tosedostat plus decitabine as compared with those given tosedostat plus IDAC (16.7 vs 10.9 months).

1.4.2.7 BH-3 mimetic drugs

1.4.2.7.1 Pan-BCL-2 inhibitor

Obatoclax mesylate is one of the first published BH-3 mimetic drugs. It binds to BCL-xL, BCL-w and MCL-1 and is a relatively weak pan-BCL-2 inhibitor (Nguyen et al., 2007). However, due to its lack of specificity, the mechanism by which the drug induces apoptosis is beyond BAK/BAX activation, resulting in non-mechanism based toxicities in an *in vitro* study (Vogler, Walter, & Dyer, 2017). A significant decrease in cell viability assessed by the 3-(4,5-dimethylthiazol-2-yl)-2,5-diphenyltetrazolium bromide (MTT) assay and a decrease in CFU-fibroblast (CFU-F) number assessed by CFU assays were observed in both wild-type and BAK/BAX double knockout mouse embryonic fibroblasts (MEFs) treated with obatoclax. The development of obatoclax mesylate was discontinued in 2013.

1.4.2.7.2 Dual BCL-2/BCL-xL inhibitor

ABT-737 and its derivative navitoclax are the victory of fragment-based drug discovery (Oltersdorf et al., 2005) in which their fragments were identified by nuclear magnetic resonance (NMR) (Shuker, Hajduk, Meadows, & Fesik, 1996) to bind pockets in the hydrophobic groove of BCL-xL. Subsequently, high affinity ligands were further developed. ABT-737 binds with high affinity to BCL-xL, BCL-2 and BCL-w but not MCL-1 and has served as a laboratory tool to research the intrinsic apoptosis pathway (Vogler et al., 2017). As insolubility is a hurdle for clinical application, ABT-737 was further modified into navitoclax to overcome this obstacle (Tse et al., 2008). Navitoclax retains the property to bind to the same BH-3 family members as ABT-737. In a phase 2 clinical study, anti-CD20 mAb rituximab in combination with long-term navitoclax treatment has shown a higher CR+PR rate as compared with rituximab alone (70% vs 35%, $P = 0.0034$) in patients with CLL (NCT01087151) (Kipps et al., 2015). A phase 1 study is ongoing in Asian patients with MPN, aiming to evaluate the safety and tolerability of navitoclax as a single agent or in combination with the JAK inhibitor ruxolitinib (NCT04041050).

Another BCL-2/BCL-xL inhibitor, S44563, has shown anti-tumour activity in uveal melanoma patient-derived xenograft (PDX) mouse models (Némati et al., 2014) and enhanced radio-sensitivity of small cell lung cancer (SCLC) H146, H69 and H196 cell lines (Loriot et al., 2014). Anti-tumour activity was also observed in a H146 xenograft mouse model.

1.4.2.7.3 Selective BCL-2 inhibitor

Venetoclax is the result of the re-engineering of navitoclax, aiming to prevent inhibition of BCL-xL which results in platelet toxicity and thrombocytopaenia (Souers et al., 2013). In a phase 1b clinical trial, the efficacy of venetoclax in combination with decitabine or azacitidine was evaluated in elderly patients with AML with intermediate or adverse cytogenetics who are ineligible for IC (NCT02203773). CR and CR+CRi rates were 35% and 66%, respectively (DiNardo et al., 2019). The rates were greater in patients with intermediate risk as compared with adverse risk (CR+CRi 74% vs 60%). Median survival was 18 months with median follow-up 7 months. In a phase 1b/2 study, the efficacy of

venetoclax in combination with LDAC was evaluated in elderly AML patients who were ineligible for IC (NCT02287233). The CR and CR+CRi rates were 26% and 62%, respectively (A. H. Wei et al., 2019). Median survival and median follow-up were approximately 12 months. In 2018, based on these data, the FDA granted "breakthrough" therapy designation for venetoclax in combination with either azacytidine or decitabine, or with LDAC for patients who are ineligible for IC. The details of venetoclax will be further described in Chapter 5.

1.4.2.7.4 Selective BCL-xL inhibitor

The first published selective inhibitor of BCL-XL was WEHI-539. The mechanism by which the drug induces apoptosis is through BAK activation (Vogler et al., 2017). However, while ABT-737 and venetoclax demonstrate potency in the low nanomolar range, WEHI-539 shows potency in the micromolar range. Therefore, A-1155463 (Tao et al., 2014) and A-1331852 (Leverson, Phillips, et al., 2015) were developed to improve the potency. To date, no clinical trials have been conducted for these agents.

1.4.2.7.5 Selective MCL-1 inhibitor

As the binding surface in the BH3 binding pocket of MCL-1 is large (Friberg et al., 2013), the development of potent MCL-1-specific inhibitors has been much slower as compared with other BH-3 mimetic drugs. Maritoclax binds to MCL-1 with micromolar affinity and induces its proteasomal degradation (Doi et al., 2012). It induces apoptosis in AML and MM cells (Vogler et al., 2017). It has been reported that the drug shows efficacy only in wild-type Jurkat cells but not in Jurkat cells lacking BAK (Doi et al., 2012; Varadarajan et al., 2015), indicating that the mechanism by which the drug induces apoptosis is through BAK/BAX activation. The efficacy of the drug was found to be dependent on MCL-1 expression status of the target cells (Gomez-Bougie et al., 2018; Varadarajan et al., 2015). In another scenario, maritoclax also induces mitochondrial fragmentation and reactive oxygen species (ROS) in cells lacking MCL-1, indicating multiple mechanisms of action of the drug (Varadarajan et al., 2015).

ML311 binds to MCL-1 with submicromolar affinity and may interact with BCL-2, but not BCL-xL (Bannister et al., 2010). UMI77 also displays submicromolar

binding of MCL-1 but not the other anti-apoptotic BCL-2 proteins (Abulwerdi et al., 2014). This was reiterated by the data showing that siRNA-mediated *MCL1* knockdown reduced the efficacy of UMI77. The mechanism by which the drug induces apoptosis is through BAK/BAX activation. UMI77 induced apoptosis in the pancreatic cancer BxPC-3 and Panc-1 cell lines (D. Wei et al., 2015).

A1210477 and S63845 bind with high affinity to MCL-1 with inhibitory constant (Ki) values of 0.45nM (Leverson, Zhang, et al., 2015) and 0.19nM (Kotschy et al., 2016), respectively. However, to induce apoptosis, micromolar concentrations are required for A1210477, whereas, nanomolar concentrations are sufficient for S63845. Both drugs induce apoptosis through BAK/BAX activation. S63845 induced apoptosis in twenty-five MM, eleven lymphoma and five CML-derived cell lines at nanomolar concentrations (Kotschy et al., 2016). In immuno-competent C57BL/6 mice bearing *Myc* driven by the IgH Eμ enhancer (Eμ-Myc) mouse lymphomas, treatment with S63845 was able to cure 70% of mice without side effects evident in normal tissues. On the other hand, A1210477 and S63845 can induce an increase in MCL-1 at the protein, but not mRNA, level (Vogler et al., 2017). The most plausible explanation is that the two drugs prevent MCL-1 from interacting with NOXA, reducing its ubiquitination. Ongoing phase 1 clinical trials are evaluating the safety and tolerability of MIK665, a derivative of S63845, in patients with AML (NCT02979366); and in patients with MM and DLBCL (NCT02992483).

1.4.2.8 Cell cycle and signalling inhibitors

1.4.2.8.1 Hedgehog inhibitor

The hedgehog (Hh) pathway regulates proliferation and differentiation during embryonic development (Shafer & Grant, 2016). Cancer stem cell (CSC) proliferation results from aberrant activation of the pathway (Campbell & Copland, 2015). The Hh pathway promotes tumour invasiveness (Sari et al., 2018). It has been reported that aberrant activation of the Hh pathway is necessary for maintenance of CD34+ Kasumi-1, Kasumi-3 and TF-1 leukaemic cell lines (Kobune et al., 2009). Glasdegib is an oral selective inhibitor of the sonic Hh receptor smoothened (SMO) involved in the Hh pathway. In a randomised phase 1b/2 clinical trial, the efficacy of treatment was evaluated, comparing

LDAC plus glasdegib vs LDAC alone in patients with AML or MDS who were ineligible for IC (NCT01546038). The CR rate was higher in the combination group (17% vs 2.3%) (J. E. Cortes et al., 2019). Median OS was higher in the combination therapy arm as compared with the single arm (8.8 vs 4.9 months, $P = 0.0004$). Glasdegib in combination with LDAC has been approved by the FDA in 2018 for patients with new diagnosed AML who are ineligible for IC. An ongoing phase 3 clinical study is evaluating the combination effect of glasdegib in combination with a "7+3" regimen in patients with AML or in combination with azacitidine if they are ineligible for IC (NCT03416179).

1.4.2.8.2 Polo-like kinases inhibitor

The polo-like kinases (PLKs) play a role in various cellular processes, including DNA replication (Song, Liu, & Liu, 2012), DNA damage response (Hyun, Hwang, Hwan, & Jang, 2014), and mitosis (Glover, Hagan, & Tavares, 1998). It has been reported that PLK is overexpressed in AML (Renner et al., 2009). In a phase 2 clinical study, the efficacy of treatment was compared between LDAC plus the PLK inhibitor volasertib vs LDAC alone in patients with R/R AML who were ineligible for IC (NCT00804856). The CR+CRi rate was higher in patients given the combination drug as compared with LDAC alone (31% vs 13.3%, $P = 0.052$) (H. Döhner et al., 2014). In the combination group, as compared with LDAC alone, median EFS was significantly prolonged (5.6 vs 2.3 months, $P = 0.021$) and median OS was longer (8.0 vs 5.2 months, $P = 0.047$). In 2013, based on these data, the FDA granted "breakthrough" therapy designation for volasertib in combination with LDAC for patients who are ineligible for IC. An ongoing phase 3 study is evaluating the efficacy of LDAC plus volasertib vs LDAC alone in elderly patients with newly diagnosed AML who are ineligible for IC (NCT01721876). Rigosertib inhibits both PLK1 and phosphatidylinositol 3-kinase (PI3K) (Okabe, Tauchi, Tanaka, Sakuta, & Ohyashiki, 2015) and induces G2/M arrest with subsequent cell death (Hyoda et al., 2015). An ongoing phase 1/2 clinical study is evaluating the safety and efficacy of rigosertib in combination with azacitidine in patients with AML or MDS (NCT01926587).

1.4.2.8.3 Wee1 inhibitor

Wee1 is a nuclear kinase belonging to the serine/threonine family of protein kinases (H. Y. Kim et al., 2016). Wee1 kinase plays an essential role at the G2 checkpoint. In the case of DNA damage, Wee1 constrains the removal of inhibitory phosphates from CDK1, keeping it inactivated, which inhibits the entry into mitosis (Schmidt et al., 2017). Hence, inhibiting Wee1 leads to an accumulation of irreparable genetic lesions with subsequent cell death (Shafer & Grant, 2016). In a phase 2 clinical trial, the safety and efficacy of the Wee1 inhibitor adavosertib with or without cytarabine was evaluated in patients with AML or MDS (NCT02666950). However, the trial was discontinued for an unspecified reason.

1.4.2.8.4 MDM2 inhibitor

MDM2 is a critical negative regulator of the p53. There are three main mechanisms by which MDM2 inhibits p53 including: **a)** MDM2 facilitates proteasomal degradation of p53 by ubiquitination through its E3 ligase activity (Chène, 2003; S. Wang, Zhao, Aguilar, Bernard, & Yang, 2017); **b)** the binding of MDM2 blocks the interaction between p53 and its targeted DNA (Freedman, Wu, & Levine, 1999; S. Wang et al., 2017; X. Wu, Bayle, Olson, & Levine, 1993); **c)** MDM2 promotes export of p53 out of the cell nucleus (Freedman et al., 1999; S. Wang et al., 2017; X. Wu et al., 1993). Thus, inhibiting MDM2 strengthens the efficacy of p53, inducing cell cycle arrest and apoptosis (Shafer & Grant, 2016). In a phase 1b study, the safety and efficacy of MDM2 inhibitor AMG 232 with or without mitogen-activated protein kinase kinase 1 and 2 (MEK1/2) inhibitor trametinib was evaluated in patients with R/R AML (NCT02016729). The CR rate was higher in the combination therapy arm as compared with the single arm (12.5% vs 0%) (Erba et al., 2019). An ongoing phase 1b clinical trial is evaluating safety and finding a recommended phase 2 dose of AMG 232 in combination with decitabine in patients with newly diagnosed or R/R AML (NCT03041688).
In a phase 3 study, the efficacy of the treatment regimen was compared between IDAC with or without MDM2 inhibitor idasanutlin in patients with R/R AML (NCT02545283). The trial has been completed but the results are not yet available. An ongoing phase 1b/2 study is evaluating the safety and efficacy of

venetoclax in combination either with MEK inhibitor cobimetinib or idasanutlin in elderly patients with R/R AML who are ineligible for IC (NCT02670044).

1.4.2.8.5 Aurora kinase inhibitor

Aurora kinases are serine/threonine kinases, including Aurora A, B, and C, which have an important role in several stages of mitosis (Willems et al., 2018). Overexpression or amplification of Aurora kinases is frequently observed in various cancers, including AML (Hartsink-Segers et al., 2013) and CML (J. Yang, Ikezoe, Nishioka, Udaka, & Yokoyama, 2014). Several Aurora kinase inhibitors have been developed and many of these are multi-kinase inhibitors that inhibit other kinases, including FLT3 (Farag, 2011). In a phase 1 clinical trial, the safety of the Aurora A kinase inhibitor alisertib in combination with a “7+3” regimen was evaluated in patients with newly diagnosed AML (NCT01779843). The CR+CRi rate was 86.4% (Fathi et al., 2017). As a consequence, a phase 2 clinical trial of alisertib in combination with a “7+3” regimen has been continued in patients with newly diagnosed high-risk AML, including elderly patients, AML with ELN adverse risk, AML with MRC, or antecedent or underlying MDS or MPN (NCT02560025). In a phase 2 study, the safety and efficacy of LDAC was compared with Aurora B kinase inhibitor barasertib in elderly patients with newly diagnosed AML (NCT00952588). The CR+CRi rate was higher in patients given barasertib (35.4% vs 11.5%, $P < 0.05$) (Kantarjian et al., 2013). Additionally, responses occurred across all cytogenetic risk groups. The median OS of patients given barasertib was higher than LDAC but not statistically significant (8.2 vs 4.5 months, $P = 0.663$). In a phase 1 clinical study, the safety of pan-Aurora kinase inhibitor AMG 900 was evaluated in patients with R/R AML or newly diagnosed patients ineligible for IC (NCT01380756). The CRi was 8.6% (Kantarjian et al., 2017). Interestingly, it has been reported that the pan-Aurora kinase inhibitor MK0457, which activates p53, in combination with MDM2 antagonist nutlin-3 synergistically induces apoptosis in OCI-AML-3 and MOLM-13 cell lines bearing wild-type p53, but not in p53-null HL-60 cells (Kojima, Konopleva, Tsao, Nakakuma, & Andreeff, 2008). Thus, further investigation of this combination is potentially beneficial.

1.4.2.8.6 Cyclin-dependent kinase inhibitors

Overactive CDK/cyclin complexes have been frequently observed in human malignancies, resulting in perturbations of the cell cycle. This is associated with amplification and overexpression of CDKs or cyclins, loss of Rb expression, inactivation of CDKIs, and loss of binding of CDKIs to CDKs (Malumbres & Barbacid, 2001, 2009; Shapiro, 2006). However, directly targeting cyclins is implausible because, rather than acting as an enzyme or receptor, they act as regulatory subunits (Tadesse, Caldon, Tilley, & Wang, 2019). Thus, CDKs are potentially a therapeutic target.

It has been reported that *HOXA7* stimulates human hepatocellular carcinoma HepG2 and QGY-7703 cell proliferation through CDK2/cyclin E1 (Y. Li et al., 2015), whereas, CDK2/cyclin A plays a role in an activation of human estrogen receptor α when transfected into human bone osteosarcoma U2-OS cell line (Rogatsky, Trowbridge, & Garabedian, 1999). With a highlight on CDK2, as a potential drug target, it has been reported that *CDK2* knockdown using shRNA and siRNA induces apoptosis in neuroblastoma myelocytomatosis oncogene (*MYCN*)-amplified neuroblastoma cell lines (Molenaar et al., 2009). siRNA-mediated *CDK2* knockdown results in marked growth inhibition through the induction of multipolar anaphases triggering apoptosis in lung cancer cell lines (Galimberti et al., 2010). In radioresistant glioblastoma cell lines, *CDK2* knockdown with shRNA in combination with radiotherapy synergistically induces apoptosis (J. Wang et al., 2016). Favourably, shRNA-mediated *CDK2* knockdown drives differentiation in AML cell lines and primary human AML cells (Ying et al., 2018). The beneficial effects of targeting CDK4/6 has also been demonstrated. In the *KMT2A-MLLT3* positive NOMO-1 and THP-1 AML cell lines, shRNA-mediated *CDK6* knockdown overcomes a block of myeloid differentiation (Placke et al., 2014). A similar result was observed in mice bearing *KMT2A-MLLT3*-driven murine leukaemia, resulting in a prolongation in their survival. In the human melanoma 518A2 and LNM1 cell lines, shRNA-mediated *CDK4* or *CDK6* knockdown significantly reduces cell proliferation and inhibits migratory capacity (Kollmann et al., 2019). *CDK4* knockdown using siRNA resulted in a decrease in Rb phosphorylation, keeping E2F inactivated, and dramatically reduced cell growth in human well-differentiated/dedifferentiated liposarcomas (WD/DDLPS) 449

and 778 cell lines (Y. X. Zhang et al., 2014). shRNA-mediated *CDK6* knockdown causes a marked inhibition of proliferation in all three small cell carcinoma of the ovary, hypercalcemic type (SCCOHT) BIN-67, SCCOHT-1, and COV434 cell lines (Xue et al., 2019). Another aspect of therapeutic CDK inhibition involves repression of CDK7 and CDK9, resulting in global transcriptional suppression (Fischer & Gianella-Borradori, 2005). It has been reported that a pan-CDKI alvocidib (also known as flavopiridol), potently inhibiting CDK9 and to a lesser extent inhibits CDKs 1, 2, 4/6, and 7. Thereby majorly targeting the transcripts with short half-lives, including the anti-apoptotic MCL-1, BCL-xL and XIAP, D-cyclins, Myc, MDM-2 (leading to p53 stabilisation), $p21^{Cip1}$, proteins whose transcription is mediated by NF-κB, and vascular endothelial growth factor (VEGF) (Lam et al., 2001). Among these, MCL-1 is shown to be critical for the survival of AML (Glaser et al., 2012), B-cell lymphoma (Michels et al., 2004), MM (B. Zhang, Gojo, & Fenton, 2002) and CLL (R. Chen et al., 2009). This provides a strong rationale to include transcriptional CDKIs in the treatment of these diseases. The combination of cell cycle and transcriptional CDKI has shown the most effective induction of apoptosis in the non–small cell lung cancer (non-SCLC) NCI-H1299 and the human bone osteosarcoma U2-OS cell lines (D. Cai, Latham, Zhang, & Shapiro, 2006, 2020). However, high structural homology within the CDK family and the lack of three-dimensional structural models for many CDKs are the major problems for a highly specific or single CDKI development (Bose et al., 2013). CDKIs currently in clinical trials and their CDK inhibition profiles are summarised in Table 1.4.2.2.7.1 (Boffo, Damato, Alfano, & Giordano, 2018; Cyclacel, 2016; Fry et al., 2004; Lapenna & Giordano, 2009; Lücking et al., 2017; MacCallum et al., 2005).

Table 1.4.2.8.6.1 CDKIs currently undergoing clinical trials and their CDK inhibition profiles (IC50) (Boffo et al., 2018; Cyclacel, 2016; Fry et al., 2004; Lapenna & Giordano, 2009; Lücking et al., 2017; MacCallum et al., 2005).

Drug class and action	Drug	CDK inhibition profile (IC50)	Phase of development in AML
Cell cycle and signaling inhibitors			
CDK inhibitors	Alvocidib (flavopiridol)	CDK9: 3 nM CDK4: 20-40 nM CDK6: 60 nM CDK1: 30-400 nM CDK2: 100 nM CDK7: 110-300 nM	2
	Seliciclib	CDK2: 100 nM CDK7: 360 nM CDK9: 810 nM	2
	Dinaciclib	CDK2: 1 nM CDK5: 1 nM CDK1: 3 nM CDK9: 4 nM	1
	TG02	CDK9: 3 nM CDK5: 4 nM CDK2: 5 nM CDK3: 8 nM CDK1: 9 nM CDK7: 37 nM	1
	SNS-032	CDK9: 4 nM CDK2: 38 nM CDK7: 62 nM	1
	Atuveciclib	CDK9: 6 nM CDK3: 890 nM CDK2: 1000nM CDK1: 1100nM CDK5: 1600nM	1
	Palbociclib	CDK4: 11 nM CDK6: 16 nM	1/2
	CYC065	CDK2: 5 nM CDK9: 26 nM CDK3: 29 nM CDK7: 193 nM	1

Cyclin-dependent kinase (CDK).

Alvocidib is the first CDKI to enter clinical trials and has been the most studied to date. It is a pan-CDKI but its primary mechanism of action is inhibiting CDK9/P-TEFb (S. H. Chao et al., 2000) which results in an inhibition of RNAPII activities (Karp et al., 2005). In a phase 1 clinical trial, a timed sequential therapy (TST) model was evaluated *in vitro* (Karp et al., 2003). Using primary human BM cells from adults with newly diagnosed AML with poor risk features, R/R AML, or ALL, it was observed that treatment with alvocidib for 24h induces a 4.3-fold increase in apoptosis as compared with NDC and pre-treatment with alvocidib also sensitised leukaemic cells to cytarabine. Subsequent study correlated a 2-fold reduction of MCL-1 and rapid induction of apoptosis in AML cell lines (B. D. Smith et al., 2015). By using leukaemic blasts from adult patients with refractory AML in a phase 1 clinical trial, it was observed that treatment with alvocidib results in a downregulation of genes encoding RNAPII, high mobility group AT-Hook 1 (HMGA1), STAT3, and E2F1 (NCT00470197) (D. M.

Nelson et al., 2011). In a phase 2 study, conducted in newly diagnosed high-risk AML patients, there was a statistically significant high efficacy of FLAM (alvocidib, cytarabine plus mitoxantrone) as compared with the standard "7+3" regimen with 1 or 2 cycles in terms of CR rate (70% vs 47%, $P = 0.003$; or 70% vs 57%, $P = 0.08$, respectively) (NCT01349972) (Zeidner et al., 2018). Nevertheless, an increase in either OS or EFS rate was not observed. Treatment-related mortality (TRM) was 70%, which is similar in both treatment arms in this study. As MCL-1 is a target of the drug, BH3 profiling is a novel therapeutic approach aiming to identify specific subsets of patients who are likely to respond to alvocidib (Dettman et al., 2015). Using receiver operating characteristic (ROC) curve analysis, factors highly predictive of a response to FLAM were identified, including NOXA priming, MDS history, and cytogenetics. Consequently, aiming to identify subsets of alvocidib-sensitive patients, these factors are included in an ongoing phase 2 study in patients with MCL-1-dependent R/R AML (NCT02520011). The purpose of this study is to assess the CR rate of FLAM as compared with cytarabine plus mitoxantrone regimen. Using the NOXA-BH3 priming assay, MCL-1 dependency is defined in this study as at least 40% Cyt c release from BM leukaemic cells treated with the NOXA peptide which specifically inhibits MCL-1. In a current phase 1 clinical trial, alvocidib in combination with a "7+3" regimen will be assessed in patients with newly diagnosed AML (NCT03298984). Correlation between the benefit of the drug combination and BH3 profiling for MCL-1 dependency is included as a secondary objective of the trial.

Seliciclib is the second CDKI to enter clinical trials in humans (Bose et al., 2013). It is an oral CDK 2, 7, and 9 inhibitor (Boffo et al., 2018). Seliciclib potently inhibited S2 and S5 RNAPII phosphorylation and suppressed a transcription of MCL-1 which induces apoptosis in the MM H929, LP-1, and RPMI 8226 cells (MacCallum et al., 2005); and in the AML U937, HL-60, and T-ALL Jurkat cells (S. Chen, Dai, Harada, Dent, & Grant, 2007). G1 and G2/M arrest, and apoptosis were seen in nine DLBCL cell lines treated with seliciclib, regardless of their karyotypic abnormalities status (Lacrima et al., 2007). Anti-tumour activity of seliciclib against MM cells in the BM microenvironment was demonstrated, with marked synergism observed when low doses of both the proteasome inhibitor bortezomib and the anthracycline doxorubicin were combined with seliciclib

(Raje et al., 2005). A phase 1 clinical trial was conducted in patients with advanced solid tumours, recruited from the Royal Marsden Hospital (Sutton) and the Beatson Oncology Centre (Glasgow). However, anti-tumour activity was not observed in this study (Benson et al., 2007). Currently, seliciclib is in phase 2 studies for the treatment of lung cancer and nasopharyngeal cancer (Raje et al., 2005).

Dinaciclib is a potent CDKs 1, 2, 5, and 9 inhibitor (Boffo et al., 2018). Using the ovarian cancer A2780 cell line, it has been reported that dinaciclib inhibited thymidine DNA incorporation and Rb phosphorylation, resulting in an induction of apoptosis (Parry et al., 2010). Moreover, total inhibition of bromodeoxyuridine (BrdU) incorporation, indicating a suppression of cell proliferation, was observed in more than 100 tumour cell lines treated with dinaciclib. A decrease in MCL-1 protein level associated with an induction of apoptosis was observed in primary human CLL cells treated with dinaciclib (Johnson et al., 2012). The effect was observed even in the patients with high-risk genomic features e.g. del(11q22.3), del(17p13.1), and the unmutated status of the immunoglobulin variable heavy chain gene (IgVH) which are associated with poor treatment response (Grever, Lucas, Johnson, & Byrd, 2007). Dinaciclib demonstrated a high efficacy in terms of anti-tumour activity and considerably prolonged survival in mice bearing *KMT2A-MLLT3*-driven murine and human leukaemias (Baker et al., 2016). In a phase 2 clinical trial, 11% of patients with relapsed MM receiving dinaciclib achieved a partial response or better (Kumar et al., 2015). In a phase 2 clinical trial, the efficacy of dinaciclib was compared with gemtuzumab ozogamicin in patients with R/R AML and the efficacy of dinaciclib in patients with ALL was evaluated (NCT00798213). Although, short-lived cytoreductive activity was observed, clinical improvement was not seen in these patients (Gojo et al., 2013). Thus, the study was terminated. In a phase 3 clinical trial, in patients with R/R CLL, the efficacy of dinaciclib was greater than an anti-CD20 mAb ofatumumab with median progression free survival rate of 13.7 vs 5.9 months, and a PR rate of 40% vs 8.3%, respectively (NCT01580228) (Ghia et al., 2017). A phase 1 clinical trial is ongoing in patients with R/R CLL, MM , and DLBCL, aiming to evaluate the safety and tolerability of dinaciclib in combination with an anti-programmed cell death protein 1 (PD-1) pembrolizumab (NCT02684617).

TG02 is an oral CDK 1, 2, 3, 5, 7, and 9 inhibitor (Boffo et al., 2018). In primary human AML cells, TG02 induced RNAPII S2 dephosphorylation and suppressed MCL-1 and XIAP protein levels, resulting in apoptosis (Pallis et al., 2012). In OCI-AML3, KG-1a, and MV4-11 AML cell lines, BH3 profiling has shown that TG02 downregulates MCL-1 and sensitises to the BAD peptide; and TG02 synergises with venetoclax which sensitises to the NOXA peptide (Pallis et al., 2017). TG02 demonstrated anti-proliferative effects in various tumour cell lines (Goh et al., 2012). It also induced cell cycle arrest and apoptosis in mutant leukaemic cells bearing the *FLT3* mutation. Tumour regression and prolonged survival in murine AML models were observed following treatment with TG02. Phase 1 clinical trials in patients with advanced haematologic malignancies i.e. relapsed AML or ALL, chronic myeloid leukaemia (CML) in blast crisis, or MDS (NCT01204164); and in small lymphocytic lymphoma or R/R CLL (NCT01699152) have been completed. The results are not yet available.

SNS-032 is a CDK 2, 7, and 9 inhibitor (Boffo et al., 2018). In HL-60 and NB4 AML cell lines and primary human AML cells, SNS-032 induced a reduction in S2 phosphorylated RNAPII and subsequent RNAPII S5 dephosphorylation was observed (Walsby, Lazenby, Pepper, & Burnett, 2011). SNS-032 in combination with cytarabine showed a synergistic effect, resulting in a downregulation of *XIAP*, *BCL2*, and *MCL1* (Walsby et al., 2011). A phase 1 clinical trial was conducted in patients with advanced CLL or MM (NCT00446342). However, limited clinical activity was observed (Tong et al., 2010).

Atuveciclib is a potent CDK9/P-TEFb inhibitor (Boffo et al., 2018). Atuveciclib reduced phosphorylation of RNAPII and reduced Myc and MCL-1 levels, triggering apoptosis in four adult T-cell leukaemia/lymphoma (ATL) cell lines, three human T-lymphotropic virus 1 (HTLV-1)-transformed cell lines, and primary human ATL cells (Narita et al., 2017). Anti-tumour activity and prolonged survival in a human ATL cell-bearing mouse model was observed. Atuveciclib displayed potent *in vitro* activity, regardless of *KMT2A*-R status, in seven AML cell lines and in non *KMT2A*-R primary human AML cells harbouring mutant *NPM1* or *FLT3*-ITD (Scholz et al., 2016). Phase 1 dose escalation studies of atuveciclib in combination with G-CSF in patients with advanced malignancies i.e. gastric cancer, triple negative breast cancer, or DLBCL (NCT01938638) and atuveciclib as a single agent in

patients with advanced acute leukaemia (NCT02345382) have been completed. The results are not yet available.

Palbociclib is an oral, second generation CDK4/6 inhibitor (DiPippo, Patel, & Barnett, 2016). To date, it is the first and only CDKI with the FDA approval in the United States for the treatment of estrogen receptor-positive (ER+)/Her2-neu negative breast cancer in combination with an aromatase inhibitor letrozole. Preclinical study has demonstrated that the benefit of *CDK6* knockdown was seen in particular in *KMT2A-MLLT3* group (Placke et al., 2014). Therefore, a phase 1b/2a clinical trial is ongoing in patients with *KMT2A*-R AML or ALL (NCT02310243).

CYC065 is a selective, orally and intravenously available, second generation CDK2/9 inhibitor (Cyclacel, 2016). Currently, phase 1 studies of CYC065 as a single therapy in patients with lung and breast cancer (NCT02552953), CYC065 in combination with venetoclax in patients with R/R AML or MDS (NCT04017546); and R/R CLL (NCT03739554), are being conducted. The details of CYC065 will be further described in Chapter 3.

1.5 Thesis hypotheses

This study has two main hypotheses:

i) AML cell lines and primary human AML cells are potentially sensitive to treatment with the novel CDK2/9 inhibitor CYC065. Inhibiting CDK9 results in an inactivation of RNAPII transcriptional elongation. It has been reported that the transcripts with short half-lives are most commonly targeted, including the anti-apoptotic MCL-1 which is shown to be critical for the survival of AML (Glaser et al., 2012). In addition, examining paired BM samples harvested before chemotherapy and at the time of leukaemic recurrence, at least a twofold increase in MCL-1 protein levels was observed in 50% of the patients (Kaufmann et al., 1998). This highlights the importance of MCL-1 for the proliferation potential of AML. Hence, the therapeutic approach for AML using MCL-1 targeting CYC065 is a rational strategy to explore.

ii) CYC065 in combination with a conventional chemotherapy cytarabine, a selective BCL-2 inhibitor venetoclax, or a hypomethylating agent azacytidine potentially elicits synergistic benefits for the treatment of AML. Because the potential inhibition target of CYC065 is MCL-1, studies combining CYC065 with drugs that have different mechanisms of action is highly relevant, i.e. targeting parallel mechanisms to potentially induce synergistic effects.

1.6 Aims and objectives

i) To assess the effects of CYC065 on growth and survival of AML cells.

ii) To confirm the mechanism of action of CYC065 in AML.

iii) To evaluate the effects of combining CYC065 with cytarabine, venetoclax, or azacitidine to target AML.

Chapter 2 Materials and methods

2.1 Materials

2.1.1 Tissue culture

Table 2.1.1.1 Plastics for Tissue Culture and Suppliers

Plastics	**Supplier**
Cell culture dish with lid	Thermo Scientific Nunc. Massachusetts, USA
Cryovial	Fisher Scientific, Loughborough, UK
Eppendorf tubes (0.5/1.5ml)	Life technologies, Paisley, UK
Falcon tubes (15ml, 50ml)	Fred Baker Scientific, Cheshire, UK
Flat bottomed culture plates (6/12/24/96-well)	Greiner bio one, Gloucestershire, UK; Thermo Scientific Nunc. Massachusetts, USA
5100 Cryo freezing container, Nalgene, 'Mr Frosty'	Sigma-Aldrich, Dorset, UK
Haemocytometer	Hawksley, Sussex, UK
Pasteur pipette (3ml)	Greiner bio one, Gloucestershire, UK
Pipette tips (p10/20/100/200/1000)	Greiner bio one, Gloucestershire, UK
Single use filter unit (0.22/0.45µm)	Sartorius Stedim Biotech, Epsom, UK
Syringes (5/10/20/50ml)	Greiner bio one, Gloucestershire, UK
Tissue culture flasks (25/75/300cm^3; non-adherent)	Greiner bio one, Gloucestershire, UK

Tissue culture flasks (25/75/300cm^3; adherent)	Thermo Scientific Nunc. Massachusetts, USA

Table 2.1.1.2 Reagents for Tissue Culture and Suppliers

Reagent	**Supplier**
Dimethylsulphoxide (DMSO)	Sigma-Aldrich, Dorset, UK
DNAse I Solution (2500U/ml)	Stemcell technologies, Grenoble, France
Dulbecco's Phosphate-buffered saline (PBS)(without Ca^{2+} and Mg^{2+})	Life technologies, Paisley, UK
Ethanol 100% molecular grade	Sigma-Aldrich, Dorset, UK
Foetal bovine serum (FBS)	Life technologies, Paisley, UK
Iscove's Modified Dulbecco's Medium (IMDM)	Life technologies, Paisley, UK
L-Glutamine (200mM)	Life technologies, Paisley, UK
2-Mercaptoethanol (0.1µM)	Sigma-Aldrich, Dorset, UK
Methocult H4034	Stemcell technologies, Grenoble, France
Penicillin-Streptomycin (Pen/Strep) (10000U/ml)	Life technologies, Paisley, UK
hFLT3L (stock – 100µg/ml)	Stemcell technologies, Grenoble, France
hIL-3 (stock – 100µg/ml)	Stemcell technologies, Grenoble, France
hIL-6 (stock – 100µg/ml)	Stemcell technologies, Grenoble, France
hSCF (stock – 100µg/ml)	Stemcell technologies, Grenoble, France

Human Serum Albumin (20%)	Scottish National Blood Transfusion Service
Resazurin (7-Hydroxy-3H-phenoxazin-3-one-10-oxide sodium salt) (R7017)	Sigma-Aldrich, Dorset, UK
Roswell Park Memorial Institute (RPMI) 1640 medium	Life technologies, Paisley, UK
Trypan blue solution (0.4%)	Thermo Fisher Scientific, Loughborough, UK

Table 2.1.1.3 Equipment for Tissue Culture and Suppliers

Equipment	**Supplier**
CompuSyn Software	ComboSyn, Inc., New Jersey, USA
Multichannel pipette	Nichiryo, Saitama, Japan
Spectramax M5 plate reader	Molecular Devices, California, USA
SoftMax Pro Software	Molecular Devices, California, USA

Table 2.1.1.4 AML Cell Lines and Characteristics

Cell line	**Disease**	**Characteristics**	**Supplier**
OCI-AML3 (ACC-582)	AML FAB M4	Established from the PB of a 57yr old male at diagnosis in 1987 Hyperdiploid karyotype - 48(45-50)<2n>X/XY, +1, +5, +8, der(1)t(1;18)(p11;q11), i(5p), del(13)(q13q21), dup(17)(q21q25) ("OCI-AML3", 2019)	DSMZ, Braunschweig, Germany

		NPM1 gene mutation (type A) and the DNMT3A R882C mutation (Lund et al., 2014)	
MOLM-13 (AC-554)	AML FAB M5a at relapse after initial RAEB	Established from PB of a 20yr old male with RAEB that developed into AML in 1995 Human hyperdiploid karyotype with 4% polyploidy - 51(48-52)<2n>XY, +8, +8, +8, +13, del(8)(p1?p2?), ins(11;9)(q23;p22p23 FLT3-ITD is present at gene level only; CBL deltaExon8 mutant; carries occult insertion effecting *KMT2A-MLLT3* (*MLL-AF9*) fusion ("MOLM-13", 2019)	DSMZ, Braunschweig, Germany
MV4-11	Biphenotypic B-myelomoncytic leukaemia	Established from a 10-year-old male at diagnosis 48, XY, t(4;11)(q21;q23), +8, +19 ("MV4-11", 2019) FLT3-ITD is present at gene and protein level; carries occult insertion effecting *KMT2A-AFF1* (*MLL-AF4*) fusion (Quentmeier, Reinhardt, Zaborski, & Drexler, 2003)	In house

Table 2.1.1.5 Cell Line Culture Conditions

Cell line	**Media conditions**
OCI-AML3	RPMI, 20% FBS, 2mM L-Glutamine, Pen/Strep (100U/ml)
MOLM-13	RPMI, 20% FBS, 2mM L-Glutamine, Pen/Strep (100U/ml)
MV4-11	RPMI, 10% FBS, 2mM L-Glutamine, Pen/Strep (100U/ml)

Table 2.1.1.6 10% Media for Cell Line Culture

Reagent	Volume
FBS	50ml
L-Glutamine (stock - 200mM)	5ml
Pen/Strep (stock - 10000U/ml)	5ml
RPMI	440ml

Table 2.1.1.7 20% Media for Cell Line Culture

Reagent	Volume
FBS	100ml
L-Glutamine (stock - 200mM)	5ml
Pen/Strep (stock - 10000U/ml)	5ml
RPMI	390ml

Table 2.1.1.8 Media for Cell Line Cryopreservation

Reagent	Volume
DMSO	5ml
FBS	45ml

Table 2.1.1.9 Media for Primary AML Cell Culture

Reagent	Volume
hFLT3L (stock – 100µg/ml)	5µl

hIL-3 (stock – 100µg/ml)	5µl
hIL-6 (stock – 100µg/ml)	5µl
hSCF (stock – 100µg/ml)	5µl
BIT (Bovine Serum Albumin [BSA]/Insulin/ Transferrin)	10ml
2-Mercaptoethanol (50mM)	0.1ml
IMDM	38.7ml
L-Glutamine (stock - 200mM)	0.5ml
Low density lipoprotein (10mg/mL)	0.2ml
Pen/Strep (stock - 10000U/ml)	0.5ml
All cytokines are made up in filter sterilised PBS and BSA (0.1%)	

Table 2.1.1.10 Media for Thawing Primary Samples

Reagent	**Volume**
DNase I (2500 U/ml)	2ml
Dulbecco's PBS (without Ca^{2+} and Mg^{2+})	418.75ml
Human Serum Albumin (20%)	25ml
Magnesium chloride (1.0M)	1.25ml
Trisodium citrate (0.155M)	53ml

Table 2.1.1.11 Reagents for CFU Assay

Reagent	Composition	Supplier
Methocult™ H4034	IMDM, methylcellulose, BSA, FBS, 2-Mercaptoethanol, recombinant human (rh)SCF, rhGM-CSF, rhG-CSF, rhIL-3, rhEPO	Stemcell technologies, Grenoble, France
Serum free media	IMDM, BSA, insulin, transferrin [BIT], 0.1μM 2-Mercaptoethanol, Pen/Strep, L-Glutamine plus a high concentration growth factor cocktail containing 10ng/mL hFLT3L, 10ng/mL hSCF, 10ng/mL hIL-3, 10ng/mL hIL-6 (Stem cell technologies)	Made in house in Vacubottle and filter sterilised

Table 2.1.1.12 Drugs Tested and Suppliers

Drug	Mechanism of action	Supplier
Azacitidine (A1907-APE)	Cytosine analogue, DNA methyl transferase (DNMT) inhibitor	Stratech Scientific Ltd, Ely, UK
Colcemid (10295892001)	Microtubule-depolymerizing drug which promotes microtubule detachment from microtubule organizing centre at high concentration	Sigma-Aldrich, Dorset, UK
CYC065	CDK2/9 inhibitor Phase 1	Cyclacel Ltd, Dundee, UK

Cytarabine (AraC; C1768)	Deoxycytidine analogue, DNA synthesis inhibitor	Sigma-Aldrich, Dorset, UK
Doramapimod (BIRB 796)	p38 MAPK inhibitor Phase 2	Stratech Scientific Ltd, Ely, UK
Sotrastaurin (S2791)	Selective pan PKC inhibitor Phase 2	Stratech Scientific Ltd, Ely, UK
Venetoclax (ABT-199; GDC-0199)	BCL-2 selective inhibitor with no activity against MCL-1	Stratech Scientific Ltd, Ely, UK

2.1.2 Molecular Studies

Table 2.1.2.1 Plastics for Molecular Studies and Suppliers

Equipment	**Supplier**
Fluidigm Dynamic Array Integrated Fluidic Circuit (48.48)	Fluidigm, San Francisco, USA
MicroAmp Optical Adhesive Film	Applied biosystems, Warrington,
Nucleotide free tips, eppendorfs and PCR tube	Applied biosystems, Warrington,
384 MicroAmp Optical Well Plates	Applied biosystems, Warrington,

Table 2.1.2.2 Molecular Reagents and Suppliers

Reagent	**Supplier**
Assay loading reagent (2X)	Fluidigm, San Francisco, USA
DNA Binding Dye Sample Loading Reagent (20X)	Fluidigm, San Francisco, USA
Exonuclease I (E. coli)	New England BioLabs

Exonuclease I reaction buffer	New England BioLabs
High-capacity cDNA reverse transcription kit (4368814) – see Table 2.1.2.4.1	Applied Biosystems, Warrington, UK
2X Multiplex pre-amplification Master Mix	Qiagen, Crawley, UK
Nuclease free water	Qiagen, Crawley, UK
Primers – see Table 2.1.2.6.8	Integrated DNA Technologies, Leuven, Belgium
RNAeasy Plus Mini kit (74136)	Qiagen, Crawley, UK
RNaseOUT™ recombinant ribonuclease inhibitor	Life technologies, Paisley, UK
SsoFast™ EvaGreen Supermix with low ROX (2X)	Bio-Rad, Hertfordshire, UK
SYBR™ Select Master Mix (4472908)	Applied Biosystems, Warrington, UK
TE Buffer pH8.0	Applied Biosystems, Warrington, UK

Table 2.1.2.3 Molecular Equipment, Software and Suppliers

Equipment	**Supplier**
Biomark™ Real-Time PCR Analysis	Fluidigm, San Francisco, USA
Fluidigm Biomark™ Analyser	Fluidigm, San Francisco, USA
Nanodrop spectrophotometer 2100	Nanodrop technologies, Wilmington, USA
Sorvall Legend T Centrifuge	DJB Labcare Ltd, Buckinghamshir UK

Taqman 7900 machine	Applied biosystems, Warrington, UK

2.1.2.4 Reverse transcription

Table 2.1.2.4.1 High-capacity cDNA Reverse Transcription Master Mix

Reagent	**Volume**
10X RT Random Primers	2µl
10X RT Buffer	2µl
25X dNTP Mix (100 mM)	0.8µl
RNaseOUT™ recombinant ribonuclease inhibitor	1µl
MultiScribe™ Reverse Transcriptase (50 U/µL)	1µl
RNA	500ng
RNase free water	13.2µl – RNA volume

Table 2.1.2.4.2 High-capacity cDNA Reverse Transcription Cycling Conditions

Temperature (ºC)	25	37	85
Time	10min	120min	5min

2.1.2.5 qRT-PCR

Table 2.1.2.5.1 qRT-PCR-Based Gene Expression Profiling

Reagent	Volume
100μM Forward primer	0.04μl
100μM Reverse primer	0.04μl
SYBR™ Select Master Mix	5μl
cDNA	From RNA 10ng
RNase free water	4.92μl – volume of cDNA

Table 2.1.2.5.2 qRT-PCR-Based Gene Expression Profiling Cycling Conditions

	Stage 1 UDG activation	Stage 2 AmpliTaq™ Fast DNA Polymerase Activation	Stage 3: Cycling conditions 40 cycles		Hold
			Denaturing	Annealing/ Extension	
Temperature (°C)	50	95	95	60	4
Time	2min	2min	15s	1min	∞

2.1.2.6 Fluidigm™ qRT-PCR

Table 2.1.2.6.1 Pre-amplification mix- Primers

Reagent	Volume
Qiagen Multiplex PCR Master Mix	2.5μl
500nM pooled primer mix – see Table 2.1.2.6.1.1	0.5μl
RNase free water	0.75μl

cDNA	1.25µl

Table 2.1.2.6.1.1 Pooled primer mixture

Reagent	**Volume**
100µM Forward primer	1µM
100µM Reverse primer	1µM
TE buffer	200µM – volume of forward and reverse primers

Table 2.1.2.6.2 Pre-amplification Cycling Conditions

	Stage 1: Initial denature	**Stage 2: Cycling conditions 18 cycles**			**Stage 3: Final extension**	**Hold**
		Denaturing	**Annealing**	**Extension**		
Temperature (°C)	94	94	60	72	72	4
Time	15min	30s	60s	40s	5min	∞

Table 2.1.2.6.3 Exonuclease I treatment mixture for use after primer pre-amplification

Reagent	**Volume***
RNase free water	1.4µl
Exonuclease I reaction buffer	0.2µl
Exonuclease I (E. coli)	0.4µl
Pre-amplified sample from Table 2.1.2.6.1	5µl

* To be diluted 1:5 by adding 18µl TE buffer after exonuclease I treatment

Table 2.1.2.6.4 Exonuclease I treatment Cycling Conditions

Temperature	37˚C	80˚C
Time	30min	15min

Table 2.1.2.6.5 Sample mixture for Fluidigm™ qRT-PCR

Reagent	**Volume**
20X DNA binding dye	0.3µl
SsoFast™ EvaGreen Supermix with low ROX	3µl
Pre-amplified/Exo I-treated sample from Table 2.1.2.6.3	2.7µl

Table 2.1.2.6.6 Assay mixture for Fluidigm™ qRT-PCR

Reagent	**Volume**
2X assay loading reagent	3µl
TE buffer	0.3µl
20µM mixed forward and reverse primers - see Table 2.1.2.6.6.1	2.7µl

Table 2.1.2.6.6.1 Mixed forward and reverse primers

Reagent	**Volume**
100µM Forward primer	2µM
100µM Reverse primer	2µM
TE buffer	6µM

Table 2.1.2.6.7 Fluidigm™ qRT-PCR Cycling conditions

	Stage 1: Initial denature	Stage 2: Cycling conditions 40 cycles		Hold
		Denaturing	Annealing	
Temperature (°C)	95	95	60	4
Time	60s	5s	20s	∞

Melt curve when primers used: 60°C to 95°C with a 1°C increase every 3 seconds

Table 2.1.2.6.8 Primers

Primer	Sequence 5´to 3´	Accession
ATM Forward	CGG AGC TGA TTG TAG CAA CAT ACT A	NM_001351834.2
ATM Reverse	CAG ATA GAG CCT GAA GTA CAC AGA G	
ATR Forward	CAG CTC TCT ATG AAG GCC ATT CAA	NM_001184.4
ATR Reverse	GTT CTA CTG TTT CAC TGT CTG TTG C	
BCL2 Forward	CCC TGT GGA TGA CTG AGT ACC	NM_000633.3
BCL2 Reverse	GTT CCA CAA AGG CAT CCC AGC	
BAK1 Forward	TCA TCG GGG ACG ACA TCA AC	NM_001188.4
BAK1 Reverse	CAA ACA GGC TGG TGG CAA TC	
BAX Forward	GAC ATT GGA CTT CCT CCG GG	NM_001291428.2
BAX Reverse	ACA GGG ACA TCA GTC GCT TC	
BIRC5 (survivin) Forward	CCA GAT GAC GAC CCC ATA GAG G	NM_001168.3
BIRC5 (survivin) Reverse	TGG CTC TTT CTC TGT CCA GTT TC	
BMF Forward	GAA CCC CAG CGA CTC TTT TA	NM_001003940.2
BMF Reverse	TTT CGG GCA ATC TGT ACC TC	
CDC25A Forward	GTC TAG ATT CTC CTG GGC CAT TG	NM_001789.3

CDC25A Reverse	CAG AAT GGC TCC TCT TCA GAG C	
CDC25B Forward	GGA TTT GTG GAC ATC CTA GAG AGT	NM_021873.3
CDC25B Reverse	ACT TGC TGT ACA TGA CGA GGT	
CDC25C Forward	CAC TCA GCT TAC CAC TTC TGC AG	NM_001790.5
CDC25C Reverse	GGG CTA CAT TTC ATT AGG TGC TGG	
CDK1 Forward	ATG AAG TGT GGC CAG AAG TG	NM_001786.5
CDK1 Reverse	CAG AAA TTC GTT TGG CTG GAT CA	
CDK2 Forward	GCT TGT TAT CGC AAA TGC TGC	NM_001290230.2
CDK2 Reverse	GAT GGG GTA CTG GCT TGG TC	
CDK3 Forward	TGG TGA CAC TGT GGT ATC GC	NM_001258.2
CDK3 Reverse	GGG CTT TTC GAG TCA CCA TC	
CDK4 Forward	CCC ATC AGC ACA GTT CGT GA	NM_000075.4
CDK4 Reverse	AAC ACC AGG GTT ACC TTG ATC TC	
CDK5 Forward	TCT TCC AGC TAC TAA AAG GGC TG	NM_004935.4
CDK5 Reverse	CAA TTT CAG CTC CCC ATT CCT G	
CDK6 Forward	CCG AAG TCT TGC TCC AGT CC	NM_001259.8
CDK6 Reverse	GTT GAT CAA CAT CTG AAC TTC CAC G	
CDK7 Forward	GTG GCC GGA CAT GTG TAG TC	NM_001324070.2
CDK7 Reverse	GCC GTA ATT CGA GCA CAT GG	
CDK9 Forward	ATG GAA AAC GAG AAG GAG GGG	NM_001261.4
CDK9 Reverse	TAG GGG GAA GCT TTG GTT CG	
CDKN1A ($p21^{Cip1}$) Forward	ACA GCA GAG GAA GAC CAT GTG	NM_000389.5
CDKN1A ($p21^{Cip1}$) Reverse	GGA GTG GTA GAA ATC TGT CAT GC	
CDKN2C ($p18^{INK4C}$) Forward	CGT CAA TGC ACA AAA TGG ATT TGG	NM_078626.3

CDKN2C ($p18^{INK4C}$) Reverse	GAA TGA CAG CGA AAC CAG TTC GG	
CDKN2D ($p19^{INK4D}$) Forward	GTG CAT CCC GAC GCC CTC AAC	NM_001800.4
CDKN2D ($p19^{INK4D}$) Reverse	TGG CAC CTT GCT TCA GCA GCT C	
CDKN3 Forward	GGT TTA TGT GCT CTT CCA GGT TG	NM_005192.4
CDKN3 Reverse	GTG CAG CTA ATT TGT CCC GAA AC	
CHEK1 Forward	GGT CAC AGG AGA GAA GGC AAT A	NM_001114122.2
CHEK1 Reverse	GGA AGA ATC TCT GAG CAT CTG G	
CHEK2 Forward	AGT GGA TCC AAA GGC ACG TT	NM_007194.4
CHEK2 Reverse	CCT GGG GTA GAG CTG TGG AT	
E2F1 Forward	GAT CAA AGC CCC TCC TGA GAC	NM_005225.3
E2F1 Reverse	ATC CCA CCT ACG GTC TCC TC	
E2F2 Forward	GGC TGG CCT ATG TGA CTT ACC	NM_004091.4
E2F2 Reverse	GGT TGT CCT CAG TCC TGT CG	
E2F4 Forward	GCT GAC ACC CTA GCT GTA CG	NM_001950.4
E2F4 Reverse	AAT CTC CCG GGT ATT GCA GC	
MCL1 Forward	GCC TTC CAA GGA TGG GTT TG	NM_182763.2
MCL1 Reverse	TAT GCC AAA CCA GCT CCT ACT C	
MYC Forward	CGT CCT CGG ATT CTC TGC TC	NM_002467.6
MYC Reverse	CTT GTT CCT CCT CAG AGT CGC	
PPP1R10 (PNUTS) Forward	TCC CCC TAG ATG AGG AGT GTT C	NM_002714.4
PPP1R10 (PNUTS) Reverse	AGA ACT GGA GGC AAC TTG GAG	
TP53 Forward	GAG CTG AAT GAG GCC TTG GA	NM_000546.6

TP53 Reverse	CTG AGT CAG GCC CTT CTG TCT T	
XIAP Forward	AGG GCT AAC TGA TTG GAA GCC	NM_001204401.2
XIAP Reverse	GTT CTT ACC AGA CAC TCC TCA AG	
Housekeeping genes		
ATP5F1B Forward	GCT GAG CTG GGC ATC TAT CC	NM_001686.4
ATP5F1B Reverse	TGG AGG GAT TTG TAG TCC TGC	
B2M Forward	TTG TCT TTC AGC AAG GAC TGG	NM_004048.4
B2M Reverse	ATG CGG CAT CTT CAA ACC TCC	
CYC1 Forward	ACT GCG GGA AGG TCT CTA CTT	NM_001916.5
CYC1 Reverse	GGG TGC CAT CGT CAA ACT CTA	
RNF20 Forward	GGT GTC TCT TCA ACG GAG GAA	NM_019592.7
RNF20 Reverse	TAG TGA GGC ATC ATC AGT GGC	
TYW1 Forward	ATT GTC ATC AAG ACG CAG GGC	NM_018264.4
TYW1 Reverse	GTT GCG AAT CCC TTC GCT GTT	
UBE2D2 Forward	CCA TGG CTC TGA AGA GAA TCC	NM_003339.3
UBE2D2 Reverse	GAT AGG GAC TGT CAT TTG GCC	

2.1.3 Protein studies

Table 2.1.3.1 Reagents for protein preparation

Reagent	Supplier
50mM Tris-HCl pH 7.5	In house
1% Nonidet p40	Sigma-Aldrich, Dorset, UK
10% Glycerol	Sigma-Aldrich, Dorset, UK
Ultrapure dH_2O	In house
cOmplete™ ULTRA tablets, Mini, EASYpack Protease Inhibitor Cocktail	Sigma-Aldrich, Dorset, UK
PhosSTOP™ phosphatase inhibitor tablets	Sigma-Aldrich, Dorset, UK
Diisopropylfluorophosphate (DIFP)	Sigma-Aldrich, Dorset, UK
4X NuPAGE™ LDS Sample Buffer	Thermo Fisher Scientific, Loughborough, UK
10X NuPAGE™ Sample Reducing Agent	Thermo Fisher Scientific, Loughborough, UK
Quick Start™ Bradford Dye Reagent	Bio-Rad, Hertfordshire, UK

Table 2.1.3.2 Solution for Protein Extraction

Protein Solubilisation Buffer	Phosphatase and Protease Inhibitor Concentrations
50mM Tris-HCl pH 7.5	cOmplete™ ULTRA 1 tablet per 10ml of solubilisation buffer
150mM NaCl	PhosSTOP™ phosphatase inhibitor 1 tablet per 10ml of solubilisation buffer
1% Nonidet P40	
10% Glycerol	

2.1.4 Western blotting

Table 2.1.4.1 Reagents and Suppliers

Reagent	Supplier
BSA Fraction V	Sigma-Aldrich, Dorset, UK
HCl	Sigma-Aldrich, Dorset, UK
Methanol, for HPLC, ≥99.9%	Sigma-Aldrich, Dorset, UK
Ultrapure dH_2O	In house
NaCl	Sigma-Aldrich, Dorset, UK
Nonfat dried skimmed milk powder	Morrisons
NuPAGE™ Antioxidant	Thermo Fisher Scientific, Loughborough, UK
NuPAGE™ MOPS SDS Running Buffer (20X)	Thermo Fisher Scientific, Loughborough, UK
NuPAGE™ Transfer Buffer (20X)	Thermo Fisher Scientific, Loughborough, UK
NuPAGE™ Tris-Acetate SDS Running Buffer (20X)	Thermo Fisher Scientific, Loughborough, UK
Precision Plus Protein™ Dual Color Standards	Bio-Rad, Hertfordshire, UK
Trizma™ base	Sigma-Aldrich, Dorset, UK
Tween™ 20	Sigma-Aldrich, Dorset, UK
ReBlot Plus Strong Antibody Stripping Solution (10X)	Merck Millipore, Watford, UK

Table 2.1.4.2 Equipment and Suppliers

Equipment	Supplier
Amersham Protran™ Premium 0.45µm nitrocellulose membrane	GE healthcare, Buckinghamshire, UK

Image Studio™ Lite Software Version 5.2	LI-COR Biosciences, Cambridge, UK
NuPAGE™ 3-8% Tris-Acetate Protein Gels, 1.5 mm, 15-well	Thermo Fisher Scientific, Loughborough, UK
NuPAGE™ 4-12% Bis-Tris Protein Gels, 1.5 mm, 15-well	Thermo Fisher Scientific, Loughborough, UK
Odyssey™ Fc Imaging System	LI-COR Biosciences, Cambridge, UK
PowerPac™ Adaptor	Bio-Rad, Hertfordshire, UK
PowerPac™ Basic Power Supply	Bio-Rad, Hertfordshire, UK
Whatman™ filter paper	GE healthcare, Buckinghamshire, UK
XCell II Blot Module	Thermo Fisher Scientific, Loughborough, UK
XCell SureLock Mini-Cell	Thermo Fisher Scientific, Loughborough, UK

Table 2.1.4.3 1X MOPS SDS or Tris-Acetate SDS running buffer

Reagent	**Volume**
Ultrapure dH_2O	950ml
20X Nupage™ MOPS SDS or 20X Tris-Acetate	50ml

Table 2.1.4.4 1X Transfer buffer, 20% Methanol

Reagent	**Volume**
Methanol, for HPLC, ≥99.9%	200ml
Ultrapure dH_2O	750ml
20X NuPAGE™ Transfer Buffer	50ml

Table 2.1.4.5 1X Tris-buffered saline, 0.1% Tween™ 20 (TBST) Buffer pH 7.5

Reagent	Concentration
NaCl	150mM
Trizma™ base	20mM
Tween™ 20	0.1% (v/v)

Table 2.1.4.6 3% BSA Blocking solution

Reagent	Volume
BSA Fraction V	3% (w/v)
1X TBST – see Table 2.1.4.5	Add up to 50ml

Table 2.1.4.7 5% Milk Blocking solution

Reagent	Volume
Nonfat Dry Milk	5% (w/v)
1X TBST – see Table 2.1.4.5	Add up to 50ml

Table 2.1.4.8 Primary antibodies

Antibody	Species	Dilution	Diluent	Manufacturer	Catalogue number
Akt (phospho S473) (D9E) XP™ (total)	Rabbit	1:1000	3% BSA	Cell Signalling Technology, Hitchin, UK	4060
Akt (total)	Mouse	1:1000	5% milk	Santa Cruz Biotechnology, Heidelberg, Germany	sc-5298

BCL-2 (phospho S70)	Rabbit	1:1000	3% BSA	Abcam, Cambridge, UK	ab28819
BCL-2 (total)	Mouse	1:1000	5% milk	Merck Millipore, Watford, UK	05-729
BCL-xL (phospho S62)	Rabbit	1:1000	3% BSA	Fisher Scientific, Loughborough, UK	44428G
BCL-xL (total)	Rabbit	1:1000	5% milk	Cell Signalling Technology, Hitchin, UK	2764
ERK1/2 (phospho T202/Y204)	Rabbit	1:1000	3% BSA	Chemicon-Millipore, Chemicon, Temecula,USA	AB3826
ERK1/2 (total)	Mouse	1:1000	5% milk	Santa Cruz Biotechnology, Heidelberg, Germany	sc-514302
GSK3β (phospho S9)	Rabbit	1:1000	3% BSA	Cell Signalling Technology, Hitchin, UK	9336
GSK3β (total)	Mouse	1:1000	5% milk	Santa Cruz Biotechnology, Heidelberg, Germany	sc-377213
GSK3β (phospho T390)	Rabbit	1:1000	3% BSA	Cell Signalling Technology, Hitchin, UK	3548
MCL-1	Rabbit	1:500	5% milk	Cell Signalling Technology, Hitchin, UK	4572S
NOXA	Mouse	1:500	5% milk	Santa Cruz Biotechnology, Heidelberg, Germany	sc-56169

p38 MAPK (phospho T180/Y182)	Rabbit	1:500	3% BSA	Cell Signalling Technology, Hitchin, UK	9211
p38 MAPK (total)	Rabbit	1:1000	5% milk	Cell Signalling Technology, Hitchin, UK	9212
PARP	Rabbit	1:1000	5% milk	Cell Signalling Technology, Hitchin, UK	9542
Phospho-PKC Substrate Motif [(R/K)XpSX(R/K)] MultiMab™ Rabbit mAb mix	Rabbit	1:1000	3% BSA	Cell Signalling Technology, Hitchin, UK	6967S
PP1α (phospho T320)	Rabbit	1:1000	3% BSA	Cell Signalling Technology, Hitchin, UK	2581
PP1α Antibody (total)	Rabbit	1:1000	5% milk	Cell Signalling Technology, Hitchin, UK	2582
Rb (phospho S780)	Rabbit	1:1000	3% BSA	Cell Signalling Technology, Hitchin, UK	9307
Rb (phospho S807/S811)	Rabbit	1:1000	3% BSA	Cell Signalling Technology, Hitchin, UK	9308
Rb (4H1) Mouse mAb (total)	Mouse	1:1000	5% milk	Cell Signalling Technology, Hitchin, UK	9309
RNAPII (phospho S2)	Rabbit	1:1000	3% BSA	Abcam, Cambridge, UK	ab70324
RNAPII (phospho S5)	Rabbit	1:1000	3% BSA	Cell Signalling Technology, Hitchin, UK	13523

RNAPII RPB1 CTD (4H8) (total)	Mouse	1:1000	5% milk	Cell Signalling Technology, Hitchin, UK	2629
SH-PTP2	Mouse	1:5000	5% milk	Santa Cruz Biotechnology, Heidelberg, Germany	sc-7384
γ-tubulin	Mouse	1:5000	5% milk	Sigma-Aldrich, Dorset, UK	T5326

Table 2.1.4.9 Secondary antibodies

Antibody	**Species**	**Dilution**	**Diluent**	**Manufacturer**	**Catalogue number**
IRDye™ 680RD Donkey anti-Mouse IgG (Red)	Mouse	1:5000	5% milk	LI-COR Biosciences, Cambridge, UK	925-68072
IRDye™ 800CW Donkey anti-Rabbit IgG (Green)	Rabbit	1:5000	5% milk	LI-COR Biosciences, Cambridge, UK	925-32213

2.1.5 Flow cytometry

Table 2.1.5.1 Plastics for flow cytometry

Plastic	Supplier
FACS tubes	Greiner bio one, Gloucestershire, UK

Table 2.1.5.2 Equipment for Flow cytometry

Equipment	Supplier
BD FACSAria™ III	BD Biosciences, Oxford, UK
BD FACSCanto™ II	BD Biosciences, Oxford, UK
BD FACSDiva™ Software	BD Biosciences, Oxford, UK
FlowJo Software	Ashland, Oregon, USA

Table 2.1.5.3 Reagents for Flow cytometry

Reagent	Supplier
Antibodies and staining reagents – see Table 2.1.5.8	-
Ethanol 100% molecular grade	Sigma-Aldrich, Dorset, UK
FACS flow solution	BD Biosciences, Oxford, UK
FACS clean solution	BD Biosciences, Oxford, UK
Cytofix/Cytoperm™ Fixation/Permeabilisation Solution Kit	BD Biosciences, Oxford, UK
FBS	Life technologies, Paisley, UK
Hank's Balanced Salt Solution (HBSS)	Life technologies, Paisley, UK
PBS tablet for 1X PBS	Sigma-Aldrich, Dorset, UK

Table 2.1.5.4 1X HBSS

Reagent	Volume
10X HBSS	5ml
Sterile water	45ml

Table 2.1.5.5 2% PBS/FBS

Reagent	Volume
1X PBS	48ml
FBS	2ml

Table 2.1.5.6 20% PBS/FBS quenching solution for CellTrace™ Violet prolifetaion assay

Reagent	Volume
1X PBS	40ml
FBS	10ml

Table 2.1.5.7 80% Ethanol fixation for cell cycle analysis

Reagent	Volume
1X PBS	10ml
Ethanol 100% molecular grade	40ml

Table 2.1.5.8 Antibodies and staining reagents for flow cytometry

Primary antibody	Fluorochrome	Manufacturer	Catalogue number
7-Aminoactinomycin D (7-AAD)	-	BD Biosciences, Oxford, UK	559925
Active caspase-3 (Rabbit)	PE	BD Biosciences, Oxford, UK	550821
Annexin V	FITC	BD Biosciences, Oxford, UK	556419
CellTrace™ Violet proliferation kit	-	Thermo Fisher Scientific, Loughborough, UK	C34557
DAPI (4',6-diamidino-2-phenylindole)	-	BD Biosciences, Oxford, UK	564907
Rabbit (DA1E) mAb IgG XP™ Isotype Control	PE	Cell Signalling Technology, Hitchin, UK	5742
Staining buffer for cell cycle analysis			
Propidium iodide (PI)/RNase staining buffer	-	BD Biosciences, Oxford, UK	550825

2.1.6 Pamgene™ multiplex serine/threonine kinases (STK) activity profiling

Table 2.1.6.1 Equipment for Pamgene™ multiplex STK activity profiling

Equipment	Supplier
PamStation™ 12 System	Pamgene International B.V., 's-Hertogenbosch, The Netherlands

STK PamChip™	Pamgene International B.V., ‘s-Hertogenbosch, The Netherlands
BioNavigator63 Software	Pamgene International B.V., ‘s-Hertogenbosch, The Netherlands
Evolve Software version 1.2	Pamgene International B.V., ‘s-Hertogenbosch, The Netherlands

Table 2.1.6.2 Reagent for Pamgene™ multiplex STK activity profiling

Reagent	**Supplier**
Halt™ Phosphatase Inhibitor Cocktail	Thermo Fisher Scientific, Loughborough, UK
Halt™ Protease Inhibitor Cocktail, EDTA free	Thermo Fisher Scientific, Loughborough, UK
Ultrapure dH_2O	In house
M-PER Mammalian Extraction Buffer	Thermo Fisher Scientific, Loughborough, UK
STK reagent kit – see Table 2.1.6.3	Pamgene International B.V., ‘s-Hertogenbosch, The Netherlands

Table 2.1.6.3 Pamgene™ multiplex STK activity profiling kit

Reagent	**Volume**
Blocking solution	
2% BSA	30µl

Sample mixture	
Sample lysate	5µl
1mM ATP solution	4µl
100X BSA	0.4µl
Ultrapure dH_2O	26.1µl
10X PK buffer	4µl
STK antibody mix	0.5µl
Detection mixture	
10X Antibody buffer	3µl
Ultrapure dH_2O	26.6µl
FITC-conjugated STK antibody	0.4µl

Table 2.1.6.4 Sample lysis buffer for Pamgene™ multiplex STK activity profiling

Reagent	Volume
Halt™ Phosphatase Inhibitor Cocktail	2µl
Halt™ Protease Inhibitor Cocktail, EDTA free	2µl
M-PER Mammalian Extraction Buffer	96µl

2.2 Methods

2.2.1 Tissue culture

2.2.1.1 Drugs and reagents

Details of all drugs used are described in Materials Table 2.1.1.12.
10mM stock solutions of CYC065, azacitidine, doramapimod, sotrastaurin and venetoclax were prepared in DMSO while cytarabine was prepared in sterile water and aliquots for single use stored at -20^{o}C. Dilutions of stock solutions were freshly prepared prior to each experiment in appropriate cell culture media. Colcemid, which was used in the proliferation assay, was stored at 4^{o}C. Cytokines were reconstituted according to manufacturer's instructions and stored in single use aliquots at -80^{o}C.

2.2.1.2 Cell culture

All cell culture experiments were performed using sterile technique in a laminar air flow hood. All cells were cultured in their specific culture media at 37^{o}C in a humidified atmosphere with 5% CO_2 (standard culture conditions).

2.2.1.2.1 AML cell lines

AML is a heterogeneous, clonal disorder with a range of morphologic, immunophenotypic, cytogenetic, and molecular characteristics. Nowadays, molecular genetics and cytogenetic alterations are stratified into favourable, intermediate and adverse risk profile according to the ELN recommendations (H. Döhner et al., 2017). In this project, OCI-AML3, MOLM-13 and MV4-11 cell lines were chosen because they carry common mutations which encompass all groups of the ELN risk profile.

OCI-AML3 cell line carries an *NPM1* and *DNMT3A* R882C mutation, two of the more common mutations identified in AML; further it belongs to the FAB M4 subgroup, myelomonocytic AML.

MV4-11 and MOLM-13 cell lines express the *FLT3* ITD mutation. MV4-11 cell line expresses the *FLT3* ITD mutation at the gene and protein level whilst the MOLM-13 cell line carries the *FLT3* ITD mutation but does not express the

protein. MOLM-13 and MV4-11 cell lines carry the *KMT2A* fusion genes, *KMT2A-MLLT3* and *KMT2A-AFF1*, respectively.

The disease phenotype of each cell line studied is further defined in Materials: Table 2.1.1.4. For experiments outlined, cells were seeded at $3x10^5$/ml and harvested at various time points for functional assays, gene and protein analysis, dependent on experimental design.

2.2.1.2.1.1 Cell line recovery post cryopreservation

Cell lines were removed from liquid nitrogen and immediately thawed at 37ºC in a water bath. Cells were added to a sterile 15ml falcon tube with a Pasteur pipette and slowly recovered by adding specific culture media drop-wise over 15min at room temperature (RT) with constant agitation. Cells were centrifuged at 300xg for 5min, the supernatant was poured off, and the pellets were resuspended in specific culture media. Cells were incubated overnight at 37ºC in a humidified atmosphere with 5% CO_2. The following day, recovery cell number and viability were assessed by trypan blue exclusion assay. Cells were seeded in standard tissue culture flasks at the concentration of $2.5x10^5$ cells/ml.

2.2.1.2.1.2 Passaging AML cell lines

AML cell lines were passaged every 2 days, back to the optimal density of $2.5x10^5$ cells/ml with fresh 37ºC warmed media, to maintain a cell density of between $1x10^5$ – $1x10^6$ cells/ml at all times in according to American Type Culture Collection (ATCC) or Leibniz-Institut Deutsche Sammlung von Mikroorganismen und Zellkulturen (DSMZ) instructions. Specific culture media as detailed in Materials: Table 2.1.1.5.

2.2.1.2.2 Cryoreservation of cell lines

Cells were resuspended at a concentration of $4\text{-}6x10^6$/ml in freezing solution (Materials: Table 2.1.1.8) and aliquoted into cryovials which were then placed in a 5100 Cryo -1ºC freezing container to provide controlled temperature reduction at -1ºC/min. Cells were stored at -80ºC for short term use, and transferred to liquid nitrogen for long term storage at -180ºC.

2.2.1.2.3 Primary cell recovery post cryopreservation

AML and normal samples were taken at diagnosis following informed consent in accordance with the Declaration of Helsinki, and approval of the Greater Glasgow and Clyde National Health Service. The source of AML samples was BM or PB as detailed in Table 5.5.1.1. For BM, heparinised samples were passed through a 100-µm cell strainer to remove fibrin filaments, micro blood clots, or fat particles. Filtered BM or PB samples were mixed with sterile PBS in a ratio of 1:1. Using 50ml falcon tubes, 30ml of diluted samples were then gently and very slowly layered on the top of 15ml of Histopaque™-1077. Then, the tubes were centrifuged at 100xg for 30min at 4ºC. After that, the buffy coat formed in the interphase between medium and Histopaque™-1077 was aspirated to recover mononuclear cells. The mononuclear cells were washed twice with 20ml of sterile PBS, centrifuged at 100xg for 10min, then aliquoted for an evaluation of the percentage of CD34 (%CD34) (detailed in Table 5.5.1.1) and cryopreserved in freezing media containing 10ml of DMSO, 5ml of 5% human albumin solution and 35ml of FBS. Normal samples used in our institute were taken from surplus leukopheresed PB of patients with non-infiltrative BM disease in remission (various types of lymphoma or myeloma). The procedure was similar to AML samples with the extra step i.e. an enrichment for CD34+ cells using the CliniMACS™ (Miltenyi Biotec) immunomagnetic beads system with the CD34+ cell yields of 95-99% before cryopreservation and stored in liquid nitrogen the cell bank until required.

25ml aliquots of thawing media (Materials: Table 2.1.1.10) were pre-warmed to 37ºC and filter sterilised (0.45µm single use filter unit). Primary AML cells were removed from liquid nitrogen and immediately thawed at 37ºC and gently transferred to the bottom of a 50ml Falcon tube using a 3ml Pasteur pipette. 15ml of thawing media was added dropwise to the cells over a 20min period at RT to enhance the DNAse I activity with constant, gentle agitation to prevent clumping. The cells were then centrifuged at 200xg for 10min and the media carefully poured off. For the second wash, the cells were gently resuspended in the remaining 10ml of thawing media. Then, the cells were centrifuged at 200xg for 10min, the media was carefully poured off, and the pellets were stained with CellTrace™ Violet for cell proliferation assay as detailed in section 2.2.1.2.4.

2.2.1.2.4 CellTrace™ Violet staining for cell proliferation assay

The principle of cell proliferation assay was to follow cell division (Salem et al., 2015). CellTrace™ Violet fluorescence intensity progressively reduced with each cell division allowing number of divisions to be calculated relative to an undivided control population.

The cell pellets from section 2.2.1.2.3 were resuspended with pre-warmed 2% PBS/FBS (Materials: Table 2.1.5.5). At this stage, an aliquot was removed for an unstained control. The remainder of the cells were resuspended in 5ml of 2%PBS/FBS to which 5µL of 5mM CellTrace™ Violet was added, to a final concentration of 5µM, and incubated in a water bath at 37°C for exactly 20min covered with aluminum foil. CellTrace™ Violet uptake was stopped by adding 45ml of cold 20% PBS/FBS (Materials: Table 2.1.5.6). Cells were centrifuged at 200xg for 10min, resuspended in AML culture media (Materials: Table 2.1.1.9) at the concentration of $1x10^6$ cells/ml in non-adherent tissue culture flasks and incubated overnight at 37°C in a humidified atmosphere with 5% CO_2. The following day, cells were centrifuged at 200xg for 10min and the pellets were resuspended in AML culture media. Cell number and viability was assessed by trypan blue dye exclusion. A recovery of 50-85% of the cryopreserved cell number was expected (detailed in Table 5.5.1.1).

2.2.1.2.5 Primary AML cell culture

The CellTrace™ Violet-positive cells were plated at the concentration of $2.5x10^5$ cells/ml in AML culture media (Materials: Table 2.1.1.9), then the compounds were added and incubated for 72h at 37°C in a humidified atmosphere with 5% CO_2 before analysis. For each experiment, an aliquot of CellTrace™ Violet-positive cells was treated with 100ng/ml colcemid, which arrests cells in metaphase and serves to determine the position of an undivided control population.

2.2.1.3 Resazurin assay

The resazurin assay is an indirect method of measuring cell viability. Metabolising cells reduce the amount of the oxidized form concomitantly with an

increase in the fluorescent intermediate, which is proportional to the number of viable cells. The assay therefore allows the rapid assessment of cell viability to a wide range of drug concentrations.

Briefly, cells (at a concentration of 0.5-1x10^4 cells per well) were cultured for 24h, 48h or 72h in 96 well plates in the presence of a serially diluted concentration of each drug, allowing for 12 different concentrations of each drug. Following culture, 50μM resazurin was added to each well and incubated at 37^{o}C for 4h. Plates were read at 535_{ex} and 590_{em} on a Spectramax M5 plate reader and analysed using SoftMax Pro software.

2.2.1.4 Cell counting and viability assessment

Cell counts were performed by trypan blue exclusion assay using a haemocytometer. 10μl of 0.4% trypan blue was added to 10μl of cells to give a 1:2 dilution from which 10μl was transferred to the haemocytometer. Cells were visualised with an inverted microscope using the 10X objective. Live and dead (blue) cells in four quadrants of the haemocytometer were counted allowing the absolute number of alive and dead cells per ml to be calculated.

Within the haemocytometer each 1mm^2 square equates to a volume of 0.1μl. The absolute cell count per ml was therefore calculated by counting the number of live cells per mm^2, dividing by the number of squares counted, multiplying by the trypan blue dilution factor (standardly 2) and then 10^4.

2.2.1.5 Synergy study

Synergism is the process by which two or more drugs are used in combination to achieve an enhanced effect (greater than the sum of the two drugs when used singly added together), for example, greater cell death. The drugs may target the same molecule or pathway through different mechanisms, or independent molecules or pathways. Further, drug synergism may allow for the use of lower doses of each drug within the combination, potentially reducing adverse reactions within the clinical setting.

In order to determine synergism, the combination effect must be greater than that which is expected from the individual drug's potencies. We used the Chou-Talalay method for drug combination based on the median-effect equation derived from the mass-action law principle (T. C. Chao & Martin, 2005). The combination index (CI) provides a quantitative definition for additive effect (CI = 1), synergism (CI < 1) or antagonism (CI > 1) in drug combinations.

Cells were seeded in 96 well plates at $1x10^4$ cells per well in media containing the test drug at varying concentrations. Two-fold serial dilutions were made with two concentration points above and below the inhibitory concentration (IC50) value (total 5 drug concentrations plus no drug and single drug controls). Cells were cultured for 72h then resazurin assay was done and data were analysed using CompuSyn software. Biological triplicates were performed.

2.2.1.6 Colony-Forming Unit assay

The CFU assay is an *in vitro* assay designed to quantify haematopoietic progenitor cells. The assay is based on the ability of haematopoietic progenitor cells to proliferate and differentiate into colonies in a semisolid media with adequate cytokine support. These colonies can be enumerated and characterised according to their unique morphology.

Methylcellulose was thawed at 4^{o}C overnight (Materials: Table 2.1.1.11). For each experimental arm a 3ml aliquot was placed into a sterile plastic vial using a 20ml syringe and brought to RT prior to use. Cell counts were performed to allow calculation of the volume of cells in media required for $1x10^4$ cells within each experimental arm. Cells were washed and resuspended in 200μl culture media (Materials: Table 2.1.1.9) then pipetted onto the 3ml methylcellulose aliquot and thoroughly mixed by inverting the tube several times. Due to the viscosity of the methylcellulose, to ensure equal division, 1.3ml was added to a 35mm tissue culture dish in duplicate. An additional 35mm culture dish containing sterile water was added to prevent culture drying. Samples were incubated for 10–14 days prior to characterising and counting the number of viable colonies using Olympus CKX41 Inverted microscope and a counting grid. The colony was defined as an aggregate of 40 or more cells (R&D, 2019) and was

categorised as CFU-G, CFU-M, CFU-GM, CFU-erythroid/Burst forming unit-erythroid (CFU-E/BFU-E), or CFU-GEMM as shown in Figure 2.2.1.6.1.

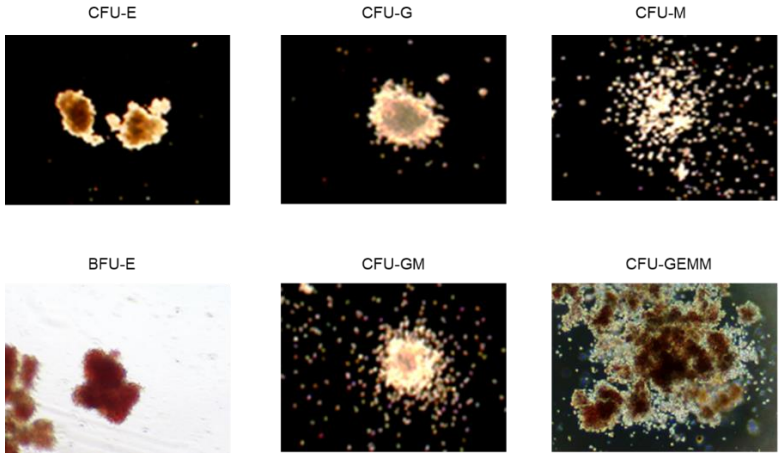

Figure 2.2.1.6.1 Colony types in the CFU assay. CFU-erythroid/Burst forming unit-erythroid (CFU-E/BFU-E). CFU-granulocyte (CFU-G). CFU-monocyte (CFU-M). CFU-granulocyte, monocyte (CFU-GM). CFU-granulocyte, erythrocyte, monocyte, megakaryocyte (CFU-GEMM).

2.2.2 Molecular studies

2.2.2.1 RNA extraction and quantification

Cells were harvested, lysed and RNA was prepared using the RNAeasy Plus Mini kit as per manufacturer's instructions.

Briefly, cells were suspended in the recommended volume for cell number of guanidine-thiocyanate-containing lysis buffer and homogenised using 26G needle. The homogenised lysate was passed through a genomic DNA removal column to remove DNA contamination. Following ethanol precipitation, the sample was added to a silica spin column that selectively binds RNA prior to washing with provided buffers to remove impurities. The column was then dried by centrifugation to remove ethanol and allow for a clean eluate. RNAse-free water was used to elute the RNA.

RNA concentration and quality were determined using a Nanodrop Spectrophotometer, using 2µl of the sample. 260nm quantifies nucleic acids. Absorbance was also recorded at 230nm and 280nm to determine purity (as a ratio to 260nm). Contamination was primarily due to protein, phenol or

carbohydrate contamination. Concentration was automatically calculated; pure RNA has an expected ratio of 2. RNA was stored at -80^{o}C until required.

2.2.2.2 cDNA synthesis

500ng of RNA was reverse transcribed to complementary DNA (cDNA) using the high-capacity cDNA reverse transcription kit according to manufacturer's instructions. This is a one-step reaction. Briefly, the mRNA, random primers and reverse transcription mixture were added to each reaction (Materials: Table 2.1.2.4.1). The 20µl sample was then cycled as outlined (Materials: Table 2.1.2.4.2).

For the purpose of reducing the false-negative results, random primers were used to ensure that the produced cDNA encompasses all regions of the mRNA. This increases the probability that 5´ends of the mRNA would be converted to cDNA as reverse transcriptase does not usually reach the 5´ends of long mRNAs. The cDNA produced for each gene is proportional to the mRNA from which it was produced.

2.2.2.3 Quantitative reverse transcription polymerase chain reaction (qRT-PCR)

qRT-PCR is a method to quantify mRNA expression (Wong & Medrano, 2005). The reactions can be performed using primers. Primers were designed in-house using National Center for Biotechnology Information (NCBI; https://www.ncbi.nlm.nih.gov/gene/)/Primer-Blast (https://www.ncbi.nlm.nih.gov/tools/primer-blast/). Briefly, the cDNA sequences of each gene of interest was identified through a Pubmed search and used to design primers. We aimed to design primers of approximately 20 base pairs with the forward and reverse primers having similar melting temperatures, ideally 60^{o}C.

2.2.2.3.1 SYBR^{TM} Green qRT-PCR

The SYBR Green dye was used to quantify the PCR products. This technique uses the SYBR Green dye to detect PCR products by binding to double-stranded DNA formed during PCR. When SYBR^{TM} Green dye is added to a sample, it immediately

binds to all double-stranded DNA present in the sample. During the PCR, DNA polymerase amplifies the target sequence, which creates the PCR products (amplicons). The SYBR™ Green dye then binds to each new copy of double-stranded DNA. As the PCR progresses, more amplicons are created. This results in an increase in fluorescence intensity proportionate to the amount of PCR product produced.

Briefly, the cDNA, primers and SYBR™ select master mix (Materials: Table 2.1.2.5.1) were added to each reaction. The 10µL reaction volumes were loaded onto 384-well plates, centrifuged and performed on a 7900 real-time PCR system. Standard thermal cycling conditions were used as per the manufacturer's instructions (Materials: Table 2.1.2.5.2). Data was acquired using SDS software and analysed using RQ manager.

The abundance or frequency of a gene of interest is measured by setting a threshold level of fluorescence. When the signal emitted by the reporter dye molecules for each gene of interest cross this point a positive, or real, signal is recorded. This is termed the cycle threshold (CT). The CT therefore represents the stage within the PCR reaction when real signal is detected over a background level. High frequency genes which cross the threshold early (after a low number of PCR cycles) will have a low CT value, with the reverse being true for low copy number genes that therefore have a high CT value.

Average CT values were calculated for each housekeeping internal control, which were then averaged to calculate the reference CT value. Average CT values for the genes of interest were calculated for each sample. Then, average CT value was subtracted from reference average to obtain ΔCT for each sample. The ΔΔCT values were calculated by subtracting ΔCT of the no drug control (NDC) from each treated sample. To show the variation between three biological replicates of calibrant samples, relative expression was shown using the $2^{-\Delta\Delta CT}$ (Rao, Huang, Zhou, & Lin, 2013).

2.2.2.3.2 Fluidigm™ qRT-PCR

The Fluidigm 48.48 Dynamic Array™ Integrated Fluidic Circuit (IFC) was used to assess the expression pattern of the genes in question. Fluidigm enables high

throughput large-scale, qRT-PCR. The design and structure of this system allows the samples and primer/probe mixes to be systematically combined into 2304 PCR reactions on 48.48 chips. Setting up a Fluidigm experiment involves four main steps: priming the chip, adding the samples (Materials: Table 2.1.2.6.5) and assays (Materials: Table 2.1.2.6.6) to the chip, loading and mixing samples and assays, and finally running the real-time experiment on the Biomark™ System.

The same principle as SYBR™ green qRT-PCR applies, though in this instance Evagreen served as the fluorescent label. The calculation step using CT values is described in Methods section 2.2.2.3.1.

2.2.2.3.2.1 Pre-amplification

Due to low-level expression of some target genes of interest, a pre-amplification step was carried out to increase the quantity of cDNA targets prior to gene expression analysis. Briefly, cDNA was incubated with a pre-amplification master mix, containing a pool of primers (Materials: Table 2.1.2.6.1). Pre-amplification was performed for target and reference genes as per manufacturer's instructions. Cycling conditions are detailed in Materials: Table 2.1.2.6.2. Residual unused primers were removed using an exonuclease I (Materials: Table 2.1.2.6.3). Cycling conditions are detailed in Materials: Table 2.1.2.6.4. Exonuclease I is used as it specifically digests single stranded DNA. The pre-amplified/exonuclease I treated cDNA was then diluted 1:5 in Tris-EDTA (TE) buffer and then stored at -20^{o}C until required.

2.2.2.3.2.2 qRT-PCR

qRT-PCR was performed using Fluidigm Biomark™ technology and data collected as per manufacturer's instructions. The 48.48 chip design was chosen (Figure 2.2.2.3.2.2.1). Briefly, the chip was first primed with line control fluid before the sample mixtures (Materials: Table 2.1.2.6.5) and the assay mixtures (Materials: Table 2.1.2.6.6) were loaded within 1h. Each chip is designed such that each sample is cycled with each primer from loading into a single well. Cycling conditions are detailed in Materials: Table 2.1.2.6.7. Internal sample control was ensured by subtracting the average of 6 housekeeping genes

(*ATP5F1B, B2M, CYC1, RNF20, TYW1 and UBE2D2*) from each gene of interest's CT value. Data were analysed using the $2^{-\Delta\Delta CT}$ method compared to NDC to show a fold change in expression (Rao et al., 2013).

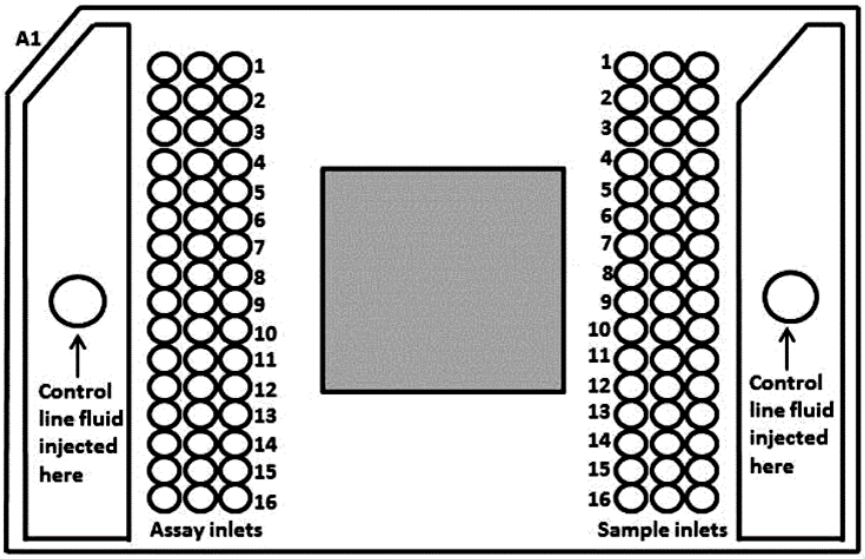

Figure 2.2.2.3.2.2.1 Illustration of a Fluidigm Biomark™ 48.48 chip.

2.2.3 Protein studies

2.2.3.1 Protein extraction and quantification

1-5x10^6 cells were harvested and washed twice in ice-cold PBS and pelleted at 300xg for 5min. After the second wash, pellets were incubated on ice for 30min with 1mM DIFP at a concentration of 1x10^6 cells per 10µl DIFP which prevents protein degradation of granulocytes during cell lysis process (Amrein & Stossel, 1980). Then, the pellets were lysed in ice-cold solubilisation buffer containing phosphatase and protease inhibitors at a concentration of 1x10^6 cells per 10µl solubilisation buffer (Materials: Table 2.1.3.2). This suspension was left on ice and vortexed every 15min for 1h, then centrifuged at 14000xg for 10min to pellet all cell debris. The supernatant was transferred to a fresh eppendorf and stored at -80^{o}C until required.

Protein concentration was quantified using the Quick Start™ Bradford Dye reagent and compared to a standard curve prepared using Quick Start™ BSA protein (Brady & Macnaughtan, 2015). This is a colorimetric protein assay based on the binding of Coomassie Brilliant Blue G-250 dye to protein and the

associated colour change from brown to blue this causes. This can be measured by visual absorbance on the Spectramax M5 plate reader at 595nm at using SoftMax Pro software.

2.2.3.2 Sample preparation for Western blotting

30µg of each cell lysate was added to appropriate amount of 10X NuPAGE™ sample reducing agent, 4X NuPAGE™ LDS sample buffer, NuPAGE™ antioxidant and ultrapure dH_2O. Sample lysates were heated to 70°C for 10min and then stored at -80°C until required.

2.2.3.3 Gel electrophoresis and protein transfer

Samples were electrophoresed using running buffer (Materials: Table 2.1.4.3) at 200V for 50min. NuPAGE™ 4-12% Bis-Tris protein gels were used to separate proteins smaller than 100kDa, whereas NuPAGE™ 3-8% Tris-Acetate protein gels were used to separate those larger than 100kDa. 0.5ml of NuPAGE™ antioxidant was added in the upper chamber within 15min before the electrophoresis.

The wet transfer method was used to transfer separated proteins to nitrocellulose membranes. Briefly, membranes and gels were saturated in cold transfer buffer with 20% methanol (Materials: Table 2.1.4.4), the gel was placed on top of the membrane and sandwiched between two 9cm x 6cm Whatman™ filter papers and 4-6 blotting pads. 0.5ml of NuPAGE™ antioxidant was added in the transfer cassette within 15min before the electroblotting. Transfer was performed at 25V on ice for 2h and membranes were stained with Ponceau S solution. Membranes were blocked with 5% milk or 3% BSA for 1h to prevent non-specific binding. Following blocking, the membrane was incubated with primary antibody (Materials: Table 2.1.4.8), and resuspended in blocking solution overnight with gentle agitation on a rocker. Unbound antibody was washed with TBST pH 7.5 (Materials: Table 2.1.4.5) three times; 5min for each wash. Secondary antibody, conjugated with infrared fluorescent dye (Materials: Table 2.1.4.9), was used at a dilution of 1:5000 and incubated for 1h. Secondary antibody was washed three times with TBST; 5min for each wash. Membranes were then placed in a tray before protein detection using the Odyssey™ Fc Imaging System. Densitometry was performed using Image Studio™ Lite software

version 5.2. For a normalisation of the densitometric analysis, the internal protein loading control was used and the adjusted densitometric unit (ADU) of treatment arms was calculated by the equation (Densitometric unit$_{(\text{internal protein loading control of NDC})}$/Densitometric unit$_{(\text{internal protein loading control of Treatment})}$) X Densitometric unit$_{(\text{Treatment})}$. The densitometry was presented as the average of the biological triplicates of fold change as compared with NDC i.e. an average of ADU$_{(\text{Treatment})}$/Densitometric unit$_{(\text{NDC})}$ and SD.

2.2.3.4 Re-probing immunoblots

The original bound antibody on nitrocellulose membranes was stripped using 1X stripping solution (Materials: Table 2.1.4.1), incubated at RT for 15-20min with agitation. The membranes were then blocked with 5% milk or 3% BSA for 10min and primary antibody was added as previously described.

2.2.4 Flow cytometry

Flow cytometry measures cell properties such as cell's size, granularity (internal complexity) and relative fluorescence intensity. An optical-to-electronic coupling system records how the cell scatters incident laser light and emits fluorescence. The principle of flow cytometry relies on the fluidic stream, which carries particles to the laser intercept to be visualised. Cells between 0.2-150μm in size are suitable for flow cytometry analysis (Hoogendoorn, 2019). Cell size is analysed using forward scatter (FSC); which is displayed on the x-axis and cellular granularity is analysed using side scatter (SSC), which is illustrated on the y-axis.

2.2.4.1 Apoptosis assessment

Apoptosis is a normal physiological process, essential for tissue homeostasis. It is characterised by certain features, including loss of membrane integrity, condensation of the cytoplasm and nucleus and internucleosomal DNA cleavage.

During the early stages of apoptosis, there is loss of membrane asymmetry with phospholipid phosphatidylserine (PS) translocating from the inner to the outer leaflet of the plasma membrane. It is this feature by which Annexin V can identify apoptotic cells. Annexin V, a calcium dependent phospholipid-binding

protein, has a high affinity for PS, binding to cells with exposed PS. When conjugated to fluorochromes, it can identify cells undergoing apoptosis by flow cytometry.

7-AAD and DAPI are nucleic acid stains distinguishing between viable and dead cells based on a loss of membrane integrity, being excluded from live cells.

2.2.4.1.1 Annexin V/7-AAD or Annexin V/DAPI staining

The principle of this experiment was to quantitatively determine the percentage of viable, early apoptotic, late apoptotic and dead cells. Cellular staining of Annexin V and 7-AAD, or Annexin V and DAPI, recording cell membrane integrity as a measure of cell viability. However, this assay is unable to distinguish between necrotic and apoptotic cell death.

Cells were harvested, washed twice with HBSS (Materials Table 2.1.5.4) and resuspended in HBSS. Fluorophore conjugated annexin V and 7-AAD or annexin V and DAPI antibodies were added (2µl of each per 100µl HBSS) and mixed well prior to incubation for 15min in the dark at RT. 300µl of HBSS was then added and the samples were analysed immediately using the BD FACSCanto™ II. $1x10^5$ events were recorded. Cell debris at the left side of the FSC-A/SSC-A plot and then clumped cells in the FSC-A/SSC-H plot were excluded, ensuring that only single cells were included in the analysis (Figure 2.2.4.1.1.1). Single-stained controls and an unstained sample were utilised to set voltages, compensation and gating. The same four rectangular gates were applied for all experimental arms.

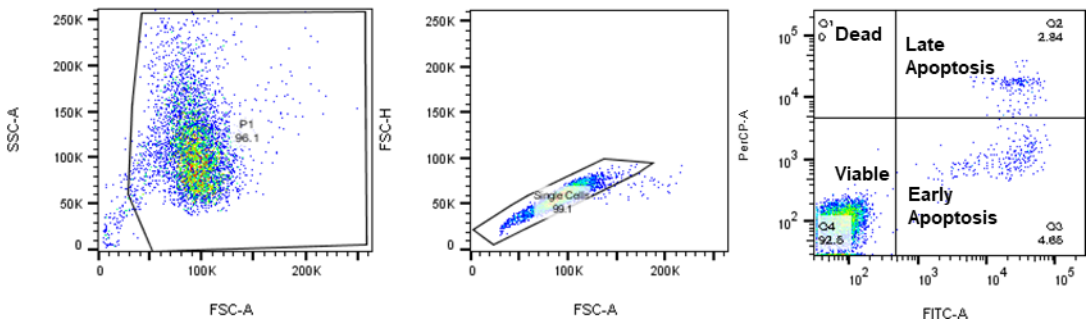

Figure 2.2.4.1.1.1 A Schematic presentation of the analysis of apoptosis assay

2.2.4.1.2 Active caspase-3 assay

Intracellular staining is needed for active caspase-3 assay. Cells were harvested and washed twice with PBS. Fixation and permeabilisation was performed using Cytofix/Cytoperm™ Fixation/Permeabilisation Solution Kit (Materials: Table 2.1.5.3) as per manufacturer's instructions. Briefly, 350µl fixation buffer was added to the pellets and incubated at 4ºC for 20min. The pellets were washed twice with 1ml permeabilisation buffer. Then, the pellets were resuspended in 40µl permeabilisation buffer and 10µl fluorophore conjugated active caspase-3 antibody was added and mixed well prior to incubation for 30min in the dark at RT. After that, the pellets were washed with 1ml permeabilisation buffer and resuspended in 400µl permeabilisation buffer. The samples were analysed immediately using the BD FACSCanto™ II. $1x10^5$ events were recorded. Cell debris at the left side of the FSC-A/SSC-A plot and then clumped cells in the FSC-A/SSC-H plot were excluded, ensuring that only single cells were included in the analysis (Figure 2.2.4.1.2.1). An unstained sample and isotype controls were utilised to set voltages and gating. Using same isotype control, the same range was applied for all experimental arms.

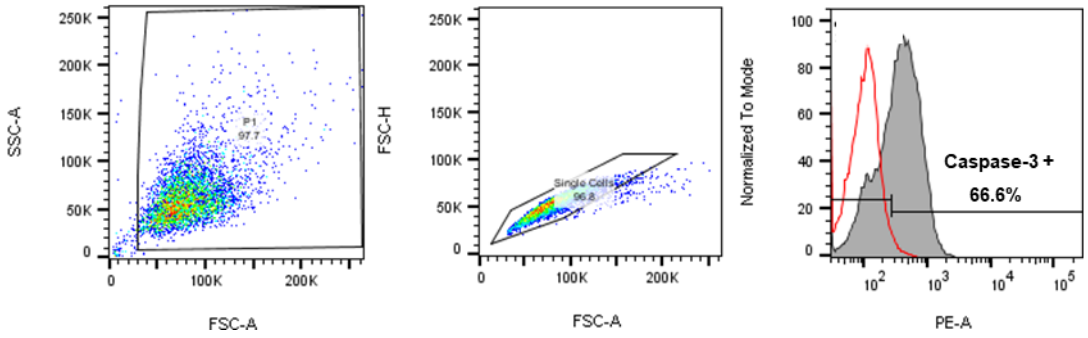

Figure 2.2.4.1.2.1 A Schematic presentation of the analysis of active caspase-3 assay. Red curve represents isotype control.

2.2.4.2 Cell cycle analysis

The principle of this experiment was to measure the proportion of cells progressing through the different stages of the cell cycle: Interphase (G0/G1, S, G2) and Mitosis (M) (Santo et al., 2015). PI is an intercalating agent, binding double stranded nucleic acids. PI is therefore capable of showing the increase in cellular DNA as the cell progresses through cell division prior to cell separation.

Cells are fixed in ethanol prior to undergoing staining in order to permeabilise the cell and allow the PI to enter and bind the DNA.

Briefly, cells were harvested, washed once with PBS, fixed in 1ml 80% ice-cold ethanol whilst gently vortexing to prevent cell clumping and stored for at least 24h at -20°C. Prior to analysis, the pellets were washed with PBS, resuspended in 500µl PI/RNase staining buffer (Materials: Table 2.1.5.8), vortexed for 30s and incubated for 15min at RT in the dark. Analysis was performed immediately using the BD FACSCanto™ II. $1x10^5$ events were recorded. Cell debris at the left side of the FSC-A/SSC-A plot and then clumped cells in the FSC-A/SSC-H plot were excluded, ensuring that only single cells were included in the analysis (Figure 2.2.4.2.1).For the analysis, in linear scale, a histogram was used to separate cells into Sub G0 which indicates apoptotic DNA fragmentation, G0/G1, S and G2/M according to the peaks and troughs seen in NDC. Determination of the width of peak was based on the peak border (Figure 2.2.4.2.1, arrows). Using FlowJo software for the analysis, the mean fluorescence intensity (MFI) of the G2/M peak was approximately double of the MFI of the G0/G1 peak, ensuring an accuracy of the analysis. Using NDC as a reference, the same width of peak was applied for all experimental arms.

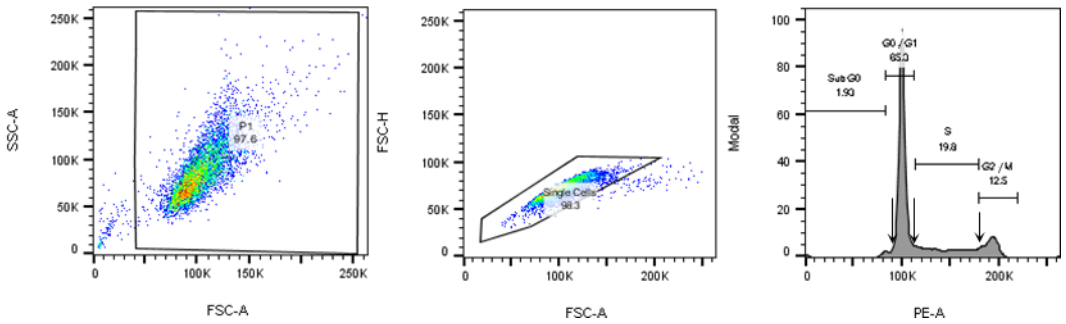

Figure 2.2.4.2.1 A Schematic presentation of the analysis of cell cycle.

2.2.4.3 Cell proliferation assay

In primary samples, CellTrace™ Violet was used as a tracing element in cell proliferation assay. The staining procedure is detailed in section 2.2.1.2.4. The cells were treated with CYC065, VEN, AraC, AZA, or the combinations for 72h. In the extra experimental arm, the cells were treated with colcemid (section 2.2.1.2.5). At 72h, simultaneously with apoptosis assay using Annexin V/7-AAD

which was detected in the FITC and PerCP channels, respectively, CellTrace™ Violet was detected in the Pacific Blue channel. In FSC-A/SSC-A plot, only viable cells were included and then clumped cells in the FSC-A/SSC-H plot were excluded, ensuring that only single cells were included in the analysis (Figure 2.2.4.3). For the analysis, in log scale, a histogram was used to trace the cell divisions. Colcemid-treated cells were used as a determinant for the position of an undivided control population (% Undivided; CTV_{max}). Determination of the width of the peak i.e. each cell division was based on the lowest points between two peaks (Figure 2.2.4.3.1, arrows). Using FlowJo software for the analysis, the MFI of the adjoining peak serially decreased by 50%, ensuring an accuracy of the analysis. Using NDC as a reference, the same width of peak was applied for all experimental arms. For normalisation, the relative fold change of the percentage of each cell division (% Div) was calculated as compared with NDC i.e. % $Undivided_{(Treatment)}$/ % $Undivided_{(NDC)}$, % $Div1_{(Treatment)}$/% $Div1_{(NDC)}$, % $Div2_{(Treatment)}$/% $Div2_{(NDC)}$, and % $Div{\geq}3_{(Treatment)}$/% $Div{\geq}3_{(NDC)}$. Then, the relative fold changes of % Div of all samples were averaged for each cell division individually (Toofan et al., 2018). Finally, means and SD of the relative fold change of % $Div_{(Treatment)}$ as compared with NDC were presented as stacked bars for each cell division (Figure 5.5.6.1C-H).

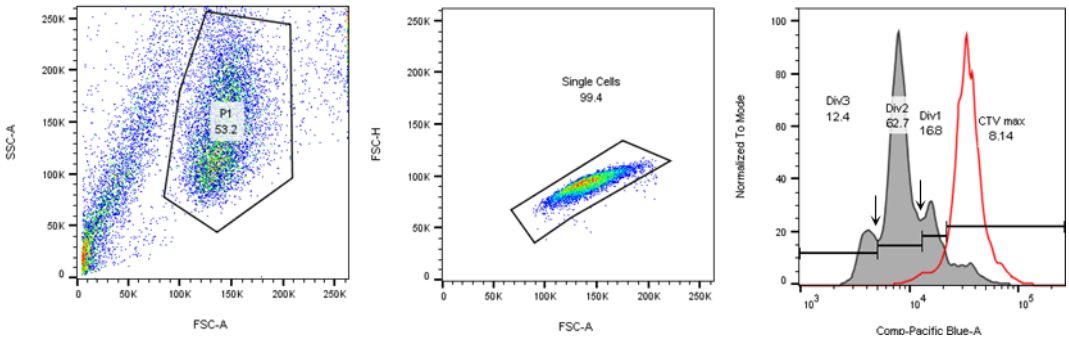

Figure 2.2.4.3.1 A Schematic presentation of the analysis of cell proliferation assay. Red curve represents colcemid-treated cells which were used as an undivided control population (CTV_{max}).

2.2.5 Pamgene™ multiplex STK activity profiling

As CYC065 has been designed to inhibit CDK2 and CDK9 activity, a high throughput STK activity profiling technique, the PamChip™ array (https://www.pamgene.com/), was used to assess kinases at an activity level (Moreira et al., 2018; Noé et al., 2019; Rosenberger et al., 2016). Specific target peptides of serine/threonine kinases are printed onto the arrays in spots and FITC-conjugated antibodies are used to quantify the phosphorylation signal by quantifying the image pixel brightness at each spot. To capture the kinetic of the reactions, the sample fluid is pumped during several cycles. Images are taken at fixed cycle intervals over the course of a reaction at varying camera exposure times.

2.2.5.1 Sample preparation

Briefly, $1x10^6$ cells were harvested, washed twice in ice-cold PBS and pelleted at 300xg for 5min. 100µl lysis buffer (Materials: Table 2.1.6.4) was added to the pellets and incubated on ice for 15min, then centrifuged at 14000xg for 10min to pellet all cell debris. The supernatant was transferred to a pre-cooled eppendorf and stored at -80°C until required. Protein concentration was quantified using the Quick Start™ Bradford Dye reagent as described in section 2.2.3.1.

2.2.5.2 STK activity profiling using PamChip™ and PamStation™ 12 system

PamChip™ arrays consist of 144 distinct peptides, each composed of 12–15 amino acids, with one or more phospho-sites. Upon incubation with a biological sample, this technology enables measurement of kinase activity using phosphorylated peptides as the readout.

Briefly, using the PamStation™ 12 machine and Evolve software version 1.2 (Materials: Table 2.1.6.1), the arrays on the STK PamChip™ (Materials: Table 2.1.6.1) were incubated with blocking solution (Materials: Table 2.1.6.3) for 30 cycles to prevent non-specific binding. The arrays were washed three times with kinase assay buffer (50mM Tris-HCl pH 7.5, 10mM $MgCl_2$, 1mM EGTA, 2mM DTT, 0.01% Brij™ 35). The sample mixture (Materials: Table 2.1.6.3) contained 0.01% BSA in kinase assay buffer supplemented with anti-phospho serine/threonine

antibodies. 1µg of protein was used, and the enzymatic assay was started by adding 100µM ATP. All sample mixtures in a total assay volume of 40µl were then applied to the arrays. The incubation mixture was pumped up and down through the porous membrane for 60 cycles. After washing of the arrays with PBST buffer (0.5% Tween™ 20/PBS), they were incubated for 1h with the detection mixture containing FITC-conjugated secondary antibody (Materials: Table 2.1.6.3).

Peptide phosphorylation was recorded after adding the secondary antibody by assessing fluorescence with a CCD camera at various exposure times (20, 50, 100 and 200ms). Raw images acquired by the camera were directly used as input of this package. One reference image was selected to detect the centres of peptide spots as well as the right and left controls. At this step, QC images showing the radius of the spots overlaid onto raw images were generated. The centres of the spots were used thereafter with the chosen radius to draw a circle on each spot, inside which the pixel brightness values were captured. The values were normalised by subtracting a background using the mean of background control spots.

2.2.5.3 Data analysis

Nominal coefficient of variation (CV) was calculated per peptide using a two-component error fit model. The CV was used as a filter to remove low intensity spots i.e. only peptides that showed nominal CV lower than 0.5 were included in the analysis. Log fold change (LFC) was calculated by the equation log2 Signal(Treatment/NDC) where signal is the pixel brightness values.
For each cell line, the experiments were done in triplicate. Comparing the profiles of CYC065-treated group with NDC, the student's t-tests were used to identify any statistically significant differences between fluorescence intensities of peptide spots. Identification of affected putative upstream kinases was performed from the peptide list using the UpKin upstream kinase prediction tool based on the Kinexus database, PamApp, in BioNavigator63 software (Materials: Table 2.1.6.1) in which a normalised kinase statistic score and specificity score were calculated. The results were displayed in kinase score plots.

2.2.6 Statistical analysis

All statistical analyses were performed using GraphPad Prism version 8. Experiments were performed at least 3 times, with 1 representative experiment shown in the results. Error bars represent the mean plus or minus standard deviation (SD). The student's t-test was used when two groups were compared. The one-way ANOVA was used to analyse multiple groups. Significant *P*-values are indicated by asterisks (****< 0.0001, *** 0.0001 to < 0.001, ** 0.001 to < 0.01, * 0.01 to < 0.05 and NS (not significant) if $P \geq 0.05$). The F distribution is a right-skewed distribution used most commonly in ANOVA. When referencing the F distribution, the numerator degrees of freedom (i.e. the number of different groups -1, $df_{\text{numerator}}$) were given first and the denominator degrees of freedom (i.e. total number of all the values combined - the number of different groups, $df_{\text{denominator}}$) were given second i.e. F ($df_{\text{numerator}}$, $df_{\text{denominator}}$). The critical values for an F distribution were generated by the GraphPad Prism software and were automatically compared with the reference values in F Table for alpha = 0.05 where $df_{\text{numerator}}$ is the column number and $df_{\text{denominator}}$ is the row number. The critical value which is greater than the reference value in the F table is considered as statistically significant which means that the differences between means of the groups compared are significantly different.

Chapter 3 Effects of CYC065 on growth and survival of AML cells, target proteins, and gene expression

3.1 Introduction

AML is one of the most common haematological malignancies, characterised by the clonal expansion of abnormal or poorly differentiated myeloid cells infiltrating the BM, blood or extramedullary tissues (H. Döhner et al., 2015). Although the treatment of AML has improved over the past few decades, in some patients, particularly elderly patients, usually defined as older than 60-65 years of age, the outcome is dismal due to the remarkable genetic complexity, epigenetic alterations, and the dynamics of the disease. TRM and resistance to chemotherapy are two major causes of treatment failure and early death. Older people are prone to poor tolerability to intensive chemotherapy because of the presence of comorbid disease, decreased ability for clearance of chemotherapy, poor performance status and susceptibility to systematic bacterial and fungal infections (Klepin & Balducci, 2009). However, longer life expectancy and possibly a cure are expected if a CR is achieved in elderly AML patients. Therefore, there are many efforts to improve the standard regimen aiming to lessen adverse drug effects e.g. intensity reduction, drug combinations, or introducing a new class of targeted therapy, to improve outcome.

Currently, several novel agents, acting through various molecular targets of AML have been introduced to combine with conventional chemotherapy or as a single agent. These include CDKI, which result in cell cycle arrest and induce apoptosis. Alvocidib, is the first pan-CDKI introduced for clinical trials in humans (Shafer & Grant, 2016), potently inhibiting at least CDKs 1, 2, 4/6, 7 and 9, as well as a number of other protein kinases (Montagnoli et al., 2008; Sedlacek, 2001). The combination regimen of alvocidib, cytarabine plus mitoxantrone (FLAM) was developed (Karp et al., 2010). A phase 2 study was conducted and revealed that there was a statistically significant higher efficacy of FLAM compared to the standard “7+3” regimen in terms of CR rate. However, improvements in terms of the overall survival and event-free survival rates were not observed (Zeidner et al., 2015, 2018). It was hypothesised that more specific target inhibition may be a solution, consequently more selective CDKIs have been developed. Seliciclib (Cyclacel Pharmaceuticals) is the second CDKI to enter clinical trials in humans (Bose et al., 2013). It is orally bioavailable inhibitor of CDKs 2, 7, and 9 (Boffo et al., 2018). Currently, seliciclib is in phase

2 studies for the treatment of lung cancer and nasopharyngeal cancer (Raje et al., 2005).

The second generation CDKI CYC065 (Cyclacel Pharmaceuticals) is an orally available 2,6,9-trisubstituted purine analogue which is designed to selectively bind to the ATP-binding site of CDK2 and CDK9 (Cyclacel, 2016) (Figure 3.1.1). Direct inhibition of CDK2 leads to G1 arrest (H. Liu, Li, Huo, Wei, & Ge, 2020; Pellerano et al., 2017) and apoptosis (Faber & Chiles, 2007; H. Liu et al., 2020; Neganova et al., 2011). The blockade of CDK9 halts RNAPII transcriptional activity and, consequently, induces apoptosis (Morales & Giordano, 2016). Indeed, inhibiting CDK9 results in a downregulation of anti-apoptotic protein MCL-1 (Gregory et al., 2015; Karp et al., 2005; H. Ma, Seebacher, Hornicek, & Duan, 2019; Polier et al., 2011; Walsby et al., 2014; Yin et al., 2014). It has been reported that inhibiting CDK9 results in global transcriptional suppression (Fischer & Gianella-Borradori, 2005). Therefore, the transcripts with short half-lives are majorly targeted, including the anti-apoptotic MCL-1 which is shown to be critical for the survival of AML (Glaser et al., 2012).

Currently, a phase 1 clinical study of CYC065 has been performed in patients with lung and breast cancer using a drug dose range of 8 to 288mg/m^2/d, administered as a 4-h intravenous infusion once every three weeks. Dose limiting toxicities were reversible, these included neutropenia, febrile neutropenia and diarrhoea (Cyclacel, 2018). A biologically effective dose was 192mg/m^2/d which corresponds to the drug concentration of 6-7μM *in vitro* (Do et al., 2018). In part 2 and 3 of this clinical trial, a more intensive schedule on days 1, 2, 8 and 9 of a three-week cycle has been evaluated in seventy patients with advanced solid tumours or lymphomas (NCT02552953).

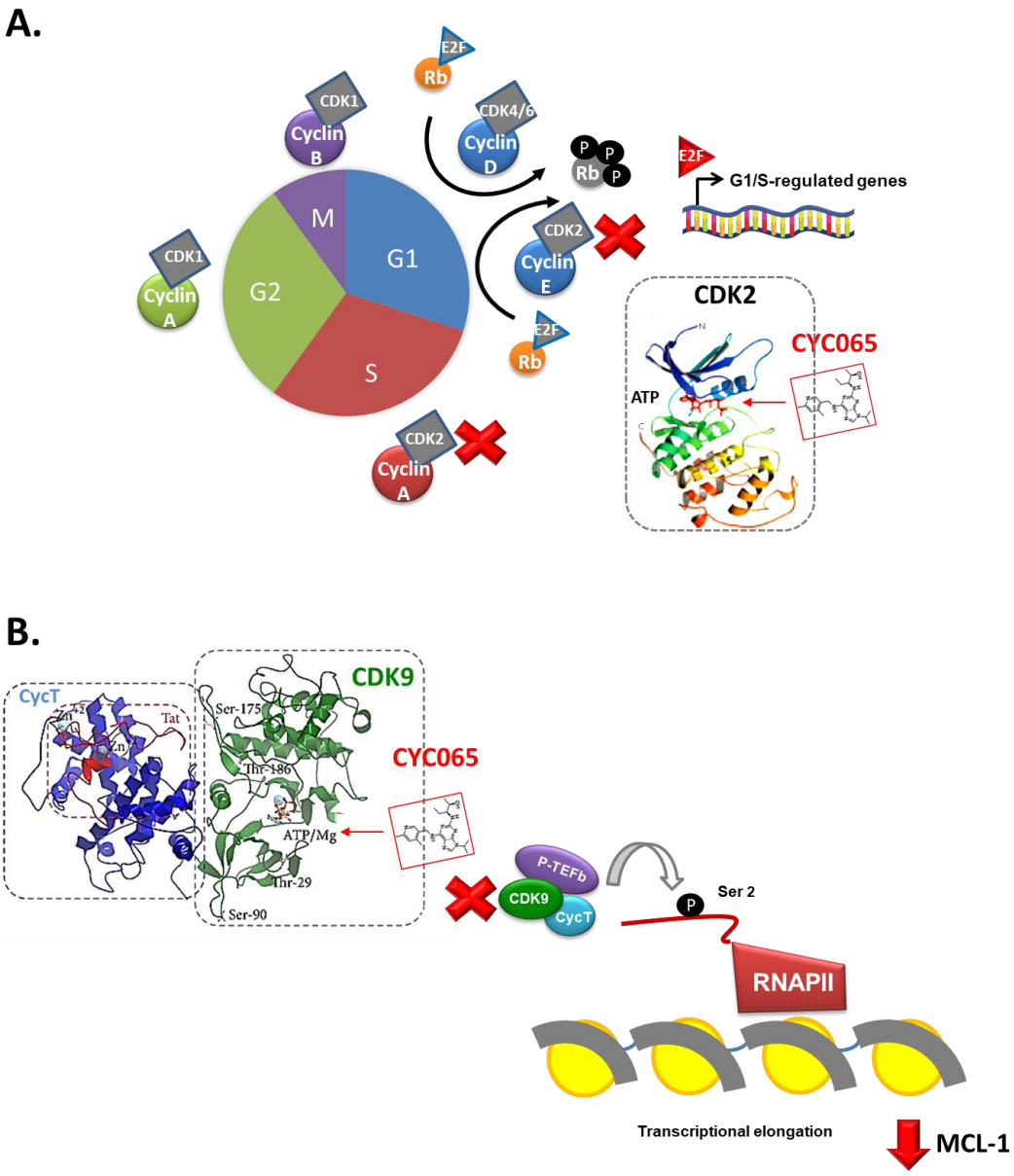

Figure 3.1.1 A schematic diagram demonstrating primary target inhibition of CYC065 (Nekhai, Petukhov, & Breuer, 2014; Ubersax & Ferrell, 2007).
CYC065 is designed to selectively bind to the ATP-binding site which inhibits the activities of (A) CDK2 which results in G1 arrest and apoptosis; and (B) CDK9 which results in an inactivation of RNAPII transcriptional elongation targeting the transcripts with short half-lives, in particular, MCL-1.

The aims of the experiments in this chapter are:

i) to assess the effects of CYC065 on growth and survival of AML cells

ii) to demonstrate target inhibition and characterise the mechanism of action of CYC065 *in vitro*

iii) to assess the effects of CYC065 on gene expression *in vitro*

3.2 Effects of CYC065 on growth and survival of AML cells

In this study, OCI-AML3, MOLM-13 and MV4-11 cell lines were chosen for preliminary study to assess the effects of CYC065 on growth and survival of AML cell lines using various methods, including; resazurin reduction, trypan blue exclusion, apoptosis, active caspase-3 assays, and cell cycle analyses.

3.2.1 Longer exposure increased CYC065 sensitivity and reduced the IC50

The IC50 of CYC065 in each cell line was assessed by resazurin reduction assays at 24h, 48h, and 72h. The IC50 for OCI-AML3 was approximately 0.69±0.07μM, 0.59±0.04μM, and 0.44±0.01μM for 24h, 48h, and 72h, respectively (Figure 3.2.1.1A). The IC50 for MOLM-13 was approximately 0.62±0.02μM, 0.31±0.06μM, and 0.25±0.01μM for 24h, 48h, and 72h, respectively (Figure 3.2.1.1B). The IC50 for MV4-11 was approximately 0.64±0.03μM, 0.56±0.01μM, and 0.52±0.01μM for 24h, 48h, and 72h, respectively (Figure 3.2.1.1C). Longer exposure to the drug increased sensitivity and reduced the IC50. Rationally, a range of doses were chosen based on the lowest IC50 at 72h of 0.25μM and 1μM to investigate further in the subsequent experiments.

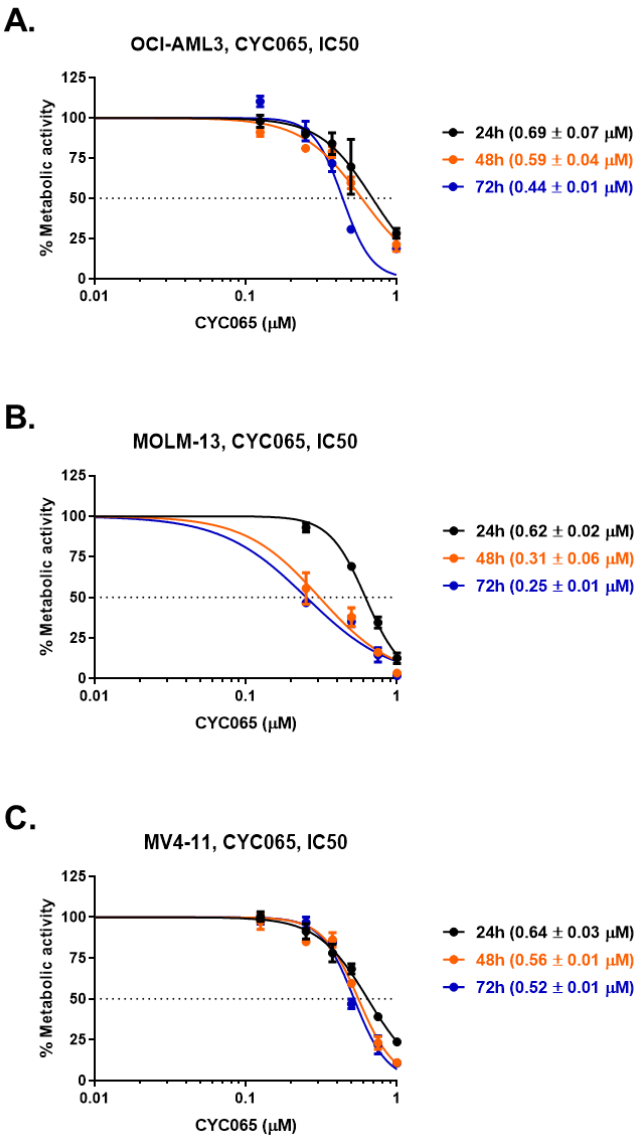

Figure 3.2.1.1 The IC50 of CYC065 at 24h, 48h and 72h in (A) OCI-AML3, (B) MOLM-13, and (C) MV4-11 cell lines using rezasurin reduction assays. The experiments were performed in technical and biological triplicates. Dots depict means ± SD.

3.2.2 A decreased number of viable cells was observed across higher CYC065 concentrations

AML cell lines were treated with various concentrations of CYC065 for up to 72h. Cell count was assessed by trypan blue exclusion assay at 24h, 48h and 72h in OCI-AML3 (Figure 3.2.2.1A), MOLM-13 (Figure 3.2.2.1B) and MV4-11 (Figure 3.2.2.1C) cell lines. It was observed that viable cell number was inversely correlated with CYC065 concentration, with cell viability decreasing as CYC065 concentration increased, particularly at the highest dose used of 1µM. Cell number was continuously increased over the period of seeding time to 72h but a greater growth inhibition was observed with increasing CYC065 concentration.

This effect was observed in all cell lines. As observed with the lower IC50s obtained for MOLM-13, 0.25µM markedly suppressed growth with higher dose of 0.5µM necessary to achieve a similar level of growth suppressing in OCI-AML3 and MV4-11, indicating that MOLM-13 are more sensitive to the drug. Of note, at 1µM of CYC065, a very low cell number seen in all AML cell lines tested indicated that the effect of CYC065 is beyond cell cycle arrest, resulting in cell toxicity.

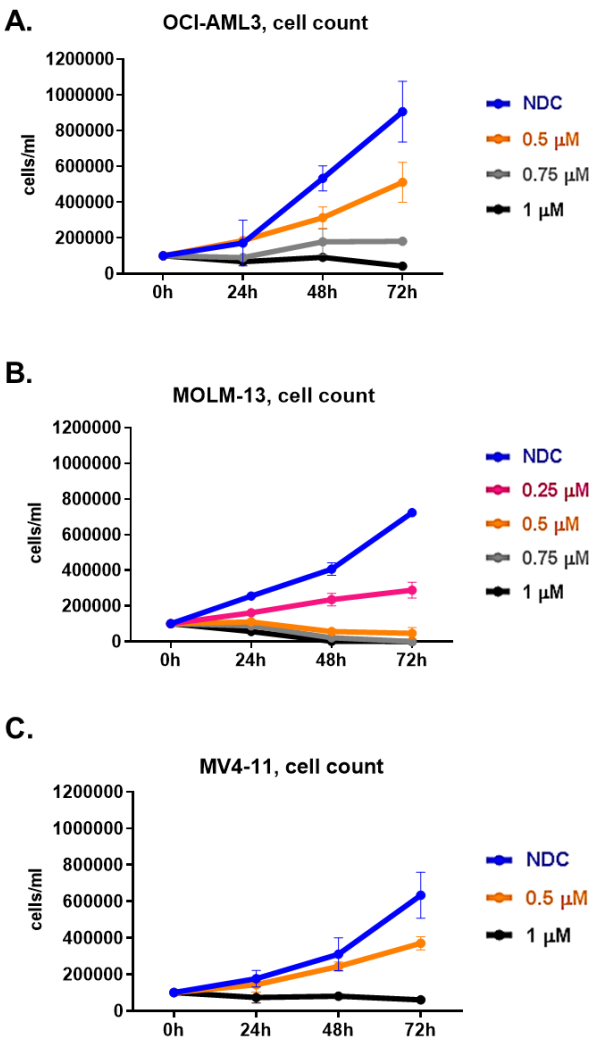

Figure 3.2.2.1 Cell count assessed by trypan blue dye exclusion of (A) OCI-AML3, (B) MOLM-13, and (C) MV4-11 cell lines treated with various concentrations of CYC065 for 24h, 48h and 72h. The experiments were performed in biological triplicates. Dots depict means ± SD.

3.2.3 Apoptosis increased as CYC065 concentration increased

AML cell lines were treated with various concentrations of CYC065 for up to 72h. Apoptosis assays using annexin V/DAPI staining were performed at 24h, 48h and 72h. Representative flow cytometry plots and flow cytometric analysis are shown in Figure 3.2.3.1. As compared with NDC, the percentage of viable cells was statistically significantly decreased with increasing CYC065 concentrations in OCI-AML3 (Figure 3.2.3.1A,B), MOLM-13 (Figure 3.2.3.1C,D), and MV4-11 cell lines (Figure 3.2.3.1E,F). As compared to the IC50 by resazurin reduction assay (section 3.2.1), a higher CYC065 concentrations were required for an induction of apoptosis in 50% of the cells for all three cell lines; 0.75μM in OCI-AML3, 0.5μM in MOLM-13, and 1μM in MV4-11 cell lines, respectively at 72h, with MOLM-13 cells being more sensitive to CYC065 treatment in line with the previous findings. Collectively, cell death was induced in all AML cell lines tested at 24h and completed at 72h following treatment with CYC065 in a dose-dependent manner.

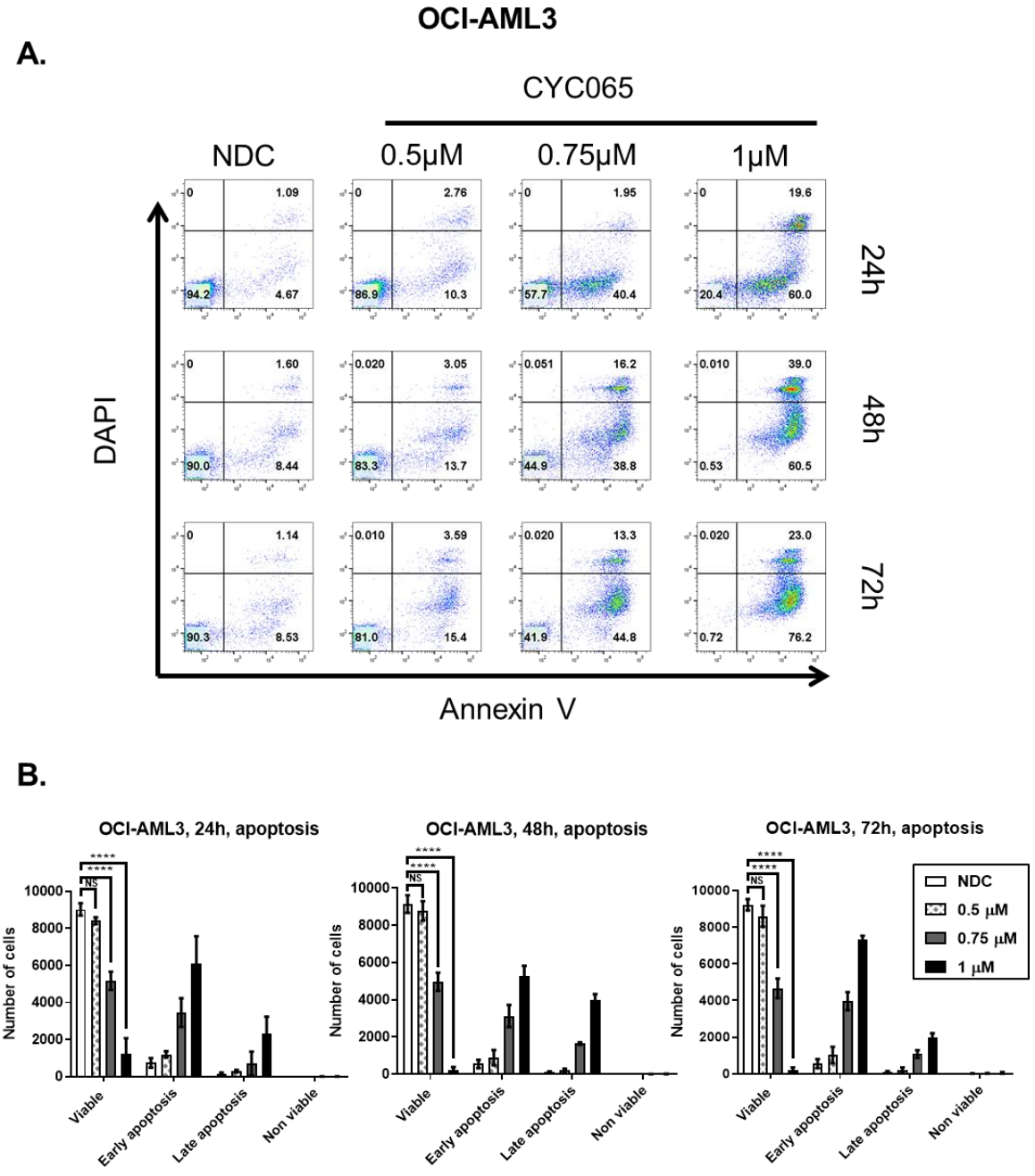

Figure 3.2.3.1 (A) Representative flow cytometry plots; and (B) Flow cytometric analysis of apoptosis assays using annexin V/DAPI of OCI-AML3 cell line treated with various concentrations of CYC065 for 24h, 48h and 72h. The experiments were performed in biological triplicates. Graphs depict means ± SD. Cell viability was compared using the one-way ANOVA, post hoc Dunnett's test ($F(3,8) = 142.7$, $P < 0.0001$, 24h; $F(3,8) = 271.6$, $P < 0.0001$, 48h; $F(3,8) = 285$, $P < 0.0001$, 72h). Significant *P*-values are indicated by asterisks (****< 0.0001, *** 0.0001 to < 0.001, ** 0.001 to < 0.01, * 0.01 to < 0.05 and NS if $P \geq 0.05$).

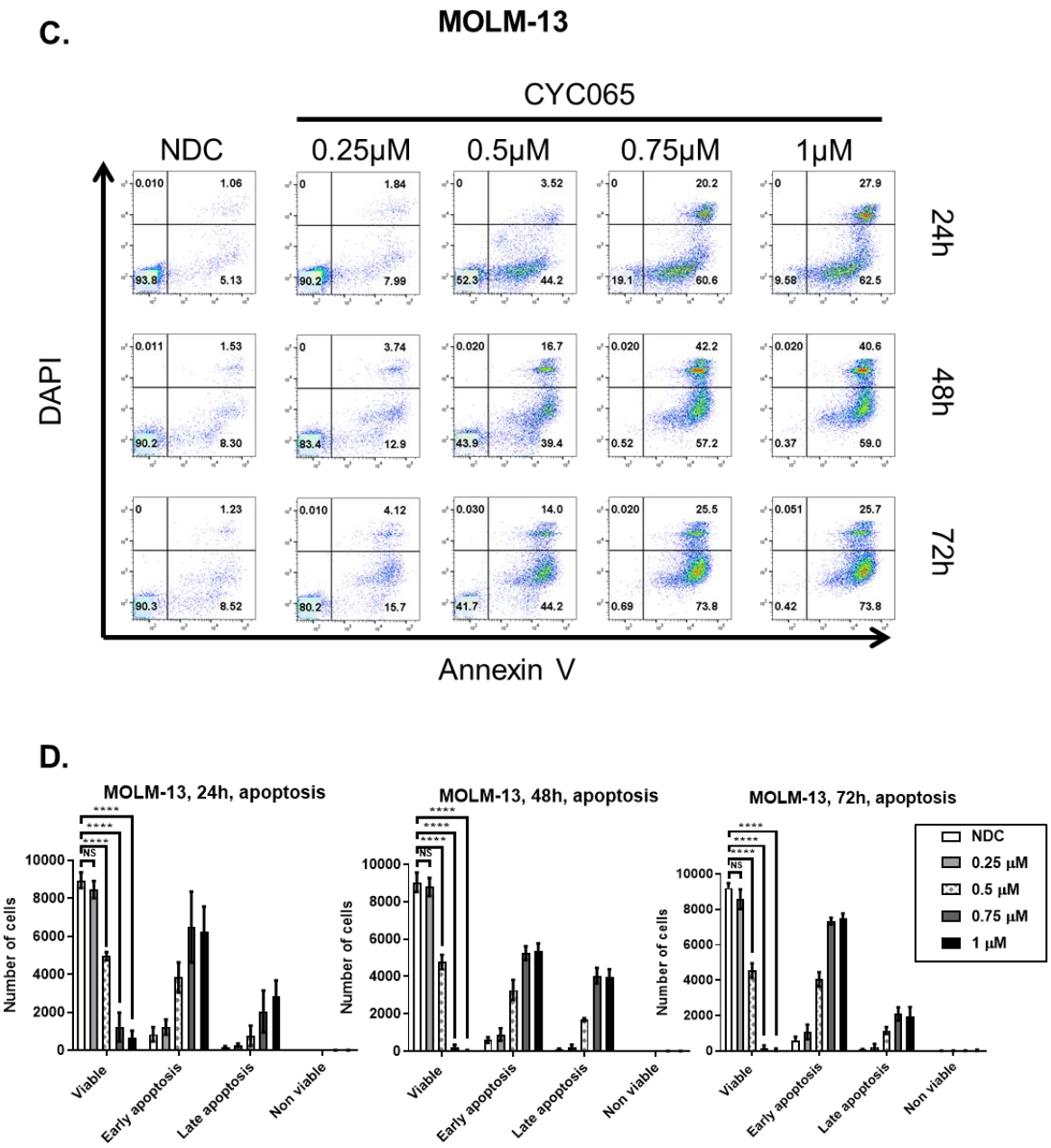

Figure 3.2.3.1 (C) Representative flow cytometry plots; and (D) Flow cytometric analysis of apoptosis assays using annexin V/DAPI of MOLM-13 cell line treated with various concentrations of CYC065 for 24h, 48h and 72h. The experiments were performed in biological triplicates. Graphs depict means ± SD. Cell viability was compared using the one-way ANOVA, post hoc Dunnett's test ($F(4,10) = 202$, $P < 0.0001$, 24h; $F(4,10) = 427.9$, $P < 0.0001$, 48h; $F(4,10) = 493.2$, $P < 0.0001$, 72h). Significant P-values are indicated by asterisks (****< 0.0001, *** 0.0001 to < 0.001, ** 0.001 to < 0.01, * 0.01 to < 0.05 and NS if $P \geq 0.05$).

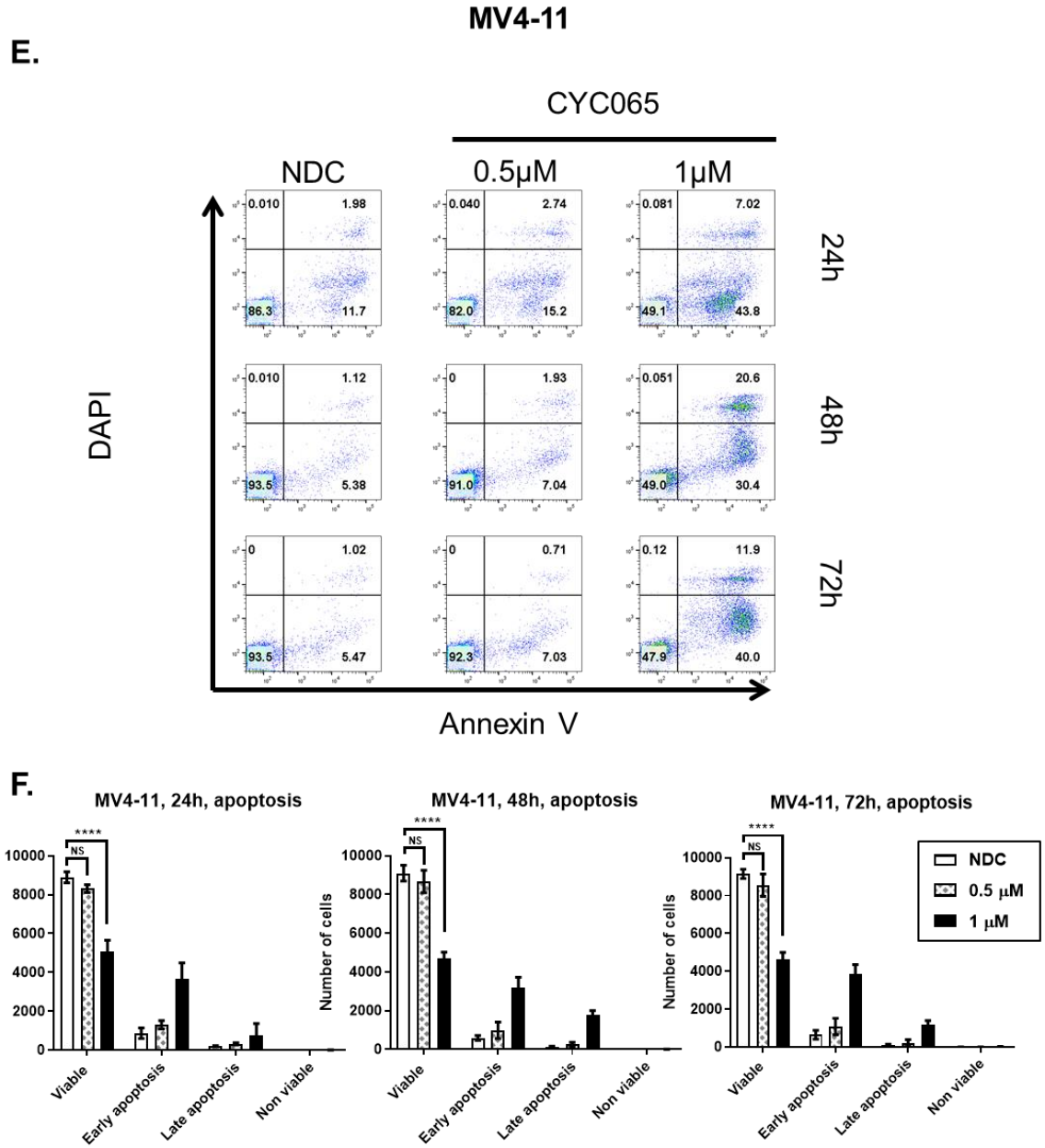

Figure 3.2.3.1 (E) Representative flow cytometry plots; and (F) Flow cytometric analysis of apoptosis assays using annexin V/DAPI of MV4-11 cell line treated with various concentrations of CYC065 for 24h, 48h and 72h. The experiments were performed in biological triplicates. Graphs depict means ± SD. Cell viability was compared using the one-way ANOVA, post hoc Dunnett's test ($F(2,6) = 85.9$, $P < 0.0001$, 24h; $F(2,6) = 87.1$, $P < 0.0001$, 48h; $F(2,6) = 96.4$, $P < 0.0001$, 72h). Significant *P*-values are indicated by asterisks (****< 0.0001, *** 0.0001 to < 0.001, ** 0.001 to < 0.01, * 0.01 to < 0.05 and NS if $P \geq 0.05$).

3.2.4 An increase in the percentage of active caspase-3-positive cells was observed with increasing CYC065 concentration

In order to confirm CYC065 was inducing early apoptosis in cells, flow cytometry was performed to measure the effector caspase, caspase-3. Active caspase-3 assays were performed at 24h, 48h, and 72h along with apoptosis assays aiming to support the results in section 3.2.3. Representative flow cytometry plots and

flow cytometric analysis are shown in Figure 3.2.4.1. As compared with NDC, it was observed that the percentage of active caspase-3-positive cells was statistically significantly increased with increasing CYC065 concentration in OCI-AML3 (Figure 3.2.4.1A,B), MOLM-13 (Figure 3.2.4.1C,D), and MV4-11 cell lines (Figure 3.2.4.1E,F). Active caspase-3 was present in approximately 50% of the cell population when OCI-AML3, MOLM-13, and MV4-11 cell lines were treated with 0.75μM, 0.5μM, and 1μM of CYC065, respectively at 72h, which is consistent with the annexin V/DAPI apoptosis assays. Hence, following treatment with CYC065, an activation of apoptosis pathway was indicated in a dose-dependent manner.

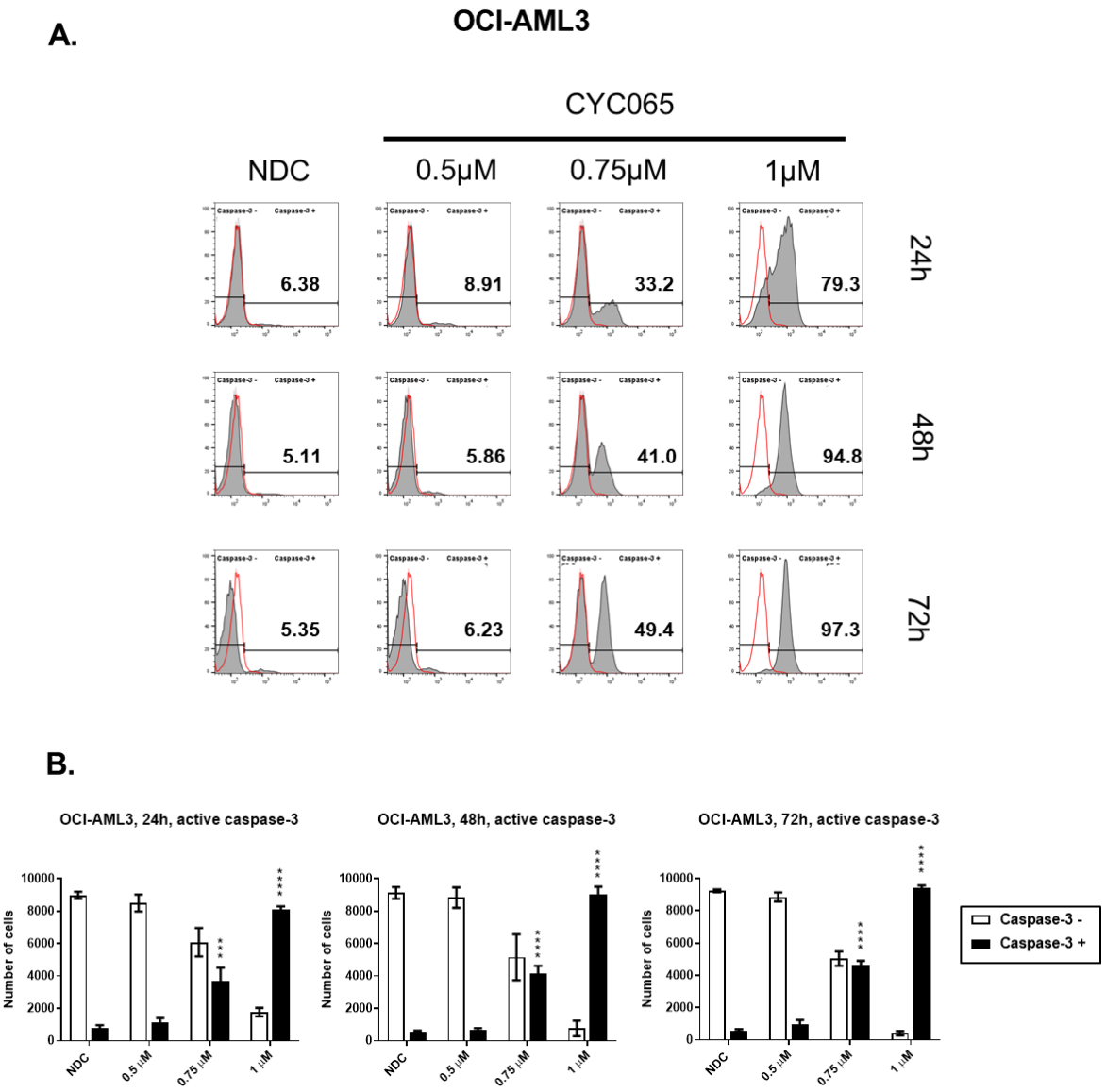

Figure 3.2.4.1 (A) Representative flow cytometry plots of active caspase-3 assay in which red curves represent isotype controls are shown; and (B) Flow cytometric analysis of the percentage of active caspase-3-positive cells of OCI-AML3 cell line treated with various concentrations of CYC065 for 24h, 48h and 72h. The experiments were performed in biological triplicates. Graphs depict means ± SD. Caspase-3-positive populations were compared using the one-way ANOVA, post hoc Dunnett's test (F (3,8) = 173.5, *P* < 0.0001, 24h; F (3,8) = 427.6, *P* < 0.0001, 48h; F (3,8) = 1012, *P* < 0.0001, 72h). Significant *P*-values are indicated by asterisks (****< 0.0001, *** 0.0001 to < 0.001, ** 0.001 to < 0.01, * 0.01 to < 0.05 and NS if *P* ≥ 0.05).

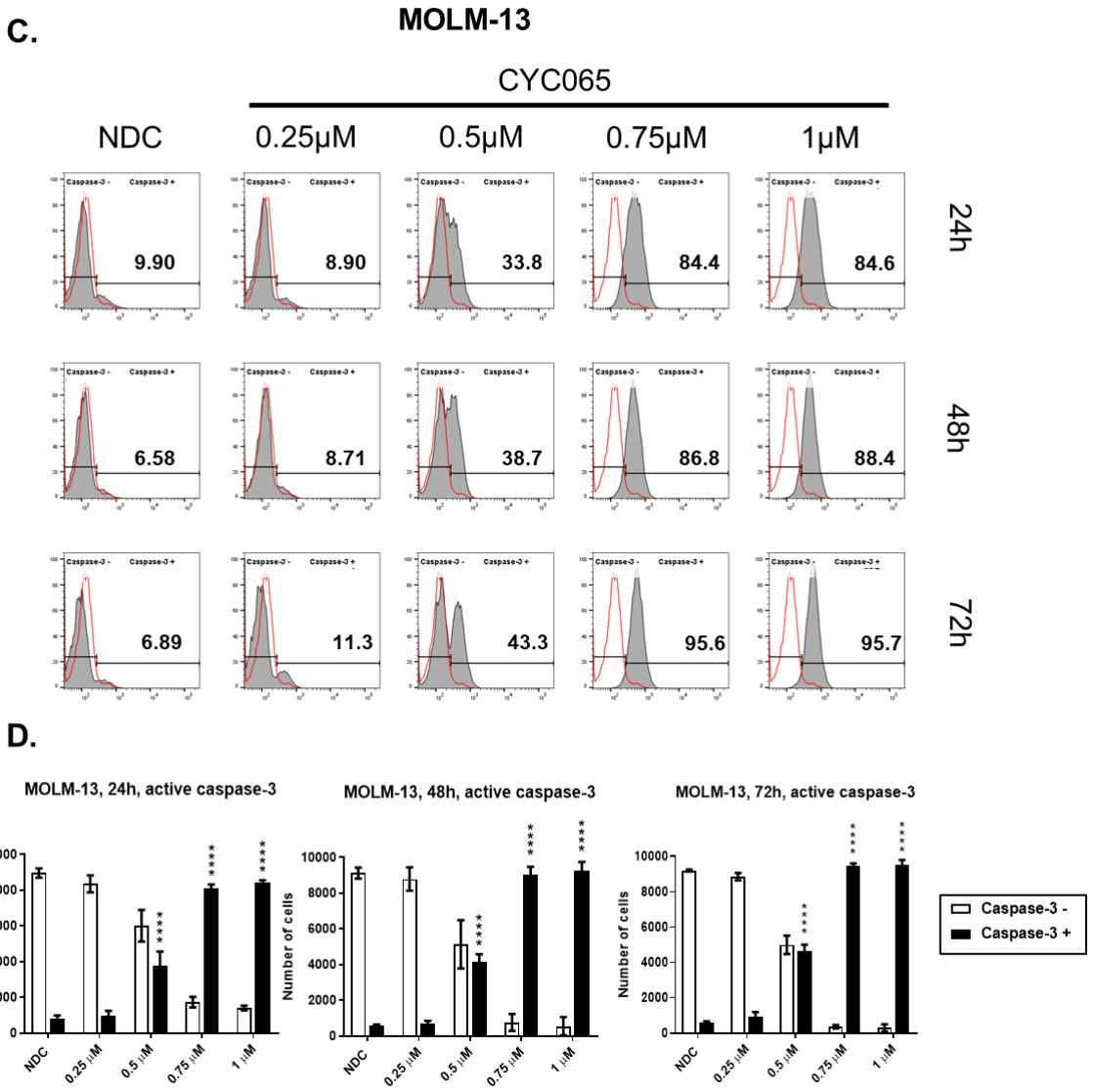

Figure 3.2.4.1 (C) Representative flow cytometry plots of active caspase-3 assay in which red curves represent isotype controls are shown; and (D) Flow cytometric analysis of the percentage of active caspase-3-positive cells of MOLM-13 cell line treated with various concentrations of CYC065 for 24h, 48h and 72h. The experiments were performed in biological triplicates. Graphs depict means ± SD. Caspase-3-positive populations were compared using the one-way ANOVA, post hoc Dunnett's test ($F(4,10) = 255.3$, $P < 0.0001$, 24h; $F(4,10) = 432.9$, $P < 0.0001$, 48h; $F(4,10) = 1060$, $P < 0.0001$, 72h). Significant *P*-values are indicated by asterisks (****< 0.0001, *** 0.0001 to < 0.001, ** 0.001 to < 0.01, * 0.01 to < 0.05 and NS if $P \geq 0.05$).

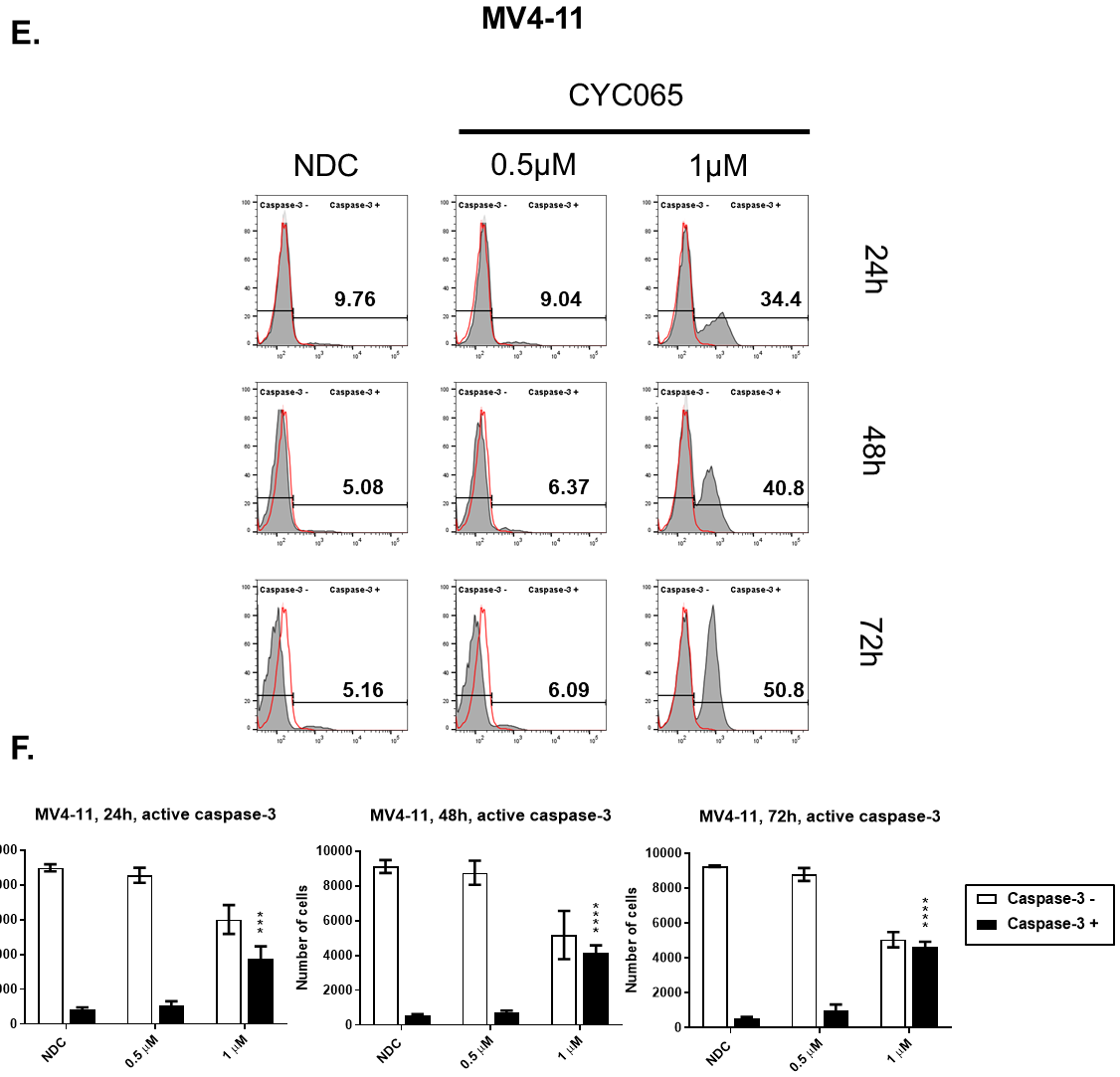

Figure 3.2.4.1 (E) Representative flow cytometry plots of active caspase-3 assay in which red curves represent isotype controls are shown; and (F) Flow cytometric analysis of the percentage of active caspase-3-positive cells of MV4-11 cell line treated with various concentrations of CYC065 for 24h, 48h and 72h. The experiments were performed in biological triplicates. Graphs depict means ± SD. Caspase-3-positive populations were compared using the one-way ANOVA, post hoc Dunnett's test ($F(2,6) = 40.9$, $P < 0.0001$, 24h; $F(2,6) = 161.6$, $P < 0.0001$, 48h; $F(2,6) = 200.7$, $P < 0.0001$, 72h). Significant *P*-values are indicated by asterisks (****< 0.0001, *** 0.0001 to < 0.001, ** 0.001 to < 0.01, * 0.01 to < 0.05 and NS if $P \geq 0.05$).

3.2.5 G1 arrest was observed at 4h in OCI-AML3 and MV4-11, but not MOLM-13 cell line, following CYC065 treatment

CYC065 inhibits CDK2 and CDK9, important kinases involved in cell cycle progression and transcription. Next, we aimed to assess the effect of CYC065 on cell cycle progression at an early timepoint, cell cycle analyses using PI staining was performed in AML cell lines following treatment with CYC065 for 4h. It was observed that the G0/G1 percentage was increased as compared with NDC, indicating G1 arrest in OCI-AML3 and MV4-11 cell lines following treatment with CYC065 at this early timepoint. By contrast, an increase in sub G0, without any other cell cycle phase, was observed in MOLM-13 cell line, indicating an induction of cell death rather than cell cycle arrest which is consistent with the data in section 3.2.1-3.2.4 showing that, compared with other cell lines, MOLM-13 cells are more sensitive to CYC065.

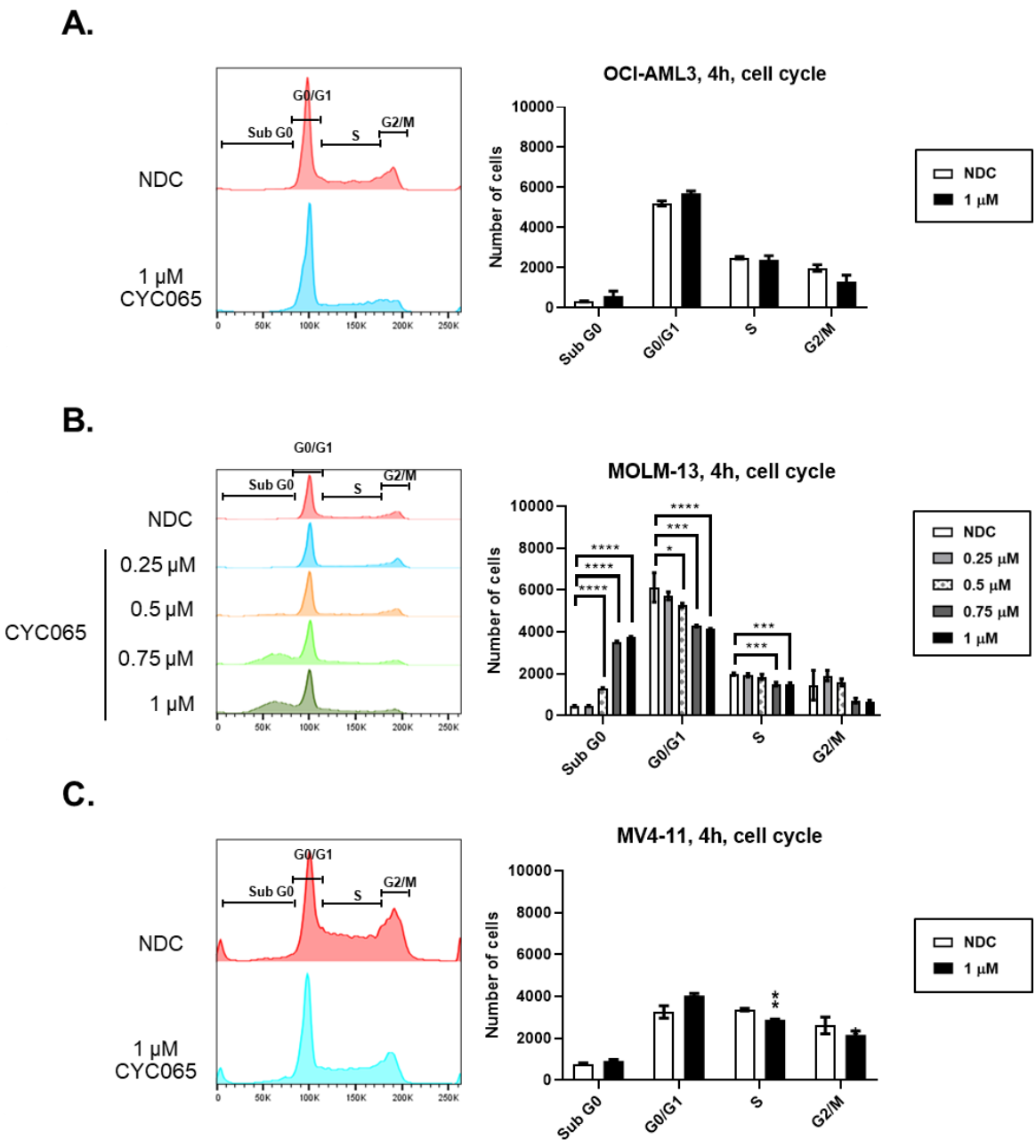

Figure 3.2.5.1 Representative flow cytometry plots and flow cytometric analysis of the cell cycle phase using PI staining of (A) OCI-AML3, (B) MOLM-13, and (C) MV4-11 cell lines treated with CYC065 for 4h. The experiments were performed in biological triplicates. Graphs depict means ± SD. Data were compared using the paired student's t-test OCI-AML3 and MV4-11 cell lines and the one-way ANOVA, post hoc Dunnett's test (Sub G0 populations; F (4,10) = 21.3, $P < 0.0001$) for MOLM-13 cell line. Significant *P*-values are indicated by asterisks (****< 0.0001, *** 0.0001 to < 0.001, ** 0.001 to < 0.01, * 0.01 to < 0.05 and NS if $P \geq 0.05$).

3.2.6 An increase in the percentage of sub G0, without an increase of any other cell cycle phase, was observed after 24h of CYC065 treatment

AML cell lines were treated with various concentrations of CYC065 for up to 72h. Cell cycle analyses using PI staining were performed at 24h, 48h and 72h. Representative flow cytometry plots and flow cytometric analysis are shown in Figure 3.2.6.1. An increase in sub G0 percentage (% Sub G0), which indicates an accumulation of apoptotic DNA fragmentation, was demonstrated across higher CYC065 concentrations, without an increase of any other cell cycle phase, indicating that cell death is fully induced after 24h in OCI-AML3 (Figure 3.2.6.1A,B), MOLM-13 (Figure 3.2.6.1C,D), and MV4-11 cell lines (Figure 3.2.6.1E,F). The results correlate with an increase in apoptosis (section 3.2.3) and the percentage of active caspase-3-postive cells observed (section 3.2.4). Collectively, in the less sensitive OCI-AML3 and MV4-11 cell lines, it can be concluded that CYC065 induced G1 arrest at the early timepoint (4h) (section 3.2.5), which was followed by cell death at 24h. By contrast, in the more sensitive MOLM-13 cell line, the drug induced apoptosis from the beginning of the treatment.

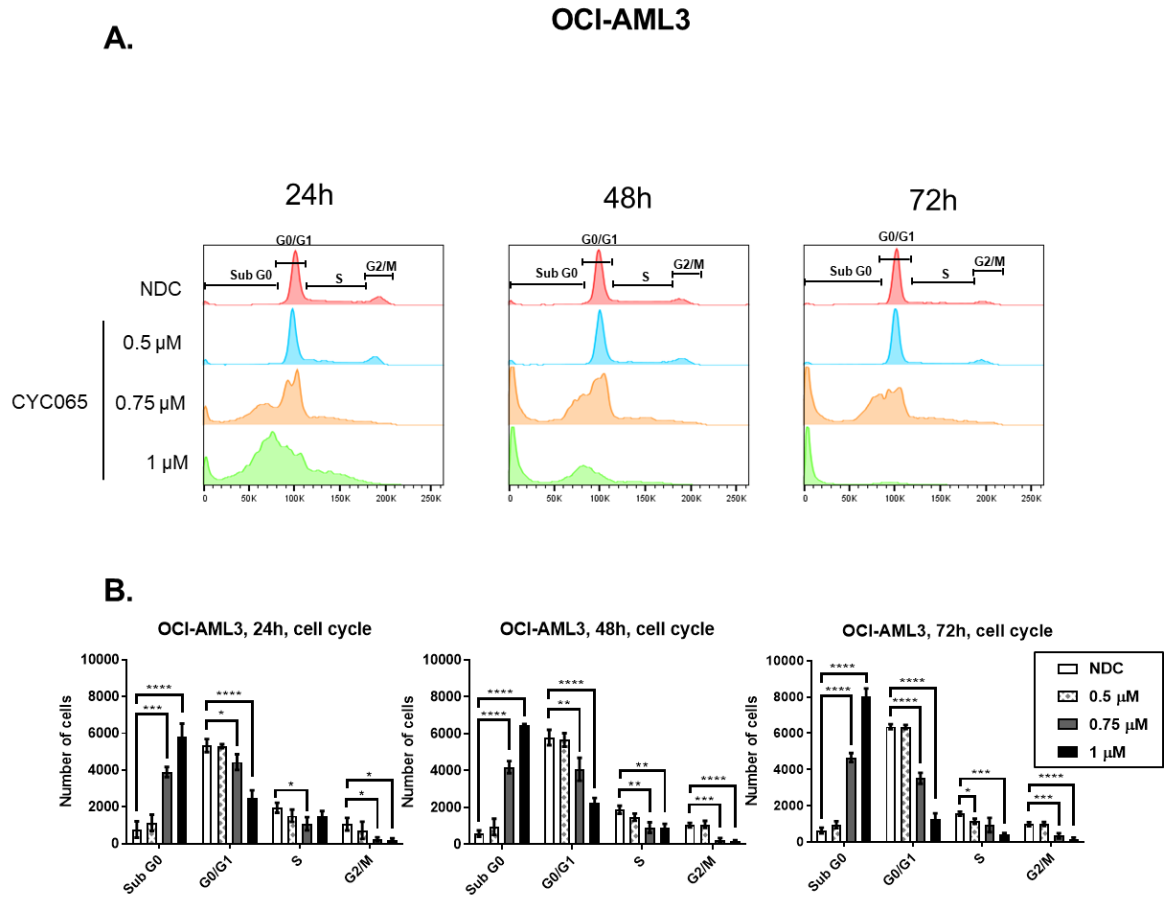

Figure 3.2.6.1 (A) Representative flow cytometry plots; and (B) Flow cytometric analysis of the cell cycle phase using PI staining of OCI-AML3 cell line treated with various concentrations of CYC065 for 24h, 48h and 72h. The experiments were performed in biological triplicates. Graphs depict means ± SD. Data were compared using the one-way ANOVA, post hoc Dunnett's test (Sub G0 populations; F (3,8) = 73.2, $P < 0.0001$, 24h; F (3,8) = 284.6, $P < 0.0001$, 48h; F (3,8) = 464.1, $P < 0.0001$, 72h). Significant *P*-values are indicated by asterisks (****< 0.0001, *** 0.0001 to < 0.001, ** 0.001 to < 0.01, * 0.01 to < 0.05 and NS if $P \geq 0.05$).

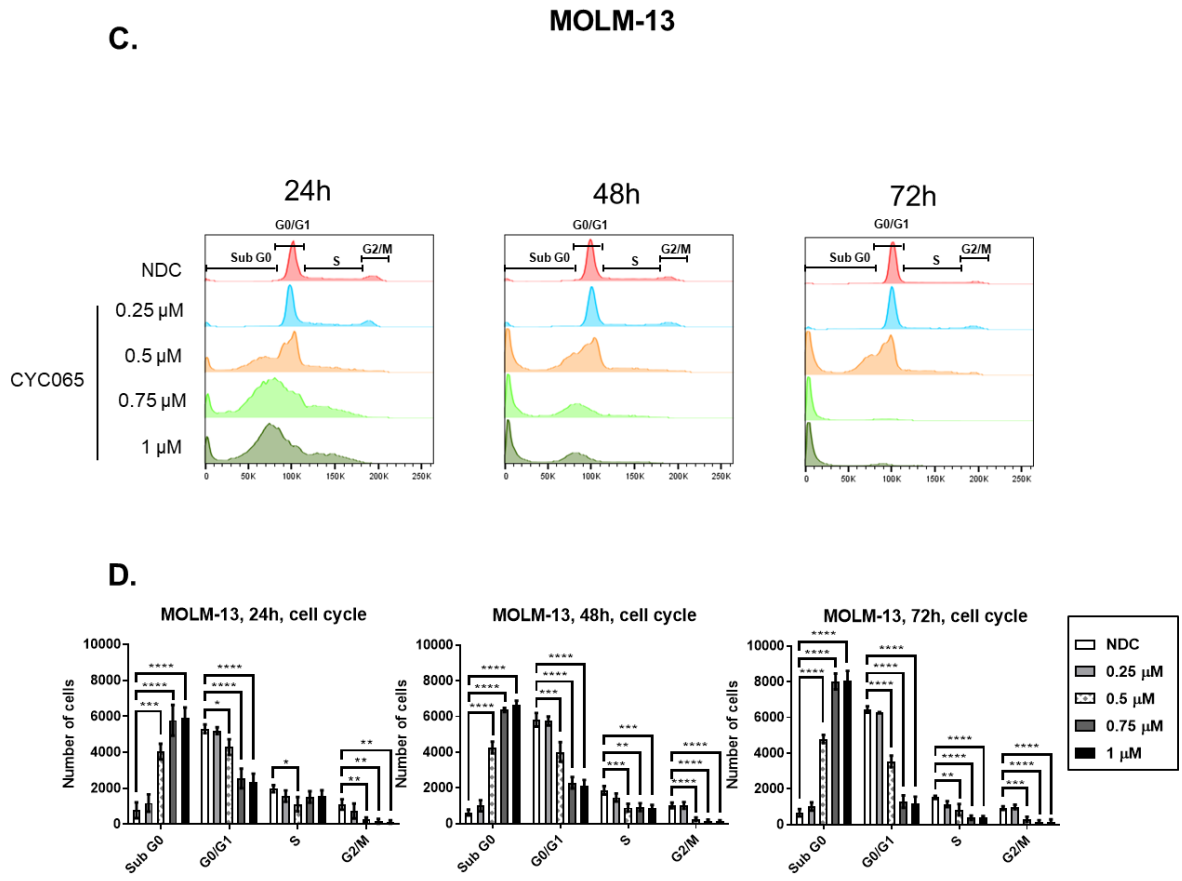

Figure 3.2.6.1 (C) Representative flow cytometry plots; and (D) Flow cytometric analysis of the cell cycle phase using PI staining of MOLM-13 cell line treated with various concentrations of CYC065 for 24h, 48h and 72h. The experiments were performed in biological triplicates. Graphs depict means ± SD. Data were compared using the one-way ANOVA, post hoc Dunnett's test (Sub G0 populations; F (4,10) = 53.2, $P < 0.0001$, 24h; F (4,10) = 413.3, $P < 0.0001$, 48h; F (4,10) = 301.4, $P < 0.0001$, 72h). Significant *P*-values are indicated by asterisks (****< 0.0001, *** 0.0001 to < 0.001, ** 0.001 to < 0.01, * 0.01 to < 0.05 and NS if $P \geq 0.05$).

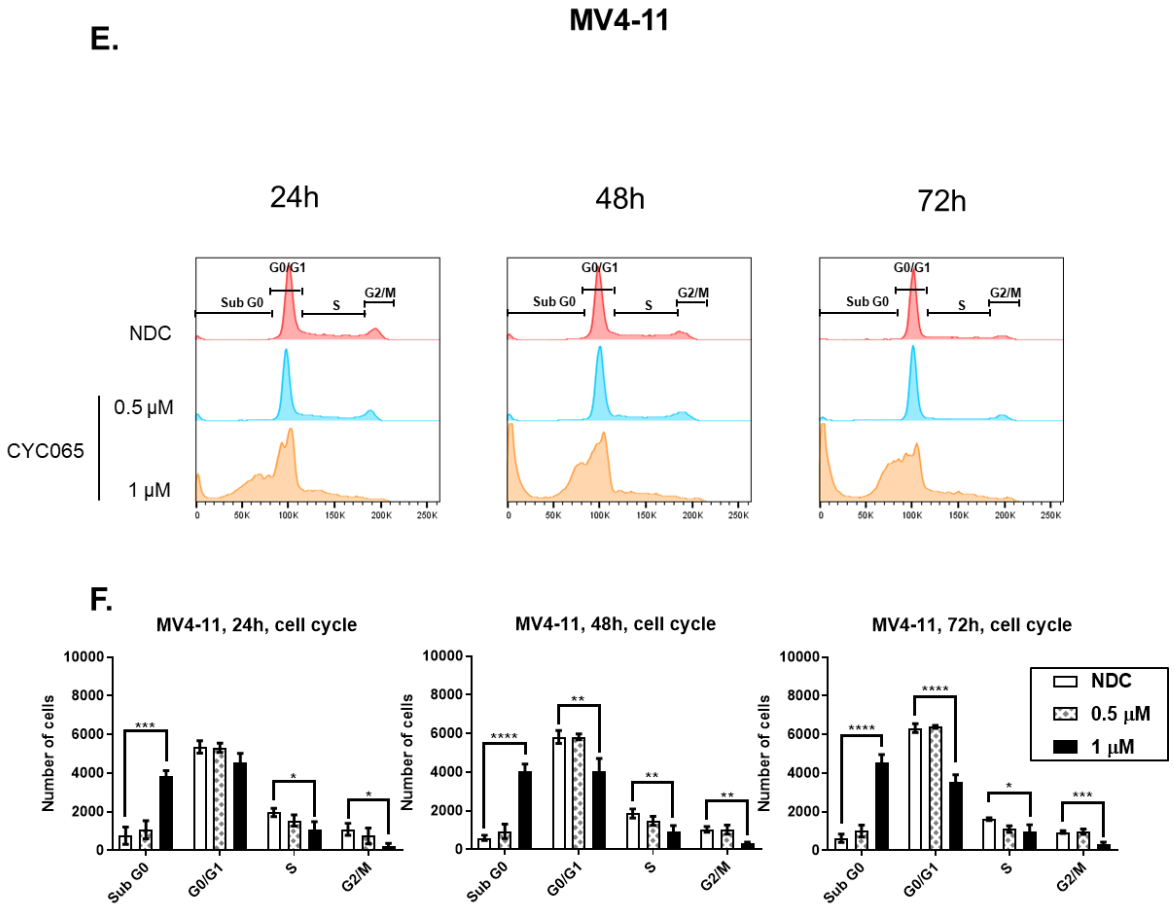

Figure 3.2.6.1 (E) Representative flow cytometry plots; and (F) Flow cytometric analysis of the cell cycle phase using PI staining of MV4-11 cell line treated with various concentrations of CYC065 for 24h, 48h and 72h. The experiments were performed in biological triplicates. Graphs depict means ± SD. Data were compared the one-way ANOVA, post hoc Dunnett's test (Sub G0 populations; F (2,6) = 53.6, *P* < 0.0001, 24h; F (2,6) = 103.8, *P* < 0.0001, 48h; F (2,6) = 143.8, *P* < 0.0001, 72h). Significant *P*-values are indicated by asterisks (****< 0.0001, *** 0.0001 to < 0.001, ** 0.001 to < 0.01, * 0.01 to < 0.05 and NS if *P* ≥ 0.05).

3.2.7 Pulsed dosing of CYC065 was sufficient to inhibit AML cell lines *in vitro*

In clinical trials to date, CYC065 has been administrated once every three weeks by IV infusion. As a consequence, in order to determine how effective the drug was over time following administration, a washout study was performed in OCI-AML3, MOLM-13, and MV4-11 cell lines. The cells were treated with various concentrations of CYC065 for 24h and then the drug was thoroughly washed out thrice and the cells were continued in culture in media only and harvested at 48h and 72h. Trypan blue exclusion assay (Figure 3.2.7.1A, OCI-AML3; B, MOLM-13; C, MV4-11), apoptosis assays (Figure 3.2.7.2A, OCI-AML3; B, MOLM-13; C, MV4-11), active caspase-3 assays (Figure 3.2.7.3A, OCI-AML3; B, MOLM-13; C, MV4-11), and cell cycle analyses (Figure 3.2.7.4A, OCI-AML3; B, MOLM-13; C,

MV4-11) were performed. After CYC065 was washed out, a slight cell recovery was observed at low concentrations in all assays analysed at 72h, however, there was no recovery of cells in any cell lines at the concentration of 1µM. Therefore, the results indicated that pulsed dosing of CYC065 was sufficient to consistently inhibit growth of AML cell lines and to induce apoptosis *in vitro*.

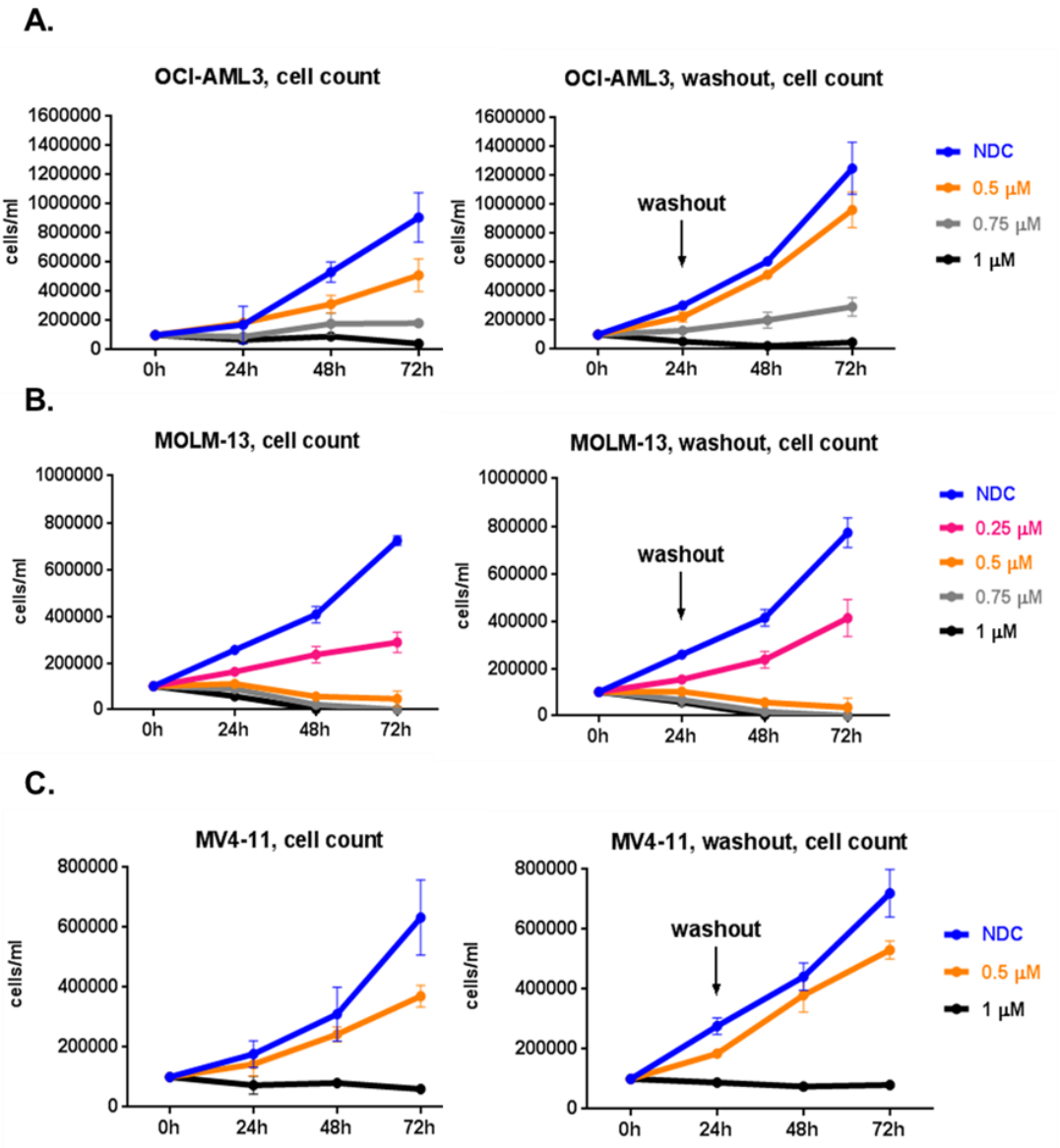

Figure 3.2.7.1 Cell count assessed by trypan blue dye exclusion of (A) OCI-AML3, (B) MOLM-13, and (C) MV4-11 cell lines treated with CYC065 at various concentrations either continuously (left panel), or with a 24h pulse treatment, followed by a washout (right panel). The experiments were performed in biological triplicates. Dots depict means ± SD.

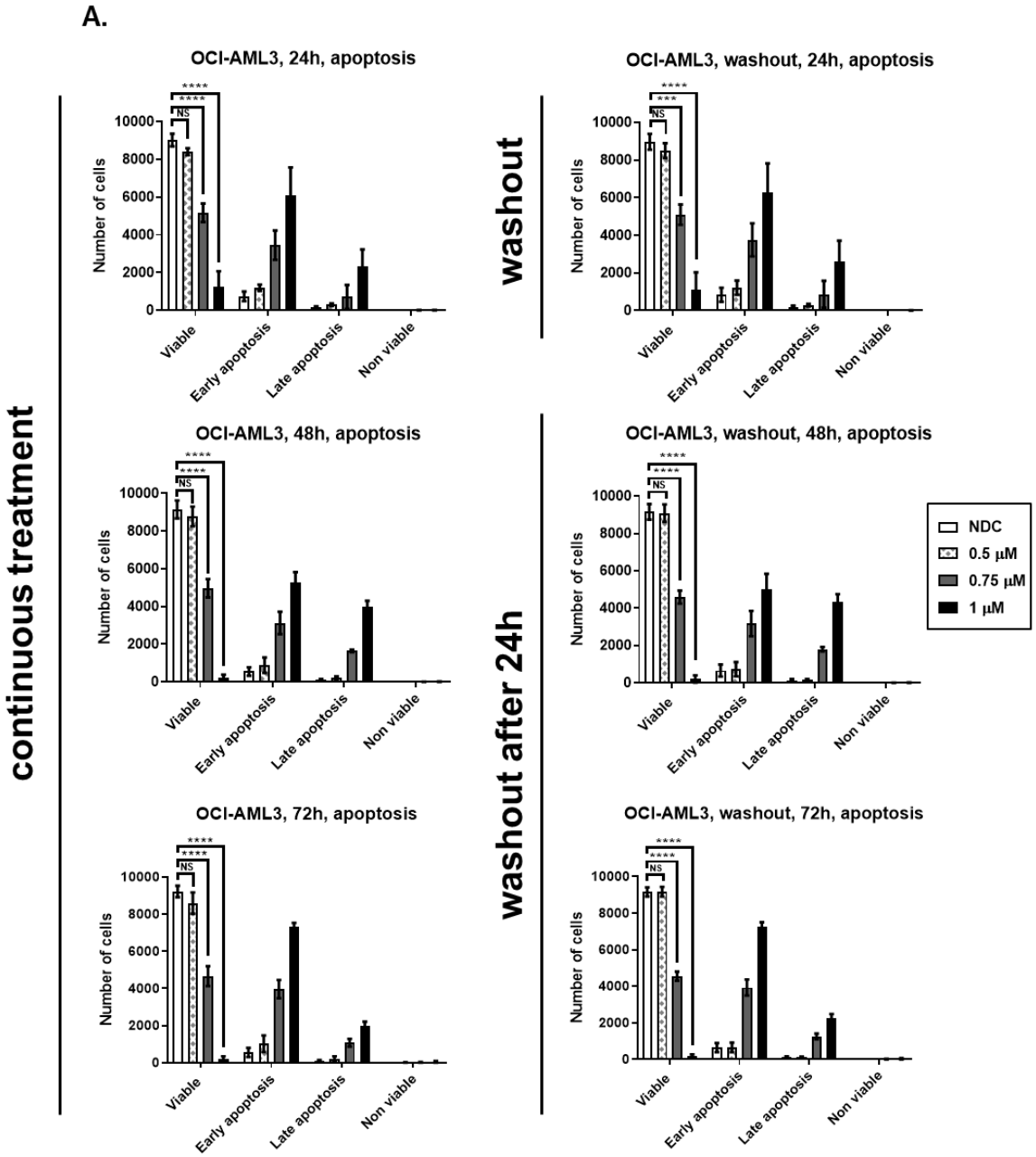

Figure 3.2.7.2 (A) Apoptosis assays of OCI-AML3 cell line treated with CYC065 at various concentrations either continuously (left panel), or with a 24h pulse treatment, followed by a washout (right panel). The experiments were performed in biological triplicates. Graphs depict means ± SD. Cell viability was compared using the one-way ANOVA. Significant *P*-values are indicated by asterisks (****< 0.0001, *** 0.0001 to < 0.001, ** 0.001 to < 0.01, * 0.01 to < 0.05 and NS if $P \geq 0.05$).

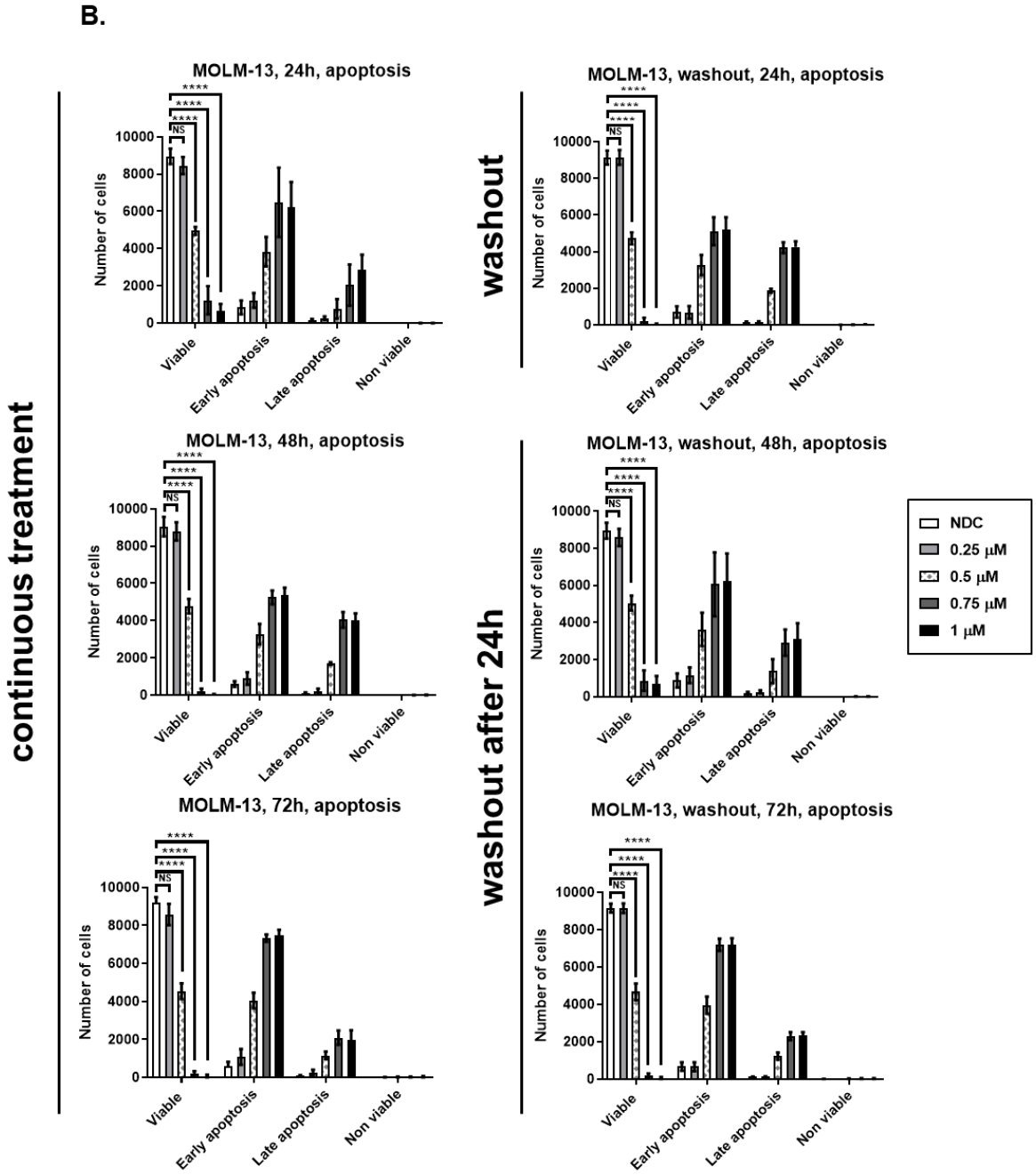

Figure 3.2.7.2 (B) Apoptosis assays of MOLM-13 cell line treated with CYC065 at various concentrations either continuously (left panel), or with a 24h pulse treatment, followed by a washout (right panel). The experiments were performed in biological triplicates. Graphs depict means ± SD. Cell viability was compared using the one-way ANOVA. Significant *P*-values are indicated by asterisks (****< 0.0001, *** 0.0001 to < 0.001, ** 0.001 to < 0.01, * 0.01 to < 0.05 and NS if $P \geq 0.05$).

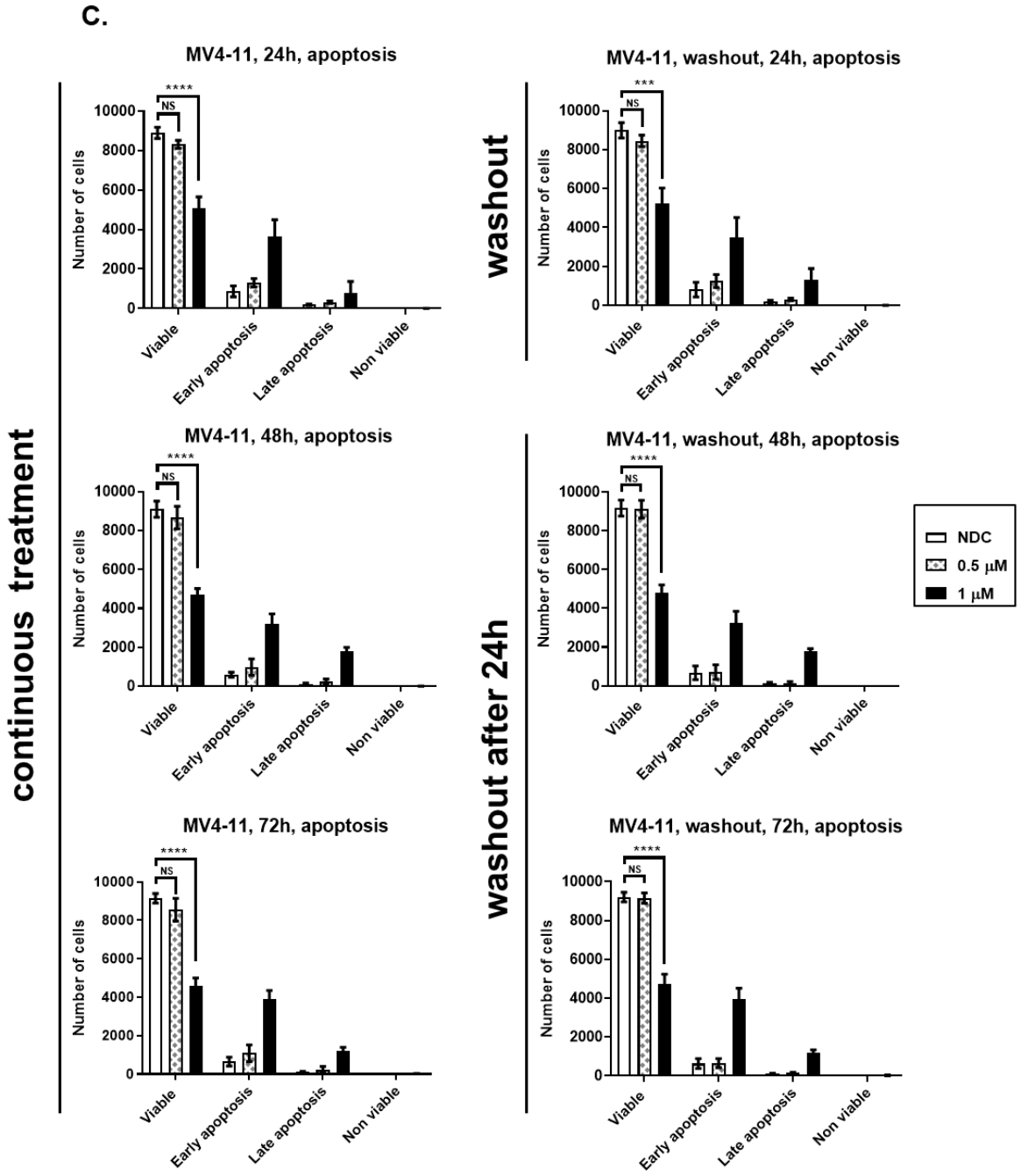

Figure 3.2.7.2 (C) Apoptosis assays of MV4-11 cell line treated with CYC065 at various concentrations either continuously (left panel), or with a 24h pulse treatment, followed by a washout (right panel). The experiments were performed in biological triplicates. Graphs depict means ± SD. Cell viability was compared using the one-way ANOVA. Significant *P*-values are indicated by asterisks (****< 0.0001, *** 0.0001 to < 0.001, ** 0.001 to < 0.01, * 0.01 to < 0.05 and NS if $P \geq 0.05$).

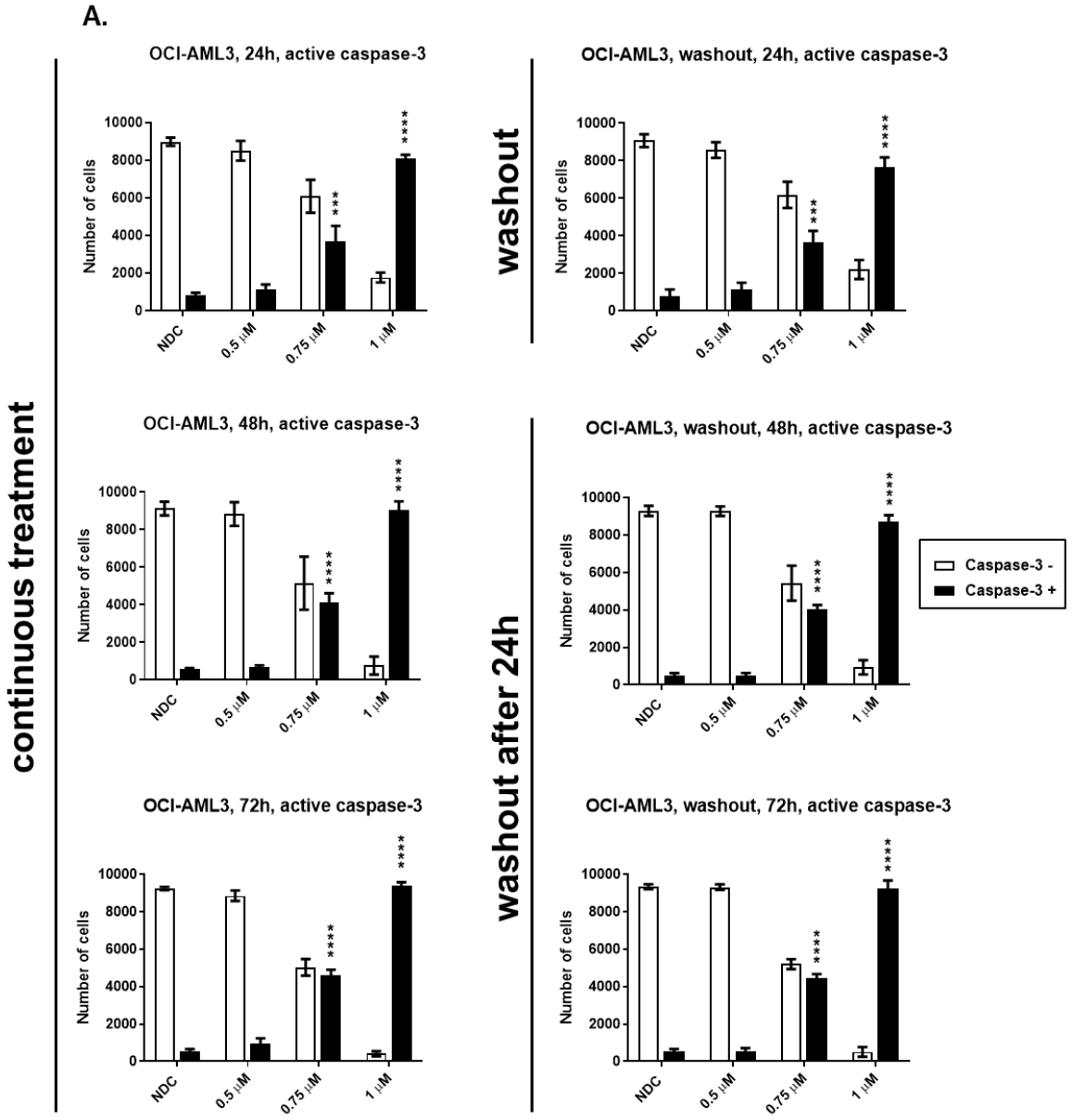

Figure 3.2.7.3 (A) Active caspase-3 assays of OCI-AML3 cell line treated with CYC065 at various concentrations either continuously (left panel), or with a 24h pulse treatment, followed by a washout (right panel). The experiments were performed in biological triplicates. Graphs depict means ± SD. Caspase-3-positive populations were compared using the one-way ANOVA. Significant *P*-values are indicated by asterisks (****< 0.0001, *** 0.0001 to < 0.001, ** 0.001 to < 0.01, * 0.01 to < 0.05 and NS if $P \geq 0.05$).

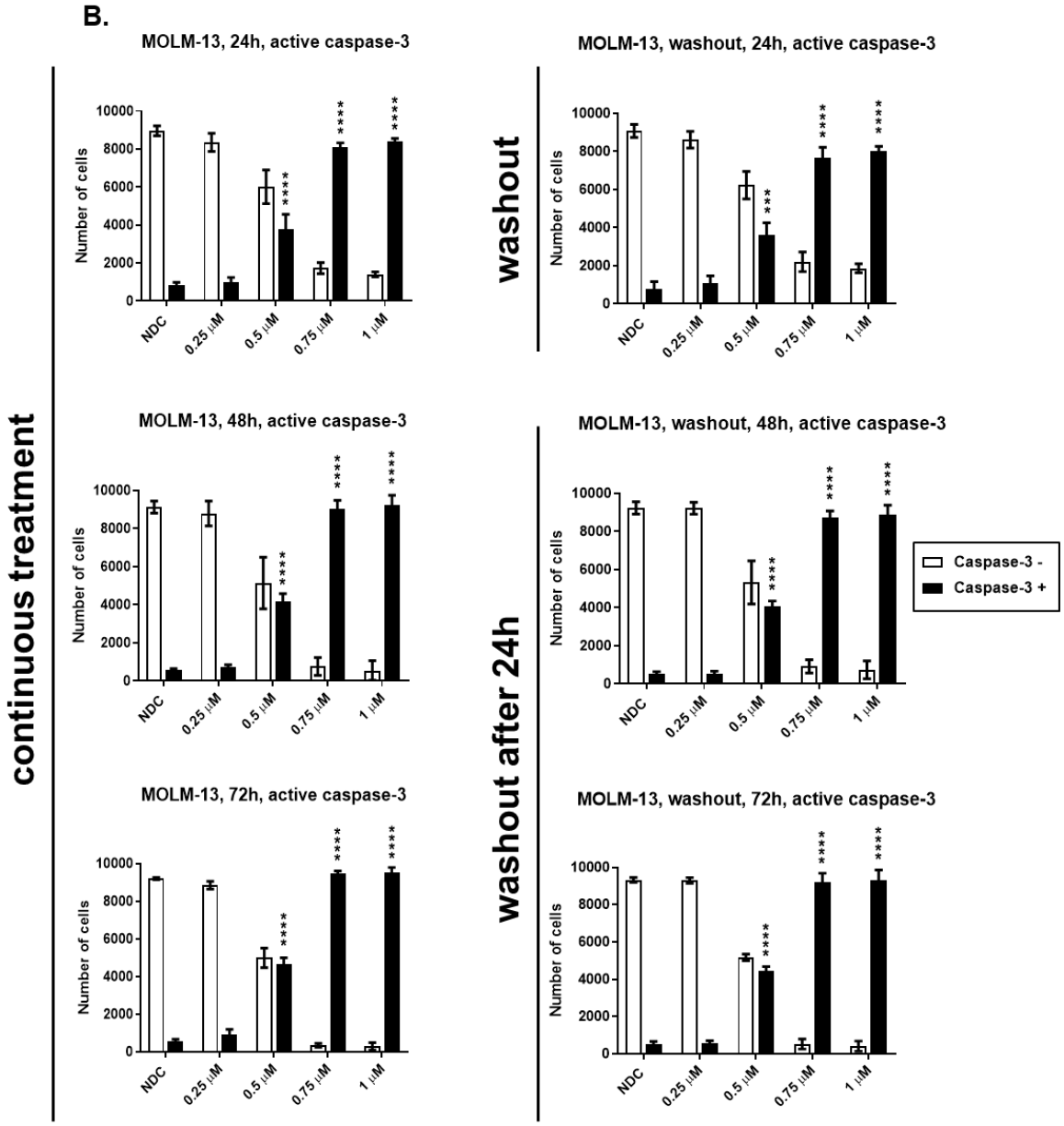

Figure 3.2.7.3 (B) Active caspase-3 assays of MOLM-13 cell line treated with CYC065 at various concentrations either continuously (left panel), or with a 24h pulse treatment, followed by a washout (right panel). The experiments were performed in biological triplicates. Graphs depict means ± SD. Caspase-3-positive populations were compared using the one-way ANOVA. Significant *P*-values are indicated by asterisks (****< 0.0001, *** 0.0001 to < 0.001, ** 0.001 to < 0.01, * 0.01 to < 0.05 and NS if $P \geq 0.05$).

C.

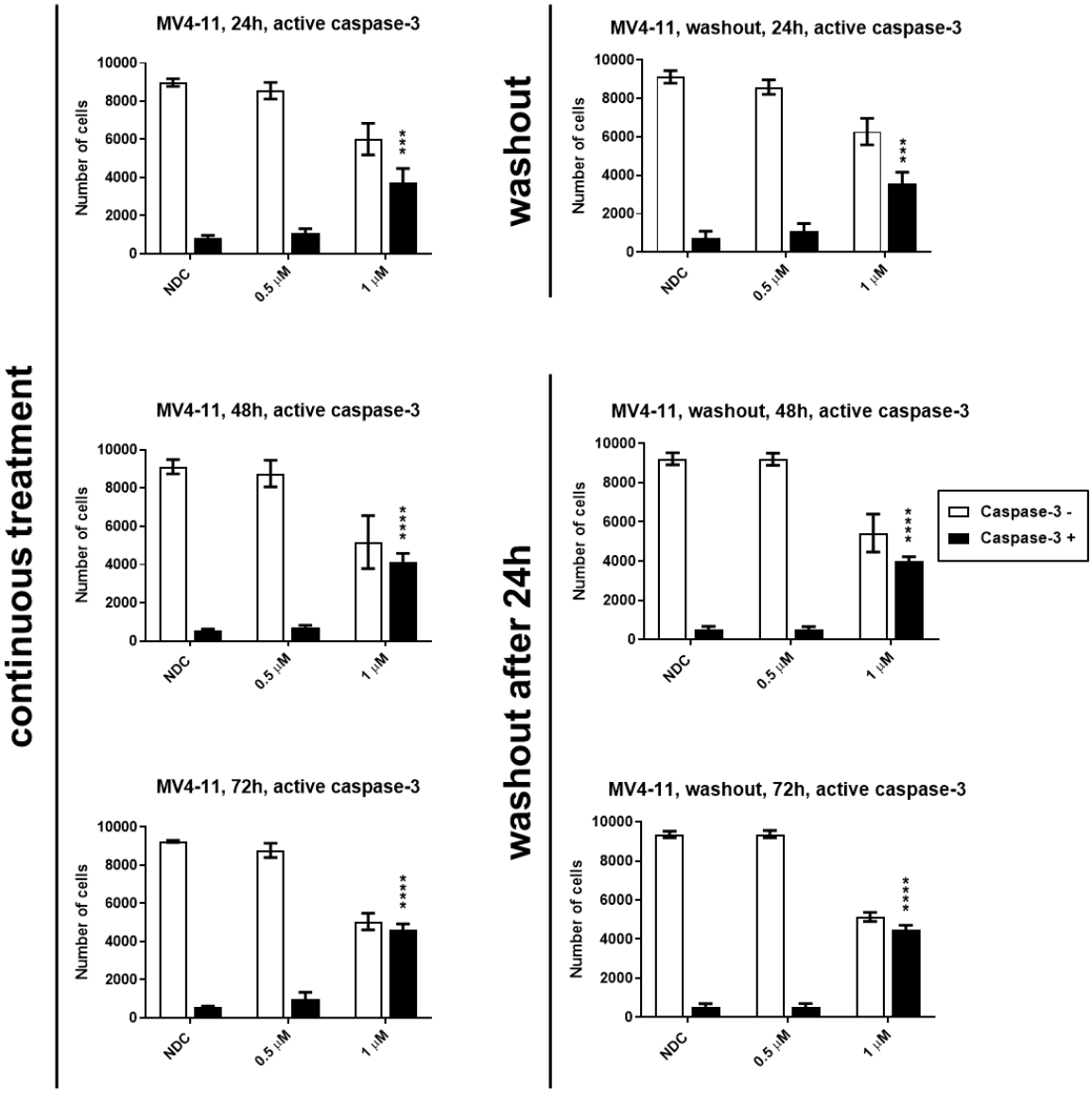

Figure 3.2.7.3 (C) Active caspase-3 assays of MV4-11 cell line treated with CYC065 at various concentrations either continuously (left panel), or with a 24h pulse treatment, followed by a washout (right panel). The experiments were performed in biological triplicates. Graphs depict means ± SD. Caspase-3-positive populations were compared using the one-way ANOVA. Significant *P*-values are indicated by asterisks (****< 0.0001, *** 0.0001 to < 0.001, ** 0.001 to < 0.01, * 0.01 to < 0.05 and NS if $P \geq 0.05$).

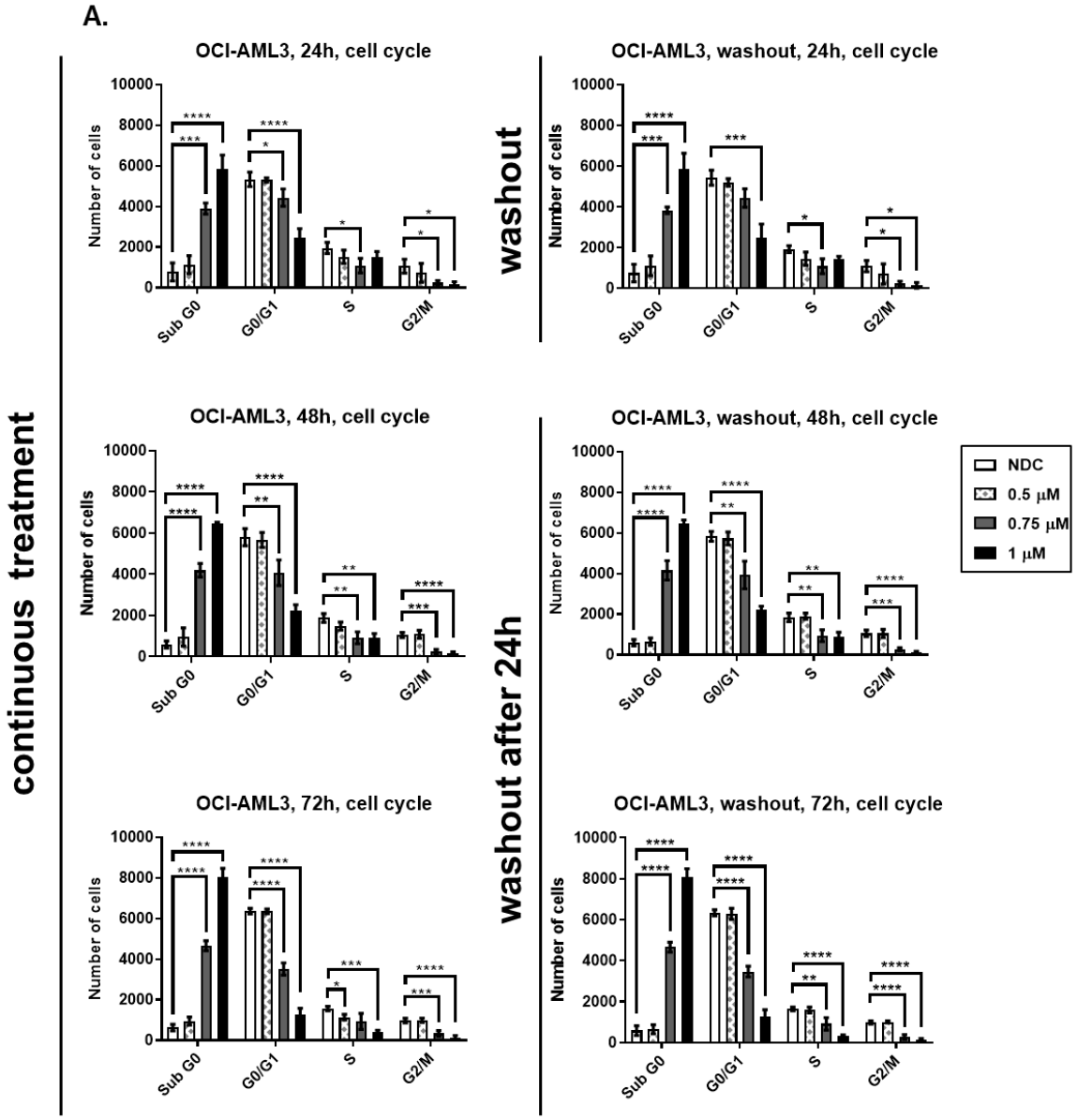

Figure 3.2.7.4 (A) Cell cycle analyses of OCI-AML3 cell line treated with CYC065 at various concentrations either continuously (left panel), or with a 24h pulse treatment, followed by a washout (right panel). The experiments were performed in biological triplicates. Graphs depict means ± SD. Data were compared using the one-way ANOVA. Significant *P*-values are indicated by asterisks (****< 0.0001, *** 0.0001 to < 0.001, ** 0.001 to < 0.01, * 0.01 to < 0.05 and NS if $P \geq 0.05$).

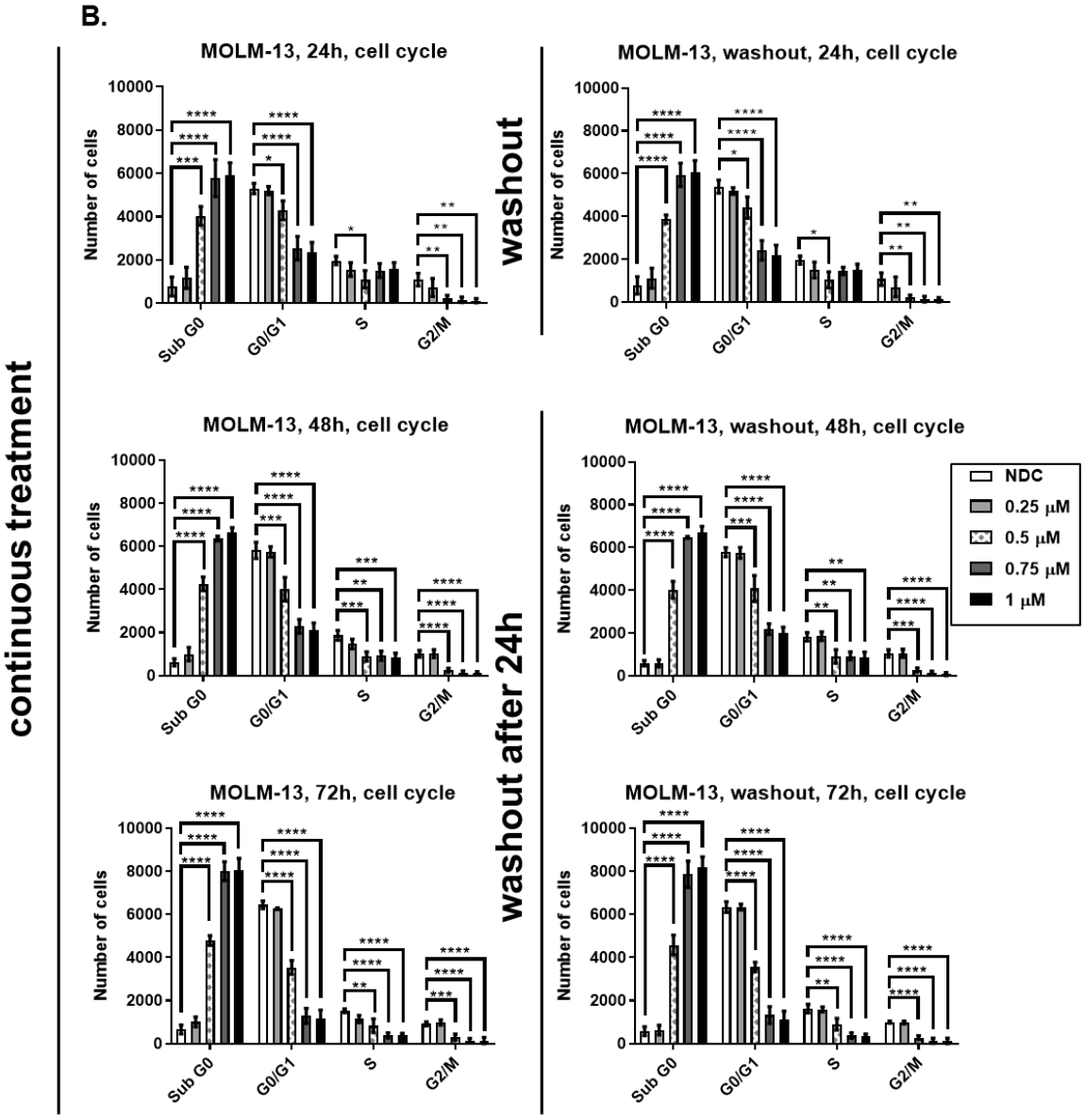

Figure 3.2.7.4 (B) Cell cycle analyses of MOLM-13 cell line treated with CYC065 at various concentrations either continuously (left panel), or with a 24h pulse treatment, followed by a washout (right panel). The experiments were performed in biological triplicates. Graphs depict means ± SD. Data were compared using the one-way ANOVA. Significant *P*-values are indicated by asterisks (****< 0.0001, *** 0.0001 to < 0.001, ** 0.001 to < 0.01, * 0.01 to < 0.05 and NS if $P \geq 0.05$).

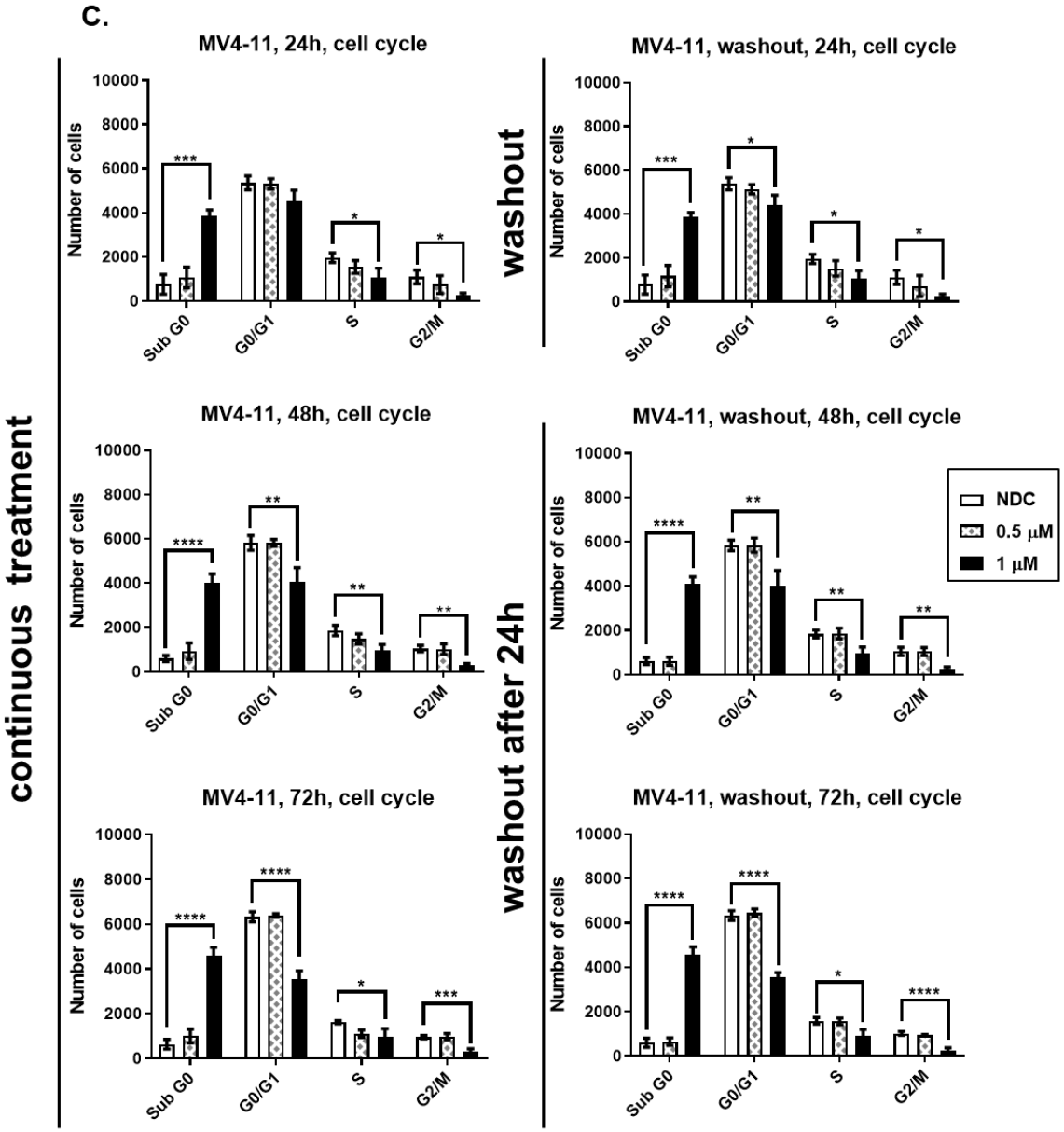

Figure 3.2.7.4 (C) Cell cycle analyses of MV4-11 cell line treated with CYC065 at various concentrations either continuously (left panel), or with a 24h pulse treatment, followed by a washout (right panel). The experiments were performed in biological triplicates. Graphs depict means ± SD. Data were compared using the one-way ANOVA. Significant *P*-values are indicated by asterisks (****< 0.0001, *** 0.0001 to < 0.001, ** 0.001 to < 0.01, * 0.01 to < 0.05 and NS if $P \geq 0.05$).

3.3 Effects of CYC065 on target proteins

OCI-AML3, MOLM-13, and MV4-11 cell lines were treated with 1μM of CYC065, for 4h and 24h. Western blotting was performed to assess the effects of CYC065 on downstream target proteins to assess its specificity. The quantification was done by densitometric analysis (Image Studio™ Lite Software Version 5.2). Where possible, the quantity of phosphorylated protein is presented as a ratio of phosphorylated to endogenous protein level. However, if the endogenous protein

is transcriptionally suppressed by the drug, a housekeeping protein was used instead as an internal protein loading control for normalisation.

3.3.1 Assessment of CDKs 1, 2, 4, 7, and 9 kinase activities following CYC065 treatment: a decrease in the endogenous level of Rb and RNAPII was observed

The aim of this experiment was to assess the activity of kinases potentially affected by CYC065. Therefore, phosphorylated and endogenous levels of the key substrates of each kinase were evaluated by Western blotting in all cell lines following treatment with CYC065 for 4h aiming to focus on the primary effect of the drug. Additionally, Western blotting at 24h-treatment was also performed for the secondary effect assessment.

At the early timepoint (4h), the function of CDK1 and CDK2 were not perturbed by CYC065 as observed by no change in the inhibitory threonine 320 (T320) phosphorylated protein phosphatase 1 alpha (PP1α)/total PP1α ratio (Figure 3.3.1.1A,B top panel) and the endogenous PP1α level in all cell lines (Figure 3.3.1.1A,B bottom panel). At 24h, there was a slight decrease of endogenous PP1α level in OCI-AML3 cell line (Figure 3.3.1.1A lane 4). Src homology 2 protein-tyrosine phosphatase (SH-PTP2) was used as an internal protein loading control. PP1 is one of the major mitotic phosphatases (Nasa & Kettenbach, 2018). At mitotic entry, most of PP1 activity is inhibited by CDK1- and CDK2-dependent phosphorylation of T320 residue on its CTD (Berndt, 1999; Dohadwala et al., 1994; Kwon, Lee, Choi, Greengard, & Nairn, 1997; C. W. Liu et al., 1999).

The function of CDK2 and CDK4 was further investigated. In MOLM-13 cell line, there was a decrease by 75% in the endogenous Rb level at 4h which resulted in a corresponding decrease of phosphorylated forms of serine 807/serine 811 (S807/S811; Figure 3.3.1.1C lane 6) and serine 780 (S780; Figure 3.3.1.1E lane 6). By contrast, in MV4-11 cell line, which is less sensitive to CYC065, S807/S811 phosphorylated Rb (Figure 3.3.1.1C lane 10) and S780 phosphorylated Rb (Figure 3.3.1.1E lane 10) remained unchanged, indicating that CDK2 and CDK4 were not affected by CYC065. SH-PTP2 was used as an internal protein loading control. During cell cycle progression, CDK4/6-cyclin D and CDK2/cyclin E are expressed in the early and late G1 phase, respectively (Santo et al., 2015). They

phosphorylate and inactivate the Rb tumour suppressor. This leads to the release of various transcription factors of the E2F group from the paused state and triggers the transition of the G1 to S phase of cell cycle. Rb phosphorylation on S807/S811 and S780 are preferred by CDK2 (Brugarolas et al., 1999; Chytil et al., 2004; Robb et al., 2018; Tetsu & McCormick, 2003) and CDK4 (H. Chen et al., 2017; Chytil et al., 2004; Kolupaeva & Janssens, 2013), respectively. However, CDK4 has also been reported to phosphorylate Rb at S807/S811 (Byth et al., 2009; Kolupaeva & Janssens, 2013; Siemeister et al., 2012).

RNAPII was used for an evaluation of CDK7 and CDK9 kinase activities. Following treatment with CYC065 for 4h, it was observed that the endogenous level of RNAPII was dramatically decreased in OCI-AML3 (Figure 3.3.1.1G lane 2; I lane 2), MOLM-13 (Figure 3.3.1.1G lane 6; I lane 6), and MV4-11 cell lines (Figure 3.3.1.1G lane 10; I lane10). This resulted in a corresponding decrease of the phosphorylated form of RNAPII. Again, SH-PTP2 was used as an internal protein loading control with changes in expression evaluated by densitometry. Interestingly, a decrease in S2 phosphorylated RNAPII (Figure 3.3.1.1J top panel) was relatively greater than in S5 phosphorylated RNAPII (Figure 3.3.1.1H top panel) in all cell lines. However, this is insufficient evidence to draw the conclusion that CYC065 directly inhibits CDK9 rather than CDK7, as the decrease in S2 phosphorylated RNAPII observed may have resulted from transcriptional suppression of the endogenous RNAPII. During transcriptional initiation, TFIIH/CDK7/cyclin H complex are recruited to the proximal promoter. CDK7 phosphorylates S5 on the CTD of RNAPII which supports the binding of the 5´mRNA capping enzyme and also activates CDK9 in P-TEFb/CDK9/cyclin T complex (Santo et al., 2015). Then, CDK9/cyclin T phosphorylates S2 on the CTD of RNAPII in order to optimise its function as a platform for several transcription factors (Santo et al., 2015; Thiel et al., 2012) which induces progressive transcriptional elongation.

Taken together, it can be implied that CDK1 and CDK2 kinase activities were not affected by CYC065 in all cell lines, whereas, the effects of the drug on CDK4, CDK7, and CDK9 activities remained unclear.

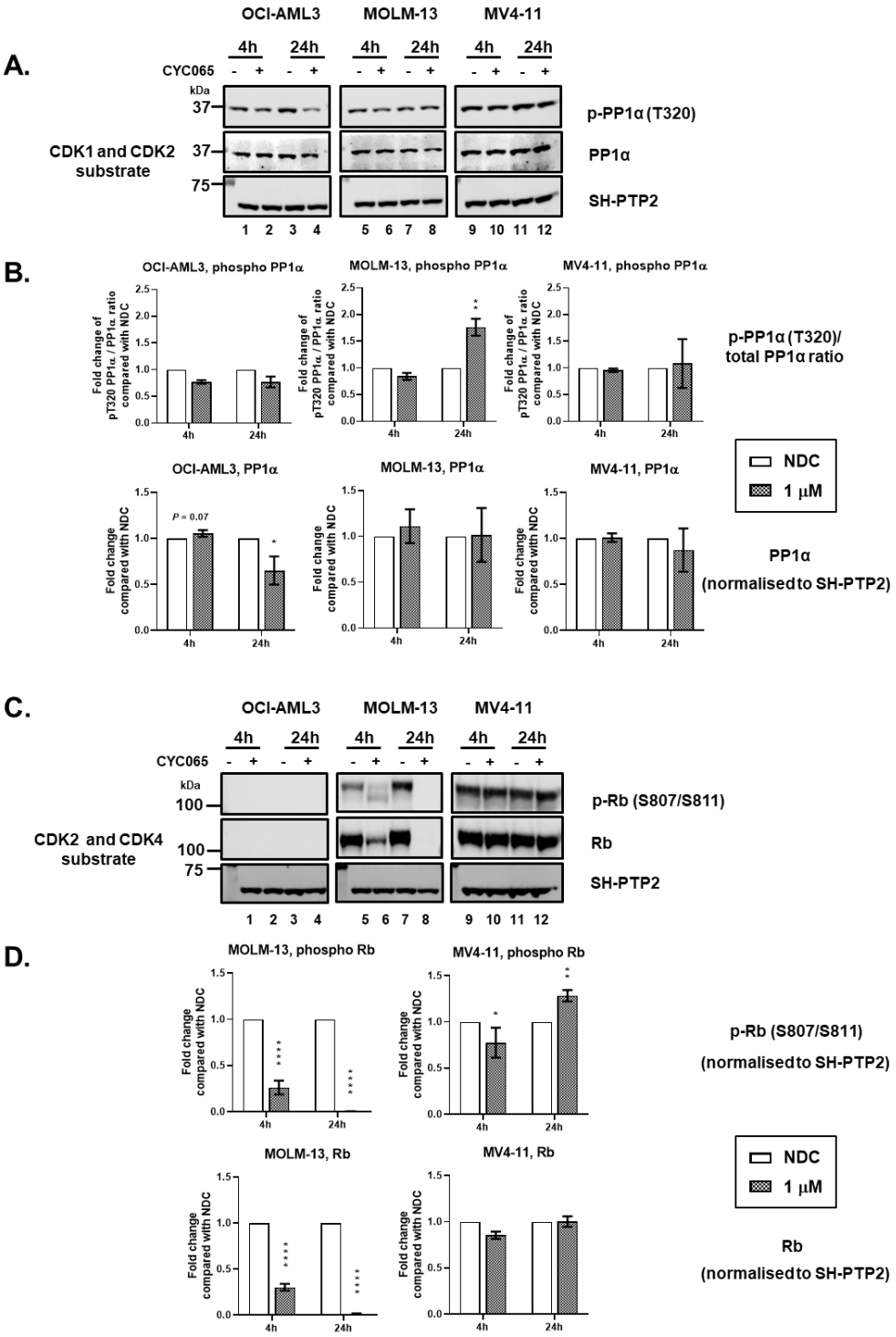

Figure 3.3.1.1 OCI-AML3, MOLM-13, and MV4-11 cell lines were treated with 1μM CYC065 for 4h and 24h. (A) Western blotting of T320 phosphorylated PP1α and the endogenous PP1α protein; and (B) normalised relative fold change of T320 phosphorylated PP1α/total PP1α ratio (top panel) and the endogenous level of PP1α protein to SH-PTP2 (bottom panel) as compared with NDC, evaluated by densitometry. The experiments were performed in biological triplicates. **(C) Western blotting of phosphorylated S807/S811 Rb and the endogenous Rb protein; and (D) normalised relative fold change of S807/S811 phosphorylated Rb (top panel) and the endogenous level of Rb protein (bottom panel) to SH-PTP2 as compared with NDC, evaluated by densitometry.** The experiments were performed in biological triplicates. Graphs depict means ± SD. Data were compared using the unpaired student's t-test. Significant *P*-values are indicated by asterisks (****< 0.0001, *** 0.0001 to < 0.001, ** 0.001 to < 0.01, * 0.01 to < 0.05 and NS if $P \geq 0.05$). Threonine 320 phosphorylated protein phosphatase 1 alpha (p-PP1α, T320). Protein phosphatase 1 alpha (PP1α). Serine 807 and serine 811 phosphorylated retinoblastoma (p-Rb, S807/S811). Retinoblastoma (Rb). Src homology 2 protein-tyrosine phosphatase (SH-PTP2).

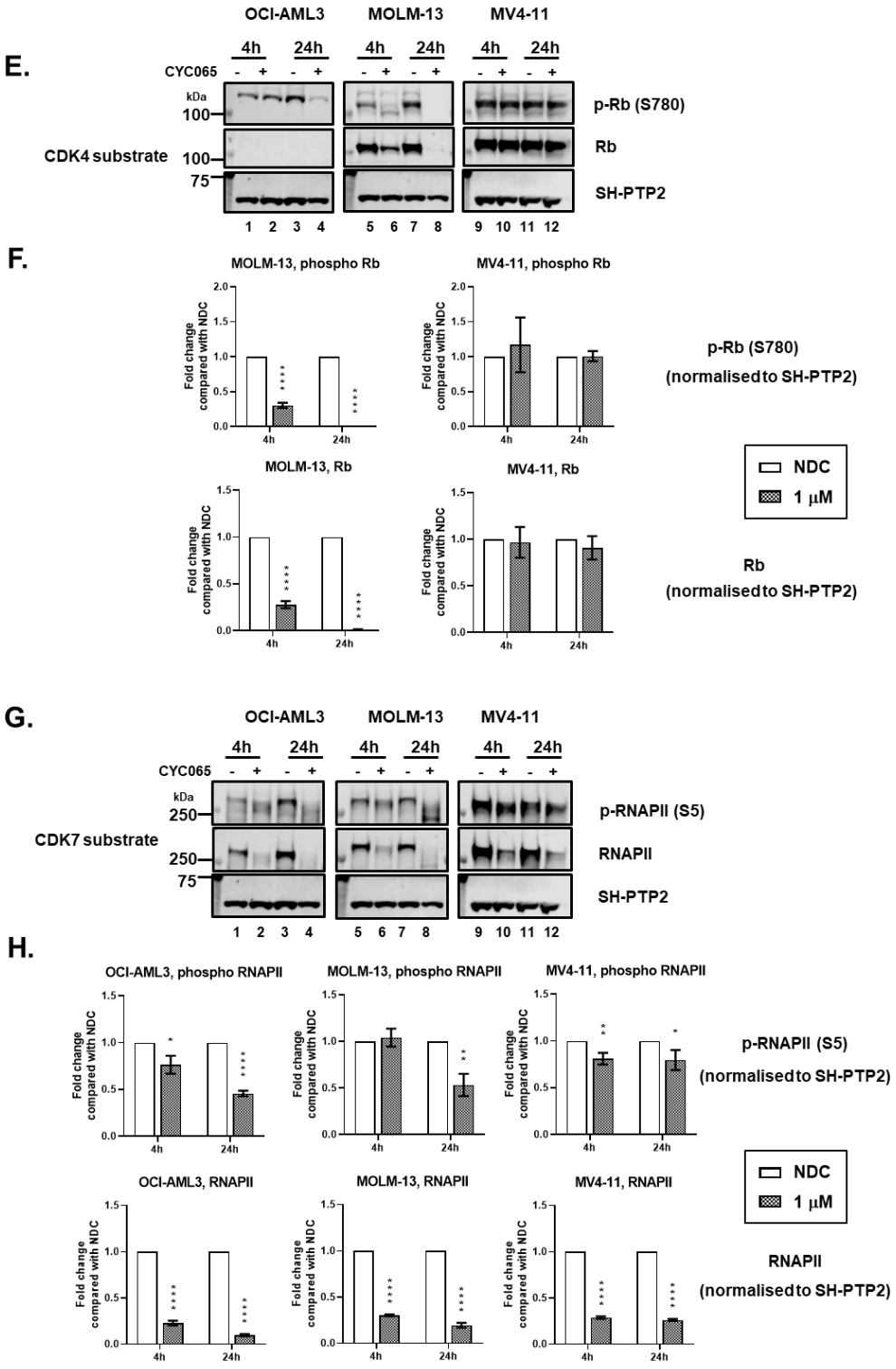

Figure 3.3.1.1 OCI-AML3, MOLM-13, and MV4-11 cell lines were treated with 1μM CYC065 for 4h and 24h. (E) Western blotting of S780 phosphorylated Rb and the endogenous Rb protein; and (F) normalised relative fold change of S780 phosphorylated Rb (top panel) and the endogenous level of Rb protein (bottom panel) to SH-PTP2 as compared with NDC, evaluated by densitometry. The experiments were performed in biological triplicates. **(G) Western blotting of S5 phosphorylated RNAPII and the endogenous RNAPII protein; and (H) normalised relative fold change of S5 phosphorylated RNAPII (top panel) and the endogenous level of RNAPII protein (bottom panel) to SH-PTP2 as compared with NDC, evaluated by densitometry.** The experiments were performed in biological triplicates. Graphs depict means ± SD. Data were compared using the unpaired student's t-test. Significant *P*-values are indicated by asterisks (****< 0.0001, *** 0.0001 to < 0.001, ** 0.001 to < 0.01, * 0.01 to < 0.05 and NS if $P \geq 0.05$). Serine 780 phosphorylated retinoblastoma (p-Rb, S780). Retinoblastoma (Rb). Serine 5 phosphorylated RNA polymerase II (p-RNAPII, S5). RNA polymerase II (RNAPII).

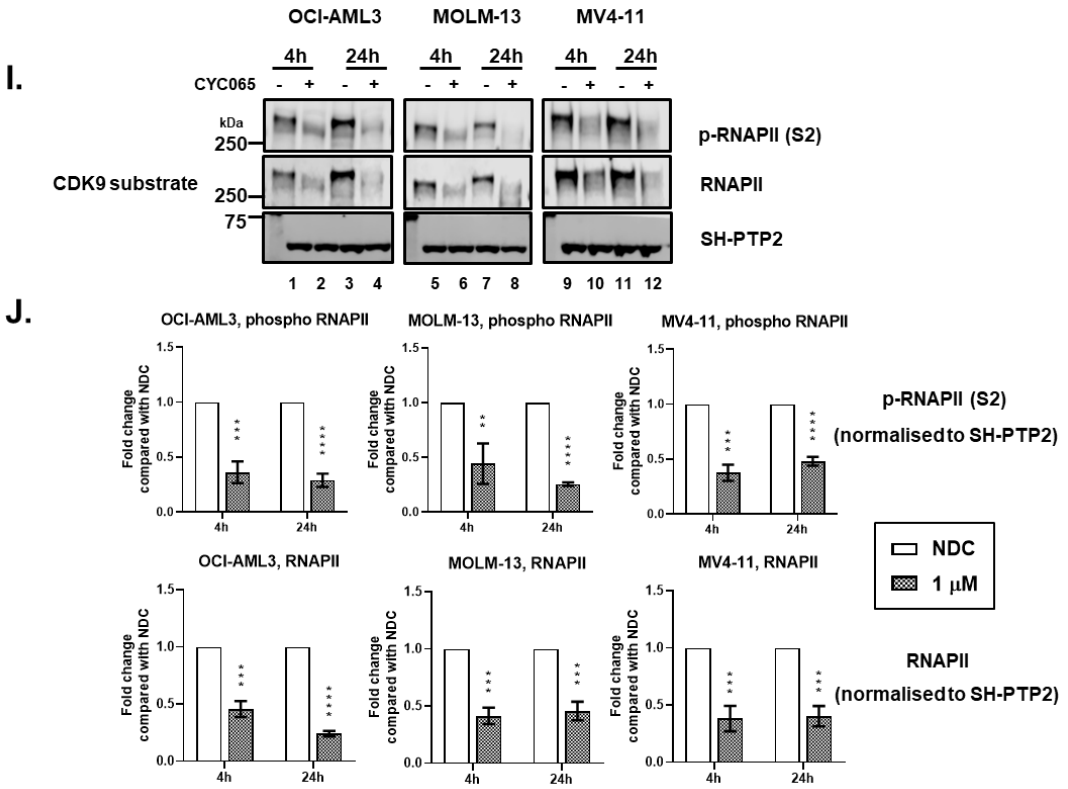

Figure 3.3.1.1 OCI-AML3, MOLM-13, and MV4-11 cell lines were treated with 1μM CYC065 for 4h and 24h. (I) Western blotting of S2 phosphorylated RNAPII and the endogenous RNAPII protein; and (J) normalised relative fold change of S2 phosphorylated RNAPII (top panel) and the endogenous level of RNAPII protein (bottom panel) to SH-PTP2 as compared with NDC, evaluated by densitometry. The experiments were performed in biological triplicates. Graphs depict means ± SD. Data were compared using the unpaired student's t-test. Significant *P*-values are indicated by asterisks (****< 0.0001, *** 0.0001 to < 0.001, ** 0.001 to < 0.01, * 0.01 to < 0.05 and NS if $P \geq 0.05$). Serine 2 phosphorylated RNA polymerase II (p-RNAPII, S2).

3.3.2 CYC065 downregulated MCL-1 resulting in rapid induction of apoptosis in AML cell lines

Following treatment with CYC065 for 4h, a transcriptional downregulation of short half-life MCL-1 protein was observed in all cell lines; OCI-AML3 (Figure 3.3.2.1A lane 2), MOLM-13 (Figure 3.3.2.1A lane 6), and MV4-11 (Figure 3.3.2.1A lane 10). The end result is apoptosis indicated by an accumulation of cleaved poly (ADP-ribose) polymerase-1 (PARP1) (Figure 3.3.2.1C). SH-PTP2 was used as an internal protein loading control. Although the total MCL-1 protein level was slightly decreased at 4h in OCI-AML3 cell line (Figure 3.3.2.1A lane 2), the level dramatically dropped at 24h (Figure 3.3.2.1A lane 4) which is consistent with the concomitant accumulation of cleaved PARP1 (Figure 3.3.2.1C lane 4).
In addition, the data showed that apoptosis was induced in approximately 80-90% of the cells after treatment with 1μM of CYC065 for 24h (Figure 3.2.3.1A,B) *in vitro*.

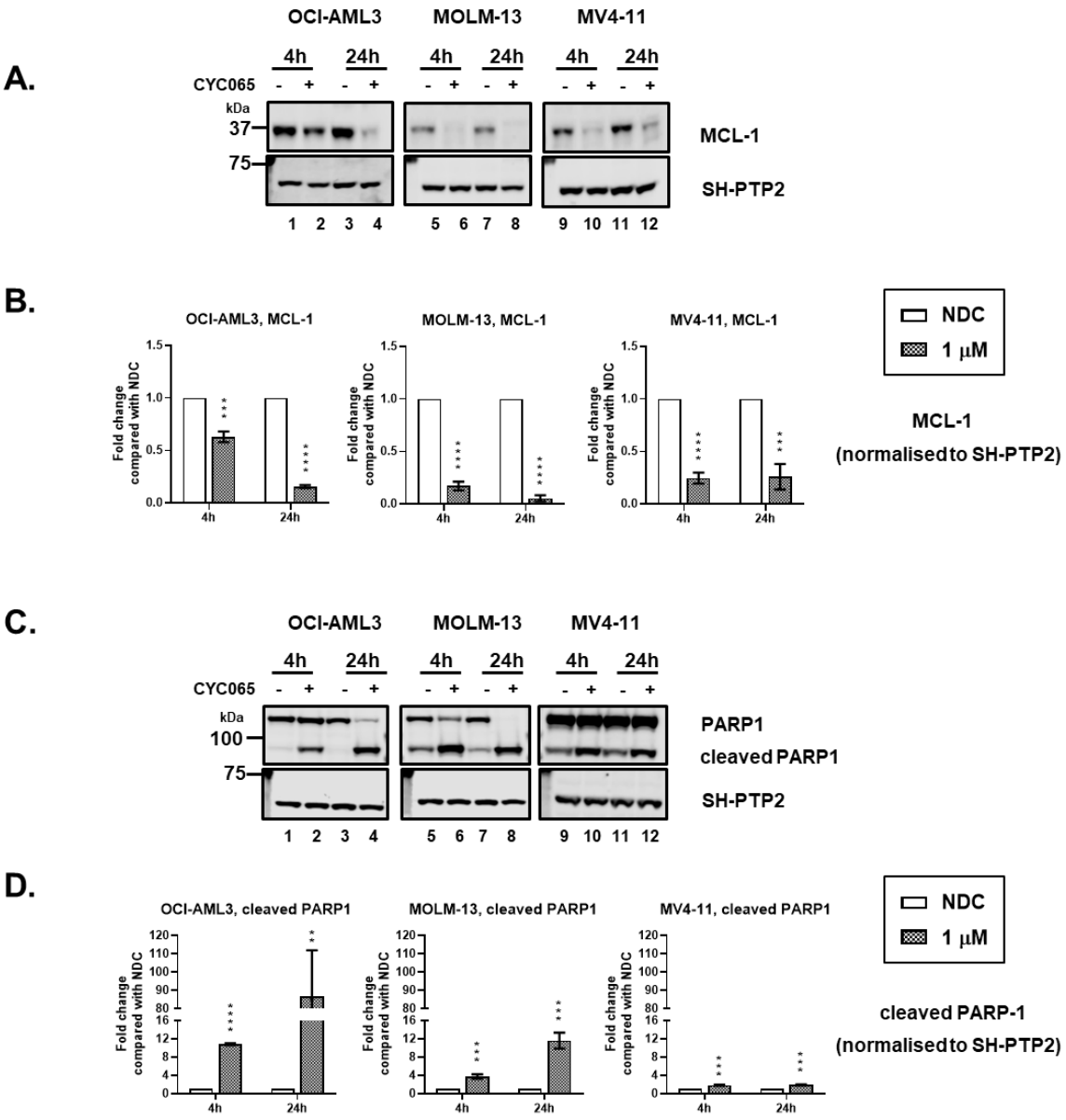

Figure 3.3.2.1 OCI-AML3, MOLM-13, and MV4-11 cell lines were treated with 1μM CYC065, for 4h and 24h. (A) Western blotting of the endogenous MCL-1 protein; and (B) normalised relative fold change of the endogenous level of MCL-1 protein to SH-PTP2 as compared with NDC, evaluated by densitometry. The experiments were performed in biological triplicates. **(C) Western blotting of total PARP1 and cleaved PARP1 protein; and (D) normalised relative fold change of cleaved PARP-1 protein to SH-PTP2 as compared with NDC, evaluated by densitometry.** The experiments were performed in biological triplicates. Graphs depict means ± SD. Data were compared using the unpaired student's t-test. Significant *P*-values are indicated by asterisks (****< 0.0001, *** 0.0001 to < 0.001, ** 0.001 to < 0.01, * 0.01 to < 0.05 and NS if $P \geq 0.05$). Myeloid cell leukemia 1 (MCL-1). Poly (ADP-ribose) polymerase-1 (PARP1). Cleaved poly (ADP-ribose) polymerase-1 (cleaved PARP1).

3.3.3 BCL-2 and BCL-xL were not the key targets of CYC065

In addition to MCL-1, the effects of CYC065 on other BCL-2 family anti-apoptotic proteins were assessed. OCI-AML3, MOLM-13 and MV4-11 cell lines were treated with 1μM CYC065 for 15min, 1h, 2h, 4h and 24h. An internal protein loading control was selected depending on the molecular weight of targets of interest. Therefore, gamma tubulin (γ-tubulin) (48kDa) was used in this experiment as the molecular weight of the target proteins is less than 30kDa. It was observed that serine 70 (S70) phosphorylated and endogenous BCL-2 protein were not significantly affected by CYC065 in all cell lines (Figure 3.3.3.1A,B). The effect of phosphorylation of BCL-2 at S70 remains controversial; it either enhances or diminishes its binding function to the mitochondrial apoptotic effectors BAX (Dai et al., 2013; Yamamoto, Ichijo, & Korsmeyer, 1999). By contrast, serine 62 (S62) phosphorylated BCL-xL/total BCL-xL ratio was increased at 4h in MV4-11 cell line (Figure 3.3.3.1C lane 17). It was observed that the endogenous level of BCL-xL was elevated at 24h in OCI-AML3 (Figure 3.3.3.1C lane 6) and MOLM-13 cell lines (Figure 3.3.3.1C lane 12). BCL-xL is phosphorylated on many sites including S62, a critical site for its response to microtubule-damaging drugs such as vinblastine (Upreti et al., 2008). Indeed, a phosphorylation at S62 results in BCL-xL to release bound BAX, promoting apoptosis. An increase in S62 phosphorylated BCL-xL observed in MV4-11 cell line potentially induces an activation of intrinsic apoptosis pathway. However, this effect was not seen in OCI-AML3 and MOLM-13 cell lines. It has been reported that BCL-xL is diminished in expression in $p53^{-/-}$ HCT116 isogenic human colorectal cancer cells treated with the CDKI seliciclib for 8h (De Leon, Cavino, D'Angelo, & Krucher, 2010). Furthermore, NOXA was evaluated. NOXA is a sensitiser/de-repressor BH3-only protein which specifically binds and inhibits MCL-1 (H. Kim et al., 2006). However, it was observed that CYC065 did not have an impact on NOXA expression (Figure 3.3.3.1E,F). Collectively, it can be implied that MCL-1 (section 3.3.2), but not BCL-2 or BCL-xL, was the key target of CYC065.

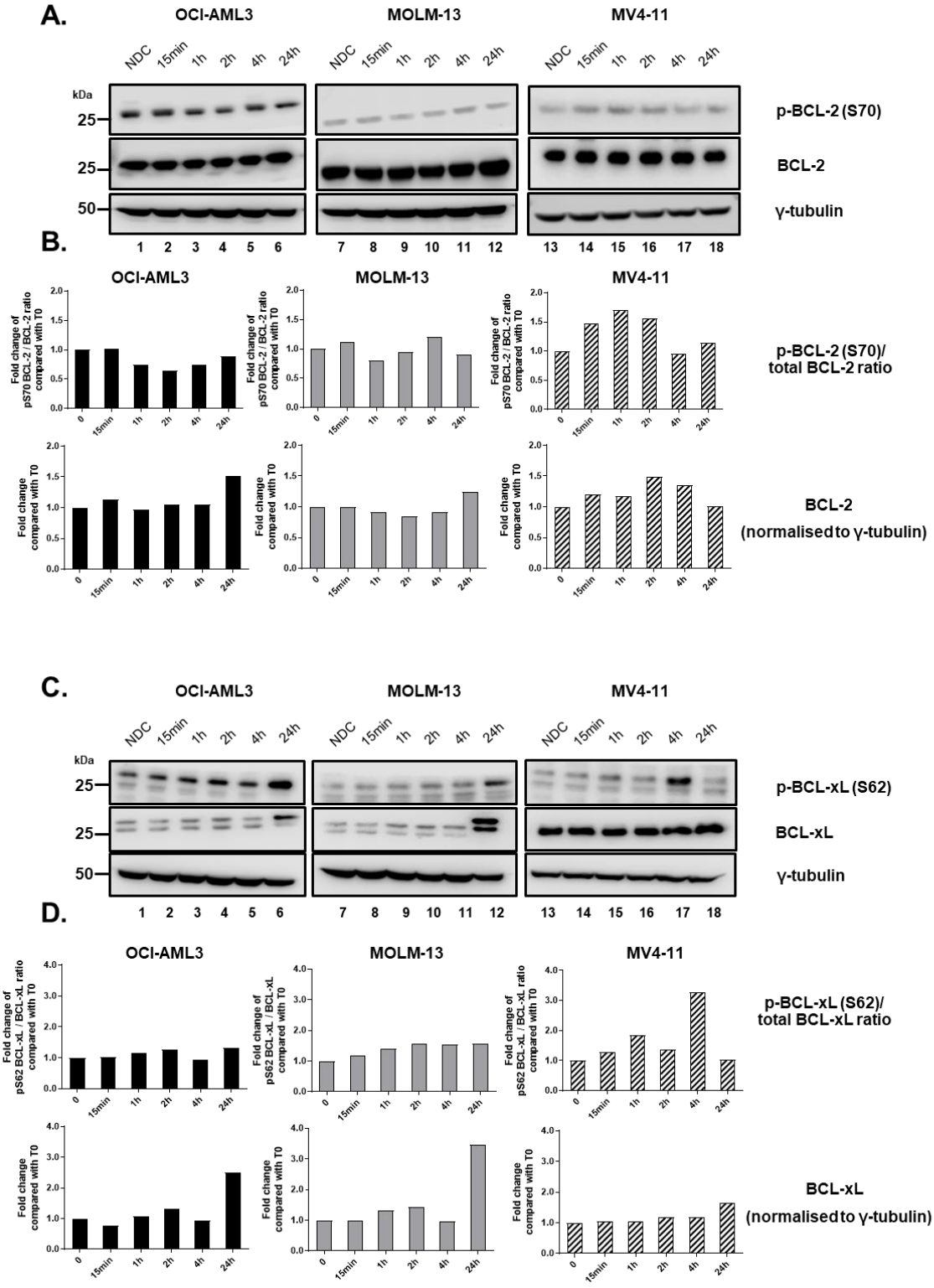

Figure 3.3.3.1 OCI-AML3, MOLM-13, and MV4-11 cell lines were treated with 1μM CYC065, for 15min, 1h, 2h, 4h and 24h. (A) Western blotting of S70 phosphorylated BCL-2 and the endogenous BCL-2 protein; and (B) normalised relative fold change of S70 phosphorylated BCL-2/total BCL-2 ratio (top panel) and the endogenous level of BCL-2 protein to γ-tubulin (bottom panel) as compared with NDC, evaluated by densitometry, n=1. (C) Western blotting of S62 phosphorylated BCL-xL and the endogenous BCL-xL protein; and (D) normalised relative fold change of S62 phosphorylated BCL-xL/total BCL-xL ratio (top panel) and the endogenous level of BCL-xL to γ-tubulin (bottom panel) as compared with NDC, evaluated by densitometry, n=1. Graphs depict means. Serine 70 phosphorylated B-cell lymphoma 2 (p-BCL-2, S70). B-cell lymphoma 2 (BCL-2). Serine 62 phosphorylated B-cell lymphoma-extra large (p-BCL-xL, S62). B-cell lymphoma-extra large (BCL-xL). Gamma tubulin (γ-tubulin).

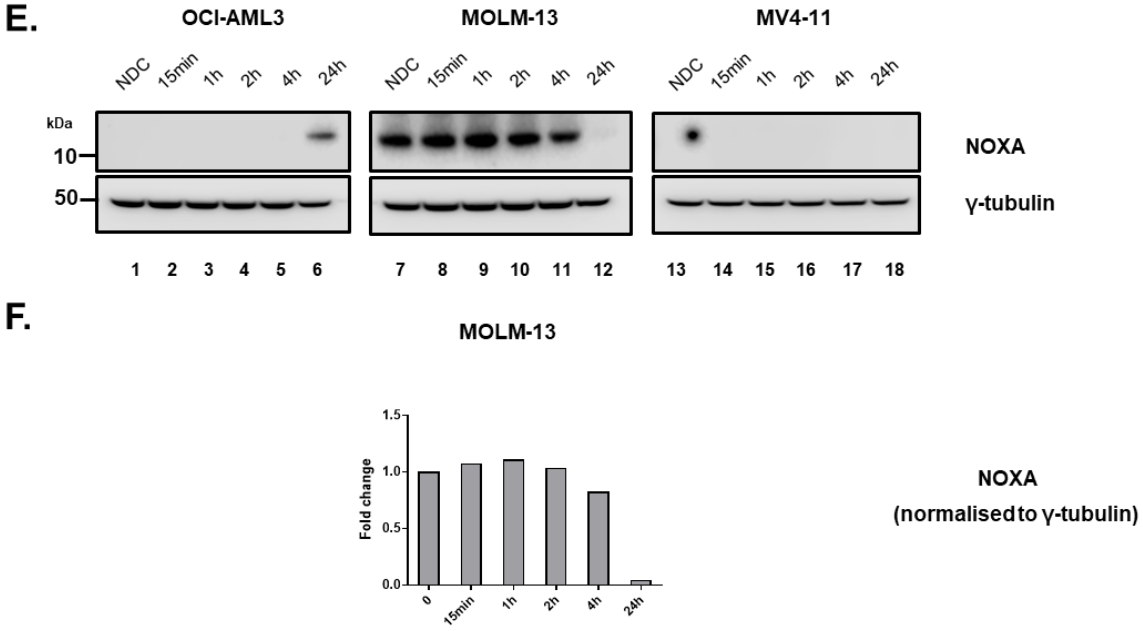

Figure 3.3.3.1 OCI-AML3, MOLM-13, and MV4-11 cell lines were treated with 1μM CYC065, for 15min, 1h, 2h, 4h and 24h. (E) Western blotting of the endogenous NOXA protein; and (F) normalised relative fold change of the endogenous level of NOXA to γ-tubulin as compared with NDC evaluated by densitometry, n=1. Graphs depict means. Phorbol-12-myristate-13-acetate-induced protein 1 (NOXA).

3.3.4 Protein kinases were altered following CYC065 treatment

As MCL-1 was rapidly and dramatically decreased following CYC065 treatment, relevant intracellular signalling pathways which control MCL-1 were investigated. At 4h, threonine 180 (T180) and tyrosine 182 (Y182) phosphorylated p38 mitogen-activated protein kinase (MAPK)/total p38 MAPK ratio was dramatically increased in MOLM-13 (Figure 3.3.4.1A lane 6), whereas, it minimally changed in MV4-11 cell lines (Figure 3.3.4.1A lane 10) and remained unchanged in OCI-AML3 (Figure 3.3.4.1A lane 2). The endogenous level of p38 MAPK was decreased in MOLM-13 cell line following treatment with CYC065 for 24h (Figure 3.3.4.1A lane 8). T180 and Y182 phosphorylation are an absolute requirement for p38 MAPK activation. Indeed, T180 is essential for its catalytic activity, whereas Y182 is required for autoactivation and substrate recognition (Askari, Beenstock, Livnah, & Engelberg, 2009).

Mutually, threonine 202/tyrosine 204 (T202/Y204) phosphorylated ERK1/2/total ERK1/2 ratio was decreased by approximately 50% in all cell lines at 4h; OCI-AML3 (Figure 3.3.4.1C lane 2), MOLM-13 (Figure 3.3.4.1C lane 6), and MV4-11 cell lines (Figure 3.3.4.1C lane 10). The phosphorylation of both tyrosine

and threonine is required for enzyme activation which is facilitated by mitogen-activated protein kinase (MEK1/2). Indeed, MEK1/2 catalyses the phosphorylation of ERK1/2 at Y204 and then T202 (Roskoski, 2012).

Serine 473 (S473) phosphorylated and endogenous level of Akt (protein kinase B) were negligibly altered at 4h in all cell lines (Figure 3.3.4.1E,F). The endogenous level of Akt was decreased in OCI-AML3 cell line following treatment with CYC065 for 24h (Figure 3.3.4.1E lane 4). Akt requires autophosphorylation at S473 site to become fully activated in a phosphoinositide 3-kinase (PI3K)-dependent kinase-1 (PDK-1)-dependent manner (Persad et al., 2001). As compared with other cell lines, a greater increase in inhibitory serine 9 (S9) phosphorylated glycogen synthase kinase 3 beta (GSK3β)/total GSK3β ratio was observed in MOLM-13 cell line (Figure 3.3.4.1G lane 6,H top panel). The endogenous level of GSK3β was decreased by 25-50% in all cell lines following treatment with CYC065 for 24h (Figure 3.3.4.1G,H bottom panel). Akt directly phosphorylates GSK3β on S9 and inactivates its activity (Thornton et al., 2008). GSK3 phosphorylates MCL-1 at serine 155 (S155), serine 159 (S159), and threonine 163 (T163) (Ding et al., 2007; Maurer, Charvet, Wagman, Dejardin, & Green, 2006; H. Yamaguchi, Hsu, & Hung, 2012). Then, the phosphorylated MCL-1 is ubiquitinated and undergoes proteasome-dependent degradation (H. Yamaguchi et al., 2012).

Taken together, following treatment with CYC065, ERK1/2 was suppressed, synchronously with a transcriptional downregulation of MCL-1 in all cell lines. Phosphorylated p38 MAPK/total p38 MAPK ratio was markedly increased only in MOLM-13 cell line, implying that stress response and apoptosis were highly induced (described in the discussion), which is consistent with the previous results showing that this cell line is most sensitive to CYC065 (section 3.2.1-3.2.6). On the other hand, Akt and GSK3β were not significantly affected by the drug, implying that a downregulation of MCL-1 observed was unlikely to be via the proteasome-dependent degradation pathway.

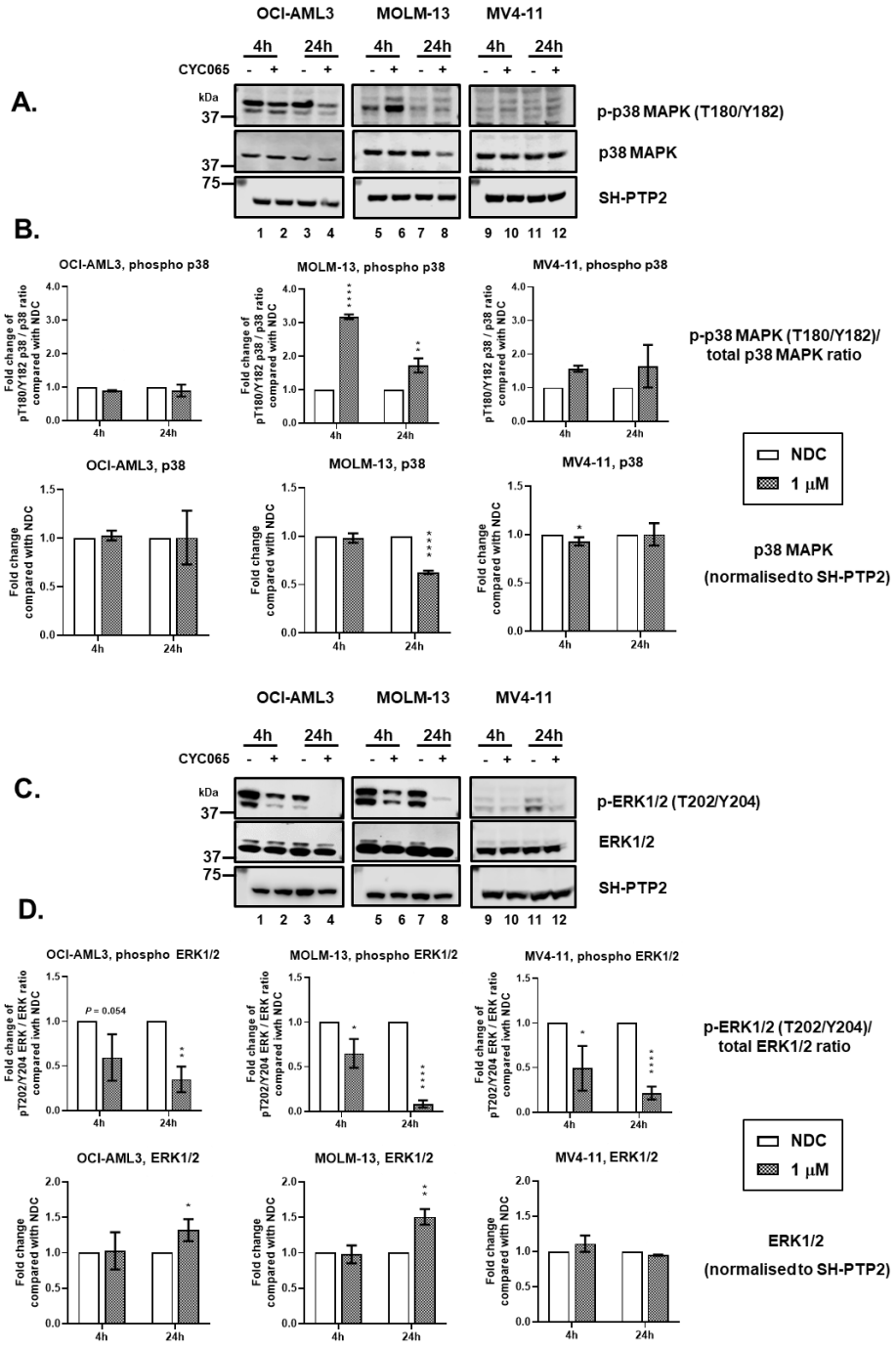

Figure 3.3.4.1 OCI-AML3, MOLM-13, and MV4-11 cell lines were treated with 1μM CYC065, for 4h and 24h. (A) Western blotting of T180/Y182 phosphorylated p38 MAPK and the endogenous p38 MAPK protein; and (B) normalised relative fold change of T180/Y182 phosphorylated p38 MAPK/total p38 MAPK ratio (top panel) and the endogenous level of p38 MAPK protein to SH-PTP2 (bottom panel) as compared with NDC, evaluated by densitometry. The experiments were performed in biological triplicates. **(C) Western blotting of T202/Y204 phosphorylated ERK1/2 and the endogenous ERK1/2 protein; and (D) normalised relative fold change of T202/Y204 phosphorylated ERK1/2/total ERK1/2 ratio (top panel) and the endogenous level of ERK1/2 protein to SH-PTP2 (bottom panel) as compared with NDC, evaluated by densitometry.** The experiments were performed in biological triplicates. Graphs depict means ± SD. Data were compared using the unpaired student's t-test. Significant *P*-values are indicated by asterisks (****< 0.0001, *** 0.0001 to < 0.001, ** 0.001 to < 0.01, * 0.01 to < 0.05 and NS if $P \geq 0.05$). Threonine 180 and tyrosine 182 phosphorylated p38 mitogen-activated protein kinase (p-p38 MAPK, T180/Y182). p38 mitogen-activated protein kinase (p38 MAPK). Threonine 202 and tyrosine 204 phosphorylated extracellular signal-regulated kinase 1 and 2 (p-ERK1/2, T202/Y204). Extracellular signal-regulated kinase 1 and 2 (ERK1/2).

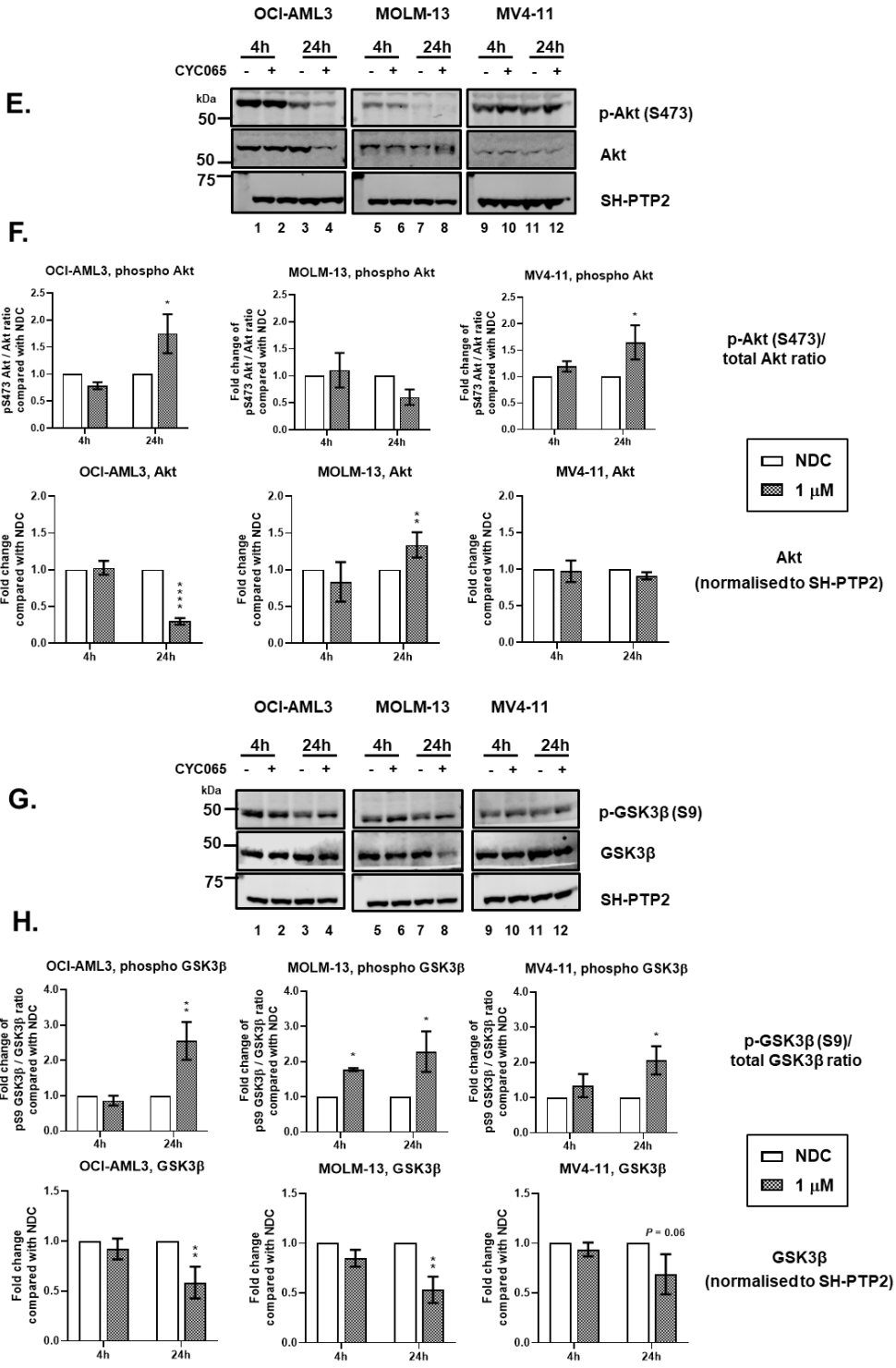

Figure 3.3.4.1 OCI-AML3, MOLM-13, and MV4-11 cell lines were treated with 1μM CYC065, for 4h and 24h. (E) Western blotting of S473 phosphorylated Akt and the endogenous Akt protein; and (F) Normalised relative fold change of S473 phosphorylated Akt/total Akt ratio (top panel) and the endogenous level of Akt protein to SH-PTP2 (bottom panel) as compared with NDC, evaluated by densitometry. The experiments were performed in biological triplicates. **(G) Western blotting of phosphorylated S9 GSK3β and the endogenous GSK3β protein; and (H) normalised relative fold change of phosphorylated S9 GSK3β/total GSK3β ratio (top panel) and the endogenous level of GSK3β protein to SH-PTP2 (bottom panel) as compared with NDC, evaluated by densitometry.** The experiments were performed in biological triplicates. Graphs depict means ± SD. Data were compared using the unpaired student's t-test. Significant *P*-values are indicated by asterisks (****< 0.0001, *** 0.0001 to < 0.001, ** 0.001 to < 0.01, * 0.01 to < 0.05 and NS if $P \geq 0.05$). Serine 473 phosphorylated protein kinase B (p-Akt, S473). Protein kinase B (Akt). Inhibitory serine 9 phosphorylated glycogen synthase kinase 3 beta (p-GSK3β, S9). Glycogen synthase kinase 3 beta (GSK3β).

3.4 Effects of CYC065 on gene expression

As CDK2 and CDK9 play important roles in transcription, the effects of CYC065 on gene expression of key transcripts involved in the cell cycle and apoptosis pathways were also investigated. OCI-AML3, MOLM-13, and MV4-11 cell lines were treated with 0.75μM, 0.5μM, and 1μM of CYC065, respectively, for 4h and 24h at which approximately 50% apoptosis of the cells was determined according to apoptosis assays (section 3.2.3). qRT-PCR of the specific target amplification (STA) was performed and data were analysed as detailed in Methods section 2.2.2.3.2.

3.4.1 Important cell cycle regulatory gene expression was suppressed after CYC065 treatment

Fold change of each gene compared with NDC is displayed in the heatmap (Figure 3.4.1.1). Expression of target genes were downregulated following CYC065 treatment, including; CDK family, transcription factors, key protein phosphatase, CDKI, DNA damage response regulator, anti-apoptotic related, and pro-apoptotic related genes (described individually below). Indeed, as the primary drug target is the point of interest rather than the secondary effect, gene expression at 4h is more relevant and is focused on here.

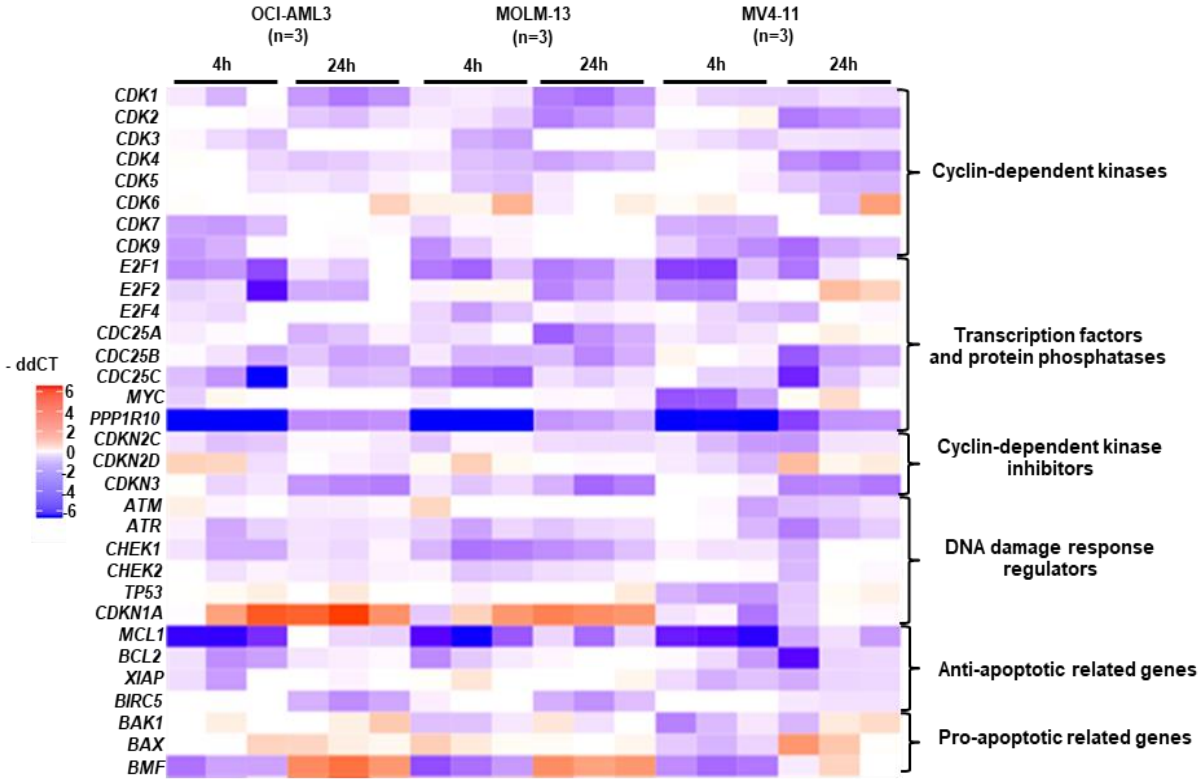

Figure 3.4.1.1 Heatmap demonstrating fold change relative to NDC of each gene in OCI-AML3, MOLM-13, and MV4-11 cell lines treated with 0.75μM, 0.5μM, and 1μM of CYC065, respectively, for 4h and 24h at which approximately 50% apoptosis of the cells was determined according to apoptosis assays. The experiments were performed in technical duplicates and biological triplicates.

3.4.2 Cyclin-dependent kinase genes: *CDK7* and *CDK9* were markedly suppressed at 4h

Fold change expression of CDK genes relative to NDC in OCI-AML3, MOLM-13, and MV4-11 cell lines following CYC065 treatment is shown in Figure 3.4.2.1. At 4h, *CDK9* was diminished in all cell lines with approximately 50% downregulation compared to NDC, whereas, *CDK7* was downregulated by 60-65% in OCI-AML3 and MV4-11 but only slightly decreased in MOLM-13 cell line. In contrast, *CDK1*, *CDK2*, *CDK3*, *CDK4*, and *CDK5* were less affected in all cell lines assessed at 4h. At 24h, *CDK1* was suppressed by 80% in OCI-AML3 and MOLM-13 cell lines, whereas, *CDK2* and *CDK4* were suppressed by 80% in MOLM-13 and MV4-11 cell lines when compared to NDC. It was observed that CYC065 did not have a significant impact on *CDK6* expression. Taken together, although CYC065 is designed to selectively bind to the ATP-binding sites of CDK2 and CDK9, it indirectly suppresses the expression of various CDK genes, with the exception of *CDK6*.

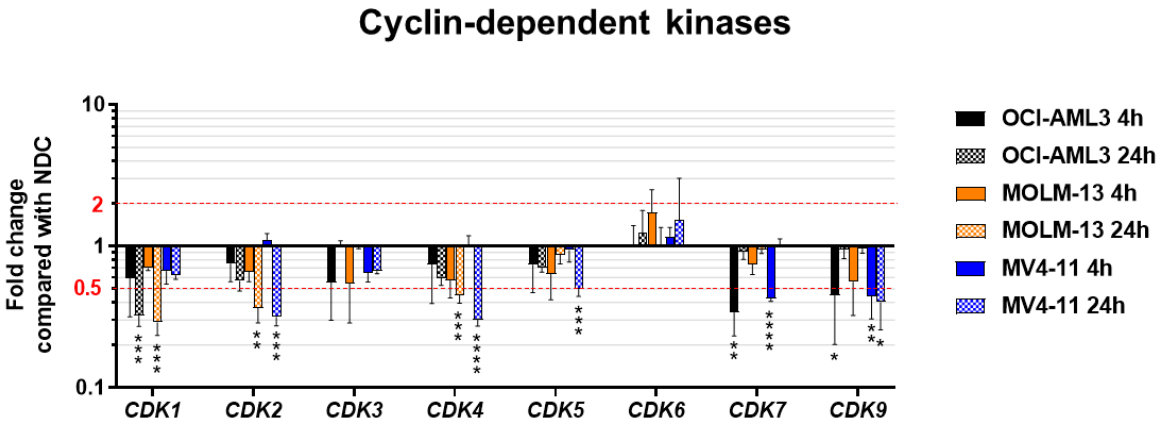

Figure 3.4.2.1 Fold change expression of CDK genes relative to NDC in OCI-AML3, MOLM-13, and MV4-11 cell lines treated with 0.75µM, 0.5µM, and 1µM of CYC065, respectively, for 4h and 24h. The experiments were performed in technical duplicates and biological triplicates. Graphs depict means ± SD. Data were compared using the unpaired student's t-test. The red lines depict two-fold increase and decrease in expression when calibrated against the NDC. Significant *P*-values are indicated by asterisks (****< 0.0001, *** 0.0001 to < 0.001, ** 0.001 to < 0.01, * 0.01 to < 0.05 and NS if $P \geq 0.05$). Cyclin-dependent kinase (CDK).

3.4.3 Transcription factor and key protein phosphatase genes: *PPP1R10* and *E2F1* were significantly downregulated at 4h in all cell lines

Fold change expression of transcription factor and key protein phosphatase genes relative to NDC in OCI-AML3, MOLM-13, and MV4-11 cell lines following CYC065 treatment is shown in Figure 3.4.3.1. Strikingly, PP1 regulatory subunit 10 (*PPP1R10*) was very significantly diminished with more than 95% downregulation at 4h in all cell lines compared to NDC. Among the E2F family, *E2F1* was decreased across all cell lines with approximately 70% downregulation at 4h. *E2F2* was suppressed by 60% in OCI-AML3 and MV4-11 cell lines, whereas, *E2F4* was negligibly affected. At 24h, *E2F1* and *E2F2* were suppressed only in MOLM-13 cell line. Considering the CDC25 family, at 4h, *CDC25B* was reduced by approximately 50%, whereas, *CDC25C* was decreased by approximately 70% in both OCI-AML3 and MOLM-13 cell lines when compared to NDC. At 24h, *CDC25B* was suppressed in all cell lines. The expression of *MYC* was decreased at 4h only in MV4-11 cell line. Collectively, following treatment with CYC065, the expression of transcription factor genes was generally suppressed, in particular, *E2F1*. In addition, the drug had a marked impact on *PPP1R10* expression, especially, at the early timepoint of 4h (discussed in section 3.5).

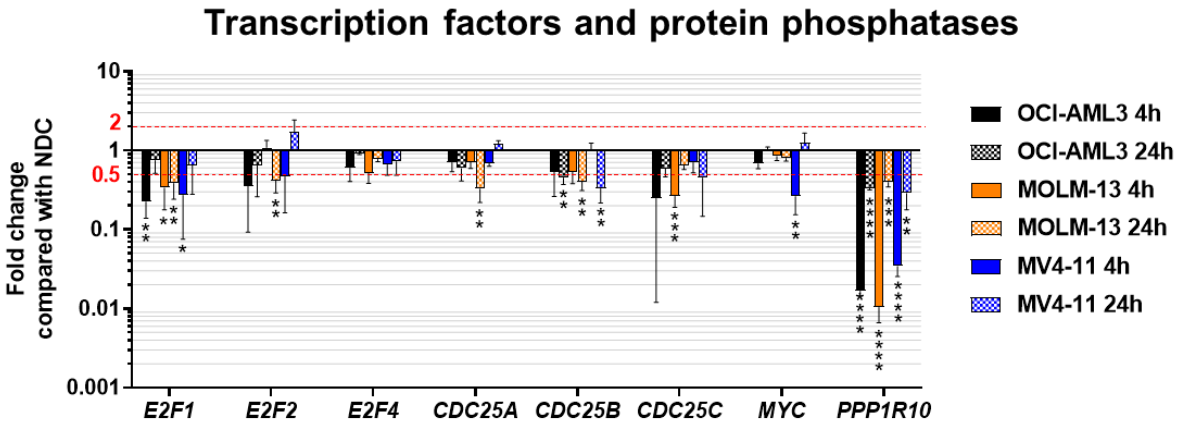

Figure 3.4.3.1 Fold change expression of transcription factor and key protein phosphatase genes relative to NDC in OCI-AML, MOLM-13, and MV4-11 cell lines treated with 0.75μM, 0.5μM, and 1μM of CYC065, respectively, for 4h and 24h. The experiments were performed in technical duplicates and biological triplicates. Graphs depict means ± SD. Data were compared using the unpaired student's t-test. The red lines depict two-fold increase and decrease in expression when calibrated against the NDC. Significant *P*-values are indicated by asterisks (****< 0.0001, *** 0.0001 to < 0.001, ** 0.001 to < 0.01, * 0.01 to < 0.05 and NS if $P \geq 0.05$). Cell division cycle (CDC). Myelocytomatosis oncogene (MYC). Protein phosphatase 1 (PP1) regulatory subunit 10 (PPP1R10).

3.4.4 Cyclin-dependent kinase inhibitor genes: *CDKN3* was markedly suppressed at 24h

Fold change expression of CDK inhibitor genes relative to NDC in OCI-AML3, MOLM-13, and MV4-11 cell lines following CYC065 treatment is shown in Figure 3.4.4.1. At 4h, it was observed that cyclin-depend kinase inhibitor 2C (*CDKN2C*) was suppressed by 50% in OCI-AML3 and MV4-11 cell lines. The expression of cyclin-depend kinase inhibitor 3 (*CDKN3*) was diminished by 80% at 24h in all cell lines when compared to NDC. Cyclin-dependent kinase inhibitor 2D (*CDKN2D*) was marginally affected by the drug. *CDKN2C* and *CDKN2D* encode $p18^{INK4C}$ and $p19^{INK4D}$, respectively, which compete with cyclin D, preventing formation of CDK4/6-cyclin D complexes (Jeffrey et al., 2000). CDKN3 dephosphorylates and inhibits CDK2 at threonine 160 (T160), whereas, cyclin A counteracts T160 dephosphorylation by CDKN3 (R. Y. Poon & Hunter, 1995). Hence, CDK2/cyclin A complex, which drives S phase, is resistance to CDKN3 (Cress, Yu, & Wu, 2017). In addition, CDKN3 also dephosphorylates and inhibits CDK1 (Nalepa et al., 2013). Taken together, CYC065 not only suppressed the expression of various CDK genes (section 3.4.2), but also suppressed the expression of some CDKI genes, in particular, *CDKN3* expression at 24h.

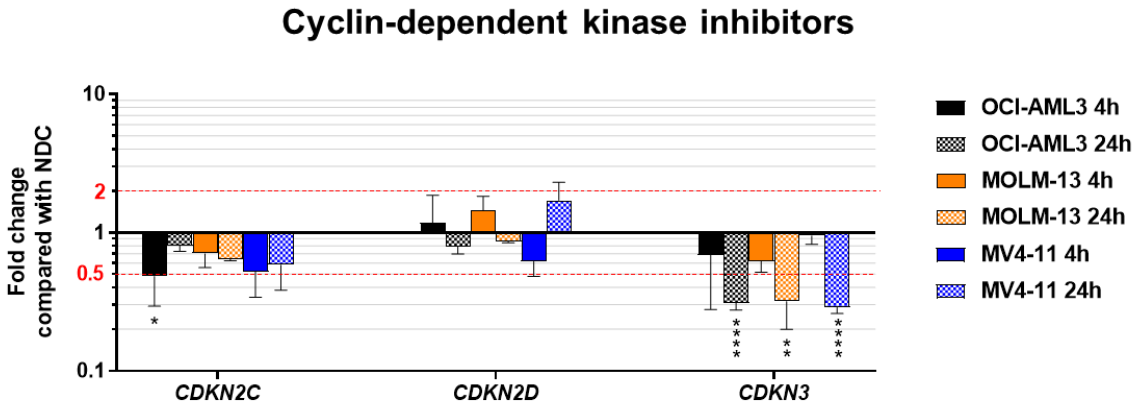

Figure 3.4.4.1 Fold change expression of CDK inhibitor genes relative to NDC in OCI-AML, MOLM-13, and MV4-11 cell lines treated with 0.75μM, 0.5μM, and 1μM of CYC065, respectively, for 4h and 24h. The experiments were performed in technical duplicates and biological triplicates. Graphs depict means ± SD. Data were compared using the unpaired student's t-test. The red lines depict two-fold increase and decrease in expression when calibrated against the NDC. Significant *P*-values are indicated by asterisks (****< 0.0001, *** 0.0001 to < 0.001, ** 0.001 to < 0.01, * 0.01 to < 0.05 and NS if $P \geq 0.05$). Cyclin-depend kinase inhibitor (CDKN).

3.4.5 DNA damage response regulator genes: *ATR* and *CHEK1* were downregulated concurrently with an upregulation of *CDKN1A* (p21^{Cip1}) at 4h in OCI-AML3 and MOLM-13 cell lines

Fold change expression of DNA damage response regulator genes relative to NDC in OCI-AML3, MOLM-13, and MV4-11 cell lines following CYC065 treatment is shown in Figure 3.4.5.1. At 4h, the expression of *ATR* and *CHEK1* were suppressed by 50% and 60%, respectively, in comparison to NDC, concurrently with an upregulation of *CDKN1A* in both OCI-AML3 and MOLM-13 cell lines. The expression of cyclin-depend kinase inhibitor 1A (*CDKN1A*), encoding p21^{Cip1}, was greater at 24h in both cell lines, indicating that the intrinsic apoptosis pathway was being activated following drug treatment (Hernandez et al., 2013). In MV4-11 cell line, the expression of *CDKN1A* was suppressed at 4h by 40%. The three cell lines assessed in this study have wild-type p53 (Morita et al., 2017; Weisberg et al., 2015). It was observed that the expression of *TP53* was decreased by approximately 60% in MV4-11 cell line. The expression of *ATR* was reduced by 60% at 24h in this cell line. It was observed that *ATM* and *CHEK2* were not significantly affected by CYC065. Collectively, *ATR* and *CHEK1* expression were markedly suppressed as compared with the other DNA damage response regulators examined. In addition, the upregulation of *CDKN1A* expression implied an activation of the intrinsic apoptosis pathway.

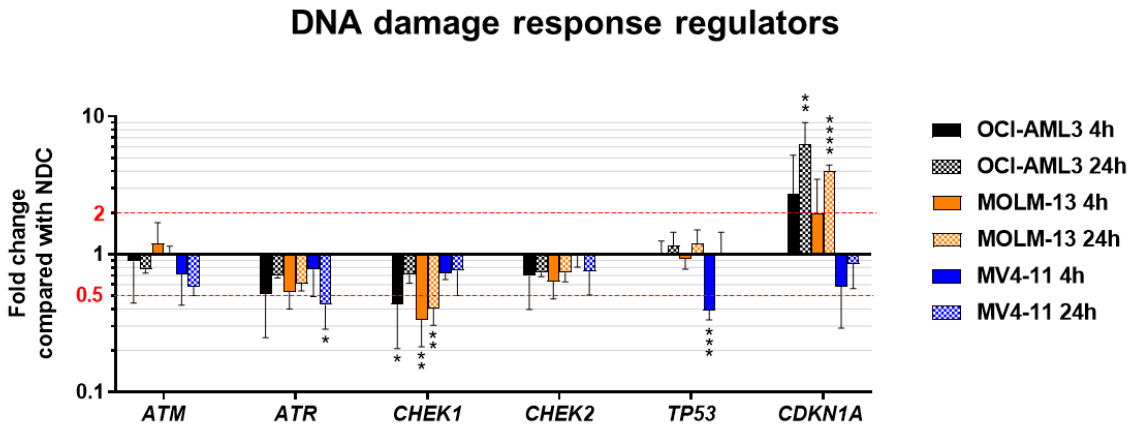

Figure 3.4.5.1 Fold change expression of DNA damage response regulator genes relative to NDC of OCI-AML, MOLM-13, and MV4-11 cell lines treated with 0.75μM, 0.5μM, and 1μM of CYC065, respectively, for 4h and 24h. The experiments were performed in technical duplicates and biological triplicates. Graphs depict means ± SD. Data were compared using the unpaired student's t-test. The red lines depict two-fold increase and decrease in expression when calibrated against the NDC. Significant *P*-values are indicated by asterisks (****< 0.0001, *** 0.0001 to < 0.001, ** 0.001 to < 0.01, * 0.01 to < 0.05 and NS if $P \geq 0.05$). Ataxia telangiectasia-mutated (ATM). Ataxia telangiectasia and Rad3 related (ATR). Checkpoint kinase (CHEK). Tumour protein p53 (TP53). Cyclin-dependent kinase inhibitor 1A (CDKN1A/p21^{Cip1}).

3.4.6 Anti-apoptotic related genes: *MCL1* had the greatest suppression

Fold change expression of anti-apoptotic related genes relative to NDC in OCI-AML3, MOLM-13, and MV4-11 cell lines following CYC065 treatment is shown in Figure 3.4.6.1. Strikingly, the expression of *MCL1* was reduced by approximately 90% at 4h in all cell lines, when compared to NDC indicating the specificity of the drug treatment for this anti-apoptotic pathway. At 4h, the drug has less effect on the expression of *BCL2* with 60%, 50%, and 40% downregulation in OCI-AML3, MOLM-13, and MV4-11 cell lines, respectively relative to NDC. The expression of *XIAP* was diminished by 40% at 4h in both OCI-AML3 and MV4-11 cell lines. At 24h, the expression of *MCL1* was decreased by 50% in MOLM-13 and MV4-11 cell lines, whereas, *BIRC5* encoding survivin was suppressed by 60% in OCI-AML3 and MOLM-13 cell lines. *BCL2* and *XIAP* were non-significantly downregulated at 24h in MV4-11 cell line. BIRC-5 and XIAP are a member of the IAP family. They function to inhibit caspase activation (Deveraux & Reed, 1999; Tamm et al., 1998). Taken together, as compared with other anti-apoptotic related genes assessed, CYC065 had a greater impact on *MCL1* expression (discussed in section 3.5). The downregulation of MCL-1 was confirmed at both gene and protein levels (section 3.3.2).

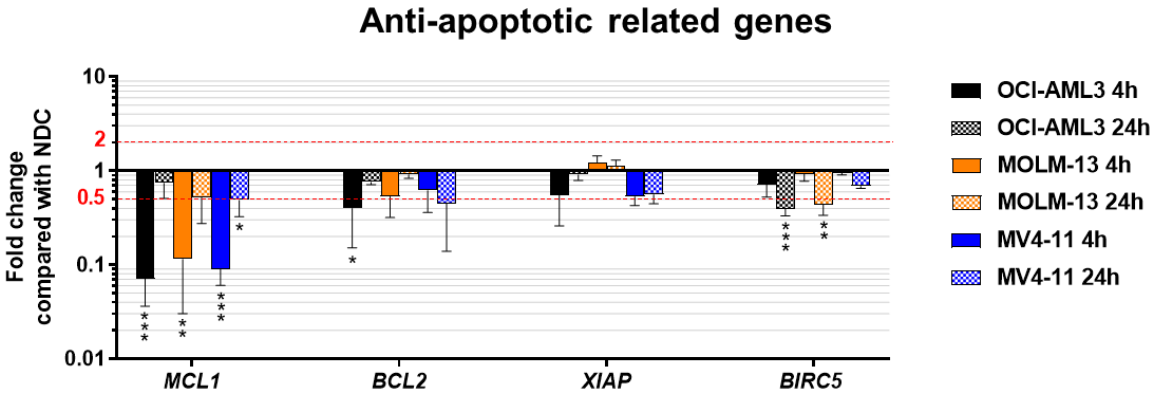

Figure 3.4.6.1 Fold change expression of anti-apoptotic related genes relative to NDC of OCI-AML, MOLM-13, and MV4-11 cell lines treated with 0.75μM, 0.5μM, and 1μM of CYC065, respectively, for 4h and 24h. The experiments were performed in technical duplicates and biological triplicates. Graphs depict means ± SD. Data were compared using the unpaired student's t-test. The red lines depict two-fold increase and decrease in expression when calibrated against the NDC. Significant *P*-values are indicated by asterisks (****< 0.0001, *** 0.0001 to < 0.001, ** 0.001 to < 0.01, * 0.01 to < 0.05 and NS if $P \geq 0.05$). Myeloid cell leukemia 1 (MCL1). B-cell lymphoma 2 (BCL2). X-linked inhibitor of apoptosis protein (XIAP). Baculoviral inhibitor of apoptosis repeat-containing 5 (BIRC5/survivin).

3.4.7 Pro-apoptotic related genes: *BMF* was downregulated at 4h and then rebounded at 24h

Fold change expression of pro-apoptotic related genes relative to NDC in OCI-AML3, MOLM-13, and MV4-11 cell lines following CYC065 treatment is shown in Figure 3.4.7.1. It was observed that the expression of *BMF* was decreased by 80% at 4h, then rebounded at 24h in all cell lines when compared to NDC. BMF is a sensitiser/de-repressor BH3 only protein which mainly binds and inhibits BCL-2 and BCL-xL (Jeng, Inoue-Yamauchi, Hsieh, & Cheng, 2018). However, it has been reported that BMF also interacts with MCL-1, but with weaker affinity (Day et al., 2005; Vogler et al., 2017). The gene expression of mitochondrial apoptotic effectors BAK and BAX were also evaluated. At 4h, the expression of *BAK1* was reduced by 40% and 50% in MOLM-13 and MV4-11 cell lines, respectively. In MV4-11 cell line, *BAX* was suppressed by 50% at 4h then upregulated at 24h when compared to NDC. Taken together, CYC065 had a great impact on the expression of *BMF* which was downregulated at 4h and then rebounded at 24h. Interestingly, among pro-apoptotic genes examined, the half-life of BAK and BAX is approximately 12h (Song et al., 2019), whereas, the half-life of BMF is shorter i.e. approximately 2h (Contreras et al., 2013) which potentially explains the greater impact.

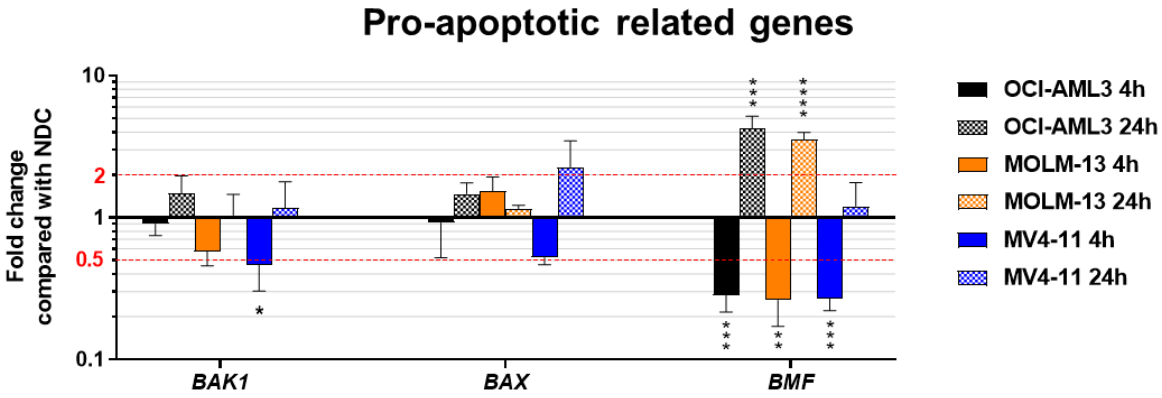

Figure 3.4.7.1 Fold change expression of pro-apoptotic related genes relative to NDC of OCI-AML, MOLM-13, and MV4-11 cell lines treated with 0.75μM, 0.5μM, and 1μM of CYC065, respectively, for 4h and 24h. The experiments were performed in technical duplicates and biological triplicates. Graphs depict means ± SD. Data were compared using the unpaired student's t-test. The red lines depict two-fold increase and decrease in expression when calibrated against the NDC. Significant *P*-values are indicated by asterisks (****< 0.0001, *** 0.0001 to < 0.001, ** 0.001 to < 0.01, * 0.01 to < 0.05 and NS if $P \geq 0.05$). B-cell lymphoma 2 antagonist/killer 1 (BAK1). B-cell lymphoma 2 Associated X (BAX). B-cell lymphoma 2 modifying factor (BMF).

3.5 Discussion

Karyotypes and the genetic mutational status are the most important predictors of resistance in AML (Estey, 2018). Therefore, OCI-AML3 (carries NPM1 and DNMT3A R882C mutations), MOLM-13 (carries *FLT3*-ITD and *KMT2A-MLLT3*), and MV4-11 (carries *FLT3*-ITD and *KMT2A-AFF1*) cell lines were used in this study. This was aiming to encompass the stratifications of major risk profiles according to the ELN recommendations (H. Döhner et al., 2017), to assess the effects of the novel CDK2/9 inhibitor CYC065 on growth and survival of AML cells.

Notably, comparing between the three cell lines, the IC50 of CYC065 in MV4-11, which carries adverse prognosis molecular abnormality, was higher than in OCI-AML3 and MOLM-13 cell lines (Figure 3.2.1.1). It was observed that the longer CYC065 exposure, the greater the cytotoxic/anti-metabolic effect on the cells, with a reduction of the IC50. This is consistent with apoptosis which was fully induced and completed by 24h and 72h, respectively, in all AML cell lines tested. To induce approximately 50% of apoptosis, 0.75μM, 0.5μM and, 1μM of CYC065 were required in OCI-AML3, MOLM-13, and MV4-11 cell lines, respectively at 72h. In addition, active caspase-3, which is a downstream effector of apoptosis and used as a hallmark apoptosis marker (Slee et al., 2001), was used to confirm annexin V/DAPI apoptosis assay findings. It was observed that the percentage of active caspase-3-positive cells was increased, and correlated with an increase in the percentage of annexin V-positive cells across higher CYC065 concentrations at 24h, 48h and 72h. Cell cycle analyses demonstrated a corresponding increase in the percentage of the sub G0 population, without an increase of any other cell cycle phase. However, G1 arrest was observed at 4h in OCI-AML3 and MV4-11 cell lines, indicating that cell cycle arrest occurred at an early time point which precedes the induction of cell death (Figure 3.2.5.1). On the other hand, cell cycle arrest was not seen in MOLM-13 cell line which is, among the three cell lines assessed in this study, the most sensitive to CYC065.

Next, the specificity of CYC065, in terms of inhibition of CDK activities, was evaluated using Western blotting for measurement of the phosphorylation level of their substrates (section 3.3.1). All cell lines were treated with 1μM of CYC065 for 4h and 24h. Using PP1 as a substrate, it was observed that CYC065

did not have an impact on CDK1 and CDK2 kinase activities (Figure 3.3.1.1A). Effects of CYC065 on the function of CDK2 and CDK4 kinase were further investigated using Rb protein. In MV4-11 cell line, it was seen that CDK2 and CDK4 were not affected by CYC065. Nevertheless, Rb protein was markedly transcriptionally suppressed in MOLM-13 cell line following CYC065 treatment and there was low expression of Rb in OCI-AML3 at baseline (Figure 3.3.1.1C,E), which means this substrate is not applicable for this cell line. Rb is a tumour suppressor and is known to play a key role in suppressing excessive cell proliferation through inhibition of cell cycle progression. It has been previously reported that a low expression of Rb protein is associated with an inferior response to conventional chemotherapy, resulting in shortened survival in AML patients (Kornblau et al., 1998; Kornblau et al., 1992; Kornblau et al., 1994). RNAPII was utilised to evaluate CDK7 and CDK9 kinase activities. However, the endogenous level of RNAPII was markedly decreased in all cell lines following treatment with CYC065 (Figure 3.3.1.1G,I). Therefore, analysing the direct effect of CYC065 on CDK7 or CDK9 activities by Western blotting was inconclusive. During the optimisation stage, it was observed that either reducing CYC065 concentration or assessing at an earlier time point (before 4h) did not work as effects of the drug on target proteins were not seen (data not shown). Consequently, the high throughput Pamgene™ STK activity profiling was also utilised aiming to elucidate these ambiguities (see Chapter 4), and better understand the effects of CYC065 on the cell cycle. Inhibiting RNAPII affects molecules essential to cancer cell survival, in particular those with short protein half-lives (Koumenis & Giaccia, 1997; Lam et al., 2001). It has been reported that the wild-type KG1a AML cells, as compared with dormant cells induced by long-term exposure to a mammalian target of rapamycin (mTOR) inhibitor, cells are more sensitive to various chemotherapies, including cytarabine, daunorubicin, azacitidine, clofarabine, and three CDKIs with activity against RNAPII - alvocodib, seliciclib and TG02 (Pallis et al., 2013). It was observed that inhibiting RNAPII by the three CDKIs strongly inhibits RNA synthesis, measuring with 5-ethynyl uridine. Interestingly, the percentage of cell reduction by RNAPII inhibitors was also significantly greater as compared with other agents. This effect was observed in both wild-type and dormant KG1a cells, and in CD34+ primary AML cells. These findings support the rationale that suppressing RNAPII

in AML cells using CDK inhibitors could be a potential beneficial therapeutic approach in combination with standard chemotherapy.

Following CYC065 treatment, it was observed that MCL-1 protein level, but not BCL-2 or BCL-xL, dramatically dropped at 4h resulting in rapid induction of apoptosis in all cell lines. It has been reported Cre-loxP-mediated *MCL1* knockout results in significant apoptosis in transformed AML cells generating by transducing mouse BM-derived HSPCs with *KMT2A-MLLT3*, *KMT2A-MLLT1*, *AML1-ETO9a*, and *HOXA9* retroviral constructs (Glaser et al., 2012). The knockout had less impact on normal HSPCs. In addition, Cre-loxP-mediated *MCL1* knockout significantly prolonged survival in mice transplanted with *KMT2A-MLLT1* transformed AML cells. These findings suggest that AML cells may be more dependent on MCL-1 than normal HSPCs. In MV4-11 cell line, however, although there was a dramatic decrease in MCL-1 level at 24h (Figure 3.3.2.1A lane 12), less apoptosis i.e. approximately 50% was observed (Figure 3.2.3.1E,F), correlating with less accumulation of cleaved PARP-1 (Figure 3.3.2.1C lane 12) comparing with other cell lines treated with 1μM of CYC065 for 24h. This indicates that the major target of CYC065 is MCL-1, but inhibiting only MCL-1 may not be sufficient for the cells to be completely eliminated. This brings forth the notion that combination studies of CYC065 with other chemotherapies are potentially beneficial. We hypothesised that targeting parallel anti-apoptotic mechanisms would induce a synergistic effect. Therefore, a selective BCL-2 inhibitor venetoclax was selected as one of the partners of CYC065 for performing combination studies (see Chapter 5).

Relevant intracellular signalling pathways which control MCL-1 were investigated. Expression of *MCL1* gene is controlled by multiple intracellular signalling pathways, including; PI3K/Akt (Longo et al., 2008; J. M. Wang et al., 1999; H. Yamaguchi et al., 2012), ERK (Booy, Henson, & Gibson, 2011; H. Yamaguchi et al., 2012), p38 MAPK (Azijli et al., 2013; Huelsemann et al., 2015) and GSK3β (H. Yamaguchi et al., 2012) pathways. ERK1/2 was suppressed synchronously with a transcriptional downregulation of MCL-1 following treatment with CYC065 for 4h in all cell lines (Figure 3.3.4.1C,D). It has been reported that the ERK inhibitor 3-(2-Aminoethyl)-5-[(4-ethoxyphenyl)methylidene]-1,3-thiazolidine-2,4-dione prevents the elevation of

MCL-1 which is transcriptionally upregulated in MCF-7 and SK-BR-3 breast cancer cell lines treated with epidermal growth factor (EGF) (Booy et al., 2011). In addition, ERK-mediated phosphorylation of MCL-1 at threonine 92 (T92) and threonine 163 (T163) (Ding et al., 2008; Domina, Vrana, Gregory, Hann, & Craig, 2004) is required for the interaction with peptidyl-prolyl cis-trans isomerase NIMA-interacting 1 (Pin1) which promotes its stability (H. Yamaguchi et al., 2012). Pin1 is a peptidyl–prolyl cis/trans isomerase that binds to specific phospho-serine/threonine-proline (pS/T-P) motifs and then isomerises its substrates, resulting in their conformational changes (Lu & Hunter, 2014). Hence, a decrease in the ERK1/2 activity observed potentially promoted a reduction in MCL-1 stability and half-life (Gores & Kaufmann, 2012). In mitoxantrone-resistant HL60/MX2 AML cells, it has been reported that treatment with the MAPK/ERK inhibitor U0126 for 30mins results in a complete inhibition of ERK1/2 phosphorylation. Subsequently, a reduction in the half-life of MCL-1, from 2.1h to approximately 1h, was also observed (Hermanson, Das, Li, & Xing, 2013), supporting the idea that MAPK inhibition in AML may be a good strategy in future combination studies.

Among the three cell lines in this study, T180/Y182 phosphorylation of p38 MAPK had the greatest increase only in MOLM-13 (Figure 3.3.4.1A,B). In the previous study, using sodium arsenite in the phaochromocytoma PC12 cell line, apoptosis induced by p38 MAPK which directly phosphorylates the serine 65 position of the pro-apoptotic BH3-protein BCL-2-like protein 11-extra long (BIM(EL)) was reported (B. Cai, Chang, Becker, Bonni, & Xia, 2006). A photosensitising ethylene glycol porphyrin derivative was applied to various cancer cell lines and the induction of apoptosis was accompanied by immediate and sustained activation of p38 MAPK resulting in caspase activation. p38 MAPK inhibitors in MEFs, derived from *p38a* knockout mice, were used to confirm that inhibiting p38 MAPK results in a decrease in induction of apoptosis in cells. In addition, preincubation of cells with scavengers of ROS attenuated p38 MAPK and caspase activation and increased cell survival (Kralova, Dvorak, Koc, & Kral, 2008). Treatment of HeLa cells with 1μM of taxol, 1μM of vincristine, or 1μM of vinblastine activated p38 MAPK and induced apoptosis. Conversely, p38 MAPK inhibitors suppressed cell death. In a p38 MAPK-dependent manner, mitogen-activated protein kinase kinase 6 (MKK6) which is a direct activator of p38 MAPK

also induced cell death by stimulating translocation of BAX from the cytosol to the mitochondria (Deacon, Mistry, Chernoff, Blank, & Patel, 2003). It was observed that Toll-like receptor 1 (TLR1) and TLR2 are upregulated on primary human CD34+CD38- AML cells. In *KMT2A-MLLT3* human AML cells, apoptosis was induced by p38 MAPK-dependent activation of caspase-3 using the TLR1/TLR2 agonist (M. Eriksson et al., 2017). Taken together, the conclusion of these studies is that apoptosis can be induced through an activation of p38 MAPK which is consistent with our results showing that apoptosis is highly induced in MOLM-13 cell line which is the most sensitive to CYC065. In addition, it has been reported that activation of p38 MAPK leads to transcriptional downregulation of MCL-1 expression (Azijli et al., 2013; Huelsemann et al., 2015).

Gene expression was studied in each cell line treated with CYC065. The doses that induce 50% apoptosis i.e. 0.75μM (Figure 3.2.3.1A,B), 0.5μM (Figure 3.2.3.1C,D), and 1μM of CYC065 (Figure 3.2.3.1E,F) were used in OCI-AML3, MOLM-13, and MV4-11 cell lines, respectively. Gene expression was generally downregulated (Figure 3.4.1.1). The most plausible explanation is that there is a global suppression resulting from a downregulation of RNAPII. At 4h, in all cell lines examined, *CDK9* (Figure 3.4.2.1), *E2F1* (Figure 3.4.3.1), *PPP1R10* (Figure 3.4.3.1), and *MCL1* (Figure 3.4.6.1) were suppressed with ≥50% downregulation. A decrease in short half-life MCL-1 transcripts highlights a potential target inhibited by CYC065, which is concordant with an alteration at the protein level (Figure 3.3.2.1A,B). Similarly, it has been reported that MCL-1 is rapidly downregulated in human multiple myeloma cell lines treated with the CDKI seliciclib for 3h, resulting in an induction of apoptosis (MacCallum et al., 2005). By using leukaemic blasts from adult patients with refractory AML in a phase 1 clinical trial, it was observed that treatment with a pan-CDKI alvocidib, which potently inhibits CDK9, results in a downregulation of various genes (NCT00470197) (D. M. Nelson et al., 2011). Among these, a downregulation of *POLR2A* (encoding the major subunit of RNAPII) and *E2F1* was seen, which is similar to the effects of CYC065 observed. Correlative studies of leukaemic BM blasts obtained before and after alvocidib showed a decrease in phosphorylation of RNAPII and the protein expression of MCL-1 in some patients who achieved CR (Karp et al., 2005).

The *PPP1R10* gene encodes a protein regulating the activity of PP1, providing a binding platform for thymocyte selection-associated high mobility group box family member 4 (TOX4) protein and tryptophan-aspartate (WD) repeat-containing protein 82 (WDR82) and a PP1 catalytic subunit (PTW/PP1) phosphatase complex which plays a role in the control of chromatin structure and cell cycle progression during the transition from M phase into interphase (J. H. Lee, You, Dobrota, & Skalnik, 2010; "PPP1R10 gene"). Indeed, it has been reported that siRNA mediated *PPP1R10* knockdown stimulates PP1 activity which results in dephosphorylation of Rb (De Leon et al., 2010) activating its growth suppressive function during each M phase exit (D. A. Nelson, Krucher, & Ludlow, 1997). This effect of *PPP1R10* knockdown is dependent on the expression of Rb which may be the case in OCI-AML3 cell line, in which Rb expression was low at the baseline; and MOLM-13 cell line in which Rb was dramatically transcriptionally suppressed following CYC065 treatment for 4h (Figure 3.3.1.1C,E). However, in MV4-11 cell line, a decrease in phosphorylated Rb/total Rb ratio was not observed either at S780 (Figure 3.3.1.1E) or S807/S811 sites (Figure 3.3.1.1C) which are PP1's dephosphorylation sites (Kolupaeva & Janssens, 2013). Moreover, an accumulation of G2/M population was not noticed in cell cycle analysis of any of the cell lines analysed at 4h (Figure 3.2.5.1). These results indicate that a decrease in *PPP1R10* expression observed might not relevant to its function and the mechanism of action of CYC065. Interestingly, it has been reported that siRNA-mediated *PPP1R10* knockdown results in a release of the tumour suppressor phosphatase and tensin homolog (PTEN) from nuclear sequestration, promoting apoptosis in HeLa cervical cancer, K562 CML, MDA-MB231 breast cancer cells (Kavela et al., 2013). Therefore, further interrogation is potentially beneficial in order to elucidate the relevance of the phenomenon observed.

For the E2F family, E2F1–3 mediate activation at G1/S transition, whereas, E2F4 is primarily responsible for quiescent cell repression (Zhu, Giangrande, & Nevins, 2004). Although E2Fs interacting with Rb plays an essential role for transcription control of both G1/S- and G2/M-regulated genes (Zhu et al., 2004), it has been reported that, in MCF-7 breast cancer cells, inhibition of E2F1 activity by inorganic sodium arsenite causes G1 arrest at 24h (Sheldon, 2017). In U937 AML cells, it was observed that treatment with low dose of alvocidib for 24h results

in a decrease in E2F1 protein level and subsequent G1 arrest (Rishi et al., 2014). In addition, a significant positive correlation between *E2F1* expression and the high level of the oncogene tribbles homolog 2 (TRIB2) protein was seen in primary AML samples. Indeed, it was discovered that TRIB2 mRNA expression is regulated by E2F1. Interestingly, shRNA-mediated *TRIB2* knockdown also resulted in G1 arrest in U937 cells. Taken together, a downregulation of *E2F1* may explain the G1 arrest seen in OCI-AML3 and MV4-11 at 4h following CYC065 treatment (Figure 3.2.5.1). However, further investigation at the transcriptional level of a set of G1/S-regulated genes e.g. *CDC6* (Witkiewicz & Knudsen, 2014; Zhu et al., 2004*),* proliferating cell nuclear antigen (*PCNA*) (Zhu et al., 2004), minichromosome maintenance complex component 7 (*MCM7*) (Witkiewicz & Knudsen, 2014), cyclin E, and cyclin A (Bartek et al., 1997; Hinds et al., 1992) is required.

In order to better understand the mechanism of action and the specificity of CYC065, parallel experiments with a focus on the knockdown of *CDK2*, *CDK9* and both *CDK2*/*CDK9* should be further studied in AML. Faber et al reported that siRNA-mediated *CDK2* knockdown for 48h results in an increase in %Sub G0 in OCI-LY3, OCI-LY8 and OCI-LY18 DLBCL cells (Faber & Chiles, 2007). Interestingly, it was observed that MCL-1 was downregulated in OCI-LY3 and OCI-LY8 at the protein level. In addition, in these DLBCL cells, an increase in %Sub G0 following siRNA-mediated knockdown of *MCL1* has also been reported. In human H1 and H9 embryonic stem cells (hESCs), it has been reported that siRNA-mediated *CDK2* knockdown for 48h leads to an activation of the G1 checkpoint, resulting in an activation of the ATM-CHK2-p53-p21 pathway and p38 MAPK and subsequent G1 arrest with a complete block of DNA replication (Neganova et al., 2011). In addition, it was observed that the knockdown of *CDK2* triggered an activation of the histone variant H2A.X which is a critical determinant of double-strand breaks (DSBs) and formation of BRCA1 and RAD52 proteins which are involved in repairing damaged DNA. Hence, G1 arrest (Figure 3.2.5.1A) and the upregulation of *CDKN1A*/p21^{Cip1} (section 3.4.5) following treatment with CYC065 for 4h observed in the OCI-AML3 cell line possibly resulted from an activation of the G1 checkpoint. In MOLM-13 cell line, upregulation of *CDKN1A*/p21^{Cip1} and activation of p38 MAPK (Figure 3.3.4.1A,B) were observed, however, the DNA damage was too severe to repair as a result of additional CDK9 inhibition (discussed below),

thereby the G1 checkpoint activation potentially led to apoptosis at the early timepoint. Recently, Lin et al reported that CRISPR/Cas9-mediated knockout of *CDK2* for 72h resulted in G1 arrest and apoptosis in A375 melanocytes (H. Liu et al., 2020). In AML cell lines and primary human AML cells, shRNA-mediated *CDK2* knockdown drives differentiation (Ying et al., 2018).

It has been reported that siRNA-mediated *CDK9* knockdown for 72h results in a decrease in the viability of U2OS and KHOS osteosarcoma cells determined by MTT assays. A decrease in S2 phosphorylated RNAPII, but not total RNAPII, as well as MCL-1 and BIRC5/survivin was observed. In CLL patient PBMCs, shRNA-mediated *CDK9* knockdown for 48h resulted in apoptosis (Walsby et al., 2014). In addition, a decrease in S2 phosphorylated RNAPII and a downregulation of *MCL1*, *XIAP* and *CCND2* (encoding cyclin D2) was observed in these cells following treatment with the CDK9 inhibitor CDKI-73 for 8h. In AML patient PBMCs, LY2857785, which inhibits CDKs 7, 8 and 9, induces a decrease in S2 phosphorylated RNAPII at an early timepoint (4h) followed by a reduction of total RNAPII after 6h (Yin et al., 2014), whereas, a decrease in total RNAPII was observed in all AML cell lines tested following treatment with CYC065 for 4h (Figure 3.3.1.1G-J). Concurrently, a reduction of MCL-1 and XIAP protein levels was observed following treatment with LY2857785 as well as an induction of apoptosis as measured by PARP cleavage in these AML patient PBMCs. In addition, the knockdown of *CDK7* and *CDK9* was performed in U2OS cells using shRNA. At 48h, it was observed that *CDK7* knockdown resulted in a decrease in S5 phosphorylated RNAPII with less impact on S2, whereas, *CDK9* knockdown led to a decrease in both S2 and S5 phosphorylated RNAPII. Total RNAPII was marginally affected by either *CDK7* or *CDK9* knockdown, suggesting that the target inhibitions of both LY2857785 and CYC065 were beyond just these CDKs. It has been reported that dinaciclib, a potent CDKs 1, 2, 5, and 9 inhibitor, strongly induces apoptosis of murine Eμ-*Myc* and human DLBCL with rapid (3h) and selective suppression of MCL-1 transcription and protein levels (Gregory et al., 2015). Using ChIP-qPCR to investigate protein-DNA interaction, S2 phosphorylated RNAPII, as a marker of CDK9 activity, was pulled down and primer sets across *MCL1* locus were used to demonstrate their binding.

Guertin et al introduced a novel normalisation strategy for ChIP-seq utilising an internal standard of unchanged peaks for reference termed “parallel factor ChIP” (Guertin, Cullen, Markowetz, & Holding, 2018). Briefly, MCF-7 breast cancer cells were treated with 0.1μM of fulvestrant for 48h to promote degradation of estrogen receptor-alpha (ER) which is via the ubiquitination pathway and the proteasome (Howell, 2006). In the parallel factor ChIP, magnetic protein G beads were incubated with anti-ER or with anti-CTCF (CCCTC-binding factor) then the beads were mixed at a ratio of 1:1. CTCF, a pervasive chromatin factor, was used as an internal control whose genomic distribution is assumed to be unchanged between NDC and fulvestrant-treated MCF-7 cells and the CTCF peaks are clearly distinguishable from the ER peak. The process of utilising a second antibody against the target chromatin avoids the need for a xenogeneic spike-in and controls for more experimental variables than conventional methods. Crosslinking using formaldehyde solution, cell lysis, chromatin digestion, immunoprecipitation, reversal of crosslinking, and DNA clean up were done. Following this, library preparation, DNA sequencing, alignment, and peak calling using MACS algorithm were performed. After normalising with CTCF signals, a dramatic reduction in ER binding was observed in the treatment arm as compared with NDC at the RARα locus, which is the known ER binding site.

This brings forth the notion of using a time-course ChIP-seq to demonstrate the correlation between CYC065 and the downregulation of *MCL1* using antibodies to pull down both S2 phosphorylated RNAPII which is a marker of CDK9 activity and, in a separate experiment, using total RNAPII as it was observed that the endogenous level of RNAPII was markedly decreased in all cell lines following treatment with CYC065 for 4h (Figure 3.3.1.1G-J) aiming to evaluate if there is a sequential effect and difference in S2 phosphorylated RNAPII and total RNAPII peaks at the *MCL1* locus when comparing CYC065 treated AML cells and NDC. However, for the parallel factor ChIP, an assurance of the stability of the reference endogenous factors across different experimental arms and an overlap of the reference and target peaks are still questionable (Blanco, Di Croce, & Aranda, 2019). Thus, in this scenario, a xenogeneic spike-in is preferred, in particular, based on the findings showing that treatment with CYC065 resulted in global gene suppression in all cell lines examined (section 3.4). In addition, the

parallel experiment of *MCL1* knockdown can be performed in AML for better understanding of the effects of CYC065.

In summary, the efficacy of CYC065 against AML was shown in this *in vitro* study. Primary target of inhibition and secondary effects of the drug were assessed by gene and protein expression studies. However, some of the results remained unclear and require further clarification. Consequently, further investigation of primary targets inhibited by CYC065 using a multiplex kinase activity profiling PamGene™ arrays was performed (Chapter 4). Moving forward to an evaluation in primary human samples and then combination studies of CYC065 with other chemotherapies were investigated (Chapter 5).

Chapter 4 Pamgene™ STK activity profiling

4.1 Introduction

Protein kinases are enzymes, which catalyse protein phosphorylation, the most common post translational modification occurring in the cell. The mechanism consists of a reversible transfer of a phosphoryl group onto specific amino acid(s) of the target protein(s). All protein kinases when activated recognise a consensus sequence to facilitate phosphorylation of their target substrate(s). This increases the functional diversity of the proteome and influences various aspects of normal physiology by activating and deactivating enzymes, receptors and regulatory proteins (Shchemelinin, Sefc, & Necas, 2006).

Over the last 15 years, there has been an improvement in array technologies to measure enzymatic activity in whole cell lysates, with the preparation of protein chips for the assessment of protein substrate interactions. In 2002, the first peptide chips were developed by the Diels-Alder-mediated immobilisation of one substrate for the tyrosine kinase c-Src on a monolayer of alkanethiolates on gold. This allowed quantitative evaluation of kinase activity (Houseman, Huh, Kron, & Mrksich, 2002).

The first-generation array was produced by Pepscan™ Systems and was commercially available in 2003. The array consisted of 192 peptides providing kinase substrates which were spotted onto branched hydro gel polymer-coated glass slides and P^{33}-γ-adenosine triphosphate (ATP) was used as a tracer. Purified protein kinase A (PKA) was used to validate the array. However, the main application of this array was from the plant biology field, but had limited funding to create a good panel quality (Diks et al., 2004; Peppelenbosch, 2012). As a result, Dr Jos Joore decided to increase the number of substrate peptides to 1176 (Peppelenbosch, 2012). This array was the first academically successful peptide-array-based kinome profiling tool and was used in high profile cancer studies e.g. alteration of cellular event in oesophageal adenocarcinoma (Izzo et al., 2007; van Baal et al., 2006; van de Winkel, Massl, Kuipers, van der Laan, & Peppelenbosch, 2013) or characterisation of signaling pathways in colorectal cancer (Tuynman, Peppelenbosch, & Richel, 2004; Tuynman et al., 2008).

Moving away from these slide-based array technologies, the Pamgene™ company has developed a platform in which samples are constantly pumped through a porous matrix, and the amount of association to a recipient molecule is assessed fluorescently. In their protein tyrosine kinase (PTK) activity profiling array, real-time kinetic reactions are measured; this differs from other microarray formats. Kinome profiling is assessed by rapid hybridisation of recipient peptide substrates as it can distinguish different affinities for substrate binding. By contrast, the serine/threonine kinase (STK) activity profiling is a non-kinetic measurement i.e. the fluorescence intensities are measured at the final step after washing (Britain, Holdbrooks, Anderson, Willey, & Bellis, 2018; A. Eriksson et al., 2014).

CYC065 has been designed to inhibit CDK2 and CDK9 activity. However, at the DNA level, most members of the kinase superfamily of enzymes share the presence of the catalytic eukaryotic protein kinase domain of approximately 250 amino acids (Z. Li et al., 2009). Therefore, specificity of CYC065 target inhibition is questionable. The current knowledge states that the preferential phosphorylation sites of CDK2 are Ser807/Ser811 of Rb protein (Brugarolas et al., 1999; Chytil et al., 2004; Tetsu & McCormick, 2003) which disrupts binding to E2F, enables cell cycling from G1 to S phase, whereas, CDK9 is known to phosphorylate Ser2 of the C-terminal domain of RNAPII (Santo et al., 2015). Based on these serine phosphorylation active sites, the STK array is preferred over the PTK array.

The aims of this experiment are;

i) to elucidate CYC065 target inhibition by assessing kinases at an activity level using the high throughput Pamgene™ STK activity profiling *in vitro*
ii) to validate the putative kinases obtained from the UpKin upstream kinase prediction tool, PamApp (Pamgene™ International B.V.), based on the Kinexus database

4.2 Variation of phosphorylation status obtained from each peptide substrate was observed in technical replicates

OCI-AML3, MOLM-13 and MV4-11 cell lines were treated with 1μM CYC065 for 4h. Treated cells and NDC were lysed and stored at -80ºC as described in Methods section 2.2.5.1 and the experiment was performed using PamChip™ and PamStation™ 12 system as detailed in Methods section 2.2.5.2.

As sensitivity and specificity of this technology is questionable, three technical replicates were examined. Nominal CV was calculated per peptide in which any CV higher than 0.5 was removed as low intensity is indicated. After removal, the STK activity profiles are shown in Figure 4.2.1A. and the percent CV (%CV) of treatment groups and NDC of each cell line was calculated as demonstrated in Figure 4.2.1B. It was observed that there were some variations of fluorescence intensities obtained from each peptide substrate in technical replicates. The variations are higher when LFC, i.e. log2 Signal(Treatment/NDC), was calculated with the average %CV of 33.7, 33.2, and 22.8 in OCI-AML3, MOLM-13, and MV4-11 cell lines, respectively (Figure 4.2.2).

Comparing the profiles of CYC065-treated group with NDC, the peptide list was obtained from the statistically significant different fluorescence intensities of each peptide spot. From the peptide list, as described in Methods section 2.2.5.3, a normalised kinase statistic score and specificity score were calculated from which the prominent affected putative upstream kinases were identified and displayed in Figure 4.3.1.1 and Figure 4.4.1.1 for the individual cell lines below.

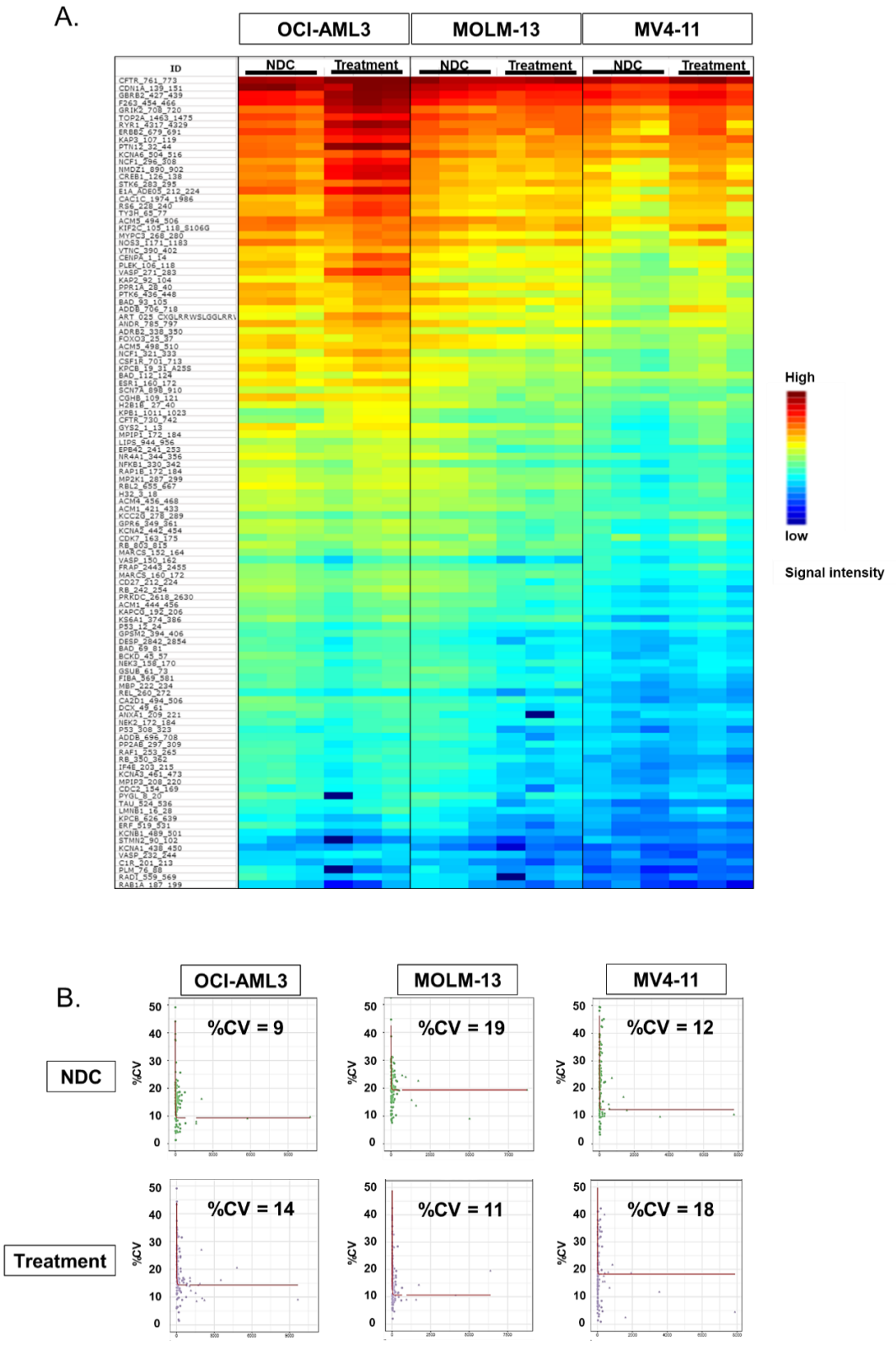

Figure 4.2.1 (A) Serine/threonine kinase activity profiles of OCI-AML3, MOLM-13 and MV4-11 cell lines treated with 1μM CYC065 for 4h or NDC. The peptides were selected according to CV as described in Methods section 2.2.5.3. **(B) The percent of coefficient of variation from three technical replicates of treatment groups and NDC of each cell line was calculated, n=1.** The percent of coefficient of variation (%CV).

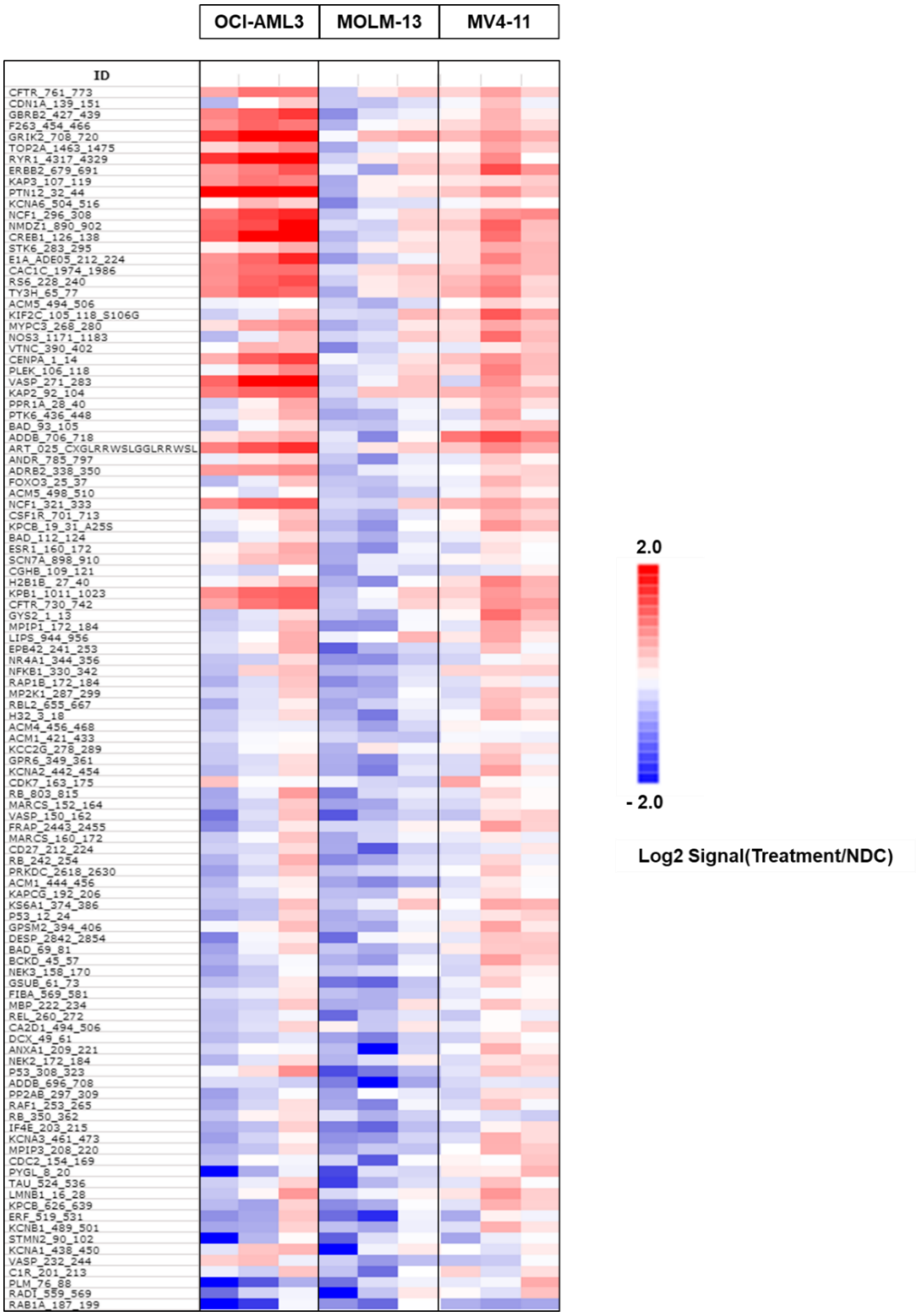

Figure 4.2.2 Log fold change of the signal intensities of 1μM CYC065-treated group as compared with NDC, i.e. log2 Signal(Treatment/NDC) where signal is the pixel brightness values, from three technical replicates of OCI-AML3, MOLM-13 and MV4-11 cell lines, n=1. %CV of log fold change was 33.7, 33.2, and 22.8 in OCI-AML3, MOLM-13, and MV4-11 cell lines, respectively.

4.3 Pamgene™ STK activity profiling in OCI-AML3 and MV4-11 cell lines treated with CYC065

4.3.1 An activation of protein kinase C was predicted

Using the UpKin upstream kinase prediction tool based on the Kinexus database (PamApp), affected putative upstream kinases were identified using the statistically significant different peptides list from Figure 4.2.2.

The specificity score measures the specificity of the kinase for its cognate peptides on the chip, with red indicating high specificity. The kinase score plots in Figure 4.3.1.1 relate the specificity score to the normalised kinase statistic score (i.e. relative kinase activity) to provide an overall score for kinase activity. In general, most of the serine/threonine kinases probed by the kinomics assay exhibited increased activation in the CYC065-treated group relative to NDC in OCI-AML3 and MV4-11 cell lines and the most prominent differentially activated kinases are shown in Figure 4.3.1.1A and Figure 4.3.1.1B, respectively. These include several members of the protein kinase C (PKC) family.

A.

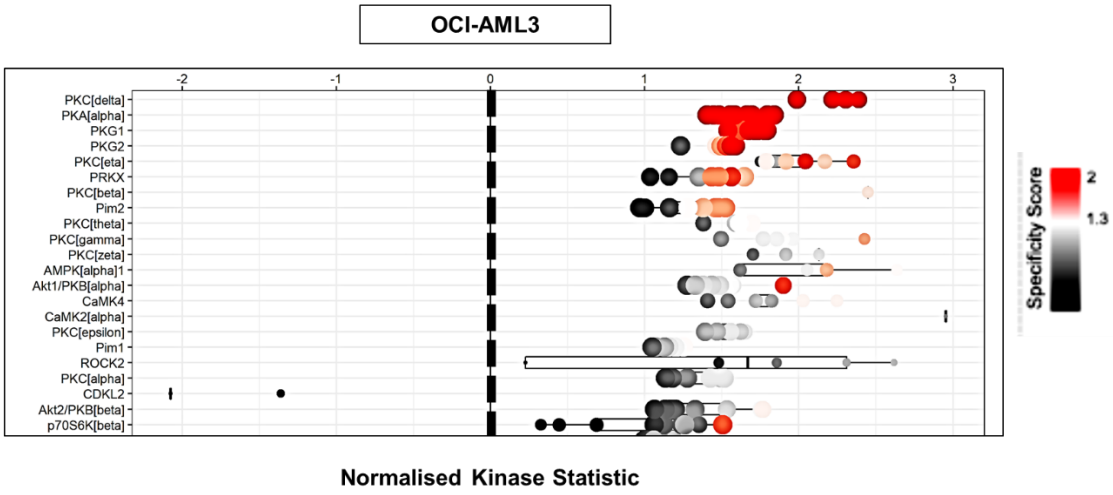

B.

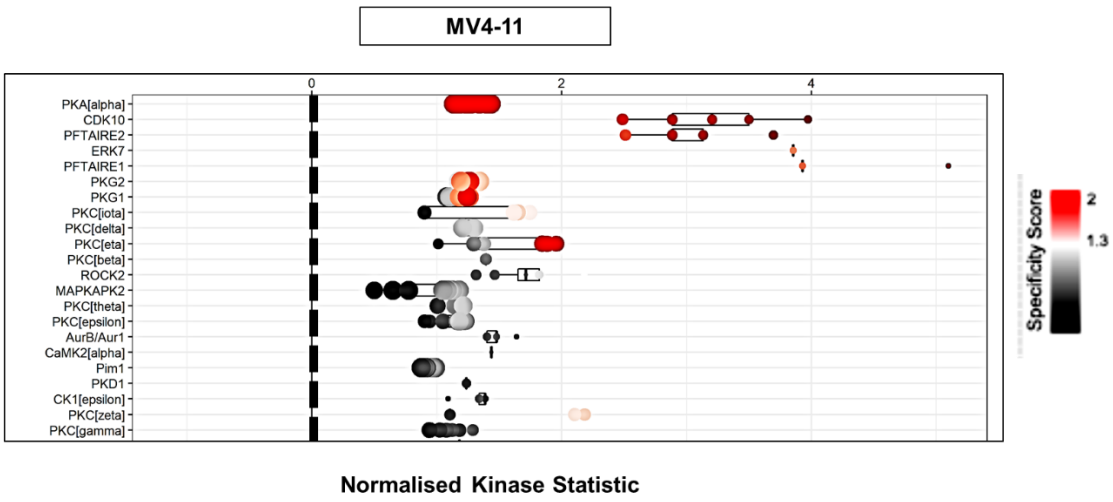

Figure 4.3.1.1 The putative kinases were identified using the UpKin upstream kinase prediction tool. Dots depict normalised kinase scores. The specificity score measures the specificity of the kinase for its cognate peptides on the chip, with red indicating high specificity. The normalised kinase scores of more than 0 indicate higher activity in CYC065-treated group relative to NDC in (A) OCI-AML3 and (B) MV4-11 cell lines.

4.3.2 Unchanged protein kinase C activity was observed in Western blotting

To validate the results from the UpKin upstream kinase prediction tool in section 4.3.1, OCI-AML3 and MV4-11 cell lines were treated with 1μM CYC065, 3μM sotrastaurin, or in combination. Sotrastaurin is a potent pan-PKC inhibitor and is currently in phase 2 clinical trial. Maximum plasma concentrations of sotrastaurin are between 1.1μM and 4.5μM (Skvara et al., 2008). Therefore, 3μM sotrastaurin was chosen with respect to a clinically achievable concentration

(Rauert-Wunderlich, Rudelius, Ott, & Rosenwald, 2016). Western blotting was performed and probed with anti phospho-PKC substrate antibody aiming to detect all proteins phosphorylated by PKC.

At 4h, which corresponded to the timepoint of STK activity profiling, it was observed that the endogenous level of all proteins phosphorylated by PKC was not increased in either OCI-AML3 (Figure 4.3.2.1A lane 2) or MV4-11 cell lines (Figure 4.3.2.1B lane 2) treated with CYC065. These results were discrepant to the results from the UpKin upstream kinase prediction tool. In addition, cells in the above-mentioned conditions were cultured for up to 24h. It was observed that there was a slight increase in the level of proteins phosphorylated by PKC in OCI-AML3 (Figure 4.3.2.1A lane 6) and MV4-11 cell lines (Figure 4.3.2.1B lane 6) treated with CYC065. All in all, using Western blotting to validate the results for OCI-AML3 and MV4-11 cell lines, it can be implied that the affected putative upstream kinases obtained from PamApp (section 4.3.1) were not valid.

The level of PKC-phosphorylated proteins was dramatically decreased when the cells were treated with a pan-PKC inhibitor sotrastaurin confirming specificity of the anti phospho-PKC substrate antibody (Figure 4.3.2.1A lane 3, 4, 7, and 8, OCI-AML3; B lane 3, 4, 7, and 8, MV4-11). γ-tubulin was used as an internal protein loading control.

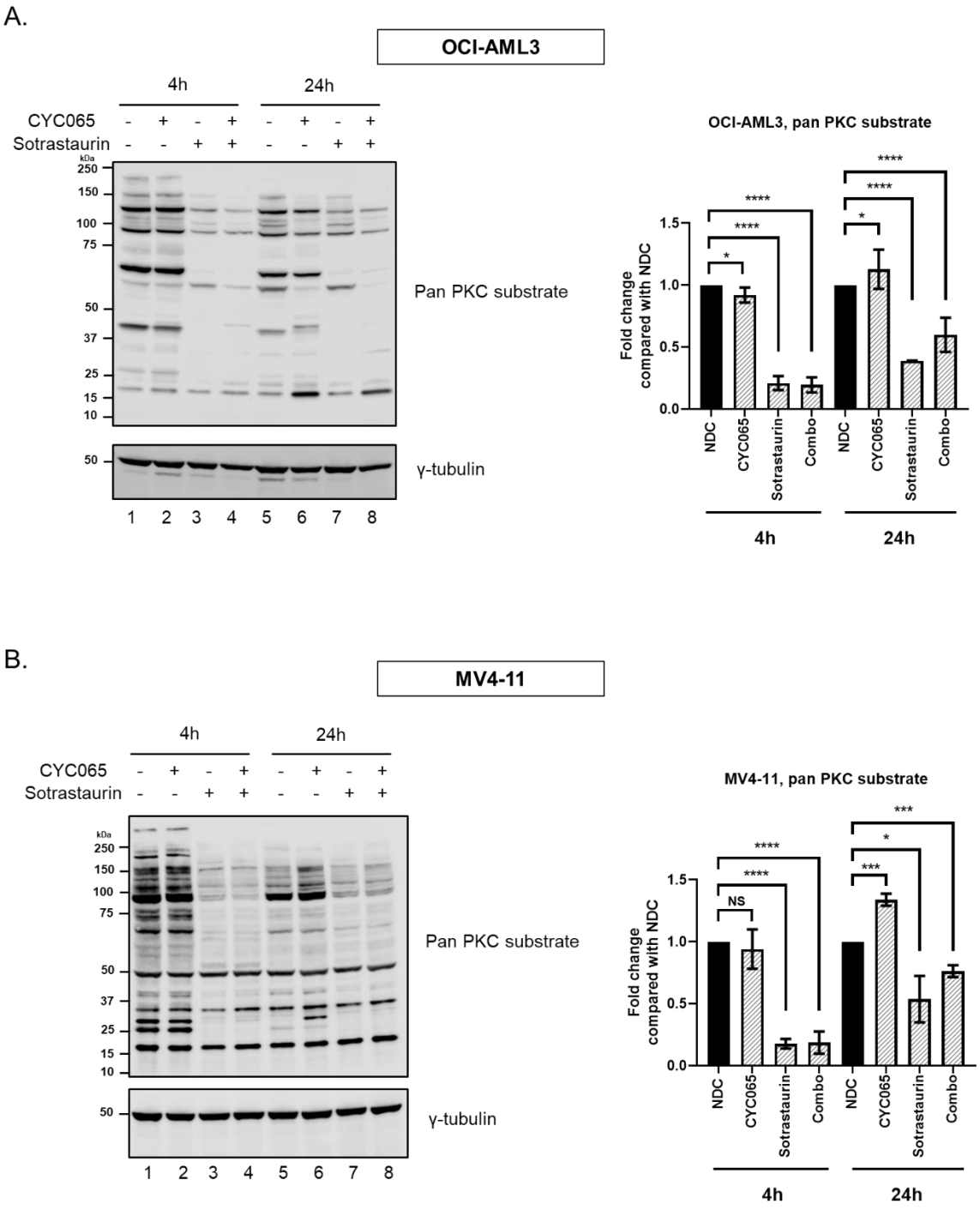

Figure 4.3.2.1 Western blotting of (A) OCI-AML3 and (B) MV4-11 cell lines treated with 1μM CYC065, 3μM sotrastaurin or in combination for 4h and 24h, which is probed with anti phospho-PKC substrate antibody to detect the endogenous level of all proteins phosphorylated by PKC, and densitometric analysis normalised to γ-tubulin (right graphs). The experiments were performed in biological triplicates. Graphs depict means ± SD. Data were compared using the unpaired student's t-test, significant *P*-values are indicated by asterisks (****< 0.0001, *** 0.0001 to < 0.001, ** 0.001 to < 0.01, * 0.01 to < 0.05 and NS if $P \geq 0.05$). Protein kinase C (PKC).

4.4 Pamgene™ STK activity profiling in MOLM-13 cell line treated with CYC065

4.4.1 A decrease in p38 MAPK activity was predicted

Compared to OCI-AML3 and MV4-11 cell lines, most of the serine/threonine kinases exhibited a decreased activity in CYC065-treated group relative to NDC in MOLM-13 cell line using the UpKin upstream kinase prediction tool, including p38-δ, p38-β and ERK1/2. In Western blotting, it was observed that T202/Y204 phosphorylated ERK1/2 decreased by approximately 50% (Figure 3.3.4.1C lane 6), whereas, T180/Y182 phosphorylated p38 MAPK 2-fold increased (Figure 3.3.4.1A lane 6) in MOLM-13 cell line treated with CYC065 for 4h. Consequently, the activity of p38 MAP kinase is questionable following treatment with CYC065.

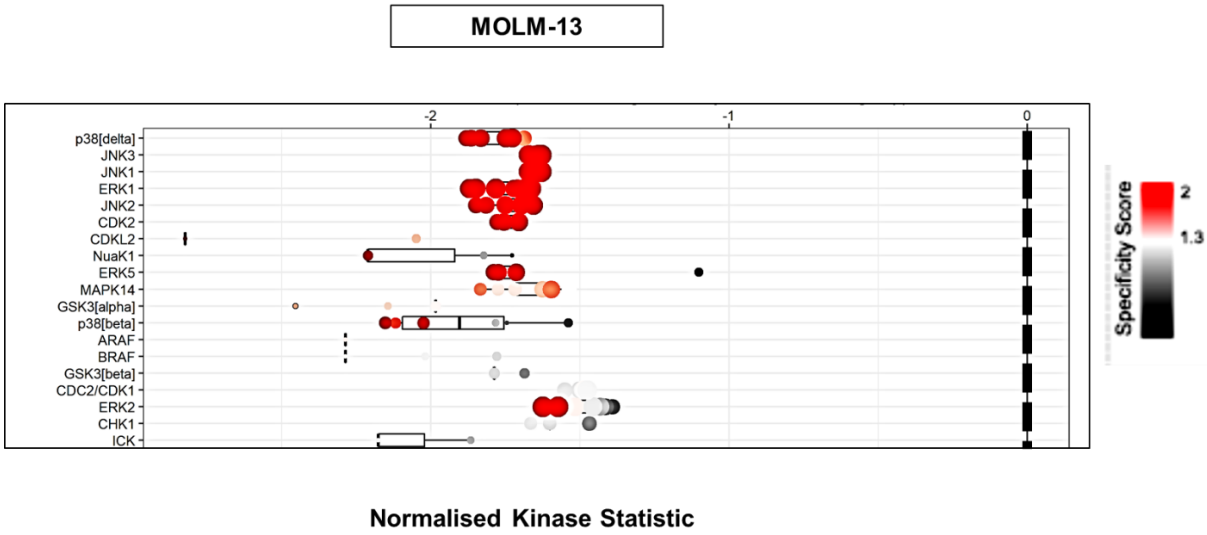

Figure 4.4.1.1 The putative kinases were identified using the UpKin upstream kinase prediction tool. Dots depict normalised kinase scores. The specificity score measures the specificity of the kinase for its cognate peptides on the chip, with red indicating high specificity. The normalised kinase scores less than 0 indicates lower activity in CYC065-treated group relative to NDC in MOLM-13 cell line.

4.4.2 An increase in p38 MAPK activity was observed in Western blotting

From the discrepant results of p38 MAPK in section 4.4.1, an inhibitory threonine 390 (T390) phosphorylation of GSK3β was studied aiming to assess its activity. MOLM-13 cell line was treated with 1μM CYC065, 0.4μM doramapimod, or in combination. Doramapimod is a pan-p38 MAPK inhibitor and is currently in phase 2 clinical trial. Plasma levels of doramapimod in humans after oral ingestion of 50mg at 3.5-5h was 0.74±0.25μM (Branger et al., 2002) and a previous study showed that 0.025–0.4μM treatment for 2h strongly inhibited phosphorylation of p38 MAPK in the human multiple myeloma MM.1S cell line (Yasui et al., 2007). Therefore, 0.4μM doramapimod was chosen for these experiments, reflecting a clinically achievable concentration.

At 4h, which corresponded to the time point of STK activity profiling, it was observed that T390 phosphorylated GSK3β/total GSK3β ratio is 18-fold increased in MOLM-13 cell line treated with CYC065 (Figure 4.4.2.1A lane 2) relative to NDC, indicating a higher activity of p38 MAPK. This result was consistent with Western blotting of T180/Y182 phosphorylated p38 MAPK level (Figure 3.3.4.1A lane 6) but discrepant to the results from the UpKin upstream kinase prediction tool (Figure 4.4.1.1). In addition, cells in the above-mentioned conditions were cultured for up to 24h. It was observed that there was a slight increase in the ratio of T390 phosphorylated GSK3β/total GSK3β in the cells treated with CYC065 (Figure 4.4.2.1A lane 6), but this did not reach statistical significance. Collectively, using Western blotting to validate the results for the MOLM-13 cell line, it can be implied that the affected putative upstream kinases obtained from PamApp (section 4.4.1) were not valid.

A level of T390 phosphorylated GSK3β/total GSK3β ratio was dramatically decreased when the cells were treated with a pan-p38 MAPK inhibitor doramapimod confirming the specificity of p38 MAPK's phosphorylation site on GSK3β and the antibody (Figure 4.4.2.1A lane 3, 4, 7 and 8). γ-tubulin was used as an internal protein loading control.

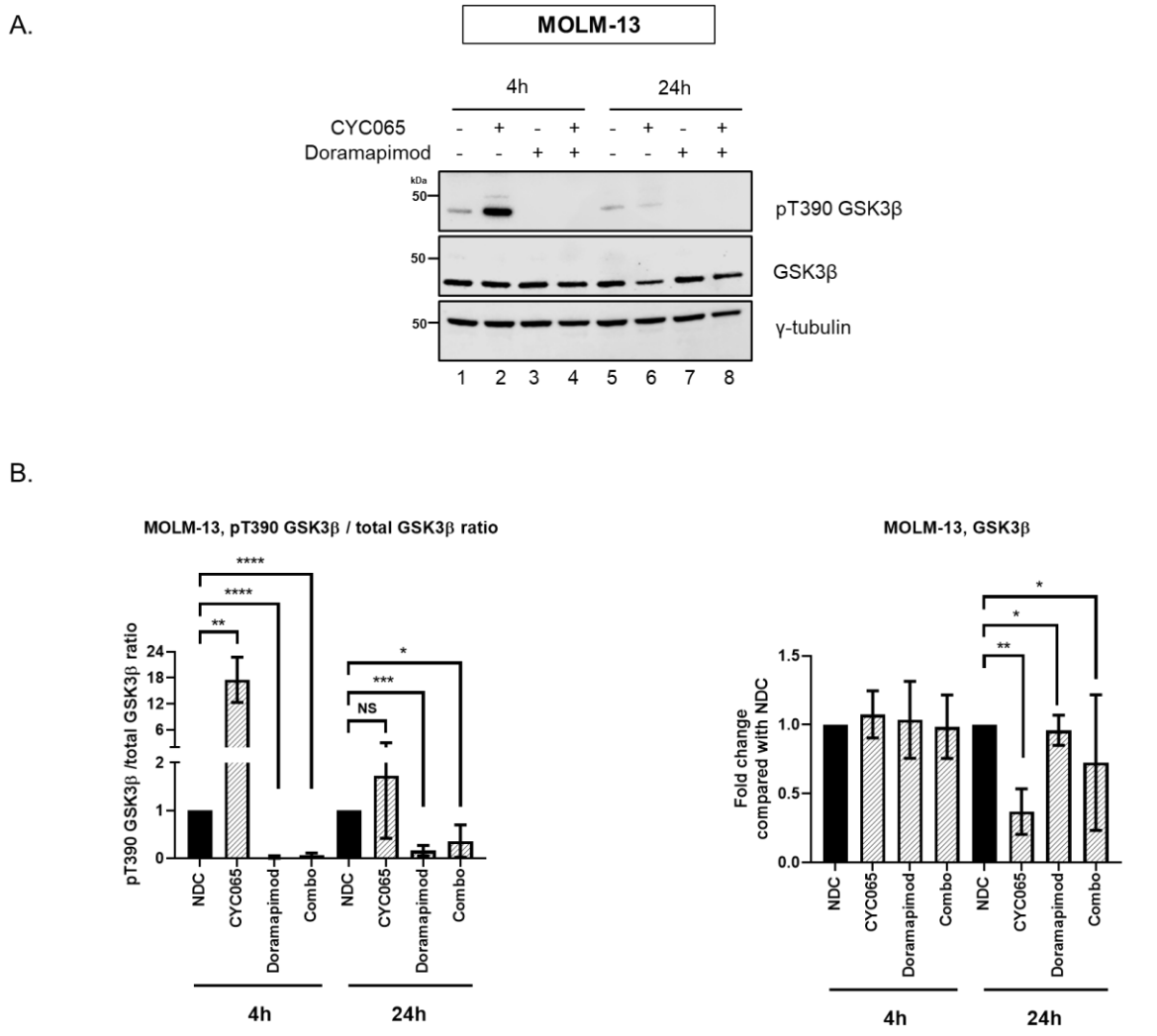

Figure 4.4.2.1 (A) Western blotting of MOLM-13 cell line treated with 1μM CYC065, 0.4μM doramapimod or in combination for 4h and 24h, which is probed with anti pT390 GSK3β or GSK3β antibody to assess p38 MAPK activity; and (B) normalised relative fold change of T390 phosphorylated GSK3β/total GSK3β ratio (left graph) and the endogenous level of GSK3β protein to SH-PTP2 (right graph) evaluated by densitometry as compared with NDC. The experiments were performed in biological triplicates. Graphs depict means ± SD. Data were compared using the unpaired student's t-test. Significant *P*-values are indicated by asterisks (****< 0.0001, *** 0.0001 to < 0.001, ** 0.001 to < 0.01, * 0.01 to < 0.05 and NS if $P \geq 0.05$). Inhibitory threonine 390 (T390) phosphorylated glycogen synthase kinase 3 beta (p-GSK3β, T390). Glycogen synthase kinase 3 beta (GSK3β).

4.5 Discussion

Pamgene™ STK activity profiling has been used in various fields of study to identify kinases involved in disease states and to profile efficacy of therapeutic drugs. Postmortem hippocampal brain tissues were used to assess the differences of STK profiles of patients diagnosed with Alzheimer's disease compared with non-demented controls. An overall decrease of protein kinase activity correlating with disease progression was found, including the Ephrin-receptor A1 (EphA1), a risk gene for Alzheimer's disease, and sarcoma tyrosine kinase (*Src*), which is involved in memory formation (Rosenberger et al., 2016). Moreira *et al*. assessed the differences of basal STK profiles of lithium excellent-responders and non-responder in patients diagnosed with bipolar disorders and they found that some of the upstream kinases are associated with lithium action (Moreira et al., 2018). Noé *et al*. assessed changes of STK profiles of non-small-cell lung cancer patients after treatment with the anti-PD-1 mAb nivolumab for 2 weeks. An activation of PI3/Akt pathway was observed (Noé et al., 2019).

Using both PTK and STK activity profiling Pamgene™ arrays, an inhibition of PTK activity was confirmed in primary AML samples treated with a novel FLT3 kinase inhibitor AKN-028, whereas, STK activity remained unchanged (A. Eriksson et al., 2014). Using the OV4 ovarian cancer cell line, which lacks endogenous beta-galactoside alpha-2,6-sialyltransferase 1 (ST6Gal1) expression, the PTK activity profiling revealed that cells with forced overexpression of ST6Gal1 exhibited increased global PTK activity. Regulated by ST6Gal1, epidermal growth factor receptor (EGFR), which is the receptor tyrosine kinase, was found to be highly activated and this was confirmed by Western blotting, whereas, the STK profiling showed that several members of PKC and the Ca^{2+}/calmodulin-dependent protein kinase (CaMK) families were activated only in the parental OV4 cell line (Britain et al., 2018). Surprisingly, none of these conclusions drawn by the STK profiling in the above-mentioned studies was validated by another confirmation method.

In this study, OCI-AML3, MOLM-13 and MV4-11 cell lines were treated with clinically relevant CYC065 concentrations of 1µM for 4h. This corresponds to the early time point in gene and protein studies because the purpose of these

experiments was to investigate the primary drug target rather than the secondary effect. Using the UpKin upstream kinase prediction tool, it was observed that most of the serine/threonine kinases probed by the kinomics assay exhibited increased activation in CYC065-treated group relative to NDC in OCI-AML3 and MV4-11 cell lines. The most prominent differentially activated kinases include several members of PKC (Figure 4.3.1.1). A previous study showed that various signal transduction pathways were activated in AML, including members of the PKC family (Kornblau et al., 2006). Western blotting was performed on 188 samples of patients with newly diagnosed, untreated AML and it was revealed that high levels of PKC-α, ERK, pERK, and pAKT were adverse factors for survival in univariate and multivariate analyses. In addition, PKC-α was shown to promote cell survival by phosphorylating BCL-2 in leukaemic cells, resulting in greater anti-apoptotic function (Jiffar et al., 2004; Ruvolo, Deng, Carr, & May, 1998). PKC-βII is crucial for breakpoint cluster region protein-abelson murine leukemia viral oncogene homolog (BCR-ABL)-mediated leukaemogenesis (Perrotti et al., 2000; Xenaki, Pierce, Underhill-Day, Whetton, & Owen-Lynch, 2004) and it promotes haematopoietic progenitor cell survival during IL-3 deprivation (Xenaki et al., 2004).

As activation of PKC was predicted (Figure 4.3.1.1), targeting PKC may synergise with CYC065 to further eliminate AML cells. However, the crucial step is to validate the results from Pamgene™ technology before drawing any conclusions. Western blotting was performed to confirm the activity of putative kinases. However, the expected increase in PKC activity was not observed in OCI-AML3 and MV4-11 cell lines treated with 1μM CYC065 for 4h (Figure 4.3.2.1). In terms of a specificity of the anti phospho-PKC substrate antibody, a pan-PKC inhibitor sotrastaurin was used to suppress PKC activity which confirmed a decrease in the endogenous level of phosphorylated PKC substrates.

For MOLM-13 cell line, by contrast, decreased serine/threonine kinase activity in CYC065-treated cells, relative to NDC, was predicted using the UpKin upstream kinase prediction tool. One of prominent differentially inactivated kinases was p38 MAPK (Figure 4.4.1.1). However, the result was contradicted by Western blotting in which an increase in the active T180/Y182 phosphorylated p38 MAPK was observed (Figure 3.3.4.1A lane 6).

It has been reported that p38 MAPK directly phosphorylates GSK3β on serine 389 (S389) in mouse or T390 in human, which inactivates its activity, in CD4+ T cells following treatment with doxorubicin or radiotherapy (Thornton et al., 2016). Phosphorylation at T390 by p38 MAPK causes an inhibition of GSK3β comparable to the phosphorylation of S9 by Akt (Thornton et al., 2016; Thornton et al., 2008). As there was a discrepancy between the results from Western blotting and the Pamgene™ technology, therefore, T390 phosphorylation on GSK3β was used to assess p38 MAPK activity. It was observed that T390 phosphorylated GSK3β/total GSK3β ratio is dramatically increased (Figure 4.4.2.1B left graph) which is synchronous with an increase in T180/Y182 phosphorylation of p38 MAPK in Western blotting (Figure 3.3.4.1A lane 6), implying an increase in its activity. Moreover, among the three cell lines in this study, T180/Y182 phosphorylation of p38 MAPK had the greatest increase only in MOLM-13 cell line, implying that apoptosis can be highly induced which is consistent with the previous results showing that this cell line is most sensitive to CYC065. In terms of a specificity of p38 MAPK's phosphorylation site on GSK3β and antibody, a pan-p38 inhibitor doramapimod was used to suppress p38 activity, and this confirmed a decrease in the level of T390 phosphorylated GSK3β/total GSK3β ratio. Collectively, using Western blotting, a concurrent increase in the protein levels of an active p38 MAPK and its substrate confirmed an activation of p38 MAPK in MOLM-13 cell line following treatment with CYC065. This refutes the results obtained from the Pamgene™ technology.

In all cell lines examined, the results obtained from Western blotting utilised for a validation were incompatible with those from Pamgene™ technology. The plausible explanations for these findings include: **a)** the immobilisation issue of peptide substrates on the array chips. An unstable peptide attachment and confirmation change of peptides are the common problems that occur during the immobilisation step (Panicker, Sun, Chen, & Yao, 2009). In addition, it has been reported that the physical property of platform, peptide secondary structure and its orientation in the immobilised state have a marked impact on the interaction between kinases and their substrates (Han et al., 2014), affecting the interpretation and final results; **b)** the analytical strategy utilised in PamApp. From three replicates, peptide substrates that showed nominal CV lower than 0.5, set by the company's bioinformaticians and statisticians, were included in

the analysis. The cut-off was very high in which a high amount of non-specific peptide substrates were included in the analytical list for a prediction of the putative kinases. Hence, the specificity was dramatically decreased; and **c)** the technical issue. Small technical issues can markedly affect the images captured by a CCD camera for the analysis, including small particles e.g. dust or fluorescence precipitates in the secondary FITC antibody, scratches on the arrays, water droplets on the camera, etc.

To our best knowledge, this is the first time that the STK profiling obtained from the UpKin upstream kinase prediction tool has been validated using alternative proteomic methods. In this study, we tried to use the high throughput Pamgene™ STK activity profiling to elucidate CYC065 target inhibition by assessing kinases at an activity level in AML cell lines. Nevertheless, the results from the confirmation method, Western blotting, were in contraindication with the Pamgene™ technology. Collectively, although the technology has been well-designed along with the sophisticated instruments, an interpretation of the results should be carefully made and validation should be performed before drawing any conclusions. Due to the poor sensitivity and specificity of the results and concerns over reproducibility, it was decided not to use the Pamgene in any further analyses and to focus on more robust proteomic techniques.

Chapter 5 Combination studies of CYC065 and venetoclax, cytarabine, or azacitidine

5.1 Introduction

Over the last 50 years, there has been a steady improvement in treatment outcome of AML. At present, the cure rate is 35-40% and 5-15% in patients younger and older than 60 years, respectively (H. Döhner et al., 2015). Nevertheless, the prognosis of AML is globally poor, with a 5-year OS of 28% (SEER, 2015), especially in the elderly as a consequence of intolerance to intensive chemotherapy and an increased number of patients with adverse cytogenetics. Therefore, novel agents, potentially with combination chemotherapy, may play a role in patients with adverse-risk AML (H. Döhner et al., 2015).

AML has been renowned for its complex clonal heterogeneity and adaptation potential. For instance, in a comparison between samples of pre- and post-treatment with the IDH2 inhibitor enasidenib of patients with relapse, it was observed that there were various patterns of clonal selection and evolution of new mutations involving different biological pathways (Quek et al., 2018). This highlights the importance of targeting these parallel mechanisms, potentially reducing the risk of relapse and improving the depth of response and overall response rate. Moreover, drug combination studies exploit opportunities for reduced drug resistance development, decreased toxicity, and efficacy improvement (Foucquier & Guedj, 2015). In this study, CYC065 in combination with venetoclax (VEN), cytarabine (AraC), or azacitidine (AZA) was assessed for efficacy against primary human AML cells. Focusing on these three partners, ongoing clinical trials with combination therapies in AML are summarised in Table 5.1.1 (Richard-Carpentier & DiNardo, 2019).

Table 5.1.1 Ongoing clinical trials with combination therapies in AML, focusing on AraC, VEN, and AZA (Richard-Carpentier & DiNardo, 2019).

Population / indication	Treatment	Phase	Identifier
Untreated AML older patients unfit for IC	VEN ± AZA	3	NCT02993523
Untreated AML older patients unfit for IC	VEN ± LDAC	3	NCT03069352
Untreated AML older patients unfit for IC	AZA + VEN	2	NCT03466294
Untreated AML older patients unfit for IC	VEN + decitabine 10 d	2	NCT03404193
Untreated AML older patients unfit for IC	VEN + LDAC + cladribine (purine nucleoside analogue) + AZA	2	NCT03586609
Untreated AML older patients unfit for IC	VEN + FLAG-ida [fludarabine (antimetabolite) + HIDAC + G-CSF + idarubicin (anthracyclines)]	2	NCT03214562
Untreated or R/R AML patients fit for IC	VEN + fludarabine + AraC + idarubicin	2	NCT03455504
Untreated or R/R AML patients fit for IC	VEN + CPX-351 (liposome-encapsulated combination of AraC and daunorubicin at a ratio of 5:1)	2	NCT03629171
Untreated or R/R AML patients fit for IC	VEN + 7+3	1b	NCT03709758
Untreated AML patients fit for IC	VEN + AZA + pevonedistat (selective NEDD8 inhibitor, inhibiting proteasome-mediated protein degradation)	1/2	NCT03862157
Untreated AML older patients unfit for IC	VEN + AZA	2	NCT03573024
Untreated AML patients 18 to 59 y old	VEN + dinaciclib (CDKs 1, 2, 5, and 9 inhibitor)	1b	NCT03484520
R/R AML	VEN + alvocidib (flavopiridol, pan-CDK inhibitor)	1b	NCT03441555
R/R AML	VEN + ruxolitinib (JAK1/2 inhibitor)	1	NCT03874052
R/R AML	VEN + gilteritinib (FLT3 inhibitor)	1	NCT03625505
R/R AML	VEN + AMG-176 (MCL-1 inhibitor)	1b	NCT03797261
R/R AML	VEN + S64315 (MCL-1 inhibitor)	1	NCT03672695
R/R AML	VEN + cobimetinib (MEK inhibitor) or VEN + idasanutlin (MDM2 inhibitor)	1b/2	NCT02670044
R/R AML	VEN + lintuzumab-^{225}Ac (anti-CD33 antibody)	1/2	NCT03867682
R/R AML	VEN + CPX-351	1	NCT03826992
R/R AML, *FLT3* mutated	VEN + quizartinib (FLT3 inhibitor)	1b/2	NCT03735875

Intensive chemotherapy (IC). Relapsed/refractory AML (R/R AML). Azacitidine (AZA). Venetoclax (VEN). Cytarabine (AraC). Low-dose cytarabine (LDAC). High-dose cytarabine (HIDAC). Cyclin-dependent kinase (CDK). Janus kinase (JAK). FMS-like tyrosine kinase 3 (FLT3). Myeloid cell leukemia 1 (MCL-1). Mitogen-activated protein/extracellular signal-regulated kinase kinase (MEK). Mouse double minute 2 homolog (MDM2).

AraC is a conventional chemotherapy, which is used in the standard “7+3” regimen (see section 1.4.1). A clinically achievable concentration of AraC for use *in vitro* is 1μM (Capizzi et al., 1983; Heasman, Zaitseva, Bowles, Rushworth, & Macewan, 2011). Several mechanisms of AraC resistance have been reported, which mostly involve enzymes in plasma which rapidly convert it into an inactive analogue, e.g. deoxycytidylate deaminase (Drake, Hande, Fuller, & Chabner, 1980) and the sterile alpha-motif and histidine-aspartate domain-containing protein 1 (SAMDH1) (Hollenbaugh et al., 2017).

VEN inhibits BCL-2's function by binding its critical hydrophobic groove, the same site that sequesters its physiologic ligands, the BH3 domain-containing pro-apoptotic proteins (Konopleva et al., 2016). If unconstrained by BCL-2, then pro-apoptotic activators and effectors are free to drive apoptosis (Elkholi et al., 2014). VEN has been approved by the FDA in 2016 for the treatment of patients with CLL with the poor prognosis cytogenetics, 17p deletion (Souers et al., 2013). In 2018, it was approved for the treatment of newly diagnosed AML patients ineligible for intensive chemotherapy i.e. conventional "7+3", by using it with LDAC i.e. 20mg/m^2/d for 10 days, or with a HMA. A clinically achievable concentration of VEN for use *in vitro* is 1μM (Anderson et al., 2016), which is corresponding to patients receiving 400mg/d. Interestingly, in a phase 2 study of single-agent VEN in patients with R/R AML, BH-3 profiling identified MCL-1 and BCL-xL as potential resistance mechanisms (Konopleva et al., 2016). An upregulation of MCL-1 and BCL-xL was observed in VEN-resistant AML cell lines generated from drug titration experiments (Lin et al., 2016). These results have been recapitulated by a study showing that siRNA-mediated knockdown of *MCL1* and BCL-2-like 1 (*BCL2L1*), encoding BCL-xL, increased VEN activity in AML cell lines (J. M. Bogenberger et al., 2014). Therefore, combining MCL-1 targeting CYC065 with VEN is a rational strategy to explore.

AZA and decitabine are two DNA methyltransferase inhibitors (DNMTi) which are approved in the USA for the treatment of patients with MDS and AML (Kihslinger & Godley, 2007). AZA is a ribonucleoside in which a counterfeit cytosine is integrated, so it is incorporated into RNA rather than into DNA. By contrast, decitabine is a deoxyribonucleoside, thus it can only incorporate into DNA. Normally, cytosine-guanine dinucleotides are recognised as substrate by the DNMTs, which form a covalent bond between the carbon-5 atom of the cytosine ring and the enzyme. This bond is reversed by a beta-elimination reaction. However, as AZA's carbon 5 is substituted by nitrogen, this bond becomes irreversible which blocks DNMTs' activity. Trapped DNMTs trigger DNA damage signaling, rendering its degradation via the ubiquitin (Ub)-proteasome pathway. Consequently, methylation marks are lost during the S phase. In many human cancers, a proportion of CpG islands are hypermethylated, and this is linked to silencing of some tumor suppressor genes (Baylin & Jones, 2011). A recent study has demonstrated that there is an increase in methylation at promotor regions of

the subset of genes rendering a decrease in their expression in OCI-AML3 cell line compared with normal HSPC, and AZA can reverse this aberrant DNA methylation resulting in re-expression of these genes (Lund et al., 2014). Only AZA, but not decitabine, is licensed in the UK. It is the first line treatment for AML patients who are not eligible for HSCT, with 20-30% blasts and multi-lineage dysplasia, intermediate-2 and high-risk MDS according to the International Prognostic Scoring System (IPSS), and chronic myelomonocytic leukaemia (CMML) with 10-29% marrow blasts without myeloproliferative disorder (NIHR, 2014). The approved dosing of AZA is 75mg/m^2/d, which is corresponding to the drug concentration of 3-11μM *in vitro* (Hollenbach et al., 2010), on days 1-7 of a 28-day cycle (Celgene, 2018). In AML cell lines, it was reported that siRNA-mediated *MCL1* and *BCL2L1* knockdown results in varying degrees of synergism with AZA (J. M. Bogenberger et al., 2014). Hence, combining MCL-1 targeting CYC065 with AZA has the potential for synergistic activity. Many mechanisms of resistance have been proposed in AZA-resistant cell lines, including mutations of nucleoside transporters which mediate uptake of the drug e.g. human equilibrative nucleoside transporters (hENTs) and concentrative nucleoside transporters (hCNTs) (Damaraju et al., 2003), mutations of reductase enzymes which catalyse the formation of deoxyribonucleotides from ribonucleotides e.g. ribonucleoside-diphosphate reductase large subunit and subunit M2 (*RRM1* and *RRM2*) (Masala et al., 2016), and mutations of kinases which facilitate phosphorylation steps e.g. uridine-cytidine kinases 1 and 2 (*UCK1* and *UCK2*) (Masala et al., 2016; Sripayap et al., 2014).

The aim of the experiments in this chapter is to investigate a synergy effect of CYC065 when being combined with a conventional chemotherapy AraC, a selective BCL-2 inhibitor VEN, or a hypomethylating agent AZA in AML cell lines and primary human AML cells *in vitro*.

5.2 Combination studies of CYC065 and VEN in AML cell lines

5.2.1 Longer exposure reduced the IC50 of VEN

The IC50 of VEN for each cell line was assessed by resazurin reduction assay at 24h, 48h and 72h. It was observed that longer exposure increased drug sensitivity and reduced the IC50. At 72h, the IC50 of VEN in OCI-AML3, MOLM-13, and MV4-11 cell lines was approximately 4.24±0.73μM (Figure 5.2.1.1A), 0.01±0.001μM (Figure 5.2.1.1B), and 0.01±0.003μM (Figure 5.2.1.1C), respectively. These IC50 values were consistent with previous publication data showing that OCI-AML3 cell line is resistant to VEN except at very high doses (J. Bogenberger et al., 2017; Ishizawa et al., 2015; R. Pan et al., 2014).

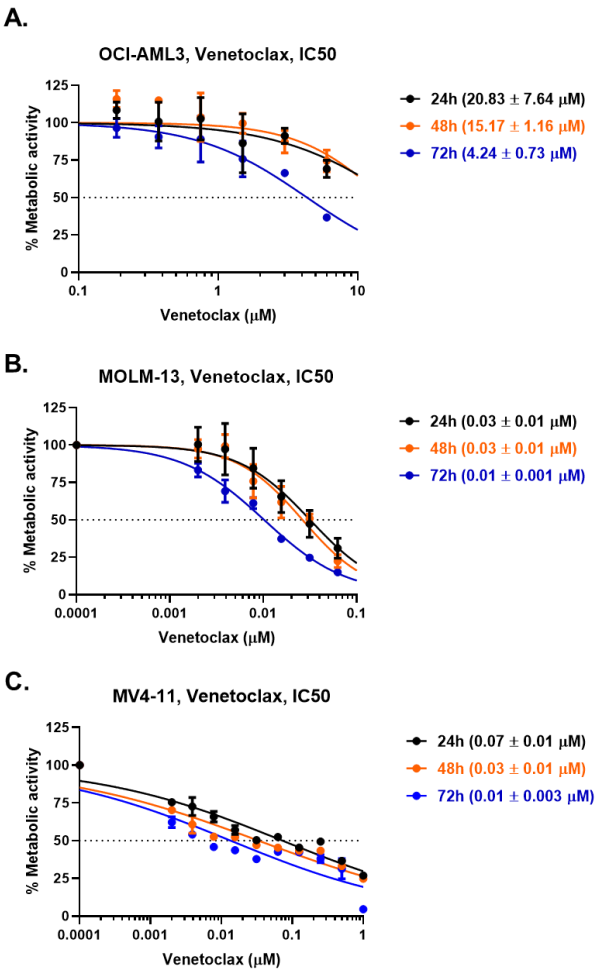

Figure 5.2.1.1 The IC50 of VEN at 24h, 48h and 72h in (A) OCI-AML3, (B) MOLM-13, and (C) MV4-11 cell lines using rezasurin reduction assay. The experiments were performed in technical and biological triplicates. Dots depict means ± SD.

5.2.2 Optimal CYC065/VEN combination ratio was investigated by synergy assays using CompuSyn software

Using the IC50 of VEN from section 5.2.1, combination studies were performed at 72h when the killing effect was maximal. CompuSyn software was used to investigate the synergism as detailed in Methods section 2.2.1.5. Preliminary results showed synergistic activity of combination of CYC065 and VEN in all cell lines. Overall, the synergistic effect was observed at 2X to 4X IC50 of CYC065. As shown in Figure 5.2.2.1 (asterisks), optimal drug combination ratios for OCI-AML3, MOLM-13, and MV4-11 cell lines were 0.88μM of CYC065 plus 1.05μM of VEN, 0.5μM of CYC065 plus 0.01μM VEN, and 1μM of CYC065 plus 0.0024μM of VEN, respectively.

For OCI-AML3 cell line, using a concentration of 0.88μM of CYC065 was not appropriate to demonstrate the synergistic effect as it was masked by too many dead cells, therefore, a concentration of 0.75μM which induces approximately 50% apoptosis (section 3.2.3) was focused instead. Using a fixed proportional reduction as previously described (Mayer et al., 2006; Palmer, 2017), the dose was reduced from 0.88μM of CYC065 plus 1.05μM of VEN to 0.75μM of CYC065 plus 0.9μM of VEN. The optimal ratio was summarised in Figure 5.2.2.1 (right panel) for each cell line, and this was applied for all further experiments, including cell count (section 5.2.3), apoptosis assays (section 5.2.4), active caspase-3 assays (section 5.2.5), and cell cycle analyses (section 5.2.6).

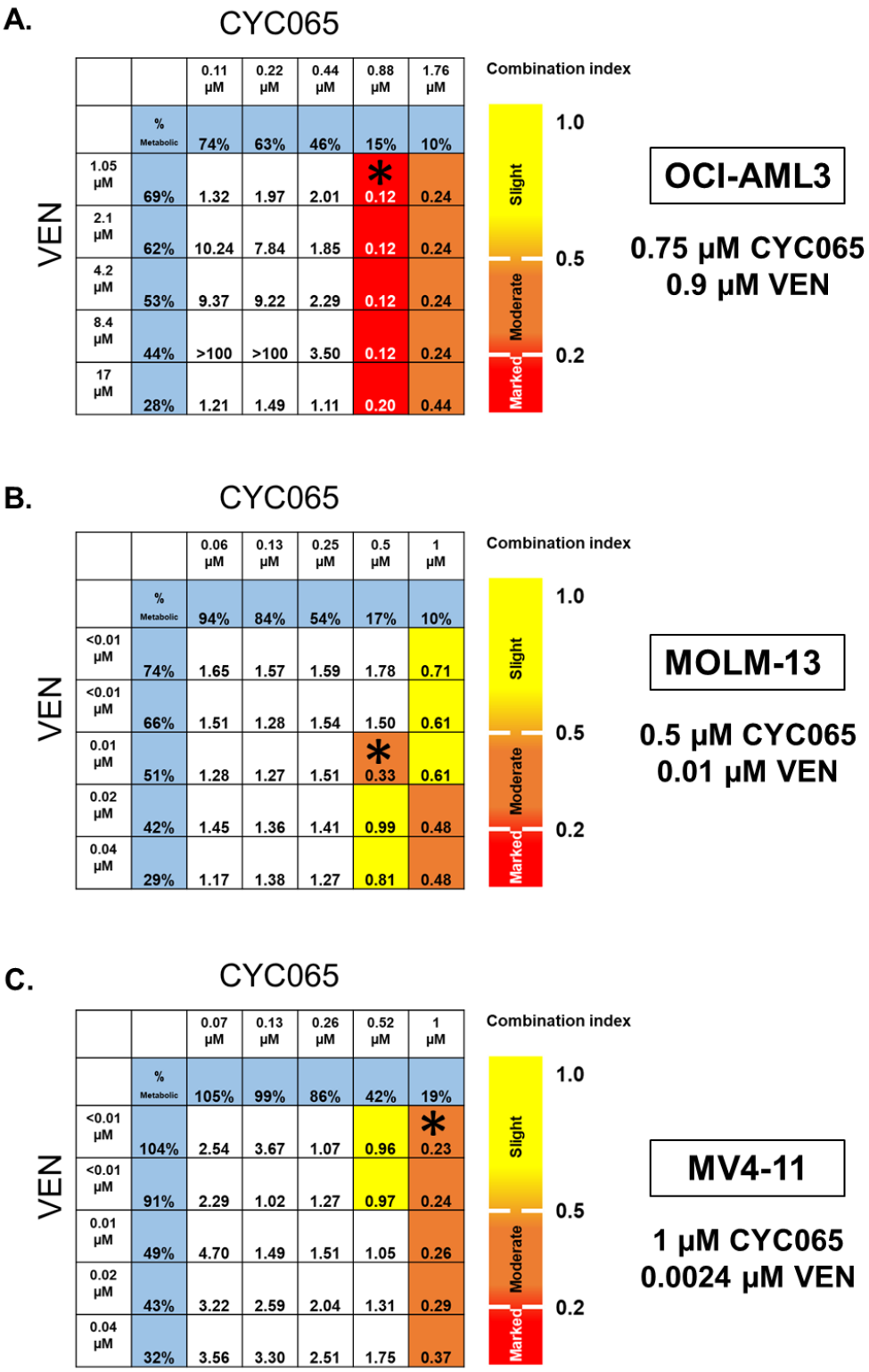

Figure 5.2.2.1 A synergy study for the combination of CYC065 and VEN added to culture for 72h in (A) OCI-AML3, (B) MOLM-13, and (C) MV4-11 cell lines. The experiments were performed in biological triplicates. By using CompuSyn software analysis, a combination index less than 1 and more than 1 indicates synergism and antagonism, respectively. A combination index less than 0.2, 0.2 to less than 0.5 and 0.5 to less than 1 indicates marked (red), moderate (orange) and slight (yellow) synergism, respectively. The most efficacious drug combination ratio was identified (asterisks) and the concentrations of CYC065 and VEN were determined for further combination studies in each cell line (right panel). Venetoclax (VEN).

5.2.3 A slight decrease in cell viability was observed in CYC065/VEN combination

Cells were treated with CYC065, VEN, or CYC065/VEN combination for 72h. Cell counting was performed using trypan blue exclusion assays.

There was only a slight decrease in cell viability in the combination arm as compared with CYC065 single treatment. However, as CYC065 concentrations used in drug combination ratios were higher than the IC50, it was not unexpected that the synergistic effect was masked. This was because of a very low cell number seen in a single treatment of CYC065 in all cell lines; OCI-AML3 (Figure 5.2.3.1A), MOLM-13 (Figure 5.2.3.1B), and MV4-11 (Figure 5.2.3.1C).

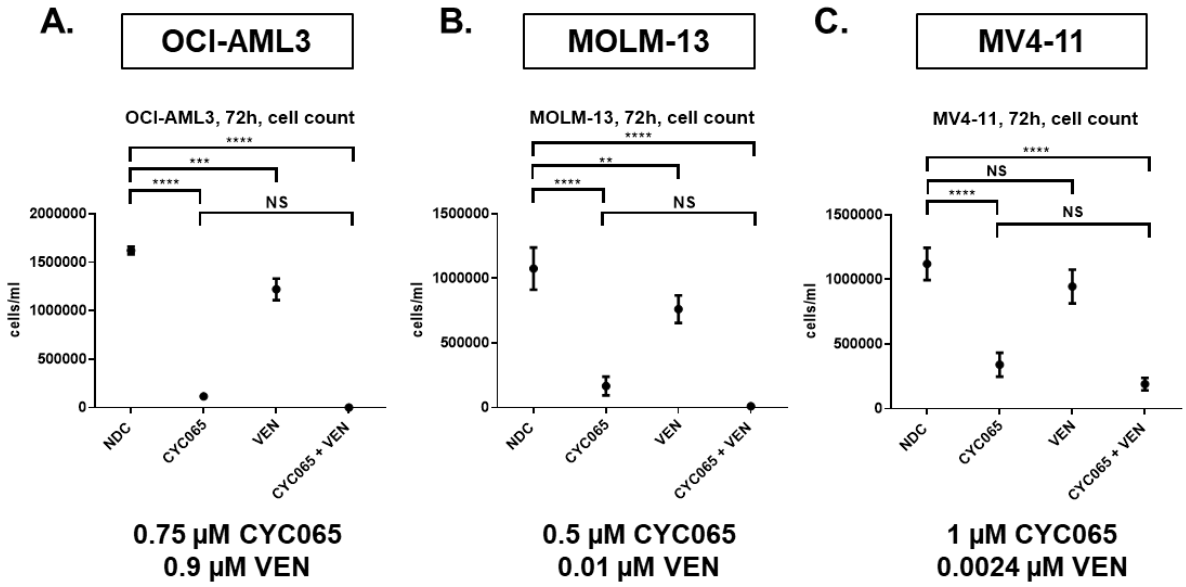

Figure 5.2.3.1 Cell number assessed by trypan blue exclusion assay of (A) OCI-AML3, (B) MOLM-13, and (C) MV4-11 cell lines treated with CYC065, VEN, or CYC065/VEN combination for 72h. The experiments were performed in biological triplicates. Drug combination ratios of each cell line were obtained from synergy assays using CompuSyn software (bottom panel). Dots depict means ± SD. Data were compared using the one-way ANOVA, post hoc Tukey's HSD test ($F(3,8) = 536.5$, $P < 0.0001$, OCI-AML3; $F(3,8) = 99.4$, $P < 0.0001$, MOLM-13; $F(3,8) = 56.7$, $P < 0.0001$, MV4-11). Significant *P*-values are indicated by asterisks (****< 0.0001, *** 0.0001 to < 0.001, ** 0.001 to < 0.01, * 0.01 to < 0.05 and NS if $P \geq 0.05$.

5.2.4 Synergistic activity of CYC065/VEN combination was observed in annexin V/DAPI apoptosis assays

Cells were treated with CYC065, VEN, or CYC065/VEN combination for 72h. The apoptosis assays were performed using annexin V/DAPI staining (Figure 5.2.4.1A,B).

In CYC065 single treatment arms, the doses of 0.75μM, 0.5μM, and 1μM were focused for OCI-AML3, MOLM-13, and MV4-11 cell lines, respectively. At these concentrations, as expected, approximately 50% apoptosis was observed in all cell lines (Figure 5.2.4.1B). Positively, there was a significant decrease in viable cells corresponding with an increase in the population of apoptotic cells in the combination arm as compared with CYC065 single treatment in OCI-AML3 (Figure 5.2.4.1B left graph) and MOLM-13 cell lines (Figure 5.2.4.1B middle graph). In MV4-11 cell line, although not statistically significant, a drop in the percentage of viable cells in the combination arm was observed (Figure 5.2.4.1B right graph).

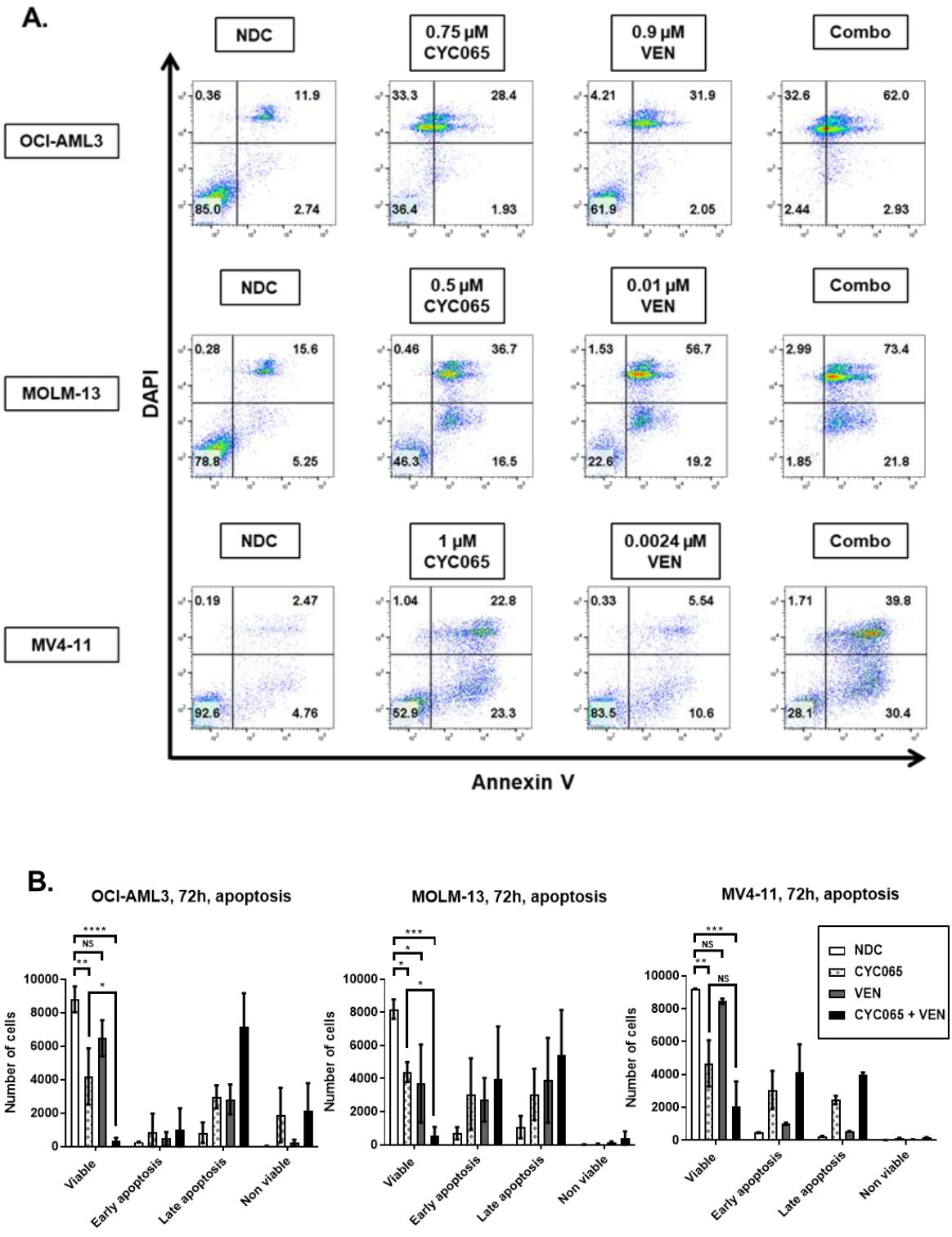

Figure 5.2.4.1 OCI-AML3, MOLM-13, and MV4-11 cell lines were treated with CYC065, VEN, or CYC065/VEN combination for 72h. Drug combination ratios obtained from synergy assays using CompuSyn software. **(A) Representative experiments flow cytometry plots of apoptosis assay using annexin V/DAPI are shown; and (B) Flow cytometric analysis of apoptosis assay.** The experiments were performed in biological triplicates. Graphs depict means ± SD. Cell viability was compared using the one-way ANOVA, post hoc Tukey's HSD test ($F(3,8) = 33.7$, $P < 0.0001$, OCI-AML3; $F(3,8) = 18$, $P = 0.0006$, MOLM-13; $F(3,8) = 30.7$, $P < 0.0001$, MV4-11). Significant *P*-values are indicated by asterisks (****< 0.0001, *** 0.0001 to < 0.001, ** 0.001 to < 0.01, * 0.01 to < 0.05 and NS if $P \geq 0.05$).

5.2.5 Synergistic activity of CYC065/VEN combination was observed in active caspase-3 assays

Cells were treated with CYC065, VEN, or CYC065/VEN combination for 72h. The active caspase-3 assays were performed (Figure 5.2.5.1A,B), aiming to confirm the results from annexin V/DAPI apoptosis assays (section 5.2.4).

In the CYC065 single treatment arms, the active caspase-3-positive population was approximately 50% in all cell lines (Figure 5.2.5.1B) which is consistent with the results from apoptosis assays (section 5.2.4). As expected, there was a significant increase in the active caspase-3-positive population in the combination arm as compared with CYC065 single treatment in all cell lines; OCI-AML3 (Figure 5.2.5.1B left graph), MOLM-13 (Figure 5.2.5.1B middle graph), and MV4-11 (Figure 5.2.5.1B right graph).

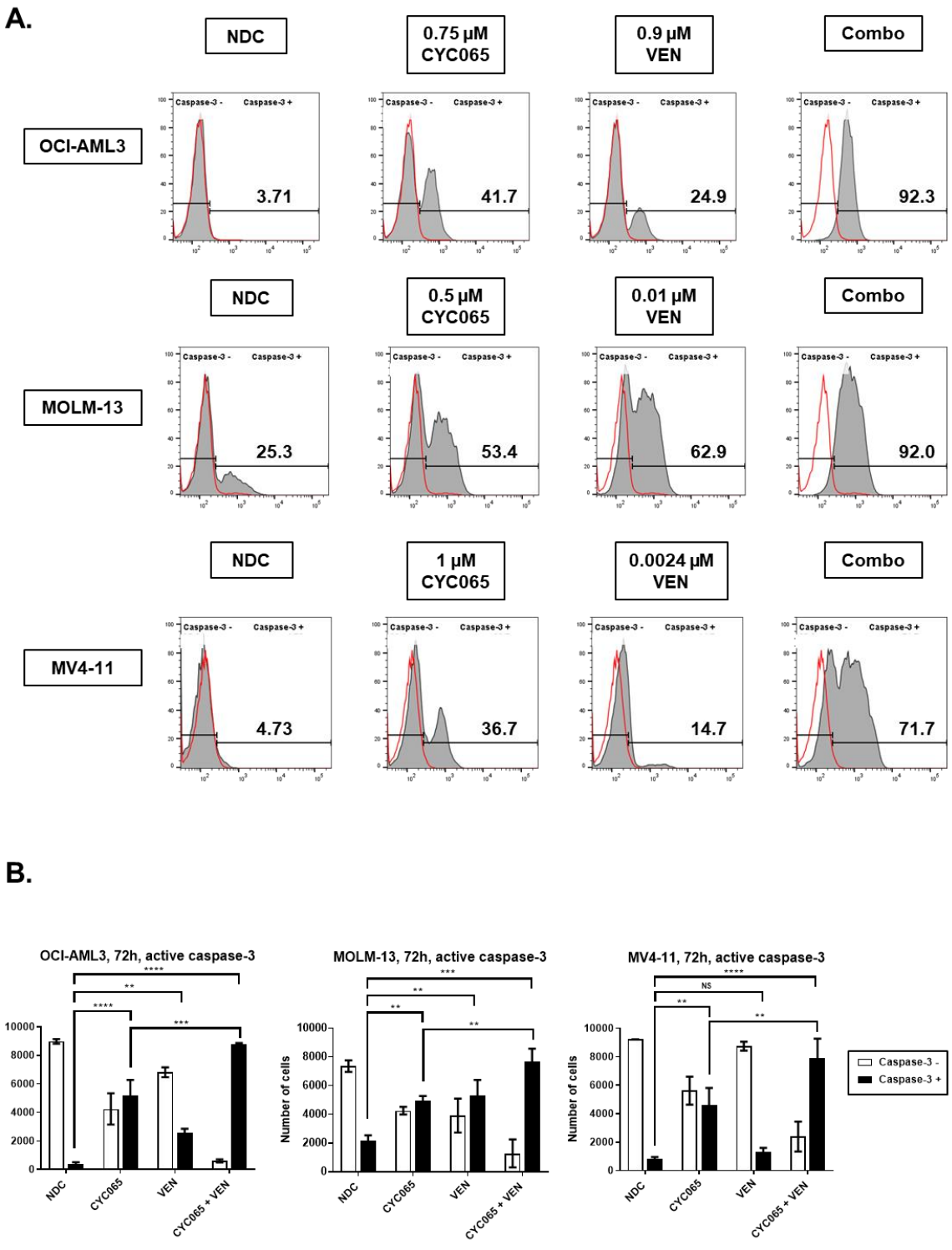

Figure 5.2.5.1 OCI-AML3, MOLM-13, and MV4-11 cell lines were treated with CYC065, VEN, or CYC065/VEN combination for 72h. Drug combination ratios obtained from synergy assays using CompuSyn software. **(A) Representative flow cytometry plots of active caspase-3 assay in which red curves represent isotype controls are shown; and B) Flow cytometric analysis of active caspase-3 assays.** The experiments were performed in biological triplicates. Graphs depict means ± SD. Caspase-3-positive populations were compared using the one-way ANOVA, post hoc Tukey's HSD test ($F(3,8) = 122.1$, $P < 0.0001$, OCI-AML3; $F(3,8) = 18$, $P < 0.0001$, MOLM-13; $F(3,8) = 40.2$, $P < 0.0001$, MV4-11). Significant *P*-values are indicated by asterisks (****< 0.0001, *** 0.0001 to < 0.001, ** 0.001 to < 0.01, * 0.01 to < 0.05 and NS if $P \geq 0.05$).

5.2.6 Synergistic activity of CYC065/VEN combination resulted in an increase in sub G0 cell population in cell cycle analyses

Cells were treated with CYC065, VEN, or CYC065/VEN combination for 72h. Cell cycle analyses were performed using PI staining (Figure 5.2.6.1A,B).

An increase in number of cells in sub G0, with corresponding reductions in all phases of active cell cycle, was observed in single treatments and combination arms. There was a significant increase in the sub G0 population in the combination arm as compared with CYC065 single treatment in OCI-AML3 (Figure 5.2.6.1B left graph) and MOLM-13 cell lines (Figure 5.2.6.1B middle graph), indicating an increase in cytotoxicity. In MV4-11 cell line, although not statistically significant, an increase in sub G0 population was seen in the combination arm as compared with single treatments (Figure 5.2.6.1B right graph).

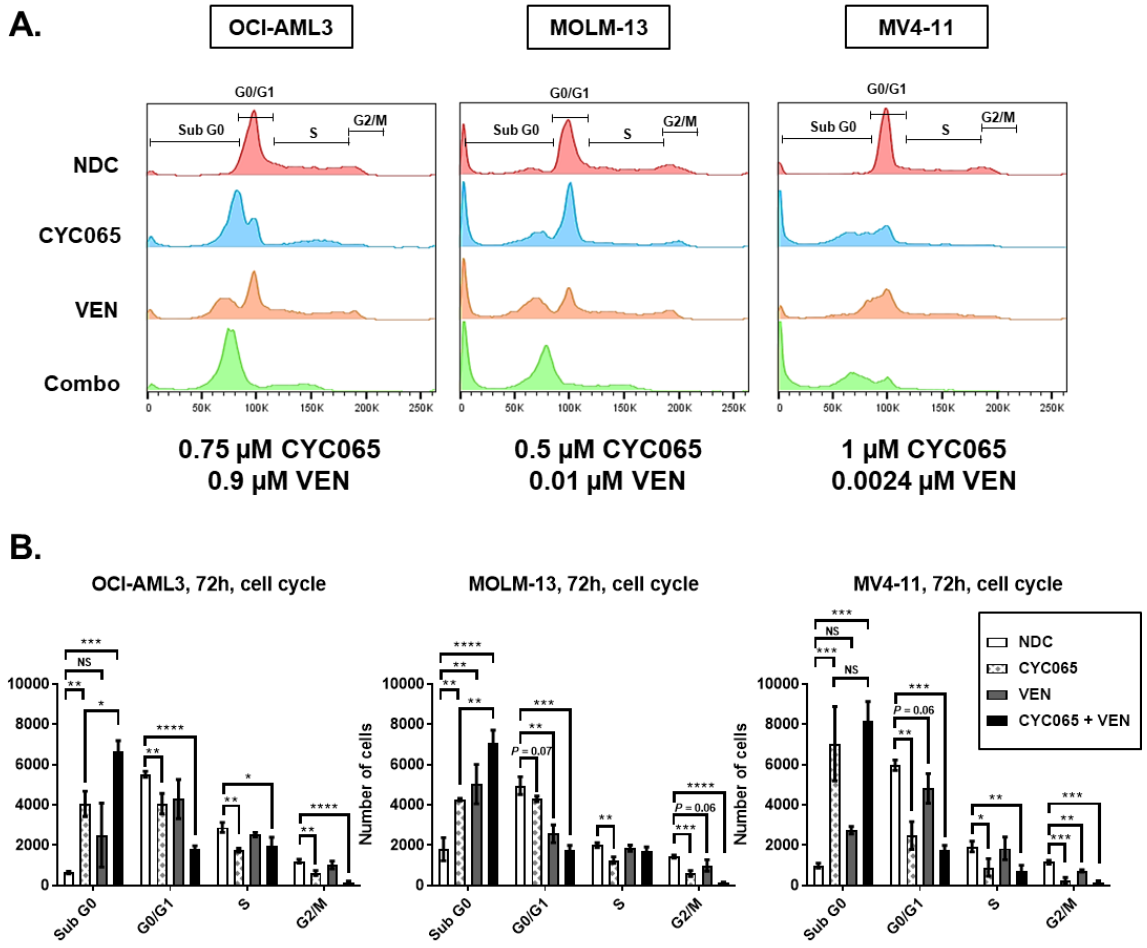

Figure 5.2.6.1 OCI-AML3, MOLM-13, and MV4-11 cell lines were treated with CYC065, VEN, or CYC065/VEN combination for 72h. Drug combination ratios obtained from synergy assays using CompuSyn software. **(A) Representative flow cytometry plots of cell cycle progression using PI staining are shown; and (B) Flow cytometric analysis of the cell cycle phase.** The experiments were performed in biological triplicates. Graphs depict means ± SD. Data were compared using the one-way ANOVA, post hoc Tukey's HSD test (Sub G0 populations; F (3,8) = 24.6, $P = 0.0002$, OCI-AML3; F (3,8) = 32.7, $P < 0.0001$, MOLM-13; F (3,8) = 32.8, $P < 0.0001$, MV4-11). Significant P-values are indicated by asterisks (****< 0.0001, *** 0.0001 to < 0.001, ** 0.001 to < 0.01, * 0.01 to < 0.05 and NS if $P \geq 0.05$).

Collectively, the synergistic effect of CYC065/VEN combination was observed in OCI-AML3 and MOLM-13 cell lines using various methods. Although not statistically significant, the trend of synergism was seen in MV4-11 cell line. Therefore, the combination effect of CYC065 and VEN was further investigated in primary human AML samples as detailed in section 5.5.

5.3 Combination studies of CYC065 and AraC in AML cell lines

5.3.1 Longer exposure reduced the IC50 of AraC

The IC50 of AraC for each cell line was assessed by resazurin reduction assay at 24h, 48h and 72h. It was observed that longer exposure increased drug sensitivity and reduced the IC50. At 24h, the IC50 of AraC was not reached in any cell line in this study at the concentrations used. At 72h, the IC50 of AraC in OCI-AML3, MOLM-13, and MV4-11 cell lines was approximately 2.18±0.33μM (Figure 5.3.1.1A), 0.41±0.04μM (Figure 5.3.1.1B), and 0.07±0.01μM (Figure 5.3.1.1C), respectively.

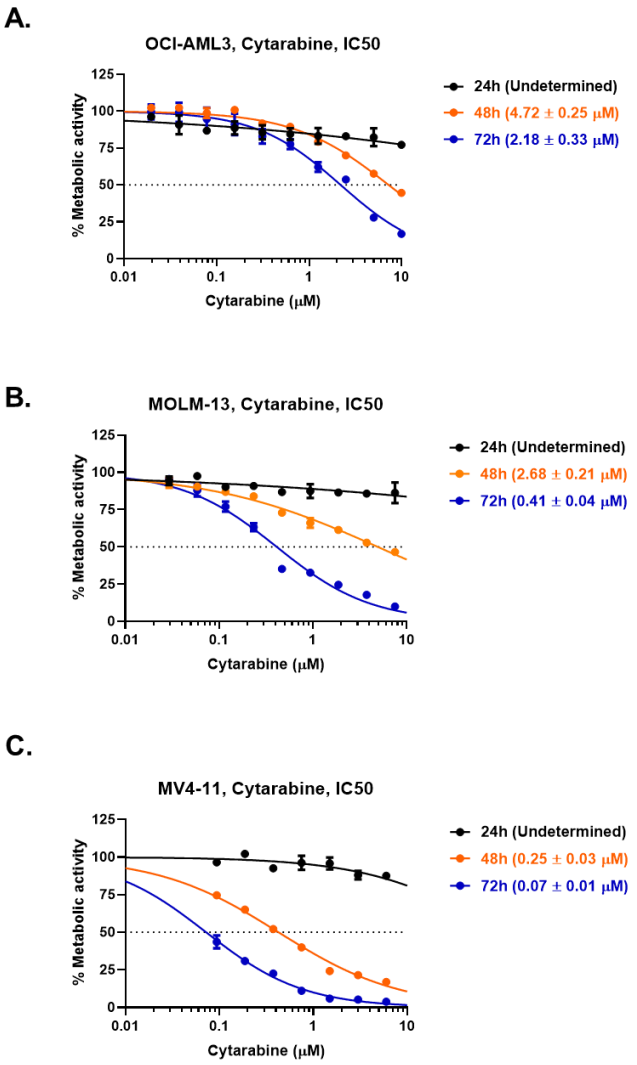

Figure 5.3.1.1 The IC50 of AraC at 24h, 48h and 72h in (A) OCI-AML3, (B) MOLM-13, and (C) MV4-11 cell lines using rezasurin reduction assay. The experiments were performed in technical and biological triplicates. Dots depict means ± SD.

5.3.2 Optimal CYC065/AraC combination ratio was investigated by synergy assay using CompuSyn software

Using the IC50 of AraC from section 5.3.1, combination studies were performed at 72h when the killing effect culminated. CompuSyn software was used to investigate the synergism as detailed in Methods section 2.2.1.5. Preliminary results showed synergistic activity of combination of CYC065 and AraC in all cell lines. Overall, the synergistic effect was observed at 2X to 4X IC50 of CYC065. As shown in Figure 5.3.2.1 (asterisks), optimal drug combination ratios of OCI-AML3, MOLM-13, and MV4-11 cell lines were 0.88μM of CYC065 plus 0.55μM of AraC, 1μM of CYC065 plus 0.1μM AraC, and 1μM of CYC065 plus 0.016μM of AraC, respectively.

For OCI-AML3 and MOLM-13 cell lines, using the concentrations of 0.88μM and 1μM of CYC065, respectively, was not appropriate to demonstrate the synergistic effect as it was masked by too many dead cells. Therefore, the concentrations of 0.75μM and 0.5μM, which induce approximately 50% apoptosis in OCI-AML3 and MOLM-13 cell lines (section 3.2.3), respectively, were focused instead. In OCI-AML3 cell line, using a fixed proportional reduction as previously described (Mayer et al., 2006; Palmer, 2017), the dose was reduced from 0.88μM of CYC065 plus 0.55μM of AraC to 0.75μM of CYC065 plus 0.47μM of AraC. In MOLM-13 cell line, it was reduced from 1μM of CYC065 plus 0.1μM of AraC to 0.5μM of CYC065 plus 0.05μM of AraC. The optimal ratio was summarised in Figure 5.3.2.1 (right panel) for each cell line which was applied for all further experiments, including cell counts (section 5.3.3), apoptosis assays (section 5.3.4), active caspase-3 assays (section 5.3.5), and cell cycle analyses (section 5.3.6).

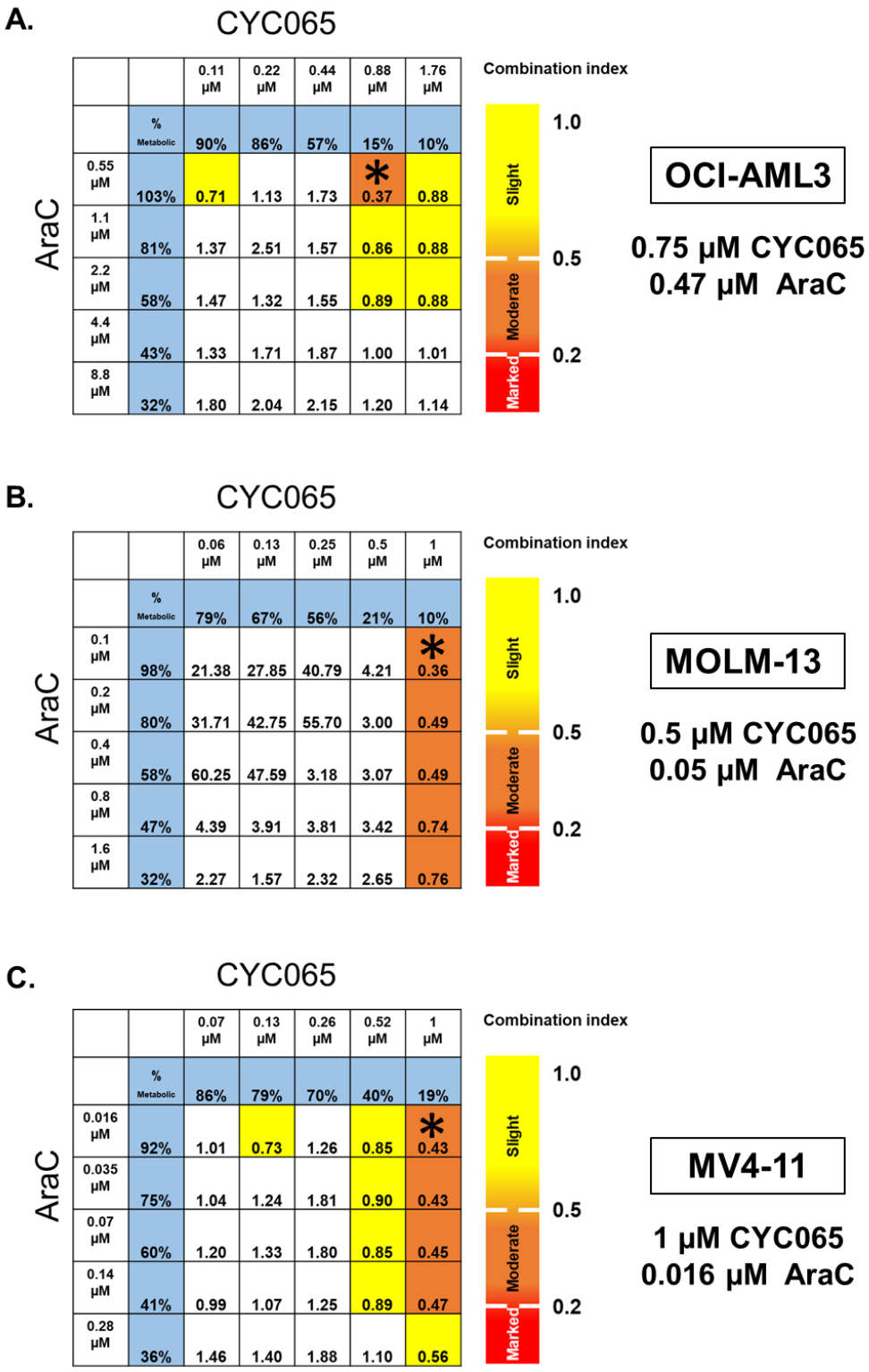

Figure 5.3.2.1 A synergy study for the combination of CYC065 and AraC added to culture for 72h in (A) OCI-AML3, (B) MOLM-13, and (C) MV4-11 cell lines. The experiments were performed in biological triplicates. By using CompuSyn software analysis, a combination index less than 1 and more than 1 indicates synergism and antagonism, respectively. A combination index less than 0.2, 0.2 to less than 0.5 and 0.5 to less than 1 indicates a marked (red), moderate (orange) and slight (yellow) synergism, respectively. The most efficacious drug combination ratio was identified (asterisks) and the concentrations of CYC065 and AraC were determined for further combination studies in each cell line (right panel). Cytarabine (AraC).

5.3.3 A slight decrease in cell viability was observed in CYC065/AraC combination

Cells were treated with CYC065, AraC, or CYC065/AraC combination for 72h. Cell counting was performed using trypan blue exclusion assay.

A dramatic decrease in cell number was seen in the CYC065 alone arm, as a result of greater than IC50 drug concentration used in drug combination ratios. As a consequence, the synergistic effect was masked i.e. only a slight decrease in cell viability was observed in the combination arm as compared with CYC065 single treatment in all cell lines; OCI-AML3 (Figure 5.3.3.1A), MOLM-13 (Figure 5.3.3.1B), and MV4-11 (Figure 5.3.3.1C).

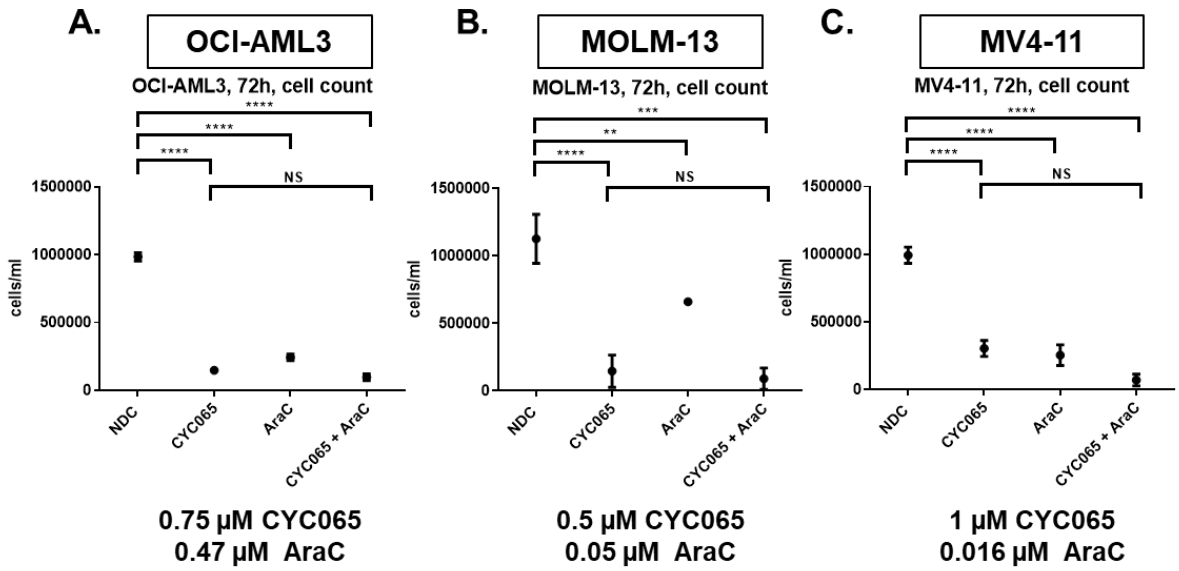

Figure 5.3.3.1 Cell number assessed by trypan blue exclusion assay of (A) OCI-AML3, (B) MOLM-13, and (C) MV4-11 cell lines treated with CYC065, AraC, or CYC065/AraC combination for 72h. The experiments were performed in biological triplicates. Drug combination ratios of each cell line were obtained from synergy assays using CompuSyn software (bottom panel). Dots depict means ± SD. Data were compared using the one-way ANOVA, post hoc Tukey's HSD test ($F(3,8) = 820.8$, $P < 0.0001$, OCI-AML3; $F(3,8) = 52.8$, $P < 0.0001$, MOLM-13; $F(3,8) = 133.1$, $P < 0.0001$, MV4-11). Significant *P*-values are indicated by asterisks (****< 0.0001, *** 0.0001 to < 0.001, ** 0.001 to < 0.01, * 0.01 to < 0.05 and NS if $P \geq 0.05$).

5.3.4 Synergistic activity of CYC065/AraC combination was observed in annexin V/DAPI apoptosis assays

Cells were treated with CYC065, AraC, or CYC065/AraC combination for 72h. The apoptosis assays were performed using annexin V/DAPI staining (Figure 5.3.4.1A,B).

In CYC065 single treatment, the doses of 0.75μM, 0.5μM, and 1μM were focused for OCI-AML3, MOLM-13, and MV4-11 cell lines, respectively. At these concentrations, approximately 50% apoptosis was observed in all cell lines (Figure 5.3.4.1B). Importantly, there was a significant decrease in viable cells, corresponding with an increase in the population of apoptotic cells in the combination arm as compared with CYC065 single treatment in all cell lines; OCI-AML3 (Figure 5.3.4.1B left graph), MOLM-13 (Figure 5.3.4.1B middle graph), and MV4-11 (Figure 5.3.4.1B right graph).

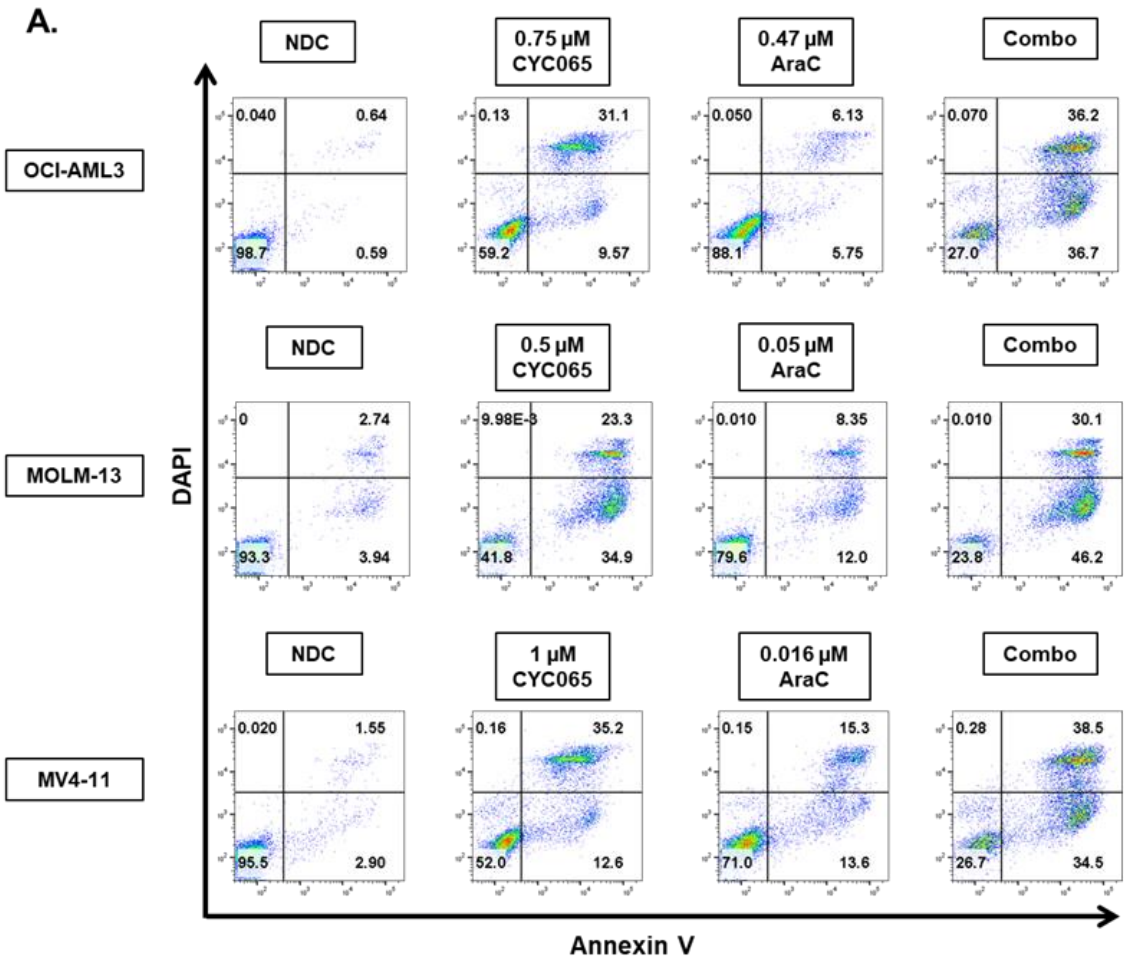

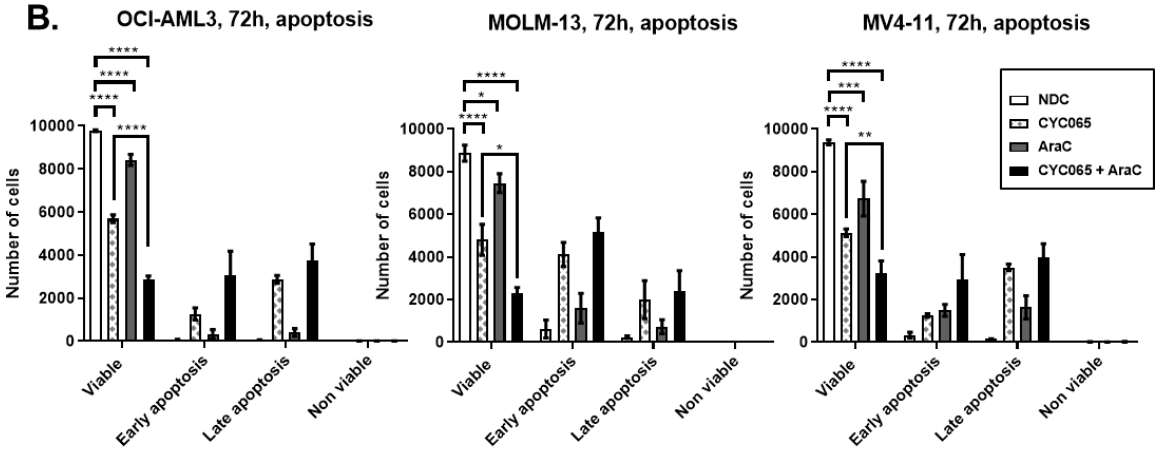

Figure 5.3.4.1 OCI-AML3, MOLM-13, and MV4-11 cell lines were treated with CYC065, AraC, or CYC065/AraC combination for 72h. Drug combination ratios obtained from synergy assays using CompuSyn software. **(A) Representative flow cytometry plots of apoptosis assay using annexin V/DAPI are shown; and (B) Flow cytometric analysis of apoptosis assay.** The experiments were performed in biological triplicates. Graphs depict means ± SD. Cell viability was compared using the one-way ANOVA, post hoc Tukey's HSD test ($F(3,8) = 85.2$, $P < 0.0001$, OCI-AML3; $F(3,8) = 120.2$, $P < 0.0001$, MOLM-13; $F(3,8) = 79.5$, $P < 0.0001$, MV4-11). Significant *P*-values are indicated by asterisks (****< 0.0001, *** 0.0001 to < 0.001, ** 0.001 to < 0.01, * 0.01 to < 0.05 and NS if $P \geq 0.05$).

5.3.5 Synergistic activity of CYC065/AraC combination was observed in active caspase-3 assays

Cells were treated with CYC065, AraC, or CYC065/AraC combination for 72h. The active caspase-3 assays were performed (Figure 5.3.5.1A,B) aiming to confirm the results from annexin V/DAPI apoptosis assays (section 5.3.4).

In CYC065 single treatment, the active caspase-3-positive population was approximately 50% of cells in all cell lines (Figure 5.3.5.1B), which is consistent with the results from the apoptosis assays (section 5.3.4). There was a significant increase in the active caspase-3-positive population in the combination arm as compared with CYC065 single treatment in all cell lines; OCI-AML3 (Figure 5.3.5.1B left graph), MOLM-13 (Figure 5.3.5.1B middle graph), and MV4-11 (Figure 5.3.5.1B right graph).

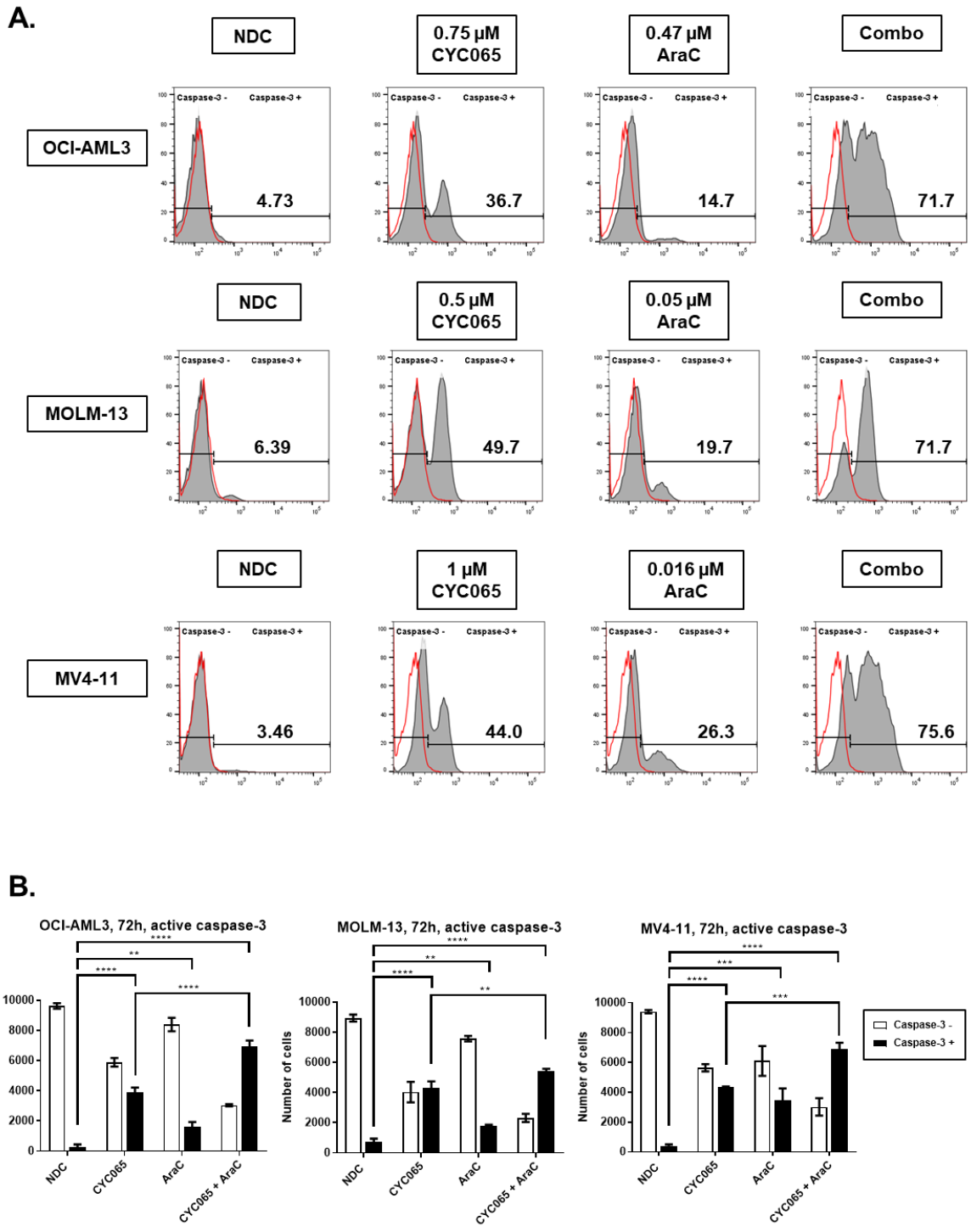

Figure 5.3.5.1 OCI-AML3, MOLM-13, and MV4-11 cell lines were treated with CYC065, AraC, or CYC065/AraC combination for 72h. Drug combination ratios obtained from synergy assays using CompuSyn software. **(A) Representative flow cytometry plots of active caspase-3 assay in which red curves represent isotype controls are shown; and (B) Flow cytometric analysis of active caspase-3 assays.** The experiments were performed in biological triplicates. Graphs depict means ± SD. Caspase-3-positive populations were compared using the one-way ANOVA, post hoc Tukey's HSD test ($F(3,8) = 129.8$, $P < 0.0001$, OCI-AML3; $F(3,8) = 125$, $P < 0.0001$, MOLM-13; $F(3,8) = 99.2$, $P < 0.0001$, MV4-11). Significant *P*-values are indicated by asterisks (****< 0.0001, *** 0.0001 to < 0.001, ** 0.001 to < 0.01, * 0.01 to < 0.05 and NS if $P \geq 0.05$).

5.3.6 Synergistic activity of CYC065/AraC combination resulted in an increase in sub G0 cell population in cell cycle analyses

Cells were treated with CYC065, AraC, or CYC065/AraC combination for 72h. Cell cycle analyses were performed using PI staining (Figure 5.3.6.1A,B).

Interestingly, an arrest in S and G2/M phases was observed with AraC single treatment in OCI-AML3 cell line only (Figure 5.3.6.1B left graph).
A significant increase in the sub G0 population in the combination arm, as compared with CYC065 single treatment, was observed in OCI-AML3 (Figure 5.3.6.1B left graph) and MV4-11 cell lines (Figure 5.3.6.1B right graph), indicating an increase in cell death. In MOLM-13 cell line, although not statistically significant, a rise in the sub G0 population was seen in the combination arm as compared with single treatments (Figure 5.3.6.1B middle graph).

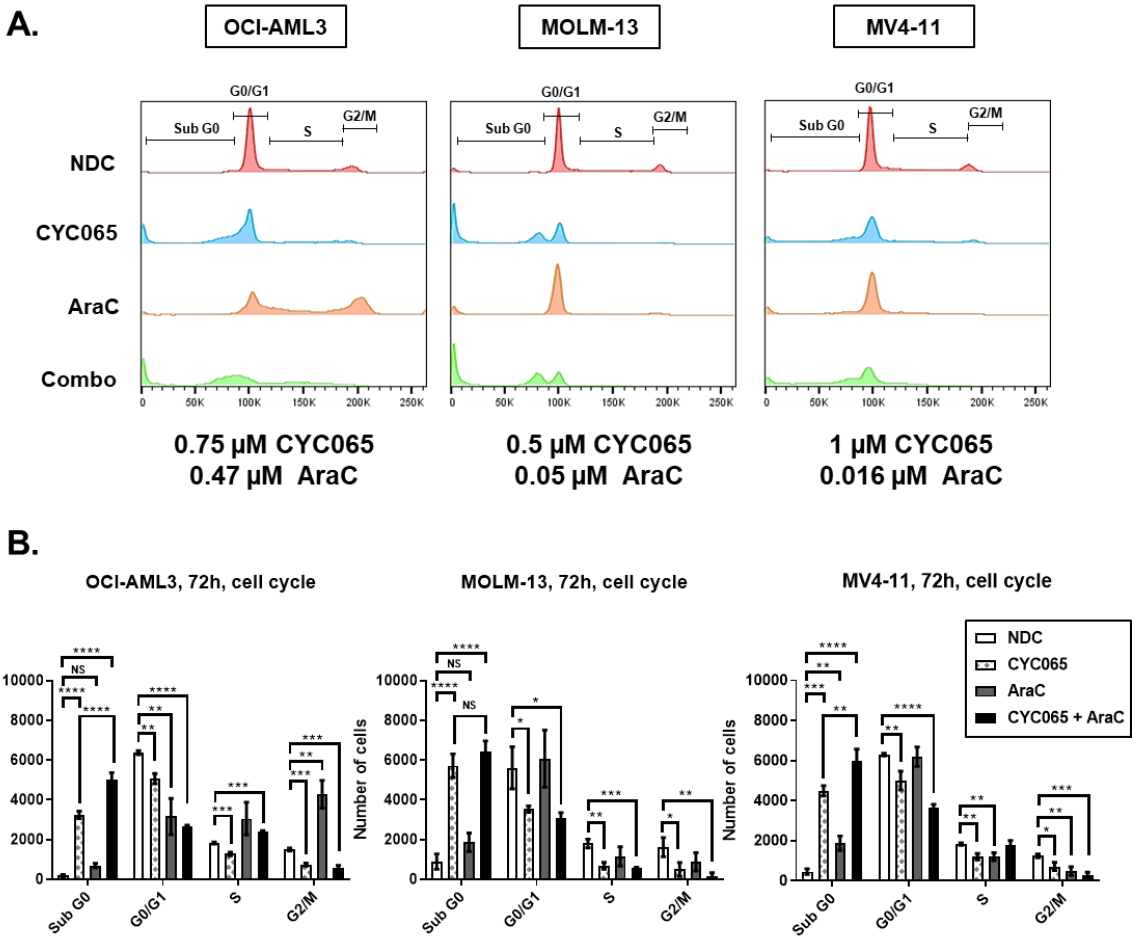

Figure 5.3.6.1 OCI-AML3, MOLM-13, and MV4-11 cell lines were treated with CYC065, AraC, or CYC065/AraC combination for 72h. Drug combination ratios obtained from synergy assays using CompuSyn software. **(A) Representative flow cytometry plots of cell cycle progression using PI staining are shown; and (B) Flow cytometric analysis of the cell cycle phase.** The experiments were performed in biological triplicates. Graphs depict means ± SD. Data were compared using the one-way ANOVA, post hoc Tukey's HSD test (Sub G0 populations; $F(3,8) = 372.9$, $P < 0.0001$, OCI-AML3; $F(3,8) = 87.8$, $P < 0.0001$, MOLM-13; $F(3,8) = 79.6$, $P < 0.0001$, MV4-11). Significant *P*-values are indicated by asterisks (****< 0.0001, *** 0.0001 to < 0.001, ** 0.001 to < 0.01, * 0.01 to < 0.05 and NS if $P \geq 0.05$).

Taken together, the synergistic effect of CYC065/AraC combination was observed in all cell lines using various methods. Therefore, the combination effect of CYC065 and AraC was further investigated in primary human AML samples as detailed in section 5.5.

5.4 Combination studies of CYC065 and AZA in AML cell lines

5.4.1 Longer exposure reduced the IC50 of AZA

The IC50 of AZA for each cell line was assessed by resazurin reduction assay at 24h, 48h and 72h. It was observed that longer exposure increased drug sensitivity and reduced the IC50. At 72h, the IC50 of AZA in OCI-AML3, MOLM-13, and MV4-11 cell lines was approximately 7.11±1.13μM (Figure 5.4.1.1A), 4.23±0.14μM (Figure 5.4.1.1B), and 10.83±0.11μM (Figure 5.4.1.1C), respectively.

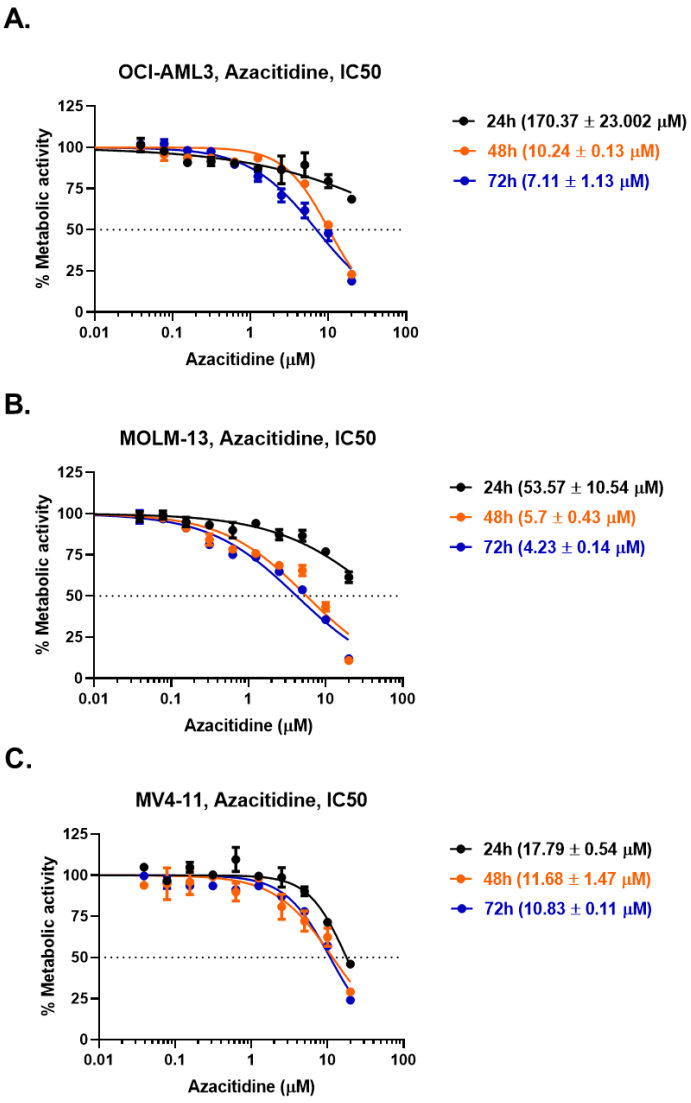

Figure 5.4.1.1 The IC50 of AZA at 24h, 48h and 72h in (A) OCI-AML3, (B) MOLM-13, and (C) MV4-11 cell lines using rezasurin reduction assay. The experiments were performed in technical and biological triplicates. Dots depict means ± SD.

5.4.2 Optimal CYC065/AZA combination ratio was investigated by synergy assay using CompuSyn software

Using the IC50 of AZA from section 5.4.1, combination studies were performed at 72h when the killing effect culminated. CompuSyn software was used to investigate the synergism as detailed in Methods section 2.2.1.5. Preliminary results showed synergistic activity of combination of CYC065 and AZA in all cell lines. Overall, the synergistic effect was observed at 2X to 4X IC50 of CYC065. As shown in Figure 5.4.2.1 (asterisks), optimal drug combination ratios for OCI-AML3, MOLM-13, and MV4-11 cell lines were 0.88μM of CYC065 plus 3.5μM of AZA, 0.5μM of CYC065 plus 2.1μM AZA, and 1μM of CYC065 plus 5.3μM of AZA, respectively.

For OCI-AML3 cell line, using a concentration of 0.88μM of CYC065 was not appropriate to demonstrate the synergistic effect as it was masked by too many dead cells, therefore, a concentration of 0.75μM which induces approximately 50% apoptosis (section 3.2.3) was focused instead. Using a fixed proportional reduction as previously described (Mayer et al., 2006; Palmer, 2017), the dose was reduced from 0.88μM of CYC065 plus 3.5μM of AZA to 0.75μM of CYC065 plus 3μM of AZA. The optimal ratio is summarised in Figure 5.4.2.1 (right panel) for each cell line, and was applied for all further experiments, including; cell count (section 5.4.3), apoptosis assays (section 5.4.4), active caspase-3 assays (section 5.4.5), and cell cycle analyses (section 5.4.6).

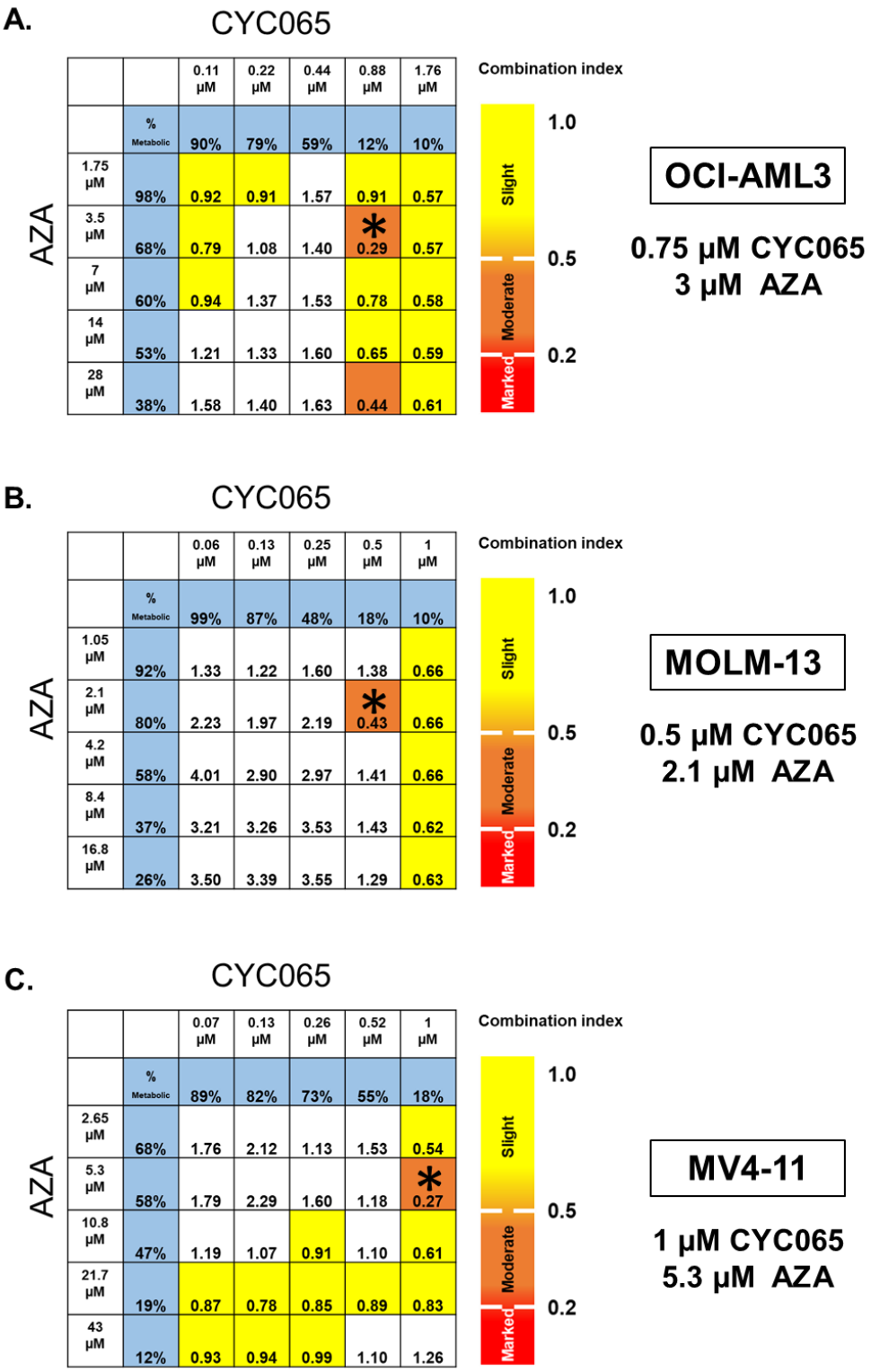

Figure 5.4.2.1 A synergy study for the combination of CYC065 and AZA added to culture for 72h in (A) OCI-AML3, (B) MOLM-13, and (C) MV4-11 cell lines. The experiments were performed in biological triplicates. By using CompuSyn software analysis, a combination index less than 1 and more than 1 indicates synergism and antagonism, respectively. A combination index less than 0.2, 0.2 to less than 0.5 and 0.5 to less than 1 indicates a marked (red), moderate (orange) and slight (yellow) synergism, respectively. The most efficacious drug combination ratio was identified (asterisks) and the concentrations of CYC065 and AZA were determined for further combination studies in each cell line (right panel). Azacitidine (AZA).

5.4.3 A slight decrease in cell viability was observed in CYC065/AZA combination

Cells were treated with CYC065, AZA, or CYC065/AZA combination for 72h. Cell counting was performed using trypan blue exclusion assay.

A dramatic decrease in cell number was seen in a single treatment of CYC065 as a result of greater than IC50 drug concentration being used in drug combination ratios. As a consequence, the synergistic effect was masked i.e. although statistically significant, only a modest drop in cell viability was observed in the combination arm as compared with CYC065 single treatment in all cell lines; OCI-AML3 (Figure 5.4.3.1A), MOLM-13 (Figure 5.4.3.1B), and MV4-11 (Figure 5.4.3.1C).

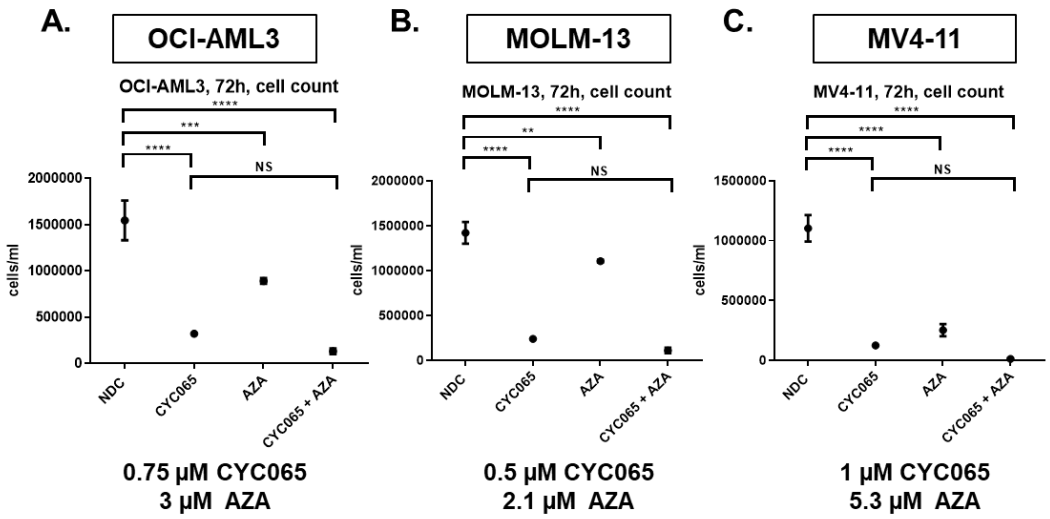

Figure 5.4.3.1 Cell number assessed by trypan blue exclusion assay of (A) OCI-AML3, (B) MOLM-13, and (C) MV4-11 cell lines treated with CYC065, AZA, or CYC065/AZA combination for 72h. The experiments were performed in biological triplicates. Drug combination ratio of each cell line was obtained from synergy assays using CompuSyn software (bottom panel). Dots depict means ± SD. Data were compared using the one-way ANOVA, post hoc Tukey's HSD test ($F(3,8) = 99.6$, $P < 0.0001$, OCI-AML3; $F(3,8) = 317.6$, $P < 0.0001$, MOLM-13; $F(3,8) = 188.8$, $P < 0.0001$, MV4-11). Significant *P*-values are indicated by asterisks (****< 0.0001, *** 0.0001 to < 0.001, ** 0.001 to < 0.01, * 0.01 to < 0.05 and NS if $P \geq 0.05$).

5.4.4 Synergistic activity of CYC065/AZA combination was observed in annexin V/DAPI apoptosis assays

Cells were treated with CYC065, AZA, or CYC065/AZA combination for 72h. The apoptosis assays were performed using annexin V/DAPI staining (Figure 5.4.4.1A,B).

In CYC065 single treatment, the doses of 0.75μM, 0.5μM, and 1μM were focused for OCI-AML3, MOLM-13, and MV4-11 cell lines, respectively. At these concentrations, approximately 50% apoptosis was observed in all cell lines (Figure 5.4.4.1B). Importantly, there was a significant decrease in viable cells, corresponding with an increase in the population of apoptotic cells in the combination arm as compared with CYC065 single treatment in all cell lines; OCI-AML3 (Figure 5.4.4.1B left graph), MOLM-13 (Figure 5.4.4.1B middle graph), and MV4-11 (Figure 5.4.4.1B right graph).

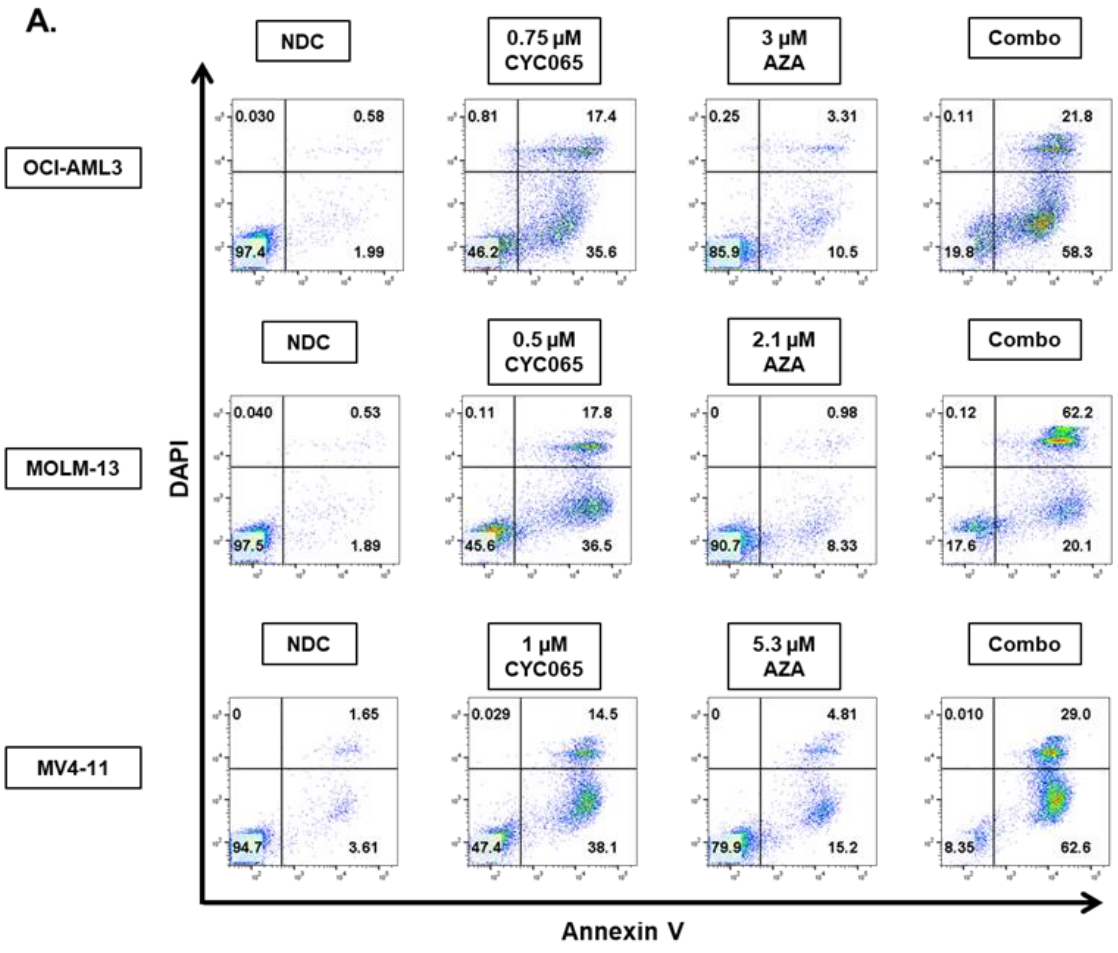

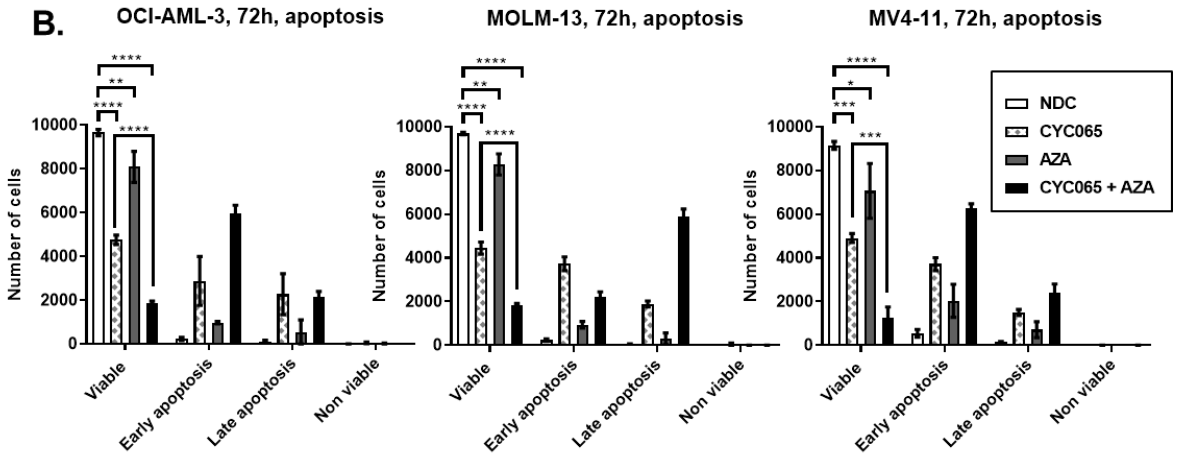

Figure 5.4.4.1 OCI-AML3, MOLM-13, and MV4-11 cell lines were treated with CYC065, AZA, or CYC065/AZA combination for 72h. Drug combination ratios were obtained from synergy assays using CompuSyn software. **(A) Representative flow cytometry plots of apoptosis assay using annexin V/DAPI are shown; (B) Flow cytometric analysis of apoptosis assay.** The experiments were performed in biological triplicates. Graphs depict means ± SD. Cell viability was compared using the one-way ANOVA, post hoc Tukey's HSD test ($F(3,8) = 85.1$, $P < 0.0001$, OCI-AML3; $F(3,8) = 82.2$, $P < 0.0001$, MOLM-13; $F(3,8) = 72$, $P < 0.0001$, MV4-11). Significant *P*-values are indicated by asterisks (****< 0.0001, *** 0.0001 to < 0.001, ** 0.001 to < 0.01, * 0.01 to < 0.05 and NS if $P \geq 0.05$).

5.4.5 Synergistic activity of CYC065/AZA combination was observed in active caspase-3 assays

Cells were treated with CYC065, AZA, or CYC065/AZA combination for 72h. The active caspase-3 assays were performed (Figure 5.4.5.1A,B) aiming to confirm the results from annexin V/DAPI apoptosis assays (section 5.4.4).

With CYC065 single agent treatment, the active caspase-3-positive population was approximately 50% of cells in all cell lines (Figure 5.4.5.1B) which is consistent with the results from the annexin V/DAPI apoptosis assay (section 5.4.4). There was a significant increase in the active caspase-3-positive population in the combination arm as compared with CYC065 single treatment in all cell lines; OCI-AML3 (Figure 5.4.5.1B left graph), MOLM-13 (Figure 5.4.5.1B middle graph), and MV4-11 (Figure 5.4.5.1B right graph).

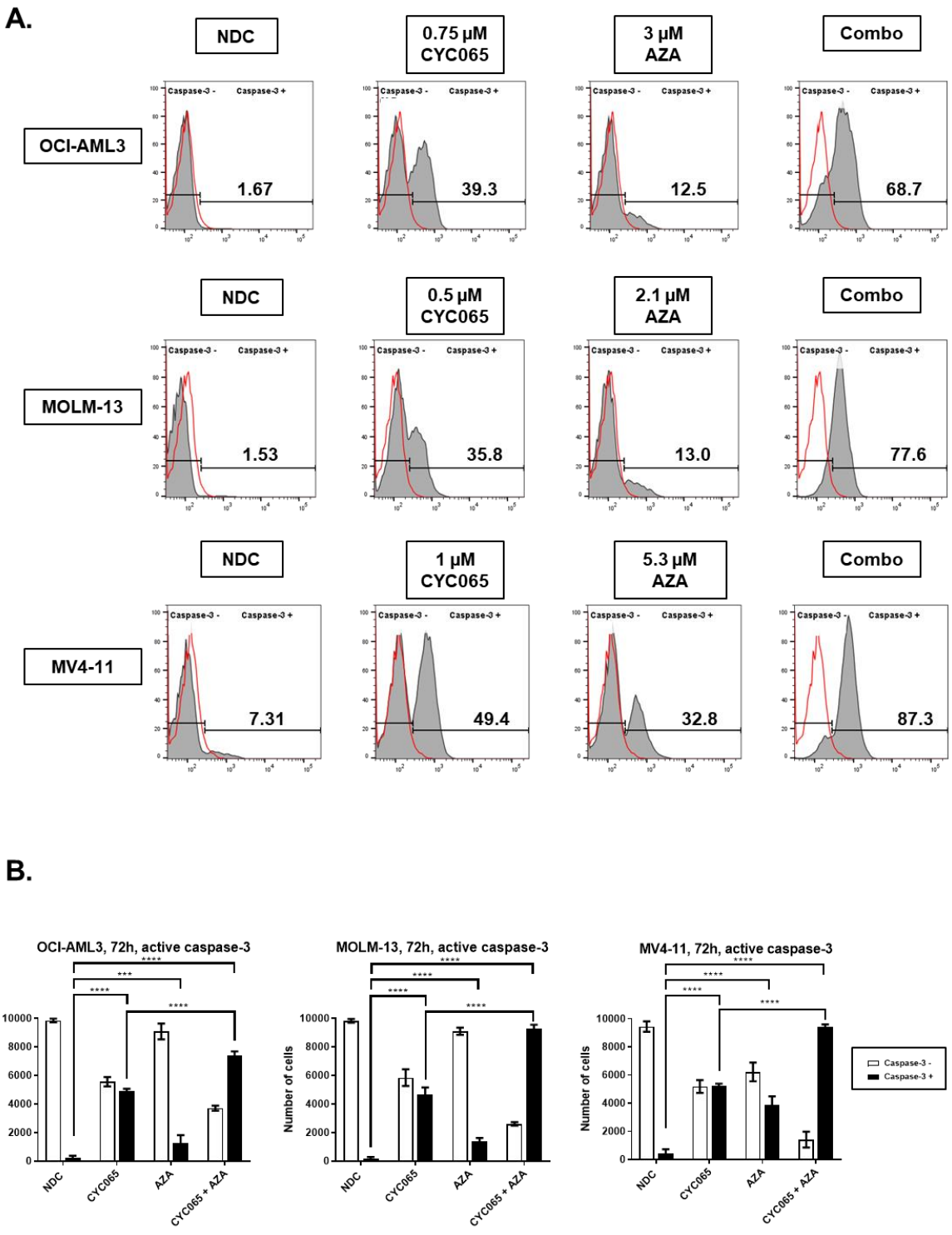

Figure 5.4.5.1 OCI-AML3, MOLM-13, and MV4-11 cell lines were treated with CYC065, AZA, or CYC065/AZA combination for 72h. Drug combination ratios obtained from synergy assays using CompuSyn software. **(A) Representative flow cytometry plots of active caspase-3 assay in which red curves represent isotype controls are shown; and (B) Flow cytometric analysis of active caspase-3 assays.** The experiments were performed in biological triplicates. Graphs depict means ± SD. Caspase-3-positive populations were compared using the one-way ANOVA, post hoc Tukey's HSD test ($F(3,8) = 86.6$, $P < 0.0001$, OCI-AML3; $F(3,8) = 96.6$, $P < 0.0001$, MOLM-13; $F(3,8) = 80.1$, $P < 0.0001$, MV4-11). Significant *P*-values are indicated by asterisks (****< 0.0001, *** 0.0001 to < 0.001, ** 0.001 to < 0.01, * 0.01 to < 0.05 and NS if $P \geq 0.05$).

5.4.6 Synergistic activity of CYC065/AZA combination resulted in an increase in sub G0 cell population in cell cycle analyses

Cells were treated with CYC065, AZA, or CYC065/AZA combination for 72h. Cell cycle analyses were performed using PI staining (Figure 5.4.6.1A,B).

An increase in sub G0, without any other cell cycle phase, was observed in single treatments and combination arms. There was a significant increase in the sub G0 population in the combination arm as compared with CYC065 single treatment in all cell lines; OCI-AML3 (Figure 5.4.6.1B left graph), MOLM-13 cell lines (Figure 5.4.6.1B middle graph), and MV4-11 (Figure 5.4.6.1B right graph), indicating a rise in cell death.

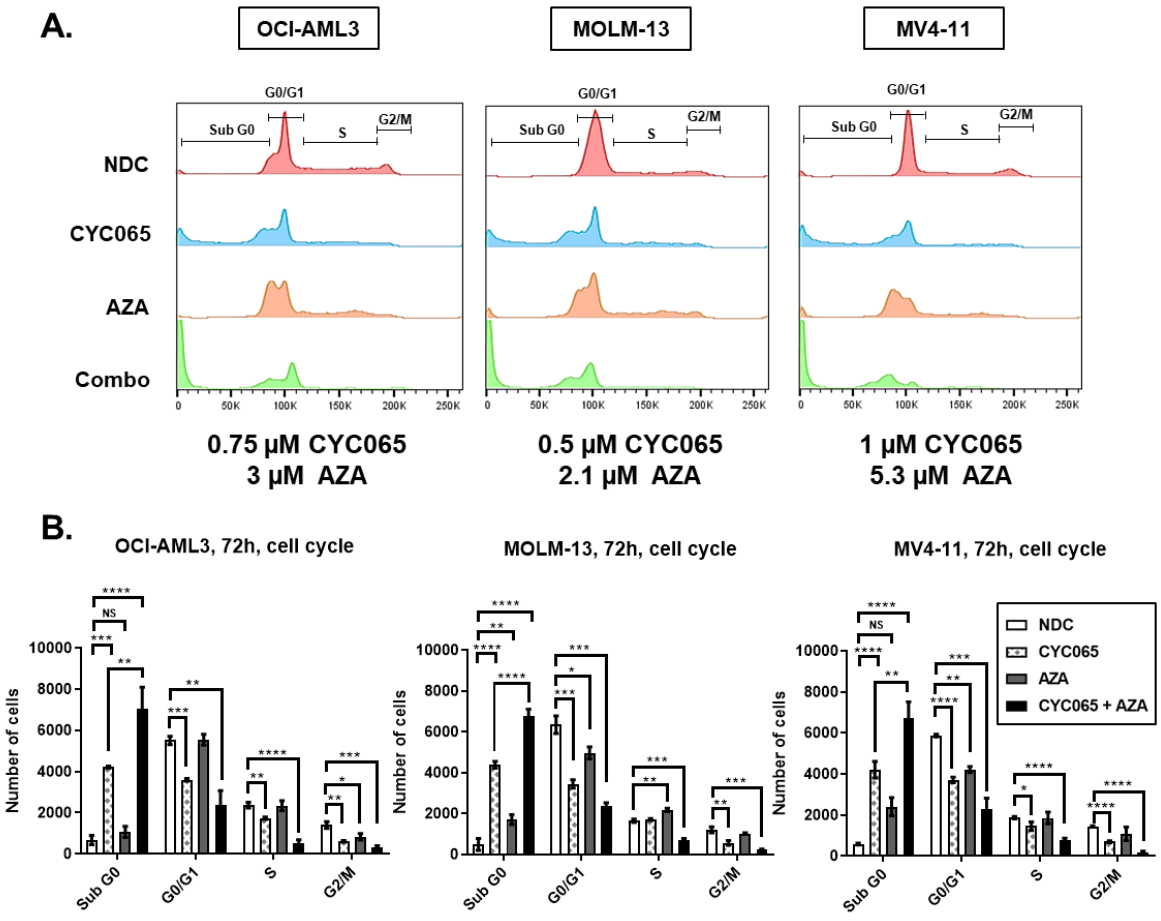

Figure 5.4.6.1 OCI-AML3, MOLM-13, and MV4-11 cell lines were treated with CYC065, AZA, or CYC065/AZA combination for 72h. Drug combination ratios were obtained from synergy assays using CompuSyn software. **(A) Representative flow cytometry plots of cell cycle progression using PI staining are shown; and (B) Flow cytometric analysis of the cell cycle phase.** The experiments were performed in biological triplicates. Graphs depict means ± SD. Data were compared using the one-way ANOVA, post hoc Tukey's HSD test (Sub G0 populations; F (3,8) = 84.9, $P < 0.0001$, OCI-AML3; F (3,8) = 92.7, $P < 0.0001$, MOLM-13; F (3,8) = 93.4, $P < 0.0001$, MV4-11). Significant *P*-values are indicated by asterisks (****< 0.0001, *** 0.0001 to < 0.001, ** 0.001 to < 0.01, * 0.01 to < 0.05 and NS if $P \geq 0.05$).

All in all, the synergistic effect of the CYC065/AZA combination was observed in all cell lines using various methods. Hence, the combination effect of CYC065 and AZA was further investigated in primary human AML samples as detailed in section 5.5.

5.5 Combination studies of CYC065 with VEN, AraC, or AZA in primary human AML samples

The synergistic effect of CYC065/VEN (section 5.2), CYC065/AraC (section 5.3), and CYC065/AZA combinations (section 5.4) was observed in all AML cell lines in this study. Therefore, further investigation of these drug combinations were performed in primary human AML samples.

5.5.1 High diversity of genetic mutations was observed for human primary AML samples

Six primary AML and three normal haematopoietic cell control samples were selected from the biobank of the Paul O'Gorman Leukaemia Research Centre. Table 5.5.1.1 shows the genetic lesions for the primary AML samples tested in this study. The common favourable, e.g. *NPM1* mutation and unfavourable mutations in AML e.g. *FLT3*-ITD, and *KMT2A*-PTD were selected for further study.

Table 5.5.1.1 Genetic lesions of primary AML samples classified by their functions.

Sample	Source	%Blasts	%CD34	%Recovery (after thawing)	Karyotype	Genetic lesions						
						Signalling genes	DNA methylation-related genes	Chromatin-modifying genes	Nucleophosmin gene	Cohesin complex genes	Spliceosome complex genes	Transcription factor fusions
AML 11	N.A.	N.A.	40.5	50	Normal		*IDH2*	*KMT2A*-PTD, *ASXL1*				
AML 12	PB	93 (PB)	71.9 (PB)	82	Monosomy 7	*FLT3*-ITD	*DNMT3A*, *IDH2*					
AML 13	PB	75 (BM) 31 (PB)	0.14 (PB)	53.5	Normal	*FLT3*-ITD	*DNMT3A*		*NPM1*	*RAD21*		
AML 14	BM	78 (BM) 80 (PB)	0.97 (BM)	73	Complex	*KIT*			*NPM1*			
AML 15	PB	33 (BM)	78.3 (PB)	85	Trisomy 11		*DNMT3A*, *IDH1*			*STAG2*	*SRSF2*	
AML 16	PB	20 (BM)	86 (PB)	50	Normal	*FLT3*-ITD	*DNMT3A*, *TET2*	*KMT2A*-PTD			*SRSF2*	*RUNX1*

Bone marrow (BM). Peripheral blood (PB). Not available (N.A.). Isocitrate dehydrogenase 1 and 2 (IDH1 and IDH2). Lysine methyltransferase 2A-partial tandem duplication (KMT2A-PTD). Additional sex combs-like 1 (ASXL1). FMS-like tyrosine kinase 3 - internal tandem duplication (FLT3-ITD). DNA methyltransferase 3 alpha (DNMT3A). Nucleophosmin 1 (NPM1). Double-strand-break repair protein rad21 (RAD21). Tyrosine-protein kinase Kit gene (KIT) Stromal antigen 2 (STAG2). Serine arginine-rich splicing factor 2 (SRSF2). Ten-eleven translocation methylcytosine dioxygenase 2 (TET2). Runt-related transcription factor 1 (RUNX1).

Initially, we proposed assessing samples with a single mutation of these genes in order to assess the efficacy of CYC065 and its synergistic activity when combined with VEN, AraC, or AZA, towards each mutation. However, those samples are not available in a real-world situation as a high diversity of genetic mutations is the nature of AML. Therefore, samples bearing isolated *NPM1* mutation, *DNMT3A* mutation, *FLT3*-ITD, *KMT2A*-PTD or their combination were utilised regardless of the presence of other genetic lesions. Normal controls were samples from patients diagnosed with non-BM infiltrative disease.

The clinically achievable concentration of CYC065 is 6-7μM (Do et al., 2018). In this study, 0.25μM (CYC1) and 0.5μM (CYC2) of CYC065 in combination with VEN, AraC, or AZA were assessed for efficacy against primary AML cells. The concentrations selected were based on previous studies (Adachi, Ishikawa, & Kiyoi, 2017; Leonard, Perry, Woodman, & Kearns, 2014; Min et al., 2017; Teh et al., 2018), i.e. 0.025μM (VEN1) and 0.5μM (VEN2) of VEN; 0.01μM (AraC1) and 0.1μM (AraC2) of AraC; 0.5μM (AZA1) and 2μM (AZA2) of AZA, aiming to cover both sensitive and more resistant groups of patient, these were still within clinically achievable concentrations i.e. 1μM of VEN (Anderson et al., 2016), 1μM of AraC (Heasman et al., 2011), and 3-11μM of AZA (Hollenbach et al., 2010). Cell counts, apoptosis assays, active caspase-3 assays, cell cycle analyses, and cell proliferation assays were performed at 72h when the culmination of killing effect was observed in AML cell lines. CFU assay were also set up at 72h and incubated for 10-14 days prior to characterising and counting the number of viable colonies.

5.5.2 A decrease in cell viability was observed in CYC065/VEN, CYC065/AraC, and CYC065/AZA combinations as compared with single treatments

Primary human AML and normal haematopoietic cells were plated at the concentration of $2.5x10^5$ cells/ml and treated with CYC065, VEN, AraC, AZA, or the combinations for 72h. Cell counting was performed using trypan blue exclusion assay. Cell number from six primary AML and three normal samples was summarised aiming to observe a global effect of the treatments.

At 72h, as an overall picture, the baseline cell number was higher in normal samples (Figure 5.5.2.1B, CYC065/VEN; D, CYC065/AraC; F, CYC065/AZA) as compared with AML samples (Figure 5.5.2.1A, CYC065/VEN; C, CYC065/AraC; E, CYC065/AZA), indicating a higher proliferative potential of the former group. It was observed that single and combination treatments had an impact on both AML and normal samples in a similar fashion. Collectively, although not statistically significant, a decrease in cell viability was seen in all drug combination pairs as compared with single treatments at both low and high concentrations in a dose-dependent manner.

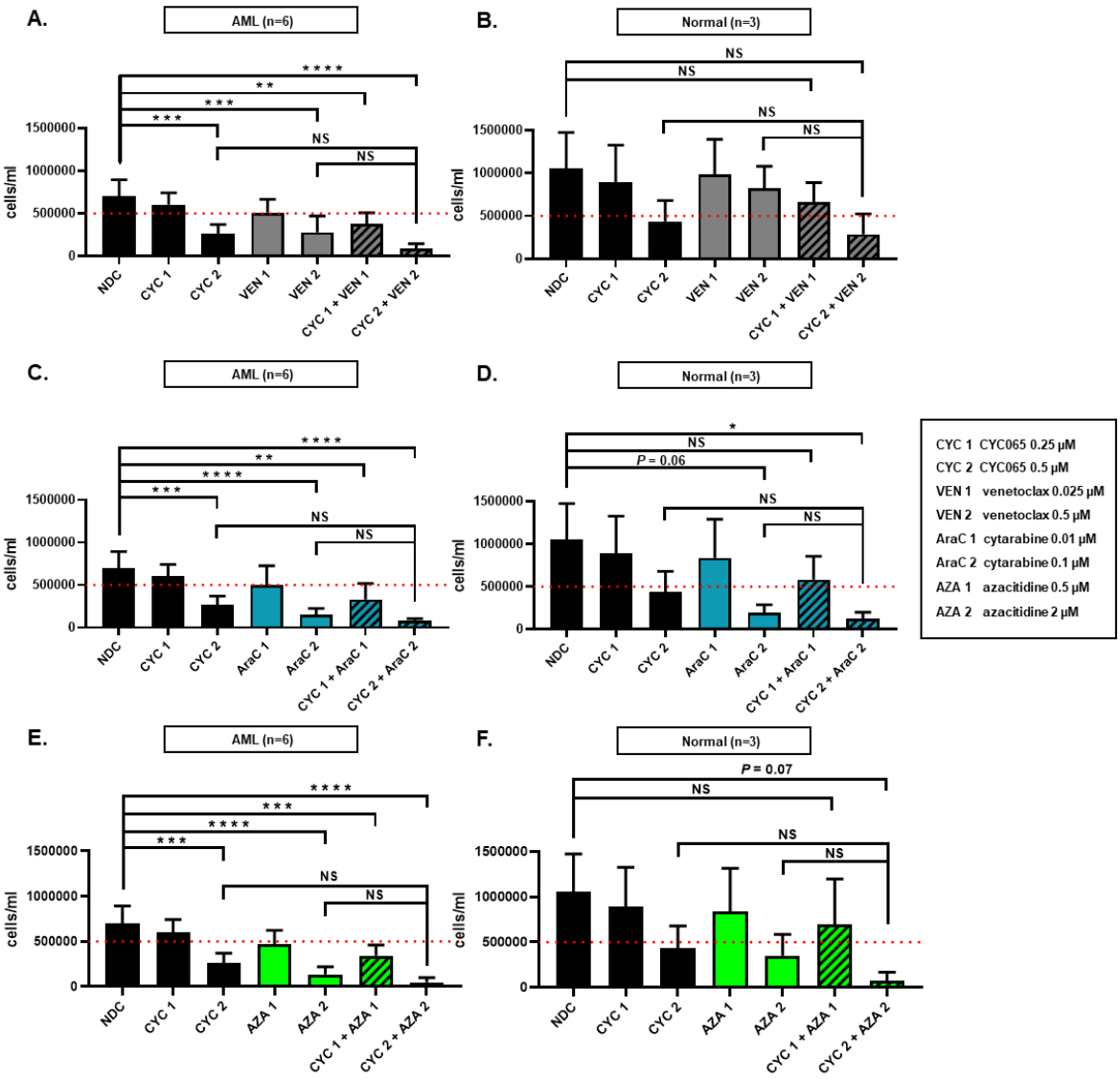

Figure 5.5.2.1 Primary human AML (n=6) or normal haematopoietic samples (n=3) were treated with CYC065, VEN, AraC, AZA, or the combinations for 72h. Summary of data analysis of cell count assessed by trypan blue dye exclusion of (A) primary AML samples and (B) normal samples treated with CYC065/VEN; (C) primary AML samples and (D) normal samples treated with CYC065/AraC; (E) primary AML samples and (F) normal samples treated with CYC065/AZA. Graphs depict means ± SD. Data were compared using the one-way ANOVA, post hoc Tukey's HSD test ([A], F (6,35) = 12.7, $P < 0.0001$; [B], F (6,14) = 2.2, $P = 0.1$; [C], F (6,35) = 13.9, $P < 0.0001$; [D], F (6,14) = 3.7, $P = 0.02$; [E], F (6,35) = 20.4, $P < 0.0001$; [F], F (6,14) = 2.6, $P = 0.0661$). Significant *P*-values are indicated by asterisks (****< 0.0001, *** 0.0001 to < 0.001, ** 0.001 to < 0.01, * 0.01 to < 0.05 and NS if $P \geq 0.05$).

5.5.3 An increase in the percentage of annexin V-positive cells was observed in CYC065/VEN, CYC065/AraC, and CYC065/AZA combinations as compared with single treatments

Primary human AML and normal haematopoietic cells were treated with CYC065, VEN, AraC, AZA, or the combinations for 72h. These cells were stained with CellTrace™ Violet, for the cell proliferation assays (section 5.5.6), which was detected at the same channel as DAPI. Hence, the apoptosis assays were performed using annexin V/7-AAD instead of annexin V/DAPI staining. The percentage of annexin V-positive cells (% Annexin V) from six primary AML and three normal samples was summarised aiming to observe a global effect of the treatments (Figure 5.5.3.1C-H).

At 72h, most of the annexin V-positive cells were within late rather than early apoptosis population (Figure 5.5.3.1A,B). In primary AML samples, % Annexin V of combination treatments as compared with single treatments were not different in any drug combination pair tested at low concentrations. At high concentrations, a slight increase in % Annexin V was observed; 82±17% in CYC2/VEN2 (as compared with 56±14% in CYC2, $P = 0.11$; and 65±21% in VEN2 alone, $P = 0.52$) (Figure 5.5.3.1C), 82±13% in CYC2/AraC2 (as compared with 56±14% in CYC2, $P = 0.11$; and 69±22% in AraC2 alone, $P = 0.81$) (Figure 5.5.3.1E), and 88±12% in CYC2/AZA2 (as compared with 56±14% in CYC2, $P = 0.01$; and 71±23% in AZA2 alone, $P = 0.44$) (Figure 5.5.3.1G). However, there was no statistically significant difference in any of these percentage changes due to the high variability of drug effect between primary patient samples. Importantly, this apoptotic effect of the drugs was not seen in normal samples treated with either single or combination treatments at low concentration. However, at high concentrations, an increase in % Annexin V of drug combinations was observed; 56±16% in CYC2/VEN2 (as compared with 34±10% in CYC2, $P = 0.03$; and 30±5% in VEN2 alone, $P = 0.008$) (Figure 5.5.3.1D), 70±5% in CYC2/AraC2 (as compared with 34±10% in CYC2, $P = 0.0002$; and 53±9% in AraC2 alone, $P = 0.09$) (Figure 5.5.3.1F), and, particularly, 85±11% in CYC2/AZA2 (as compared with 34±10% in CYC2, $P = 0.0002$; and 55±19% in AZA2 alone, $P = 0.02$) (Figure 5.5.3.1H). Taken together, although not statistically significant, an increase in % Annexin V was seen in all drug combination pairs as compared with single treatments in AML samples at both low and high concentrations in a dose-

dependent manner. The combinations had an impact on normal cells only at high concentrations.

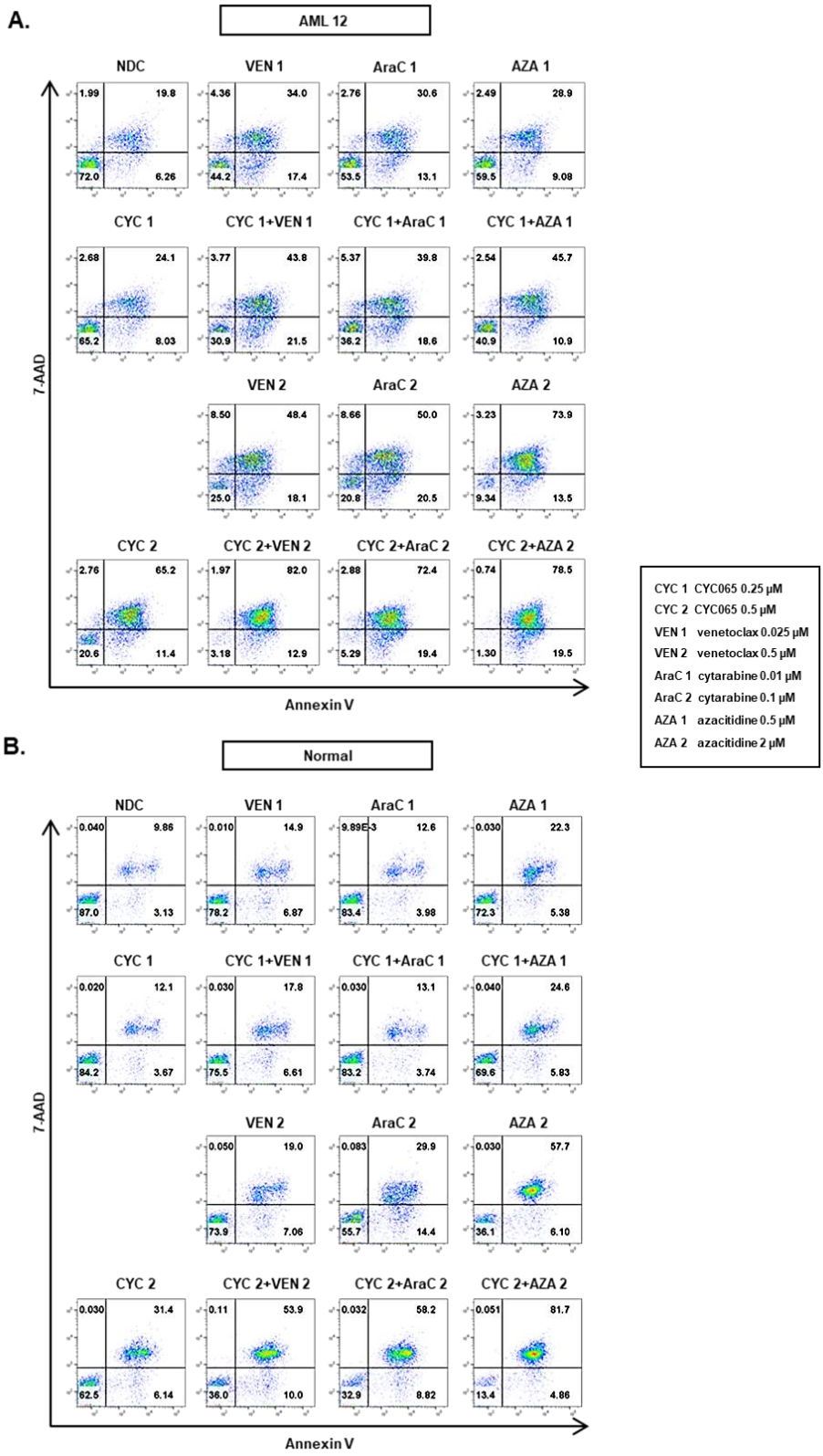

Figure 5.5.3.1 Primary human AML or normal haematopoietic samples were treated with CYC065, VEN, AraC, AZA, or the combinations for 72h. Representative flow cytometry plots of apoptosis assay using annexin V/7-AAD staining of (A) primary AML sample (AML 12); and (B) normal sample are shown.

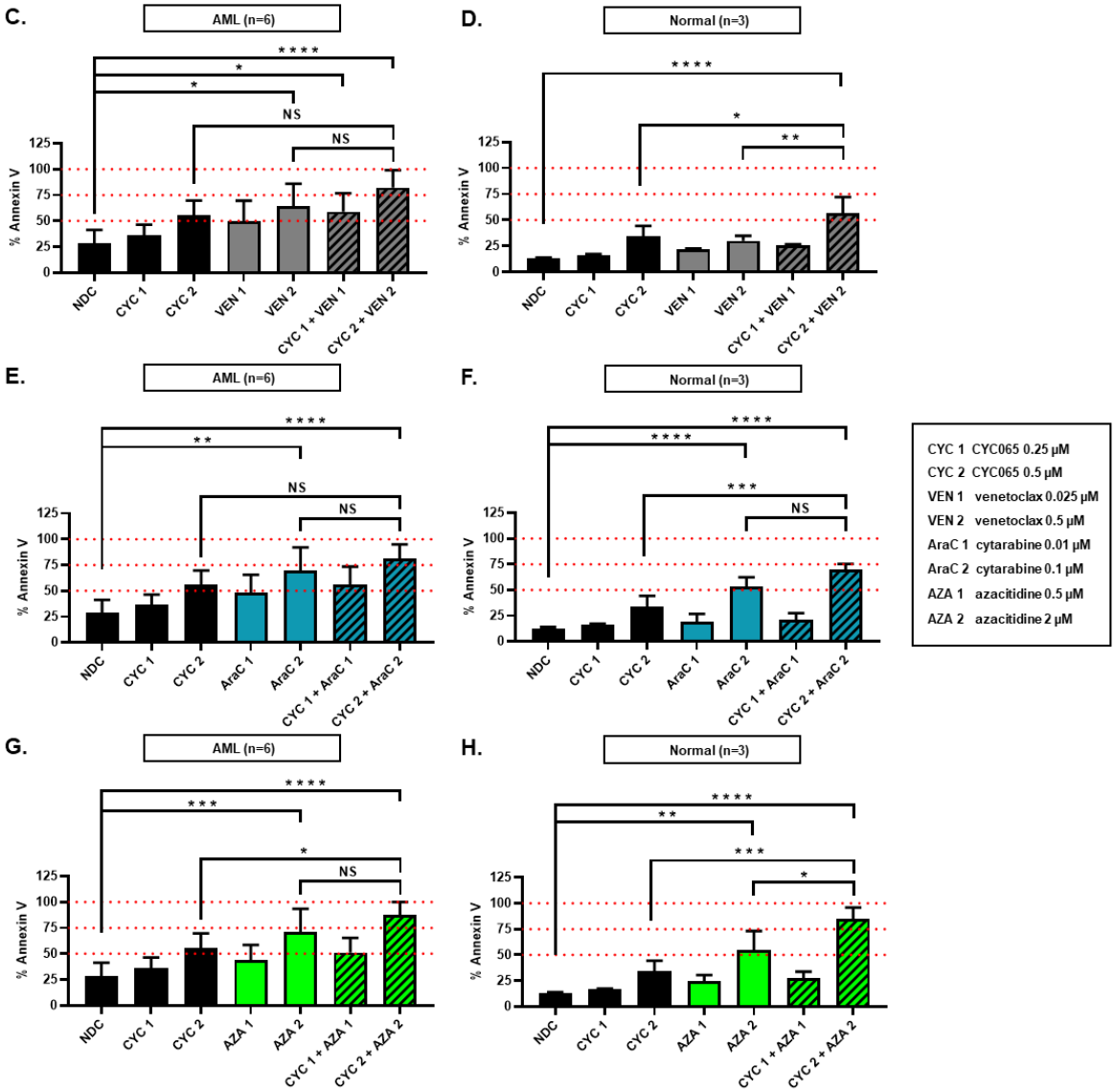

Figure 5.5.3.1 Primary human AML (n=6) or normal haematopoietic samples (n=3) were treated with CYC065, VEN, AraC, AZA, or the combinations for 72h. Summary of flow cytometric analysis of the percentage of annexin V-positive cells of (C) primary AML samples and (D) normal samples treated with CYC065/VEN; (E) primary AML samples and (F) normal samples treated with CYC065/AraC; (G) primary AML samples and (H) normal samples treated with CYC065/AZA. Graphs depict means ± SD. Data were compared using the one-way ANOVA, post hoc Tukey's HSD test ([C], F (6,35) = 7, $P < 0.0001$; [D], F (6,14) = 11.7, $P < 0.0001$; [E], F (6,35) = 7.7, $P < 0.0001$; [F], F (6,14) = 31.2, $P < 0.0001$; [G], F (6,35) = 11.2, $P < 0.0001$; [H], F (6,14) = 20.7, $P < 0.0001$). Significant *P*-values are indicated by asterisks (****< 0.0001, *** 0.0001 to < 0.001, ** 0.001 to < 0.01, * 0.01 to < 0.05 and NS if $P \geq 0.05$).

5.5.4 An increase in the percentage of active caspase-3-postive cells was observed in CYC065/VEN, CYC065/AraC, and CYC065/AZA combinations as compared with single treatments

Primary human AML and normal haematopoietic cells were treated with CYC065, VEN, AraC, AZA, or the combinations for 72h. The active caspase-3 assays were performed in parallel with the annexin V/7-AAD apoptosis assays (section 5.5.3). The percentage of active caspase-3-positive cells (% Caspase-3) from six primary AML and three normal samples was summarised aiming to observe a global effect of the treatments (Figure 5.5.4.1C-H).

As an overall picture, % Caspase-3 was consistent with % Annexin V. In primary AML samples, % Caspase-3 of combination treatments, as compared with single treatments, was not significantly different in any drug combination pair tested at low concentrations. At high concentrations, a slight increase in % Caspase-3 was observed; 84±12% in CYC2/VEN2 (as compared with 56±14% in CYC2, $P = 0.02$; and 65±18% in VEN2 alone, $P = 0.27$) (Figure 5.5.4.1C), 87±6% in CYC2/AraC2 (as compared with 56±14% in CYC2, $P = 0.01$; and 69±20% in AraC2 alone, $P = 0.4$) (Figure 5.5.4.1E), and 91±4% in CYC2/AZA2 (as compared with 56±14% in CYC2, $P = 0.0006$; and 74±17% in AZA2 alone, $P = 0.32$) (Figure 5.5.4.1G). The synergistic effect of the drugs was not seen in normal samples treated with either single or combination treatments at low concentration. However, at high concentrations, an increase in % Caspase-3 of drug combinations was observed; 50±15% in CYC2/VEN2 (as compared with 33±9% in CYC2, $P = 0.09$; and 26±3% in VEN2 alone, $P = 0.008$) (Figure 5.5.4.1D), 65±7% in CYC2/AraC2 (as compared with 33±9% in CYC2, $P = 0.001$; and 45±12% in AraC2 alone, $P = 0.05$) (Figure 5.5.4.1F) and, particularly, 80±11% in CYC2/AZA2 (as compared with 33±9% in CYC2, $P = 0.0001$; and 47±14% in AZA2 alone, $P = 0.003$) (Figure 5.5.4.1H). Collectively, although not statistically significant, an increase in % Caspase-3 was seen in all drug combination pairs as compared with single treatments in AML samples at both low and high concentrations in a dose-dependent manner. The combinations had an impact on normal cells only at high concentrations. These results confirmed the apoptosis assays in section 5.5.3.

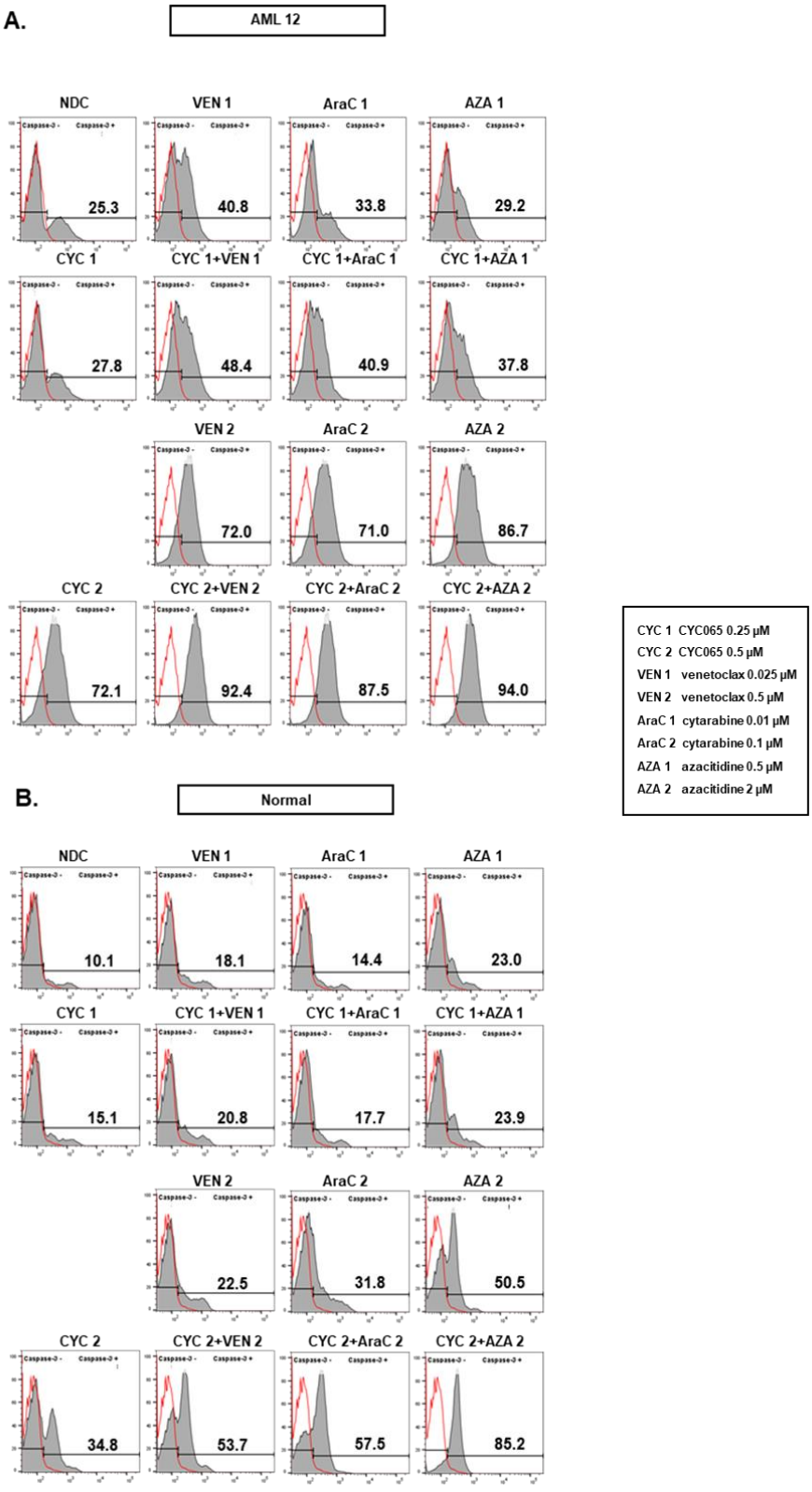

Figure 5.5.4.1 Primary human AML or normal haematopoietic samples were treated with CYC065, VEN, AraC, AZA, or the combinations for 72h. Representative flow cytometry plots of active caspase-3 assay of (A) primary AML sample (AML 12); and (B) normal sample. Red curves represent isotype controls.

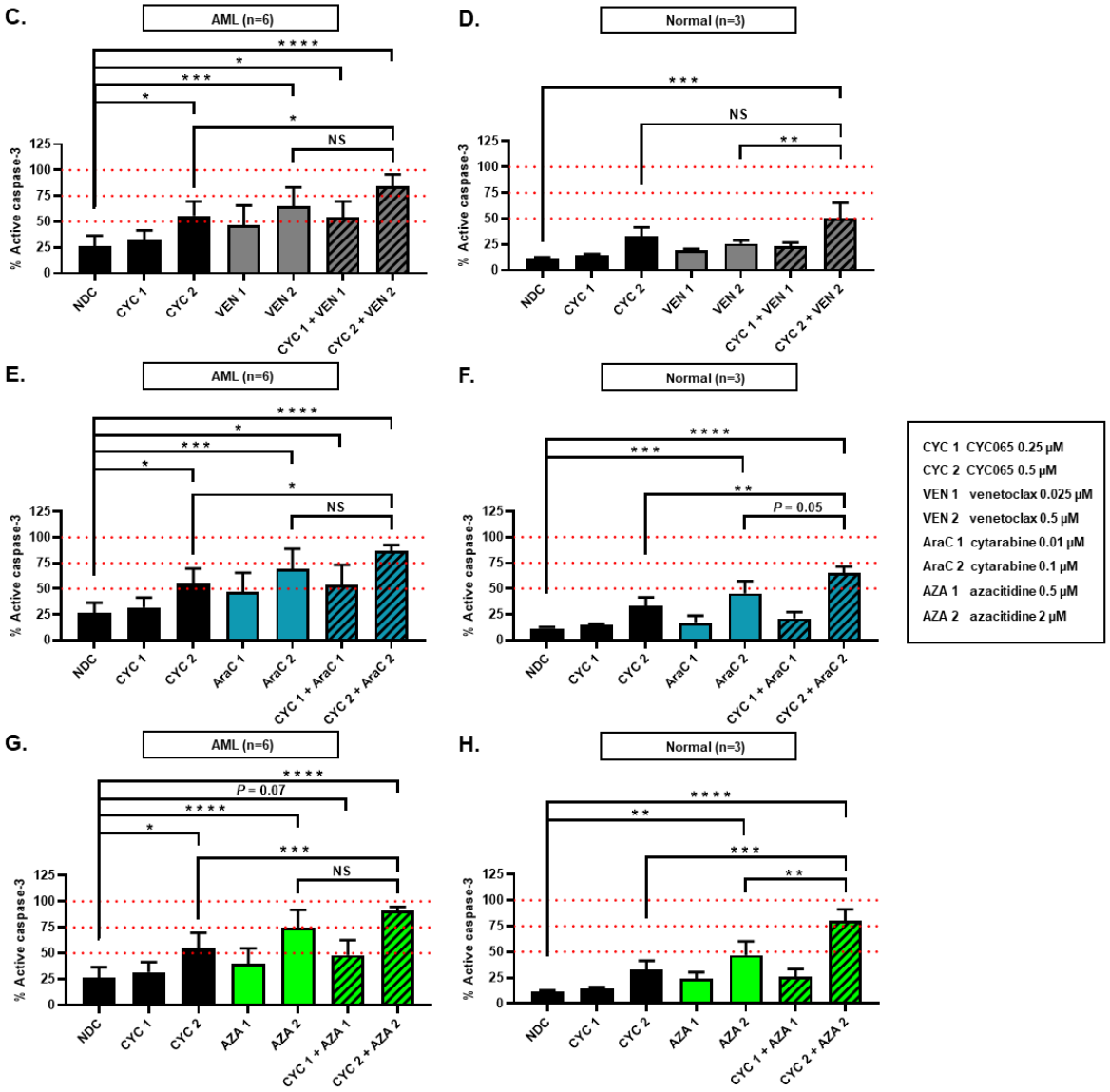

Figure 5.5.4.1 Primary human AML (n=6) or normal haematopoietic samples (n=3) were treated with CYC065, VEN, AraC, AZA, or the combinations for 72h. Summary of flow cytometric analysis of the percentage of active caspase-3-positive cells of (C) primary AML samples and (D) normal samples treated with CYC065/VEN; (E) primary AML samples and (F) normal samples treated with CYC065/AraC; (G) primary AML samples and (H) normal samples treated with CYC065/AZA. Graphs depict means ± SD. Data were compared using the one-way ANOVA, post hoc Tukey's HSD test ([C], F (6,35) = 11.4, $P < 0.0001$; [D], F (6,14) = 11, $P = 0.0001$; [E], F (6,35) = 11.8, $P < 0.0001$; [F], F (6,14) = 23.2, $P < 0.0001$; [G], F (6,35) = 19.8, $P < 0.0001$; [H], F (6,14) = 24.2, $P < 0.0001$). Significant *P*-values are indicated by asterisks (****< 0.0001, *** 0.0001 to < 0.001, ** 0.001 to < 0.01, * 0.01 to < 0.05 and NS if $P \geq 0.05$).

5.5.5 An increase in sub G0 population in cell cycle analyses was observed in CYC065/VEN, CYC065/AraC, and CYC065/AZA combinations as compared with single treatments

Primary human AML and normal haematopoietic cells were treated with CYC065, VEN, AraC, AZA, or the combinations for 72h. Cell cycle analyses was performed using PI staining. The percentage of cells in each cell cycle phase from six primary AML and three normal samples was summarised aiming to observe a global effect of the treatments (Figure 5.5.5.1C-H).

Overall, an increase in the percentage of sub G0 population (% Sub G0) was observed in the treatment arms without any other cell cycle phase, indicating an accumulation of cell death at 72h rather than cell cycle arrest. This is not unexpected regarding to the results in section 3.2.5-3.2.6 in which G1 arrest was observed in AML cell lines treated with CYC065 for 4h and then, after 24h, cell death was fully induced. In primary AML samples, % Sub G0 of combination treatments as compared with single treatments was not different in any drug combination pair tested at low concentrations. At high concentrations, a slight increase in % Sub G0 was observed; 76±10% in CYC2/VEN2 (as compared with 58±13% in CYC2, $P = 0.25$; and 63±17% in VEN2 alone, $P = 0.6$) (Figure 5.5.5.1C), 75±7% in CYC2/AraC2 (as compared with 58±13% in CYC2, $P = 0.32$; and 62±19% in AraC2 alone, $P = 0.66$) (Figure 5.5.5.1E), and 82±8% in CYC2/AZA2 (as compared with 58±13% in CYC2, $P = 0.02$; and 66±17% in AZA2 alone, $P = 0.3$) (Figure 5.5.5.1G). The effect of the drugs was not seen in normal samples treated with either single or combination treatments at low concentration. At high concentrations, an increase in % Sub G0 of drug combinations was observed; 58±14% in CYC2/VEN2 (as compared with 37±11% in CYC2, $P = 0.04$; and 33±4% in VEN2 alone, $P = 0.01$) (Figure 5.5.5.1D), 62±5% in CYC2/AraC2 (as compared with 37±11% in CYC2, $P = 0.003$; and 45±3% in AraC2 alone, $P = 0.04$) (Figure 5.5.5.1F), and 69±9% in CYC2/AZA2 (as compared with 37±11% in CYC2, $P = 0.02$; and 53±15% in AZA2 alone, $P = 0.4$) (Figure 5.5.5.1H). Taken together, although not statistically significant, an increase in % Sub G0 was seen in all drug combination pairs as compared with single treatments at both low and high concentrations in a dose-dependent manner. The combinations had an impact on normal cells only at high concentrations. These results were consistent with apoptosis (section 5.5.3) and active caspase-3 assays (section 5.5.4).

A.

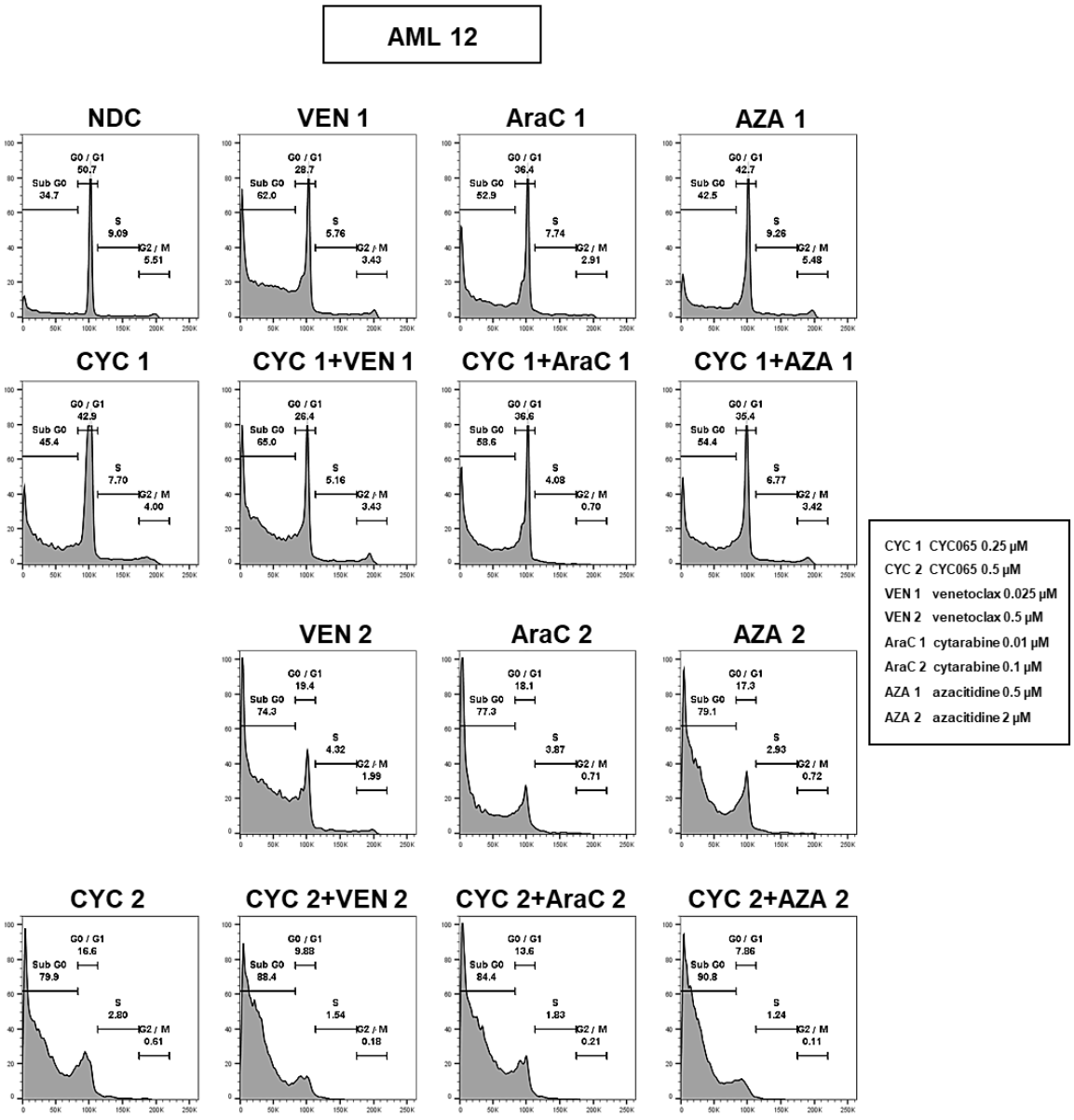
AML 12
NDC
Sub G0 34.7
G0 / G1 50.7
S 9.09
G2 / M 5.51
VEN 1
Sub G0 62.0
G0 / G1 28.7
S 5.76
G2 / M 3.43
AraC 1
Sub G0 52.9
G0 / G1 36.4
S 7.74
G2 / M 2.91
AZA 1
Sub G0 42.5
G0 / G1 42.7
S 9.26
G2 / M 5.48
CYC 1
Sub G0 45.4
G0 / G1 42.9
S 7.70
G2 / M 4.00
CYC 1+VEN 1
Sub G0 65.0
G0 / G1 26.4
S 5.16
G2 / M 3.43
CYC 1+AraC 1
Sub G0 58.6
G0 / G1 36.6
S 4.08
G2 / M 0.70
CYC 1+AZA 1
Sub G0 54.4
G0 / G1 35.4
S 6.77
G2 / M 3.42
VEN 2
Sub G0 74.3
G0 / G1 19.4
S 4.32
G2 / M 1.99
AraC 2
Sub G0 77.3
G0 / G1 18.1
S 3.87
G2 / M 0.71
AZA 2
Sub G0 79.1
G0 / G1 17.3
S 2.93
G2 / M 0.72
CYC 2
Sub G0 79.9
G0 / G1 16.6
S 2.80
G2 / M 0.61
CYC 2+VEN 2
Sub G0 88.4
G0 / G1 9.88
S 1.54
G2 / M 0.18
CYC 2+AraC 2
Sub G0 84.4
G0 / G1 13.6
S 1.83
G2 / M 0.21
CYC 2+AZA 2
Sub G0 90.8
G0 / G1 7.86
S 1.24
G2 / M 0.11
CYC 1 CYC065 0.25 µM
CYC 2 CYC065 0.5 µM
VEN 1 venetoclax 0.025 µM
VEN 2 venetoclax 0.5 µM
AraC 1 cytarabine 0.01 µM
AraC 2 cytarabine 0.1 µM
AZA 1 azacitidine 0.5 µM
AZA 2 azacitidine 2 µM

B.

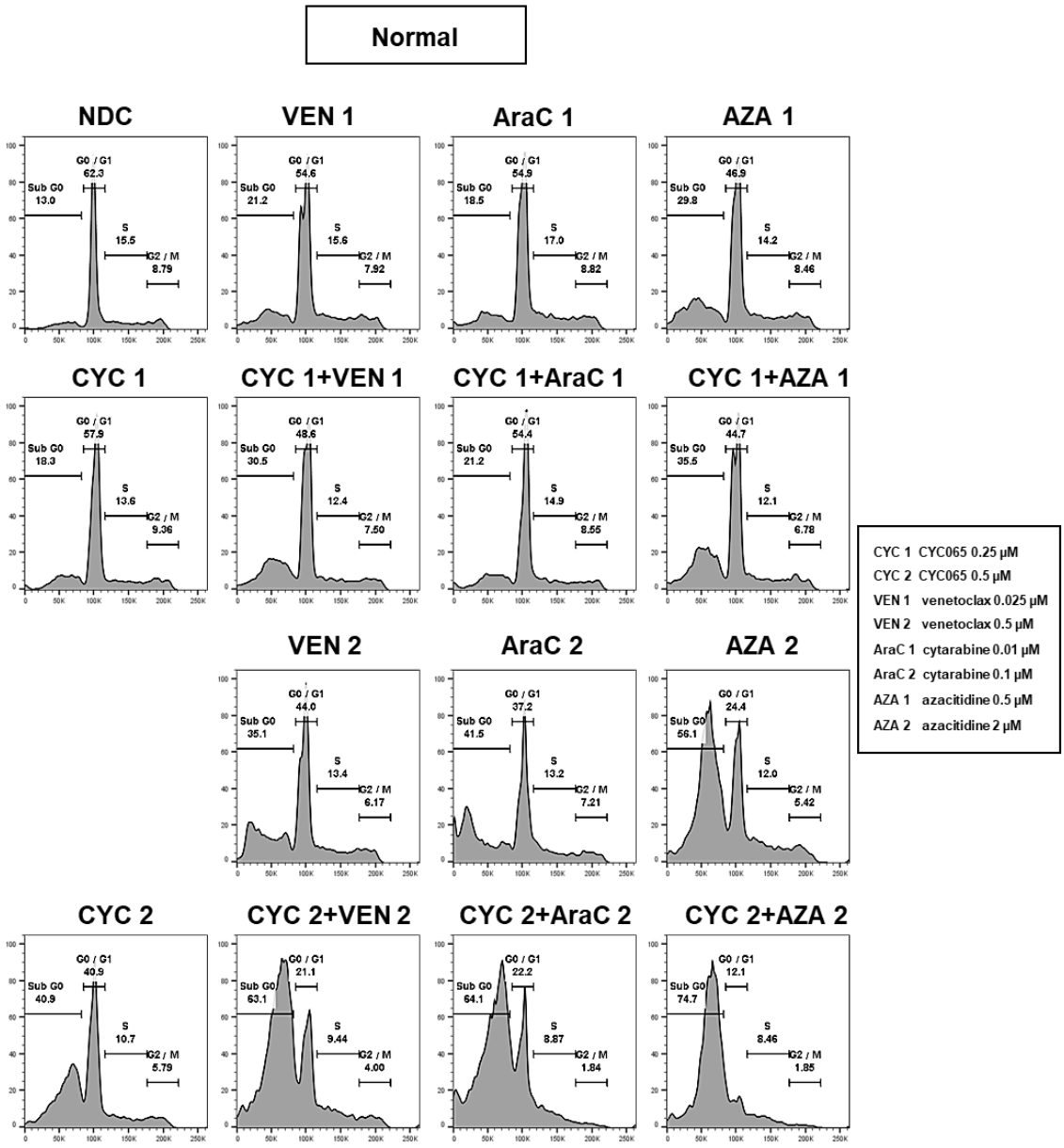

Figure 5.5.5.1 Primary human AML or normal haematopoietic samples were treated with CYC065, VEN, AraC, AZA, or the combinations for 72h. Representative flow cytometry plots of cell cycle progression using PI staining of (A) primary AML sample (AML 12); and (B) normal sample.

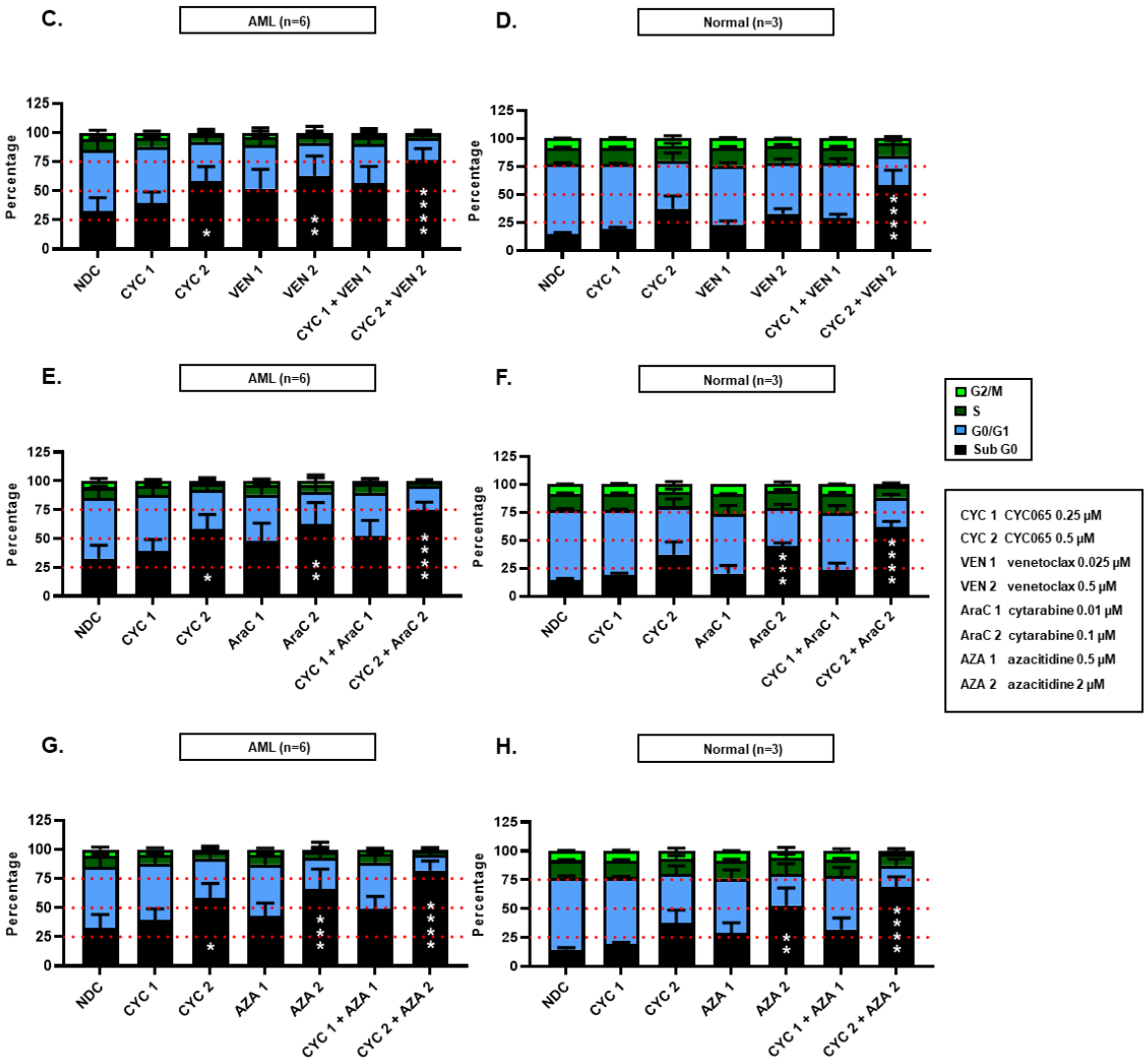

Figure 5.5.5.1 Primary human AML (n=6) or normal haematopoietic samples (n=3) were treated with CYC065, VEN, AraC, AZA, or the combinations for 72h. Summary of flow cytometric analysis of cell cycle phase of (C) primary AML samples and (D) normal samples treated with CYC065/VEN; (E) primary AML samples and (F) normal samples treated with CYC065/AraC; (G) primary AML samples and (H) normal samples treated with CYC065/AZA. Graphs depict means ± SD. Data were compared using the one-way ANOVA, post hoc Tukey's HSD test (Sub G0 populations; [C], F (6,35) = 7.2, $P < 0.0001$; [D], F (6,14) = 12.1, $P < 0.0001$; [E], F (6,35) = 7.2, $P < 0.0001$; [F], F (6,14) = 24.1, $P < 0.0001$; [G], F (6,35) = 12.5, $P < 0.0001$; [H], F (6,14) = 12.1, $P < 0.0001$). Significant *P*-values are indicated by asterisks (****< 0.0001, *** 0.0001 to < 0.001, ** 0.001 to < 0.01, * 0.01 to < 0.05 and NS if $P \geq 0.05$).

5.5.6 Therapeutic window was observed in cell proliferation assays in CYC065/AZA combination

Primary human AML and normal haematopoietic cells were treated with CYC065, VEN, AraC, AZA, or the combinations for 72h. Cell proliferation assays were performed using CellTrace™ Violet staining. The percentage of each cell division from six primary AML and three normal samples was summarised aiming to observe a global effect of the treatments (Figure 5.5.6.1C-H).

Overall, a higher percentage of cells undergoing ≥3 divisions (Div3) in normal samples was observed (Figure 5.5.6.1B) when compared to primary AML samples (Figure 5.5.6.1A), indicating greater sensitivity of AML cells to chemotherapies. In primary AML samples, the synergism was seen in CYC2/AZA2 combination, with an increase in the fold change (FC) of undivided cells normalised to NDC (Undivided FC) of 7.1±4.2 as compared with 2.6±0.7 (P = 0.001) and 3.1±1.6 (P = 0.005) in a single treatment of CYC2 and AZA2, respectively (Figure 5.5.6.1G). These results indicate a favourable therapeutic window at these concentrations as normal samples in this combination displayed Undivided FC of 0.94±0.28 as compared with 2.48±0.47 (P = 0.003) and 0.15±0.02 (P = 0.2) in a single treatment of CYC2 and AZA2, respectively (Figure 5.5.6.1H). By contrast, although an increase in Undivided FC was seen in CYC2/AraC2 combination as compared with a single treatment in primary AML samples (Figure 5.5.6.1E), this combination also had a marked impact on normal cells (Figure 5.5.6.1F). The difference between CYC2/VEN2 and a single treatment was not observed in either primary AML (Figure 5.5.6.1C) or normal cells (Figure 5.5.6.1D). Collectively, these findings indicate a potential therapeutic window for combination treatments of CYC2 with AZA2 in AML.

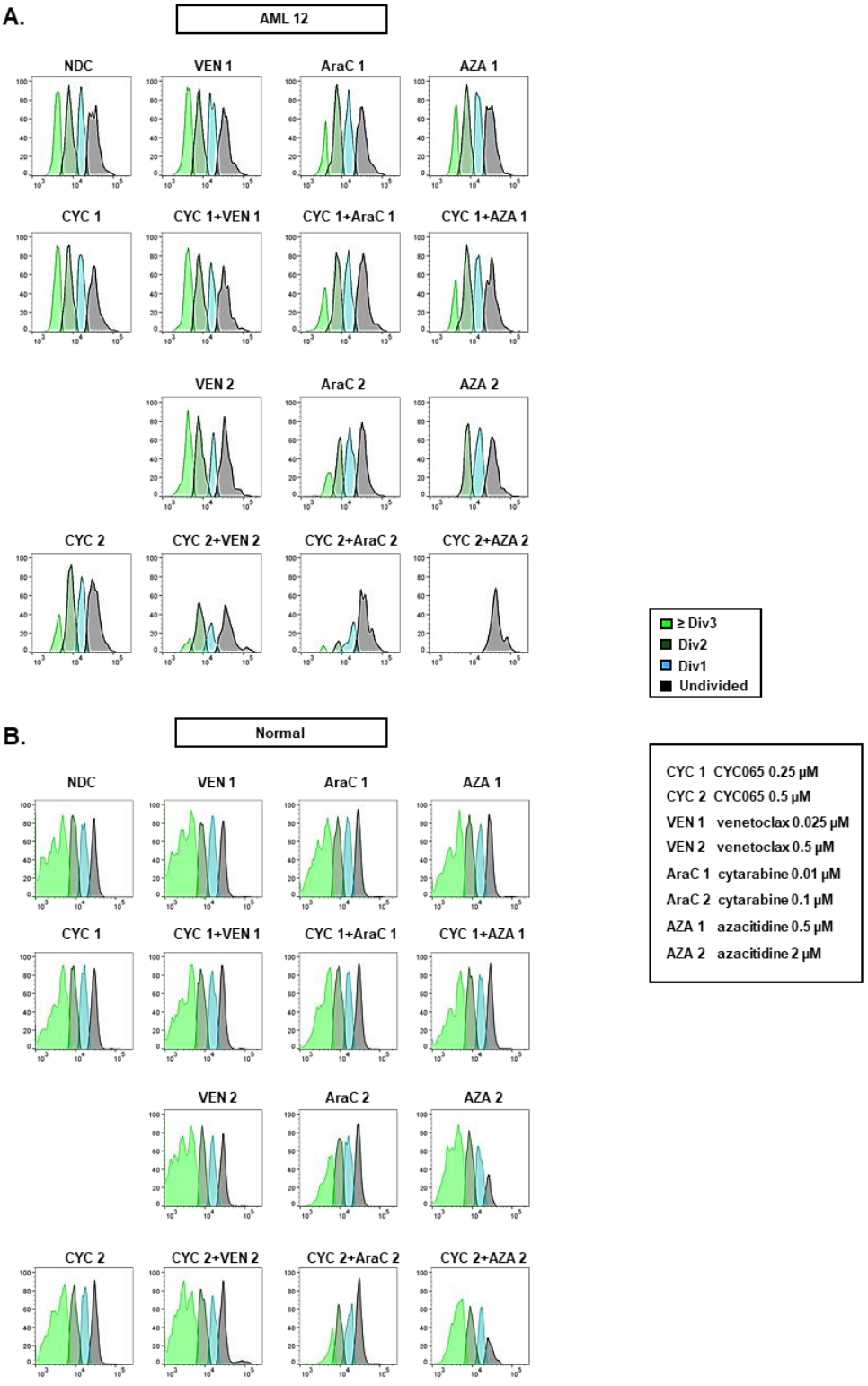

Figure 5.5.6.1 Primary human AML or normal haematopoietic samples were treated with CYC065, VEN, AraC, AZA, or the combinations for 72h. Representative flow cytometry plots of cell proliferation assay using CellTrace™ Violet staining of (A) primary AML sample (AML 12); and (B) normal sample. Division (Div).

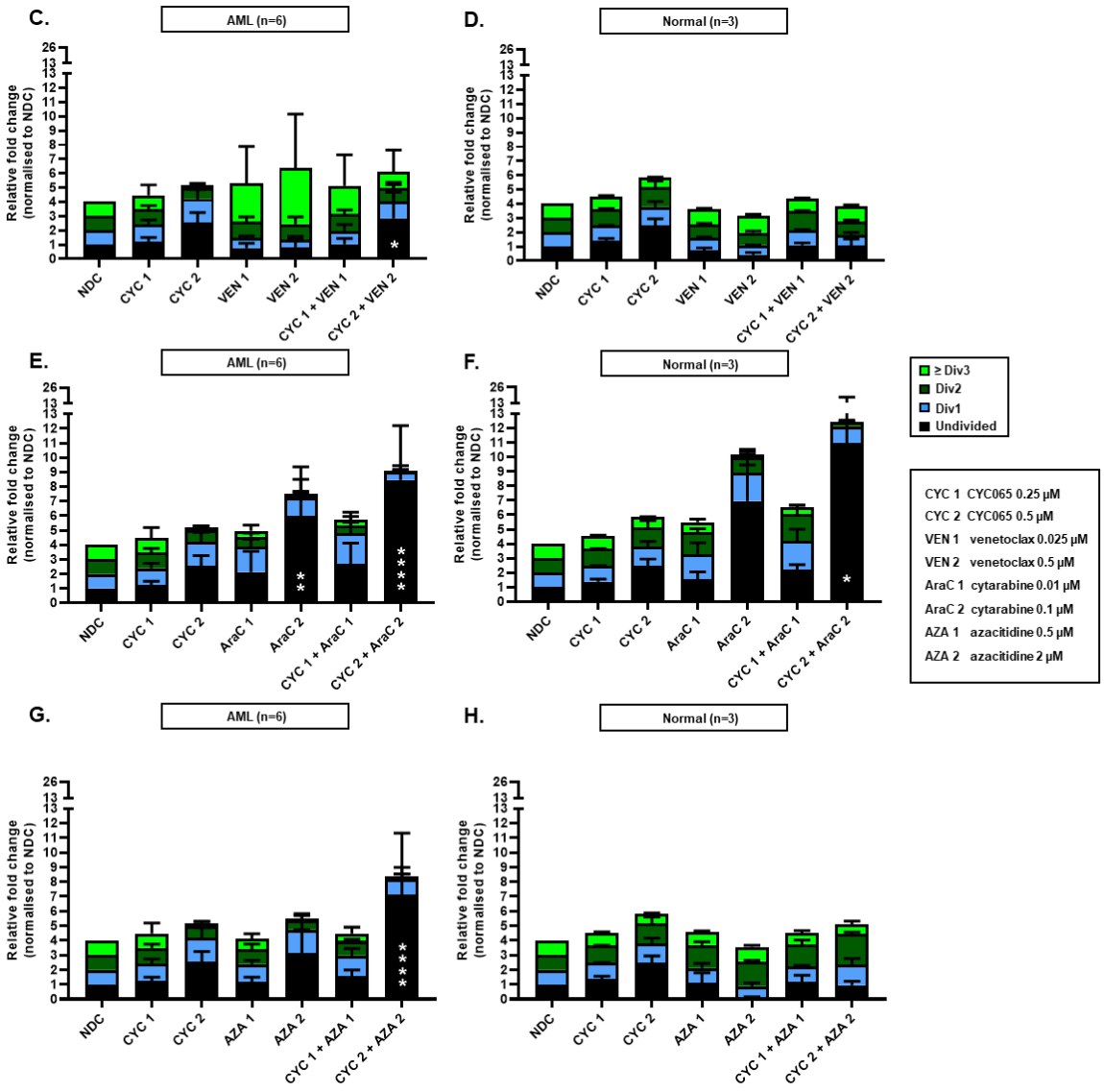

Figure 5.5.6.1 Primary human AML (n=6) or normal haematopoietic samples (n=3) were treated with CYC065, VEN, AraC, AZA, or the combinations for 72h. Summary of flow cytometric analysis of cell proliferation of (C) primary AML samples and (D) normal samples treated with CYC065/VEN; (E) primary AML samples and (F) normal samples treated with CYC065/AraC; (G) primary AML samples and (H) normal samples treated with CYC065/AZA. Graphs depict means ± SD. Data were compared using the one-way ANOVA, post hoc Tukey's HSD test (Undivided populations; [C], $F(6,35) = 4.5$, $P = 0.002$; [D], $F(6,14) = 16.5$, $P < 0.0001$; [E], $F(6,35) = 10.6$, $P < 0.0001$; [F], $F(6,14) = 4.8$, $P = 0.008$; [G], $F(6,35) = 9.6$, $P < 0.0001$; [H], $F(6,14) = 10.1$, $P = 0.0002$).

5.5.7 A decrease in colony number, regardless of colony type, was observed in the colony-forming unit assays

The CFU assay was used to study the alteration of proliferation and differentiation pattern of haematopoietic progenitor cells, by their ability to form colonies in a semisolid medium, after drug treatment in both single and combination arms. Primary human AML cells were treated with CYC065, VEN, AraC, AZA, or the combinations for 72h. The CFU assay was set up and incubated for 10-14 days prior to characterising and counting the number of viable colonies (Figure 5.5.7.1A-O).

In primary AML samples, colonies grew from only two out of six samples. The majority of the colonies were CFU-M, indicating a poorly differentiated status (Figure 5.5.7.1A; D, CYC065/VEN; H, CYC065/AraC; L, CYC065/AZA). In the two samples where data were available, a decrease in total colony number was seen in all drug combination pairs as compared with single treatments at both low and high concentrations in a dose-dependent manner (Figure 5.5.7.1F, CYC065/VEN; J, CYC065/AraC; N, CYC065/AZA). By contrast, in normal samples, the colonies grew very well from all three samples with the presence of a variety of types of colonies, indicating normal differentiation (Figure 5.5.7.1B,C; E, CYC065/VEN; I, CYC065/AraC; M, CYC065/AZA). However, after drug treatments, an inhibitory effect was observed in the same fashion as seen in primary AML samples. Although not statistically significant, a decrease in total colony number was observed in each combination arm as compared with single arms (Figure 5.5.7.1G, CYC065/VEN; K, CYC065/AraC; O, CYC065/AZA), regardless of colony type (Figure 5.5.7.1E, CYC065/VEN; I, CYC065/AraC; M, CYC065/AZA).
In addition, in terms of morphology, a slight decrease in colony size was also seen in each combination arm as compared with single arms (Figure 5.5.7.1B,C). Collectively, the results indicate that CYC065 had an impact not only on AML cells, but also the more primitive CFU-M in AML samples and various types of haematopoietic progenitor cells in normal samples.

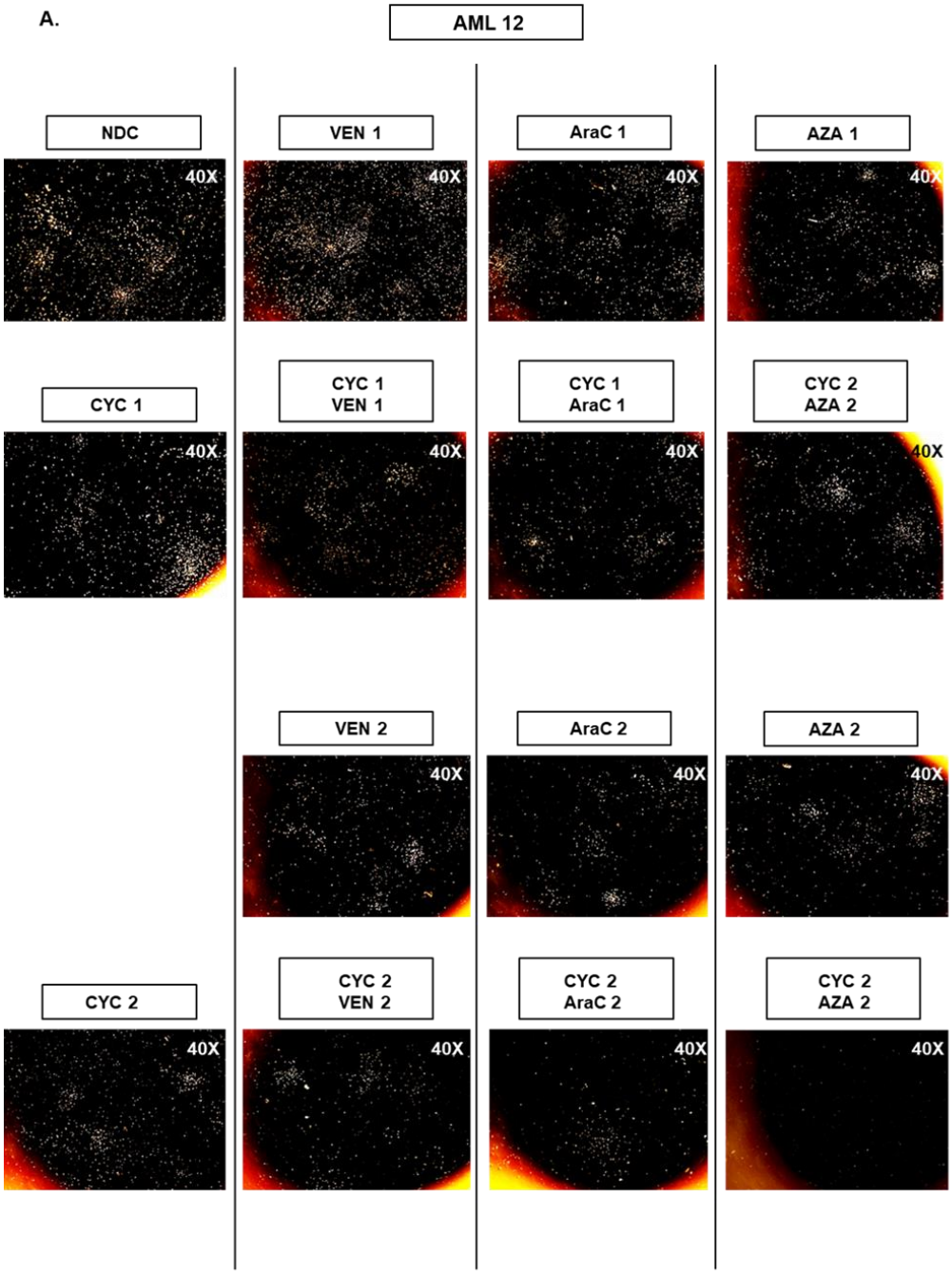
A.
AML 12
NDC
VEN 1
AraC 1
AZA 1
CYC 1
CYC 1
VEN 1
CYC 1
AraC 1
CYC 2
AZA 2
VEN 2
AraC 2
AZA 2
CYC 2
CYC 2
VEN 2
CYC 2
AraC 2
CYC 2
AZA 2
40X
CYC 1 CYC065 0.25 µM
CYC 2 CYC065 0.5 µM
VEN 1 venetoclax 0.025 µM
VEN 2 venetoclax 0.5 µM
AraC 1 cytarabine 0.01 µM
AraC 2 cytarabine 0.1 µM
AZA 1 azacitidine 0.5 µM
AZA 2 azacitidine 2 µM

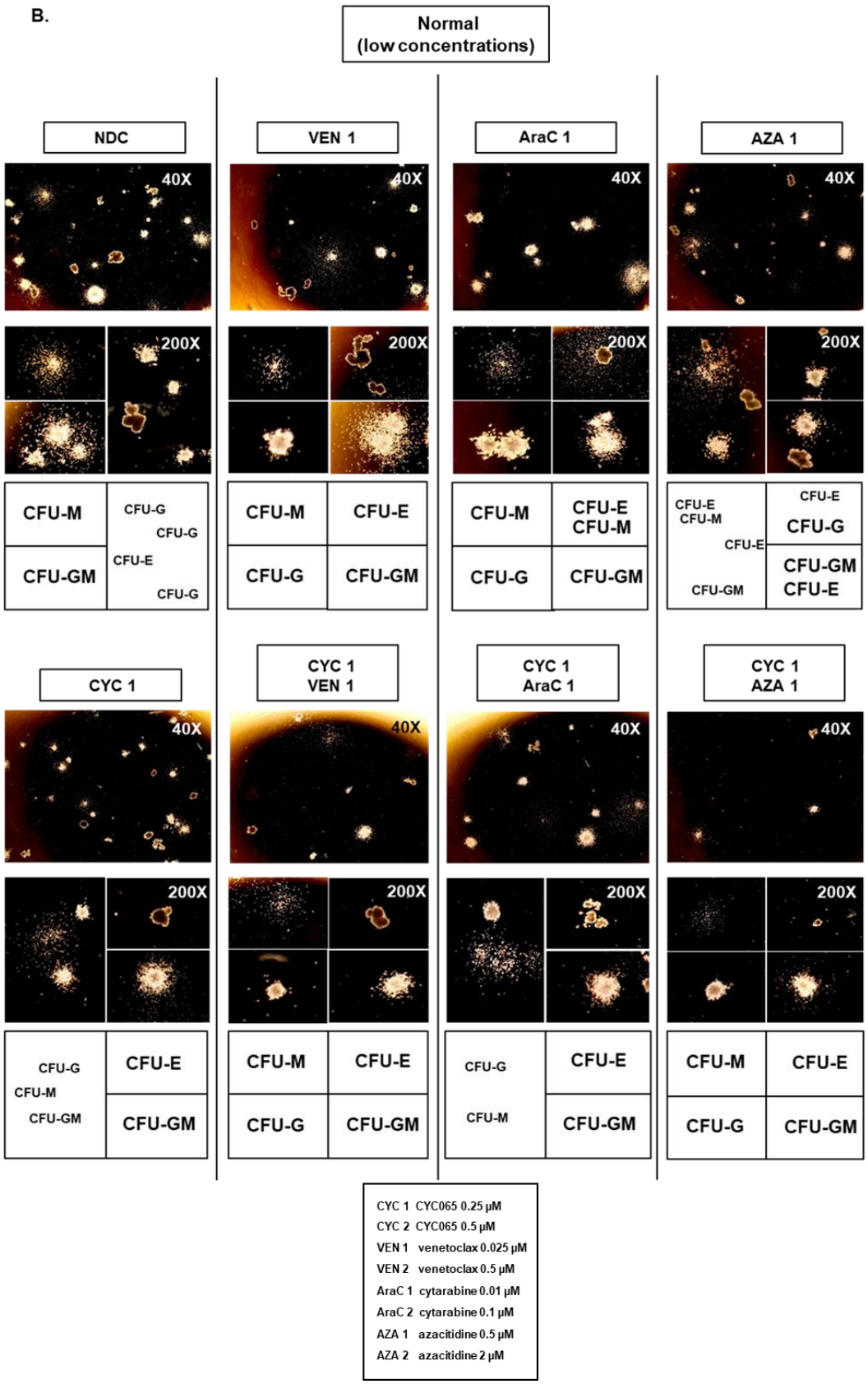
B.
Normal
(low concentrations)
NDC
40X
200X
CFU-M
CFU-G
CFU-G
CFU-E
CFU-GM
CFU-G
VEN 1
40X
200X
CFU-M
CFU-E
CFU-G
CFU-GM
AraC 1
40X
200X
CFU-M
CFU-E
CFU-M
CFU-G
CFU-GM
AZA 1
40X
200X
CFU-E
CFU-M
CFU-E
CFU-E
CFU-G
CFU-GM
CFU-GM
CFU-E
CYC 1
40X
200X
CFU-G
CFU-M
CFU-GM
CFU-E
CFU-GM
CYC 1
VEN 1
40X
200X
CFU-M
CFU-E
CFU-G
CFU-GM
CYC 1
AraC 1
40X
200X
CFU-G
CFU-E
CFU-M
CFU-GM
CYC 1
AZA 1
40X
200X
CFU-M
CFU-E
CFU-G
CFU-GM
CYC 1 CYC065 0.25 µM
CYC 2 CYC065 0.5 µM
VEN 1 venetoclax 0.025 µM
VEN 2 venetoclax 0.5 µM
AraC 1 cytarabine 0.01 µM
AraC 2 cytarabine 0.1 µM
AZA 1 azacitidine 0.5 µM
AZA 2 azacitidine 2 µM

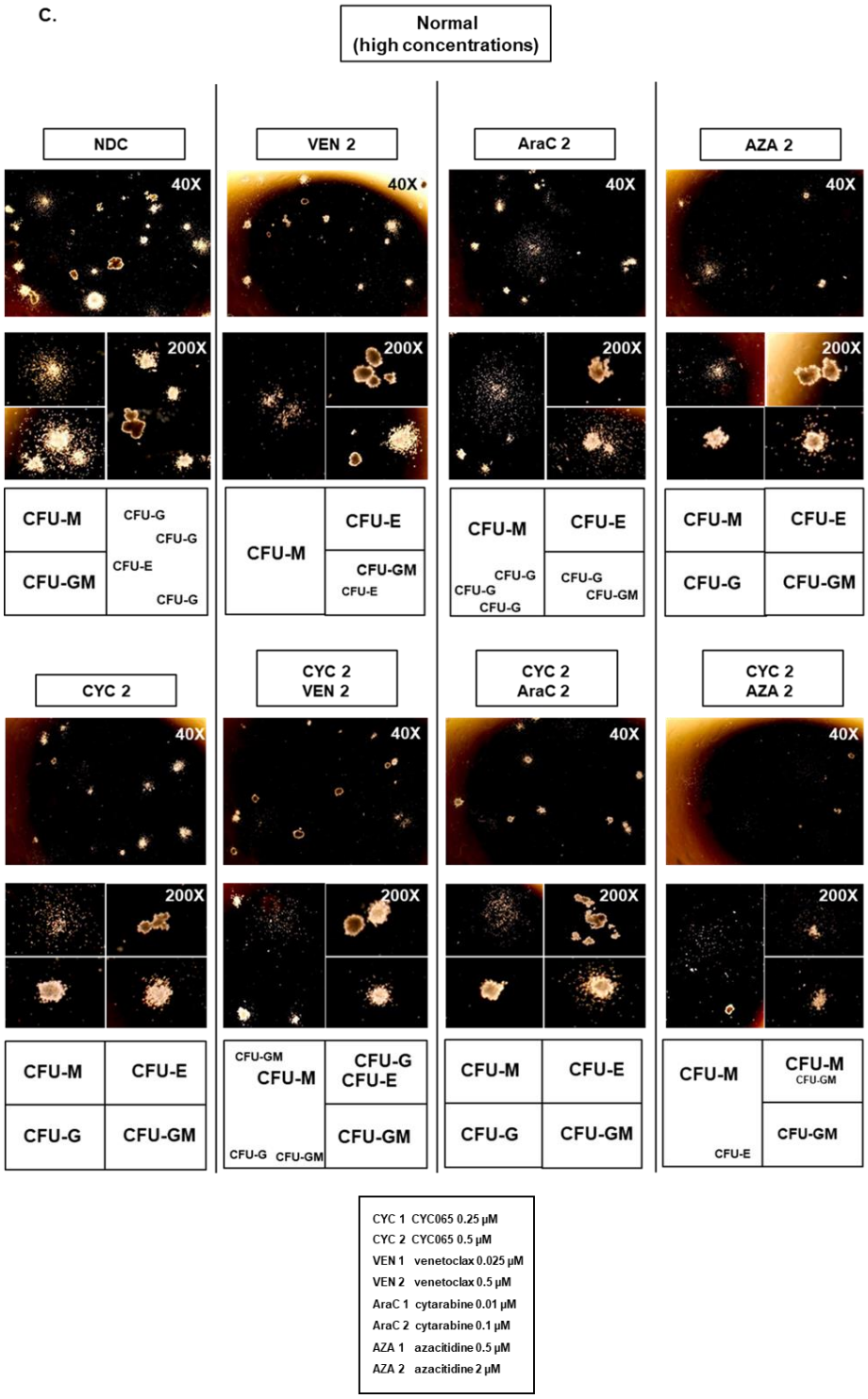

Figure 5.5.7.1 Primary human AML (n=2) or normal haematopoietic samples (n=3) were treated with CYC065, VEN, AraC, AZA, or the combinations for 72h. Representative experiments of CFU assay of (A) primary AML sample (AML 12); and (B) normal sample (low concentrations) and (C) normal sample (high concentrations). The experiment was set up as duplicate plates for each arm containing $1x10^4$ cells. Colony type is labelled at the bottom of each figure. Colony-forming unit-granulocyte, monocyte (CFU-GM), Colony-forming unit-monocyte (CFU-M). Colony-forming unit-granulocyte (CFU-G). Colony-forming unit erythroid (CFU-E).

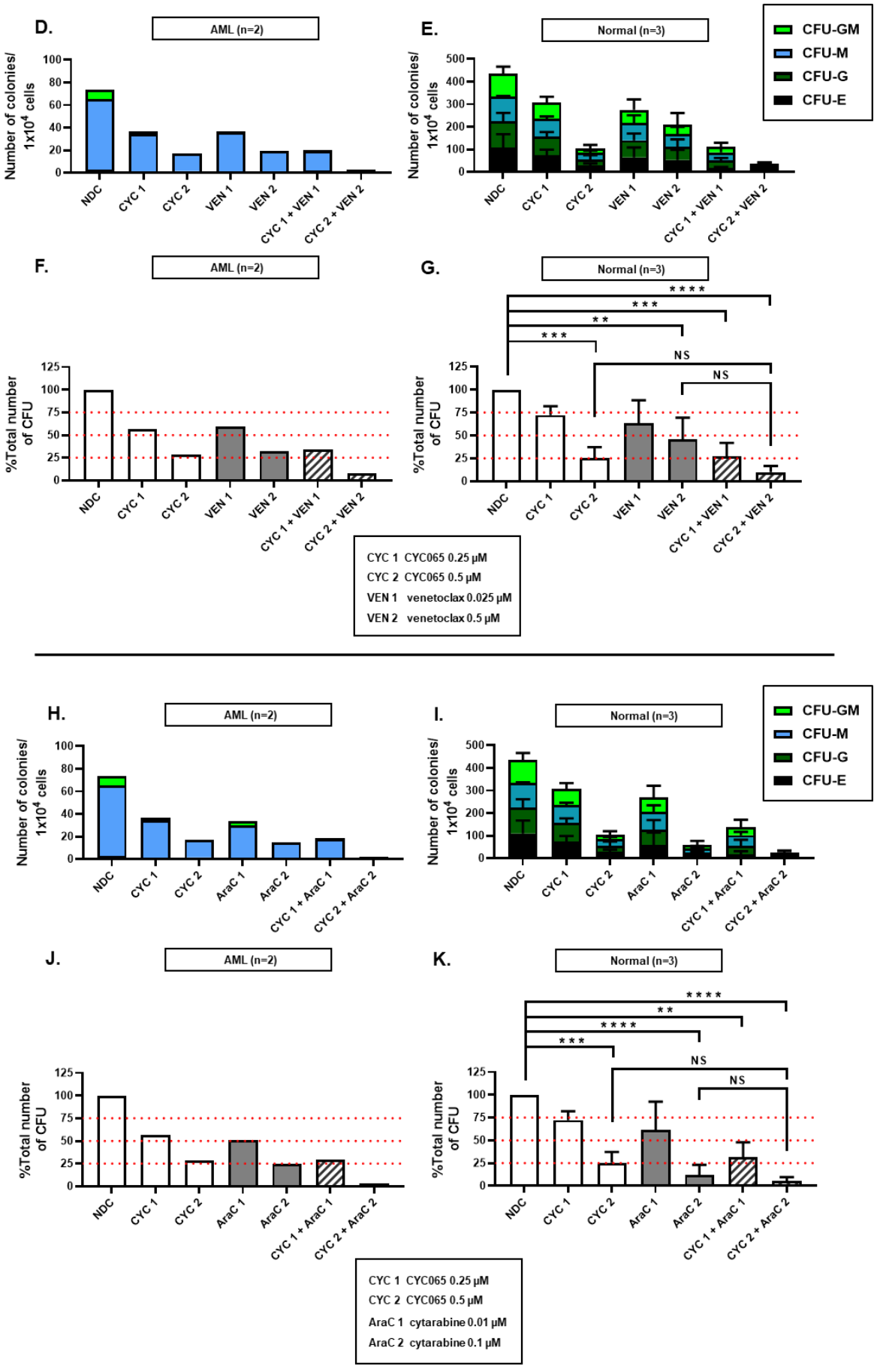
D.
AML (n=2)
Number of colonies/ 1x10^4 cells
E.
Normal (n=3)
CFU-GM
CFU-M
CFU-G
CFU-E
F.
AML (n=2)
%Total number of CFU
G.
Normal (n=3)
****
***
**
***
NS
NS
NDC
CYC 1
CYC 2
VEN 1
VEN 2
CYC 1 + VEN 1
CYC 2 + VEN 2
CYC 1 CYC065 0.25 µM
CYC 2 CYC065 0.5 µM
VEN 1 venetoclax 0.025 µM
VEN 2 venetoclax 0.5 µM
H.
AML (n=2)
I.
Normal (n=3)
AraC 1
AraC 2
CYC 1 + AraC 1
CYC 2 + AraC 2
J.
AML (n=2)
K.
Normal (n=3)
AraC 1 cytarabine 0.01 µM
AraC 2 cytarabine 0.1 µM

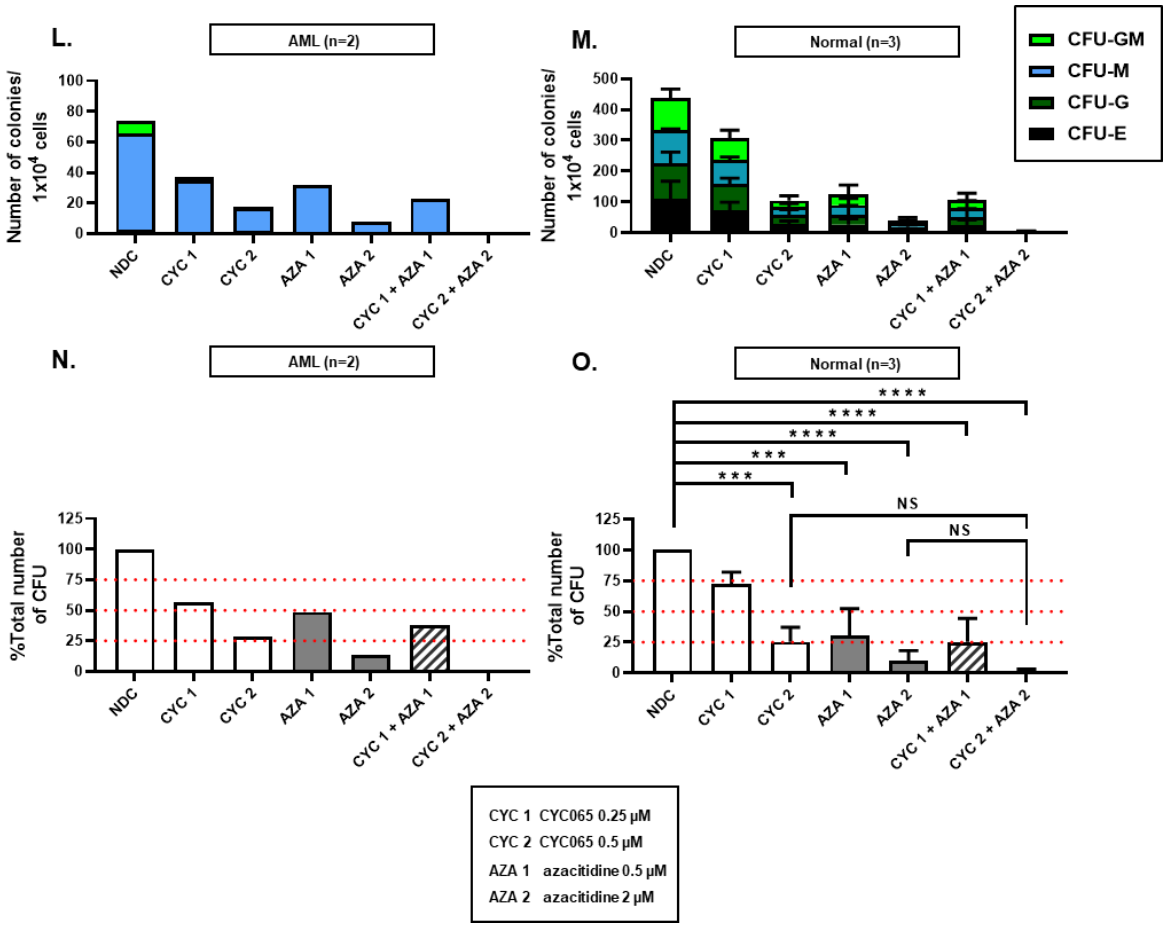

Figure 5.5.7.1 Primary human AML (n=2) or normal haematopoietic samples (n=3) were treated with CYC065, VEN, AraC, AZA, or the combinations for 72h. Summary of colony number categorised by type of (D) primary AML samples and (E) normal samples; and the percentage of total CFU number normalised to NDC of (F) primary AML samples and (G) normal samples treated with CYC065/VEN. Summary of colony number categorised by type of (H) primary AML samples and (I) normal samples; and the percentage of total CFU number normalised to NDC of (J) primary AML samples and (K) normal samples treated with CYC065/AraC. Summary of colony number categorised by type of (L) primary AML samples and (M) normal samples; and the percentage of total CFU number normalised to NDC of (N) primary AML samples and (O) normal samples treated with CYC065/AZA. Graphs depict means ± SD. Data were compared using the one-way ANOVA, post hoc Tukey's HSD test ([G], F (6,14) = 12.4, $P < 0.0001$; [K], F (6,14) = 15.8, $P < 0.0001$; [O], F (6,14) = 22.7, $P < 0.0001$). Significant *P*-values are indicated by asterisks (****< 0.0001, *** 0.0001 to < 0.001, ** 0.001 to < 0.01, * 0.01 to < 0.05 and NS if $P \geq 0.05$).

5.6 Discussion

Whereas the goal of AML treatment in younger patients is cure with intensive chemotherapy, the optimal treatment decision for elderly, usually defined as older than 60 years of age, is controversial. For the elderly patients, approaches include palliative care only, less intensive chemotherapy, standard chemotherapy, or offering the patient entry into a clinical trial (Eleni, Nicholas, & Alexandros, 2010). Treatment-related mortality and resistance to chemotherapy are two major causes of treatment failure. Older people are prone to poor tolerability which often leads to them being ineligible for intensive chemotherapy because of the presence of comorbid disease, decreased ability for clearance of chemotherapy, poor performance status and poor tolerance and susceptibility to systematic bacterial and fungal infections (Klepin & Balducci, 2009). However, longer life expectancy and possibly a cure are expected if a CR is achieved in elderly AML patients. Therefore, there are many efforts to improve the standard AML treatment regimens, especially in older patients, aiming to lessen adverse drug effects. The possible interventions include intensity reduction, introducing a new class of chemotherapy or targeted small molecule inhibitor, or drug combinations. Moreover, combination studies are potentially beneficial for patients with adverse-risk cytogenetics and patients with R/R AML for which a specific salvage regimen is not available.

In this study, CYC065 in combination with VEN, AraC, or AZA was assessed for efficacy against AML cells. The major target of CYC065 is MCL-1, therefore, a selective BCL-2 inhibitor VEN was selected aiming to target the parallel mechanisms, whilst potentially inducing a synergistic effect. AraC is used in the current standard therapy regimens for induction and consolidation of AML. A novel treatment algorithm in which intensive chemotherapy “7+3” regimen is combined with newly developed molecularly targeted therapies has rapidly evolved (Richard-Carpentier & DiNardo, 2019). Hence, the combination study of AraC and CYC065, as a potential candidate, was evaluated here. AML is known to carry aberrant hypermethylation resulting in silencing of genes involved in cell proliferation and differentiation (Lund et al., 2014). Thus, a benefit of combining CYC065 with the hypomethylating agent AZA may be obtained and therefore warranted investigation.

In parallel with the study of CYC065 as a single agent in Chapter 3, OCI-AML3, MOLM-13, and MV4-11 cell lines were preliminarily tested in combination studies. Initially, the IC50 of VEN, AraC, and AZA of each cell line was assessed by resazurin reduction assay at 24h, 48h, and 72h. It was observed that the killing effect culminated at 72h, the timepoint which was decided to be used for the rest of the experiments. Combination studies using CompuSyn software were performed to investigate the most efficacious drug combination ratios. Overall, the synergistic effect of CYC065/VEN, CYC065/AraC, and CYC065/AZA combinations was seen at 2X to 4X IC50 of CYC065. However, clinically relevant concentrations of 0.75μM, 0.5μM, and 1μM were selected for OCI-AML3, MOLM-13, and MV4-11 cell lines, respectively, instead of using such a high concentration of CYC065, which would potentially mask the synergistic activity. A fixed proportional reduction in the drug concentrations was used (Mayer et al., 2006; Palmer, 2017), this was based on the ratio obtained from CompuSyn software (section 5.2.2, CYC065/VEN; section 5.3.2, CYC065/AraC; section 5.4.2, CYC065/AZA). In the trypan blue exclusion assays, nevertheless, the synergistic effect was still masked at these reduced CYC065 doses (section 5.2.3, CYC065/VEN; section 5.3.3, CYC065/AraC; section 5.4.3, CYC065/AZA). However, the synergistic effect of CYC065/VEN, CYC065/AraC, and CYC065/AZA combinations were observed in apoptosis assays in which a significant decrease in the percentage of viable cells in the combination arm was seen as compared with single treatments (section 5.2.4, CYC065/VEN; section 5.3.4, CYC065/AraC; section 5.4.4, CYC065/AZA). These results were consistent with an increase in the percentage of active caspase-3-positive cells in the combination arm (section 5.2.5, CYC065/VEN; section 5.3.5, CYC065/AraC; section 5.4.5, CYC065/AZA) and were reiterated with a rise in sub G0 population in cell cycle analyses (section 5.2.6, CYC065/VEN; section 5.3.6, CYC065/AraC; section 5.4.6, CYC065/AZA). Collectively, the synergistic effect of CYC065/VEN, CYC065/AraC, and CYC065/AZA combinations were observed in the three cell lines in this study using various methods. Taken together, these preliminary data provided a strong rationale for continuing CYC065/VEN, CYC065/AraC, and CYC065/AZA combination studies in primary human AML samples.

In primary AML samples, the concentrations selected were based on previous publications (Adachi et al., 2017; Leonard et al., 2014; Min et al., 2017; Teh et

al., 2018), i.e. 0.025μM (VEN1) and 0.5μM (VEN2) of VEN, 0.01μM (AraC1) and 0.1μM (AraC2) of AraC, and 0.5μM (AZA1) and 2μM (AZA2) of AZA, aiming to cover both very and less sensitive groups of patients. The drug concentrations used are still far below those used clinically and maximally tolerated plasma concentrations in patients; i.e. 1μM of VEN (Anderson et al., 2016), 1μM of AraC (Capizzi et al., 1983; Heasman et al., 2011), and 3-11μM of AZA (Hollenbach et al., 2010) as stated in the introduction. Trypan blue exclusion, apoptosis, active caspase-3, cell proliferation, CFU assays, and cell cycle analyses were used to assess the killing and synergistic effect of drug combinations. The data from six primary AML and three normal control samples were averaged and the results summarized, aiming to observe the overall effect of the treatments and determine their efficacy in AML.

In general, the results from all assays were in agreement. An increase in % Annexin V (section 5.5.3) in the apoptosis assay was concordant with a rise in % Caspase-3 in active caspase-3 assays (section 5.5.4) and an elevation of % Sub G0 in cell cycle analyses (section 5.5.5). As an overall picture, it was observed that primary AML samples, compared with normal samples, were more sensitive to CYC065, VEN, AraC, and AZA i.e. AML cells apoptosed at low concentrations whereas normal cells did not (Figure 5.5.3.1, apoptosis assays; Figure 5.5.4.1, active caspase-3 assays; Figure 5.5.5.1, cell cycle analyses). In primary AML samples, although not statistically significant, a decrease in cell number (Figure 5.5.2.1A, CYC065/VEN; C, CYC065/AraC; E, CYC065/AZA) synchronously with an increase in % Annexin V (Figure 5.5.3.1C, CYC065/VEN; E, CYC065/AraC; G, CYC065/AZA), % Caspase-3 (Figure 5.5.4.1C, CYC065/VEN; E, CYC065/AraC; G, CYC065/AZA), and % Sub G0 (Figure 5.5.5.1C, CYC065/VEN; E, CYC065/AraC; G, CYC065/AZA) was seen in all drug combination pairs as compared with single treatments at both low and high concentrations in a dose-dependent manner. By contrast, normal cells experienced toxicity only at high concentrations of single and combination treatments with the exception of a single treatment of CYC2 and VEN2 in which the killing effect was modest as evaluated with apoptosis assays (Figure 5.5.3.1D, CYC065/VEN; F, CYC065/AraC; H, CYC065/AZA), active caspase-3 assays (Figure 5.5.4.1D, CYC065/VEN; F, CYC065/AraC; H, CYC065/AZA), and cell cycle analyses (Figure 5.5.5.1D, CYC065/VEN; F, CYC065/AraC; H, CYC065/AZA).

In the cell proliferation assays, CYC2/AZA2 combination showed the synergistic effect in cell division arrest in primary AML (Figure 5.5.6.1G) but not in normal control samples (Figure 5.5.6.1H), thus, a therapeutic window was observed. Nevertheless, using the concentration of CYC2, the concentration of AZA2 would still need to be tapered in order to reduce toxicity to normal cells (Figure 5.5.3.1H, apoptosis assays; Figure 5.5.4.1H, active caspase-3 assays; Figure 5.5.5.1H, cell cycle analyses). By contrast, slight and marked blocking effects in cell division was observed in normal samples at low and high concentrations, respectively, in single and combination treatments of AraC, indicating cell toxicity (Figure 5.5.6.1F). For the CFU assays, although representing a small proportion of primary AML samples, a decrease in colony number, in which the majority of the colonies were CFU-M, was seen in combination arms as compared with single treatments in a dose-dependent manner (Figure 5.5.7.1D, CYC065/VEN; H, CYC065/AraC; L, CYC065/AZA). The same effect was observed in normal samples in which a decline in colony number was seen regardless of colony type (Figure 5.5.7.1E, CYC065/VEN; I, CYC065/AraC; M, CYC065/AZA).

The responses to the treatment of CYC2 in combination with VEN2, AraC2, or AZA2 of each primary AML sample are summarised in Table 5.6.1. Changes <25% and >50% are considered as slight and marked responses, respectively, or moderate if between 25-50%, when combination arms were compared with single treatments with results consistent in at least two assays, i.e. apoptosis, active-caspase-3, cell cycle analyses, or cell proliferation assays, to assign the response status. It was observed that the more complex the molecular genetic lesions or complexity of karyotype, the less efficacious the combination therapy was. A variable response of these primary samples was the most plausible explanation for statistically insignificant results when a global effect of the treatments was evaluated. Nonetheless, an insufficient number of cases could introduce overinterpretation and these promising findings need evaluation in a larger cohort of patient samples in order to determine whether there is cohort of patients who would benefit from this combinational therapeutic approach. Consequently, it is inappropriate to draw any conclusions at present.

Table 5.6.1 Genetic lesions of primary AML samples classified by their functions and their responsive statuses to combination treatments.

Sample	Karyotype	Genetic lesions							Synergy status		
		Signalling genes	DNA methylation-related genes	Chromatin-modifying genes	Nucleo-phosmin gene	Cohesin complex genes	Spliceosome complex genes	Transcrip-tion factor fusions	CYC2/ VEN2	CYC2/ AraC2	CYC2/ AZA2
AML 11	Normal		*IDH2*	*KMT2A*-PTD, *ASXL1*					Moderate	Moderate	Marked
AML12	Monosomy 7	*FLT3*-ITD	*DNMT3A*, *IDH2*						Marked	Moderate	Marked
AML 13	Normal	*FLT3*-ITD	*DNMT3A*		*NPM1*	*RAD21*			Slight/ Moderate	Slight	Moderate/ Marked
AML 14	Complex	*KIT*			*NPM1*				Slight	Slight	Slight
AML 15	Trisomy 11		*DNMT3A*, *IDH1*			*STAG2*	*SRSF2*		Slight	Slight	Slight
AML 16	Normal	*FLT3*-ITD	*DNMT3A*, *TET2*	*KMT2A*-PTD			*SRSF2*	*RUNX1*	Slight	Slight	Slight

Changes <25% and >50% are considered as slight and marked response, respectively, or moderate if between 25-50%, when combination arms were compared with single treatments. The results must be consistent in at least two assays, i.e. apoptosis, active-caspase3, cell cycle analyses, or proliferation assays, to assign the responsive status. 0.5μM of CYC065 (CYC2). 0.5μM of venetoclax (VEN2). 0.1μM of cytarabine (AraC2). 2μM of azacitidine (AZA2). Isocitrate dehydrogenase 1 and 2 (IDH1 and IDH2). Lysine Methyltransferase 2A-partial tandem duplication (KMT2A-PTD). Additional sex combs-like 1 (ASXL1). FMS-like tyrosine kinase 3 - internal tandem duplication (FLT3-ITD). DNA methyltransferase 3 alpha (DNMT3A). Nucleophosmin 1 (NPM1). Double-strand-break repair protein rad21 (RAD21). Tyrosine-protein kinase Kit gene (KIT) Stromal antigen 2 (STAG2). Serine arginine-rich splicing factor 2 (SRSF2). Ten-eleven translocation methylcytosine dioxygenase 2 (TET2). Runt-related transcription factor 1 (RUNX1).

In other cancers, targeting MCL-1 and BCL-2 has also shown encouraging results. It has been reported that shRNA-mediated *MCL1* knockdown in CHP126, KCNR and SJNB12 neuroblastoma cell lines resulted in an increase in sensitivity to VEN assessed by the MTT assay (Bate-Eya et al., 2016). The same effect was observed in these cell lines when the small molecule MCL-1 inhibitor A-1210477 was combined with VEN. In cell cycle analysis, % Sub G0 was significantly increased in combination arms as compared with single treatments when the KCNR cell line was treated with either A-1210477 or VEN for 72h. Phillips et al reported that the novel CDK9 inhibitor A-1592668 in combination with VEN showed the synergistic effect in VEN-resistant SU-DHL-4, OCI-Ly1 199R, and SC-1 199R B-cell lymphoma cell lines assessed by the CellTiter-Glo™ luminescent cell viability assay (Phillips et al., 2019). This combination resulted in greater tumor growth inhibition over single treatments in a SU-DHL-4 xenograft model. In addition, two AML PDX mouse models, in which one of them carries *FLT3*-ITD, were used.

It was observed that A-1592668/VEN combination provided a significant survival advantage over single treatments, which was associated with a decline in the percentage of engraftment. These findings were recapitulated by a study in AML using the pan-CDKI alvocidib, which reduces MCL-1, in combination with VEN (J. Bogenberger et al., 2017). VEN-sensitive MOLM-13 and MV4-11 cell lines and VEN-resistant OCI-AML3 and THP-1 cell lines were tested. It was observed that addition of alvocidib resulted in potent dose-dependent reduction of the IC50 of VEN in both VEN-sensitive and –resistant cells. Combination studies using CalcuSyn software displayed synergistic activity when clinically achievable concentration of 0.08-0.16μM of alvocidib was used in combination with all doses of VEN tested, the similar pattern seen in this study (Figure 5.2.2.1). In addition, an increase in % Annexin V was observed in response to the combination beyond the additive effects of either single agent. CYC065 in combination with VEN has shown synergistic killing activity of CLL cells *in vitro*. The combination of IC50 concentrations of CYC065 and VEN for 24h decreased the viability of CLL cells by over 90% in the lymph node mimicking microenvironment (C. Rong et al., 2018). Currently, an ongoing phase 1 clinical trial for CYC065 in combination with VEN is evaluating the drug safety in 25 outpatients with R/R AML or MDS (NCT04017546); and R/R CLL (NCT03739554). A four-week cycle is planned i.e. all patients will receive CYC065 over 4h-infusion once every 2 weeks on day 1 and day 15 in combination with VEN. In another study, using Calcusyn software, synergistic activity was seen in combination studies of CDKs 2,7, and 9 inhibitor SNS-032 and AraC in twenty five primary AML samples and the NB4 and HL-60 cell lines (Walsby et al., 2011), supporting the validity of combinational approaches for AML. In preliminary experiments, Kim et al reported that pre-treatment with alvocidib reduced the IC50 of AZA in MV4-11 cell line (W. Kim et al., 2018). In the same manner seen in CYC065/AZA combination, alvocidib in combination with AZA also increased % Caspase-3 as compared with single treatments. In a MOLM-13 xenograft model, the combination showed greater tumor growth inhibition over single treatments.

However, it may be questionable whether combination of CDKI and cell cycle-active agents e.g. AraC or anthracyclines is appropriate. For this issue, the better approach is timed sequential therapy (TST). For example, in FLAM (alvocidib, AraC plus mitoxantrone) regimen, alvocidib is administered as an

initial cytoreductive agent for 3 days (50mg/m^2 days 1-3). After this, the remaining leukemic cells can be recruited into the cell cycle and thus be kinetically ripe for targeting by the 72-h continuous administration of AraC beginning on day 6 (667mg/m^2/d continuous infusion days 6-8) and 40mg/m^2 of mitoxantrone on day 9. In a phase 2 study, there was a statistically significant high efficacy of FLAM as compared with 1 or 2 cycles of the standard "7+3" regimen in terms of a CR rate (70% vs 47%, $P = 0.003$; or 70% vs 57%, $P = 0.08$, respectively). Nevertheless, an increase in either OS or EFS rate was not observed (NCT01349972) (Zeidner et al., 2015, 2018). Potentially, this may be due to a higher toxicity of the combination regimen based on the preliminary data showing the impact of CYC065/AraC combination on normal cells in this study. The approach of TST has been recapitulated by a study showing that, in primary AML cells, pre-treatment with CDK4/6 inhibitor palbociclib for 24h to induce G1 arrest and then cultured in fresh medium for 12h to allow re-entry into S phase before the addition of AraC induces more apoptosis than co-treatment of both drugs at the same time (Yang et al., 2015). Hence, TST by priming cells with CDKI prior to introducing cell cycle-active agents e.g. AraC or anthracyclines is potentially optimal approach for the future work.

Collectively, this preliminary study has demonstrated a synergistic effect of CYC065 when combining with a selective BCL-2 inhibitor VEN, a conventional chemotherapy AraC, or a hypomethylating agent AZA in AML cell lines.
A variable response to the combinations was observed in primary human AML cells, highlighting the need for a more personalised medicine approach to improve outcomes in AML. As a global effect, although not statistically significant, the advantage of combining CYC065 to VEN, AraC, or AZA was seen. Favourably, using cell proliferation assays, a therapeutic window was observed in CYC065/AZA combination. However, the impact on normal cells seen in apoptosis, active caspase-3 assays, and cell cycle analyses of CYC065/AZA combination was still problematic. Consequently, finding the most appropriate concentrations of CYC065/AZA combinations will be required to reduce the toxicity in patients.

Chapter 6 Positive findings and general discussion, conclusions, and future directions

6.1 Positive findings and general discussion

Although the treatment outcome of AML has steadily improved over the past few decades, nonetheless, the prognosis of patients is still dismal, in particular, in the elderly and patients with adverse-risk cytogenetics. In this study, the effects of a newly developed CDK2/9 inhibitor CYC065 on growth and survival of AML cells was interrogated. Preliminarily, OCI-AML3 (carries *NPM1* and *DNMT3A* R882C mutations), MOLM-13 (carries *FLT3*-ITD and *KMT2A-MLLT3*) and MV4-11 (carries *FLT3*-ITD and *KMT2A-AFF1*) cell lines were selected aiming to encompass the stratifications of major risk profiles according to the ELN recommendation (H. Döhner et al., 2017).

CYC065 showed efficacy against AML cells in a dose-dependent manner, evaluated by various methods including trypan blue exclusion, resazurin reduction, apoptosis, active caspase-3 assays, and cell cycle analyses. G1 arrest was observed at an early timepoint (4h) in OCI-AML3 and MV4-11 cell lines. Western blotting was performed aiming to elucidate the primary targets of the drug. A downregulation of MCL-1 at 4h was consistently seen in all cell lines at both gene and protein levels, preceding apoptosis which was fully induced at 24h and culminated at 72h. Relevant intracellular signalling pathways controlling MCL-1 were investigated. A decrease in T202/Y204 phosphorylated ERK1/2 was consistently observed in all cell lines, whereas, p38 MAPK was highly activated only in MOLM-13 cell line, indicating that the stress response and apoptosis is markedly induced at 4h. A decrease in the ERK1/2 activity observed potentially reduced MCL-1 stability. Inhibition of CDK2 and CDK9 was evaluated by measuring the phosphorylation level at S807/811 on Rb protein and S2 on the CTD of RNAPII, respectively. However, the impact of the drug on CDK2 was not seen in MV4-11 cell line, whereas, Rb protein was transcriptionally suppressed in MOLM-13 and was very lowly expressed in OCI-AML3 cell lines. Transcriptional suppression of RNAPII, resulting in a corresponding decrease of its phosphorylated forms, this was observed in all cell lines. As the direct inhibition of CDK2 and CDK9 of CYC065 was inconclusive, high throughput Pamgene™ STK activity profiling was used to further interrogate the affected kinases at their activity level. Although the kinase screen identified several promising targets to interrogate, the confirmatory results from Western blotting, were in

contraindication with the Pamgene™ technology. By using Pamgene™ STK activity profiling, the activation of several members of PKC was identified in CYC065-treated group relative to NDC in OCI-AML3 and MV4-11 cell lines. However, it was demonstrated by Western blotting that PKC activity remained unchanged. In MOLM-13, most of the serine/threonine kinases exhibited a decreased activity in CYC065-treated group relative to NDC, including p38 MAPK. By using Western blotting, nevertheless, a significant increase in phosphorylated p38 MAPK level was observed which is consistent with an increase in the phosphorylation of its substrate, indicating a higher activity of p38 MAPK. Due to the poor reliability of the results and concerns over reproducibility, it was decided not to use the Pamgene in any further analyses.

For this issue, there are various options available for further investigation in the future. Conventionally, by performing an immunoprecipitation to capture specifically the correct CDK of interest using specific antibody-coated beads, and then incubate with labelled ATP (usually radioactive e.g. [γ-^{32}P]-ATP) and a suitable substrate. Next, the eluates are applied to polyacrylamide gel and transferred to the electrophoresis membrane. Finally, phosphorimaging is performed to assess the phosphorylation level of the substrate. This is followed by immunoblotting in order to assess immunoprecipitation of the CDKs of interest which is used as internal protein loading control for a normalisation (Bankston, Ku, & Feng, 2017). Nonetheless, labour-intensiveness and potentially harmful radiation are disadvantages of this method. Outsourcing using this technology is also available (Reactionbiology, 2020). In addition, CDK kinase activity may be measured with a commercially available kit using technology based on fluorescence resonance energy transfer (FRET) technique (PerkinElmer, 2020; Phillips et al., 2019). Briefly, acceptor fluorophore-labeled peptide substrate is phosphorylated by the kinase of interest. The phosphorylated site on the substrate is recognised by donor fluorophore-labeled anti-phospho antibody. Finally, the donor fluorophore is excited which results in energy transferring to the acceptor fluorophore, rendering a detectable fluorescence emission signal at the final step. The assay is performed in a 96-well plate. Alternatively, rather than using peptide substrates, phosphoproteomics profiling using high performance liquid chromatography (HPLC) with tandem mass spectrometry (MS/MS) can be performed to generate a global view of serine, threonine, and

tyrosine phosphorylation within the sample rather than focusing specifically on a selected subset of phosphorylated peptides (Wu et al., 2019). In each experimental arm, samples will be labelled with different isotopes which can be performed by various methods e.g. stable-isotope labelling of amino acids in cell culture (SILAC) during cell culture or it can be done after cell fractionation using stable-isotope labelling through chemical modification of peptides e.g. iTRAQ (Nita-Lazar, Saito-Benz, & White, 2008) or dimethyl labelling (Lin et al., 2015). After labelling, isotope-tagged samples from all experiment arms will be pooled for an enrichment. Briefly, the procedure can be divided in four stages (Y. Liu & Chance, 2014) include: **a)** cell fractionation and protein digestion; **b)** enrichment of phosphopeptides aiming to increase the sensitivity of detection. Current methods for enriching phosphopeptides prominently include strong cation exchange (SCX) chromatography which separates phosphopeptides from non-phosphopeptides by their solution charge state, whereas, immobilised metal affinity chromatography (IMAC) and titanium dioxide (TiO_2) are based on the high affinity of phosphate group to metal ions (Lin et al., 2015); **c)** analysis via LC coupled with MS/MS; and **d)** localisation and quantification of phosphosites/phosphoproteins using bioinformatics approach. The peaks of different samples can be distinguished and compared due to the different atomic mass of isotope tagged.

Expression of target genes were downregulated following CYC065 treatment, including CDK family, transcription factor, key protein phosphatase, CDKI, DNA damage response regulator, anti-apoptotic related, and pro-apoptotic related genes. At an early timepoint (4h), the expression of *CDK9* and transcription factor *E2F1* was decreased in all cell lines with ≥50% downregulation. Anti-apoptotic related gene *MCL1* was consistently markedly suppressed, indicating the on-target specificity of the drug treatment. *PPP1R10*, which plays a role in cell cycle progression during the transition from M phase into interphase (J. H. Lee et al., 2010; "PPP1R10 gene"), was drastically downregulated in all cell lines. Nonetheless, an accumulation of the G2/M population was not seen in cell cycle analysis of any of the cell lines analysed. A downregulation of *E2F1* may explain the G1 arrest but a set of G1/S-regulated genes needs to be further explored. On the other hand, some pro-apoptotic proteins e.g. *CDKN1A*/$p21^{Cip1}$ were upregulated, indicating that the intrinsic apoptosis pathway was being activated

following drug treatment. These findings confirm the efficacy of CYC065 and provide a potential 'gene signature' of downstream target genes that can be employed for future studies and potentially incorporated as a biomarker readout in future clinical trials.

VEN, AraC, and AZA were chosen to be used in combination studies with CYC065. Initially, the three cell lines (OCI-AML3, MOLM-13 and MV4-11) were preliminarily investigated for synergistic activity of the combinations with CYC065 using CompuSyn software. In all cell lines, it was observed that 2X to 4X IC50 CYC065 in combination with the three partners was the optimal combination ratio. Nevertheless, it was decided to reduce the concentrations of CYC065 to 0.5μM, 0.75μM, and 1μM for OCI-AML3, MOLM-13 and MV4-11 cell lines, respectively, to avoid masking synergistic activity with higher drug concentrations. Individually, the reduction was in a dose-proportional fashion with respect to the combination ratio obtained from the software. Positively, the synergistic activity was confirmed by various methods, including apoptosis, active caspase-3 assays and cell cycle analyses. A combination of CYC065 with VEN, AraC, or AZA was rational and of further interest, thus, the experiments were extended into six primary human AML and three normal samples.

Trypan blue exclusion, apoptosis, active caspase-3, cell proliferation, CFU assays, and cell cycle analyses were used to assess the killing and synergistic effect of drug combinations at 72h on primary AML samples. Consistency between the assays i.e. % Annexin V, % Caspase-3, and % Sub G0, was seen. As a global effect, although not statistically significant, CYC065/VEN, CYC065/AraC, and CYC065/AZA combinations showed additional effects over the single agent activity. However, the impact on normal cells was still problematic. Favourably, in cell proliferation assay, a therapeutic window was observed in CYC065/AZA combination in which normal cells were not affected. Nonetheless, the doses of CYC065 and AZA would need to be adjusted to minimise the impact on normal cells seen in apoptosis, caspase-3 assays, and cell cycle analyses.

Considering the six primary AML samples individually, the treatment response variability associated with the high diversity of genetic mutations observed, stressing the importance of individual genetic profiling and targeted therapy.

With reference to the 2017 ELN risk stratification (H. Döhner et al., 2017), nowadays, NGS and potentially exome sequencing and genome wide assays (Kuo, Mar, Lindsley, & Lindeman, 2017), are being developed to replace single gene assays, and this will facilitate more rapid and improved prognostic scoring systems (Estey, 2018). Although immediate treatment once AML is diagnosed may not be possible in all patients, a slight delay of therapy i.e. 4-8 days had been shown to have no deleterious effect on outcome after accounting for other prognostic covariates (Bertoli et al., 2013). Moreover, immediately initiating an ineffective regimen may lead to more fatalities than a delay of therapy resulting from NGS results pending (Estey, 2018), and then patients being signposted by their molecular results to the most appropriate therapy.

Over the past few years, many targeted therapies, as part of the therapeutic arsenal, for patients with AML have rapidly emerged (Figure 6.1.1) (Richard-Carpentier & DiNardo, 2019). These include FLT3 inhibitors midostaurin (Stone et al., 2017) and gilteritinib (Perl et al., 2019), anti-CD33 GO (Hills et al., 2014), IDH1 inhibitor ivosidenib (DiNardo, Stein, et al., 2018), IDH2 inhibitor enasidenib (Roboz et al., 2014), and BCL-2 inhibitor VEN (A. H. Wei et al., 2019).

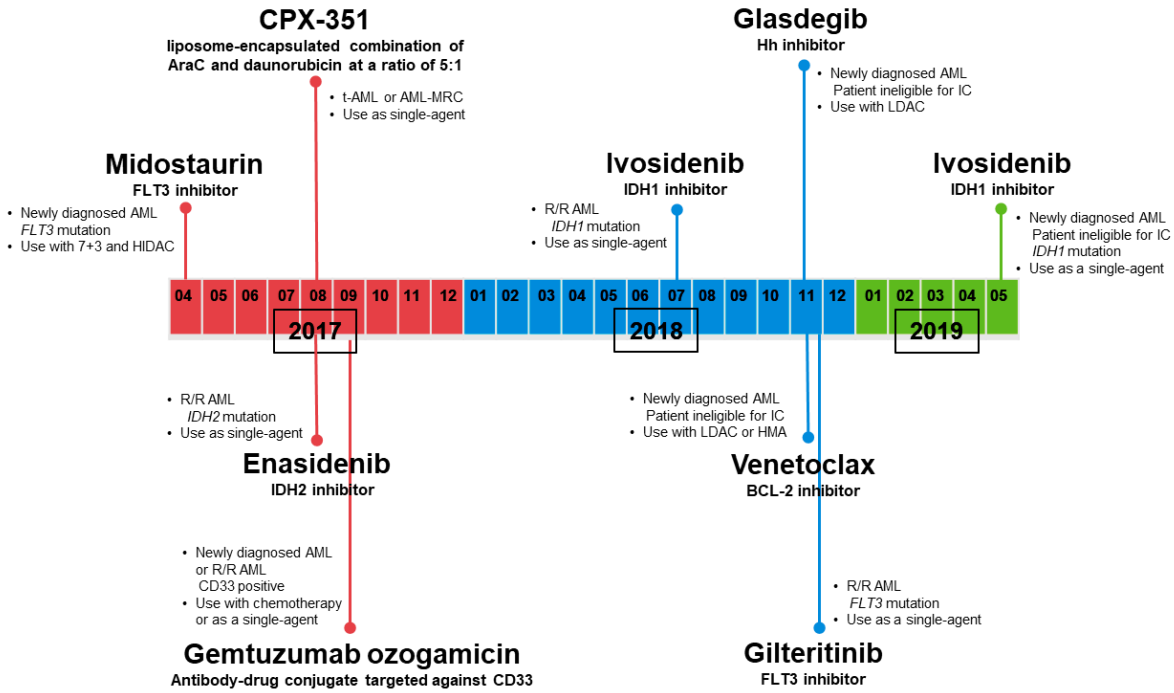

Figure 6.1.1 Novel targeted therapies approved by the FDA for the treatment of AML (Richard-Carpentier & DiNardo, 2019). Relapsed/refractory AML (R/R AML). Therapy-related AML (t-AML). AML with myelodysplasia-related changes (AML-MRC). Isocitrate dehydrogenase 1 and 2 (IDH1 and IDH2). FMS-like tyrosine kinase 3 - internal tandem duplication (FLT3-ITD). Hedgehog signalling pathway (Hh). B-cell lymphoma 2 (BCL-2). Intensive chemotherapy (IC). Low-dose cytarabine (LDAC). High-dose cytarabine (HIDAC). Hypomethylating agent (HMA).

Based on clinical trials, a novel therapeutic approach, including these targeted agents will be available for newly diagnosed AML patients in the near future (Figure 6.1.2) (Richard-Carpentier & DiNardo, 2019). Briefly, apart from patient medical history, the comprehensive profiling, including morphology, immunophenotyping, cytogenetics, and gene mutation screening, should be the additional step to select the best available therapy. In clinical trials, it has been reported that VEN/LDAC (A. H. Wei et al., 2019), VEN/AZA or decitabine (DiNardo et al., 2019; DiNardo, Pratz, et al., 2018), LDAC/glasdegib combinations (J. E. Cortes et al., 2019) improve outcomes as compared with conventional care in elderly patients with newly diagnosed AML who are ineligible to receive IC. CPX-351 improves overall survival rate over the standard "7+3" regimen in fit patients with therapy-related AML or AML-MRC (Lancet et al., 2018). Anti-CD33 GO should be added to the standard "7+3" in patients with newly diagnosed or R/R AML with favourable- or intermediate-risk cytogenetics with CD33 positive (Hills et al., 2014).

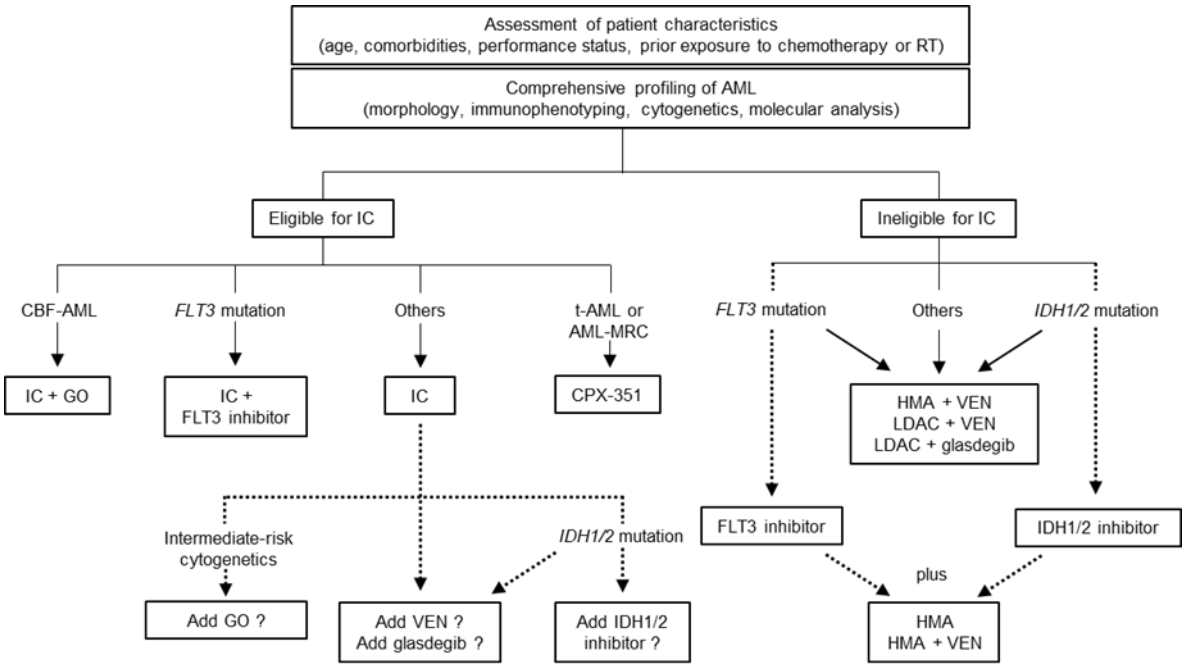

Figure 6.1.2 Therapeutic approach for newly diagnosed AML patients (Richard-Carpentier & DiNardo, 2019). Dotted lines indicate therapeutic options of unclear benefit, for which additional research is needed. Radiotherapy (RT). Core binding factor AML (CBF-AML). Therapy-related AML (t-AML). FMS-like tyrosine kinase 3 (FLT3). Isocitrate dehydrogenase 1 and 2 (IDH1 and IDH2). AML with myelodysplasia-related changes (AML-MRC). Intensive chemotherapy (IC). Gemtuzumab ozogamicin (GO). Low-dose cytarabine (LDAC). Hypomethylating agent (HMA). Venetoclax (VEN).

6.2 Conclusions

CYC065 has been designed to inhibit CDK2 and CDK9 activity. In this study, targets inhibition was interrogated from gene to protein and kinase activity levels. A simplified illustration of the effects of CYC065 is demonstrated in Figure 6.2.1 based on our data and on what is previously known about cell cycle progression. At an early timepoint (4h), a downregulation of RNAPII was observed, resulting in an inhibition of transcription. Among the BCL-2 family, a dramatic reduction in short half-life MCL-1 level was seen at both gene and protein level, highlighting on-target inhibition by CYC065. Various intracellular signalling pathways and transcription factors were perturbed. ERK1/2 was consistently suppressed in all cell lines, synchronously with a transcriptional downregulation of MCL-1. p38 MAPK was activated only in MOLM-13 cell line, which is most sensitive to CYC065, implying that the stress response and apoptosis are highly induced. A transcriptional downregulation of Rb was seen in MOLM-13 cell line. A decrease in gene expression of *E2F1* was demonstrated, which potentially leads to G1 arrest was observed in OCI-AML3 and MV4-11 cell lines following treatment with CYC065 for 4h.

As summarised in Figure 6.2.2, based on what is previously known about the intrinsic apoptosis pathway, a rapid decrease in MCL-1 level perturbs a balance in the BCL-2 family which leads directly to activator BH3-only proteins (yellow) binding BAK and BAX (blue), resulting in their homo-oligomerisation and MOMP. A decrease in the expression of *BMF* was also observed. After MOMP, pro-apoptotic proteins within the mitochondrial intermembrane space e.g., Cyt c, Smac and HtrA2 are released. Cyt c binds to Apaf-1 to form the apoptosome. Once formed, the apoptosome can then recruit and activate the inactive pro-caspase-9. Following this, active caspase-9 then activates caspase-3, 6, and 7 which results in subsequent multiple proteolytic events. Simultaneously, Smac and HtrA2 inhibit the IAP family members XIAP and BIRC5, releasing caspases from being repressed.

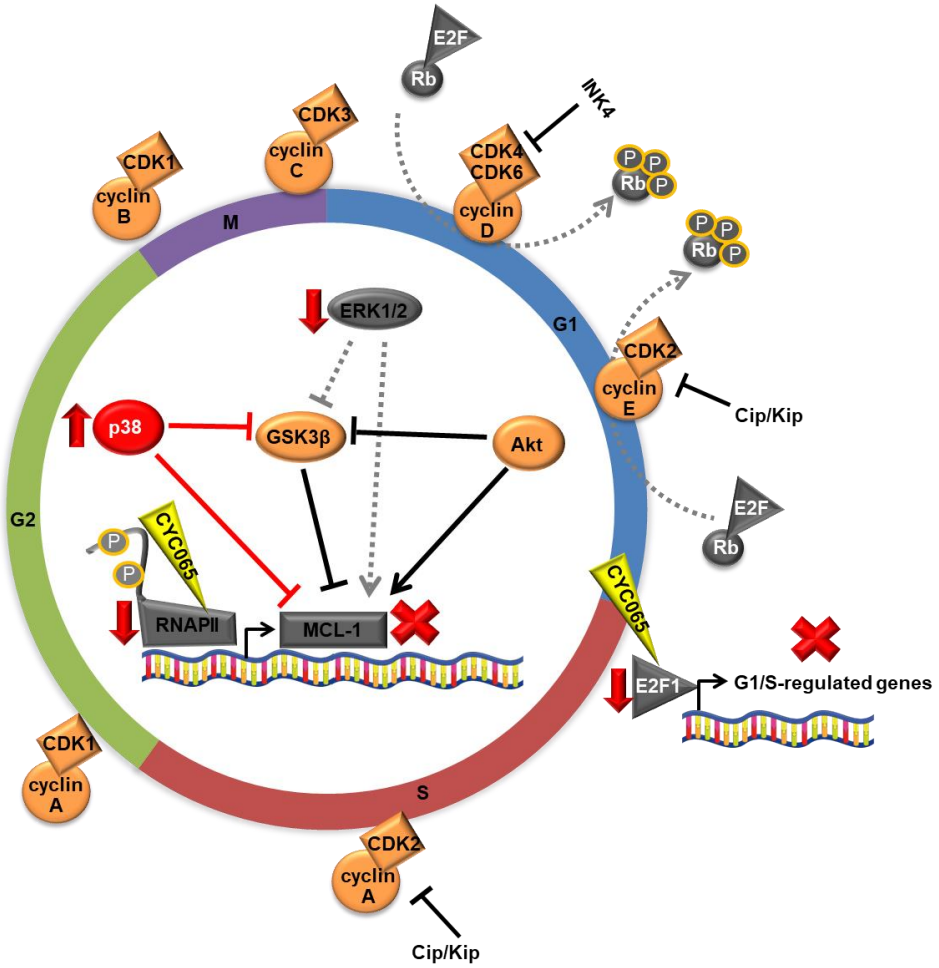

Figure 6.2.1 A schematic diagram of the effects of CYC065 at early time point (4h). RNA polymerase II (RNAPII). Myeloid cell leukemia 1 (MCL-1). p38 mitogen-activated protein kinase (p38). Extracellular signal-regulated kinase 1 and 2 (ERK1/2). Protein kinase B (Akt). Glycogen synthase kinase 3 beta (GSK3β). Retinoblastoma tumour suppressor (Rb). E2F transcription factor 1 (E2F1). Cyclin-dependent kinase (CDK). Cyclin-dependent kinase interacting protein/Kinase inhibitory protein (Cip/Kip). Inhibitors of cyclin-dependent kinase 4 (INK4). Gap 1 phase (G1). Synthesis phase (S). Gap 2 phase (G2). Mitotic phase (M).

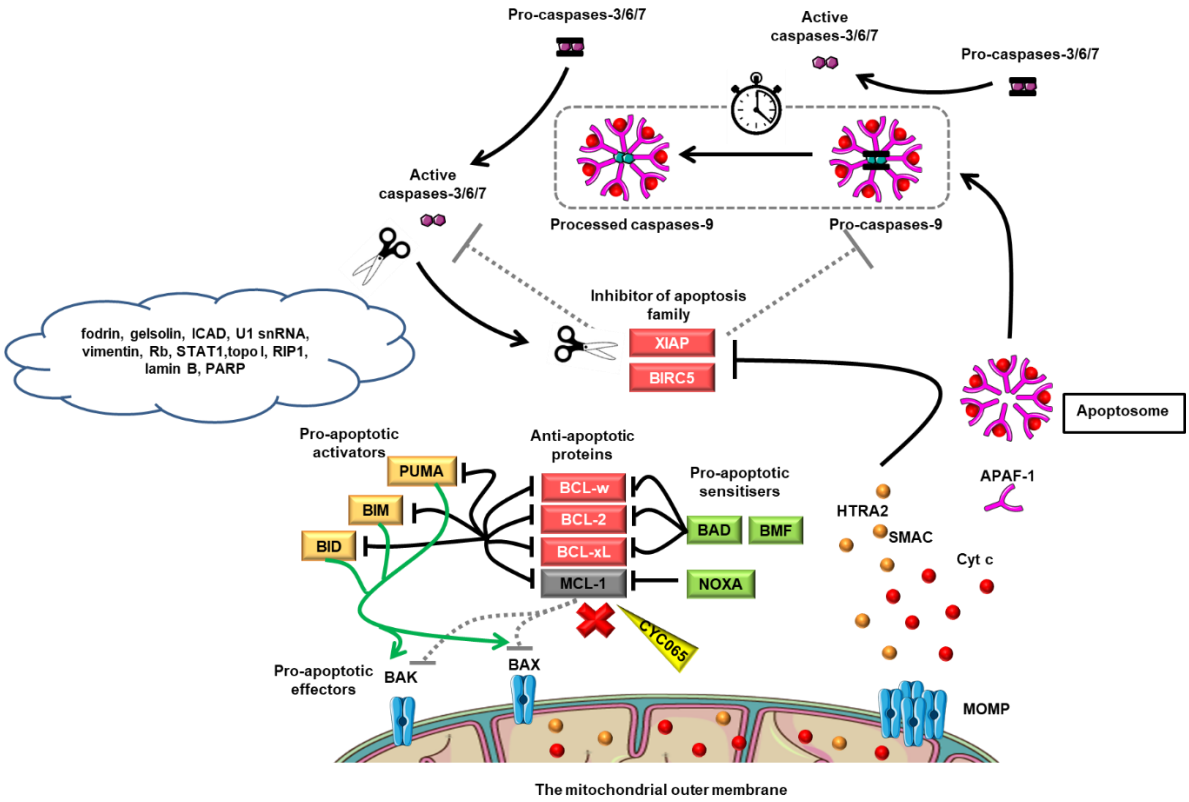

Figure 6.2.2 A schematic diagram of the intrinsic apoptosis pathway perturbed by CYC065. B-cell lymphoma 2 (BCL-2). B-cell lymphoma-extra large (BCL-xL). B-cell lymphoma 2-like protein 2 (BCL-w). Myeloid cell leukemia 1 (MCL-1). B-cell lymphoma 2-associated death promoter (BAD). B-cell lymphoma 2 modifying factor (BMF). phorbol-12-myristate-13-acetate-induced protein 1 (NOXA). B-cell lymphoma 2-like protein 11 (BIM). BH3 interacting-domain death agonist (BID). p53 upregulated modulator of apoptosis (PUMA). B-cell lymphoma 2 homologous antagonist/killer (BAK). B-cell lymphoma 2-associated X protein (BAX). Mitochondrial outer membrane permeabilisation (MOMP). Cytochrome c (Cyt c). Second mitochondria-derived activator of caspases (SMAC). High-temperature requirement A serine peptidase 2 (HTRA2). Apoptotic protease activating factor-1 (APAF-1).

The efficacy of the novel CDK2/9 inhibitor CYC065 as a single agent or in conjunction with frontline AML chemotherapeutics was seen in cell lines and primary human samples, in particular, CYC065/AZA combination, highlighting the potential of CYC065 for a novel therapeutic approach. This work emphasises the importance of individual genetic profiling as a critical step prior to initiating therapy for AML, stressing the need for a more personalised medicine approach to improve outcomes in AML.

6.3 Future Directions

In this study, the specificity of CYC065 in inhibiting CDK2/9 is not yet clearly elucidated. Thus, further investigation is required which could include CDK activity profiling using FRET technique or phosphoproteomics profiling using HPLC-MS/MS as discussed in section 6.1. To improve the combination studies, TST should be considered, in particular, for the combination of CDKI and cell cycle-active agents.

It has been reported that the BM niche exerts a protective effect on leukaemic cells through cell-cell contact and through emission of signalling molecules which stimulate anti-apoptotic pathways (Crane, Jeffery, & Morrison, 2017). As a result, the efficacy of chemotherapeutic drugs may be reduced. This brings forth the notion that evaluation of the efficacy of CYC065 in the BM microenvironment either alone or in combination with other partners. Initially, experiments using AML cell lines co-cultured with the HS-5 human BM stromal cell line is planned. The efficacy of CYC065 either as a single agent or in combination with VEN, AraC, or AZA will be assessed using various methods. The results from the co-culture conditions will be compared with the data in this study. After that, it would be interesting to further investigate the interaction using a 3D BM niche model. Currently, there are various BM niche models available e.g. 3D hollow fibre bioreactor systems (3DHFR) (Rödling et al., 2017), organ-on-a-chip technologies (Torisawa et al., 2014), and BM microenvironment models developed using magnetically levitated mesenchymal stem cells (MSCs) cultured in collagen hydrogels (Lewis et al., 2017).

Personalised medicine and targeted therapy are the current trend for the therapeutic approach in AML, thereby many novel agents have been developed aiming to hit specific molecular targets. Among these, MCL-1 is shown to be critical for the survival of AML. However, it has been reported that direct MCL-1 inhibition results in the disruption of mitochondrial morphology and dynamics as well as disorganisation of the actin cytoskeleton which leads to cardiotoxicity (Rasmussen et al., 2020).

As it was observed that MCL-1 is the key target of CYC065, therefore, it is worthwhile to assess whether CYC065 is more effective for an MCL-1-dependent cell population with reduced toxicity to the organism as a whole. Moving forward, an *in vivo* study would be an essential step with an ultimate aim of applying CYC065 in clinical practice, mainly focused on targeting MCL-1. Wunderlich et al reported that NSGS mice (NOD/SCID IL2Rγnull SCF/IL-3/GM-CSF) have a better engraftment potency as compared with NS (NOD/SCID), NSG (NOD/SCID IL2Rγnull), or NSS (NOD/SCID SCF/IL-3/GM-CSF) mice (Wunderlich et al., 2018). Hence, NSGS mice would be selected for future study and are available in-house.

The first step is to perform dose-escalation studies to determine the maximum tolerated dose (MTD) of CYC065 in 8-12-week-old NSGS mice which will be administrated via tail vain injection on days 1, 2, 8 and 9 of a three-week cycle, similar to the human strategy. Then, low and high doses of CYC065 will be selected aiming to evaluate whether the effect is dose-dependent. In parallel, a xenograft transplantation model will be established. Among twenty-one AML cell lines, it has been reported that NB-4, HL-60, THP-1, KG-1, and MV4-11 cell lines are less dependent, whereas, U-937, MOLM-16, OCI-AML3, MOLM-13 and MUTZ-2 cell lines are more dependent on MCL-1, as identified by NOXA priming (Ishizawa et al., 2015). The cell lines will be transplanted via tail vein injection into two sets of sub-lethally irradiated (200 cGy) NSGS mice. After establishing disseminated leukaemia, DMSO and two doses CYC065 will be injected and weekly chimerism analyses will be assessed in murine PB using anti-human CD45 (hCD45) and anti-human CD33 (hCD33) (Ramsey et al., 2018).

The first set of xenograft NSGS mice would be euthanised at 4 weeks. The percentage of hCD45 would be evaluated in their blood, spleen, and BM. Spleen would be weighed and spleen-to-body weight ratio calculated. For the second set, the mice would be followed until death, and survival evaluated by Kaplan–Meier analysis. Finally, the efficacy of CYC065 would be compared between MCL-1-dependent and MCL-1-independent xenograft NSGS mice. If there is statistically significant different between the two groups, AML patient-derived xenograft (PDX) models would be generated, again, using MCL-1-dependent and MCL-1-independent patient samples. Following this, combination studies of low

dose of CYC065 and the best combination partner, identified by aforementioned 3D BM niche experiment, can be performed in the PDX mice.

References

Abdel-Wahab, O., & Levine, R. L. (2013). Mutations in epigenetic modifiers in the pathogenesis and therapy of acute myeloid leukemia. *Blood, 121*(18), 3563-3572. doi:10.1182/blood-2013-01-451781

Abraham, R. T. (2001). Cell cycle checkpoint signaling through the ATM and ATR kinases. *Genes Dev, 15*(17), 2177-2196. doi:10.1101/gad.914401

Abulwerdi, F., Liao, C., Liu, M., Azmi, A. S., Aboukameel, A., Mady, A. S., . . . Nikolovska-Coleska, Z. (2014). A novel small-molecule inhibitor of mcl-1 blocks pancreatic cancer growth in vitro and in vivo. *Mol Cancer Ther, 13*(3), 565-575. doi:10.1158/1535-7163.MCT-12-0767

Adachi, Y., Ishikawa, Y., & Kiyoi, H. (2017). Identification of volasertib-resistant mechanism and evaluation of combination effects with volasertib and other agents on acute myeloid leukemia. *Oncotarget, 8*(45), 78452-78465. doi:10.18632/oncotarget.19632

Alharbi, R. A., Pettengell, R., Pandha, H. S., & Morgan, R. (2013). The role of HOX genes in normal hematopoiesis and acute leukemia. *Leukemia, 27*(5), 1000-1008. doi:10.1038/leu.2012.356

Allan, A. L., Albanese, C., Pestell, R. G., & LaMarre, J. (2001). Activating transcription factor 3 induces DNA synthesis and expression of cyclin D1 in hepatocytes. *J Biol Chem, 276*(29), 27272-27280. doi:10.1074/jbc.M103196200

Amrein, P. C., & Stossel, T. P. (1980). Prevention of degradation of human polymorphonuclear leukocyte proteins by diisopropylfluorophosphate. *Blood, 56*(3), 442-447.

Anderson, M. A., Deng, J., Seymour, J. F., Tam, C., Kim, S. Y., Fein, J., . . . Roberts, A. W. (2016). The BCL2 selective inhibitor venetoclax induces rapid onset apoptosis of CLL cells in patients via a TP53-independent mechanism. *Blood, 127*(25), 3215-3224. doi:10.1182/blood-2016-01-688796

Arai, F., Hirao, A., Ohmura, M., Sato, H., Matsuoka, S., Takubo, K., . . . Suda, T. (2004). Tie2/angiopoietin-1 signaling regulates hematopoietic stem cell quiescence in the bone marrow niche. *Cell, 118*(2), 149-161. doi:10.1016/j.cell.2004.07.004

Arber, D. A., Orazi, A., Hasserjian, R., Thiele, J., Borowitz, M. J., Le Beau, M. M., . . . Vardiman, J. W. (2016). The 2016 revision to the World Health Organization classification of myeloid neoplasms and acute leukemia. *Blood, 127*(20), 2391-2405. doi:10.1182/blood-2016-03-643544

Askari, N., Beenstock, J., Livnah, O., & Engelberg, D. (2009). p38alpha is active in vitro and in vivo when monophosphorylated at threonine 180. *Biochemistry, 48*(11), 2497-2504. doi:10.1021/bi900024v

Ayton, P. M., & Cleary, M. L. (2001). Molecular mechanisms of leukemogenesis mediated by MLL fusion proteins. *Oncogene, 20*(40), 5695-5707. doi:10.1038/sj.onc.1204639

Azijli, K., Yuvaraj, S., van Roosmalen, I., Flach, K., Giovannetti, E., Peters, G. J., . . . Kruyt, F. A. (2013). MAPK p38 and JNK have opposing activities on

TRAIL-induced apoptosis activation in NSCLC H460 cells that involves RIP1 and caspase-8 and is mediated by Mcl-1. *Apoptosis, 18*(7), 851-860. doi:10.1007/s10495-013-0829-3

Bacher, U., Haferlach, T., Alpermann, T., Zenger, M., Kröger, N., Beelen, D. W., . . . Haferlach, C. (2010). Comparison of cytogenetic clonal evolution patterns following allogeneic hematopoietic transplantation versus conventional treatment in patients at relapse of AML. *Biol Blood Marrow Transplant, 16*(12), 1649-1657. doi:10.1016/j.bbmt.2010.06.007

Baker, A., Gregory, G. P., Verbrugge, I., Kats, L., Hilton, J. J., Vidacs, E., . . . Johnstone, R. W. (2016). The CDK9 Inhibitor Dinaciclib Exerts Potent Apoptotic and Antitumor Effects in Preclinical Models of MLL-Rearranged Acute Myeloid Leukemia. *Cancer Res, 76*(5), 1158-1169. doi:10.1158/0008-5472.CAN-15-1070

Baldridge, M. T., King, K. Y., Boles, N. C., Weksberg, D. C., & Goodell, M. A. (2010). Quiescent haematopoietic stem cells are activated by IFN-gamma in response to chronic infection. *Nature, 465*(7299), 793-797. doi:10.1038/nature09135

Bankston, A. N., Ku, L., & Feng, Y. (2017). Active Cdk5 Immunoprecipitation and Kinase Assay. *Bio Protoc, 7*(13). doi:10.21769/BioProtoc.2363

Bannister, T., Koenig, M., He, Y., Mishra, J., Spicer, T., Minond, D., . . . Hodder, P. (2010). ML311: A Small Molecule that Potently and Selectively Disrupts the Protein-Protein Interaction of Mcl- 1 and Bim: A Probe for Studying Lymphoid Tumorigenesis. In *Probe Reports from the NIH Molecular Libraries Program*. Bethesda, MD: National Institutes of Health.

Barragán, E., Cervera, J., Bolufer, P., Ballester, S., Martín, G., Fernández, P., . . . Sanz, M. A. (2004). Prognostic implications of Wilms' tumor gene (WT1) expression in patients with de novo acute myeloid leukemia. *Haematologica, 89*(8), 926-933.

Bartek, J., & Lukas, J. (2001). Mammalian G1- and S-phase checkpoints in response to DNA damage. *Curr Opin Cell Biol, 13*(6), 738-747.

Bartek, J., Bartkova, J., & Lukas, J. (1997). The retinoblastoma protein pathway in cell cycle control and cancer. *Exp Cell Res, 237*(1), 1-6. doi:10.1006/excr.1997.3776

Bate-Eya, L. T., den Hartog, I. J., van der Ploeg, I., Schild, L., Koster, J., Santo, E. E., . . . Dolman, M. E. (2016). High efficacy of the BCL-2 inhibitor ABT199 (venetoclax) in BCL-2 high-expressing neuroblastoma cell lines and xenografts and rational for combination with MCL-1 inhibition. *Oncotarget, 7*(19), 27946-27958. doi:10.18632/oncotarget.8547

Baylin, S. B., & Jones, P. A. (2011). A decade of exploring the cancer epigenome - biological and translational implications. *Nat Rev Cancer, 11*(10), 726-734. doi:10.1038/nrc3130

Becker, P. S. (2016). Clonal Hematopoiesis: The Seeds of Leukemia or Innocuous Bystander? *Blood, 13*(1).

Bellissimo, D. C., & Speck, N. A. (2017). Mutations in Inherited and Sporadic Leukemia. *Front Cell Dev Biol, 5*, 111. doi:10.3389/fcell.2017.00111

Benson, C., White, J., De Bono, J., O'Donnell, A., Raynaud, F., Cruickshank, C., . . . Twelves, C. (2007). A phase I trial of the selective oral cyclin-dependent kinase inhibitor seliciclib (CYC202; R-Roscovitine), administered twice daily for 7 days every 21 days. *Br J Cancer, 96*(1), 29-37. doi:10.1038/sj.bjc.6603509

Berndt, N. (1999). Protein dephosphorylation and the intracellular control of the cell number. *Front Biosci, 4*, D22-42. doi:10.2741/berndt

Bertoli, S., Bérard, E., Huguet, F., Huynh, A., Tavitian, S., Vergez, F., . . . Récher, C. (2013). Time from diagnosis to intensive chemotherapy initiation does not adversely impact the outcome of patients with acute myeloid leukemia. *Blood, 121*(14), 2618-2626. doi:10.1182/blood-2012-09-454553

Bitoun, E., Oliver, P. L., & Davies, K. E. (2007). The mixed-lineage leukemia fusion partner AF4 stimulates RNA polymerase II transcriptional elongation and mediates coordinated chromatin remodeling. *Hum Mol Genet, 16*(1), 92-106. doi:10.1093/hmg/ddl444

Blanco, E., Di Croce, L., & Aranda, S. (2019). Comparative ChIP-seq (Comp-ChIP-seq): a novel computational methodology for genome-wide analysis. *bioRxiv*, 532622. doi:10.1101/532622

Blazek, D., Kohoutek, J., Bartholomeeusen, K., Johansen, E., Hulinkova, P., Luo, Z., . . . Peterlin, B. M. (2011). The Cyclin K/Cdk12 complex maintains genomic stability via regulation of expression of DNA damage response genes. Genes Dev, 25(20), 2158-2172. doi:10.1101/gad.16962311

Boffo, S., Damato, A., Alfano, L., & Giordano, A. (2018). CDK9 inhibitors in acute myeloid leukemia. *J Exp Clin Cancer Res, 37*(1), 36. doi:10.1186/s13046-018-0704-8

Bogenberger, J. M., Kornblau, S. M., Pierceall, W. E., Lena, R., Chow, D., Shi, C. X., . . . Tibes, R. (2014). BCL-2 family proteins as 5-Azacytidine-sensitizing targets and determinants of response in myeloid malignancies. *Leukemia, 28*(8), 1657-1665. doi:10.1038/leu.2014.44

Bogenberger, J., Whatcott, C., Hansen, N., Delman, D., Shi, C. X., Kim, W., . . . Tibes, R. (2017). Combined venetoclax and alvocidib in acute myeloid leukemia. *Oncotarget, 8*(63), 107206-107222. doi:10.18632/oncotarget.22284

Boissel, N., Cayuela, J. M., Preudhomme, C., Thomas, X., Grardel, N., Fund, X., . . . Dombret, H. (2002). Prognostic significance of FLT3 internal tandem repeat in patients with de novo acute myeloid leukemia treated with reinforced courses of chemotherapy. *Leukemia, 16*(9), 1699-1704. doi:10.1038/sj.leu.2402622

Boissel, N., Leroy, H., Brethon, B., Philippe, N., de Botton, S., Auvrignon, A., . . . Groups, L. A. M. d. l. E. L. C. (2006). Incidence and prognostic impact of c-Kit, FLT3, and Ras gene mutations in core binding factor acute myeloid leukemia (CBF-AML). *Leukemia, 20*(6), 965-970. doi:10.1038/sj.leu.2404188

Bonetti, P., Davoli, T., Sironi, C., Amati, B., Pelicci, P. G., & Colombo, E. (2008). Nucleophosmin and its AML-associated mutant regulate c-Myc turnover through Fbw7 gamma. *J Cell Biol, 182*(1), 19-26. doi:10.1083/jcb.200711040

Booy, E. P., Henson, E. S., & Gibson, S. B. (2011). Epidermal growth factor regulates Mcl-1 expression through the MAPK-Elk-1 signalling pathway contributing to cell survival in breast cancer. *Oncogene, 30*(20), 2367-2378. doi:10.1038/onc.2010.616

Bose, P., Simmons, G. L., & Grant, S. (2013). Cyclin-dependent kinase inhibitor therapy for hematologic malignancies. *Expert Opin Investig Drugs, 22*(6), 723-738. doi:10.1517/13543784.2013.789859

Brady, P. N., & Macnaughtan, M. A. (2015). Evaluation of colorimetric assays for analyzing reductively methylated proteins: Biases and mechanistic insights. *Anal Biochem, 491*, 43-51. doi:10.1016/j.ab.2015.08.027

Branger, J., van den Blink, B., Weijer, S., Madwed, J., Bos, C. L., Gupta, A., . . . van der Poll, T. (2002). Anti-inflammatory effects of a p38 mitogen-activated protein kinase inhibitor during human endotoxemia. *J Immunol, 168*(8), 4070-4077. doi:10.4049/jimmunol.168.8.4070

Bratton, S. B., & Salvesen, G. S. (2010). Regulation of the Apaf-1-caspase-9 apoptosome. *J Cell Sci, 123*(Pt 19), 3209-3214. doi:10.1242/jcs.073643

Britain, C. M., Holdbrooks, A. T., Anderson, J. C., Willey, C. D., & Bellis, S. L. (2018). Sialylation of EGFR by the ST6Gal-I sialyltransferase promotes EGFR activation and resistance to gefitinib-mediated cell death. *J Ovarian Res, 11*(1), 12. doi:10.1186/s13048-018-0385-0

Brugarolas, J., Moberg, K., Boyd, S. D., Taya, Y., Jacks, T., & Lees, J. A. (1999). Inhibition of cyclin-dependent kinase 2 by p21 is necessary for retinoblastoma protein-mediated G1 arrest after gamma-irradiation. *Proc Natl Acad Sci U S A, 96*(3), 1002-1007. doi:10.1073/pnas.96.3.1002

Byth, K. F., Thomas, A., Hughes, G., Forder, C., McGregor, A., Geh, C., . . . Wilkinson, R. W. (2009). AZD5438, a potent oral inhibitor of cyclin-dependent kinases 1, 2, and 9, leads to pharmacodynamic changes and potent antitumor effects in human tumor xenografts. *Mol Cancer Ther, 8*(7), 1856-1866. doi:10.1158/1535-7163.MCT-08-0836

Cai, B., Chang, S. H., Becker, E. B., Bonni, A., & Xia, Z. (2006). p38 MAP kinase mediates apoptosis through phosphorylation of BimEL at Ser-65. *J Biol Chem, 281*(35), 25215-25222. doi:10.1074/jbc.M512627200

Cai, D., Latham, V. M., Zhang, X., & Shapiro, G. I. (2006). Combined depletion of cell cycle and transcriptional cyclin-dependent kinase activities induces apoptosis in cancer cells. *Cancer Res, 66*(18), 9270-9280. doi:10.1158/0008-5472.CAN-06-1758

Cai, D., Latham, V. M., Zhang, X., & Shapiro, G. I. (2020). Correction: Combined Depletion of Cell Cycle and Transcriptional Cyclin-Dependent Kinase Activities Induces Apoptosis in Cancer Cells. *Cancer Res, 80*(2), 361. doi:10.1158/0008-5472.CAN-19-3524

Campbell, V., & Copland, M. (2015). Hedgehog signaling in cancer stem cells: a focus on hematological cancers. *Stem Cells Cloning, 8*, 27-38. doi:10.2147/SCCAA.S58613

Cao, L., Chen, F., Yang, X., Xu, W., Xie, J., & Yu, L. (2014). Phylogenetic analysis of CDK and cyclin proteins in premetazoan lineages. *BMC Evol Biol, 14*, 10. doi:10.1186/1471-2148-14-10

Cao, L., Kim, S., Xiao, C., Wang, R. H., Coumoul, X., Wang, X., . . . Deng, C. X. (2006). ATM-Chk2-p53 activation prevents tumorigenesis at an expense of organ homeostasis upon Brca1 deficiency. *EMBO J, 25*(10), 2167-2177. doi:10.1038/sj.emboj.7601115

Capizzi, R. L., Yang, J. L., Cheng, E., Bjornsson, T., Sahasrabudhe, D., Tan, R. S., & Cheng, Y. C. (1983). Alteration of the pharmacokinetics of high-dose ara-C by its metabolite, high ara-U in patients with acute leukemia. *J Clin Oncol, 1*(12), 763-771. doi:10.1200/JCO.1983.1.12.763

Castaigne, S., Pautas, C., Terré, C., Raffoux, E., Bordessoule, D., Bastie, J. N., . . . Association, A. L. F. (2012). Effect of gemtuzumab ozogamicin on survival of adult patients with de-novo acute myeloid leukaemia (ALFA-0701): a randomised, open-label, phase 3 study. *Lancet, 379*(9825), 1508-1516. doi:10.1016/S0140-6736(12)60485-1

Celgene. (2018). VIDAZA (azacitidine for injection) [package insert]. In. Summit, NJ: Celgene corporation.

Chao, S. H., Fujinaga, K., Marion, J. E., Taube, R., Sausville, E. A., Senderowicz, A. M., . . . Price, D. H. (2000). Flavopiridol inhibits P-TEFb and blocks HIV-1 replication. *J Biol Chem, 275*(37), 28345-28348. doi:10.1074/jbc.C000446200

Chao, T. C., & Martin, N. (2005). CompuSyn for drug combinations: PC Software and User's Guide: a computer program for quantitation of synergism and antagonism in drug combinations, and the determination of IC 50 and ED 50 and LD 50 values. Paramus (NJ): ComboSyn. Retrieved from http://www.compusyn.com/

Chaput, D., Kirouac, L., Stevens, S. M., & Padmanabhan, J. (2016). Potential role of PCTAIRE-2, PCTAIRE-3 and P-Histone H4 in amyloid precursor protein-dependent Alzheimer pathology. Oncotarget, 7(8), 8481-8497. doi:10.18632/oncotarget.7380

Chen, H., Xu, X., Wang, G., Zhang, B., Xin, G., Liu, J., . . . Zhang, C. (2017). CDK4 protein is degraded by anaphase-promoting complex/cyclosome in mitosis and reaccumulates in early G. *J Biol Chem, 292*(24), 10131-10141. doi:10.1074/jbc.M116.773226

Chen, L., & Flies, D. B. (2013). Molecular mechanisms of T cell co-stimulation and co-inhibition. *Nat Rev Immunol, 13*(4), 227-242. doi:10.1038/nri3405

Chen, R., Chen, Y., Frame, S., Blake, D., Wierda, W. G., Zheleva, D., & Plunkett, W. (2018). *Strategic combination of the cyclin-dependent kinase inhibitor CYC065 with venetoclax to target anti-apoptotic proteins in chronic lymphocytic leukemia*. Paper presented at the AACR Annual Meeting, Chicago, Illinois, the USA. http://www.abstractsonline.com/pp8/#!/4562/presentation/4821

Chen, R., Wierda, W. G., Chubb, S., Hawtin, R. E., Fox, J. A., Keating, M. J., . . . Plunkett, W. (2009). Mechanism of action of SNS-032, a novel cyclin-dependent kinase inhibitor, in chronic lymphocytic leukemia. *Blood, 113*(19), 4637-4645. doi:10.1182/blood-2008-12-190256

Chen, S., Dai, Y., Harada, H., Dent, P., & Grant, S. (2007). Mcl-1 down-regulation potentiates ABT-737 lethality by cooperatively inducing Bak activation and Bax translocation. *Cancer Res, 67*(2), 782-791. doi:10.1158/0008-5472.CAN-06-3964

Chen, Y. J., Dominguez-Brauer, C., Wang, Z., Asara, J. M., Costa, R. H., Tyner, A. L., . . . Raychaudhuri, P. (2009). A conserved phosphorylation site within the forkhead domain of FoxM1B is required for its activation by cyclin-CDK1. J Biol Chem, 284(44), 30695-30707. doi:10.1074/jbc.M109.007997

Chène, P. (2003). Inhibiting the p53-MDM2 interaction: an important target for cancer therapy. *Nat Rev Cancer, 3*(2), 102-109. doi:10.1038/nrc991

Cheng, K., Sportoletti, P., Ito, K., Clohessy, J. G., Teruya-Feldstein, J., Kutok, J. L., & Pandolfi, P. P. (2010). The cytoplasmic NPM mutant induces myeloproliferation in a transgenic mouse model. *Blood, 115*(16), 3341-3345. doi:10.1182/blood-2009-03-208587

Cheson, B. D., Bennett, J. M., Kopecky, K. J., Büchner, T., Willman, C. L., Estey, E. H., . . . International Working Group for Diagnosis, S. o. R. C., T.eatment Outcomes, and Reporting Standards for Therapeutic Trials in Acute Myeloid Leukemia. (2003). Revised recommendations of the International Working Group for Diagnosis, Standardization of Response Criteria, Treatment Outcomes, and Reporting Standards for Therapeutic

Trials in Acute Myeloid Leukemia. *J Clin Oncol, 21*(24), 4642-4649. doi:10.1200/JCO.2003.04.036

Chipuk, J. E., Fisher, J. C., Dillon, C. P., Kriwacki, R. W., Kuwana, T., & Green, D. R. (2008). Mechanism of apoptosis induction by inhibition of the anti-apoptotic BCL-2 proteins. *Proc Natl Acad Sci U S A, 105*(51), 20327-20332. doi:10.1073/pnas.0808036105

Chytil, A., Waltner-Law, M., West, R., Friedman, D., Aakre, M., Barker, D., & Law, B. (2004). Construction of a cyclin D1-Cdk2 fusion protein to model the biological functions of cyclin D1-Cdk2 complexes. *J Biol Chem, 279*(46), 47688-47698. doi:10.1074/jbc.M405938200

Cimmino, L., Dolgalev, I., Wang, Y., Yoshimi, A., Martin, G. H., Wang, J., . . . Aifantis, I. (2017). Restoration of TET2 Function Blocks Aberrant Self-Renewal and Leukemia Progression. *Cell, 170*(6), 1079-1095.e1020. doi:10.1016/j.cell.2017.07.032

Classon, M., & Harlow, E. (2002). The retinoblastoma tumour suppressor in development and cancer. *Nat Rev Cancer, 2*(12), 910-917. doi:10.1038/nrc950

Colombo, E., Marine, J. C., Danovi, D., Falini, B., & Pelicci, P. G. (2002). Nucleophosmin regulates the stability and transcriptional activity of p53. *Nat Cell Biol, 4*(7), 529-533. doi:10.1038/ncb814

Contreras, A. U., Mebratu, Y., Delgado, M., Montano, G., Hu, C. A., Ryter, S. W., . . . Tesfaigzi, Y. (2013). Deacetylation of p53 induces autophagy by suppressing Bmf expression. *J Cell Biol, 201*(3), 427-437. doi:10.1083/jcb.201205064

Cooper, G. M. (2000). The Eukaryotic Cell Cycle. In *The cell : a molecular approach* (2nd ed.). Washington, D.C.: ASM Press.

Cortes, J. E., Heidel, F. H., Hellmann, A., Fiedler, W., Smith, B. D., Robak, T., . . . Heuser, M. (2019). Randomized comparison of low dose cytarabine with or without glasdegib in patients with newly diagnosed acute myeloid leukemia or high-risk myelodysplastic syndrome. *Leukemia, 33*(2), 379-389. doi:10.1038/s41375-018-0312-9

Cortes, J., Feldman, E., Yee, K., Rizzieri, D., Advani, A. S., Charman, A., . . . Kantarjian, H. (2013). Two dosing regimens of tosedostat in elderly patients with relapsed or refractory acute myeloid leukaemia (OPAL): a randomised open-label phase 2 study. *Lancet Oncol, 14*(4), 354-362. doi:10.1016/S1470-2045(13)70037-8

Coudé, M. M., Braun, T., Berrou, J., Dupont, M., Bertrand, S., Masse, A., . . . Gardin, C. (2015). BET inhibitor OTX015 targets BRD2 and BRD4 and decreases c-MYC in acute leukemia cells. *Oncotarget, 6*(19), 17698-17712. doi:10.18632/oncotarget.4131

Craddock, C. F., Houlton, A. E., Quek, L. S., Ferguson, P., Gbandi, E., Roberts, C., . . . Vyas, P. (2017). Outcome of Azacitidine Therapy in Acute Myeloid Leukemia Is not Improved by Concurrent Vorinostat Therapy but Is Predicted by a Diagnostic Molecular Signature. *Clin Cancer Res, 23*(21), 6430-6440. doi:10.1158/1078-0432.CCR-17-1423

Crane, G. M., Jeffery, E., & Morrison, S. J. (2017). Adult haematopoietic stem cell niches. *Nat Rev Immunol, 17*(9), 573-590. doi:10.1038/nri.2017.53

Cress, W. D., Yu, P., & Wu, J. (2017). Expression and alternative splicing of the cyclin-dependent kinase inhibitor-3 gene in human cancer. *Int J Biochem Cell Biol, 91*(Pt B), 98-101. doi:10.1016/j.biocel.2017.05.013

CRUK. (2016). Acute myeloid leukaemia (AML) statistics. Retrieved from https://www.cancerresearchuk.org/health-professional/cancer-statistics/statistics-by-cancer-type/leukaemia-aml#heading-Five

Cyclacel. (2016). Highly-selective clinical stage CDK2/9 inhibitor with targeted development potential in hematological malignancies and solid tumors.

Cyclacel. (2018). Cyclacel Announces Presentation of Phase 1 Clinical Data for CDK Inhibitor CYC065 at AACR 2018 Annual Meeting. Retrieved from http://investor.cyclacel.com/news-releases/news-release-details/cyclacel-announces-presentation-phase-1-clinical-data-cdk

Czabotar, P. E., Westphal, D., Dewson, G., Ma, S., Hockings, C., Fairlie, W. D., . . . Colman, P. M. (2013). Bax crystal structures reveal how BH3 domains activate Bax and nucleate its oligomerization to induce apoptosis. *Cell, 152*(3), 519-531. doi:10.1016/j.cell.2012.12.031

Dai, H., Ding, H., Meng, X. W., Lee, S. H., Schneider, P. A., & Kaufmann, S. H. (2013). Contribution of Bcl-2 phosphorylation to Bak binding and drug resistance. *Cancer Res, 73*(23), 6998-7008. doi:10.1158/0008-5472.CAN-13-0940

Damaraju, V. L., Damaraju, S., Young, J. D., Baldwin, S. A., Mackey, J., Sawyer, M. B., & Cass, C. E. (2003). Nucleoside anticancer drugs: the role of nucleoside transporters in resistance to cancer chemotherapy. *Oncogene, 22*(47), 7524-7536. doi:10.1038/sj.onc.1206952

Dave, U. P., & Koury, M. J. (2016). Structure of the marrow and the hematopoietic microenvironment. In K. Kaushansky, M. A. Lichtman, & J. T. Prchal (Eds.), *Williams Hematology* (9th ed., pp. 53-84). New York: McGraw-Hill.

Day, C. L., Chen, L., Richardson, S. J., Harrison, P. J., Huang, D. C., & Hinds, M. G. (2005). Solution structure of prosurvival Mcl-1 and characterization of its binding by proapoptotic BH3-only ligands. *J Biol Chem, 280*(6), 4738-4744. doi:10.1074/jbc.M411434200

De Leon, G., Cavino, M., D'Angelo, M., & Krucher, N. A. (2010). PNUTS knockdown potentiates the apoptotic effect of Roscovitine in breast and colon cancer cells. *Int J Oncol, 36*(5), 1269-1275. doi:10.3892/ijo_00000611

Deacon, K., Mistry, P., Chernoff, J., Blank, J. L., & Patel, R. (2003). p38 Mitogen-activated protein kinase mediates cell death and p21-activated kinase mediates cell survival during chemotherapeutic drug-induced mitotic arrest. *Mol Biol Cell, 14*(5), 2071-2087. doi:10.1091/mbc.e02-10-0653

Del Principe, M. I., Buccisano, F., Maurillo, L., Sconocchia, G., Cefalo, M., Consalvo, M. I., . . . Venditti, A. (2016). Minimal Residual Disease in Acute Myeloid Leukemia of Adults: Determination, Prognostic Impact and Clinical Applications. *Mediterr J Hematol Infect Dis, 8*(1), e2016052. doi:10.4084/MJHID.2016.052

Desagher, S., Osen-Sand, A., Nichols, A., Eskes, R., Montessuit, S., Lauper, S., . . . Martinou, J. C. (1999). Bid-induced conformational change of Bax is responsible for mitochondrial cytochrome c release during apoptosis. *J Cell Biol, 144*(5), 891-901. doi:10.1083/jcb.144.5.891

Dettman, E. J., Warner, S. L., Doykan, C., Arn, M., Blake, N., & Bearss, D. J. (2015). Mitochondrial profiling in AML patients treated with an alvocidib containing regimen reveals MCL1 dependency in responder bone marrow [abstract]. *Cancer Res, 75*.

Deveraux, Q. L., & Reed, J. C. (1999). IAP family proteins--suppressors of apoptosis. *Genes Dev, 13*(3), 239-252. doi:10.1101/gad.13.3.239

Dick, J. E., Bhatia, M., Gan, O., Kapp, U., & Wang, J. C. (1997). Assay of human stem cells by repopulation of NOD/SCID mice. *Stem Cells, 15 Suppl 1*, 199-203; discussion 204-197. doi:10.1002/stem.5530150826

Diks, S. H., Kok, K., O'Toole, T., Hommes, D. W., van Dijken, P., Joore, J., & Peppelenbosch, M. P. (2004). Kinome profiling for studying lipopolysaccharide signal transduction in human peripheral blood mononuclear cells. *J Biol Chem, 279*(47), 49206-49213. doi:10.1074/jbc.M405028200

DiNardo, C. D., & Cortes, J. E. (2016). Mutations in AML: prognostic and therapeutic implications. *Hematology Am Soc Hematol Educ Program, 2016*(1), 348-355. doi:10.1182/asheducation-2016.1.348

DiNardo, C. D., Pratz, K. W., Letai, A., Jonas, B. A., Wei, A. H., Thirman, M., . . . Pollyea, D. A. (2018). Safety and preliminary efficacy of venetoclax with decitabine or azacitidine in elderly patients with previously untreated acute myeloid leukaemia: a non-randomised, open-label, phase 1b study. *Lancet Oncol, 19*(2), 216-228. doi:10.1016/S1470-2045(18)30010-X

DiNardo, C. D., Pratz, K., Pullarkat, V., Jonas, B. A., Arellano, M., Becker, P. S., . . . Letai, A. (2019). Venetoclax combined with decitabine or azacitidine in treatment-naive, elderly patients with acute myeloid leukemia. *Blood, 133*(1), 7-17. doi:10.1182/blood-2018-08-868752

DiNardo, C. D., Stein, E. M., de Botton, S., Roboz, G. J., Altman, J. K., Mims, A. S., . . . Kantarjian, H. M. (2018). Durable Remissions with Ivosidenib in IDH1-Mutated Relapsed or Refractory AML. *N Engl J Med, 378*(25), 2386-2398. doi:10.1056/NEJMoa1716984

Ding, Q., He, X., Hsu, J. M., Xia, W., Chen, C. T., Li, L. Y., . . . Hung, M. C. (2007). Degradation of Mcl-1 by beta-TrCP mediates glycogen synthase kinase 3-induced tumor suppression and chemosensitization. *Mol Cell Biol, 27*(11), 4006-4017. doi:10.1128/MCB.00620-06

Ding, Q., Huo, L., Yang, J. Y., Xia, W., Wei, Y., Liao, Y., . . . Hung, M. C. (2008). Down-regulation of myeloid cell leukemia-1 through inhibiting Erk/Pin 1 pathway by sorafenib facilitates chemosensitization in breast cancer. *Cancer Res, 68*(15), 6109-6117. doi:10.1158/0008-5472.CAN-08-0579

DiPippo, A. J., Patel, N. K., & Barnett, C. M. (2016). Cyclin-Dependent Kinase Inhibitors for the Treatment of Breast Cancer: Past, Present, and Future. *Pharmacotherapy, 36*(6), 652-667. doi:10.1002/phar.1756

Do, K. T., Chau, N., Wolanski, A., Beardslee, B., Hassinger, F., Bhushan, K., . . . Shapiro, G. I. (2018). Abstract CT037: Phase I safety, pharmacokinetic and pharmacodynamic study of CYC065, a cyclin dependent kinase inhibitor, in patients with advanced cancers (NCT02552953). Cancer Research, 78(13 Supplement), CT037-CT037. doi:10.1158/1538-7445.am2018-ct037

Dohadwala, M., da Cruz e Silva, E. F., Hall, F. L., Williams, R. T., Carbonaro-Hall, D. A., Nairn, A. C., . . . Berndt, N. (1994). Phosphorylation and inactivation of protein phosphatase 1 by cyclin-dependent kinases. *Proc Natl Acad Sci U S A, 91*(14), 6408-6412. doi:10.1073/pnas.91.14.6408

Döhner, H., Estey, E. H., Amadori, S., Appelbaum, F. R., Büchner, T., Burnett, A. K., . . . LeukemiaNet, E. (2010). Diagnosis and management of acute myeloid leukemia in adults: recommendations from an international expert panel, on behalf of the European LeukemiaNet. *Blood, 115*(3), 453-474. doi:10.1182/blood-2009-07-235358

Döhner, H., Estey, E., Grimwade, D., Amadori, S., Appelbaum, F. R., Büchner, T., . . . Bloomfield, C. D. (2017). Diagnosis and management of AML in adults: 2017 ELN recommendations from an international expert panel. *Blood, 129*(4), 424-447. doi:10.1182/blood-2016-08-733196

Döhner, H., Lübbert, M., Fiedler, W., Fouillard, L., Haaland, A., Brandwein, J. M., . . . Maertens, J. (2014). Randomized, phase 2 trial of low-dose cytarabine with or without volasertib in AML patients not suitable for induction therapy. *Blood, 124*(9), 1426-1433. doi:10.1182/blood-2014-03-560557

Döhner, H., Weisdorf, D. J., & Bloomfield, C. D. (2015). Acute Myeloid Leukemia. *N Engl J Med, 373*(12), 1136-1152. doi:10.1056/NEJMra1406184

Döhner, K., Schlenk, R. F., Habdank, M., Scholl, C., Rücker, F. G., Corbacioglu, A., . . . Döhner, H. (2005). Mutant nucleophosmin (NPM1) predicts favorable prognosis in younger adults with acute myeloid leukemia and normal cytogenetics: interaction with other gene mutations. *Blood, 106*(12), 3740-3746. doi:10.1182/blood-2005-05-2164

Doi, K., Li, R., Sung, S. S., Wu, H., Liu, Y., Manieri, W., . . . Wang, H. G. (2012). Discovery of marinopyrrole A (maritoclax) as a selective Mcl-1 antagonist that overcomes ABT-737 resistance by binding to and targeting Mcl-1 for proteasomal degradation. *J Biol Chem, 287*(13), 10224-10235. doi:10.1074/jbc.M111.334532

Domina, A. M., Vrana, J. A., Gregory, M. A., Hann, S. R., & Craig, R. W. (2004). MCL1 is phosphorylated in the PEST region and stabilized upon ERK activation in viable cells, and at additional sites with cytotoxic okadaic acid or taxol. *Oncogene, 23*(31), 5301-5315. doi:10.1038/sj.onc.1207692

Dorand, R. D., Nthale, J., Myers, J. T., Barkauskas, D. S., Avril, S., Chirieleison, S. M., . . . Petrosiute, A. (2016). Cdk5 disruption attenuates tumor PD-L1 expression and promotes antitumor immunity. Science, 353(6297), 399-403. doi:10.1126/science.aae0477

Dos Santos Paparidis, N. F., & Canduri, F. (2018). The Emerging Picture of CDK11: Genetic, Functional and Medicinal Aspects. Curr Med Chem, 25(8), 880-888. doi:10.2174/0929867324666170815102036

Drake, J. C., Hande, K. R., Fuller, R. W., & Chabner, B. A. (1980). Cytidine and deoxycytidylate deaminase inhibition by uridine analogs. *Biochem Pharmacol, 29*(5), 807-811.

Duployez, N., Marceau-Renaut, A., Boissel, N., Petit, A., Bucci, M., Geffroy, S., . . . Preudhomme, C. (2016). Comprehensive mutational profiling of core binding factor acute myeloid leukemia. *Blood, 127*(20), 2451-2459. doi:10.1182/blood-2015-12-688705

Durand, E. M., & Zon, L. I. (2010). Newly emerging roles for prostaglandin E2 regulation of hematopoiesis and hematopoietic stem cell engraftment. *Curr Opin Hematol, 17*(4), 308-312. doi:10.1097/MOH.0b013e32833a888c

Eleni, L. D., Nicholas, Z. C., & Alexandros, S. (2010). Challenges in treating older patients with acute myeloid leukemia. *J Oncol, 2010*, 943823. doi:10.1155/2010/943823

Elkholi, R., Floros, K. V., & Chipuk, J. E. (2011). The Role of BH3-Only Proteins in Tumor Cell Development, Signaling, and Treatment. *Genes Cancer, 2*(5), 523-537. doi:10.1177/1947601911417177

Elkholi, R., Renault, T. T., Serasinghe, M. N., & Chipuk, J. E. (2014). Putting the pieces together: How is the mitochondrial pathway of apoptosis regulated in cancer and chemotherapy? *Cancer Metab, 2*, 16. doi:10.1186/2049-3002-2-16

Elmer, J. J., Christensen, M. D., Barua, S., Lehrman, J., Haynes, K. A., & Rege, K. (2016). The histone deacetylase inhibitor Entinostat enhances polymer-mediated transgene expression in cancer cell lines. *Biotechnol Bioeng, 113*(6), 1345-1356. doi:10.1002/bit.25898

Erba, H. P., Becker, P. S., Shami, P. J., Grunwald, M. R., Flesher, D. L., Zhu, M., . . . Wang, E. S. (2019). Phase 1b study of the MDM2 inhibitor AMG 232 with or without trametinib in relapsed/refractory acute myeloid leukemia. *Blood Adv, 3*(13), 1939-1949. doi:10.1182/bloodadvances.2019030916

Eriksson, A., Kalushkova, A., Jarvius, M., Hilhorst, R., Rickardson, L., Kultima, H. G., . . . Höglund, M. (2014). AKN-028 induces cell cycle arrest, downregulation of Myc associated genes and dose dependent reduction of tyrosine kinase activity in acute myeloid leukemia. *Biochem Pharmacol, 87*(2), 284-291. doi:10.1016/j.bcp.2013.10.022

Eriksson, M., Peña-Martínez, P., Ramakrishnan, R., Chapellier, M., Högberg, C., Glowacki, G., . . . Järås, M. (2017). Agonistic targeting of TLR1/TLR2 induces p38 MAPK-dependent apoptosis and NFκB-dependent differentiation of AML cells. *Blood Adv, 1*(23), 2046-2057. doi:10.1182/bloodadvances.2017006148

Essers, M. A., Offner, S., Blanco-Bose, W. E., Waibler, Z., Kalinke, U., Duchosal, M. A., & Trumpp, A. (2009). IFNalpha activates dormant haematopoietic stem cells in vivo. *Nature, 458*(7240), 904-908. doi:10.1038/nature07815

Estey, E. H. (2018). Acute myeloid leukemia: 2019 update on risk-stratification and management. *Am J Hematol, 93*(10), 1267-1291. doi:10.1002/ajh.25214

Faber, A. C., & Chiles, T. C. (2007). Inhibition of cyclin-dependent kinase-2 induces apoptosis in human diffuse large B-cell lymphomas. *Cell Cycle, 6*(23), 2982-2989. doi:10.4161/cc.6.23.4994

Faber, Z. J., Chen, X., Gedman, A. L., Boggs, K., Cheng, J., Ma, J., . . . Downing, J. R. (2016). The genomic landscape of core-binding factor acute myeloid leukemias. *Nat Genet, 48*(12), 1551-1556. doi:10.1038/ng.3709

Falini, B., Mecucci, C., Tiacci, E., Alcalay, M., Rosati, R., Pasqualucci, L., . . . Party, G. A. L. W. (2005). Cytoplasmic nucleophosmin in acute myelogenous leukemia with a normal karyotype. *N Engl J Med, 352*(3), 254-266. doi:10.1056/NEJMoa041974

Fang, J., Ying, H., Mao, T., Fang, Y., Lu, Y., Wang, H., . . . Gu, J. (2017). Upregulation of CD11b and CD86 through LSD1 inhibition promotes myeloid differentiation and suppresses cell proliferation in human monocytic leukemia cells. *Oncotarget, 8*(49), 85085-85101. doi:10.18632/oncotarget.18564

Farag, S. S. (2011). The potential role of Aurora kinase inhibitors in haematological malignancies. *Br J Haematol, 155*(5), 561-579. doi:10.1111/j.1365-2141.2011.08898.x

Fathi, A. T., Wander, S. A., Blonquist, T. M., Brunner, A. M., Amrein, P. C., Supko, J., . . . Chen, Y. B. (2017). Phase I study of the aurora A kinase inhibitor alisertib with induction chemotherapy in patients with acute myeloid leukemia. *Haematologica, 102*(4), 719-727. doi:10.3324/haematol.2016.158394

Federici, L., & Falini, B. (2013). Nucleophosmin mutations in acute myeloid leukemia: a tale of protein unfolding and mislocalization. *Protein Sci, 22*(5), 545-556. doi:10.1002/pro.2240

Fischer, P. M., & Gianella-Borradori, A. (2005). Recent progress in the discovery and development of cyclin-dependent kinase inhibitors. *Expert Opin Investig Drugs, 14*(4), 457-477. doi:10.1517/13543784.14.4.457

Foucquier, J., & Guedj, M. (2015). Analysis of drug combinations: current methodological landscape. *Pharmacol Res Perspect, 3*(3), e00149. doi:10.1002/prp2.149

Freedman, D. A., Wu, L., & Levine, A. J. (1999). Functions of the MDM2 oncoprotein. *Cell Mol Life Sci, 55*(1), 96-107. doi:10.1007/s000180050273

Freeman, S. D., Virgo, P., Couzens, S., Grimwade, D., Russell, N., Hills, R. K., & Burnett, A. K. (2013). Prognostic relevance of treatment response measured by flow cytometric residual disease detection in older patients with acute myeloid leukemia. *J Clin Oncol, 31*(32), 4123-4131. doi:10.1200/JCO.2013.49.1753

Frezza, C., Cipolat, S., Martins de Brito, O., Micaroni, M., Beznoussenko, G. V., Rudka, T., . . . Scorrano, L. (2006). OPA1 controls apoptotic cristae remodeling independently from mitochondrial fusion. *Cell, 126*(1), 177-189. doi:10.1016/j.cell.2006.06.025

Friberg, A., Vigil, D., Zhao, B., Daniels, R. N., Burke, J. P., Garcia-Barrantes, P. M., . . . Fesik, S. W. (2013). Discovery of potent myeloid cell leukemia 1 (Mcl-1) inhibitors using fragment-based methods and structure-based design. *J Med Chem, 56*(1), 15-30. doi:10.1021/jm301448p

Fry, D. W., Harvey, P. J., Keller, P. R., Elliott, W. L., Meade, M., Trachet, E., . . . Toogood, P. L. (2004). Specific inhibition of cyclin-dependent kinase 4/6 by PD 0332991 and associated antitumor activity in human tumor xenografts. *Mol Cancer Ther, 3*(11), 1427-1438.

Fuchs, Y., & Steller, H. (2011). Programmed cell death in animal development and disease. *Cell, 147*(4), 742-758. doi:10.1016/j.cell.2011.10.033

Galbraith, M. D., Allen, M. A., Bensard, C. L., Wang, X., Schwinn, M. K., Qin, B., . . . Espinosa, J. M. (2013). HIF1A employs CDK8-mediator to stimulate RNAPII elongation in response to hypoxia. Cell, 153(6), 1327-1339. doi:10.1016/j.cell.2013.04.048

Galimberti, F., Thompson, S. L., Liu, X., Li, H., Memoli, V., Green, S. R., . . . Dmitrovsky, E. (2010). Targeting the cyclin E-Cdk-2 complex represses lung cancer growth by triggering anaphase catastrophe. *Clin Cancer Res, 16*(1), 109-120. doi:10.1158/1078-0432.CCR-09-2151

Galluzzi, L., Bravo-San Pedro, J. M., Kepp, O., & Kroemer, G. (2016). Regulated cell death and adaptive stress responses. *Cell Mol Life Sci, 73*(11-12), 2405-2410. doi:10.1007/s00018-016-2209-y

Galluzzi, L., Kepp, O., & Kroemer, G. (2016). Mitochondrial regulation of cell death: a phylogenetically conserved control. *Microb Cell, 3*(3), 101-108. doi:10.15698/mic2016.03.483

Galluzzi, L., Vitale, I., Aaronson, S. A., Abrams, J. M., Adam, D., Agostinis, P., . . . Kroemer, G. (2018). Molecular mechanisms of cell death: recommendations of the Nomenclature Committee on Cell Death 2018. *Cell Death Differ, 25*(3), 486-541. doi:10.1038/s41418-017-0012-4

Ganjam, G. K., Terpolilli, N. A., Diemert, S., Eisenbach, I., Hoffmann, L., Reuther, C., . . . Culmsee, C. (2018). Cylindromatosis mediates neuronal cell death in vitro and in vivo. *Cell Death Differ, 25*(8), 1394-1407. doi:10.1038/s41418-017-0046-7

Gao, H., Jin, S., Song, Y., Fu, M., Wang, M., Liu, Z., . . . Zhan, Q. (2005). B23 regulates GADD45a nuclear translocation and contributes to GADD45a-

induced cell cycle G2-M arrest. *J Biol Chem, 280*(12), 10988-10996. doi:10.1074/jbc.M412720200

Gavathiotis, E., Suzuki, M., Davis, M. L., Pitter, K., Bird, G. H., Katz, S. G., . . . Walensky, L. D. (2008). BAX activation is initiated at a novel interaction site. *Nature, 455*(7216), 1076-1081. doi:10.1038/nature07396

Gavet, O., & Pines, J. (2010). Activation of cyclin B1-Cdk1 synchronizes events in the nucleus and the cytoplasm at mitosis. *J Cell Biol, 189*(2), 247-259. doi:10.1083/jcb.200909144

Gélinas, C., & White, E. (2005). BH3-only proteins in control: specificity regulates MCL-1 and BAK-mediated apoptosis. *Genes Dev, 19*(11), 1263-1268. doi:10.1101/gad.1326205

Genovese, G., Kähler, A. K., Handsaker, R. E., Lindberg, J., Rose, S. A., Bakhoum, S. F., . . . McCarroll, S. A. (2014). Clonal hematopoiesis and blood-cancer risk inferred from blood DNA sequence. *N Engl J Med, 371*(26), 2477-2487. doi:10.1056/NEJMoa1409405

Ghia, P., Scarfò, L., Perez, S., Pathiraja, K., Derosier, M., Small, K., . . . Patton, N. (2017). Efficacy and safety of dinaciclib vs ofatumumab in patients with relapsed/refractory chronic lymphocytic leukemia. *Blood, 129*(13), 1876-1878. doi:10.1182/blood-2016-10-748210

Gillissen, B., Essmann, F., Hemmati, P. G., Richter, A., Oztop, I., Chinnadurai, G., . . . Daniel, P. T. (2007). Mcl-1 determines the Bax dependency of Nbk/Bik-induced apoptosis. *J Cell Biol, 179*(4), 701-715. doi:10.1083/jcb.200703040

Glaser, S. P., Lee, E. F., Trounson, E., Bouillet, P., Wei, A., Fairlie, W. D., . . . Strasser, A. (2012). Anti-apoptotic Mcl-1 is essential for the development and sustained growth of acute myeloid leukemia. *Genes Dev, 26*(2), 120-125. doi:10.1101/gad.182980.111

GLOBOCAN. (2012). Estimated Cancer Incidence, Mortality and Prevalence Worldwide, 2012. Retrieved from https://www.who.int/selection_medicines/committees/expert/20/applications/AML_APL.pdf?ua=1

Glover, D. M., Hagan, I. M., & Tavares, A. A. (1998). Polo-like kinases: a team that plays throughout mitosis. *Genes Dev, 12*(24), 3777-3787. doi:10.1101/gad.12.24.3777

Godley, L. A., & Shimamura, A. (2017). Genetic predisposition to hematologic malignancies: management and surveillance. *Blood, 130*(4), 424-432. doi:10.1182/blood-2017-02-735290

Goh, K. C., Novotny-Diermayr, V., Hart, S., Ong, L. C., Loh, Y. K., Cheong, A., . . . Wood, J. M. (2012). TG02, a novel oral multi-kinase inhibitor of CDKs, JAK2 and FLT3 with potent anti-leukemic properties. *Leukemia, 26*(2), 236-243. doi:10.1038/leu.2011.218

Gojo, I., Sadowska, M., Walker, A., Feldman, E. J., Iyer, S. P., Baer, M. R., . . . Bannerji, R. (2013). Clinical and laboratory studies of the novel cyclin-dependent kinase inhibitor dinaciclib (SCH 727965) in acute leukemias. *Cancer Chemother Pharmacol, 72*(4), 897-908. doi:10.1007/s00280-013-2249-z

Gomez-Bougie, P., Dousset, C., Descamps, G., Schnitzler, A., Audiger, L., Tessier, A., . . . Amiot, M. (2018). The selectivity of Marinopyrrole A to induce apoptosis in MCL1. *Br J Haematol, 180*(1), 157-159. doi:10.1111/bjh.14293

Gore, S. D., Baylin, S., Sugar, E., Carraway, H., Miller, C. B., Carducci, M., . . . Herman, J. G. (2006). Combined DNA methyltransferase and histone

deacetylase inhibition in the treatment of myeloid neoplasms. *Cancer Res, 66*(12), 6361-6369. doi:10.1158/0008-5472.CAN-06-0080

Gores, G. J., & Kaufmann, S. H. (2012). Selectively targeting Mcl-1 for the treatment of acute myelogenous leukemia and solid tumors. *Genes Dev, 26*(4), 305-311. doi:10.1101/gad.186189.111

Gregory, G. P., Hogg, S. J., Kats, L. M., Vidacs, E., Baker, A. J., Gilan, O., . . . Shortt, J. (2015). CDK9 inhibition by dinaciclib potently suppresses Mcl-1 to induce durable apoptotic responses in aggressive MYC-driven B-cell lymphoma in vivo. *Leukemia, 29*(6), 1437-1441. doi:10.1038/leu.2015.10

Grever, M. R., Lucas, D. M., Johnson, A. J., & Byrd, J. C. (2007). Novel agents and strategies for treatment of p53-defective chronic lymphocytic leukemia. *Best Pract Res Clin Haematol, 20*(3), 545-556. doi:10.1016/j.beha.2007.03.005

Grimwade, D., Hills, R. K., Moorman, A. V., Walker, H., Chatters, S., Goldstone, A. H., . . . Group, N. C. R. I. A. L. W. (2010). Refinement of cytogenetic classification in acute myeloid leukemia: determination of prognostic significance of rare recurring chromosomal abnormalities among 5876 younger adult patients treated in the United Kingdom Medical Research Council trials. *Blood, 116*(3), 354-365. doi:10.1182/blood-2009-11-254441

Gröschel, S., Sanders, M. A., Hoogenboezem, R., Zeilemaker, A., Havermans, M., Erpelinck, C., . . . Valk, P. J. (2015). Mutational spectrum of myeloid malignancies with inv(3)/t(3;3) reveals a predominant involvement of RAS/RTK signaling pathways. *Blood, 125*(1), 133-139. doi:10.1182/blood-2014-07-591461

Grove, C. S., & Vassiliou, G. S. (2014). Acute myeloid leukaemia: a paradigm for the clonal evolution of cancer? *Dis Model Mech, 7*(8), 941-951. doi:10.1242/dmm.015974

Gruber, T. A., & Rubnitz, J. E. (2018). Acute Myeloid Leukemia in Children. In R. Hoffman, L. E. Silberstein, J. I. Weitz, M. E. Salama, E. J. Benz, Jr., H. E. Heslop, J. Anastasi, & S. A. Abutalib (Eds.), *Hematology* (7th ed., pp. 981-993): Elsevier.

Guen, V. J., Gamble, C., Lees, J. A., & Colas, P. (2017). The awakening of the CDK10/Cyclin M protein kinase. Oncotarget, 8(30), 50174-50186. doi:10.18632/oncotarget.15024

Guertin, M. J., Cullen, A. E., Markowetz, F., & Holding, A. N. (2018). Parallel factor ChIP provides essential internal control for quantitative differential ChIP-seq. *Nucleic Acids Res, 46*(12), e75. doi:10.1093/nar/gky252

Haferlach, T., Nagata, Y., Grossmann, V., Okuno, Y., Bacher, U., Nagae, G., . . . Ogawa, S. (2014). Landscape of genetic lesions in 944 patients with myelodysplastic syndromes. *Leukemia, 28*(2), 241-247. doi:10.1038/leu.2013.336

Han, X., Liu, Y., Wu, F. G., Jansensky, J., Kim, T., Wang, Z., . . . Chen, Z. (2014). Different interfacial behaviors of peptides chemically immobilized on surfaces with different linker lengths and via different termini. *J Phys Chem B, 118*(11), 2904-2912. doi:10.1021/jp4122003

Hartsink-Segers, S. A., Zwaan, C. M., Exalto, C., Luijendijk, M. W., Calvert, V. S., Petricoin, E. F., . . . Den Boer, M. L. (2013). Aurora kinases in childhood acute leukemia: the promise of aurora B as therapeutic target. *Leukemia, 27*(3), 560-568. doi:10.1038/leu.2012.256

Harvey, S. L., Charlet, A., Haas, W., Gygi, S. P., & Kellogg, D. R. (2005). Cdk1-dependent regulation of the mitotic inhibitor Wee1. *Cell, 122*(3), 407-420. doi:10.1016/j.cell.2005.05.029

Haupt, S., Berger, M., Goldberg, Z., & Haupt, Y. (2003). Apoptosis - the p53 network. *J Cell Sci, 116*(Pt 20), 4077-4085. doi:10.1242/jcs.00739

He, R., Oliveira, J. L., Hoyer, J. D., & Viswanatha, D. S. (2018). Molecular Hematopathology. In E. D. Hsi (Ed.), *Hematopathology A volume in Foundations in Diagnostic Pathology* (Third ed., pp. 712-760): Elsevier.

Heasman, S. A., Zaitseva, L., Bowles, K. M., Rushworth, S. A., & Macewan, D. J. (2011). Protection of acute myeloid leukaemia cells from apoptosis induced by front-line chemotherapeutics is mediated by haem oxygenase-1. *Oncotarget, 2*(9), 658-668. doi:10.18632/oncotarget.321

Heath, E. M., Chan, S. M., Minden, M. D., Murphy, T., Shlush, L. I., & Schimmer, A. D. (2017). Biological and clinical consequences of NPM1 mutations in AML. *Leukemia, 31*(4), 798-807. doi:10.1038/leu.2017.30

Hengst, L., Göpfert, U., Lashuel, H. A., & Reed, S. I. (1998). Complete inhibition of Cdk/cyclin by one molecule of p21(Cip1). *Genes Dev, 12*(24), 3882-3888. doi:10.1101/gad.12.24.3882

Henley, S. A., & Dick, F. A. (2012). The retinoblastoma family of proteins and their regulatory functions in the mammalian cell division cycle. *Cell Div, 7*(1), 10. doi:10.1186/1747-1028-7-10

Hermanson, D. L., Das, S. G., Li, Y., & Xing, C. (2013). Overexpression of Mcl-1 confers multidrug resistance, whereas topoisomerase IIß downregulation introduces mitoxantrone-specific drug resistance in acute myeloid leukemia. *Mol Pharmacol, 84*(2), 236-243. doi:10.1124/mol.113.086140

Hernandez, A. M., Colvin, E. S., Chen, Y. C., Geiss, S. L., Eller, L. E., & Fueger, P. T. (2013). Upregulation of p21 activates the intrinsic apoptotic pathway in ß-cells. *Am J Physiol Endocrinol Metab, 304*(12), E1281-1290. doi:10.1152/ajpendo.00663.2012

Heuser, M., Thol, F., & Ganser, A. (2016). Clonal Hematopoiesis of Indeterminate Potential. *Dtsch Arztebl Int, 113*(18), 317-322. doi:10.3238/arztebl.2016.0317

Hills, R. K., Castaigne, S., Appelbaum, F. R., Delaunay, J., Petersdorf, S., Othus, M., . . . Burnett, A. K. (2014). Addition of gemtuzumab ozogamicin to induction chemotherapy in adult patients with acute myeloid leukaemia: a meta-analysis of individual patient data from randomised controlled trials. *Lancet Oncol, 15*(9), 986-996. doi:10.1016/S1470-2045(14)70281-5

Hinds, P. W., Mittnacht, S., Dulic, V., Arnold, A., Reed, S. I., & Weinberg, R. A. (1992). Regulation of retinoblastoma protein functions by ectopic expression of human cyclins. *Cell, 70*(6), 993-1006. doi:10.1016/0092-8674(92)90249-c

Hirao, A., Cheung, A., Duncan, G., Girard, P. M., Elia, A. J., Wakeham, A., . . . Mak, T. W. (2002). Chk2 is a tumor suppressor that regulates apoptosis in both an ataxia telangiectasia mutated (ATM)-dependent and an ATM-independent manner. *Mol Cell Biol, 22*(18), 6521-6532. doi:10.1128/mcb.22.18.6521-6532.2002

Hodgson, G. S., & Bradley, T. R. (1979). Properties of haematopoietic stem cells surviving 5-fluorouracil treatment: evidence for a pre-CFU-S cell? *Nature, 281*(5730), 381-382. doi:10.1038/281381a0

Hogge, D. E., Lansdorp, P. M., Reid, D., Gerhard, B., & Eaves, C. J. (1996). Enhanced detection, maintenance, and differentiation of primitive human hematopoietic cells in cultures containing murine fibroblasts engineered to produce human steel factor, interleukin-3, and granulocyte colony-stimulating factor. *Blood, 88*(10), 3765-3773.

Hollenbach, P. W., Nguyen, A. N., Brady, H., Williams, M., Ning, Y., Richard, N., . . . MacBeth, K. J. (2010). A comparison of azacitidine and decitabine activities in acute myeloid leukemia cell lines. *PLoS One, 5*(2), e9001. doi:10.1371/journal.pone.0009001

Hollenbaugh, J. A., Shelton, J., Tao, S., Amiralaei, S., Liu, P., Lu, X., . . . Kim, B. (2017). Substrates and Inhibitors of SAMHD1. *PLoS One, 12*(1), e0169052. doi:10.1371/journal.pone.0169052

Hoogendoorn, K. H. (2019). Advanced Therapies: Clinical, Non-clinical and Quality Considerations. In D. Crommelin, R. Sindelar, & B. Meibohm (Eds.), *Pharmaceutical Biotechnology* (5th ed., pp. 357-402). Cham: Springer.

Hou, H. A., Chou, W. C., Kuo, Y. Y., Liu, C. Y., Lin, L. I., Tseng, M. H., . . . Tien, H. F. (2015). TP53 mutations in de novo acute myeloid leukemia patients: longitudinal follow-ups show the mutation is stable during disease evolution. *Blood Cancer J, 5*, e331. doi:10.1038/bcj.2015.59

Hou, H. A., Huang, T. C., Lin, L. I., Liu, C. Y., Chen, C. Y., Chou, W. C., . . . Tien, H. F. (2010). WT1 mutation in 470 adult patients with acute myeloid leukemia: stability during disease evolution and implication of its incorporation into a survival scoring system. *Blood, 115*(25), 5222-5231. doi:10.1182/blood-2009-12-259390

Houseman, B. T., Huh, J. H., Kron, S. J., & Mrksich, M. (2002). Peptide chips for the quantitative evaluation of protein kinase activity. *Nat Biotechnol, 20*(3), 270-274. doi:10.1038/nbt0302-270

Howell, A. (2006). Pure oestrogen antagonists for the treatment of advanced breast cancer. *Endocr Relat Cancer, 13*(3), 689-706. doi:10.1677/erc.1.00846

Hsu, H., Xiong, J., & Goeddel, D. V. (1995). The TNF receptor 1-associated protein TRADD signals cell death and NF-kappa B activation. *Cell, 81*(4), 495-504. doi:10.1016/0092-8674(95)90070-5

Hua, P., Kronsteiner, B., van der Garde, M., Ashley, N., Hernandez, D., Tarunina, M., . . . Watt, S. M. (2019). Single-cell assessment of transcriptome alterations induced by Scriptaid in early differentiated human haematopoietic progenitors during ex vivo expansion. *Sci Rep, 9*(1), 5300. doi:10.1038/s41598-019-41803-z

Huelsemann, M. F., Patz, M., Beckmann, L., Brinkmann, K., Otto, T., Fandrey, J., . . . Frenzel, L. P. (2015). Hypoxia-induced p38 MAPK activation reduces Mcl-1 expression and facilitates sensitivity towards BH3 mimetics in chronic lymphocytic leukemia. *Leukemia, 29*(4), 981-984. doi:10.1038/leu.2014.320

Hwang, B., Lee, J. H., & Bang, D. (2018). Single-cell RNA sequencing technologies and bioinformatics pipelines. *Exp Mol Med, 50*(8), 96. doi:10.1038/s12276-018-0071-8

Hyoda, T., Tsujioka, T., Nakahara, T., Suemori, S., Okamoto, S., Kataoka, M., & Tohyama, K. (2015). Rigosertib induces cell death of a myelodysplastic syndrome-derived cell line by DNA damage-induced G2/M arrest. *Cancer Sci, 106*(3), 287-293. doi:10.1111/cas.12605

Hyun, S. Y., Hwang, H. I., Hwan, H. I., & Jang, Y. J. (2014). Polo-like kinase-1 in DNA damage response. *BMB Rep, 47*(5), 249-255. doi:10.5483/bmbrep.2014.47.5.061

Ikeda, H., Kanakura, Y., Tamaki, T., Kuriu, A., Kitayama, H., Ishikawa, J., . . . Griffin, J. D. (1991). Expression and functional role of the proto-oncogene c-kit in acute myeloblastic leukemia cells. *Blood, 78*(11), 2962-2968.

Ishizawa, J., Kojima, K., McQueen, T., Ruvolo, V., Chachad, D., Nogueras-Gonzalez, G. M., . . . Andreeff, M. (2015). Mitochondrial Profiling of Acute Myeloid Leukemia in the Assessment of Response to Apoptosis Modulating Drugs. *PLoS One, 10*(9), e0138377. doi:10.1371/journal.pone.0138377
Ishizawa, J., Kojima, K., McQueen, T., Ruvolo, V., Chachad, D., Nogueras-Gonzalez, G. M., . . . Andreeff, M. (2015). Mitochondrial Profiling of Acute Myeloid Leukemia in the Assessment of Response to Apoptosis Modulating Drugs. *PLoS One, 10*(9), e0138377. doi:10.1371/journal.pone.0138377
Issa, J. P., Garcia-Manero, G., Huang, X., Cortes, J., Ravandi, F., Jabbour, E., . . . Kantarjian, H. M. (2015). Results of phase 2 randomized study of low-dose decitabine with or without valproic acid in patients with myelodysplastic syndrome and acute myelogenous leukemia. *Cancer, 121*(4), 556-561. doi:10.1002/cncr.29085

Izzo, J. G., Luthra, R., Sims-Mourtada, J., Chao, K. S., Lee, J. H., Wu, T. T., . . . Ajani, J. A. (2007). Emerging molecular targets in esophageal cancers. *Gastrointest Cancer Res, 1*(4 Suppl 2), S3-6.

Jaiswal, S., Fontanillas, P., Flannick, J., Manning, A., Grauman, P. V., Mar, B. G., . . . Ebert, B. L. (2014). Age-related clonal hematopoiesis associated with adverse outcomes. *N Engl J Med, 371*(26), 2488-2498. doi:10.1056/NEJMoa1408617

Jalili, M., Yaghmaie, M., Ahmadvand, M., Alimoghaddam, K., Mousavi, S. A., Vaezi, M., & Ghavamzadeh, A. (2018). Prognostic Value of RUNX1 Mutations in AML: A Meta-Analysis. *Asian Pac J Cancer Prev, 19*(2), 325-329. doi:10.22034/APJCP.2018.19.2.325

Jeffrey, P. D., Tong, L., & Pavletich, N. P. (2000). Structural basis of inhibition of CDK-cyclin complexes by INK4 inhibitors. *Genes Dev, 14*(24), 3115-3125. doi:10.1101/gad.851100

Jeng, P. S., Inoue-Yamauchi, A., Hsieh, J. J., & Cheng, E. H. (2018). BH3-Dependent and Independent Activation of BAX and BAK in Mitochondrial Apoptosis. *Curr Opin Physiol, 3*, 71-81. doi:10.1016/j.cophys.2018.03.005

Jiffar, T., Kurinna, S., Suck, G., Carlson-Bremer, D., Ricciardi, M. R., Konopleva, M., . . . Ruvolo, P. P. (2004). PKC alpha mediates chemoresistance in acute lymphoblastic leukemia through effects on Bcl2 phosphorylation. *Leukemia, 18*(3), 505-512. doi:10.1038/sj.leu.2403275

Johnson, A. J., Yeh, Y. Y., Smith, L. L., Wagner, A. J., Hessler, J., Gupta, S., . . . Byrd, J. C. (2012). The novel cyclin-dependent kinase inhibitor dinaciclib (SCH727965) promotes apoptosis and abrogates microenvironmental cytokine protection in chronic lymphocytic leukemia cells. *Leukemia, 26*(12), 2554-2557. doi:10.1038/leu.2012.144

Kagoya, Y., Yoshimi, A., Kataoka, K., Nakagawa, M., Kumano, K., Arai, S., . . . Kurokawa, M. (2014). Positive feedback between NF-κB and TNF-α promotes leukemia-initiating cell capacity. *J Clin Invest, 124*(2), 528-542. doi:10.1172/JCI68101

Kantarjian, H. M., Martinelli, G., Jabbour, E. J., Quintás-Cardama, A., Ando, K., Bay, J. O., . . . Investigators, S.-A. (2013). Stage I of a phase 2 study assessing the efficacy, safety, and tolerability of barasertib (AZD1152) versus low-dose cytosine arabinoside in elderly patients with acute myeloid leukemia. *Cancer, 119*(14), 2611-2619. doi:10.1002/cncr.28113

Kantarjian, H. M., Schuster, M. W., Jain, N., Advani, A., Jabbour, E., Gamelin, E., . . . Sekeres, M. A. (2017). A phase 1 study of AMG 900, an orally administered pan-aurora kinase inhibitor, in adult patients with acute myeloid leukemia. *Am J Hematol, 92*(7), 660-667. doi:10.1002/ajh.24736

Karp, J. E., Blackford, A., Smith, B. D., Alino, K., Seung, A. H., Bolaños-Meade, J., . . . Wright, J. J. (2010). Clinical activity of sequential flavopiridol, cytosine arabinoside, and mitoxantrone for adults with newly diagnosed, poor-risk acute myelogenous leukemia. *Leuk Res, 34*(7), 877-882. doi:10.1016/j.leukres.2009.11.007

Karp, J. E., Passaniti, A., Gojo, I., Kaufmann, S., Bible, K., Garimella, T. S., . . . Bauer, K. S. (2005). Phase I and pharmacokinetic study of flavopiridol followed by 1-beta-D-arabinofuranosylcytosine and mitoxantrone in relapsed and refractory adult acute leukemias. *Clin Cancer Res, 11*(23), 8403-8412. doi:10.1158/1078-0432.CCR-05-1201

Karp, J. E., Ross, D. D., Yang, W., Tidwell, M. L., Wei, Y., Greer, J., . . . Colevas, A. D. (2003). Timed sequential therapy of acute leukemia with flavopiridol: in vitro model for a phase I clinical trial. *Clin Cancer Res, 9*(1), 307-315.

Kato, K. M., Liu, X., Oki, H., Ogasawara, S., Nakamura, T., Saidoh, N., . . . Kato, Y. (2014). Isocitrate dehydrogenase mutation is frequently observed in giant cell tumor of bone. *Cancer Sci, 105*(6), 744-748. doi:10.1111/cas.12413

Kaufmann, S. H., Karp, J. E., Svingen, P. A., Krajewski, S., Burke, P. J., Gore, S. D., & Reed, J. C. (1998). Elevated expression of the apoptotic regulator Mcl-1 at the time of leukemic relapse. *Blood, 91*(3), 991-1000.

Kaushansky, K. (2016). Hematopoietic stem cells, progenitors, and cytokines. In K. Kaushansky, M. A. Lichtman, & J. T. Prchal (Eds.), *Williams Hematology* (9th ed., pp. 257–278). New York: McGraw-Hill.

Kavela, S., Shinde, S. R., Ratheesh, R., Viswakalyan, K., Bashyam, M. D., Gowrishankar, S., . . . Maddika, S. (2013). PNUTS functions as a proto-oncogene by sequestering PTEN. *Cancer Res, 73*(1), 205-214. doi:10.1158/0008-5472.CAN-12-1394

Kihslinger, J. E., & Godley, L. A. (2007). The use of hypomethylating agents in the treatment of hematologic malignancies. *Leuk Lymphoma, 48*(9), 1676-1695. doi:10.1080/10428190701493910

Kim, E., Ilagan, J. O., Liang, Y., Daubner, G. M., Lee, S. C., Ramakrishnan, A., . . . Abdel-Wahab, O. (2015). SRSF2 Mutations Contribute to Myelodysplasia by Mutant-Specific Effects on Exon Recognition. *Cancer Cell, 27*(5), 617-630. doi:10.1016/j.ccell.2015.04.006

Kim, H. Y., Cho, Y., Kang, H., Yim, Y. S., Kim, S. J., Song, J., & Chun, K. H. (2016). Targeting the WEE1 kinase as a molecular targeted therapy for gastric cancer. *Oncotarget, 7*(31), 49902-49916. doi:10.18632/oncotarget.10231

Kim, H., Rafiuddin-Shah, M., Tu, H. C., Jeffers, J. R., Zambetti, G. P., Hsieh, J. J., & Cheng, E. H. (2006). Hierarchical regulation of mitochondrion-dependent apoptosis by BCL-2 subfamilies. *Nat Cell Biol, 8*(12), 1348-1358. doi:10.1038/ncb1499

Kim, J. E., Lim, J. H., Jeon, G. S., Shin, J. Y., Ahn, S. W., Kim, S. H., . . . Sung, J. J. (2017). Extrinsic Apoptosis Pathway Altered by Glycogen Synthase Kinase-3β Inhibitor Influences the Net Drug Effect on NSC-34 Motor Neuron-Like Cell Survival. *Biomed Res Int, 2017*, 4163839. doi:10.1155/2017/4163839

Kim, W., Whatcott, C., Siddiqui-Jain, A., Anthony, S., Bearss, D. J., & warner, S. L. (2018). *The CDK9 Inhibitor, Alvocidib, Potentiates the Non-Clinical Activity of Azacytidine or Decitabine in an MCL-1-Dependent Fashion,*

Supporting Clinical Exploration of a Decitabine and Alvocidib Combination. Paper presented at the The 60th ASH, San Diego, CA.

Kipps, T. J., Eradat, H., Grosicki, S., Catalano, J., Cosolo, W., Dyagil, I. S., . . . Pylypenko, H. (2015). A phase 2 study of the BH3 mimetic BCL2 inhibitor navitoclax (ABT-263) with or without rituximab, in previously untreated B-cell chronic lymphocytic leukemia. *Leuk Lymphoma, 56*(10), 2826-2833. doi:10.3109/10428194.2015.1030638

Kirschbaum, M., Gojo, I., Goldberg, S. L., Bredeson, C., Kujawski, L. A., Yang, A., . . . Issa, J. P. (2014). A phase 1 clinical trial of vorinostat in combination with decitabine in patients with acute myeloid leukaemia or myelodysplastic syndrome. *Br J Haematol, 167*(2), 185-193. doi:10.1111/bjh.13016

Klein, K., Kaspers, G., Harrison, C. J., Beverloo, H. B., Reedijk, A., Bongers, M., . . . Gibson, B. (2015). Clinical Impact of Additional Cytogenetic Aberrations, cKIT and RAS Mutations, and Treatment Elements in Pediatric t(8;21)-AML: Results From an International Retrospective Study by the International Berlin-Frankfurt-Münster Study Group. *J Clin Oncol, 33*(36), 4247-4258. doi:10.1200/JCO.2015.61.1947

Klepin, H. D., & Balducci, L. (2009). Acute myelogenous leukemia in older adults. *Oncologist, 14*(3), 222-232. doi:10.1634/theoncologist.2008-0224

Kobune, M., Takimoto, R., Murase, K., Iyama, S., Sato, T., Kikuchi, S., . . . Kato, J. (2009). Drug resistance is dramatically restored by hedgehog inhibitors in CD34+ leukemic cells. *Cancer Sci, 100*(5), 948-955. doi:10.1111/j.1349-7006.2009.01111.x

Kohoutek, J., & Blazek, D. (2012). Cyclin K goes with Cdk12 and Cdk13. Cell Div, 7, 12. doi:10.1186/1747-1028-7-12

Kojima, K., Konopleva, M., Tsao, T., Nakakuma, H., & Andreeff, M. (2008). Concomitant inhibition of Mdm2-p53 interaction and Aurora kinases activates the p53-dependent postmitotic checkpoints and synergistically induces p53-mediated mitochondrial apoptosis along with reduced endoreduplication in acute myelogenous leukemia. *Blood, 112*(7), 2886-2895. doi:10.1182/blood-2008-01-128611

Kollmann, K., Briand, C., Bellutti, F., Schicher, N., Blunder, S., Zojer, M., & Hoeller, C. (2019). The interplay of CDK4 and CDK6 in melanoma. *Oncotarget, 10*(14), 1346-1359. doi:10.18632/oncotarget.26515

Kolupaeva, V., & Janssens, V. (2013). PP1 and PP2A phosphatases--cooperating partners in modulating retinoblastoma protein activation. *FEBS J, 280*(2), 627-643. doi:10.1111/j.1742-4658.2012.08511.x

Konda, N., Arvind, P. P., & Shah, S. (2013). Pharmaceutical development and compatibility studies on cytarabine injection. *Asian J Pharm Clin Res, 6*(3), 142-145.

Konopleva, M., Pollyea, D. A., Potluri, J., Chyla, B., Hogdal, L., Busman, T., . . . Letai, A. (2016). Efficacy and Biological Correlates of Response in a Phase II Study of Venetoclax Monotherapy in Patients with Acute Myelogenous Leukemia. *Cancer Discov, 6*(10), 1106-1117. doi:10.1158/2159-8290.CD-16-0313

Kornblau, S. M., Andreeff, M., Hu, S. X., Xu, H. J., Patel, S., Theriault, A., . . . Benedict, W. F. (1998). Low and maximally phosphorylated levels of the retinoblastoma protein confer poor prognosis in newly diagnosed acute myelogenous leukemia: a prospective study. *Clin Cancer Res, 4*(8), 1955-1963.

Kornblau, S. M., Womble, M., Qiu, Y. H., Jackson, C. E., Chen, W., Konopleva, M., . . . Andreeff, M. (2006). Simultaneous activation of multiple signal transduction pathways confers poor prognosis in acute myelogenous leukemia. *Blood, 108*(7), 2358-2365. doi:10.1182/blood-2006-02-003475

Kornblau, S. M., Xu, H. J., del Giglio, A., Hu, S. X., Zhang, W., Calvert, L., . . . Trujillo, J. (1992). Clinical implications of decreased retinoblastoma protein expression in acute myelogenous leukemia. *Cancer Res, 52*(17), 4587-4590.

Kornblau, S. M., Xu, H. J., Zhang, W., Hu, S. X., Beran, M., Smith, T. L., . . . Deisseroth, A. B. (1994). Levels of retinoblastoma protein expression in newly diagnosed acute myelogenous leukemia. *Blood, 84*(1), 256-261.

Kotschy, A., Szlavik, Z., Murray, J., Davidson, J., Maragno, A. L., Le Toumelin-Braizat, G., . . . Geneste, O. (2016). The MCL1 inhibitor S63845 is tolerable and effective in diverse cancer models. *Nature, 538*(7626), 477-482. doi:10.1038/nature19830

Koumenis, C., & Giaccia, A. (1997). Transformed cells require continuous activity of RNA polymerase II to resist oncogene-induced apoptosis. *Mol Cell Biol, 17*(12), 7306-7316. doi:10.1128/mcb.17.12.7306

Koya, J., Kataoka, K., Sato, T., Bando, M., Kato, Y., Tsuruta-Kishino, T., . . . Kurokawa, M. (2016). DNMT3A R882 mutants interact with polycomb proteins to block haematopoietic stem and leukaemic cell differentiation. *Nat Commun, 7*, 10924. doi:10.1038/ncomms10924

Kralova, J., Dvorak, M., Koc, M., & Kral, V. (2008). p38 MAPK plays an essential role in apoptosis induced by photoactivation of a novel ethylene glycol porphyrin derivative. *Oncogene, 27*(21), 3010-3020. doi:10.1038/sj.onc.1210960

Krivtsov, A. V., & Armstrong, S. A. (2007). MLL translocations, histone modifications and leukaemia stem-cell development. *Nat Rev Cancer, 7*(11), 823-833. doi:10.1038/nrc2253

Kumar, S. K., LaPlant, B., Chng, W. J., Zonder, J., Callander, N., Fonseca, R., . . . Consortium, M. P. (2015). Dinaciclib, a novel CDK inhibitor, demonstrates encouraging single-agent activity in patients with relapsed multiple myeloma. *Blood, 125*(3), 443-448. doi:10.1182/blood-2014-05-573741

Kuo, F. C., Mar, B. G., Lindsley, R. C., & Lindeman, N. I. (2017). The relative utilities of genome-wide, gene panel, and individual gene sequencing in clinical practice. *Blood, 130*(4), 433-439. doi:10.1182/blood-2017-03-734533

Kurki, S., Peltonen, K., Latonen, L., Kiviharju, T. M., Ojala, P. M., Meek, D., & Laiho, M. (2004). Nucleolar protein NPM interacts with HDM2 and protects tumor suppressor protein p53 from HDM2-mediated degradation. *Cancer Cell, 5*(5), 465-475.

Kuwana, T., Bouchier-Hayes, L., Chipuk, J. E., Bonzon, C., Sullivan, B. A., Green, D. R., & Newmeyer, D. D. (2005). BH3 domains of BH3-only proteins differentially regulate Bax-mediated mitochondrial membrane permeabilization both directly and indirectly. *Mol Cell, 17*(4), 525-535. doi:10.1016/j.molcel.2005.02.003

Kwok, K. K., Vincent, E. C., & Gibson, J. N. (2017). Antineoplastic Drugs. In F. J. Dowd, B. S. Johnson, & A. J. Mariotti (Eds.), *Pharmacology and Therapeutics for Dentistry* (7th ed., pp. 530-562): Mosby.

Kwon, Y. G., Lee, S. Y., Choi, Y., Greengard, P., & Nairn, A. C. (1997). Cell cycle-dependent phosphorylation of mammalian protein phosphatase 1 by

cdc2 kinase. *Proc Natl Acad Sci U S A, 94*(6), 2168-2173. doi:10.1073/pnas.94.6.2168

Lacrima, K., Rinaldi, A., Vignati, S., Martin, V., Tibiletti, M. G., Gaidano, G., . . . Bertoni, F. (2007). Cyclin-dependent kinase inhibitor seliciclib shows in vitro activity in diffuse large B-cell lymphomas. *Leuk Lymphoma, 48*(1), 158-167. doi:10.1080/10428190601026562

Lam, L. T., Pickeral, O. K., Peng, A. C., Rosenwald, A., Hurt, E. M., Giltnane, J. M., . . . Staudt, L. M. (2001). Genomic-scale measurement of mRNA turnover and the mechanisms of action of the anti-cancer drug flavopiridol. *Genome Biol, 2*(10), RESEARCH0041. doi:10.1186/gb-2001-2-10-research0041

Lancet, J. E., Uy, G. L., Cortes, J. E., Newell, L. F., Lin, T. L., Ritchie, E. K., . . . Medeiros, B. C. (2018). CPX-351 (cytarabine and daunorubicin) Liposome for Injection Versus Conventional Cytarabine Plus Daunorubicin in Older Patients With Newly Diagnosed Secondary Acute Myeloid Leukemia. *J Clin Oncol, 36*(26), 2684-2692. doi:10.1200/JCO.2017.77.6112

Lapenna, S., & Giordano, A. (2009). Cell cycle kinases as therapeutic targets for cancer. *Nat Rev Drug Discov, 8*(7), 547-566. doi:10.1038/nrd2907

Larson, R. A., Sievers, E. L., Stadtmauer, E. A., Löwenberg, B., Estey, E. H., Dombret, H., . . . Appelbaum, F. R. (2005). Final report of the efficacy and safety of gemtuzumab ozogamicin (Mylotarg) in patients with CD33-positive acute myeloid leukemia in first recurrence. *Cancer, 104*(7), 1442-1452. doi:10.1002/cncr.21326

Lee, J. H., You, J., Dobrota, E., & Skalnik, D. G. (2010). Identification and characterization of a novel human PP1 phosphatase complex. *J Biol Chem, 285*(32), 24466-24476. doi:10.1074/jbc.M110.109801

Lee, L. Y., Hernandez, D., Rajkhowa, T., Smith, S. C., Raman, J. R., Nguyen, B., . . . Levis, M. (2017). Preclinical studies of gilteritinib, a next-generation FLT3 inhibitor. *Blood, 129*(2), 257-260. doi:10.1182/blood-2016-10-745133

Leist, M., & Jäättelä, M. (2001). Four deaths and a funeral: from caspases to alternative mechanisms. *Nat Rev Mol Cell Biol, 2*(8), 589-598. doi:10.1038/35085008

Leonard, S. M., Perry, T., Woodman, C. B., & Kearns, P. (2014). Sequential treatment with cytarabine and decitabine has an increased anti-leukemia effect compared to cytarabine alone in xenograft models of childhood acute myeloid leukemia. *PLoS One, 9*(1), e87475. doi:10.1371/journal.pone.0087475

Leonardi, M., Perna, E., Tronnolone, S., Colecchia, D., & Chiariello, M. (2019). Activated kinase screening identifies the. Autophagy, 15(2), 312-326. doi:10.1080/15548627.2018.1517855

Leong, S. M., Tan, B. X., Bte Ahmad, B., Yan, T., Chee, L. Y., Ang, S. T., . . . Lim, T. M. (2010). Mutant nucleophosmin deregulates cell death and myeloid differentiation through excessive caspase-6 and -8 inhibition. *Blood, 116*(17), 3286-3296. doi:10.1182/blood-2009-12-256149

LeRoy, G., Rickards, B., & Flint, S. J. (2008). The double bromodomain proteins Brd2 and Brd3 couple histone acetylation to transcription. *Mol Cell, 30*(1), 51-60. doi:10.1016/j.molcel.2008.01.018

Letai, A., Bassik, M. C., Walensky, L. D., Sorcinelli, M. D., Weiler, S., & Korsmeyer, S. J. (2002). Distinct BH3 domains either sensitize or activate mitochondrial apoptosis, serving as prototype cancer therapeutics. *Cancer Cell, 2*(3), 183-192. doi:10.1016/s1535-6108(02)00127-7

Leverson, J. D., Phillips, D. C., Mitten, M. J., Boghaert, E. R., Diaz, D., Tahir, S. K., . . . Souers, A. J. (2015). Exploiting selective BCL-2 family inhibitors to dissect cell survival dependencies and define improved strategies for cancer therapy. *Sci Transl Med, 7*(279), 279ra240. doi:10.1126/scitranslmed.aaa4642

Leverson, J. D., Zhang, H., Chen, J., Tahir, S. K., Phillips, D. C., Xue, J., . . . Souers, A. J. (2015). Potent and selective small-molecule MCL-1 inhibitors demonstrate on-target cancer cell killing activity as single agents and in combination with ABT-263 (navitoclax). *Cell Death Dis, 6*, e1590. doi:10.1038/cddis.2014.561

Levis, M., & Small, D. (2003). FLT3: ITDoes matter in leukemia. *Leukemia, 17*(9), 1738-1752. doi:10.1038/sj.leu.2403099

Lewin, J., Soria, J. C., Stathis, A., Delord, J. P., Peters, S., Awada, A., . . . Massard, C. (2018). Phase Ib Trial With Birabresib, a Small-Molecule Inhibitor of Bromodomain and Extraterminal Proteins, in Patients With Selected Advanced Solid Tumors. *J Clin Oncol, 36*(30), 3007-3014. doi:10.1200/JCO.2018.78.2292

Lewis, N. S., Lewis, E. E., Mullin, M., Wheadon, H., Dalby, M. J., & Berry, C. C. (2017). Magnetically levitated mesenchymal stem cell spheroids cultured with a collagen gel maintain phenotype and quiescence. *J Tissue Eng, 8*, 2041731417704428. doi:10.1177/2041731417704428

Ley, T. J., Ding, L., Walter, M. J., McLellan, M. D., Lamprecht, T., Larson, D. E., . . . Wilson, R. K. (2010). DNMT3A mutations in acute myeloid leukemia. *N Engl J Med, 363*(25), 2424-2433. doi:10.1056/NEJMoa1005143

Ley, T. J., Miller, C., Ding, L., Raphael, B. J., Mungall, A. J., Robertson, A., . . . Network, C. G. A. R. (2013). Genomic and epigenomic landscapes of adult de novo acute myeloid leukemia. *N Engl J Med, 368*(22), 2059-2074. doi:10.1056/NEJMoa1301689

Li, B., Ni Chonghaile, T., Fan, Y., Madden, S. F., Klinger, R., O'Connor, A. E., . . . Gallagher, W. M. (2017). Therapeutic Rationale to Target Highly Expressed CDK7 Conferring Poor Outcomes in Triple-Negative Breast Cancer. Cancer Res, 77(14), 3834-3845. doi:10.1158/0008-5472.CAN-16-2546

Li, S., Garrett-Bakelman, F. E., Chung, S. S., Sanders, M. A., Hricik, T., Rapaport, F., . . . Mason, C. E. (2016). Distinct evolution and dynamics of epigenetic and genetic heterogeneity in acute myeloid leukemia. *Nat Med, 22*(7), 792-799. doi:10.1038/nm.4125

Li, Y., Yang, X. H., Fang, S. J., Qin, C. F., Sun, R. L., Liu, Z. Y., . . . Li, G. (2015). HOXA7 stimulates human hepatocellular carcinoma proliferation through cyclin E1/CDK2. *Oncol Rep, 33*(2), 990-996. doi:10.3892/or.2014.3668

Li, Z., Luo, R. T., Mi, S., Sun, M., Chen, P., Bao, J., . . . Thirman, M. J. (2009). Consistent deregulation of gene expression between human and murine MLL rearrangement leukemias. *Cancer Res, 69*(3), 1109-1116. doi:10.1158/0008-5472.CAN-08-3381

Liang, K., Gao, X., Gilmore, J. M., Florens, L., Washburn, M. P., Smith, E., & Shilatifard, A. (2015). Characterization of human cyclin-dependent kinase 12 (CDK12) and CDK13 complexes in C-terminal domain phosphorylation, gene transcription, and RNA processing. Mol Cell Biol, 35(6), 928-938. doi:10.1128/MCB.01426-14

Lin, K. H., Winter, P. S., Xie, A., Roth, C., Martz, C. A., Stein, E. M., . . . Wood, K. C. (2016). Targeting MCL-1/BCL-XL Forestalls the Acquisition of

Resistance to ABT-199 in Acute Myeloid Leukemia. *Sci Rep, 6*, 27696. doi:10.1038/srep27696

Lin, L. L., Hsu, C. L., Hu, C. W., Ko, S. Y., Hsieh, H. L., Huang, H. C., & Juan, H. F. (2015). Integrating Phosphoproteomics and Bioinformatics to Study Brassinosteroid-Regulated Phosphorylation Dynamics in Arabidopsis. *BMC Genomics, 16*, 533. doi:10.1186/s12864-015-1753-4

Linnekin, D. (1999). Early signaling pathways activated by c-Kit in hematopoietic cells. *Int J Biochem Cell Biol, 31*(10), 1053-1074.

Liu, C. W., Wang, R. H., Dohadwala, M., Schönthal, A. H., Villa-Moruzzi, E., & Berndt, N. (1999). Inhibitory phosphorylation of PP1alpha catalytic subunit during the G(1)/S transition. *J Biol Chem, 274*(41), 29470-29475. doi:10.1074/jbc.274.41.29470

Liu, E., Li, X., Yan, F., Zhao, Q., & Wu, X. (2004). Cyclin-dependent kinases phosphorylate human Cdt1 and induce its degradation. *J Biol Chem, 279*(17), 17283-17288. doi:10.1074/jbc.C300549200

Liu, H., Cheng, E. H., & Hsieh, J. J. (2009). MLL fusions: pathways to leukemia. *Cancer Biol Ther, 8*(13), 1204-1211. doi:10.4161/cbt.8.13.8924

Liu, H., Li, Z., Huo, S., Wei, Q., & Ge, L. (2020). Induction of G0/G1 phase arrest and apoptosis by CRISPR/Cas9-mediated knockout of CDK2 in A375 melanocytes. *Mol Clin Oncol, 12*(1), 9-14. doi:10.3892/mco.2019.1952

Liu, Y., & Chance, M. R. (2014). Integrating phosphoproteomics in systems biology. *Comput Struct Biotechnol J, 10*(17), 90-97. doi:10.1016/j.csbj.2014.07.003

Liu, Z. G., Hsu, H., Goeddel, D. V., & Karin, M. (1996). Dissection of TNF receptor 1 effector functions: JNK activation is not linked to apoptosis while NF-kappaB activation prevents cell death. *Cell, 87*(3), 565-576. doi:10.1016/s0092-8674(00)81375-6

Lo-Coco, F., Cimino, G., Breccia, M., Noguera, N. I., Diverio, D., Finolezzi, E., . . . Mandelli, F. (2004). Gemtuzumab ozogamicin (Mylotarg) as a single agent for molecularly relapsed acute promyelocytic leukemia. *Blood, 104*(7), 1995-1999. doi:10.1182/blood-2004-04-1550

Longo, P. G., Laurenti, L., Gobessi, S., Sica, S., Leone, G., & Efremov, D. G. (2008). The Akt/Mcl-1 pathway plays a prominent role in mediating antiapoptotic signals downstream of the B-cell receptor in chronic lymphocytic leukemia B cells. *Blood, 111*(2), 846-855. doi:10.1182/blood-2007-05-089037

Loriot, Y., Mordant, P., Dugue, D., Geneste, O., Gombos, A., Opolon, P., . . . Deutsch, E. (2014). Radiosensitization by a novel Bcl-2 and Bcl-XL inhibitor S44563 in small-cell lung cancer. *Cell Death Dis, 5*, e1423. doi:10.1038/cddis.2014.365

Loyer, P., Cariou, S., Glaise, D., Bilodeau, M., Baffet, G., & Guguen-Guillouzo, C. (1996). Growth factor dependence of progression through G1 and S phases of adult rat hepatocytes in vitro. Evidence of a mitogen restriction point in mid-late G1. *J Biol Chem, 271*(19), 11484-11492. doi:10.1074/jbc.271.19.11484

Lu, Z., & Hunter, T. (2014). Prolyl isomerase Pin1 in cancer. *Cell Res, 24*(9), 1033-1049. doi:10.1038/cr.2014.109

Lücking, U., Scholz, A., Lienau, P., Siemeister, G., Kosemund, D., Bohlmann, R., . . . Brands, M. (2017). Identification of Atuveciclib (BAY 1143572), the First Highly Selective, Clinical PTEFb/CDK9 Inhibitor for the Treatment of Cancer. *ChemMedChem, 12*(21), 1776-1793. doi:10.1002/cmdc.201700447

Luis, T. C., Naber, B. A., Roozen, P. P., Brugman, M. H., de Haas, E. F., Ghazvini, M., . . . Staal, F. J. (2011). Canonical wnt signaling regulates hematopoiesis in a dosage-dependent fashion. *Cell Stem Cell, 9*(4), 345-356. doi:10.1016/j.stem.2011.07.017

Lund, K., Cole, J. J., VanderKraats, N. D., McBryan, T., Pchelintsev, N. A., Clark, W., . . . Adams, P. D. (2014). DNMT inhibitors reverse a specific signature of aberrant promoter DNA methylation and associated gene silencing in AML. *Genome Biol, 15*(8), 406. doi:10.1186/s13059-014-0406-2

Luskin, M. R., & Stone, R. M. (2017). Can Minimal Residual Disease Determination in Acute Myeloid Leukemia Be Used in Clinical Practice? *J Oncol Pract, 13*(8), 471-480. doi:10.1200/JOP.2017.021675

Ma, H., Seebacher, N. A., Hornicek, F. J., & Duan, Z. (2019). Cyclin-dependent kinase 9 (CDK9) is a novel prognostic marker and therapeutic target in osteosarcoma. *EBioMedicine, 39*, 182-193. doi:10.1016/j.ebiom.2018.12.022

Ma, T., Van Tine, B. A., Wei, Y., Garrett, M. D., Nelson, D., Adams, P. D., . . . Harper, J. W. (2000). Cell cycle-regulated phosphorylation of p220(NPAT) by cyclin E/Cdk2 in Cajal bodies promotes histone gene transcription. *Genes Dev, 14*(18), 2298-2313. doi:10.1101/gad.829500

Ma, Z., Wu, Y., Jin, J., Yan, J., Kuang, S., Zhou, M., . . . Guo, A. Y. (2013). Phylogenetic analysis reveals the evolution and diversification of cyclins in eukaryotes. *Mol Phylogenet Evol, 66*(3), 1002-1010. doi:10.1016/j.ympev.2012.12.007

MacCallum, D. E., Melville, J., Frame, S., Watt, K., Anderson, S., Gianella-Borradori, A., . . . Green, S. R. (2005). Seliciclib (CYC202, R-Roscovitine) induces cell death in multiple myeloma cells by inhibition of RNA polymerase II-dependent transcription and down-regulation of Mcl-1. *Cancer Res, 65*(12), 5399-5407. doi:10.1158/0008-5472.CAN-05-0233

Maheswaran, S., Park, S., Bernard, A., Morris, J. F., Rauscher, F. J., Hill, D. E., & Haber, D. A. (1993). Physical and functional interaction between WT1 and p53 proteins. *Proc Natl Acad Sci U S A, 90*(11), 5100-5104. doi:10.1073/pnas.90.11.5100

Mailand, N., & Diffley, J. F. (2005). CDKs promote DNA replication origin licensing in human cells by protecting Cdc6 from APC/C-dependent proteolysis. *Cell, 122*(6), 915-926. doi:10.1016/j.cell.2005.08.013

Malaise, M., Steinbach, D., & Corbacioglu, S. (2009). Clinical implications of c-Kit mutations in acute myelogenous leukemia. *Curr Hematol Malig Rep, 4*(2), 77-82. doi:10.1007/s11899-009-0011-8

Mallo, M., & Alonso, C. R. (2013). The regulation of Hox gene expression during animal development. *Development, 140*(19), 3951-3963. doi:10.1242/dev.068346

Malumbres, M. (2014). Cyclin-dependent kinases. Genome Biol, 15(6), 122. doi:10.1186/gb4184

Malumbres, M., & Barbacid, M. (2001). To cycle or not to cycle: a critical decision in cancer. *Nat Rev Cancer, 1*(3), 222-231. doi:10.1038/35106065

Malumbres, M., & Barbacid, M. (2009). Cell cycle, CDKs and cancer: a changing paradigm. *Nat Rev Cancer, 9*(3), 153-166. doi:10.1038/nrc2602

Marais, A., Ji, Z., Child, E. S., Krause, E., Mann, D. J., & Sharrocks, A. D. (2010). Cell cycle-dependent regulation of the forkhead transcription factor FOXK2 by CDK·cyclin complexes. J Biol Chem, 285(46), 35728-35739. doi:10.1074/jbc.M110.154005

Marcucci, G., Metzeler, K. H., Schwind, S., Becker, H., Maharry, K., Mrózek, K., . . . Bloomfield, C. D. (2012). Age-related prognostic impact of different types of DNMT3A mutations in adults with primary cytogenetically normal acute myeloid leukemia. *J Clin Oncol, 30*(7), 742-750. doi:10.1200/JCO.2011.39.2092

Masala, E., Valencia, A. B., Sanna, A., Brogi, A., Zaroili, L., & Santini, V. (2016). *Resistance to Azacitidine Is Determined at Cellular Level By Lower Expression of Nucleoside Metabolizing Enzymes*. Paper presented at the 58th ASH annual meeting, Washington, D.C. http://www.bloodjournal.org/content/128/22/5129?sso-checked=true

Mateyak, M. K., Obaya, A. J., & Sedivy, J. M. (1999). c-Myc regulates cyclin D-Cdk4 and -Cdk6 activity but affects cell cycle progression at multiple independent points. *Mol Cell Biol, 19*(7), 4672-4683. doi:10.1128/mcb.19.7.4672

Maton, A., Hopkins, J. J., LaHart, S., Quon, W. D., Wright, M., & Jill, D. (1997). *Cells: Building Blocks of Life*. Upper Saddle River, NJ: Prentice Hall.

Maurer, U., Charvet, C., Wagman, A. S., Dejardin, E., & Green, D. R. (2006). Glycogen synthase kinase-3 regulates mitochondrial outer membrane permeabilization and apoptosis by destabilization of MCL-1. *Mol Cell, 21*(6), 749-760. doi:10.1016/j.molcel.2006.02.009

Mawad, R., Becker, P. S., Hendrie, P., Scott, B., Wood, B. L., Dean, C., . . . Pagel, J. M. (2016). Phase II study of tosedostat with cytarabine or decitabine in newly diagnosed older patients with acute myeloid leukaemia or high-risk MDS. *Br J Haematol, 172*(2), 238-245. doi:10.1111/bjh.13829

Mayer, L. D., Harasym, T. O., Tardi, P. G., Harasym, N. L., Shew, C. R., Johnstone, S. A., . . . Janoff, A. S. (2006). Ratiometric dosing of anticancer drug combinations: controlling drug ratios after systemic administration regulates therapeutic activity in tumor-bearing mice. *Mol Cancer Ther, 5*(7), 1854-1863. doi:10.1158/1535-7163.MCT-06-0118

Mead, A. J., Linch, D. C., Hills, R. K., Wheatley, K., Burnett, A. K., & Gale, R. E. (2007). FLT3 tyrosine kinase domain mutations are biologically distinct from and have a significantly more favorable prognosis than FLT3 internal tandem duplications in patients with acute myeloid leukemia. *Blood, 110*(4), 1262-1270. doi:10.1182/blood-2006-04-015826

Medeiros, B. C., Fathi, A. T., DiNardo, C. D., Pollyea, D. A., Chan, S. M., & Swords, R. (2017). Isocitrate dehydrogenase mutations in myeloid malignancies. *Leukemia, 31*(2), 272-281. doi:10.1038/leu.2016.275

Mehta, G. D., Kumar, R., Srivastava, S., & Ghosh, S. K. (2013). Cohesin: functions beyond sister chromatid cohesion. *FEBS Lett, 587*(15), 2299-2312. doi:10.1016/j.febslet.2013.06.035

Metcalf, D. (2007). On hematopoietic stem cell fate. *Immunity, 26*(6), 669-673. doi:10.1016/j.immuni.2007.05.012

Meyer, C., Hofmann, J., Burmeister, T., Gröger, D., Park, T. S., Emerenciano, M., . . . Marschalek, R. (2013). The MLL recombinome of acute leukemias in 2013. *Leukemia, 27*(11), 2165-2176. doi:10.1038/leu.2013.135

Micheau, O., & Tschopp, J. (2003). Induction of TNF receptor I-mediated apoptosis via two sequential signaling complexes. *Cell, 114*(2), 181-190. doi:10.1016/s0092-8674(03)00521-x

Michels, J., O'Neill, J. W., Dallman, C. L., Mouzakiti, A., Habens, F., Brimmell, M., . . . Packham, G. (2004). Mcl-1 is required for Akata6 B-lymphoma cell survival and is converted to a cell death molecule by efficient caspase-

mediated cleavage. *Oncogene, 23*(28), 4818-4827. doi:10.1038/sj.onc.1207648

Min, C., Moore, N., Shearstone, J. R., Quayle, S. N., Huang, P., van Duzer, J. H., . . . Yang, M. (2017). Selective Inhibitors of Histone Deacetylases 1 and 2 Synergize with Azacitidine in Acute Myeloid Leukemia. *PLoS One, 12*(1), e0169128. doi:10.1371/journal.pone.0169128

Mirza, K. M. (2019). Hematopoiesis. In E. Keohane, C. Otto, & J. Walenga (Eds.), *Rodak's Hematology: Clinical Principles and Applications* (6th ed., pp. 43-61). St. Louis, Missouri: Elsevier/Saunders.

Mishra, B. P., Zaffuto, K. M., Artinger, E. L., Org, T., Mikkola, H. K., Cheng, C., . . . Ernst, P. (2014). The histone methyltransferase activity of MLL1 is dispensable for hematopoiesis and leukemogenesis. *Cell Rep, 7*(4), 1239-1247. doi:10.1016/j.celrep.2014.04.015

Molenaar, J. J., Ebus, M. E., Geerts, D., Koster, J., Lamers, F., Valentijn, L. J., . . . Caron, H. N. (2009). Inactivation of CDK2 is synthetically lethal to MYCN over-expressing cancer cells. *Proc Natl Acad Sci U S A, 106*(31), 12968-12973. doi:10.1073/pnas.0901418106

MOLM-13. (2019). Retrieved from https://www.dsmz.de/collection/catalogue/details/culture/ACC-554

Montagnoli, A., Valsasina, B., Croci, V., Menichincheri, M., Rainoldi, S., Marchesi, V., . . . Santocanale, C. (2008). A Cdc7 kinase inhibitor restricts initiation of DNA replication and has antitumor activity. *Nat Chem Biol, 4*(6), 357-365. doi:10.1038/nchembio.90

Moore, H. E., Davenport, E. L., Smith, E. M., Muralikrishnan, S., Dunlop, A. S., Walker, B. A., . . . Davies, F. E. (2009). Aminopeptidase inhibition as a targeted treatment strategy in myeloma. *Mol Cancer Ther, 8*(4), 762-770. doi:10.1158/1535-7163.MCT-08-0735

Morales, F., & Giordano, A. (2016). Overview of CDK9 as a target in cancer research. *Cell Cycle, 15*(4), 519-527. doi:10.1080/15384101.2016.1138186

Moreira, J., Noé, G., Rangarajan, S., Courtin, C., Etain, B., Geoffroy, P. A., . . . Marie-Claire, C. (2018). Lithium effects on serine-threonine kinases activity: High throughput kinomic profiling of lymphoblastoid cell lines from excellent-responders and non-responders bipolar patients. *World J Biol Psychiatry*, 1-8. doi:10.1080/15622975.2018.1487078

Morita, K., Suzuki, K., Maeda, S., Matsuo, A., Mitsuda, Y., Tokushige, C., . . . Kamikubo, Y. (2017). Genetic regulation of the RUNX transcription factor family has antitumor effects. *J Clin Invest, 127*(7), 2815-2828. doi:10.1172/JCI91788

Mueller, D., Bach, C., Zeisig, D., Garcia-Cuellar, M. P., Monroe, S., Sreekumar, A., . . . Slany, R. K. (2007). A role for the MLL fusion partner ENL in transcriptional elongation and chromatin modification. *Blood, 110*(13), 4445-4454. doi:10.1182/blood-2007-05-090514

MV4-11. (2019). Retrieved from https://www.lgcstandards-atcc.org/Products/All/CRL-9591.aspx?geo_country=gb

Naik, S. H., Perié, L., Swart, E., Gerlach, C., van Rooij, N., de Boer, R. J., & Schumacher, T. N. (2013). Diverse and heritable lineage imprinting of early haematopoietic progenitors. *Nature, 496*(7444), 229-232. doi:10.1038/nature12013

Nalepa, G., Barnholtz-Sloan, J., Enzor, R., Dey, D., He, Y., Gehlhausen, J. R., . . . Clapp, W. (2013). The tumor suppressor CDKN3 controls mitosis. *J Cell Biol, 201*(7), 997-1012. doi:10.1083/jcb.201205125

Narita, T., Ishida, T., Ito, A., Masaki, A., Kinoshita, S., Suzuki, S., . . . Iida, S. (2017). Cyclin-dependent kinase 9 is a novel specific molecular target in adult T-cell leukemia/lymphoma. *Blood, 130*(9), 1114-1124. doi:10.1182/blood-2016-09-741983

Nasa, I., & Kettenbach, A. N. (2018). Coordination of Protein Kinase and Phosphoprotein Phosphatase Activities in Mitosis. *Front Cell Dev Biol, 6*, 30. doi:10.3389/fcell.2018.00030

Neganova, I., Vilella, F., Atkinson, S. P., Lloret, M., Passos, J. F., von Zglinicki, T., . . . Lako, M. (2011). An important role for CDK2 in G1 to S checkpoint activation and DNA damage response in human embryonic stem cells. *Stem Cells, 29*(4), 651-659. doi:10.1002/stem.620

Nekhai, S., Petukhov, M., & Breuer, D. (2014). Regulation of CDK9 activity by phosphorylation and dephosphorylation. *Biomed Res Int, 2014*, 964964. doi:10.1155/2014/964964

Nelson, D. A., Krucher, N. A., & Ludlow, J. W. (1997). High molecular weight protein phosphatase type 1 dephosphorylates the retinoblastoma protein. *J Biol Chem, 272*(7), 4528-4535. doi:10.1074/jbc.272.7.4528

Nelson, D. M., Joseph, B., Hillion, J., Segal, J., Karp, J. E., & Resar, L. M. (2011). Flavopiridol induces BCL-2 expression and represses oncogenic transcription factors in leukemic blasts from adults with refractory acute myeloid leukemia. *Leuk Lymphoma, 52*(10), 1999-2006. doi:10.3109/10428194.2011.591012

Némati, F., de Montrion, C., Lang, G., Kraus-Berthier, L., Carita, G., Sastre-Garau, X., . . . Decaudin, D. (2014). Targeting Bcl-2/Bcl-XL induces antitumor activity in uveal melanoma patient-derived xenografts. *PLoS One, 9*(1), e80836. doi:10.1371/journal.pone.0080836

Nemet, J., Jelicic, B., Rubelj, I., & Sopta, M. (2014). The two faces of Cdk8, a positive/negative regulator of transcription. Biochimie, 97, 22-27. doi:10.1016/j.biochi.2013.10.004

Nerlov, C. (2004). C/EBPalpha mutations in acute myeloid leukaemias. *Nat Rev Cancer, 4*(5), 394-400. doi:10.1038/nrc1363

Nguyen, M., Marcellus, R. C., Roulston, A., Watson, M., Serfass, L., Murthy Madiraju, S. R., . . . Shore, G. C. (2007). Small molecule obatoclax (GX15-070) antagonizes MCL-1 and overcomes MCL-1-mediated resistance to apoptosis. *Proc Natl Acad Sci U S A, 104*(49), 19512-19517. doi:10.1073/pnas.0709443104

NICE. (2018). Liposomal cytarabine and daunorubicin for untreated acute myeloid leukaemia.

Nigro, J. M., Baker, S. J., Preisinger, A. C., Jessup, J. M., Hostetter, R., Cleary, K., . . . Devilee, P. (1989). Mutations in the p53 gene occur in diverse human tumour types. *Nature, 342*(6250), 705-708. doi:10.1038/342705a0

NIHR. (2014). Azacitidine (Vidaza) for acute myeloid leukaemia – first line. Retrieved from http://www.io.nihr.ac.uk/report/azacitidine-vidaza-for-acute-myeloid-leukaemia-first-line/

Nikanjam, M., Capparelli, E. V., Lancet, J. E., Louie, A., & Schiller, G. (2018). Persistent cytarabine and daunorubicin exposure after administration of novel liposomal formulation CPX-351: population pharmacokinetic assessment. *Cancer Chemother Pharmacol, 81*(1), 171-178. doi:10.1007/s00280-017-3484-5

Nilsson, S. K., Johnston, H. M., Whitty, G. A., Williams, B., Webb, R. J., Denhardt, D. T., . . . Haylock, D. N. (2005). Osteopontin, a key component of the hematopoietic stem cell niche and regulator of

primitive hematopoietic progenitor cells. *Blood, 106*(4), 1232-1239. doi:10.1182/blood-2004-11-4422

Nita-Lazar, A., Saito-Benz, H., & White, F. M. (2008). Quantitative phosphoproteomics by mass spectrometry: past, present, and future. *Proteomics, 8*(21), 4433-4443. doi:10.1002/pmic.200800231

Noé, G., Bellesoeur, A., Golmard, L., Thomas-Schoemann, A., Boudou-Rouquette, P., Tiako Meyo, M., . . . Vidal, M. (2019). Differential Kinase Activation in Peripheral Blood Mononuclear Cells from Non-Small-Cell Lung Cancer Patients Treated with Nivolumab. *Cancers (Basel), 11*(6). doi:10.3390/cancers11060762

Notta, F., Zandi, S., Takayama, N., Dobson, S., Gan, O. I., Wilson, G., . . . Dick, J. E. (2016). Distinct routes of lineage development reshape the human blood hierarchy across ontogeny. *Science, 351*(6269), aab2116. doi:10.1126/science.aab2116

Ochsenbein, A. F., Riether, C., Bacher, U., Müller, R., Höpner, S., Banz, Y., . . . Pabst, T. (2018). Argx-110 Targeting CD70, in Combination with Azacitidine, Shows Favorable Safety Profile and Promising Anti-Leukemia Activity in Newly Diagnosed AML Patients in an Ongoing Phase 1/2 Clinical Trial. *Blood*(132), 2680.

OCI-AML3. (2019). Retrieved from https://www.dsmz.de/collection/catalogue/details/culture/ACC-582

O'Connor, C. (2008). Cell Division: Stages of Mitosis. Retrieved from https://www.nature.com/scitable/topicpage/mitosis-and-cell-division-205/#

Okabe, S., Tauchi, T., Tanaka, Y., Sakuta, J., & Ohyashiki, K. (2015). Efficacy of the polo-like kinase inhibitor rigosertib, alone or in combination with Abelson tyrosine kinase inhibitors, against break point cluster region-c-Abelson-positive leukemia cells. *Oncotarget, 6*(24), 20231-20240. doi:10.18632/oncotarget.4047

Okada, Y., Feng, Q., Lin, Y., Jiang, Q., Li, Y., Coffield, V. M., . . . Zhang, Y. (2005). hDOT1L links histone methylation to leukemogenesis. *Cell, 121*(2), 167-178. doi:10.1016/j.cell.2005.02.020

Okuda, M., Horn, H. F., Tarapore, P., Tokuyama, Y., Smulian, A. G., Chan, P. K., . . . Fukasawa, K. (2000). Nucleophosmin/B23 is a target of CDK2/cyclin E in centrosome duplication. *Cell, 103*(1), 127-140.

Oltersdorf, T., Elmore, S. W., Shoemaker, A. R., Armstrong, R. C., Augeri, D. J., Belli, B. A., . . . Rosenberg, S. H. (2005). An inhibitor of Bcl-2 family proteins induces regression of solid tumours. *Nature, 435*(7042), 677-681. doi:10.1038/nature03579

Ossenkoppele, G., & Schuurhuis, G. J. (2016). MRD in AML: does it already guide therapy decision-making? *Hematology Am Soc Hematol Educ Program, 2016*(1), 356-365. doi:10.1182/asheducation-2016.1.356

Ostronoff, F., Othus, M., Ho, P. A., Kutny, M., Geraghty, D. E., Petersdorf, S. H., . . . Meshinchi, S. (2013). Mutations in the DNMT3A exon 23 independently predict poor outcome in older patients with acute myeloid leukemia: a SWOG report. *Leukemia, 27*(1), 238-241. doi:10.1038/leu.2012.168

Othus, M., Sekeres, M. A., Nand, S., Garcia-Manero, G., Appelbaum, F. R., Erba, H. P., & Estey, E. H. (2016). Complete remissions (CRs) with Azacitidine regimens compared to CRs with 7+3 induction chemotherapy and the effect on overall survival. *Blood, 128*, 1613.

Ou, C. Y., Poon, V. Y., Maeder, C. I., Watanabe, S., Lehrman, E. K., Fu, A. K., . . . Shen, K. (2010). Two cyclin-dependent kinase pathways are essential

for polarized trafficking of presynaptic components. Cell, 141(5), 846-858. doi:10.1016/j.cell.2010.04.011

Ou-Yang, J., Huang, L. H., & Sun, X. X. (2017). Cyclin-Dependent Kinase 14 Promotes Cell Proliferation, Migration and Invasion in Ovarian Cancer by Inhibiting Wnt Signaling Pathway. Gynecol Obstet Invest, 82(3), 230-239. doi:10.1159/000447632

Pallis, M., Abdul-Aziz, A., Burrows, F., Seedhouse, C., Grundy, M., & Russell, N. (2012). The multi-kinase inhibitor TG02 overcomes signalling activation by survival factors to deplete MCL1 and XIAP and induce cell death in primary acute myeloid leukaemia cells. *Br J Haematol, 159*(2), 191-203. doi:10.1111/bjh.12018

Pallis, M., Burrows, F., Ryan, J., Grundy, M., Seedhouse, C., Abdul-Aziz, A., . . . Russell, N. (2017). Complementary dynamic BH3 profiles predict co-operativity between the multi-kinase inhibitor TG02 and the BH3 mimetic ABT-199 in acute myeloid leukaemia cells. *Oncotarget, 8*(10), 16220-16232. doi:10.18632/oncotarget.8742

Pallis, M., Burrows, F., Whittall, A., Boddy, N., Seedhouse, C., & Russell, N. (2013). Efficacy of RNA polymerase II inhibitors in targeting dormant leukaemia cells. *BMC Pharmacol Toxicol, 14*, 32. doi:10.1186/2050-6511-14-32

Palmer, A. (2017). Assessing drug synergy in combination therapies. Retrieved from http://lincs.hms.harvard.edu/wordpress/wp-content/uploads/2017/08/ICSB_Part3_Assessing_drug_combination.pdf

Pan, R., Hogdal, L. J., Benito, J. M., Bucci, D., Han, L., Borthakur, G., . . . Letai, A. G. (2014). Selective BCL-2 inhibition by ABT-199 causes on-target cell death in acute myeloid leukemia. *Cancer Discov, 4*(3), 362-375. doi:10.1158/2159-8290.CD-13-0609

Pan, Z. Q., Kentsis, A., Dias, D. C., Yamoah, K., & Wu, K. (2004). Nedd8 on cullin: building an expressway to protein destruction. *Oncogene, 23*(11), 1985-1997. doi:10.1038/sj.onc.1207414

Panicker, R. C., Sun, H., Chen, G. Y., & Yao, S. Q. (2009). Peptide-Based Microarray. In K. Dill, R. Liu, & P. Grodzinsky (Eds.), *Microarrays: Preparation, Microfluidics, Detection Methods, and Biological Applications* (pp. 139-168). New York, USA: Springer.

Papaemmanuil, E., Gerstung, M., Bullinger, L., Gaidzik, V. I., Paschka, P., Roberts, N. D., . . . Campbell, P. J. (2016). Genomic Classification and Prognosis in Acute Myeloid Leukemia. *N Engl J Med, 374*(23), 2209-2221. doi:10.1056/NEJMoa1516192

Parry, D., Guzi, T., Shanahan, F., Davis, N., Prabhavalkar, D., Wiswell, D., . . . Lees, E. M. (2010). Dinaciclib (SCH 727965), a novel and potent cyclin-dependent kinase inhibitor. *Mol Cancer Ther, 9*(8), 2344-2353. doi:10.1158/1535-7163.MCT-10-0324

Paschka, P., Marcucci, G., Ruppert, A. S., Mrózek, K., Chen, H., Kittles, R. A., . . . B, C. a. L. G. (2006). Adverse prognostic significance of KIT mutations in adult acute myeloid leukemia with inv(16) and t(8;21): a Cancer and Leukemia Group B Study. *J Clin Oncol, 24*(24), 3904-3911. doi:10.1200/JCO.2006.06.9500

Pedersen-Bjergaard, J., Christiansen, D. H., Desta, F., & Andersen, M. K. (2006). Alternative genetic pathways and cooperating genetic abnormalities in the pathogenesis of therapy-related myelodysplasia and acute myeloid leukemia. *Leukemia, 20*(11), 1943-1949. doi:10.1038/sj.leu.2404381

Pellerano, M., Tcherniuk, S., Perals, C., Ngoc Van, T. N., Garcin, E., Mahuteau-Betzer, F., . . . Morris, M. C. (2017). Targeting Conformational Activation of CDK2 Kinase. *Biotechnol J*. doi:10.1002/biot.201600531

Peppelenbosch, M. P. (2012). Kinome profiling. *Scientifica (Cairo), 2012*, 306798. doi:10.6064/2012/306798

PerkinElmer. (2020). LANCE TR-FRET. Retrieved from https://www.perkinelmer.com/lab-products-and-services/application-support-knowledgebase/lance/lance-tr-fret-kinase.html

Perl, A. E., Martinelli, G., Cortes, J. E., Neubauer, A., Berman, E., Paolini, S., . . . Levis, M. J. (2019). Gilteritinib or Chemotherapy for Relapsed or Refractory FLT3-Mutated AML. *N Engl J Med, 381*(18), 1728-1740. doi:10.1056/NEJMoa1902688

Perrotti, D., Iervolino, A., Cesi, V., Cirinná, M., Lombardini, S., Grassilli, E., . . . Calabretta, B. (2000). BCR-ABL prevents c-jun-mediated and proteasome-dependent FUS (TLS) proteolysis through a protein kinase CbetaII-dependent pathway. *Mol Cell Biol, 20*(16), 6159-6169. doi:10.1128/mcb.20.16.6159-6169.2000

Perry, M. J. (2008). *The Chemotherapy source book*. Philadelphia: Wolters Kluwer Health/Lippincott Williams & Wilkins.

Persad, S., Attwell, S., Gray, V., Mawji, N., Deng, J. T., Leung, D., . . . Dedhar, S. (2001). Regulation of protein kinase B/Akt-serine 473 phosphorylation by integrin-linked kinase: critical roles for kinase activity and amino acids arginine 211 and serine 343. *J Biol Chem, 276*(29), 27462-27469. doi:10.1074/jbc.M102940200

Peterlin, B. M., & Price, D. H. (2006). Controlling the elongation phase of transcription with P-TEFb. Mol Cell, 23(3), 297-305. doi:10.1016/j.molcel.2006.06.014

Petropoulos, S., Edsgärd, D., Reinius, B., Deng, Q., Panula, S. P., Codeluppi, S., . . . Lanner, F. (2016). Single-Cell RNA-Seq Reveals Lineage and X Chromosome Dynamics in Human Preimplantation Embryos. *Cell, 167*(1), 285. doi:10.1016/j.cell.2016.08.009

Phillips, D. C., Jin, S., Gregory, G. P., Zhang, Q., Xue, J., Zhao, X., . . . Souers, A. J. (2019). A novel CDK9 inhibitor increases the efficacy of venetoclax (ABT-199) in multiple models of hematologic malignancies. *Leukemia*. doi:10.1038/s41375-019-0652-0

Placke, T., Faber, K., Nonami, A., Putwain, S. L., Salih, H. R., Heidel, F. H., . . . Fröhling, S. (2014). Requirement for CDK6 in MLL-rearranged acute myeloid leukemia. *Blood, 124*(1), 13-23. doi:10.1182/blood-2014-02-558114

Ploemacher, R. E., van Os, R., van Beurden, C. A., & Down, J. D. (1992). Murine haemopoietic stem cells with long-term engraftment and marrow repopulating ability are more resistant to gamma-radiation than are spleen colony forming cells. *Int J Radiat Biol, 61*(4), 489-499. doi:10.1080/09553009214551251

Polier, G., Ding, J., Konkimalla, B. V., Eick, D., Ribeiro, N., Köhler, R., . . . Li-Weber, M. (2011). Wogonin and related natural flavones are inhibitors of CDK9 that induce apoptosis in cancer cells by transcriptional suppression of Mcl-1. *Cell Death Dis, 2*, e182. doi:10.1038/cddis.2011.66

Poon, I. K., Lucas, C. D., Rossi, A. G., & Ravichandran, K. S. (2014). Apoptotic cell clearance: basic biology and therapeutic potential. *Nat Rev Immunol, 14*(3), 166-180. doi:10.1038/nri3607

Poon, R. Y., & Hunter, T. (1995). Dephosphorylation of Cdk2 Thr160 by the cyclin-dependent kinase-interacting phosphatase KAP in the absence of cyclin. *Science, 270*(5233), 90-93. doi:10.1126/science.270.5233.90

Pozo, K., Castro-Rivera, E., Tan, C., Plattner, F., Schwach, G., Siegl, V., . . . Bibb, J. A. (2013). The role of Cdk5 in neuroendocrine thyroid cancer. Cancer Cell, 24(4), 499-511. doi:10.1016/j.ccr.2013.08.027

PPP1R10 gene. Retrieved from https://www.genecards.org/cgi-bin/carddisp.pl?gene=PPP1R10

Prebet, T., Sun, Z., Figueroa, M. E., Ketterling, R., Melnick, A., Greenberg, P. L., . . . Tallman, M. S. (2014). Prolonged administration of azacitidine with or without entinostat for myelodysplastic syndrome and acute myeloid leukemia with myelodysplasia-related changes: results of the US Leukemia Intergroup trial E1905. *J Clin Oncol, 32*(12), 1242-1248. doi:10.1200/JCO.2013.50.3102

Quek, L., David, M. D., Kennedy, A., Metzner, M., Amatangelo, M., Shih, A., . . . Vyas, P. (2018). Clonal heterogeneity of acute myeloid leukemia treated with the IDH2 inhibitor enasidenib. *Nat Med, 24*(8), 1167-1177. doi:10.1038/s41591-018-0115-6

Quek, L., Otto, G. W., Garnett, C., Lhermitte, L., Karamitros, D., Stoilova, B., . . . Vyas, P. (2016). Genetically distinct leukemic stem cells in human CD34- acute myeloid leukemia are arrested at a hemopoietic precursor-like stage. *J Exp Med, 213*(8), 1513-1535. doi:10.1084/jem.20151775

Quentmeier, H., Reinhardt, J., Zaborski, M., & Drexler, H. G. (2003). FLT3 mutations in acute myeloid leukemia cell lines. *Leukemia, 17*(1), 120-124. doi:10.1038/sj.leu.2402740

Quigley, J. G., Means, R. T., & Glader, B. (2014). The birth, life, and death of red blood cells: Erythropoiesis, the mature red blood cell, and cell destruction. In J. P. Greer, D. A. Arber, & B. Glader (Eds.), *Wintrobe's Clinical Hematology* (13th ed., pp. 83–124). Philadelphia: Wolters Kluwer Health/Lippincott Williams & Wilkins.

R&D. (2019). The Human Colony Forming Cell (CFC) Assay using Methylcellulose-based Media. Retrieved from https://www.rndsystems.com/resources/protocols/human-colony-forming-cell-cfc-assay-using-methylcellulose-based-media

Raje, N., Kumar, S., Hideshima, T., Roccaro, A., Ishitsuka, K., Yasui, H., . . . Anderson, K. C. (2005). Seliciclib (CYC202 or R-roscovitine), a small-molecule cyclin-dependent kinase inhibitor, mediates activity via down-regulation of Mcl-1 in multiple myeloma. *Blood, 106*(3), 1042-1047. doi:10.1182/blood-2005-01-0320

Rakheja, D., Konoplev, S., Medeiros, L. J., & Chen, W. (2012). IDH mutations in acute myeloid leukemia. *Hum Pathol, 43*(10), 1541-1551. doi:10.1016/j.humpath.2012.05.003

Rampal, R., & Figueroa, M. E. (2016). Wilms tumor 1 mutations in the pathogenesis of acute myeloid leukemia. *Haematologica, 101*(6), 672-679. doi:10.3324/haematol.2015.141796

Ramsey, H. E., Fischer, M. A., Lee, T., Gorska, A. E., Arrate, M. P., Fuller, L., . . . Savona, M. R. (2018). A Novel MCL1 Inhibitor Combined with Venetoclax Rescues Venetoclax-Resistant Acute Myelogenous Leukemia. *Cancer Discov, 8*(12), 1566-1581. doi:10.1158/2159-8290.CD-18-0140

Rao, X., Huang, X., Zhou, Z., & Lin, X. (2013). An improvement of the 2ˆ(-delta delta CT) method for quantitative real-time polymerase chain reaction data analysis. *Biostat Bioinforma Biomath, 3*(3), 71-85.

Rasmussen, M. L., Taneja, N., Neininger, A. C., Wang, L., Robertson, G. L., Riffle, S. N., . . . Gama, V. (2020). MCL-1 Inhibition by Selective BH3 Mimetics Disrupts Mitochondrial Dynamics Causing Loss of Viability and Functionality of Human Cardiomyocytes. *iScience, 23*(4), 101015. doi:10.1016/j.isci.2020.101015

Rauert-Wunderlich, H., Rudelius, M., Ott, G., & Rosenwald, A. (2016). Targeting protein kinase C in mantle cell lymphoma. *Br J Haematol, 173*(3), 394-403. doi:10.1111/bjh.13973

Ravandi, F., Kantarjian, H., Faderl, S., Garcia-Manero, G., O'Brien, S., Koller, C., . . . Beran, M. (2010). Outcome of patients with FLT3-mutated acute myeloid leukemia in first relapse. *Leuk Res, 34*(6), 752-756. doi:10.1016/j.leukres.2009.10.001

Ravandi, F., Walter, R. B., & Freeman, S. D. (2018). Evaluating measurable residual disease in acute myeloid leukemia. *Blood Adv, 2*(11), 1356-1366. doi:10.1182/bloodadvances.2018016378

Reactionbiology. (2020). Kinase Assays: 600+ Kinases Assays Available for HTS and Profiling. Retrieved from http://reactionbiology.com/webapps/site/kinaseassay.aspx?gclid=Cj0KCQiAmsrxBRDaARIsANyiD1p32K_MxxolKC54RcoXE5-ZFWEI8cPV65b9IJPZr4FvXoga1HB-dcIaArtTEALw_wcB

Read, A. P., & Strachan, T. (1999). Cancer Genetics. In *Human Molecular Genetics 2*. New York: Wiley.

Ren, S., & Rollins, B. J. (2004). Cyclin C/cdk3 promotes Rb-dependent G0 exit. *Cell, 117*(2), 239-251. doi:10.1016/s0092-8674(04)00300-9

Renatus, M., Stennicke, H. R., Scott, F. L., Liddington, R. C., & Salvesen, G. S. (2001). Dimer formation drives the activation of the cell death protease caspase 9. *Proc Natl Acad Sci U S A, 98*(25), 14250-14255. doi:10.1073/pnas.231465798

Renault, T. T., & Chipuk, J. E. (2014). Death upon a kiss: mitochondrial outer membrane composition and organelle communication govern sensitivity to BAK/BAX-dependent apoptosis. *Chem Biol, 21*(1), 114-123. doi:10.1016/j.chembiol.2013.10.009

Renner, A. G., Dos Santos, C., Recher, C., Bailly, C., Créancier, L., Kruczynski, A., . . . Manenti, S. (2009). Polo-like kinase 1 is overexpressed in acute myeloid leukemia and its inhibition preferentially targets the proliferation of leukemic cells. *Blood, 114*(3), 659-662. doi:10.1182/blood-2008-12-195867

Richard-Carpentier, G., & DiNardo, C. D. (2019). Single-agent and combination biologics in acute myeloid leukemia. *Hematology Am Soc Hematol Educ Program, 2019*(1), 548-556. doi:10.1182/hematology.2019000059

Riether, C., Schürch, C. M., Bührer, E. D., Hinterbrandner, M., Huguenin, A. L., Hoepner, S., . . . Ochsenbein, A. F. (2017). CD70/CD27 signaling promotes blast stemness and is a viable therapeutic target in acute myeloid leukemia. *J Exp Med, 214*(2), 359-380. doi:10.1084/jem.20152008

Rishi, L., Hannon, M., Salomè, M., Hasemann, M., Frank, A. K., Campos, J., . . . Keeshan, K. (2014). Regulation of Trib2 by an E2F1-C/EBPα feedback loop in AML cell proliferation. *Blood, 123*(15), 2389-2400. doi:10.1182/blood-2013-07-511683

Robb, C. M., Kour, S., Contreras, J. I., Agarwal, E., Barger, C. J., Rana, S., . . . Natarajan, A. (2018). Characterization of CDK(5) inhibitor, 20-223 (aka CP668863) for colorectal cancer therapy. *Oncotarget, 9*(4), 5216-5232. doi:10.18632/oncotarget.23749

Roboz, G. J., Rosenblat, T., Arellano, M., Gobbi, M., Altman, J. K., Montesinos, P., . . . Giles, F. J. (2014). International randomized phase III study of elacytarabine versus investigator choice in patients with relapsed/refractory acute myeloid leukemia. *J Clin Oncol, 32*(18), 1919-1926. doi:10.1200/JCO.2013.52.8562

Rödling, L., Schwedhelm, I., Kraus, S., Bieback, K., Hansmann, J., & Lee-Thedieck, C. (2017). 3D models of the hematopoietic stem cell niche under steady-state and active conditions. *Sci Rep, 7*(1), 4625. doi:10.1038/s41598-017-04808-0

Rogatsky, I., Trowbridge, J. M., & Garabedian, M. J. (1999). Potentiation of human estrogen receptor alpha transcriptional activation through phosphorylation of serines 104 and 106 by the cyclin A-CDK2 complex. *J Biol Chem, 274*(32), 22296-22302. doi:10.1074/jbc.274.32.22296

Romesser, P. B., Perlman, D. H., Faller, D. V., Costello, C. E., McComb, M. E., & Denis, G. V. (2009). Development of a malignancy-associated proteomic signature for diffuse large B-cell lymphoma. *Am J Pathol, 175*(1), 25-35. doi:10.2353/ajpath.2009.080707

Rong, C., Yuling, C., Sheelagh, F., David, B., G., W. W., Daniella, Z., & William, P. (2018). *Strategic combination of the cyclin-dependent kinase inhibitor CYC065 with venetoclax to target anti-apoptotic proteins in chronic lymphocytic leukemia.* Paper presented at the AACR Annual Meeting 2018, Chicago, Illinois, the USA.

Rong, Y., Cheng, L., Ning, H., Zou, J., Zhang, Y., Xu, F., . . . Fu, X. Y. (2006). Wilms' tumor 1 and signal transducers and activators of transcription 3 synergistically promote cell proliferation: a possible mechanism in sporadic Wilms' tumor. *Cancer Res, 66*(16), 8049-8057. doi:10.1158/0008-5472.CAN-06-1172

Rosenberger, A. F., Hilhorst, R., Coart, E., García Barrado, L., Naji, F., Rozemuller, A. J., . . . van der Vies, S. M. (2016). Protein Kinase Activity Decreases with Higher Braak Stages of Alzheimer's Disease Pathology. *J Alzheimers Dis, 49*(4), 927-943. doi:10.3233/JAD-150429

Roskoski, R. (2012). ERK1/2 MAP kinases: structure, function, and regulation. *Pharmacol Res, 66*(2), 105-143. doi:10.1016/j.phrs.2012.04.005

Rossmann, M. P., Orkin, S. H., & Chute, J. P. (2018). Hematopoietic stem cell biology. In R. Hoffman, E. J. Benz, & L. E. Silberstein (Eds.), *Hematology Basic Principles and Practice* (7th ed., pp. 95-110). Philadelphia: Elsevier.

Ruvolo, P. P., Deng, X., Carr, B. K., & May, W. S. (1998). A functional role for mitochondrial protein kinase Calpha in Bcl2 phosphorylation and suppression of apoptosis. *J Biol Chem, 273*(39), 25436-25442. doi:10.1074/jbc.273.39.25436

Salem, B., Miner, S., Hensel, N. F., Battiwalla, M., Keyvanfar, K., Stroncek, D. F., . . . Barrett, A. J. (2015). Quantitative activation suppression assay to evaluate human bone marrow-derived mesenchymal stromal cell potency. *Cytotherapy, 17*(12), 1675-1686. doi:10.1016/j.jcyt.2015.08.008

Samali, A., Zhivotovsky, B., Jones, D., Nagata, S., & Orrenius, S. (1999). Apoptosis: cell death defined by caspase activation. *Cell Death Differ, 6*(6), 495-496. doi:10.1038/sj.cdd.4400520

Santo, L., Siu, K. T., & Raje, N. (2015). Targeting Cyclin-Dependent Kinases and Cell Cycle Progression in Human Cancers. *Semin Oncol, 42*(6), 788-800. doi:10.1053/j.seminoncol.2015.09.024

Sari, I. N., Phi, L. T. H., Jun, N., Wijaya, Y. T., Lee, S., & Kwon, H. Y. (2018). Hedgehog Signaling in Cancer: A Prospective Therapeutic Target for Eradicating Cancer Stem Cells. *Cells, 7*(11). doi:10.3390/cells7110208

Sato, H., Wheat, J. C., Steidl, U., & Ito, K. (2016). DNMT3A and TET2 in the Pre-Leukemic Phase of Hematopoietic Disorders. *Front Oncol, 6*, 187. doi:10.3389/fonc.2016.00187

Schmalbrock, L. K., Bonifacio, L., Bill, M., Jentzsch, M., Schubert, K., Grimm, J., . . . Schwind, S. (2018). Prognostic relevance of DNMT3A R882 mutations in AML patients undergoing non-myeloablative conditioning hematopoietic stem cell transplantation. *Bone Marrow Transplant, 53*(5), 640-643. doi:10.1038/s41409-017-0060-x

Schmidt, M., Rohe, A., Platzer, C., Najjar, A., Erdmann, F., & Sippl, W. (2017). Regulation of G2/M Transition by Inhibition of WEE1 and PKMYT1 Kinases. *Molecules, 22*(12). doi:10.3390/molecules22122045

Scholz, A., Oellerich, T., Hussain, A., Lindner, S., Luecking, U., & Walter, A. O. (2016). BAY 1143572, a first-in-class, highly selective, potent and orally available inhibitor of PTEFb/CDK9 currently in Phase I, shows convincing antitumor activity in preclinical models of acute myeloid leukemia (AML) [abstract]. *Cancer Res*(76).

Schütze, S., Tchikov, V., & Schneider-Brachert, W. (2008). Regulation of TNFR1 and CD95 signalling by receptor compartmentalization. *Nat Rev Mol Cell Biol, 9*(8), 655-662. doi:10.1038/nrm2430

Schuurhuis, G. J., Heuser, M., Freeman, S., Béné, M. C., Buccisano, F., Cloos, J., . . . Ossenkoppele, G. J. (2018). Minimal/measurable residual disease in AML: a consensus document from the European LeukemiaNet MRD Working Party. *Blood, 131*(12), 1275-1291. doi:10.1182/blood-2017-09-801498

Schwartz, G. W., Manning, B., Zhou, Y., Velu, P., Bigdeli, A., Astles, R., . . . Faryabi, R. B. (2019). Classes of ITD Predict Outcomes in AML Patients Treated with FLT3 Inhibitors. *Clin Cancer Res, 25*(2), 573-583. doi:10.1158/1078-0432.CCR-18-0655

Scorrano, L., Ashiya, M., Buttle, K., Weiler, S., Oakes, S. A., Mannella, C. A., & Korsmeyer, S. J. (2002). A distinct pathway remodels mitochondrial cristae and mobilizes cytochrome c during apoptosis. *Dev Cell, 2*(1), 55-67. doi:10.1016/s1534-5807(01)00116-2

Sedlacek, H. H. (2001). Mechanisms of action of flavopiridol. *Crit Rev Oncol Hematol, 38*(2), 139-170. doi:10.1016/s1040-8428(00)00124-4

SEER. (2015). Cancer Stat Facts: Leukemia - Acute Myeloid Leukemia (AML). Retrieved from https://seer.cancer.gov/statfacts/html/amyl.html

Segawa, K., Kurata, S., Yanagihashi, Y., Brummelkamp, T. R., Matsuda, F., & Nagata, S. (2014). Caspase-mediated cleavage of phospholipid flippase for apoptotic phosphatidylserine exposure. *Science, 344*(6188), 1164-1168. doi:10.1126/science.1252809

Shafer, D., & Grant, S. (2016). Update on rational targeted therapy in AML. *Blood Rev, 30*(4), 275-283. doi:10.1016/j.blre.2016.02.001

Shapiro, G. I. (2006). Cyclin-dependent kinase pathways as targets for cancer treatment. *J Clin Oncol, 24*(11), 1770-1783. doi:10.1200/JCO.2005.03.7689

Shchemelinin, I., Sefc, L., & Necas, E. (2006). Protein kinases, their function and implication in cancer and other diseases. *Folia Biol (Praha), 52*(3), 81-100.

Sheldon, L. A. (2017). Inhibition of E2F1 activity and cell cycle progression by arsenic via retinoblastoma protein. *Cell Cycle, 16*(21), 2058-2072. doi:10.1080/15384101.2017.1338221

Shen, C. (2019). Nucleic Acids: DNA and RNA. In C. Shen (Ed.), *Diagnostic Molecular Biology* (pp. 1-25): Academic press.

Sherr, C. J. (2006). Divorcing ARF and p53: an unsettled case. *Nat Rev Cancer, 6*(9), 663-673. doi:10.1038/nrc1954

Sherr, C. J., & Roberts, J. M. (1999). CDK inhibitors: positive and negative regulators of G1-phase progression. *Genes Dev, 13*(12), 1501-1512. doi:10.1101/gad.13.12.1501

Shiraishi, Y., Fujimoto, A., Furuta, M., Tanaka, H., Chiba, K., Boroevich, K. A., . . . Nakagawa, H. (2014). Integrated analysis of whole genome and transcriptome sequencing reveals diverse transcriptomic aberrations driven by somatic genomic changes in liver cancers. PLoS One, 9(12), e114263. doi:10.1371/journal.pone.0114263

Shuker, S. B., Hajduk, P. J., Meadows, R. P., & Fesik, S. W. (1996). Discovering high-affinity ligands for proteins: SAR by NMR. *Science, 274*(5292), 1531-1534. doi:10.1126/science.274.5292.1531

Siemeister, G., Lücking, U., Wengner, A. M., Lienau, P., Steinke, W., Schatz, C., . . . Ziegelbauer, K. (2012). BAY 1000394, a novel cyclin-dependent kinase inhibitor, with potent antitumor activity in mono- and in combination treatment upon oral application. *Mol Cancer Ther, 11*(10), 2265-2273. doi:10.1158/1535-7163.MCT-12-0286

Skvara, H., Dawid, M., Kleyn, E., Wolff, B., Meingassner, J. G., Knight, H., . . . Jung, T. (2008). The PKC inhibitor AEB071 may be a therapeutic option for psoriasis. *J Clin Invest, 118*(9), 3151-3159. doi:10.1172/JCI35636

Slee, E. A., Adrain, C., & Martin, S. J. (2001). Executioner caspase-3, -6, and -7 perform distinct, non-redundant roles during the demolition phase of apoptosis. *J Biol Chem, 276*(10), 7320-7326. doi:10.1074/jbc.M008363200

Smith, A. M., LaValle, T., Ketkar, S., Ramakrishnan, S. M., Miller, C. A., & Ley, T. J. (2019). $DNMT3A^{R882}$ alters the epigenome of hematopoietic cells. *Blood, 134*.

Smith, B. D., Warner, S. L., C., W., A., S.-J., Bahr, B., & Dettman, E. (2015). An alvocidib-containing regimen is highly effective in AML patients through a mechanism dependent on MCL1 expression and function [abstract]. *J Clin Oncol*(33).

Smitheman, K. N., Severson, T. M., Rajapurkar, S. R., McCabe, M. T., Karpinich, N., Foley, J., . . . Mohammad, H. P. (2019). Lysine specific demethylase 1 inactivation enhances differentiation and promotes cytotoxic response when combined with all-. *Haematologica, 104*(6), 1156-1167. doi:10.3324/haematol.2018.199190

Song, B., Liu, X. S., & Liu, X. (2012). Polo-like kinase 1 (Plk1): an Unexpected Player in DNA Replication. *Cell Div, 7*, 3. doi:10.1186/1747-1028-7-3

Song, T., Wang, P., Yu, X., Wang, A., Chai, G., Fan, Y., & Zhang, Z. (2019). Systems analysis of phosphorylation-regulated Bcl-2 interactions establishes a model to reconcile the controversy over the significance of Bcl-2 phosphorylation. *Br J Pharmacol, 176*(3), 491-504. doi:10.1111/bph.14555

Souers, A. J., Leverson, J. D., Boghaert, E. R., Ackler, S. L., Catron, N. D., Chen, J., . . . Elmore, S. W. (2013). ABT-199, a potent and selective BCL-2 inhibitor, achieves antitumor activity while sparing platelets. *Nat Med, 19*(2), 202-208. doi:10.1038/nm.3048

Spencer, D. H., Russler-Germain, D. A., Ketkar, S., Helton, N. M., Lamprecht, T. L., Fulton, R. S., . . . Ley, T. J. (2017). CpG Island Hypermethylation Mediated by DNMT3A Is a Consequence of AML Progression. *Cell, 168*(5), 801-816.e813. doi:10.1016/j.cell.2017.01.021

Sportoletti, P., Grisendi, S., Majid, S. M., Cheng, K., Clohessy, J. G., Viale, A., . . . Pandolfi, P. P. (2008). Npm1 is a haploinsufficient suppressor of myeloid and lymphoid malignancies in the mouse. *Blood, 111*(7), 3859-3862. doi:10.1182/blood-2007-06-098251

Sripayap, P., Nagai, T., Uesawa, M., Kobayashi, H., Tsukahara, T., Ohmine, K., . . . Ozawa, K. (2014). Mechanisms of resistance to azacitidine in human leukemia cell lines. *Exp Hematol, 42*(4), 294-306.e292. doi:10.1016/j.exphem.2013.12.004

Steensma, D. P., Bejar, R., Jaiswal, S., Lindsley, R. C., Sekeres, M. A., Hasserjian, R. P., & Ebert, B. L. (2015). Clonal hematopoiesis of indeterminate potential and its distinction from myelodysplastic syndromes. *Blood, 126*(1), 9-16. doi:10.1182/blood-2015-03-631747

Stein, E. M. (2018). Enasidenib, a targeted inhibitor of mutant IDH2 proteins for treatment of relapsed or refractory acute myeloid leukemia. *Future Oncol, 14*(1), 23-40. doi:10.2217/fon-2017-0392

Stein, E. M., DiNardo, C. D., Pollyea, D. A., Fathi, A. T., Roboz, G. J., Altman, J. K., . . . Tallman, M. S. (2017). Enasidenib in mutant *IDH2* relapsed or refractory acute myeloid leukemia. *Blood, 130*(6), 722-731. doi:10.1182/blood-2017-04-779405

Stennicke, H. R., Deveraux, Q. L., Humke, E. W., Reed, J. C., Dixit, V. M., & Salvesen, G. S. (1999). Caspase-9 can be activated without proteolytic processing. *J Biol Chem, 274*(13), 8359-8362. doi:10.1074/jbc.274.13.8359

Stone, R. M., Mandrekar, S. J., Sanford, B. L., Laumann, K., Geyer, S., Bloomfield, C. D., . . . Döhner, H. (2017). Midostaurin plus Chemotherapy for Acute Myeloid Leukemia with a FLT3 Mutation. *N Engl J Med, 377*(5), 454-464. doi:10.1056/NEJMoa1614359

Stratton, M. R., Campbell, P. J., & Futreal, P. A. (2009). The cancer genome. *Nature, 458*(7239), 719-724. doi:10.1038/nature07943

Strom, S. P. (2016). Current practices and guidelines for clinical next-generation sequencing oncology testing. *Cancer Biol Med, 13*(1), 3-11. doi:10.28092/j.issn.2095-3941.2016.0004

Stubbington, M. J. T., Lönnberg, T., Proserpio, V., Clare, S., Speak, A. O., Dougan, G., & Teichmann, S. A. (2016). T cell fate and clonality inference from single-cell transcriptomes. *Nat Methods, 13*(4), 329-332. doi:10.1038/nmeth.3800

Suresh, B., Lee, J., Kim, K. S., & Ramakrishna, S. (2016). The Importance of Ubiquitination and Deubiquitination in Cellular Reprogramming. *Stem Cells Int, 2016*, 6705927. doi:10.1155/2016/6705927

Sutherland, H. J., Hogge, D. E., & Eaves, C. J. (1993). Growth factor regulation of the maintenance and differentiation of human long-term culture-initiating cells (LTC-IC). *Leukemia, 7 Suppl 2*, S122-125.

Swerdlow, S. H., Campo, E., & Harris, N. L. (2008). *WHO Classification of Tumours of Haematopoietic and Lymphoid Tissues* (4th ed.). Lyn,France: IARC Press.

Swords, R. T., Coutre, S., Maris, M. B., Zeidner, J. F., Foran, J. M., Cruz, J., . . . Savona, M. R. (2018). Pevonedistat, a first-in-class NEDD8-activating enzyme inhibitor, combined with azacitidine in patients with AML. *Blood, 131*(13), 1415-1424. doi:10.1182/blood-2017-09-805895

Swords, R. T., Erba, H. P., DeAngelo, D. J., Bixby, D. L., Altman, J. K., Maris, M., . . . Medeiros, B. C. (2015). Pevonedistat (MLN4924), a First-in-Class NEDD8-activating enzyme inhibitor, in patients with acute myeloid leukaemia and myelodysplastic syndromes: a phase 1 study. *Br J Haematol, 169*(4), 534-543. doi:10.1111/bjh.13323

Swords, R. T., Kelly, K. R., Smith, P. G., Garnsey, J. J., Mahalingam, D., Medina, E., . . . Carew, J. S. (2010). Inhibition of NEDD8-activating enzyme: a novel approach for the treatment of acute myeloid leukemia. *Blood, 115*(18), 3796-3800. doi:10.1182/blood-2009-11-254862

Tadesse, S., Caldon, E. C., Tilley, W., & Wang, S. (2019). Cyclin-Dependent Kinase 2 Inhibitors in Cancer Therapy: An Update. *J Med Chem, 62*(9), 4233-4251. doi:10.1021/acs.jmedchem.8b01469

Takahashi, S. (2011). Downstream molecular pathways of FLT3 in the pathogenesis of acute myeloid leukemia: biology and therapeutic implications. *J Hematol Oncol, 4*, 13. doi:10.1186/1756-8722-4-13

Tamm, I., Wang, Y., Sausville, E., Scudiero, D. A., Vigna, N., Oltersdorf, T., & Reed, J. C. (1998). IAP-family protein survivin inhibits caspase activity and apoptosis induced by Fas (CD95), Bax, caspases, and anticancer drugs. *Cancer Res, 58*(23), 5315-5320.

Tan, P., Wei, A., Mithraprabhu, S., Cummings, N., Liu, H. B., Perugini, M., . . . Spencer, A. (2014). Dual epigenetic targeting with panobinostat and azacitidine in acute myeloid leukemia and high-risk myelodysplastic syndrome. *Blood Cancer J, 4*, e170. doi:10.1038/bcj.2013.68

Tao, Z. F., Hasvold, L., Wang, L., Wang, X., Petros, A. M., Park, C. H., . . . Souers, A. J. (2014). Discovery of a Potent and Selective BCL-XL Inhibitor with in Vivo Activity. *ACS Med Chem Lett, 5*(10), 1088-1093. doi:10.1021/ml5001867

Taylor, A. (1993). Aminopeptidases: structure and function. *FASEB J, 7*(2), 290-298. doi:10.1096/fasebj.7.2.8440407

Teh, T. C., Nguyen, N. Y., Moujalled, D. M., Segal, D., Pomilio, G., Rijal, S., . . . Wei, A. H. (2018). Enhancing venetoclax activity in acute myeloid leukemia by co-targeting MCL1. *Leukemia, 32*(2), 303-312. doi:10.1038/leu.2017.243

Tetsu, O., & McCormick, F. (2003). Proliferation of cancer cells despite CDK2 inhibition. *Cancer Cell, 3*(3), 233-245.

Thiel, A. T., Huang, J., Lei, M., & Hua, X. (2012). Menin as a hub controlling mixed lineage leukemia. *Bioessays, 34*(9), 771-780. doi:10.1002/bies.201200007

Thol, F., Bollin, R., Gehlhaar, M., Walter, C., Dugas, M., Suchanek, K. J., . . . Heuser, M. (2014). Mutations in the cohesin complex in acute myeloid leukemia: clinical and prognostic implications. *Blood, 123*(6), 914-920. doi:10.1182/blood-2013-07-518746

Thol, F., Damm, F., Lüdeking, A., Winschel, C., Wagner, K., Morgan, M., . . . Heuser, M. (2011). Incidence and prognostic influence of DNMT3A mutations in acute myeloid leukemia. *J Clin Oncol, 29*(21), 2889-2896. doi:10.1200/JCO.2011.35.4894

Thol, F., Heuser, M., & Ganser, A. (2015). Myelodysplastic syndromes. *Internist (Berl), 56*(4), 364-373. doi:10.1007/s00108-014-3598-3

Thornton, T. M., Delgado, P., Chen, L., Salas, B., Krementsov, D., Fernandez, M., . . . Rincón, M. (2016). Inactivation of nuclear GSK3β by Ser(389) phosphorylation promotes lymphocyte fitness during DNA double-strand break response. *Nat Commun, 7*, 10553. doi:10.1038/ncomms10553

Thornton, T. M., Pedraza-Alva, G., Deng, B., Wood, C. D., Aronshtam, A., Clements, J. L., . . . Rincon, M. (2008). Phosphorylation by p38 MAPK as an alternative pathway for GSK3beta inactivation. *Science, 320*(5876), 667-670. doi:10.1126/science.1156037

Tibbetts, M. D., Zheng, L., & Lenardo, M. J. (2003). The death effector domain protein family: regulators of cellular homeostasis. *Nat Immunol, 4*(5), 404-409. doi:10.1038/ni0503-404

Tickenbrock, L., Klein, H. U., Trento, C., Hascher, A., Göllner, S., Bäumer, N., . . . Group, S. A. L. (2011). Increased HDAC1 deposition at hematopoietic promoters in AML and its association with patient survival. *Leuk Res, 35*(5), 620-625. doi:10.1016/j.leukres.2010.11.006

Till, J. E., & McCulloch, E. A. (1961). A direct measurement of the radiation sensitivity of normal mouse bone marrow cells. *Radiat Res, 14*, 213-222.

Timofeev, O., Cizmecioglu, O., Settele, F., Kempf, T., & Hoffmann, I. (2010). Cdc25 phosphatases are required for timely assembly of CDK1-cyclin B at the G2/M transition. *J Biol Chem, 285*(22), 16978-16990. doi:10.1074/jbc.M109.096552

Tong, W. G., Chen, R., Plunkett, W., Siegel, D., Sinha, R., Harvey, R. D., . . . Wierda, W. G. (2010). Phase I and pharmacologic study of SNS-032, a potent and selective Cdk2, 7, and 9 inhibitor, in patients with advanced chronic lymphocytic leukemia and multiple myeloma. *J Clin Oncol, 28*(18), 3015-3022. doi:10.1200/JCO.2009.26.1347

Toofan, P., Busch, C., Morrison, H., O'Brien, S., Jørgensen, H., Copland, M., & Wheadon, H. (2018). Chronic myeloid leukaemia cells require the bone morphogenic protein pathway for cell cycle progression and self-renewal. *Cell Death Dis, 9*(9), 927. doi:10.1038/s41419-018-0905-2

Torisawa, Y. S., Spina, C. S., Mammoto, T., Mammoto, A., Weaver, J. C., Tat, T., . . . Ingber, D. E. (2014). Bone marrow-on-a-chip replicates hematopoietic niche physiology in vitro. *Nat Methods, 11*(6), 663-669. doi:10.1038/nmeth.2938

Trapnell, C., Cacchiarelli, D., Grimsby, J., Pokharel, P., Li, S., Morse, M., . . . Rinn, J. L. (2014). The dynamics and regulators of cell fate decisions are revealed by pseudotemporal ordering of single cells. *Nat Biotechnol, 32*(4), 381-386. doi:10.1038/nbt.2859

Tse, C., Shoemaker, A. R., Adickes, J., Anderson, M. G., Chen, J., Jin, S., . . . Elmore, S. W. (2008). ABT-263: a potent and orally bioavailable Bcl-2 family inhibitor. *Cancer Res, 68*(9), 3421-3428. doi:10.1158/0008-5472.CAN-07-5836

Tuynman, J. B., Peppelenbosch, M. P., & Richel, D. J. (2004). COX-2 inhibition as a tool to treat and prevent colorectal cancer. *Crit Rev Oncol Hematol, 52*(2), 81-101. doi:10.1016/j.critrevonc.2004.08.004

Tuynman, J. B., Vermeulen, L., Boon, E. M., Kemper, K., Zwinderman, A. H., Peppelenbosch, M. P., & Richel, D. J. (2008). Cyclooxygenase-2 inhibition inhibits c-Met kinase activity and Wnt activity in colon cancer. *Cancer Res, 68*(4), 1213-1220. doi:10.1158/0008-5472.CAN-07-5172

Ubersax, J. A., & Ferrell, J. E. (2007). Mechanisms of specificity in protein phosphorylation. *Nat Rev Mol Cell Biol, 8*(7), 530-541. doi:10.1038/nrm2203

University of Chicago, H. M. C. R. T. (2016). How I diagnose and manage individuals at risk for inherited myeloid malignancies. *Blood, 128*(14), 1800-1813. doi:10.1182/blood-2016-05-670240

Upreti, M., Galitovskaya, E. N., Chu, R., Tackett, A. J., Terrano, D. T., Granell, S., & Chambers, T. C. (2008). Identification of the major phosphorylation site in Bcl-xL induced by microtubule inhibitors and analysis of its functional significance. *J Biol Chem, 283*(51), 35517-35525. doi:10.1074/jbc.M805019200

van Baal, J. W., Diks, S. H., Wanders, R. J., Rygiel, A. M., Milano, F., Joore, J., . . . Krishnadath, K. K. (2006). Comparison of kinome profiles of Barrett's esophagus with normal squamous esophagus and normal gastric cardia. *Cancer Res, 66*(24), 11605-11612. doi:10.1158/0008-5472.CAN-06-1370

van de Winkel, A., Massl, R., Kuipers, E. J., van der Laan, L. J., & Peppelenbosch, M. P. (2013). Digestive disease week 2011: highlights of clinical and preclinical research on Barrett's esophagus and associated esophageal adenocarcinoma. *Dis Esophagus, 26*(2), 130-140. doi:10.1111/j.1442-2050.2012.01340.x

van Lochem, E. G., van der Velden, V. H., Wind, H. K., te Marvelde, J. G., Westerdaal, N. A., & van Dongen, J. J. (2004). Immunophenotypic differentiation patterns of normal hematopoiesis in human bone marrow: reference patterns for age-related changes and disease-induced shifts. *Cytometry B Clin Cytom, 60*(1), 1-13. doi:10.1002/cyto.b.20008

Varadarajan, S., Poornima, P., Milani, M., Gowda, K., Amin, S., Wang, H. G., & Cohen, G. M. (2015). Maritoclax and dinaciclib inhibit MCL-1 activity and induce apoptosis in both a MCL-1-dependent and -independent manner. *Oncotarget, 6*(14), 12668-12681. doi:10.18632/oncotarget.3706

Verfaillie, C. (2003). Regulation of hematopoiesis. In S. N. Wickramasinghe & J. McCullough (Eds.), *Blood and Bone Marrow Pathology*. New York: Churchill Livingstone.

Verhaak, R. G., Goudswaard, C. S., van Putten, W., Bijl, M. A., Sanders, M. A., Hugens, W., . . . Valk, P. J. (2005). Mutations in nucleophosmin (NPM1) in acute myeloid leukemia (AML): association with other gene abnormalities and previously established gene expression signatures and their favorable prognostic significance. *Blood, 106*(12), 3747-3754. doi:10.1182/blood-2005-05-2168

Vogler, M., Walter, H. S., & Dyer, M. J. S. (2017). Targeting anti-apoptotic BCL2 family proteins in haematological malignancies - from pathogenesis to treatment. *Br J Haematol, 178*(3), 364-379. doi:10.1111/bjh.14684

Vosberg, S., & Greif, P. A. (2019). Clonal evolution of acute myeloid leukemia from diagnosis to relapse. *Genes Chromosomes Cancer, 58*(12), 839-849. doi:10.1002/gcc.22806

Walsby, E., Lazenby, M., Pepper, C., & Burnett, A. K. (2011). The cyclin-dependent kinase inhibitor SNS-032 has single agent activity in AML cells and is highly synergistic with cytarabine. *Leukemia, 25*(3), 411-419. doi:10.1038/leu.2010.290

Walsby, E., Pratt, G., Shao, H., Abbas, A. Y., Fischer, P. M., Bradshaw, T. D., . . . Pepper, C. (2014). A novel Cdk9 inhibitor preferentially targets tumor cells and synergizes with fludarabine. *Oncotarget, 5*(2), 375-385. doi:10.18632/oncotarget.1568

Walter, M. J. (2015). What came first: MDS or AML? *Blood, 125*(9), 1357-1358. doi:10.1182/blood-2015-01-621193

Walter, R. B., Appelbaum, F. R., Estey, E. H., & Bernstein, I. D. (2012). Acute myeloid leukemia stem cells and CD33-targeted immunotherapy. *Blood, 119*(26), 6198-6208. doi:10.1182/blood-2011-11-325050

Walter, R. B., Buckley, S. A., Pagel, J. M., Wood, B. L., Storer, B. E., Sandmaier, B. M., . . . Appelbaum, F. R. (2013). Significance of minimal residual disease before myeloablative allogeneic hematopoietic cell transplantation for AML in first and second complete remission. *Blood, 122*(10), 1813-1821. doi:10.1182/blood-2013-06-506725

Walter, R. B., Kantarjian, H. M., Huang, X., Pierce, S. A., Sun, Z., Gundacker, H. M., . . . Estey, E. H. (2010). Effect of complete remission and responses less than complete remission on survival in acute myeloid leukemia: a combined Eastern Cooperative Oncology Group, Southwest Oncology Group, and M. D. Anderson Cancer Center Study. *J Clin Oncol, 28*(10), 1766-1771. doi:10.1200/JCO.2009.25.1066

Wang, J. M., Chao, J. R., Chen, W., Kuo, M. L., Yen, J. J., & Yang-Yen, H. F. (1999). The antiapoptotic gene mcl-1 is up-regulated by the phosphatidylinositol 3-kinase/Akt signaling pathway through a transcription factor complex containing CREB. *Mol Cell Biol, 19*(9), 6195-6206.

Wang, J., Yang, T., Xu, G., Liu, H., Ren, C., Xie, W., & Wang, M. (2016). Cyclin-Dependent Kinase 2 Promotes Tumor Proliferation and Induces Radio Resistance in Glioblastoma. *Transl Oncol, 9*(6), 548-556. doi:10.1016/j.tranon.2016.08.007

Wang, S., Zhao, Y., Aguilar, A., Bernard, D., & Yang, C. Y. (2017). Targeting the MDM2-p53 Protein-Protein Interaction for New Cancer Therapy: Progress and Challenges. *Cold Spring Harb Perspect Med, 7*(5). doi:10.1101/cshperspect.a026245

Weber, J. D., Taylor, L. J., Roussel, M. F., Sherr, C. J., & Bar-Sagi, D. (1999). Nucleolar Arf sequesters Mdm2 and activates p53. *Nat Cell Biol, 1*(1), 20-26. doi:10.1038/8991

Wei, A. H., Strickland, S. A., Hou, J. Z., Fiedler, W., Lin, T. L., Walter, R. B., . . . Roboz, G. J. (2019). Venetoclax Combined With Low-Dose Cytarabine for Previously Untreated Patients With Acute Myeloid Leukemia: Results From a Phase Ib/II Study. *J Clin Oncol, 37*(15), 1277-1284. doi:10.1200/JCO.18.01600

Wei, D., Zhang, Q., Schreiber, J. S., Parsels, L. A., Abulwerdi, F. A., Kausar, T., . . . Morgan, M. A. (2015). Targeting mcl-1 for radiosensitization of pancreatic cancers. *Transl Oncol, 8*(1), 47-54. doi:10.1016/j.tranon.2014.12.004

Weisberg, E., Halilovic, E., Cooke, V. G., Nonami, A., Ren, T., Sanda, T., . . . Griffin, J. D. (2015). Inhibition of Wild-Type p53-Expressing AML by the Novel Small Molecule HDM2 Inhibitor CGM097. *Mol Cancer Ther, 14*(10), 2249-2259. doi:10.1158/1535-7163.MCT-15-0429

Weiss, R. B. (1992). The anthracyclines: will we ever find a better doxorubicin? *Semin Oncol, 19*(6), 670-686.

Whitman, S. P., Liu, S., Vukosavljevic, T., Rush, L. J., Yu, L., Liu, C., . . . Caligiuri, M. A. (2005). The MLL partial tandem duplication: evidence for recessive gain-of-function in acute myeloid leukemia identifies a novel patient subgroup for molecular-targeted therapy. *Blood, 106*(1), 345-352. doi:10.1182/blood-2005-01-0204

Whitman, S. P., Maharry, K., Radmacher, M. D., Becker, H., Mrózek, K., Margeson, D., . . . Bloomfield, C. D. (2010). FLT3 internal tandem duplication associates with adverse outcome and gene- and microRNA-expression signatures in patients 60 years of age or older with primary cytogenetically normal acute myeloid leukemia: a Cancer and Leukemia

Group B study. *Blood, 116*(18), 3622-3626. doi:10.1182/blood-2010-05-283648

Wiles, E. T., & Selker, E. U. (2017). H3K27 methylation: a promiscuous repressive chromatin mark. *Curr Opin Genet Dev, 43*, 31-37. doi:10.1016/j.gde.2016.11.001

Willems, E., Dedobbeleer, M., Digregorio, M., Lombard, A., Lumapat, P. N., & Rogister, B. (2018). The functional diversity of Aurora kinases: a comprehensive review. *Cell Div, 13*, 7. doi:10.1186/s13008-018-0040-6

Winters, A. C., & Bernt, K. M. (2017). MLL-Rearranged Leukemias-An Update on Science and Clinical Approaches. *Front Pediatr, 5*, 4. doi:10.3389/fped.2017.00004

Witkiewicz, A. K., & Knudsen, E. S. (2014). Retinoblastoma tumor suppressor pathway in breast cancer: prognosis, precision medicine, and therapeutic interventions. *Breast Cancer Res, 16*(3), 207. doi:10.1186/bcr3652

Wolber, E. M., Dame, C., Fahnenstich, H., Hofmann, D., Bartmann, P., Jelkmann, W., & Fandrey, J. (1999). Expression of the thrombopoietin gene in human fetal and neonatal tissues. *Blood, 94*(1), 97-105.

Wong, M. L., & Medrano, J. F. (2005). Real-time PCR for mRNA quantitation. *Biotechniques, 39*(1), 75-85. doi:10.2144/05391RV01

Wouters, B. J., Löwenberg, B., Erpelinck-Verschueren, C. A., van Putten, W. L., Valk, P. J., & Delwel, R. (2009). Double CEBPA mutations, but not single CEBPA mutations, define a subgroup of acute myeloid leukemia with a distinctive gene expression profile that is uniquely associated with a favorable outcome. *Blood, 113*(13), 3088-3091. doi:10.1182/blood-2008-09-179895

Wu, H., Coskun, V., Tao, J., Xie, W., Ge, W., Yoshikawa, K., . . . Sun, Y. E. (2010). Dnmt3a-dependent nonpromoter DNA methylation facilitates transcription of neurogenic genes. *Science, 329*(5990), 444-448. doi:10.1126/science.1190485

Wu, X., Bayle, J. H., Olson, D., & Levine, A. J. (1993). The p53-mdm-2 autoregulatory feedback loop. *Genes Dev, 7*(7A), 1126-1132. doi:10.1101/gad.7.7a.1126

Wu, X., Xing, X., Dowlut, D., Zeng, Y., Liu, J., & Liu, X. (2019). Integrating phosphoproteomics into kinase-targeted cancer therapies in precision medicine. *J Proteomics, 191*, 68-79. doi:10.1016/j.jprot.2018.03.033

Wunderlich, M., Chou, F. S., Sexton, C., Presicce, P., Chougnet, C. A., Aliberti, J., & Mulloy, J. C. (2018). Improved multilineage human hematopoietic reconstitution and function in NSGS mice. *PLoS One, 13*(12), e0209034. doi:10.1371/journal.pone.0209034

Xenaki, D., Pierce, A., Underhill-Day, N., Whetton, A. D., & Owen-Lynch, P. J. (2004). Bcr-Abl-mediated molecular mechanism for apoptotic suppression in multipotent haemopoietic cells: a role for PKCbetaII. *Cell Signal, 16*(2), 145-156. doi:10.1016/s0898-6568(03)00101-3

Xie, M., Lu, C., Wang, J., McLellan, M. D., Johnson, K. J., Wendl, M. C., . . . Ding, L. (2014). Age-related mutations associated with clonal hematopoietic expansion and malignancies. *Nat Med, 20*(12), 1472-1478. doi:10.1038/nm.3733

Xu, W., Yang, H., Liu, Y., Yang, Y., Wang, P., Kim, S. H., . . . Xiong, Y. (2011). Oncometabolite 2-hydroxyglutarate is a competitive inhibitor of α-ketoglutarate-dependent dioxygenases. *Cancer Cell, 19*(1), 17-30. doi:10.1016/j.ccr.2010.12.014

Xue, Y., Meehan, B., Macdonald, E., Venneti, S., Wang, X. Q. D., Witkowski, L., . . . Huang, S. (2019). CDK4/6 inhibitors target SMARCA4-determined cyclin D1 deficiency in hypercalcemic small cell carcinoma of the ovary. *Nat Commun, 10*(1), 558. doi:10.1038/s41467-018-06958-9

Yamada, A., Arakaki, R., Saito, M., Kudo, Y., & Ishimaru, N. (2017). Dual Role of Fas/FasL-Mediated Signal in Peripheral Immune Tolerance. *Front Immunol, 8*, 403. doi:10.3389/fimmu.2017.00403

Yamaguchi, H., Hsu, J. L., & Hung, M. C. (2012). Regulation of ubiquitination-mediated protein degradation by survival kinases in cancer. *Front Oncol, 2*, 15. doi:10.3389/fonc.2012.00015

Yamaguchi, R., Lartigue, L., Perkins, G., Scott, R. T., Dixit, A., Kushnareva, Y., . . . Newmeyer, D. D. (2008). Opa1-mediated cristae opening is Bax/Bak and BH3 dependent, required for apoptosis, and independent of Bak oligomerization. *Mol Cell, 31*(4), 557-569. doi:10.1016/j.molcel.2008.07.010

Yamamoto, K., Ichijo, H., & Korsmeyer, S. J. (1999). BCL-2 is phosphorylated and inactivated by an ASK1/Jun N-terminal protein kinase pathway normally activated at G(2)/M. *Mol Cell Biol, 19*(12), 8469-8478.

Yanagi, T., & Matsuzawa, S. (2015). PCTAIRE1/PCTK1/CDK16: a new oncotarget? Cell Cycle, 14(4), 463-464. doi:10.1080/15384101.2015.1006539

Yang, C., Boyson, C. A., Di Liberto, M., Huang, X., Hannah, J., Dorn, D. C., . . . Zhou, P. (2015). CDK4/6 Inhibitor PD 0332991 Sensitizes Acute Myeloid Leukemia to Cytarabine-Mediated Cytotoxicity. *Cancer Res, 75*(9), 1838-1845. doi:10.1158/0008-5472.CAN-14-2486

Yang, J., Ikezoe, T., Nishioka, C., Udaka, K., & Yokoyama, A. (2014). Bcr-Abl activates AURKA and AURKB in chronic myeloid leukemia cells via AKT signaling. *Int J Cancer, 134*(5), 1183-1194. doi:10.1002/ijc.28434

Yang, L., Rau, R., & Goodell, M. A. (2015). DNMT3A in haematological malignancies. *Nat Rev Cancer, 15*(3), 152-165. doi:10.1038/nrc3895

Yang, Z., He, N., & Zhou, Q. (2008). Brd4 recruits P-TEFb to chromosomes at late mitosis to promote G1 gene expression and cell cycle progression. *Mol Cell Biol, 28*(3), 967-976. doi:10.1128/MCB.01020-07

Yang, Z., Zheng, C., Thiriet, C., & Hayes, J. J. (2005). The core histone N-terminal tail domains negatively regulate binding of transcription factor IIIA to a nucleosome containing a 5S RNA gene via a novel mechanism. *Mol Cell Biol, 25*(1), 241-249. doi:10.1128/MCB.25.1.241-249.2005

Yao, G. (2014). Modelling mammalian cellular quiescence. *Interface Focus, 4*(3), 20130074. doi:10.1098/rsfs.2013.0074

Yasui, H., Hideshima, T., Ikeda, H., Jin, J., Ocio, E. M., Kiziltepe, T., . . . Anderson, K. C. (2007). BIRB 796 enhances cytotoxicity triggered by bortezomib, heat shock protein (Hsp) 90 inhibitor, and dexamethasone via inhibition of p38 mitogen-activated protein kinase/Hsp27 pathway in multiple myeloma cell lines and inhibits paracrine tumour growth. *Br J Haematol, 136*(3), 414-423. doi:10.1111/j.1365-2141.2006.06443.x

Yin, T., Lallena, M. J., Kreklau, E. L., Fales, K. R., Carballares, S., Torrres, R., . . . Du, J. (2014). A novel CDK9 inhibitor shows potent antitumor efficacy in preclinical hematologic tumor models. *Mol Cancer Ther, 13*(6), 1442-1456. doi:10.1158/1535-7163.MCT-13-0849

Ying, M., Shao, X., Jing, H., Liu, Y., Qi, X., Cao, J., . . . He, Q. (2018). Ubiquitin-dependent degradation of CDK2 drives the therapeutic

differentiation of AML by targeting PRDX2. *Blood, 131*(24), 2698-2711. doi:10.1182/blood-2017-10-813139

Yoshizato, T., Dumitriu, B., Hosokawa, K., Makishima, H., Yoshida, K., Townsley, D., . . . Ogawa, S. (2015). Somatic Mutations and Clonal Hematopoiesis in Aplastic Anemia. *N Engl J Med, 373*(1), 35-47. doi:10.1056/NEJMoa1414799

Yu, Y., Maggi, L. B., Brady, S. N., Apicelli, A. J., Dai, M. S., Lu, H., & Weber, J. D. (2006). Nucleophosmin is essential for ribosomal protein L5 nuclear export. *Mol Cell Biol, 26*(10), 3798-3809. doi:10.1128/MCB.26.10.3798-3809.2006

Zeidner, J. F., Foster, M. C., Blackford, A. L., Litzow, M. R., Morris, L. E., Strickland, S. A., . . . Karp, J. E. (2015). Randomized multicenter phase II study of flavopiridol (alvocidib), cytarabine, and mitoxantrone (FLAM) versus cytarabine/daunorubicin (7+3) in newly diagnosed acute myeloid leukemia. *Haematologica, 100*(9), 1172-1179. doi:10.3324/haematol.2015.125849

Zeidner, J. F., Foster, M. C., Blackford, A. L., Litzow, M. R., Morris, L. E., Strickland, S. A., . . . Karp, J. E. (2018). Final results of a randomized multicenter phase II study of alvocidib, cytarabine, and mitoxantrone versus cytarabine and daunorubicin (7 + 3) in newly diagnosed high-risk acute myeloid leukemia (AML). *Leuk Res, 72*, 92-95. doi:10.1016/j.leukres.2018.08.005

Zhang, B., Gojo, I., & Fenton, R. G. (2002). Myeloid cell factor-1 is a critical survival factor for multiple myeloma. *Blood, 99*(6), 1885-1893. doi:10.1182/blood.v99.6.1885

Zhang, Y. X., Sicinska, E., Czaplinski, J. T., Remillard, S. P., Moss, S., Wang, Y., . . . Wagner, A. J. (2014). Antiproliferative effects of CDK4/6 inhibition in CDK4-amplified human liposarcoma in vitro and in vivo. *Mol Cancer Ther, 13*(9), 2184-2193. doi:10.1158/1535-7163.MCT-14-0387

Zhang, Y., Chen, X., Gueydan, C., & Han, J. (2018). Plasma membrane changes during programmed cell deaths. *Cell Res, 28*(1), 9-21. doi:10.1038/cr.2017.133

Zhao, J., Kennedy, B. K., Lawrence, B. D., Barbie, D. A., Matera, A. G., Fletcher, J. A., & Harlow, E. (2000). NPAT links cyclin E-Cdk2 to the regulation of replication-dependent histone gene transcription. *Genes Dev, 14*(18), 2283-2297.

Zhou, J. X., & Li, X. (2015). Apoptosis in Polycystic Kidney Disease: From Pathogenesis to Treatment. In X. Li (Ed.), *Polycystic kidney disease* (1st ed., pp. 197-230). Brisbane, Australia: Codon Publications.

Zhu, W., Giangrande, P. H., & Nevins, J. R. (2004). E2Fs link the control of G1/S and G2/M transcription. *EMBO J, 23*(23), 4615-4626. doi:10.1038/sj.emboj.7600459

Zuber, J., Shi, J., Wang, E., Rappaport, A. R., Herrmann, H., Sison, E. A., . . . Vakoc, C. R. (2011). RNAi screen identifies Brd4 as a therapeutic target in acute myeloid leukaemia. *Nature, 478*(7370), 524-528. doi:10.1038/nature10334